

Development of the Enantioselective Oxidation of Secondary Alcohols and Natural Products Total Synthesis

Thesis by

Jeffrey T. Bagdanoff

In Partial Fulfillment of the Requirements

for the Degree of

Doctor of Philosophy



California Institute of Technology

Pasadena, California

2005

(Thesis Defended August 5, 2005)

© 2005

Jeffrey Thomas Bagdanoff

All Rights Reserved

For
Claire Weatherhead

Acknowledgements

The Stoltz group has collaborated to establish a work environment alive with creativity, based in mutual respect, and fortified with an amazing work ethic. It has been a truly rewarding experience to watch the lab grow from a group of friends, unsure of our common purpose but eager to find out, into a mature research force.

I'd like to first thank Brian for providing me with an excellent example of exactly what a successful, well-balanced scientist is. He has been a great motivator, mentor, teacher and friend over the years and I am constantly impressed at his ability to develop his students. That man knows what he is doing.

While every member of the group, past and present, has had an impact on me in my time here I would like to single out a few people. I'd like to thank all of my collaborators over the years, including Doug Behenna and, more recently, Jen Stockdill, for their diligent work on zoanthenol. While a number of people have contributed to various aspects of a rich palladium program, I'd like especially to thank Eric Ferriera, Raissa Trend, and Dave Ebner for keeping oxidation exciting and expanding my understanding of palladium catalysis. I'd like to thank Eric Ashley for pretending to not have a photographic memory and brightly outshining me during those early years as my baymate. (I was probably "in over my head" when I first got here.) I'd like to thank Uttam Tambar, Ryan Zeidan, Yeeman Ramtohul, and the Reverend Joel Austin for the many adventurous nights that made my last few years of bachelorhood here at Caltech memorable.

Which brings me to my bride-to-be. I need to thank Claire for standing by my side during the challenging times and lighting my way. I have the deepest gratitude for the love, patience and support she has given to me. I will work hard to return those gifts in our new life together.

Finally, I would like to thank my dad for setting the bar high, and my mom for helping my chin to reach it during my earliest years.

Abstract

Oxidation is a fundamental process in chemistry and biology. In synthetic chemistry, there are several methods for the asymmetric oxidation of organic substrates. Classically, these methods have focused on the delivery of a heteroatom from a reagent or catalyst to a prochiral substrate. What have historically been underdeveloped are enantioselective oxidation methods that do not involve the transfer of a heteroatom, but rather are defined by the enantioselective dehydrogenation of an organic substrate. This type of oxidative transformation was investigated using a palladium(II) catalyst system.

A palladium-catalyzed oxidative kinetic resolution of secondary alcohols was developed. Key features of the catalytic system include the use of (–)-sparteine as the source of chiral relay, and molecular oxygen as the sole stoichiometric oxidant. Under the described catalytic system, a number of benzylic and allylic alcohols have been oxidized in an enantioselective manner, to provide a ketone and residual alcohol in high enantiomeric excess and excellent yield.

Subsequent to the original system, the systematic investigation of a number of mechanistic hypotheses involving the role of exogenous bases and H-bonding additives prompted the discovery of new reaction conditions displaying greatly enhanced reactivity, selectivity, atom economy, and generality. The net result of these improvements was a catalytic system effective in oxidative desymmetrization of a number of complex *meso*-diols. Ultimately, these advances have permitted our method to be applied towards a number of synthetic endeavors, including the key step in the total synthesis of the natural product alkaloid (–)-lobeline.

Table of Contents

Acknowledgements.....	iv
Abstract.....	vi
Table of Contents.....	vii
List of Schemes.....	xi
List of Figures.....	xiv
List of Tables.....	xxi
Abbreviations.....	xxii

Section I.

Chapter 1 **Progress Toward the Total Synthesis of Zoanthenol**

I. Introduction.....	1
<i>Zoanthid natural products</i>	<i>1</i>
<i>Background</i>	<i>2</i>
<i>Retrosynthesis</i>	<i>6</i>
<i>Mechanistic Considerations</i>	<i>8</i>
 II. Results and Discussion	9
<i>Retrosynthetic analysis of the DEFG ring precursor</i>	<i>9</i>
<i>Synthetic Route from the Chiral Pool</i>	<i>10</i>
<i>Synthetic Route from Glycidol</i>	<i>11</i>

	<i>Synthetic Route from a Hetero-Diels-Alder Reaction</i>	13
	<i>Endgame for the Total Synthesis</i>	14
III.	Conclusion	15
IV.	Experimental Section	16
	<i>Materials and Methods</i>	16
	<i>Preparative Procedures</i>	17
IV.	Notes and References	23
V.	Appendix	25

Section II.

Chapter 2 **Development and Application of the Oxidative Kinetic**

Resolution of 2°-Alcohols by Catalytic Palladium

I.	Introduction	55
	<i>Enantioselective Oxidation Background</i>	55
	<i>The Original Oxidative Kinetic Resolution (OKR)</i>	57
II.	Results and Discussion	59

	<i>The Role of Exogenous Base and Alcohol Additives</i>	59
	<i>The Mechanistic Role of Potential H-Bond Donors</i>	72
	<i>Application to the Desymmetrization of Complex Meso-Diols</i>	82
	<i>Application to Pharmaceutical Intermediates</i>	89
	<i>L-Type Ligand Studies</i>	90
	<i>X-Type Ligand Studies</i>	98
III.	Conclusion	106
IV.	Experimental Section	108
	<i>Materials and Methods</i>	108
	<i>General Procedures</i>	110
	<i>Preparative Procedures</i>	116
V.	Notes and References	139
VI.	Appendix	145

Chapter 3 Total Synthesis of (–)-Lobeline and (–)-Sedamine by Palladium-Catalyzed Enantioselective Oxidation

I.	Introduction	230
	<i>Enantioselective Oxidation</i>	230

<i>Piperidine Natural Products</i>	232
<i>Proposed Biogenesis</i>	233
<i>Retrosynthesis</i>	235
<i>Results and Discussion</i>	236
<i>Preliminary Results</i>	236
<i>Revised Retrosynthesis</i>	241
<i>Total Synthesis of (–)-Lobeline</i>	241
<i>Features of the Oxidative Desymmetrization</i>	253
<i>Total Synthesis of (+)-Sedamine and (–)-Sedamine</i>	256
<i>Acidic Polonovski-Type Demethylation</i>	258
II. Conclusion	262
III. Experimental Section	
<i>Materials and Methods</i>	264
<i>Preparative Procedures</i>	266
IV. Notes and References	301
IV. Appendix	304

List of Schemes

Chapter 1

Scheme 1.	Miyashita's intramolecular Diels-Alder reaction	2
Scheme 2.	Synthesis of the Diels-Alder substrate	3
Scheme 3.	Endgame for Miashitas' norzoanthamine synthesis	4
Scheme 4.	Williams' synthetic studies on norzoanthamine AB-rings	4
Scheme 5.	Williams' tandem amination cyclization	5
Scheme 6.	Degradation of a sugar	10
Scheme 7.	Synthetic route from glycidol.....	11
Scheme 8.	Advancing to the final retron.....	12
Scheme 9.	Enantioselective hetero-Diels-Alder reaction	13
Scheme 10.	Advancing enantiopure synthetic intermediates	14
Scheme 11.	Endgame for zoanthenol	14

Chapter 2

Scheme 1.	Uemuras' protocol for the oxidation of alcohols	55
Scheme 2.	β -Silicon effect in cation stabilization	65
Scheme 3.	Tandem oxidation/intermolecular Si-transfer	65
Scheme 4.	Formation of a (sp) Pd(II) carbonate complex	72
Scheme 5.	Retrosynthesis of a polymethoxydiene	83
Scheme 6.	Variable ether arrays from a common source	84

Scheme 7.	Advancing the <i>anti</i> -ether array	85
Scheme 8.	Advancing the <i>syn</i> -ether array	86
Scheme 9.	Establishing relative stereochemistry	86
Scheme 10.	Enantioselective oxidative <i>meso</i> -diol desymmetrization	87
Scheme 11.	Homologation to the skipped framework	88
Scheme 12.	Regioselective formation of a palladium-alkoxide	100
Scheme 13.	A palladium phenoxide	102

Chapter 3

Scheme 1.	Epimerization pathway	234
Scheme 2.	Attempted ring hydrogenation route	237
Scheme 3.	Attempted tropenone route	239
Scheme 4.	Small quantities of a key intermediate	239
Scheme 5.	Diastereoselective reduction	240
Scheme 6.	Retrosynthesis of (–)-lobeline	241
Scheme 7.	Advancing the piperidine	242
Scheme 8.	Functionalizing the piperidine ring	243
Scheme 9.	Completion of the <i>meso</i> -diol	244
Scheme 10.	OKR on an advanced lobeline intermediate	246
Scheme 11.	Attempted methylation	246
Scheme 12.	Dynamic precipitation of (–)-lobeline	250
Scheme 13.	Derivatization to a HPLC tractable analogue	251
Scheme 14.	Previous enantioselective synthesis.....	257

Scheme 15.	OKR of a sedamine intermediate	257
Scheme 16.	Demethylation problem	259
Scheme 17.	Mechanism for the Polonovski demethylation	259
Scheme 18.	Modified Polonovski demethylation	260
Scheme 19.	Lobeline demethylation	262

List of Figures

Chapter 1

Figure 1.	Zoanthamine natural products	1
Figure 2.	Retrosynthetic analysis of zoanthenol.....	7
Figure 3.	A reasonable mechanism for the cyclization	8
Figure 4.	Retrosynthesis of caprolactam 33	11
Figure 5.	X-ray structure of phthalamide adduct 57	12
Figure 6.	Hetero-Diels-Alder catalyst	13

Appendix 1

Figure A1.1	¹ HNMR (300 MHz, CDCl ₃) of compound 63	27
Figure A1.2	Infrared spectrum (thin film/NaCl) of compound 63	28
Figure A1.3	¹³ CNMR (125 MHz, CDCl ₃) of compound 63	28
Figure A1.4	¹ HNMR (300 MHz, CDCl ₃) of compound 37	29
Figure A1.5	Infrared spectrum (thin film/NaCl) of compound 37	30
Figure A1.6	¹³ CNMR (125 MHz, CDCl ₃) of compound 37	30
Figure A1.7	¹ HNMR (300 MHz, CDCl ₃) of compound 64	31
Figure A1.8	Infrared spectrum (thin film/NaCl) of compound 64	32
Figure A1.9	¹³ CNMR (125 MHz, CDCl ₃) of compound 64	32
Figure A1.10	¹ HNMR (300 MHz, CDCl ₃) of compound 65	33
Figure A1.11	Infrared spectrum (thin film/NaCl) of compound 65	34
Figure A1.12	¹³ CNMR (125 MHz, CDCl ₃) of compound 65	34
Figure A1.13	¹ HNMR (300 MHz, CDCl ₃) of compound 57	35
Figure A1.14	Infrared spectrum (thin film/NaCl) of compound 57	36
Figure A1.15	¹³ CNMR (125 MHz, CDCl ₃) of compound 57	36
Figure A1.16	¹ HNMR (300 MHz, CDCl ₃) of compound 58	37
Figure A1.17	Infrared spectrum (thin film/NaCl) of compound 58	38
Figure A1.18	¹³ CNMR (125 MHz, CDCl ₃) of compound 58	38
Figure A1.19	¹ HNMR (300 MHz, CDCl ₃) of compound 59	39
Figure A1.20	Infrared spectrum (thin film/NaCl) of compound 59	40
Figure A1.21	¹³ CNMR (125 MHz, CDCl ₃) of compound 59	40
Figure A1.22	¹ HNMR (300 MHz, CDCl ₃) of compound 33	41

Figure A1.23	Infrared spectrum (thin film/NaCl) of compound 33	42
Figure A1.24	^{13}C NMR (125 MHz, CDCl_3) of compound 33	42
X-ray crystal structure report 1	43

Chapter 2

Figure 1.	Principles of an oxidative kinetic resolution.....	56
Figure 2.	X-Ray crystal structure of $\text{Pd}(\text{sp})\text{Cl}_2$	58
Figure 3.	Plausible mechanism for Pd catalyzed oxidation.....	60
Figure 4.	The potential role of Cs_2CO_3	64
Figure 5.	Crystal structure of $(\text{sp})\text{Pd}(\text{CO}_3)$	73
Figure 6.	Plausible mechanism involving H-bonding species	74
Figure 7.	Resolution vs. desymmetrization	83
Figure 8.	The chirality of (–)-sparteine	91
Figure 9.	Synthetic diamine vs. natural (–)-sparteine chiral pocket.....	92
Figure 10.	Bispinidones, bispinidines, and (–)-sparteine	93
Figure 11.	Calculated lowest energy pathway	98
Figure 12.	A model for asymmetric induction	101
Figure 13.	Crystal structure of $(\text{sp})\text{Pd}^{\text{II}}(\text{pentafluoropenoxide})$	103
Figure 14.	Experimental setup	110

Appendix 2

Figure A2.1	^1H NMR (300 MHz, CDCl_3) of compound 72	146
Figure A2.2	Infrared spectrum (thin film/NaCl) of compound 72	147
Figure A2.3	^{13}C NMR (125 MHz, CDCl_3) of compound 72	147
Figure A2.4	^1H NMR (300 MHz, CDCl_3) of compound 88	148

Figure A2.5	Infrared spectrum (thin film/NaCl) of compound 88	149
Figure A2.6	¹³ CNMR (125 MHz, CDCl ₃) of compound 88	149
Figure A2.7	¹ HNMR (300 MHz, CDCl ₃) of compound 96	150
Figure A2.8	Infrared spectrum (thin film/NaCl) of compound 96	151
Figure A2.9	¹³ CNMR (125 MHz, CDCl ₃) of compound 96	151
Figure A2.10	¹ HNMR (300 MHz, CDCl ₃) of compound 98	152
Figure A2.11	Infrared spectrum (thin film/NaCl) of compound 98	153
Figure A2.12	¹³ CNMR (125 MHz, CDCl ₃) of compound 98	153
Figure A2.13	¹ HNMR (300 MHz, CDCl ₃) of compound 99	154
Figure A2.14	Infrared spectrum (thin film/NaCl) of compound 99	155
Figure A2.15	¹³ CNMR (125 MHz, CDCl ₃) of compound 99	155
Figure A2.16	¹ HNMR (300 MHz, CDCl ₃) of compound 100	156
Figure A2.17	Infrared spectrum (thin film/NaCl) of compound 100	157
Figure A2.18	¹³ CNMR (125 MHz, CDCl ₃) of compound 100	157
Figure A2.19	¹ HNMR (300 MHz, CDCl ₃) of compound 101	158
Figure A2.20	Infrared spectrum (thin film/NaCl) of compound 101	159
Figure A2.21	¹³ CNMR (125 MHz, CDCl ₃) of compound 101	159
Figure A2.22	¹ HNMR (300 MHz, CDCl ₃) of compound 102	160
Figure A2.23	Infrared spectrum (thin film/NaCl) of compound 102	161
Figure A2.24	¹³ CNMR (125 MHz, CDCl ₃) of compound 102	161
Figure A2.25	¹ HNMR (300 MHz, CDCl ₃) of compound 103	162
Figure A2.26	Infrared spectrum (thin film/NaCl) of compound 103	163
Figure A2.27	¹³ CNMR (125 MHz, CDCl ₃) of compound 103	163
Figure A2.28	¹ HNMR (300 MHz, CDCl ₃) of compound 104	164
Figure A2.29	Infrared spectrum (thin film/NaCl) of compound 104	165
Figure A2.30	¹³ CNMR (125 MHz, CDCl ₃) of compound 104	165
Figure A2.31	¹ HNMR (300 MHz, CDCl ₃) of compound 105	166
Figure A2.32	Infrared spectrum (thin film/NaCl) of compound 105	167
Figure A2.33	¹³ CNMR (125 MHz, CDCl ₃) of compound 105	167
Figure A2.34	¹ HNMR (300 MHz, CDCl ₃) of compound 106	168
Figure A2.35	¹ HNMR NOE1 (300 MHz, CDCl ₃) of compound 106	169
Figure A2.36	¹ HNMR NOE2 (300 MHz, CDCl ₃) of compound 106	170
Figure A2.37	Infrared spectrum (thin film/NaCl) of compound 106	171
Figure A2.38	¹³ CNMR (125 MHz, CDCl ₃) of compound 106	171
Figure A2.39	¹ HNMR (300 MHz, CDCl ₃) of compound (–)- 107	172
Figure A2.40	Infrared spectrum (thin film/NaCl) of compound (–)- 107	173
Figure A2.41	¹³ CNMR (125 MHz, CDCl ₃) of compound (–)- 107	173
Figure A2.42	¹ HNMR (300 MHz, CDCl ₃) of compound 107a	174
Figure A2.43	Infrared spectrum (thin film/NaCl) of compound 107a	175
Figure A2.44	¹³ CNMR (125 MHz, CDCl ₃) of compound 107a	175
Figure A2.45	¹ HNMR (300 MHz, CDCl ₃) of compound (–)- 108	176
Figure A2.46	Infrared spectrum (thin film/NaCl) of compound (–)- 108	177
Figure A2.47	¹³ CNMR (125 MHz, CDCl ₃) of compound (–)- 108	177
Figure A2.48	¹ HNMR (300 MHz, CDCl ₃) of compound (–)- 109	178
Figure A2.49	Infrared spectrum (thin film/NaCl) of compound (–)- 109	179
Figure A2.50	¹³ CNMR (125 MHz, CDCl ₃) of compound (–)- 109	179

Figure A2.51	¹ HNMR (300 MHz, CDCl ₃) of compound 109a	181
Figure A2.52	Infrared spectrum (thin film/NaCl) of compound 109a	181
Figure A2.53	¹³ CNMR (125 MHz, CDCl ₃) of compound 109a	181
Figure A2.54	¹ HNMR (300 MHz, CDCl ₃) of compound 111	182
Figure A2.55	Infrared spectrum (thin film/NaCl) of compound 111	183
Figure A2.56	¹³ CNMR (125 MHz, CDCl ₃) of compound 111	183
Figure A2.57	¹ HNMR (300 MHz, CDCl ₃) of compound 112	184
Figure A2.58	Infrared spectrum (thin film/NaCl) of compound 112	185
Figure A2.59	¹³ CNMR (125 MHz, CDCl ₃) of compound 112	185
Figure A2.60	¹ HNMR (300 MHz, CDCl ₃) of compound 113	186
Figure A2.61	Infrared spectrum (thin film/NaCl) of compound 113	186
Figure A2.62	¹³ CNMR (125 MHz, CDCl ₃) of compound 113	187
Figure A2.63	¹ HNMR (300 MHz, CDCl ₃) of compound 114	188
Figure A2.64	Infrared spectrum (thin film/NaCl) of compound 114	189
Figure A2.65	¹³ CNMR (125 MHz, CDCl ₃) of compound 114	189
Figure A2.66	¹ HNMR (300 MHz, CDCl ₃) of compound 145	190
Figure A2.67	Infrared spectrum (thin film/NaCl) of compound 145	191
Figure A2.68	¹³ CNMR (125 MHz, CDCl ₃) of compound 145	191
Figure A2.69	¹ HNMR (300 MHz, CDCl ₃) of compound 146	193
Figure A2.70	Infrared spectrum (thin film/NaCl) of compound 146	193
Figure A2.71	¹³ CNMR (125 MHz, CDCl ₃) of compound 146	193
Figure A2.72	¹ HNMR (300 MHz, CDCl ₃) of compound 159	194
Figure A2.73	Infrared spectrum (thin film/NaCl) of compound 159	195
Figure A2.74	¹³ CNMR (125 MHz, CDCl ₃) of compound 159	195
X-ray crystal structure report 2.....		196
X-ray crystal structure report 3.....		208
X-ray crystal structure report 4.....		218

Chapter 3

Figure 1.	Structures of piperidine natural products	232
Figure 2.	Proposed biogenesis of (–)-lobeline	234
Figure 3.	Lobeline derived from a <i>meso</i> -diol	235
Figure 4.	Stereochemical rationale for hydride addition	243
Figure 5.	X-ray crystal structure of diol 206 (lobelanine)	245
Figure 6.	Predicted solution phase conformations	247
Figure 7.	Steric congestion about the 3°-amine in (–)-lobeline	249

Figure 8.	OKR vs. oxidative desymmetrization	254
Figure 9.	Retrosynthesis of sedamine alkaloids	256
Figure 10.	Proposed mechanism of the modified Polonovski	261
Figure 11.	Experimental setup	286

Appendix 3

Figure A3.1	¹ HNMR (300 MHz, CDCl ₃) of compound (<i>cis:trans</i>)- 162	305
Figure A3.2	IR spectrum (thin film/NaCl) of compound (<i>cis:trans</i>)- 162	306
Figure A3.3	¹³ CNMR (125 MHz, CDCl ₃) of compound (<i>cis:trans</i>)- 162	306
Figure A3.4	¹ HNMR (300 MHz, CDCl ₃) of compound 162	307
Figure A3.5	Infrared spectrum (thin film/NaCl) of compound 162	308
Figure A3.6	¹³ CNMR (125 MHz, CDCl ₃) of compound 162	308
Figure A3.7	¹ HNMR (300 MHz, CDCl ₃) of compound (–)- 163	309
Figure A3.8	Infrared spectrum (thin film/NaCl) of compound (–)- 163	310
Figure A3.9	¹³ CNMR (125 MHz, CDCl ₃) of compound (–)- 163	310
Figure A3.10	¹ HNMR (300 MHz, CDCl ₃) of compound (+)- 163	311
Figure A3.11	Infrared spectrum (thin film/NaCl) of compound (+)- 163	312
Figure A3.12	¹³ CNMR (125 MHz, CDCl ₃) of compound (+)- 163	312
Figure A3.13	¹ HNMR (300 MHz, D ₆ -DMSO) of compound 177	313
Figure A3.14	Infrared spectrum (KBr pellet) of compound 177	314
Figure A3.15	¹³ CNMR (125 MHz, D ₆ -DMSO) of compound 177	314
Figure A3.16	¹ HNMR (300 MHz, CDCl ₃) of compound 180	315
Figure A3.17	Infrared spectrum (thin film/NaCl) of compound 180	316
Figure A3.18	¹³ CNMR (125 MHz, CDCl ₃) of compound 180	316
Figure A3.19	¹ HNMR (300 MHz, CDCl ₃) of compound 182	317
Figure A3.20	Infrared spectrum (thin film/NaCl) of compound 182	317
Figure A3.21	¹³ CNMR (125 MHz, CDCl ₃) of compound 182	318
Figure A3.22	¹ HNMR (300 MHz, CDCl ₃) of compound 186	319
Figure A3.23	Infrared spectrum (thin film/NaCl) of compound 186	319
Figure A3.24	¹³ CNMR (125 MHz, CDCl ₃) of compound 186	320
Figure A3.25	¹ HNMR (300 MHz, CDCl ₃) of compound 187	321
Figure A3.26	Infrared spectrum (thin film/NaCl) of compound 187	322
Figure A3.27	¹³ CNMR (125 MHz, CDCl ₃) of compound 187	322
Figure A3.28	¹ HNMR (300 MHz, CDCl ₃) of compound 188	323
Figure A3.29	Infrared spectrum (thin film/NaCl) of compound 188	324
Figure A3.30	¹³ CNMR (125 MHz, CDCl ₃) of compound 188	324
Figure A3.31	¹ HNMR (300 MHz, CDCl ₃) of compound 190	325
Figure A3.32	Infrared spectrum (thin film/NaCl) of compound 190	326
Figure A3.33	¹³ CNMR (125 MHz, CDCl ₃) of compound 190	326
Figure A3.34	¹ HNMR (300 MHz, CDCl ₃) of compound 191	327

Figure A3.35	Infrared spectrum (thin film/NaCl) of compound 191	328
Figure A3.36	¹³ CNMR (125 MHz, CDCl ₃) of compound 191	328
Figure A3.37	¹ HNMR (300 MHz, CDCl ₃) of compound 193	329
Figure A3.38	Infrared spectrum (thin film/NaCl) of compound 193	330
Figure A3.39	¹³ CNMR (125 MHz, CDCl ₃) of compound 193	330
Figure A3.40	¹ HNMR (300 MHz, CDCl ₃) of compound 194	331
Figure A3.41	Infrared spectrum (thin film/NaCl) of compound 194	332
Figure A3.42	¹³ CNMR (125 MHz, CDCl ₃) of compound 194	332
Figure A3.43	¹ HNMR (300 MHz, CDCl ₃) of compound (–)- 194	333
Figure A3.44	Infrared spectrum (thin film/NaCl) of compound (–)- 194	334
Figure A3.45	¹³ CNMR (125 MHz, CDCl ₃) of compound (–)- 194	334
Figure A3.46	¹ HNMR (300 MHz, CDCl ₃) of compound (+)- 195	335
Figure A3.47	Infrared spectrum (thin film/NaCl) of compound (+)- 195	336
Figure A3.48	¹³ CNMR (125 MHz, CDCl ₃) of compound (+)- 195	336
Figure A3.49	¹ HNMR (300 MHz, CDCl ₃) of compound (–)- 195	337
Figure A3.50	Infrared spectrum (thin film/NaCl) of compound (–)- 195	338
Figure A3.51	¹³ CNMR (125 MHz, CDCl ₃) of compound (–)- 195	338
Figure A3.52	¹ HNMR (300 MHz, CDCl ₃) of compound (±)- 196	339
Figure A3.53	Infrared spectrum (thin film/NaCl) of compound (±)- 196	340
Figure A3.54	¹³ CNMR (125 MHz, CDCl ₃) of compound (±)- 196	340
Figure A3.55	¹ HNMR (300 MHz, CDCl ₃) of compound (±)- 199	341
Figure A3.56	Infrared spectrum (thin film/NaCl) of compound (±)- 199	342
Figure A3.57	¹³ CNMR (125 MHz, CDCl ₃) of compound (±)- 199	342
Figure A3.58	¹ HNMR (300 MHz, CDCl ₃) of compound (–)- 201	343
Figure A3.59	Infrared spectrum (thin film/NaCl) of compound (–)- 201	344
Figure A3.60	¹³ CNMR (125 MHz, CDCl ₃) of compound (–)- 201	344
Figure A3.61	¹ HNMR (300 MHz, CDCl ₃) of compound (±)- 202	345
Figure A3.62	Infrared spectrum (thin film/NaCl) of compound (±)- 202	346
Figure A3.63	¹³ CNMR (125 MHz, CDCl ₃) of compound (±)- 202	346
Figure A3.64	¹ HNMR (300 MHz, CDCl ₃) of compound (±)- 203	347
Figure A3.65	Infrared spectrum (thin film/NaCl) of compound (±)- 203	348
Figure A3.66	¹³ CNMR (125 MHz, CDCl ₃) of compound (±)- 203	348
Figure A3.67	¹ HNMR (300 MHz, CDCl ₃) of compound (±)- 204	349
Figure A3.68	Infrared spectrum (thin film/NaCl) of compound (±)- 204	350
Figure A3.69	¹³ CNMR (125 MHz, CDCl ₃) of compound (±)- 204	350
Figure A3.70	¹ HNMR (300 MHz, CDCl ₃) of compound 205	350
Figure A3.71	Infrared spectrum (thin film/NaCl) of compound 205	352
Figure A3.72	¹³ CNMR (125 MHz, CDCl ₃) of compound 205	352
Figure A3.73	¹ HNMR (300 MHz, CDCl ₃) of compound 206	353
Figure A3.74	Infrared spectrum (thin film/NaCl) of compound 206	354
Figure A3.75	¹³ CNMR (125 MHz, CDCl ₃) of compound 206	354
Figure A3.76	¹ HNMR (300 MHz, CDCl ₃) of compound 208	355
Figure A3.77	Infrared spectrum (thin film/NaCl) of compound 208	356
Figure A3.78	¹³ CNMR (125 MHz, CDCl ₃) of compound 208	356
Figure A3.79	¹ HNMR (300 MHz, CDCl ₃) of compound 217	357
Figure A3.80	Infrared spectrum (thin film/NaCl) of compound 217	358

Figure A3.81	^{13}C NMR (125 MHz, CDCl_3) of compound 217	358
Figure A3.82	^1H NMR (300 MHz, CDCl_3) of compound 218	359
Figure A3.83	Infrared spectrum (thin film/ NaCl) of compound 218	360
Figure A3.84	^{13}C NMR (125 MHz, CDCl_3) of compound 218	360
Figure A3.85	^1H NMR (300 MHz, CDCl_3) of compound 219	361
Figure A3.86	Infrared spectrum (thin film/ NaCl) of compound 219	362
Figure A3.87	^{13}C NMR (125 MHz, CDCl_3) of compound 219	362
X-ray crystal structure report 5.....		363

List of Tables

Chapter 2

Table 1.	The original oxidative kinetic resolution.....	57
Table 2.	<i>In situ</i> catalyst formation	59
Table 3.	Additive effects on the OKR.....	61
Table 4.	Effect of excess (–)-sparteine.....	63
Table 5.	Effect of an oxidatively inert alcohol	67
Table 6.	Effect of oxidatively inert alcohols on the OKR.....	68
Table 7.	Cumulative additive effects	70
Table 8.	Cs ₂ CO ₃ / <i>t</i> -BuOH-modified OKR	71
Table 9.	Impact of solvent on reaction rate	76
Table 10.	C–D stretch of CDCl ₃	77
Table 11.	Scope of the CHCl ₃ conditions	79
Table 12.	Comparison of oxidation performance	80
Table 13.	Effect of O ₂ concentration	81
Table 14.	Monoamine and diamine ligands	94
Table 15.	Impact of ligand structure on conversion	96
Table 16.	Effect of sodium phenoxide salts on the OKR	104

Chapter 3

Table 1.	Scope of the original palladium catalyzed OKR	230
Table 2.	Evolution of the palladium catalyzed OKR	231
Table 3.	Impact of <i>N</i> -protecting groups on the OKR	236

List of Abbreviations

$[\alpha]_D$	specific rotation at wavelength of sodium D line
aq.	aqueous
Ar	aryl
atm	atmosphere
BBN	borabicyclo[3.3.1]nonane
Bn	benzyl
Boc	<i>tert</i> -butyloxycarbonyl
bp	boiling point
br	broad
Bu	butyl
<i>i</i> -Bu	isobutyl
<i>n</i> -Bu	<i>n</i> -butyl
<i>t</i> -Bu	<i>tert</i> -butyl
Bz	benzoyl
<i>c</i>	concentration for specific rotation measurements
° C	degrees Celsius
calc'd	calculated
cat.	catalytic
comp	complex
d	doublet
DCC	dicyclohexylcarbodiimide

DCE	1,2-dichloroethane
DIBAL	diisobutylaluminum hydride
DMAP	4-dimethylaminopyridine
DMF	<i>N,N</i> -dimethylformamide
DMSO	dimethylsulfoxide
dr	diastereomeric ratio
ee	enantiomeric excess
EI	electrospray ionization
equiv	equivalents
Et	ethyl
EtOAc	ethyl acetate
FAB	fast atom bombardment
g	grams
GC	gas chromatography
[H]	reduction
h	hour(s)
h ν	light
HPLC	high performance liquid chromatography
HRMS	high resolution mass spectroscopy
Hz	hertz
Imid.	Imidazole
IR	infrared
<i>J</i>	coupling constant

Kcal	kilocalories
L	liter
LAH	lithium aluminum hydride
M	metal or molar
m	milli or multiplet or meters
m/z	mass to charge ratio
μ	micro
Me	methyl
MHz	megahertz
min	minutes
mol	moles
mmol	millimoles
mp	melting point
MS	molecular sieves
Ms	methanesulfonyl
N	normal
nbd	norbornadiene
NMO	<i>N</i> -methylmorpholine <i>N</i> -oxide
NMR	nuclear magnetic resonance
NOE	nuclear Overhouser effect
[O]	oxidation
OKR	oxidative kinetic resolution
Ph	phenyl

PhH	benzene
p <i>K</i> _a	acidity constant
ppm	parts per million
<i>i</i> -Pr	isopropyl
q	quartet
ref	reference
R _F	retention factor
s	singlet or selectivity factor
sp	(–)-sparteine
t	triplet
TBAF	tetrabutylammonium fluoride
TBS	<i>tert</i> -butyldimethylsilyl
TCA	trichloroacetic acid
Tf	trifluoromethanesulfonyl
TFA	trifluoroacetic acid
THF	tetrahydrofuran
TLC	thin-layer chromatography
TMS	trimethylsilyl
v/v	volume to volume
w/v	weight to volume

Chapter 1

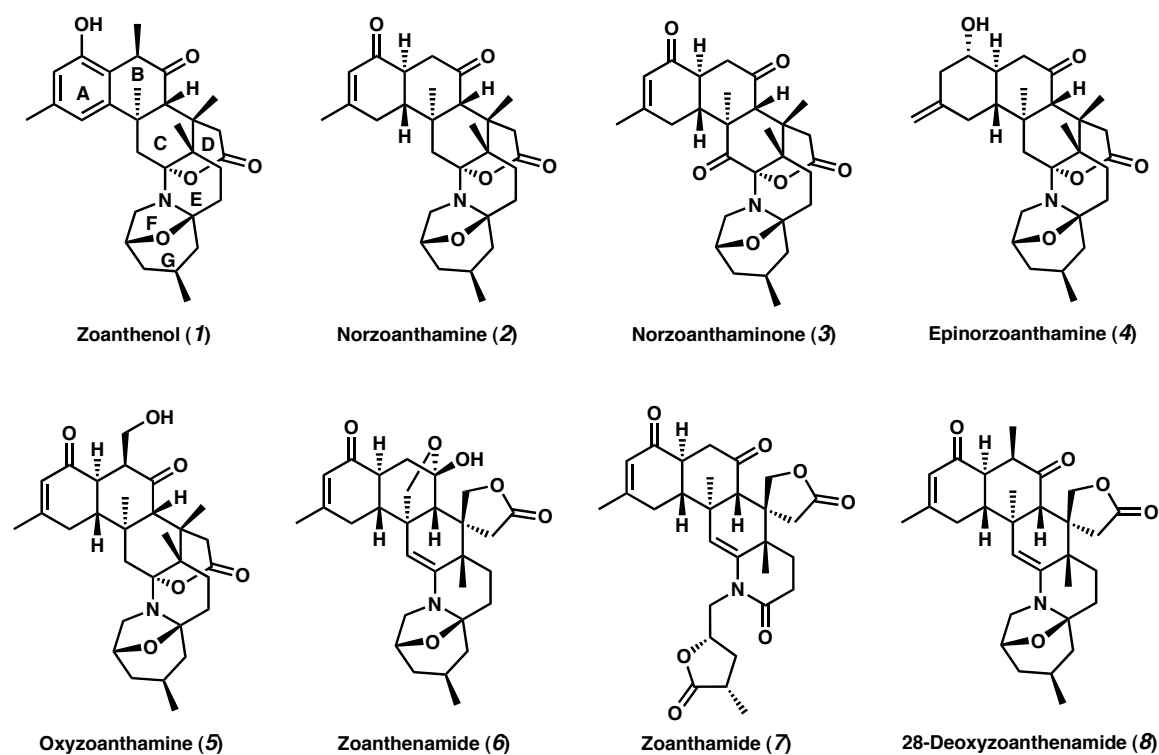
Progress Toward the Total Synthesis of Zoanthenol

I. Introduction

Zoanthid Natural Products

Zoanthenol **1** (Figure 1) is a member of the zoanthamine family of natural products, isolated from marine polyps (*Zoanthus sp.*) in 1999 off of the coast of India.¹ While zoanthenol **1** is a selective inhibitor of collagen-induced human platelet aggregation,² the range of zoanthus alkaloids exhibit interesting biological activities.

Figure 1. Zoanthamine natural products

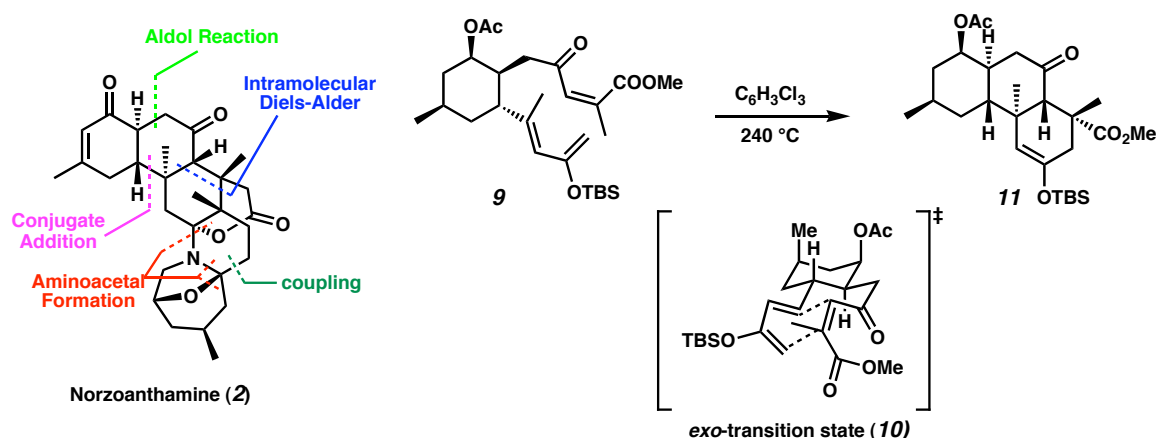


For example, norzoanthamine **2**, norzoanthaminone **3**, epinorzoanthamine **4**, and oxyzoanthamine **5** are all P388 murine leukemia inhibitors. Norzoanthamine **2** is also a potent antiosteoporotic due to its inhibitory activity against interleukin-6, and has been shown to counteract decreases in bone weight and strength in ovariectomized mice.³ Additionally, zoanthenamide **6**, zoanthamide **7**, and 28-deoxyzoanthenamide **8** all inhibit inflammation induced by phorbol myristate acetate (PMA) in a mouse-ear model.

Background

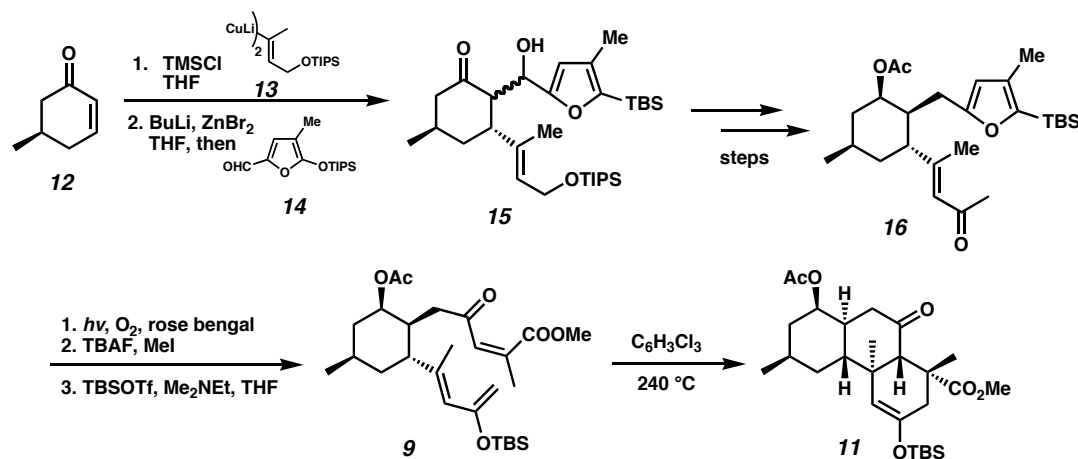
Despite the large structural diversity of the zoanthus alkaloids, the fact that several years have passed since their structural elucidation, and a number of relevant synthetic studies have been published, only a single total synthesis of a zoanthus alkaloid has been reported to date.⁴ The total synthesis of norzoanthamine was completed in 2004 by Miyashita and coworkers. As shown in Scheme 1, they dissected the structure of norzoanthamine **2** by a number of bond disconnections, with the key step in their synthesis resting on the formation of the ABC ring system.

Scheme 1. Miyashita's intramolecular Diels-Alder reaction

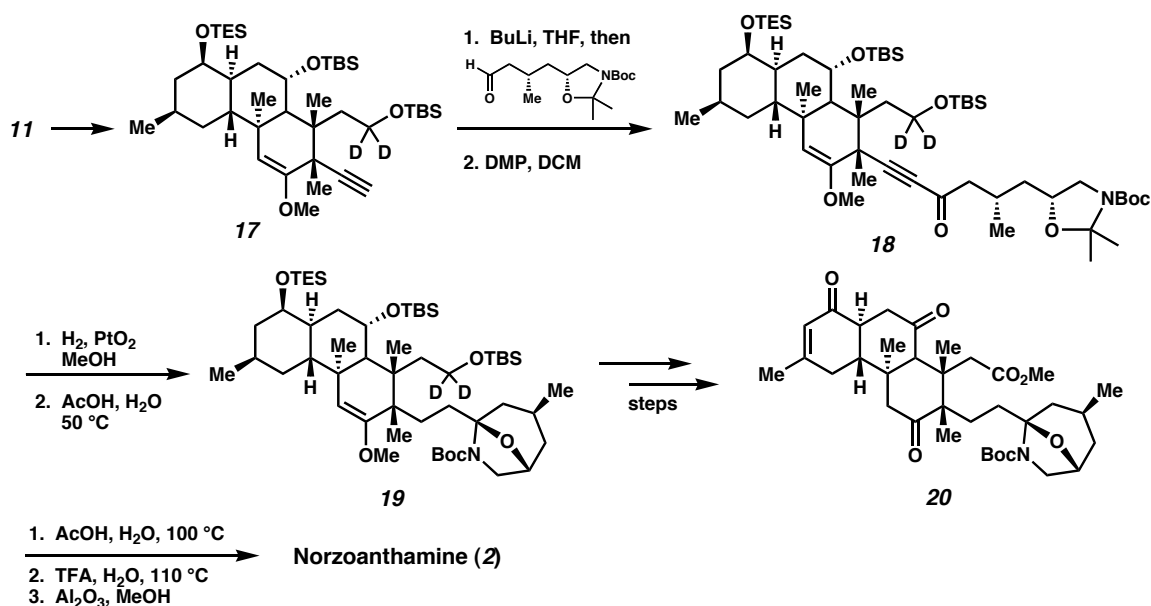


They constructed the tricycle with an intramolecular Diels-Alder reaction of triene **9**, which proceeded *via* *exo*-transition state **10** to form **11** as a mixture of cycloadducts in 98% combined yield. The intramolecular Diels-Alder substrate **9** was synthesized in 14 steps from the known chiral enone **12** by sequential C–C bond forming reactions including a diastereoselective cuprate addition with cuprate **13** and an aldol reaction with aldehyde **14** (Scheme 2), to provide furanol **15**. After elaboration of **15** to enone **16**, the tethered diene/dienophile pair are unveiled after functional group manipulation to provide Diels-Alder substrate **9**.

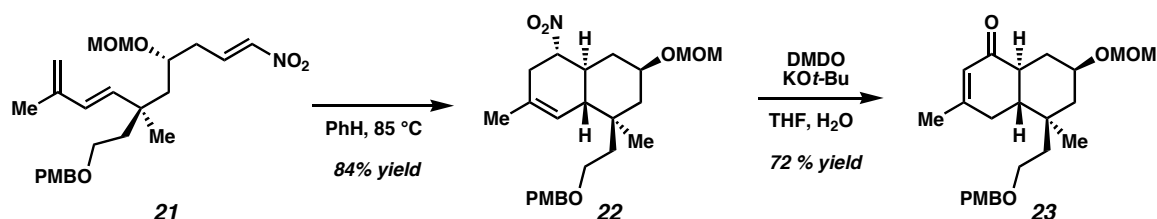
Scheme 2. Synthesis of the Diels-Alder substrate



After the Diels-Alder reaction, tricycle **11** is further elaborated into alkyne **17** in 14 synthetic steps (Scheme 3). Fragment coupling between alkyne **17** and an aldehyde occurs by nucleophilic attack to provide yne-one **18** after oxidation. Following reduction of the yne-one, the acetonide is selectively removed upon exposure to mild acid, and the system cyclizes to form hemi-aminal **19**, which is converted into triketone **20** in several steps. At this stage, the final aminal cyclization event is triggered by strongly acidic conditions and the final product is free-based to provide norzoanthamine **2**.

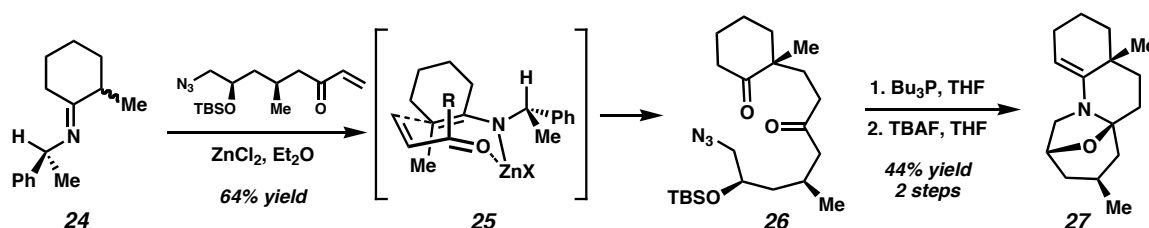
Scheme 3. Endgame for Miashita's norzoanthamine synthesis

Aside from the total synthesis of norzoanthamine **2**, a number of other groups have conducted synthetic studies toward a number of zoanthamine alkaloids. The Williams group synthesized the AB-rings of norzoanthamine **2** using an intramolecular Diels-Alder reaction of ene-diyne **21** to establish the bicyclic carbon framework **22** (Scheme 4).⁵ Subsequently, a Nef reaction completes the synthesis of enone **23**, present in the A-ring of norzoanthamine **2** (Figure 1).

Scheme 4. Williams' synthetic studies on norzoanthamine AB-rings

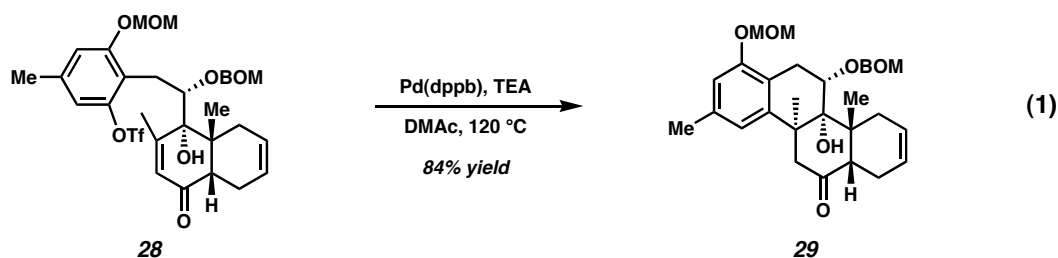
Williams also published an approach to the CEEG ring system of zoanthid alkaloids involving a diastereoselective conjugate addition directed by the chiral enamine **24**, which may proceed through contact pair **25** (Scheme 5). A minimization of non-bonding allylic interactions of the chiral controller unit present in transition state **25** dictates the facial approach of the enone opposite to the phenyl group.

Scheme 5. Williams' tandem amination cyclization

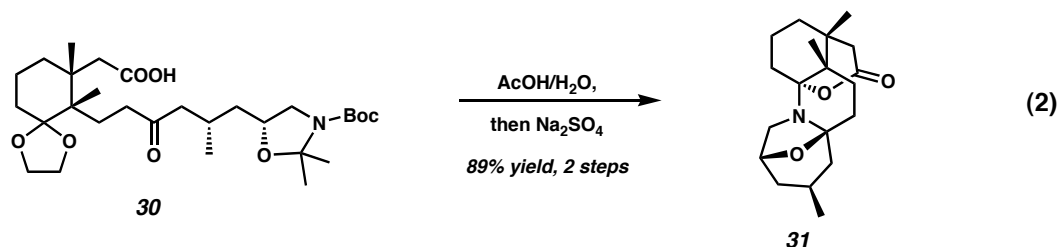


While transition structure **25** rationalizes the stereochemical outcome of the metallo-enamine reaction, reactions of this type may progress through an aza-ene mechanism with concerted proton transfer, or *via* formation of a hetero-Diels-Alder dihydropyran with subsequent isomerization.⁶ In either event, the Michael adduct **26** was obtained in good yield and diastereoselectivity. Subsequently, a tandem Staudinger reaction/intramolecular aza-Wittig condensation provided **27** after desilylation.⁷

In other synthetic studies aimed at zoanthid natural products, Hirama and coworkers demonstrate progress toward zoanthenol **1** using an intramolecular Heck reaction of aryl triflate **28** to close the B-ring with high diastereoselectivity to provide **29** in good yield (eq 1).⁸



Finally, Kobayashi has completed a diastereoselective synthesis of the CDEFG-ring system **31** in good yield by demonstrating the biogenic acid-catalyzed tandem aminal cyclization on protected amino-alcohol **30** (eq 2).⁹



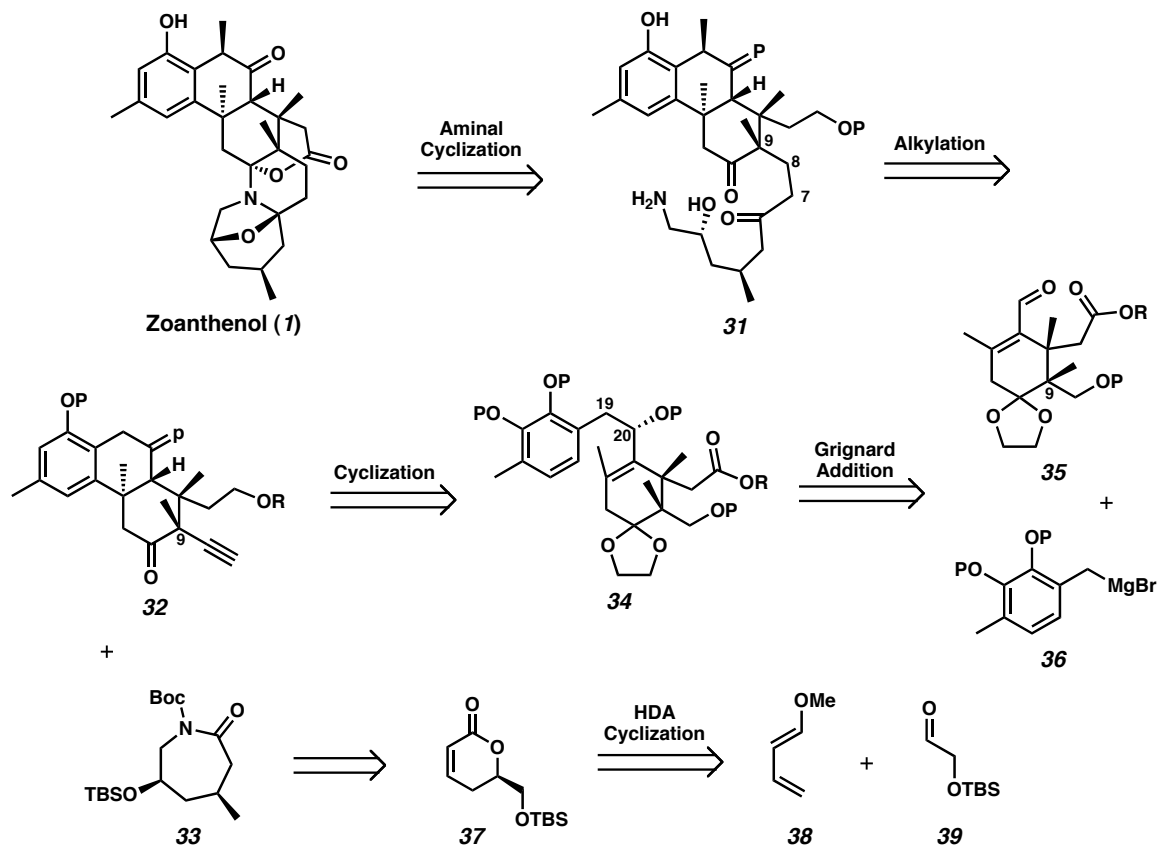
While there are a number of published synthetic studies towards zoanthid natural products, they remain formidable targets for total synthesis, as only norzoanthamine **2** has been synthesized. Intrigued by its structural complexity, we initiated synthetic studies towards the enantioselective total synthesis of zoanthenol **1**.

Retrosynthetic Analysis

Zoanthenol presents a stimulating challenge for total synthesis owing to its intricate array of nine stereocenters, including three quaternary stereocenters, and complex polycyclic architecture. Furthermore, the heteroatom distribution in the lower four rings constitutes an unusual bis-aminal ring system. The complex structure of zoanthenol **1** allows for late stage disconnection of the aminal moiety (Figure 2), immediately reducing the heptacyclic natural product to a tricyclic system appended with a linear fragment as

shown in structure **31**. Another C–C bond disconnection reduces **31** into tricycle **32** and caprolactam **33**. Fragment **32** may be disconnected to provide the cyclization substrate **34**, which is constructed from aldehyde **35** and Grignard **36**.

Figure 2. Retrosynthetic analysis of zoanthanol

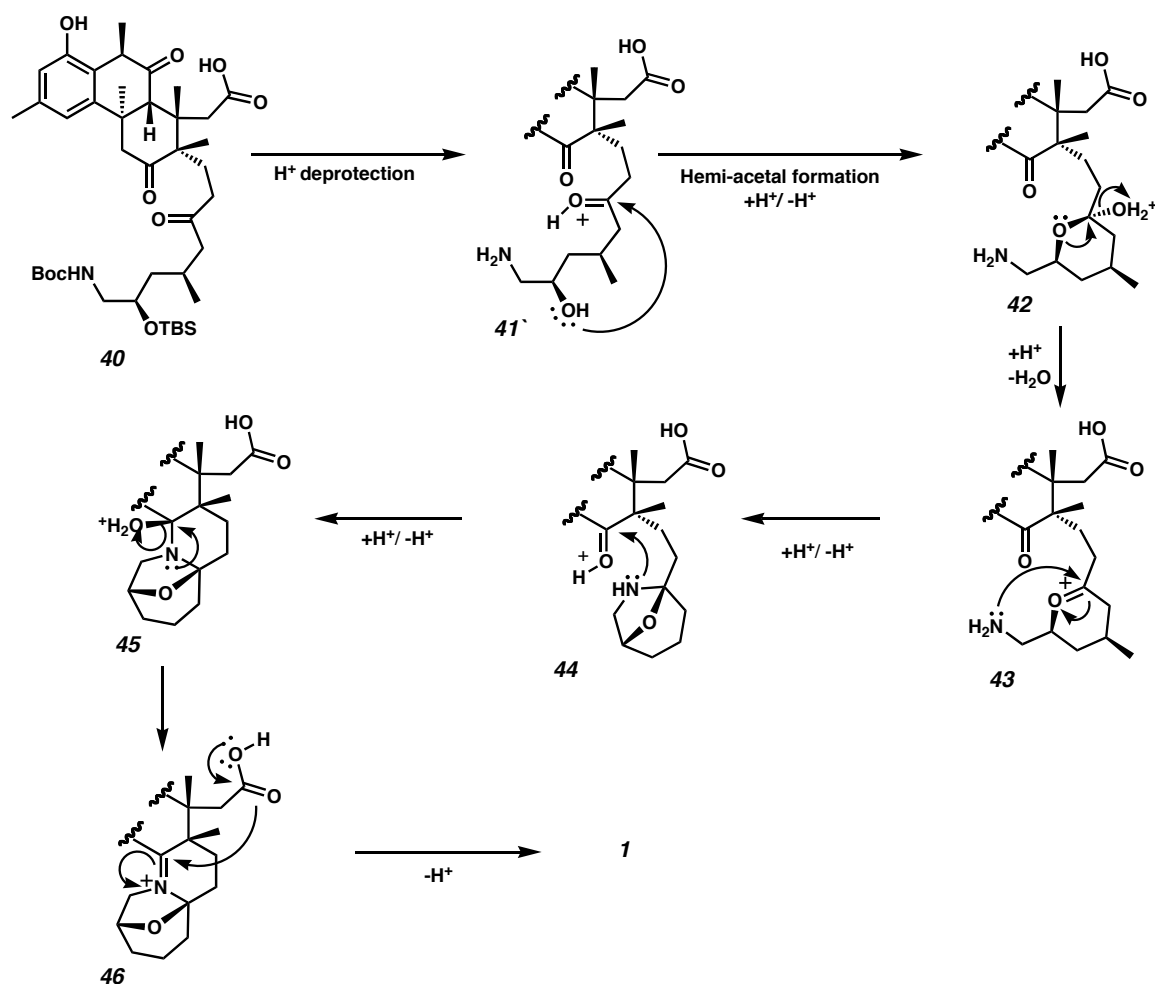


Synthetic studies on tricycle **32** are currently under pursuit by graduate students Doug Behenna and Jennifer Stockdill, and will not be detailed here. Instead, this discussion will focus on the synthesis of caprolactam **33**, which is accessible through the unsaturated lactone **37**. Intermediate **37** is in turn generated directly from diene **38** and aldehyde **39** by an enantioselective hetero-Diels-Alder reaction.

Mechanistic Considerations of the Tandem Aminal Cyclization

The disconnection from zoanthanol **1** to amino alcohol **31** (Figure 2) suggests the biogenesis of zoanthanol.¹ The fully constructed aminal ring system likely represents one end of an intricate equilibrium. A plausible mechanism for the proposed synthetic cyclization event, shown in Figure 3, is based on the assumptions that 1) full deprotection occurs before any bond forming event and that 2) five- and six-membered ring acetal formation is much faster than any higher membered ring.

Figure 3. A reasonable mechanism for the cyclization



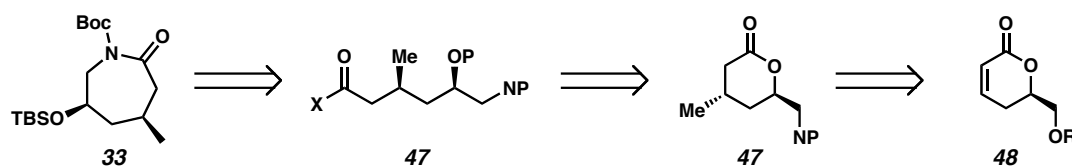
Under acidic conditions, full deprotection of advanced carbocycle **40** results in amino alcohol **41**, which is likely to form the kinetically favored six-membered hemi-acetal **42**. After protonation of the hemi-acetal, donation of the lone pair from the newly formed ether produces oxo-carbenium ion **43**. The oxo-carbenium ion is suitably disposed for attack by the nearby nitrogen lone pair to close the bicyclic aминаl **44**. After proton shift, the resulting аминаl **45** may now close as a six-membered ring, forming iminium ion **46**. The iminium ion is subsequently quenched upon nucleophilic attack of the nearby carbonyl, closing the final six-membered ring to provide zoanthenol (**1**).

II. Results and Discussion

Retrosynthetic analysis of the DEFG ring precursor

Early on, we identified caprolactam **33** as an essential fragment in the total synthesis of zoanthenol (Figure 4). Simple disconnection across the amide functionality provides the protected linear amino-alcohol **47**, which may be constructed from a six-membered lactone **47**, a more common structural subunit than the seven-membered lactam **33**. Further retrosynthetic removal of a methyl equivalent from lactone **47** provides the known α,β -unsaturated δ -lactone **48**.¹⁰

Figure 4. Retrosynthesis of caprolactam **33**



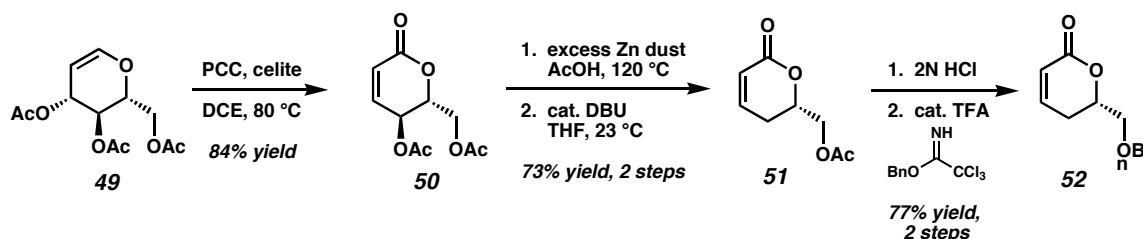
With a clearly defined set of goals (i.e., synthesis of caprolactam **33** via a δ -lactone of type **48**), we began synthetic efforts to determine a fast and efficient enantioselective synthesis of this major natural product fragment present in many of the zoanthid natural products, including zoanthenol **1**.

Synthetic Route from the Chiral Pool

Our first efforts focused on utilizing the chiral pool as a starting point for the synthesis of an α,β -unsaturated lactone of type **48**. Literature preparations detail the synthesis of several intermediates *en route* to lactone **48** from tri-O-acetyl-*D*-glucal **49**.¹¹ While both enantiomers of the required sugar are commercially available, tri-O-acetyl-*D*-glucal **49** is much cheaper than the (*L*)-enantiomer, which is ultimately required for the synthesis of zoanthid natural products according to our synthetic plan. To minimize the cost of materials, initial synthetic investigation was conducted on the inexpensive (*D*)-glucal.

Starting from tri-O-acetyl-*D*-glucal **49**, unsaturated lactone **50** was accessed in good yield by PCC oxidation according to known methods (Scheme 6).¹² The extraneous acetate was removed by reductive deconjugation with activated Zn dust in acetic acid, providing lactone **51**, upon re-conjugation by treatment with catalytic DBU.¹² Following removal of the acetate group, our initial attempts at protection with a more suitable group were unproductive because intermediates related to **51** were very sensitive to base, and the route was abandoned in favor of another approach (see Scheme 7). Ultimately, mild acidic conditions for the benzyl protection were developed, providing δ -lactone **52**, which was identical to material produced by published methods.¹³

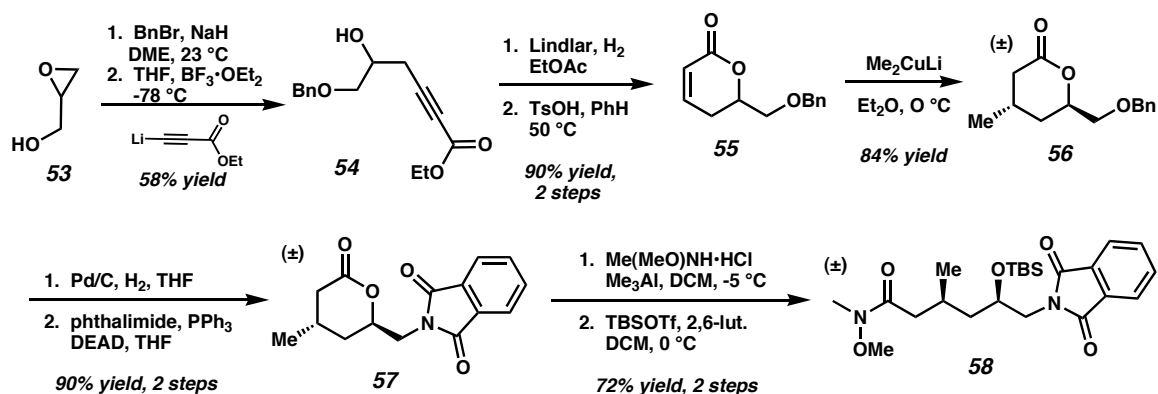
Scheme 6. Sugar route



Synthetic Route from Glycidol

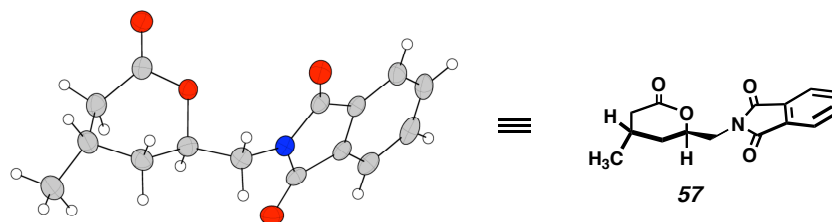
Despite the initial appeal of utilizing the chiral pool as the starting point for the synthesis of enone **52**, both the necessity to alter protecting groups, and the initial difficulty in doing so, prompted the exploration of a route starting from racemic glycidol **53**. The enantioselective route could be secured upon completion of the racemic route from readily available (*S*)-glycidol.^{14,15} According to literature preparations, the sequence began with benzyl protection of racemic glycidol **53**, followed by nucleophilic epoxide opening with the anion of ethyl propiolate to provide the known alkyne **54** (Scheme 7).¹⁶

Scheme 7. Synthetic route from glycidol

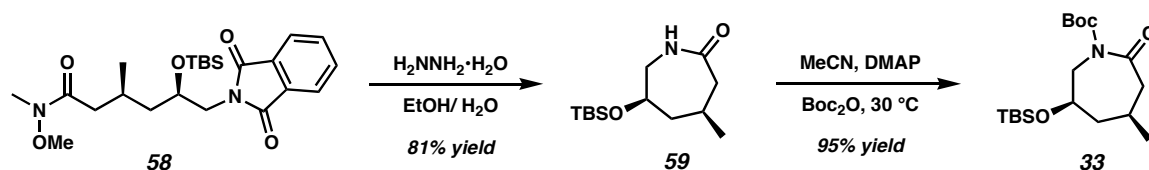


Unsaturated lactone **55** was quickly accessed through Lindlar reduction of alkyne **54**, followed by cyclization upon exposure to mild acid. With the suitably protected lactone **55** in hand, a highly diastereoselective cuprate addition with the Gilman reagent proceeded smoothly, yielding scaleable quantities of the saturated lactone **56** as a single observed diastereomer. Installation of the primary amine was accomplished through hydrogenolysis of the benzyl ether, followed by a Mitsunobu reaction with phthalimide, providing the crystalline intermediate **57**. X-ray analysis of **57** confirms the relative stereochemistry resulting from the cuprate addition (Figure 5).

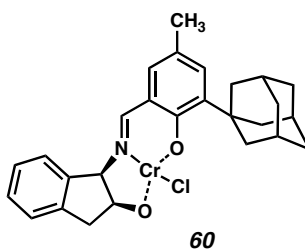
Figure 5. X-ray structure of phthalimide adduct **57**



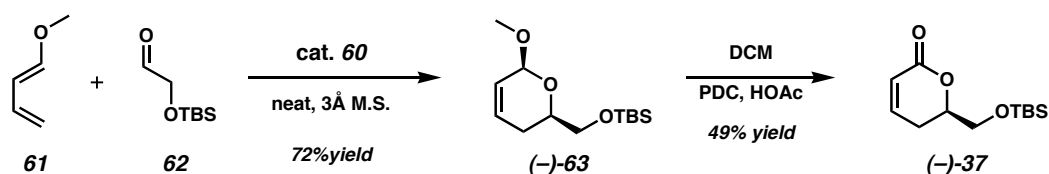
The Weinreb amide **58** was prepared from lactone **57** and the intermediate alcohol was immediately trapped as the TBS ether to prevent the facile closure to starting material, generating amide **58** (Scheme 7). Decomposition of the phthalimide moiety present in **58** with hydrazine hydrate in refluxing ethanol released the latent amine functionality, which immediately cyclized to provide caprolactam **59** (Scheme 8). Protection of the amide as the *t*-butylcarbamate provided **33**, a key retron for the total synthesis of **1**.

Scheme 8. Advancing to the final retron*Synthesis of key lactone via a hetero-Diels Alder cyclization.*

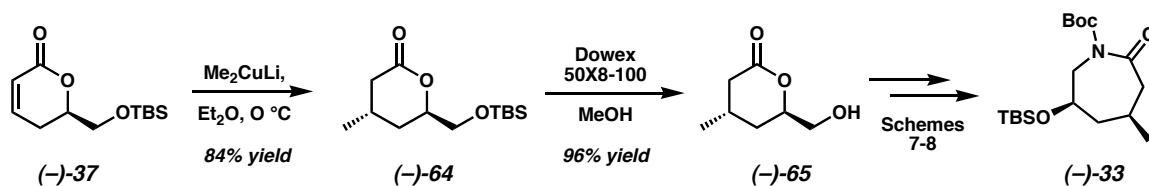
Despite having developed a reaction sequence readily applicable to enantioselective synthesis, our attentions were soon drawn to a more direct route to an equivalent of key lactone **52**. Jacobsen et al. have demonstrated that the chromium complex **60** is an effective catalyst for enantioselective hetero-Diels-Alder (HDA) reactions between aldehydes and electron rich dienes.⁶

Figure 6. Jacobsen hetero-Diels-Alder catalyst

According to their method,¹⁷ simply by combining the diene **61**, the aldehyde **62**, and a catalytic quantity of chromium catalyst **60**, we observed the highly diastereo- and enantioselective synthesis of glycol (–)-**63** in 72% yield and >99% ee. Subsequent PDC oxidation of glycol (–)-**63** in the presence of wet acetic acid provided enone (–)-**37** (Scheme 9).

Scheme 9. Enantioselective hetero-Diels-Alder reaction

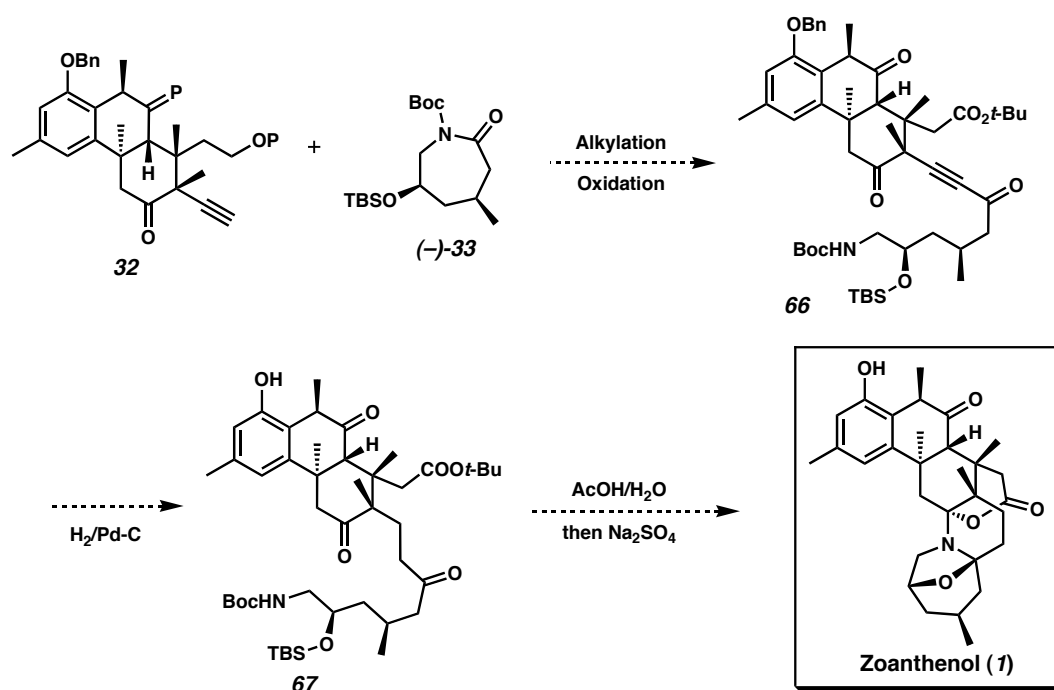
Conjugate addition with the Gilman reagent into unsaturated lactone **(-)-37** provided the *anti*-disubstituted lactone **(-)-64** as a single observed diastereomer (Scheme 10). Mild desilylation in the presence of a resin-bound acid source provided the unprotected alcohol **(-)-65**, which was elaborated to the caprolactam **(-)-33** as previously described (Schemes 7-8). All intermediates in the enantioselective route were analytically identical to those in the racemic route by ^1H NMR and ^{13}C NMR analysis.

Scheme 10. Advancing enantiopure synthetic intermediates*Endgame for the Total Synthesis of Zoanthanol*

Upon completion of the ABC ring **32**, fragment coupling with caprolactam **(-)-33** will provide yne-one **66** after oxidation (Scheme 11).¹⁸ After deprotection and further oxidation, hydrogenolysis of both the alkyne and the benzyl ether present in **66** is expected to generate the advanced intermediate **67**. Treatment with acid is expected to

initiate the ultimate tandem aminal cyclization, completing the total synthesis of zoanthenol **1**.

Scheme 11. Endgame for zoanthenol



III. Conclusion

With the goal of establishing a synthetic route to enantiopure caprolactam (–)-**33**, three routes to the key δ -lactone of type **44** were explored. Our initial plan to derive the desired lactone from the chiral pool was soon abandoned due to preliminary synthetic difficulties. A more modern method utilizing glycidol as the starting material was explored, resulting in successful delivery of the racemic caprolactam **33**. Ultimately, enantiopure δ -lactone (–)-**37** was obtained by means of a highly diastereoselective and

enantioselective hetero-Diels-Alder cyclization. Key features of the subsequent synthesis include a highly diastereoselective cuprate addition and a protecting group strategy for the masking of the reactive amino alcohol moiety. The enantiopure caprolactam (–)-**33** generated by the detailed method is expected to be a competent electrophile for coupling with the appropriate nucleophile of alkynyl-tricycle **32**. After fragment coupling, only a few synthetic transformations are expected to complete the total synthesis of zoanthenol **1**.

IV. Experimental Section

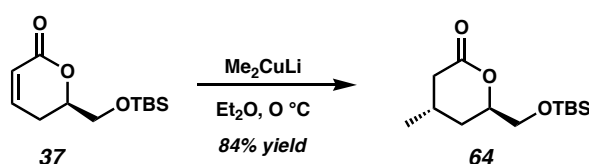
Materials and Methods

Unless stated otherwise, reactions were conducted in flame-dried glassware using anhydrous solvents (either freshly distilled or passed through activated alumina columns). All reactions were conducted under an inert atmosphere of dry nitrogen or argon, unless otherwise stated. All commercially obtained reagents were used as received. When required, commercial reagents were purified following the guidelines of Perrin and Armarego.¹⁹ Reaction temperatures were controlled using an IKAmag temperature modulator. Thin-layer chromatography (TLC) was conducted with E. Merck silica gel 60 F254 pre-coated plates (0.25 mm) and visualized using a combination of UV, anisaldehyde, ceric ammonium molybdate, and potassium permanganate staining. ICN silica gel (particle size 0.032–0.063 mm) was used for flash chromatography using the method described by Still.²⁰

¹H NMR spectra were recorded on a Varian Mercury 300 (at 300 MHz), a Varian Inova 500 (at 500 MHz), and are reported relative to residual protio solvent signals. Data for ¹H NMR spectra are reported as follows: chemical shift (δ ppm), multiplicity (s = singlet, d = doublet, t = triplet, q = quartet, m = multiplet), coupling constant (Hz), and integration. ¹³C NMR spectra were recorded on a Varian Mercury 300 (at 75 MHz) and are reported relative to residual protio solvent signals. Data for ¹³C NMR spectra are reported in terms of chemical shift. IR spectra were recorded on a Perkin Elmer Paragon 1000 spectrometer and are reported in frequency of absorption (cm^{-1}). Optical rotations were measured with a Jasco P-1010 polarimeter (Na lamp, 589 nm). HPLC analysis was performed on a Hewlet-Packard 1100 Series HPLC (UV detector at 245 nm) equipped

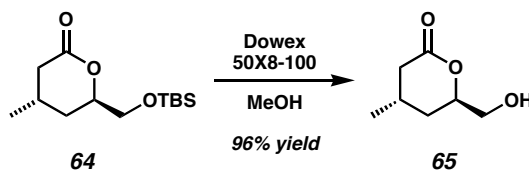
with the following Chiralcel columns: OD-H (25 cm), OD guard (5 cm), AD (25 cm), OJ (25 cm) and OB-H (25 cm). High resolution mass spectra were obtained from the California Institute of Technology Mass Spectral Facility.

Preparative Procedures

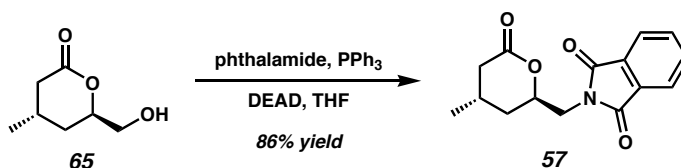


β -Me, δ -Lactone (64). MeLi (1.3 M in ether, 5.8 mL, 7.56 mmol) was added to a stirring slurry of CuI (714 mg, 3.89 mmol) in diethyl ether cooled to $-78\text{ }^\circ\text{C}$. The vessel was warmed to $0\text{ }^\circ\text{C}$ for 15 min, then cooled again to $-78\text{ }^\circ\text{C}$. A solution of the α,β -unsaturated lactone **37** (471 mg, 1.95 mmol) in diethyl ether (4 mL) was then carefully added along the cooled inner walls of the reaction flask. After 1 h, the reaction mixture was quenched by the slow addition of saturated aq ammonium chloride (15 mL) at $-78\text{ }^\circ\text{C}$. The reaction flask was gradually warmed to ambient temperature for 30 min, then diluted with ether (30 mL). The biphasic mixture was transferred to a separatory funnel and shaken vigorously to dissolve solids. The organic layer was washed with saturated aq ammonium chloride (2 x 20 mL), then brine (1 x 10 mL), dried over magnesium sulfate and concentrated. The resulting material was purified by flash chromatography over silica gel (25% EtOAc:hexane eluent) to yield δ -lactone **64** (422 mg, 84% yield, $R_f = 0.20$ in 25% EtOAc:hexane) as a clear oil: ^1H NMR (300 MHz, CDCl_3) δ 4.47-4.40 (m, 1H), 3.70-3.73 (m, 2H), 2.55 (dd, $J=16.3, 5.1$ Hz, 1H), 2.18-2.29 (m, 1H), 2.12 (dd, $J=16.4, 8.9$ Hz, 1H), 1.90-1.99 (m, 1H), 1.52-1.60 (m, 1H), 1.05 (d, $J=6.6$ Hz, 3H), 0.87 (s, 9H), 0.06 (s, 6H); ^{13}C NMR (75 MHz, CDCl_3) δ 171.7, 77.8, 65.1, 38.1, 31.7, 26.2, 24.1, 21.4, 18.6,

5.00; IR (neat) 1743 cm^{-1} ; HRMS (FAB⁺) m/z calc'd for $[\text{C}_{13}\text{H}_{26}\text{O}_3\text{Si}]^+$: 201.0947, found 201.0950; $[\alpha]_{\text{D}}^{20}$ -25.027° ($c=1$, CDCl_3).

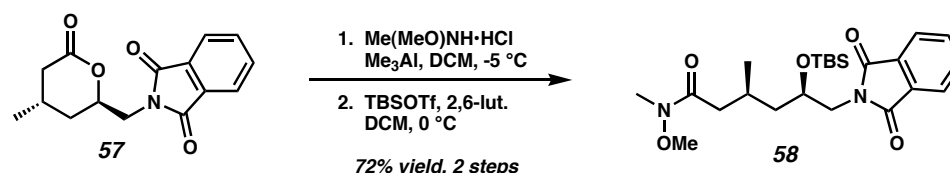


Alcohol 65. The lactone (100 mg, 0.39 mmol) was dissolved in methanol (5.0 mL) and added to a reaction flask equipped with Dowex 50X8-100 cation exchange resin (1.0 g). The mixture was stirred at ambient temperature for 3 h, then filtered. The resin was washed with methanol (2 x 5 mL) and the combined organics were concentrated. The crude material was dried overnight under high vacuum to yield the alcohol **65** (53 mg, 96% yield, R_{F} = 0.18 in 80% EtOAc:hexane) as a clear oil: ^1H NMR (300 MHz, CDCl_3) δ 4.47-4.52 (m, 1H), 3.75 (dd, $J=12.3$, 3.6 Hz, 1H), 3.66 (dd, $J=12.1$, 5.8 Hz, 1H), 2.69 (br s, 1H), 2.53-2.58 (m, 1H), 2.13-2.23 (m, 2H), 1.88-1.97 (m, 1H), 1.49-1.57 (m, 1H), 1.08 (d, $J=6.0$ Hz, 3H); ^{13}C NMR (75 MHz, CDCl_3) δ 172.3, 78.2, 65.1, 37.8, 31.1, 24.3, 21.4; IR (neat) 1722.4 cm^{-1} ; HRMS (FAB⁺) m/z calc'd for $[\text{C}_7\text{H}_{12}\text{O}_3]^+$: 144.0786, found 144.0787; $[\alpha]_{\text{D}}^{20}$ -162.147° ($c=1$, CDCl_3).



Phthalimide (57). To a stirred solution of alcohol **65** (1.48 g, 10.28 mmol) in tetrahydrofuran (30 mL) was added triphenyl phosphine (2.83 g 10.79 mmol), then

phthalimide (1.59 g, 10.76 mmol). Once all reagents had dissolved, the reaction mixture was cooled to 0 °C and DEAD (1.707 mL, 10.79 mmol) was added dropwise to the stirred solution. The reaction flask was then warmed to 30 °C for 12 h, then concentrated. The concentrated reaction mixture was flashed over silica (4:1 hexanes/EtOAc eluent). The resulting solid was recrystallized from dichloromethane to provide phthalimide **57** (2.42 g, 86% yield, R_F = 0.16 in 40% EtOAc:hexane) as a white solid: m.p. 118-120 °C; ^1H NMR (300 MHz, CDCl_3) δ 7.82-7.88 (m, 2H), 7.71-7.76 (m, 2H), 4.74-4.83 (m, 1H), 4.04 (dd, J =15.0, 8.3 Hz, 1H), 3.78 (dd, J =15.0, 5.5 Hz, 1H), 2.63 (dd, J =16.6, 5.4 Hz, 1H), 2.28 (m, 1H), 2.16 (dd, J =16.5, 9.1 Hz, 1H), 1.86 (m, 1H), 1.66 (m, 1H), 1.09 (d, J =6.9 Hz, 3H); ^{13}C NMR (300 MHz, CDCl_3) δ 170.9, 168.1, 134.4, 132.0, 123.7, 74.1, 41.9, 37.9, 32.8, 24.0, 21.5; IR (neat) 1773.9, 1715.8 cm^{-1} ; HRMS (FAB^+) m/z calc'd for $[\text{C}_{15}\text{H}_{16}\text{NO}_4]^+$: 274.1079, found 274.1076; $[\alpha]_D^{20}$ -68.6255° (c =1, CDCl_3).

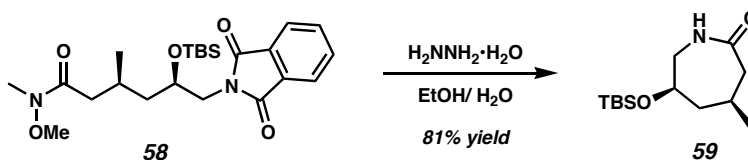


Weinreb Amide (58). Trimethylaluminum (2.0 M in toluene, 10.32 mL, 20.64 mmol) was slowly added to a stirred solution of *N,O*-dimethylhydroxylamine hydrochloride (2.01 g, 16.80 mmol) in dichloromethane (40 mL) cooled to $-10\text{ }^\circ\text{C}$. The solution was stirred for 20 min before the dropwise addition of the Mitsunobu adduct **57** (2.26 g, 8.23 mmol) in dichloromethane (10 mL). The reaction temperature was maintained at $-10\text{ }^\circ\text{C}$ for 30 min before the addition of saturated sodium bicarbonate (20

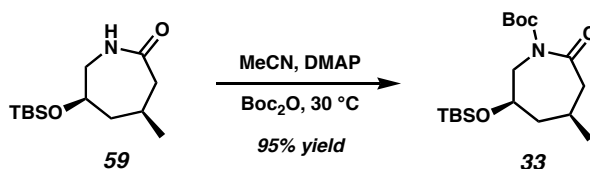
mL). The reaction mixture was then allowed to warm to room temperature. The crude reaction mixture was diluted with dichloromethane (30 mL) and brine (20 mL) to dissipate emulsions during extraction. The crude was transferred to a separatory funnel and the organic layer was separated. The aqueous layer was extracted with dichloromethane (2 x 30 mL). The combined organic layers were washed with brine (1 x 30 mL), then dried and concentrated to a volume of 10 mL over a rotovap pot temperature of 15 °C.

The crude amide was diluted with dichloromethane (20 mL) and cooled to 0 °C. To the cooled, stirred solution was added TBSOTf (3.79 mL, 16.51 mmol) followed by 2,6-lutidine (1.442 mL, 12.38 mmol). The solution was maintained at 0 °C for 20 min, then quenched by addition of saturated ammonium chloride (20 mL). The biphasic mixture was allowed to warm to room temperature while stirring vigorously, then transferred to a separatory funnel. The organic layer was separated and the aqueous layer was extracted with dichloromethane (2 x 20 mL). The combined organics were washed with saturated sodium bicarbonate solution (1 x 15 mL) and water (1 x 15 mL), then dried over magnesium sulfate and concentrated. The resulting crude product was flashed over silica gel (20% EtOAc:hexanes eluent) to provide Weinreb amide **58** (2.58g, 72% yield, R_F = 0.30 in 40% EtOAc:hexane) as an oil: ^1H NMR (300 MHz, CDCl_3) δ 7.82 (dd, J =5.4, 3.1 Hz, 2H), 7.70 (dd, J =5.6, 2.9 Hz, 2H), 4.05-4.14 (m, 1H), 3.68-3.78 (m, 2H), 3.65 (s, 3H), 3.14 (s, 3H), 2.38-2.45 (m, 1H), 2.18-2.29 (m, 1H), 1.51-1.60 (m, 1H), 1.38-1.47 (m, 1H), 1.03 (d, J =6.3 Hz, 3H), 0.76 (s, 9H), -0.01 (s, 3H), -0.20 (s, 3H); ^{13}C NMR (300 MHz, CDCl_3) δ 168.5, 134.1, 132.3, 123.3, 68.3, 61.5, 44.0, 43.7, 39.7, 32.3, 26.9, 26.0, 20.8, 18.1, -4.3, -4.4; IR (neat) 3473.5, 2955.4, 2857.3, 1774.2, 1714.5, 1660.3

cm^{-1} ; HRMS m/z calc'd for $[\text{C}_{23}\text{H}_{37}\text{N}_2\text{O}_5\text{Si}]^+$: 449.2472, found 449.2470; $[\alpha]_D^{20}$ -29.7° ($c=1$, CDCl_3).



Caprolactam 59. To a solution of **58** (2.848 g, 6.55 mmol) in absolute ethanol was added hydrazine monohydrate (1.75 mL, 32.77 mmol) and deionized water (0.39 mL). The solution was heated to 90°C for 4 h. The reaction was then cooled in an ice bath and the thick cottony solids were filtered. The filtrate was then concentrated to a solid. The crude solid was taken up in EtOAc (50 mL), cooled in an ice bath, and filtered over a pad of Celite, rinsing with portions of EtOAc (2 x 20 mL). The organics were then dried over sodium sulfate and concentrated. The crude solid was subjected to chromatography over silica gel (30% EtOAc:hexane eluent) to yield the unprotected caprolactam **59** (1.633g, 81% yield, $R_f=0.22$ in 50% EtOAc:hexane) as a white solid: m.p. $79-81^\circ\text{C}$; ^1H NMR (300 MHz, CDCl_3) δ 6.27 (br s, 1H), 3.56-3.65 (m, 1H), 3.18-3.28 (m, 1H), 3.01-3.10 (m, 1H), 2.38 (dd, $J=13.7, 11.0$ Hz, 1H), 2.25 (dd, $J=12.1, 1.7$ Hz, 1H), 1.96-2.04 (m, 1H), 1.83-1.93 (m, 1H), 1.36 (q, $J=11.8$ Hz, 1H), 1.04 (d, $J=6.9$ Hz, 3H), 0.86 (s, 9H), 0.05 (s, 6H); ^{13}C NMR (300 MHz, CDCl_3) δ 177.3, 71.0, 49.7, 48.9, 44.2, 28.6, 26.1, 24.8, 18.4, $-4.2, -4.4$; IR (neat) 3239.9, 2929.8, 2857.6, 1673.1 cm^{-1} ; HRMS (EI^+) m/z calc'd for $[\text{C}_{13}\text{H}_{28}\text{NO}_2\text{Si}]^+$: 242.1576, found 242.1576; $[\alpha]_D^{20}$ -15.0° ($c=1$, CDCl_3).

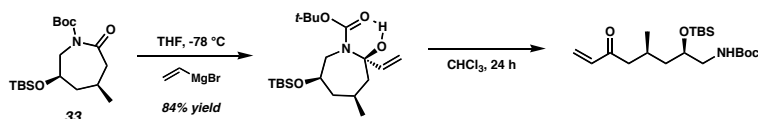


***N*-Boc-caprolactam (33).** To a solution of **33** (853 mg, 3.313 mmol) in acetonitrile (40 ml) was added *t*-butyl carbonate anhydride (1.81 g, 8.28 mmol). After the *t*-butyl carbonate anhydride had completely dissolved, *N,N*-dimethylamino pyridine (1.01 g, 8.28 mmol) was added in several small portions. The resulting dark-brown solution was stirred for 10 min at ambient temperature, then warmed to 35 °C. After 5 hours, the reaction was quenched by addition of water (20 mL). The mixture was transferred to a separatory funnel and extracted with EtOAc (4 x 30 mL). The combined organics were washed with brine (1 x 30 mL), dried over sodium sulfate, and concentrated to give a brown waxy solid, which was purified by flash chromatography over silica (10% EtOAc:hexane) to provide *N*-Boc-caprolactam **33** (1.314 g, 95% yield, R_F = 0.22 in 10% EtOAc:hexane) as a waxy solid: m.p. 77-78°; ^1H NMR (300 MHz, CDCl_3) δ 4.11 (dt, J =14.8, 1.8 Hz, 1H), 3.63 (tdd, J =22.0, 4.9, 2.2 Hz, 1H), 3.33 (dd, J =15.0, 9.5 Hz, 1H), 2.56 (dd, J =14.1, 10.9 Hz, 1H), 2.41 (d, J =14.3 Hz, 1H), 1.96-2.03 (m, 1H), 1.87-1.94 (m, 1H), 1.51 (s, 9H), 1.27-1.39 (m, 1H), 1.04 (d, J =6.6 Hz, 3H), 0.87 (s, 9H), 0.09 (s, 3H), 0.07 (s, 3H); ^{13}C NMR (300 MHz, CDCl_3) δ 174.1, 152.5, 83.4, 70.4, 52.4, 47.7, 47.0, 28.4, 28.1, 26.1, 24.5, 18.4, 4.3, 4.4; IR (neat) 2932.4, 1710.2, 1645.1 cm^{-1} ; HRMS m/z calc'd for $[\text{C}_{18}\text{H}_{36}\text{NO}_4\text{Si}]^+$: 358.2414, found 358.2426; $[\alpha]_D^{20}$ -48.0° (c =1, CDCl_3).

IV. Notes and References

- (1) (a) Rao, C.B.; Anjaneyula, A.S.; Sarma, N.S.; Venkatateswarlu, Y.; Rosser, R.M.; Faulkner, D. J.; Chen, M. H.; Clardy J. *J. Am. Chem. Soc.* **1984**, *106*, 7983. (b) Rao, C. B.; Anjaneyula, A. S.; Sarma, N. S.; Venkatateswarlu, Y.; Rosser, R. M.; Faulkner, D. J. *J. Org. Chem.* **1985**, *50*, 3757. (c) Rao, C.B.; Rao, D.V.; Raju, V.S.; Raju, B.W.; Sullivan, B.W.; Faulkner, D.J. *Heterocycles* **1989**, *28*, 103. (d) Fukuzawa, S.; Hayashi, Y.; Uemura, D.; Nagatsu, A.; Yamada, K.; Ijyuin, Y. *Heterocycl. Commun.* **1995**, *1*, 207.
- (2) Villar, R. M.; Gil-Longo, J.; Daranas, A. H.; Souto, M. L.; Fernández, J. J.; Peixinho, S.; Barral, M. A.; Santafé, G.; Rodríguez, J.; Jiménez, C. *Bioorg. Med. Chem.* **2003**, *11*, 2301.
- (3) Kuramoto, M.; Hiyashi, K.; Fujitani, Y.; Yamaguchi, K.; Tsuji, T.; Yamada, K.; Ijuin, Y.; Uemura, D. *Tetrahedron Lett.* **1997**, *38*, 5683.
- (4) Miyashita, M.; Sasaki, M.; Hattori, I.; Sakai, M.; Tanino, K., *Science* **2004**, *305*, 495.
- (5) Williams, D. R.; Brugel, T. A. *Org. Lett.* **2000**, *2*, 1023.
- (6) Hickmott, P.W. *The Chemistry of Enamines, Part 1* John Wiley & Sons, Inc.: New York, 1994, 843-871.
- (7) Williams, D. R.; Cortez, G. S. *Tetrahedron Lett.* **1998**, *39*, 2675.
- (8) Hirai, G.; Koizumi, Y.; Moharram, S. M.; Oguri, H.; Hiram, M. *Org. Lett.* **2002**, *4*, 1627.
- (9) Hikage, N.; Furukawa, H.; Takao, K.; Kobayashi, S. *Chem. Pharm. Bull.* **2000**, *48*, 1370.
- (10) The lactone is a common synthetic intermediate used in the synthesis of several natural products, including compactin and mevinoline. For references, see: (a) Bauer, T.; Chapuis, C.; Jezewski, A.; Kozak, J.; Jurczak, J. *Tetrahedron: Asymm.* **1996**, *7*, 1391. (b) Cardani, S.; Scolastico, C.; Villa, R. *Tetrahedron* **1990**, *46*, 7283. (c) Bauer, T.; Kozak, J.; Chapuis, C.; Jurczak, J. *J. Chem. Soc., Chem. Commun.* **1990**, *17*, 1178.
- (11) (a) Roth, B. D.; Roark, W. H. *Tetrahedron Lett.* **1988**, *29*, 1255. (b) Lichtenthaler, F. W.; Lorenz, K.; Ma, W. *Tetrahedron Lett.* **1987**, *28*, 47. (c) Rollin, P.; Sinay, P. *Carbohydrate Res.* **1981**, *98*, 139.

- (12) Roth, B. D.; Roark, H. *Tetrahedron Lett.* **1988**, 29, 1255.
- (13) Synthesized from a Diels-Alder reaction using a chiral controller, see: Bauer, T.; Chapuis, C.; Jezewski, A.; Kozak, J.; Jurczak, J. *Tetrahedron: Asymm.* **1996**, 7, 1391.
- (14) (a) Takano, S.; Shimazaki, Y.; Moriya, M.; Ogasawara, K. *Chem. Lett.* **1990**, 1177. (b) Takano, S.; Shimazaki, Y.; Iwabuchi, Y.; Ogasawara, K. *Tetrahedron Lett.* **1990**, 31, 3619.
- (15) Furrow, M.E.; Schaus, S. E.; Jacobsen, E. N. *J. Org. Chem.* **1998**, 63, 6776-6777.
- (16) Prepared according to the procedure given by: Oizumi, M.; Takahashi, M.; Ogasawara, K. *Syn. Lett.* **1997**, 9, 1111.
- (17) Dossetter, A. G.; Jamison, T. F.; Jacobsen, E. N. *Angew. Chem. Int. Ed.* **1999**, 38, 2398-2400.
- (18) Caprolactam **33** is expected to be an excellent coupling partner for a single electrophilic addition, without competing double anion addition. In a test reaction (see below) with excess vinyl magnesium bromide, the tetrahedral intermediate was an isolable intermediate, which collapsed to the linear species upon standing.



- (19) Perrin, D. D.; Armarego, W. L. F. *Purification of Laboratory Chemicals*; 3rd ed., Pergamon Press, Oxford, 1988.
- (20) Still, W. C.; Kahn, M.; Mitra, A. J. *J. Org. Chem.* **1978**, 43, 2923.

APPENDIX ONE

Spectra Relevant to Chapter 1: Progress Toward the Total Synthesis of Zoanthenol

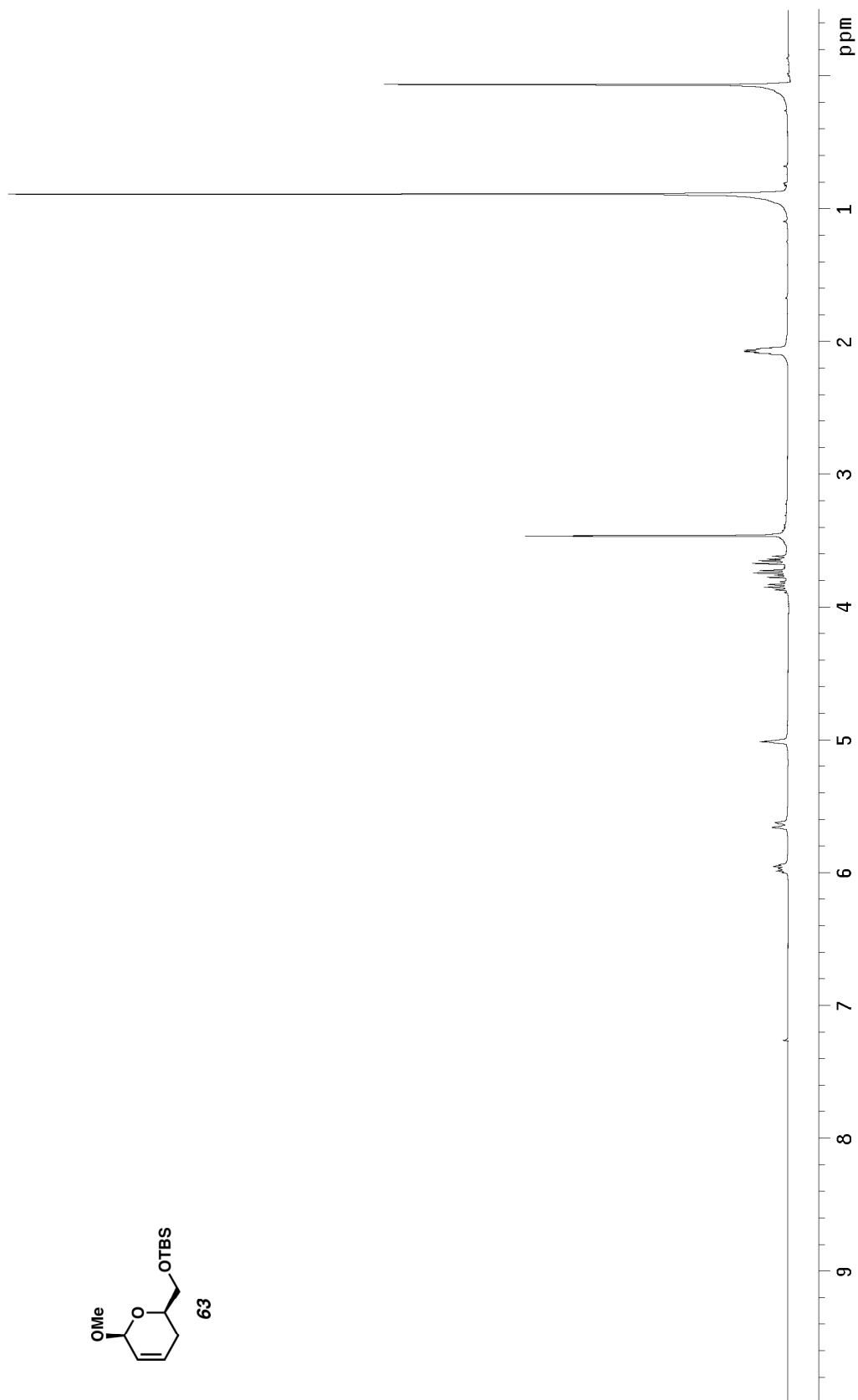
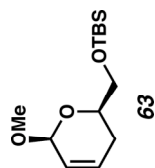


Figure A1.1 ¹H NMR (300 MHz, CDCl₃) of compound **63**.

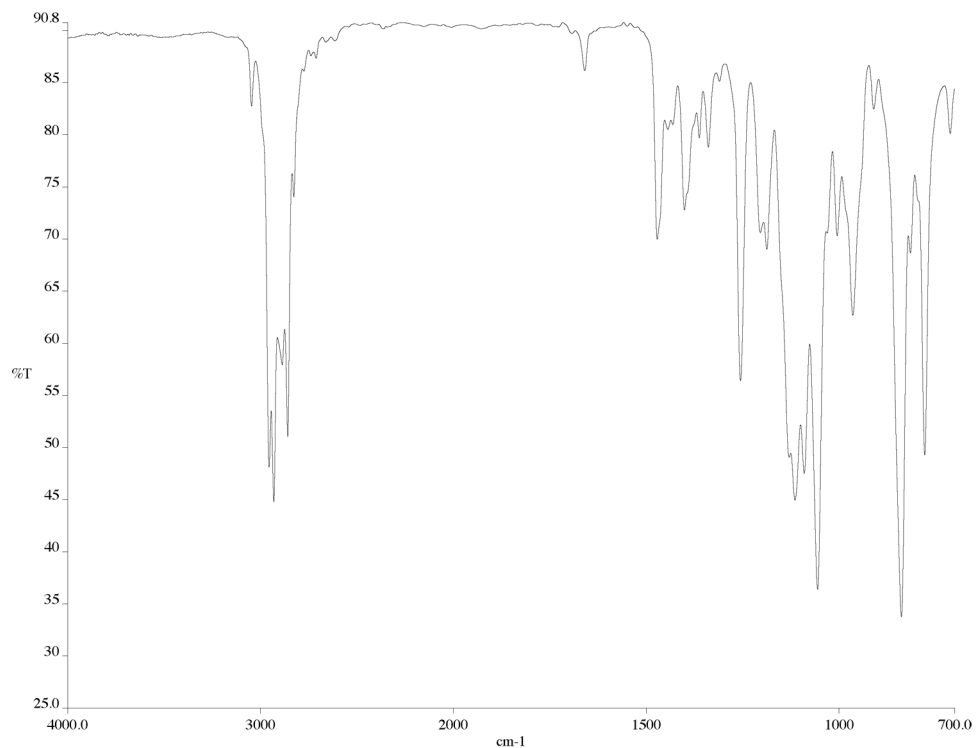


Figure A1.2 Infrared spectrum (thin film/NaCl) of compound **63**.

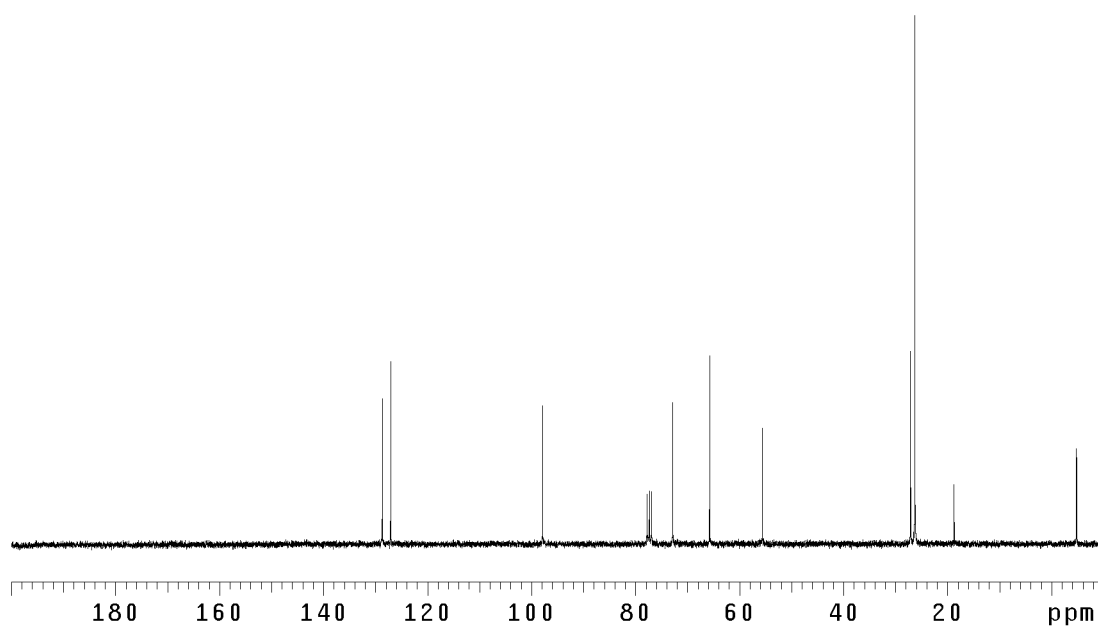
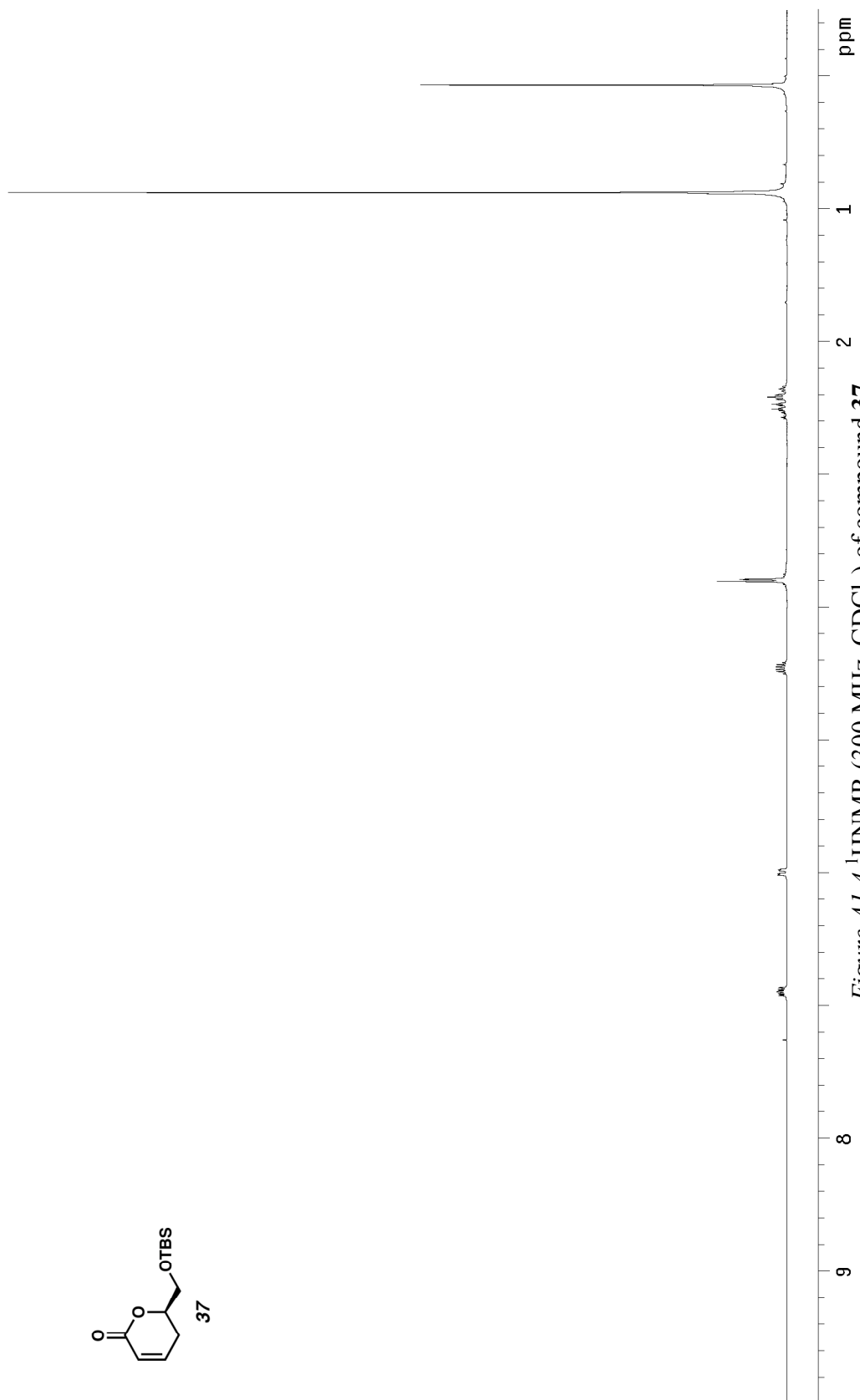
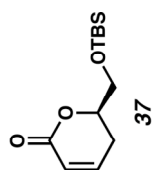


Figure A1.3 ¹³CNMR (125 MHz, CDCl₃) of compound **63**.



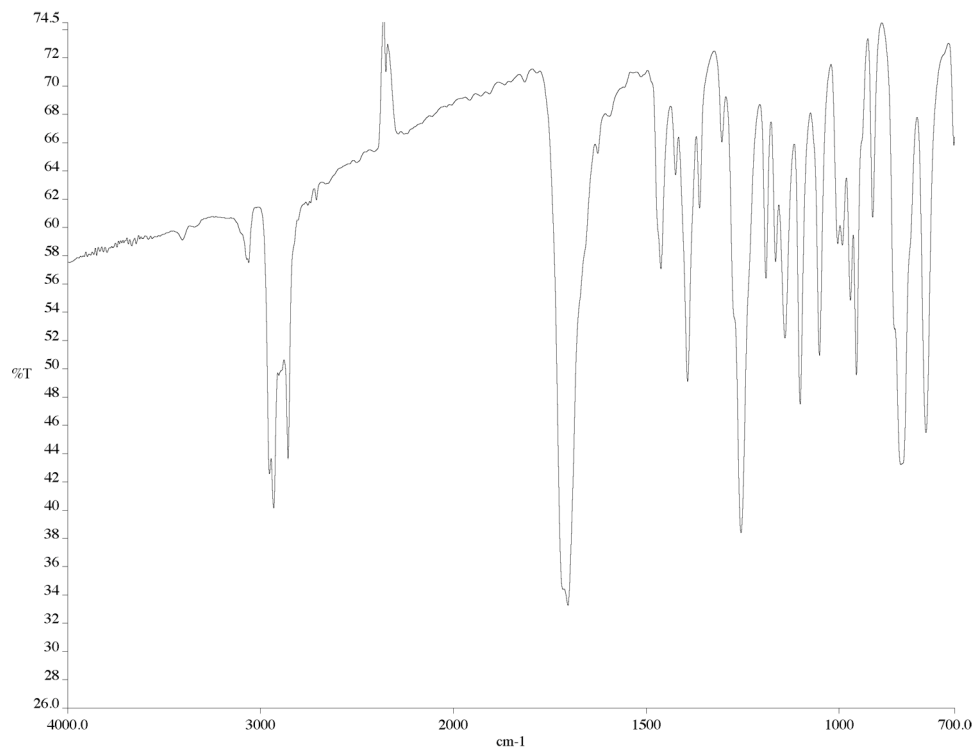


Figure A1.5 Infrared spectrum (thin film/NaCl) of compound **37**.

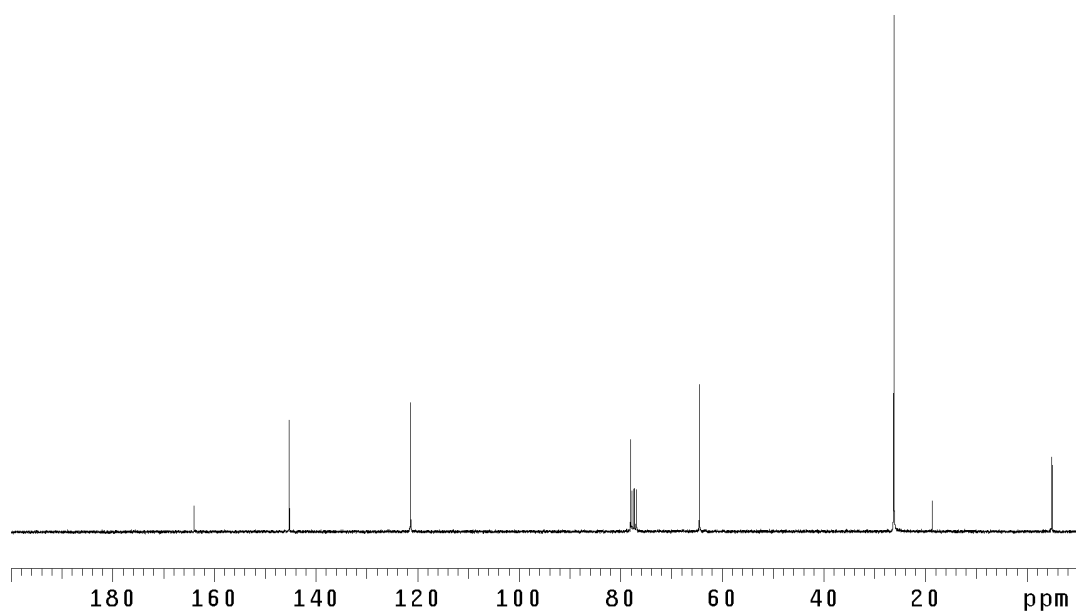


Figure A1.6 ¹³CNMR (125 MHz, CDCl₃) of compound **37**.

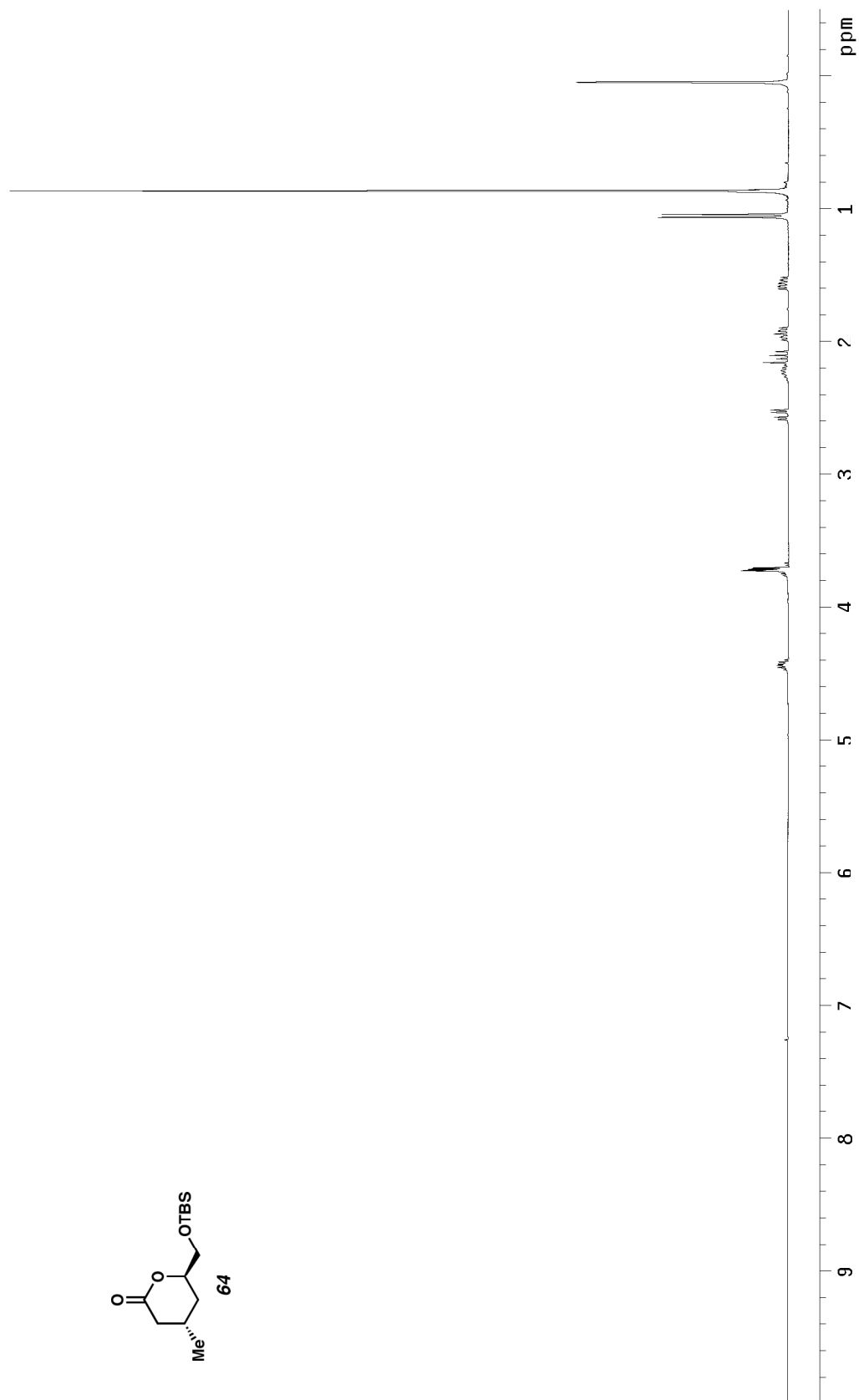
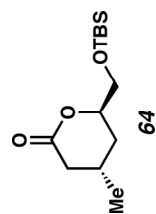


Figure A1.7 ¹H NMR (300 MHz, CDCl₃) of compound **64**.

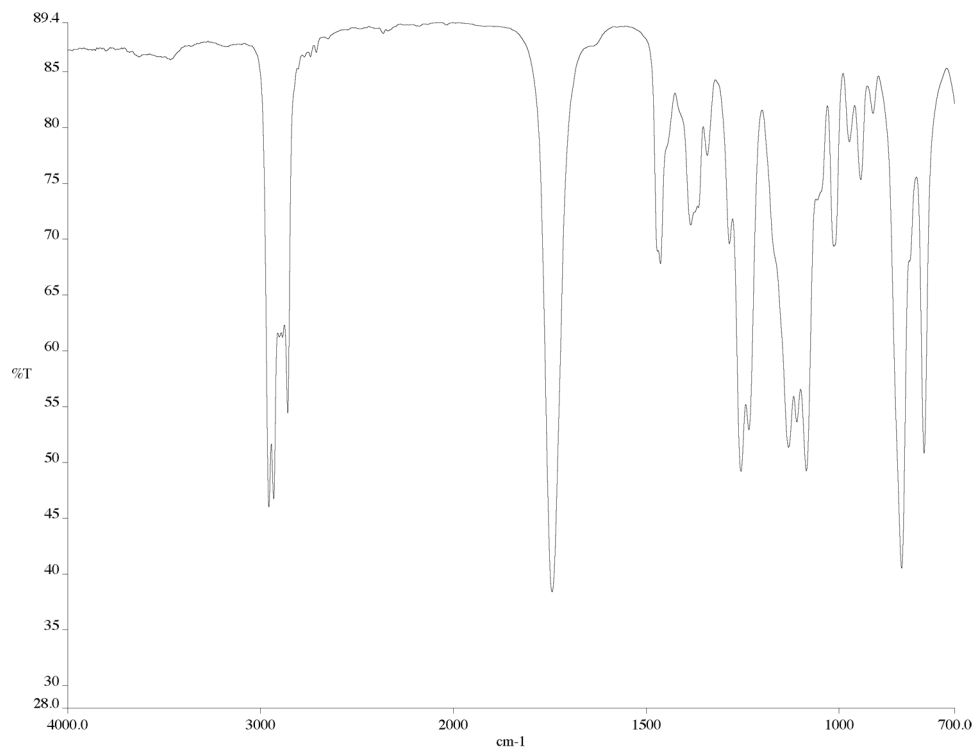


Figure A1.8 Infrared spectrum (thin film/NaCl) of compound **64**.

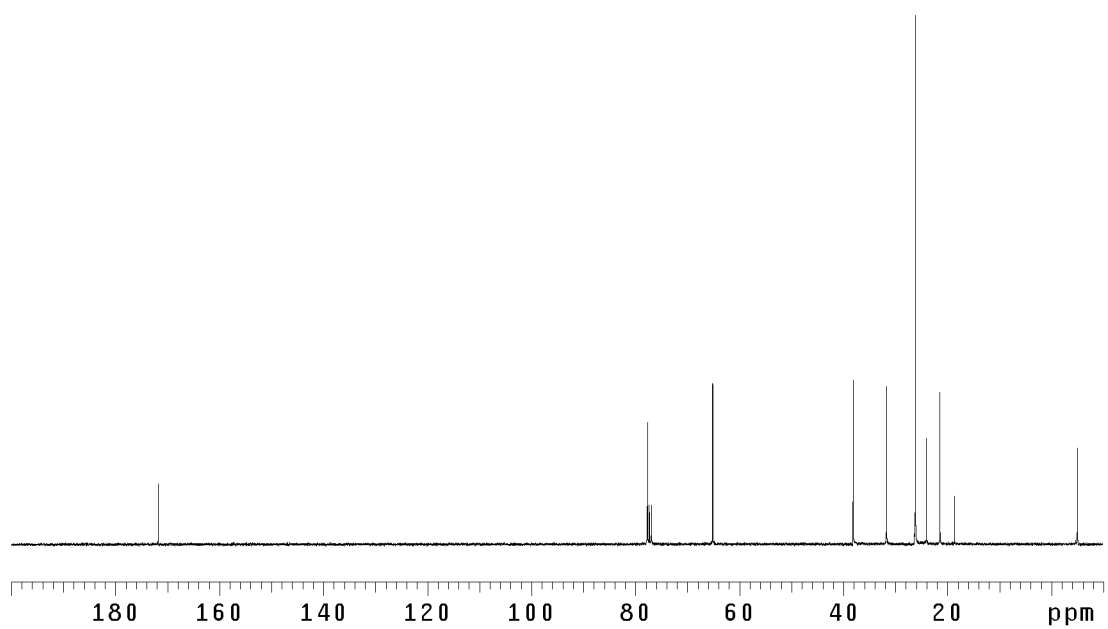


Figure A1.9 ¹³CNMR (125 MHz, CDCl₃) of compound **64**.

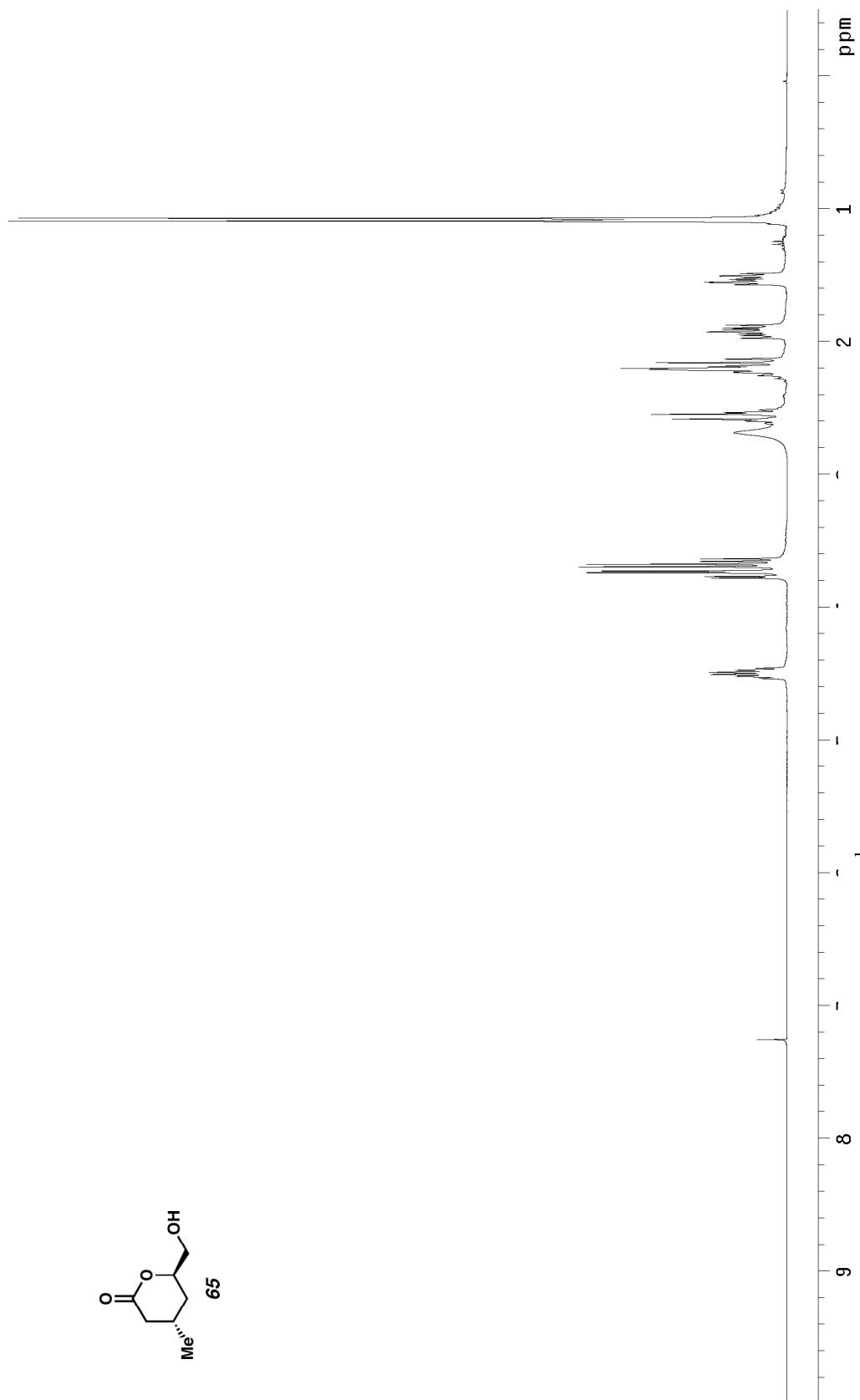
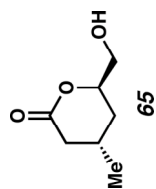


Figure A1.10 ¹H NMR (300 MHz, CDCl₃) of compound **65**.

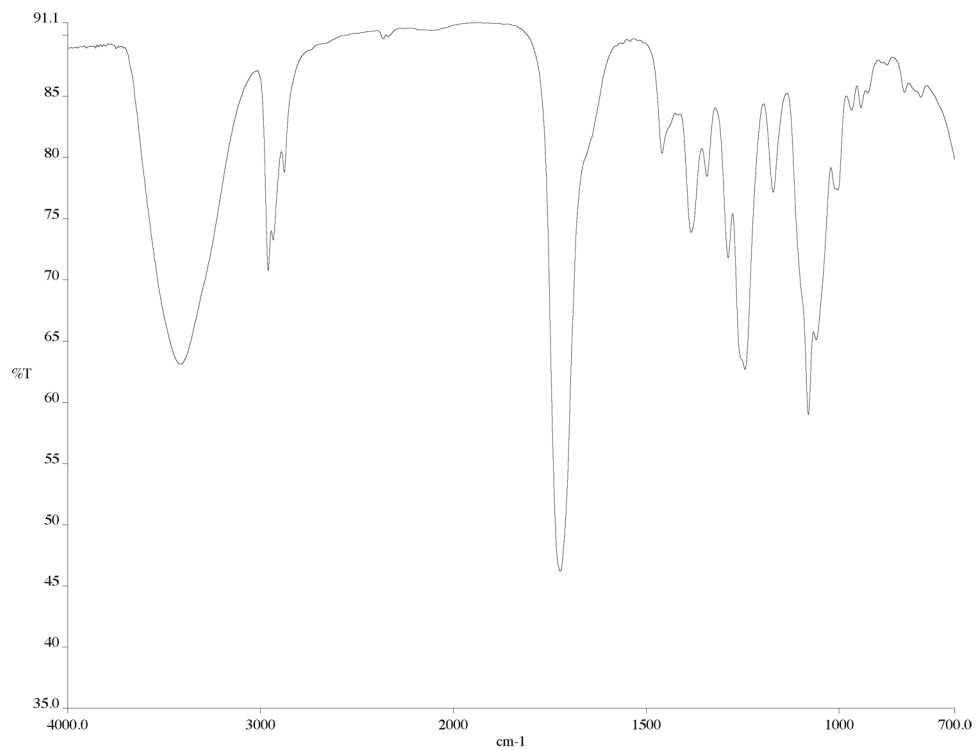


Figure A1.11 Infrared spectrum (thin film/NaCl) of compound **65**.

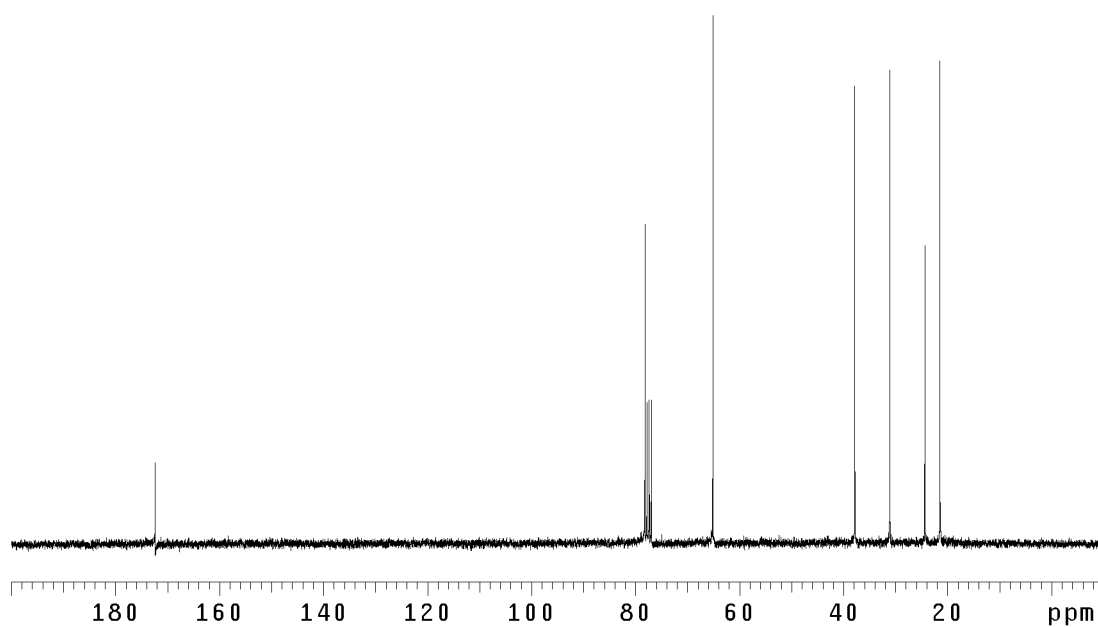


Figure A1.12 ¹³CNMR (125 MHz, CDCl₃) of compound **65**.

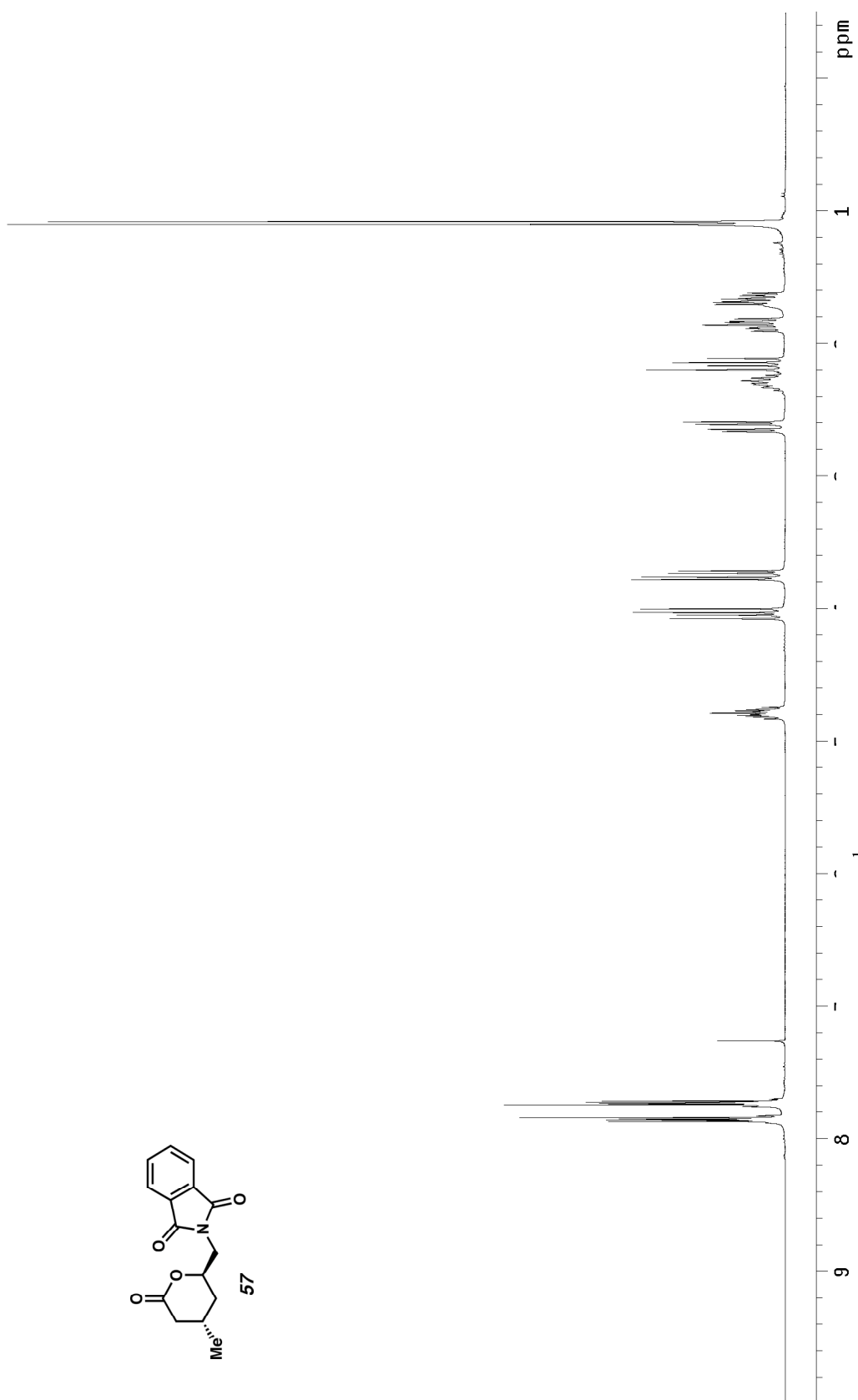


Figure A1.13 ¹H NMR (300 MHz, CDCl₃) of compound **57**.

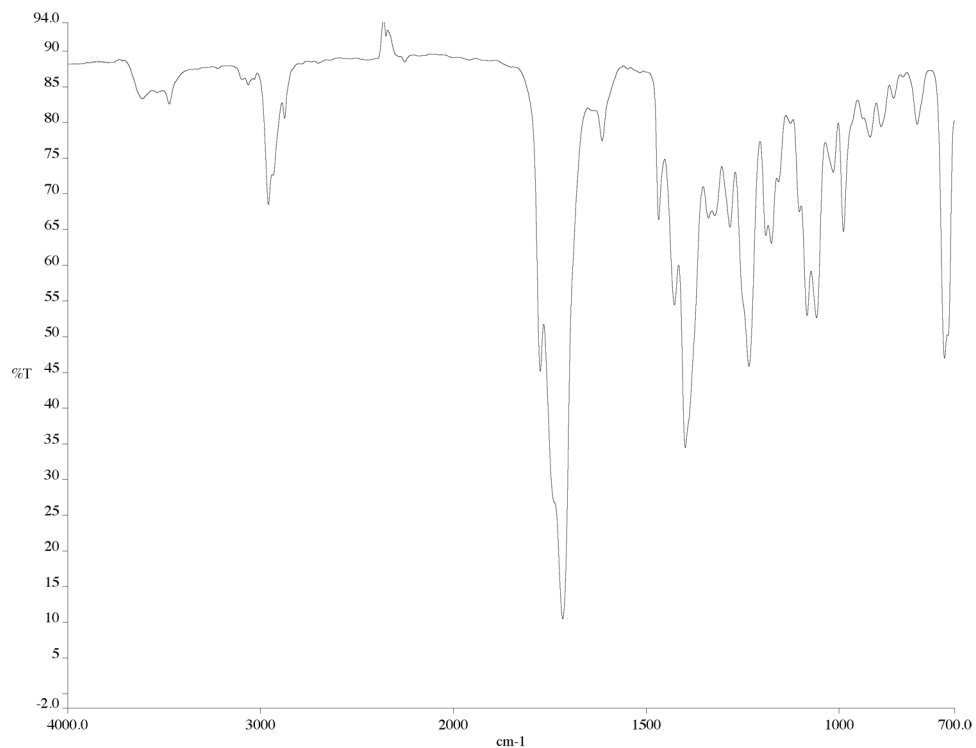


Figure A1.14 Infrared spectrum (thin film/NaCl) of compound **57**.

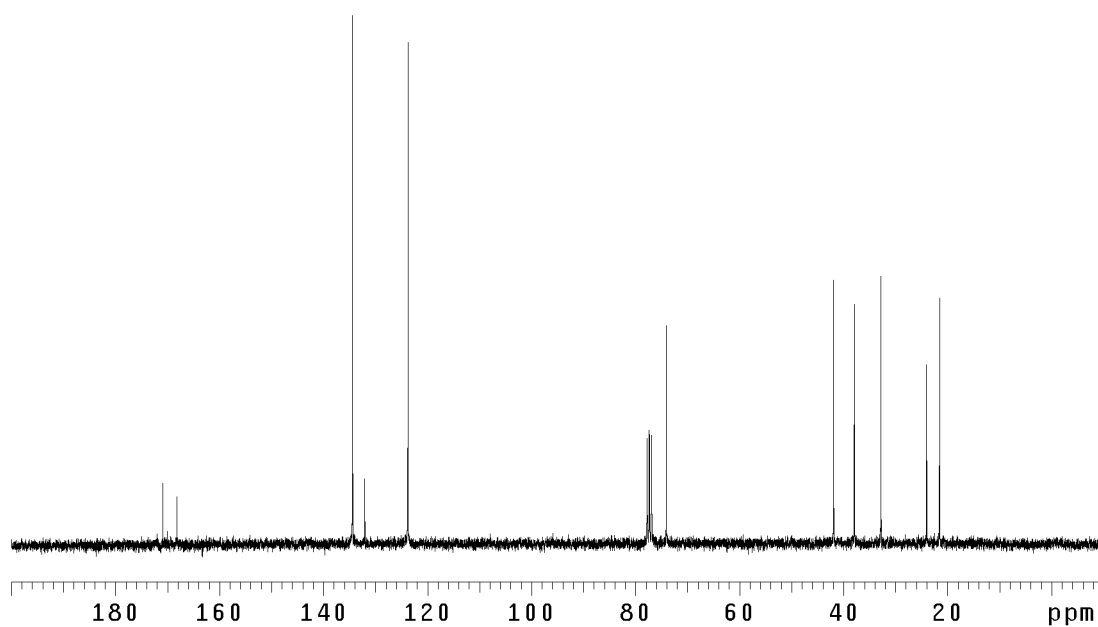


Figure A1.15 ¹³CNMR (125 MHz, CDCl₃) of compound **57**.

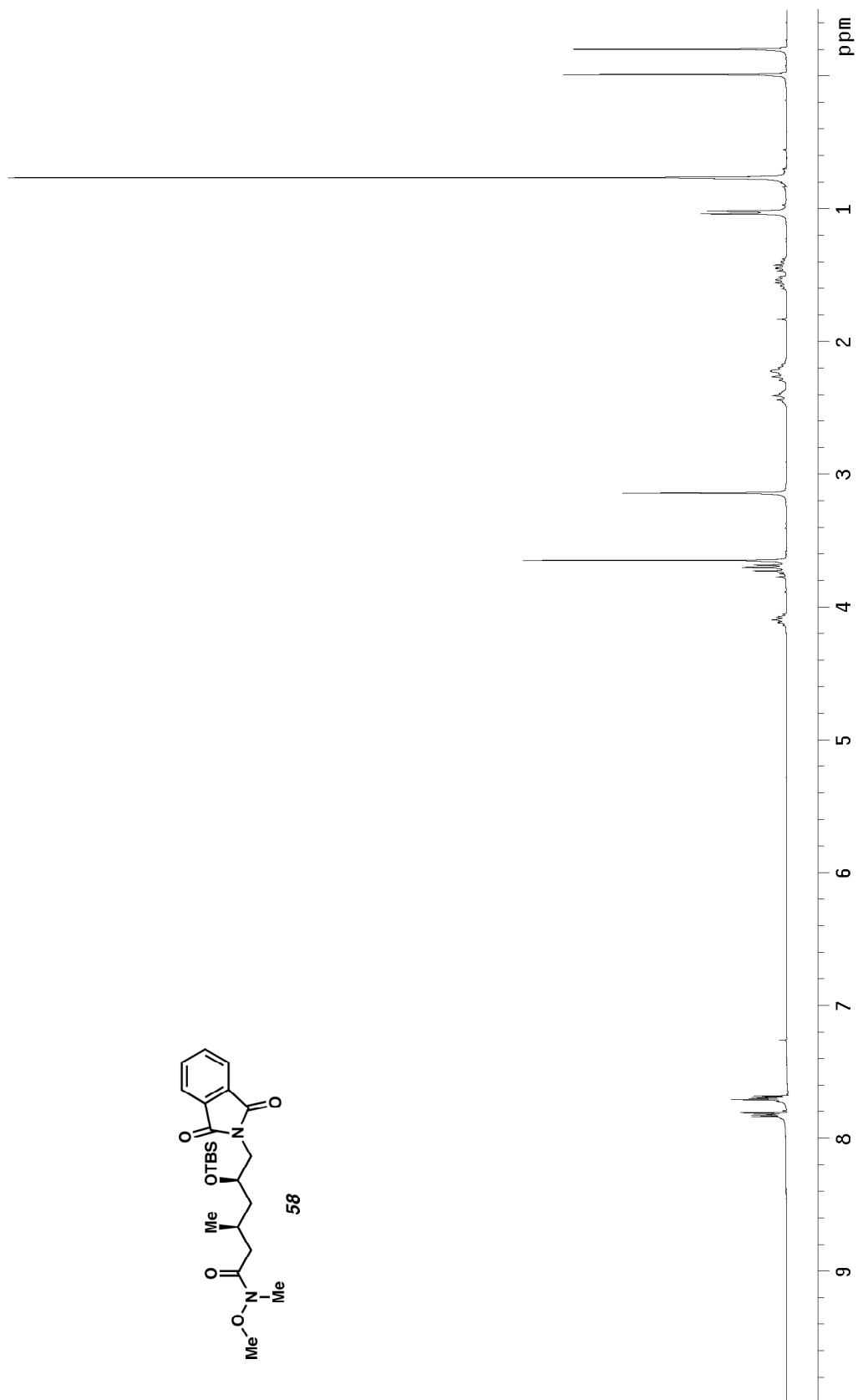
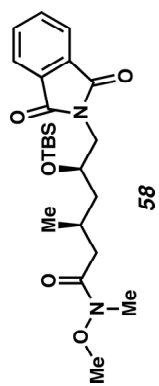


Figure A1.16 ^1H NMR (300 MHz, CDCl_3) of compound **58**.

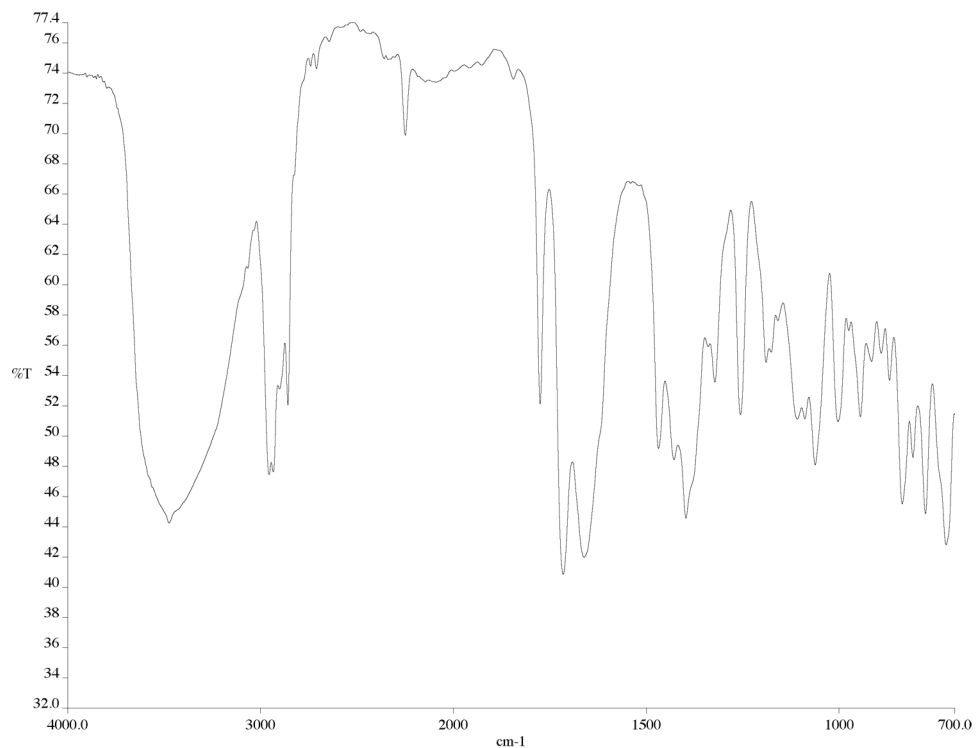


Figure A1.17 Infrared spectrum (thin film/NaCl) of compound **58**.

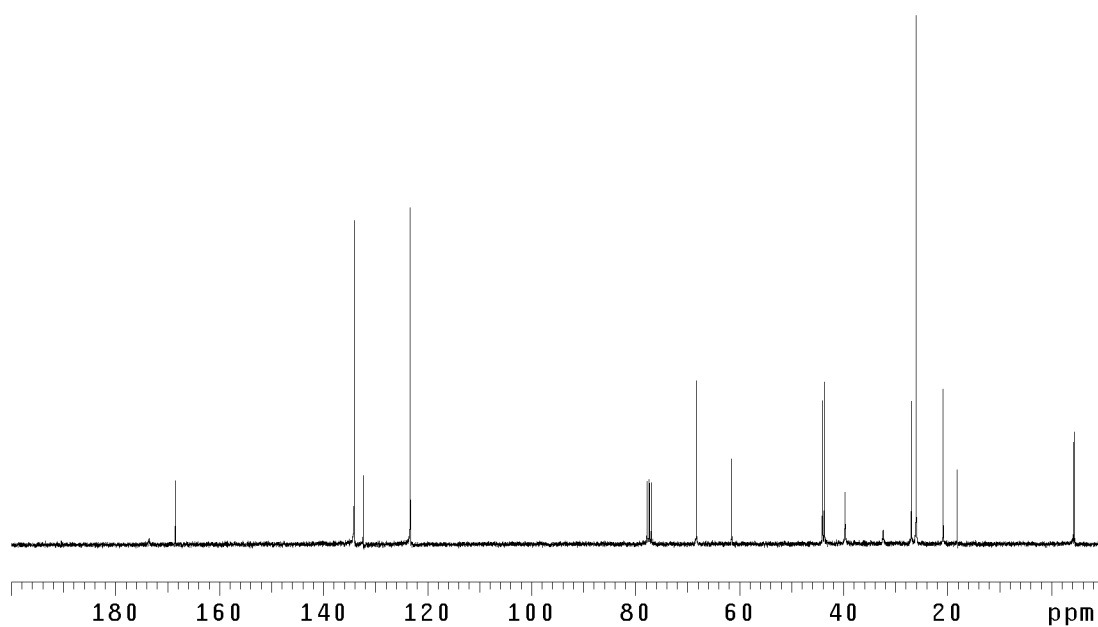


Figure A1.18 ¹³CNMR (125 MHz, CDCl₃) of compound **58**.

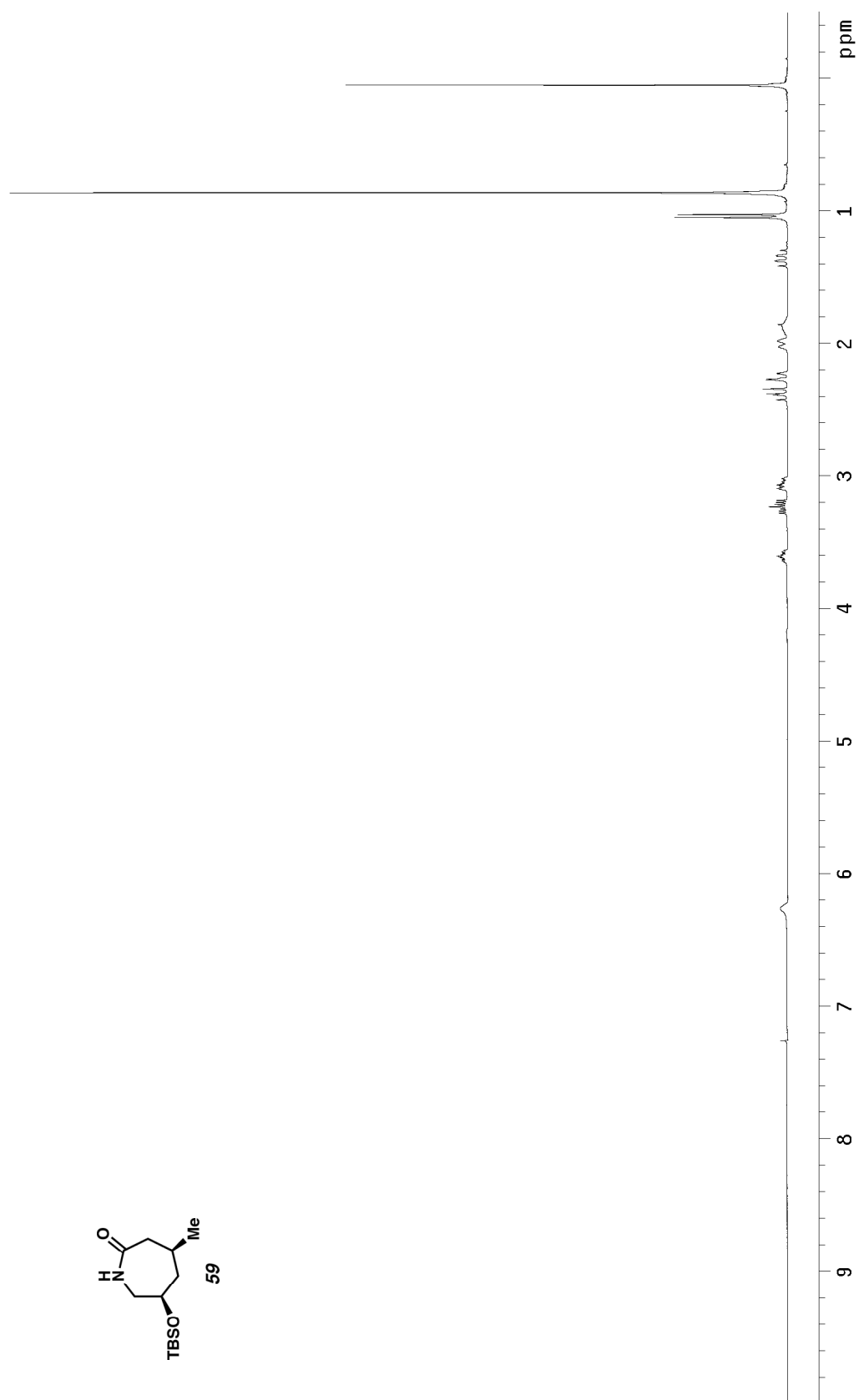


Figure A1.19 ^1H NMR (300 MHz, CDCl_3) of compound **59**.

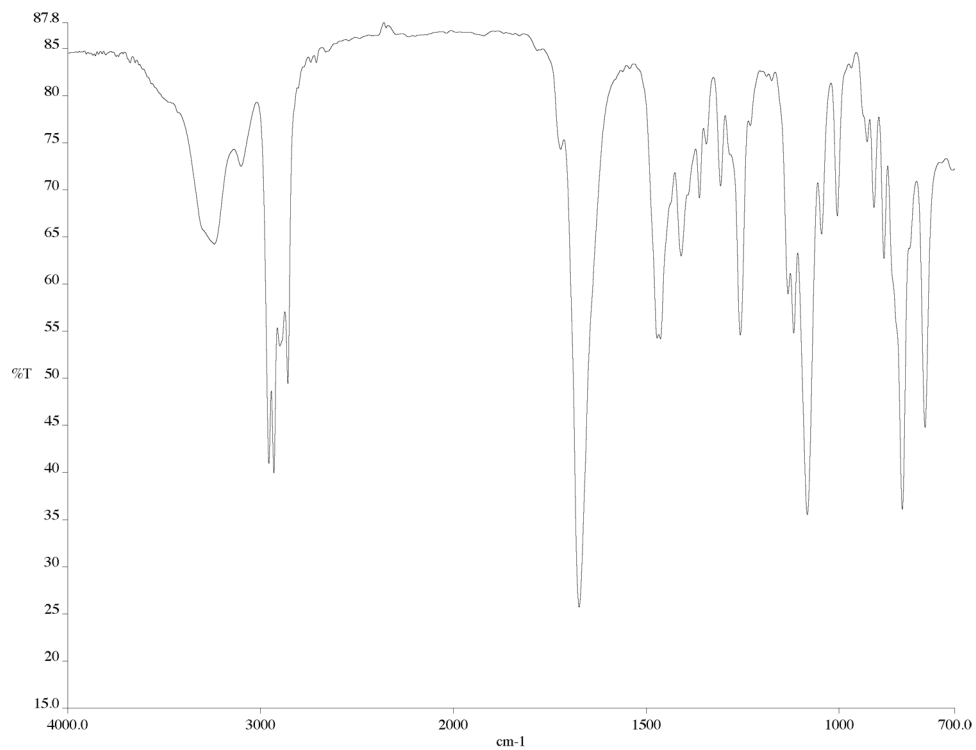


Figure A1.20 Infrared spectrum (thin film/NaCl) of compound **59**.

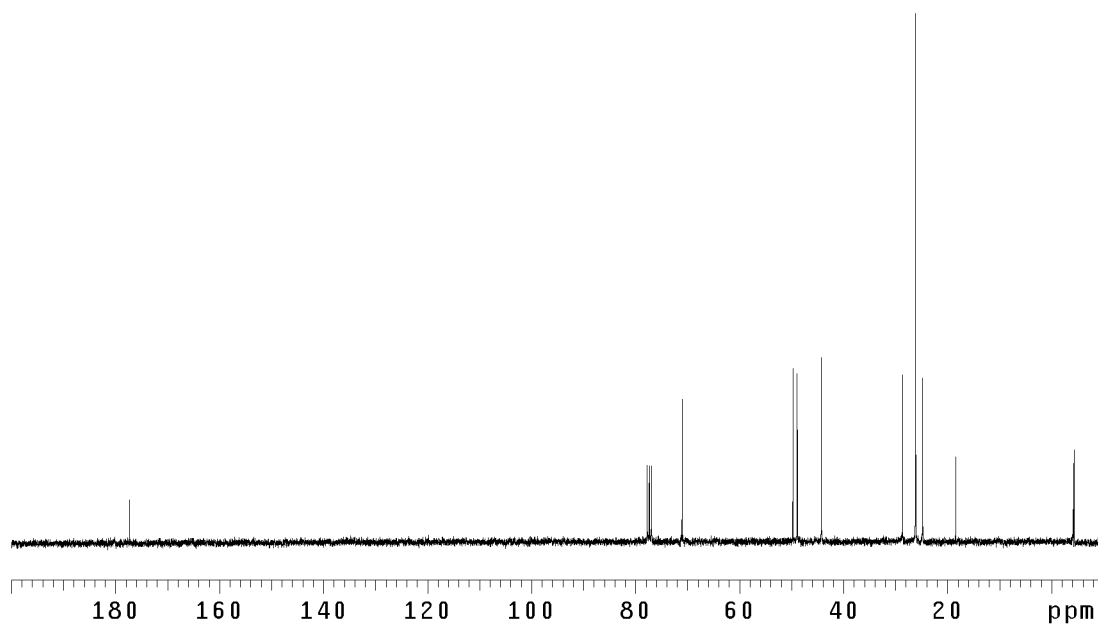


Figure A1.21 ¹³CNMR (125 MHz, CDCl₃) of compound **59**.

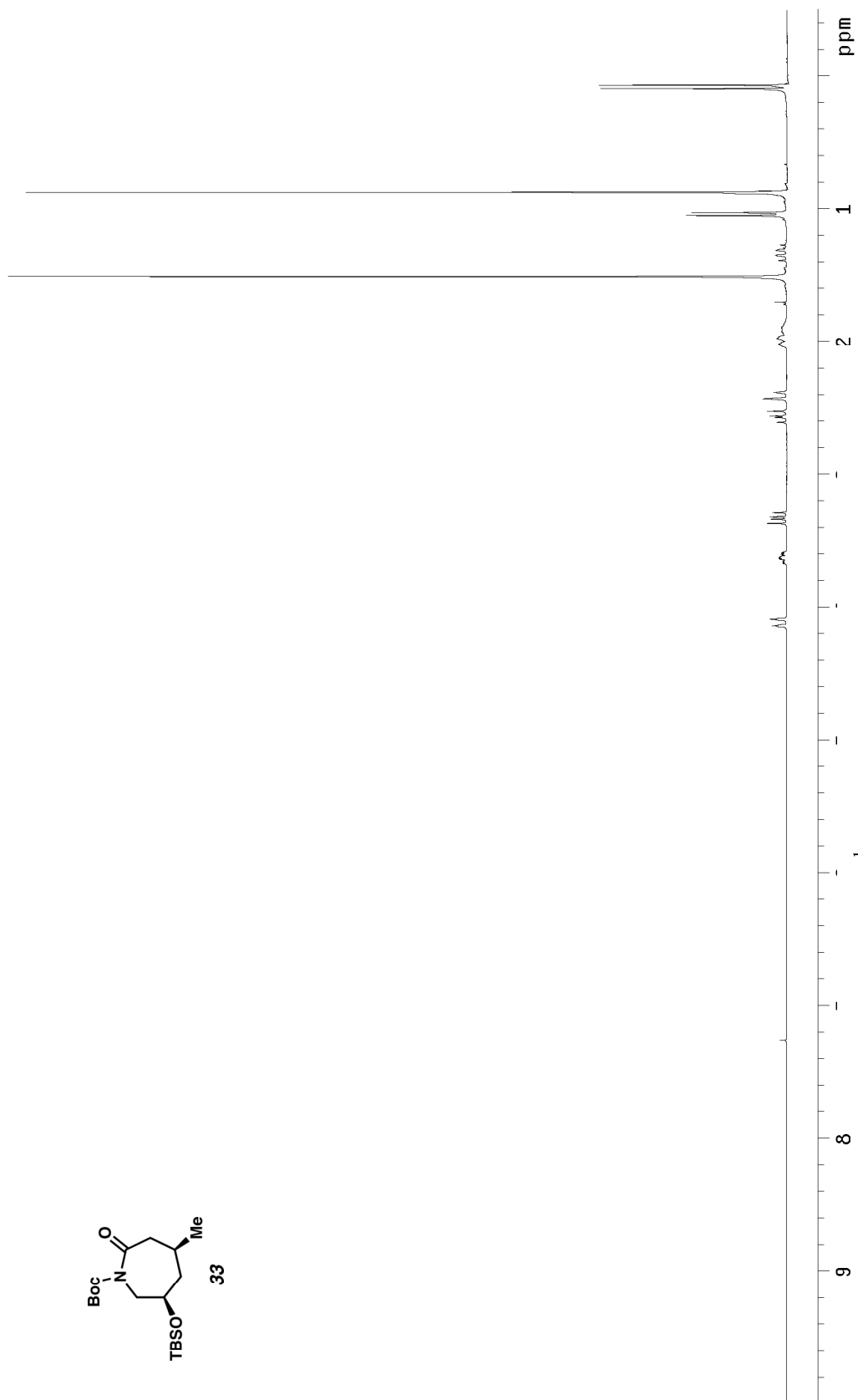
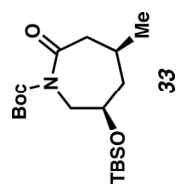


Figure A1.22 ¹H NMR (300 MHz, CDCl₃) of compound **33**.

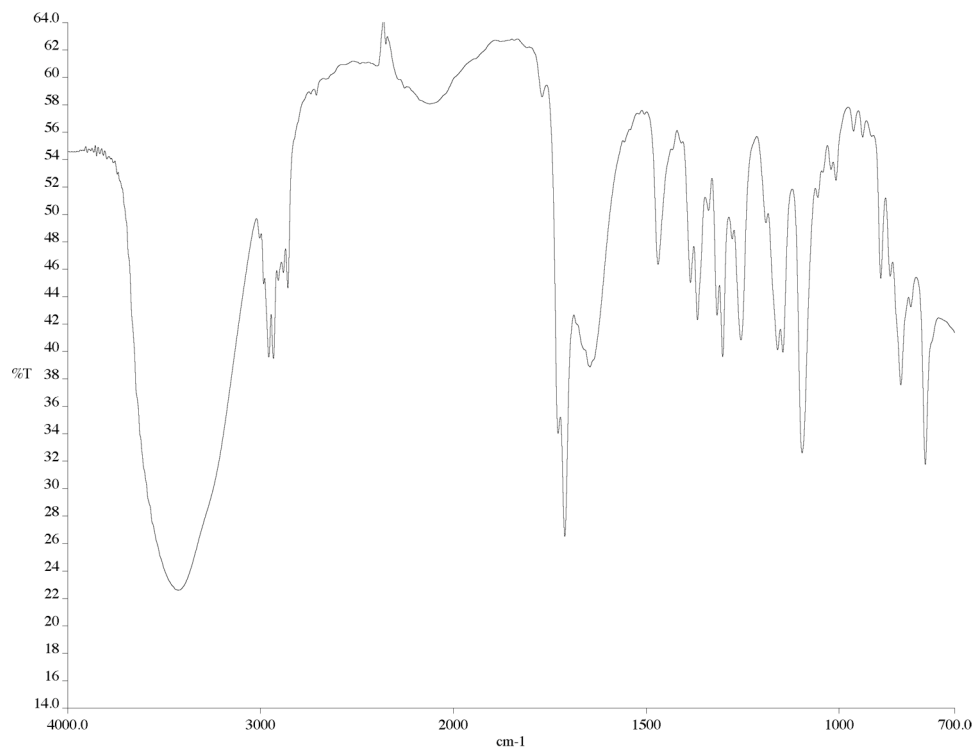


Figure A1.23 Infrared spectrum (thin film/NaCl) of compound **33**.

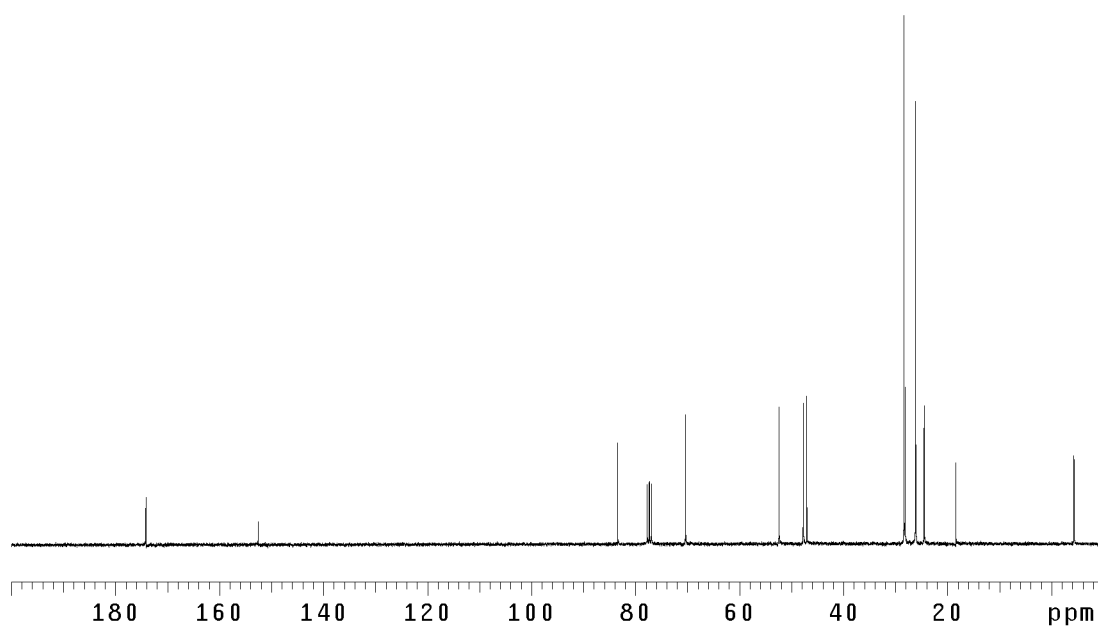
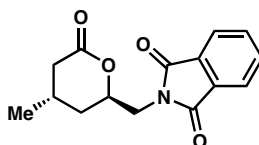


Figure A1.24 ¹³CNMR (125 MHz, CDCl₃) of compound **33**.

X-Ray Crystallographic Data

**2-(((2*R*,4*S*)-4-methyl-6-oxotetrahydro-2*H*-pyran-2-yl)
methyl)isoindoline-1,3-dione**



Contents

Table 1.	Crystal data
Figures	Figures for publication
Table 2.	Atomic coordinates
Table 3.	Selected bond distances and angles
Table 4.	Full bond distances and angles (for deposit)
Table 5.	Anisotropic displacement parameters

Table 1. Crystal data and structure refinement for JTB01 (CCDC 181862).

Empirical formula	C ₁₅ H ₁₅ NO ₄	
Formula weight	273.28	
Crystallization solvent	Heptane/ethylacetate	
Crystal habit	Tabular	
Crystal size	0.53 x 0.30 x 0.24 mm ³	
Crystal color	Colorless	
Data Collection		
Preliminary Photos	Rotation	
Type of diffractometer	Bruker P4	
Wavelength	0.71073 Å MoK α	
Data Collection Temperature	98(2) K	
θ range for 7982 reflections used in lattice determination	2.33 to 27.55°	
Unit cell dimensions	a = 7.0241(7) Å b = 19.2892(19) Å c = 10.3911(10) Å	β = 109.578(2)°
Volume	1326.5(2) Å ³	
Z	4	
Crystal system	Monoclinic	
Space group	P2 ₁ /n	
Density (calculated)	1.368 Mg/m ³	
F(000)	576	
Data collection program	Bruker SMART v5.054	
θ range for data collection	2.11 to 27.89°	
Completeness to θ = 27.89°	94.1 %	
Index ranges	-9 ≤ h ≤ 8, -25 ≤ k ≤ 25, -13 ≤ l ≤ 13	
Data collection scan type	ω scans at 5 ϕ settings	
Data reduction program	Bruker SAINT v6.022	
Reflections collected	18272	
Independent reflections	2992 [R _{int} = 0.0434]	
Absorption coefficient	0.100 mm ⁻¹	
Absorption correction	None	
Max. and min. transmission	0.9764 and 0.9489	

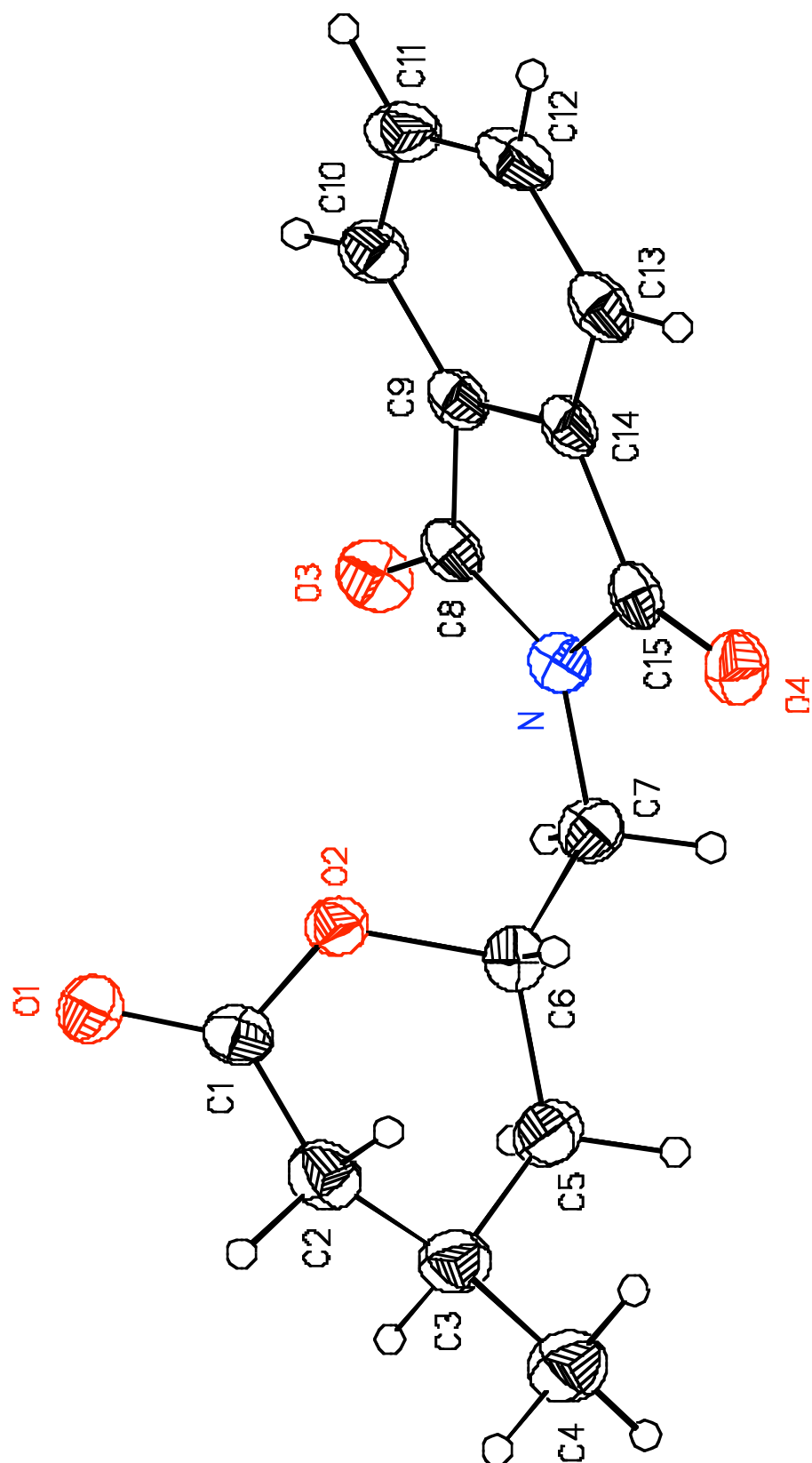
Table 1 (cont.)**Structure Solution and Refinement**

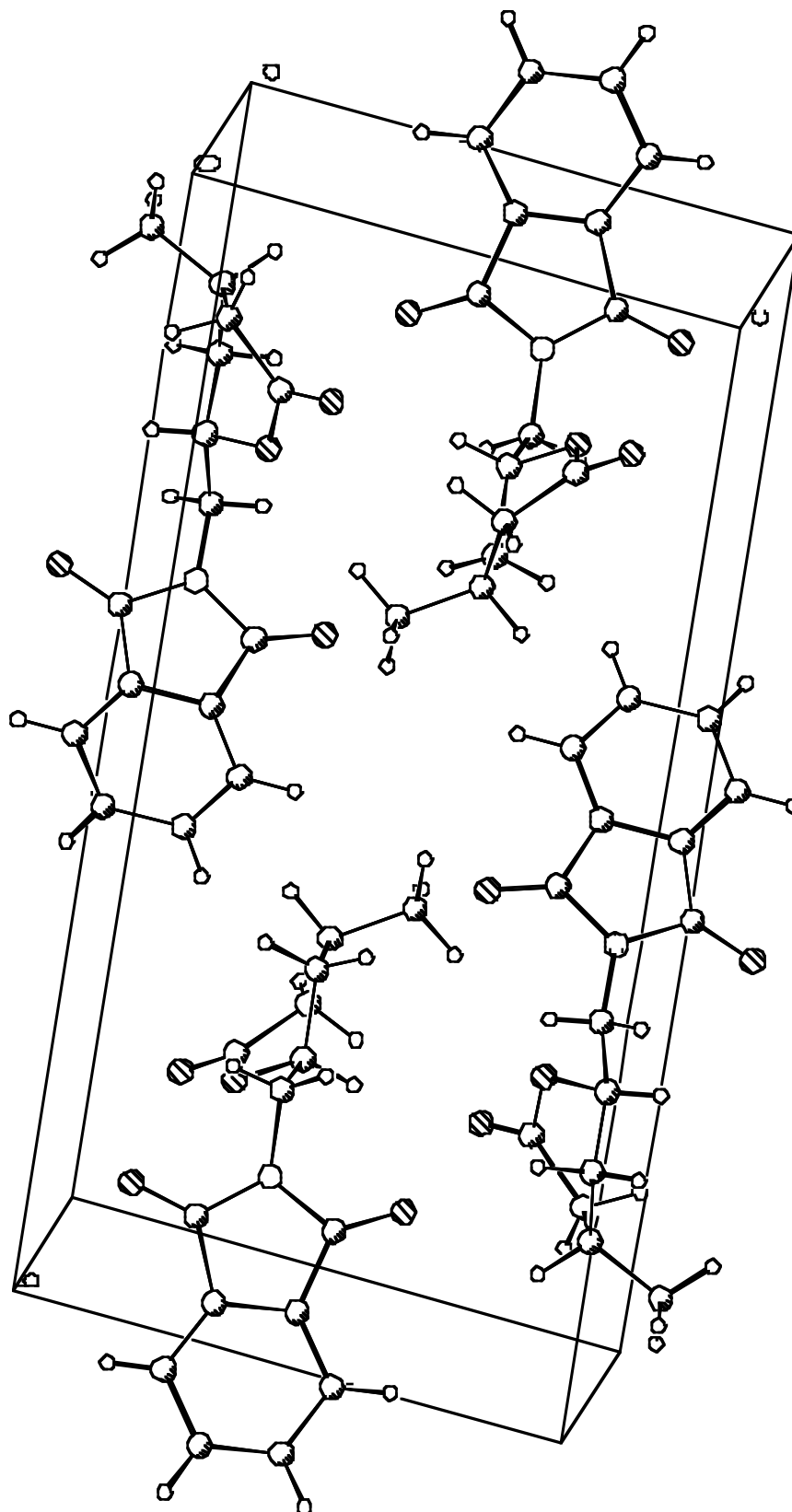
Structure solution program	SHELXS-97 (Sheldrick, 1990)
Primary solution method	Direct methods
Secondary solution method	Difference Fourier map
Hydrogen placement	Difference Fourier map
Structure refinement program	SHELXL-97 (Sheldrick, 1997)
Refinement method	Full matrix least-squares on F^2
Data / restraints / parameters	2992 / 0 / 241
Treatment of hydrogen atoms	Unrestrained
Goodness-of-fit on F^2	2.274
Final R indices [$I > 2\sigma(I)$, 2323 reflections]	$R1 = 0.0428$, $wR2 = 0.0682$
R indices (all data)	$R1 = 0.0579$, $wR2 = 0.0692$
Type of weighting scheme used	Sigma
Weighting scheme used	$w = 1/\sigma^2(F_o^2)$
Max shift/error	0.000
Average shift/error	0.000
Largest diff. peak and hole	0.298 and -0.245 e. \AA^{-3}

Special Refinement Details

Refinement of F^2 against ALL reflections. The weighted R-factor (wR) and goodness of fit (S) are based on F^2 , conventional R-factors (R) are based on F , with F set to zero for negative F^2 . The threshold expression of $F^2 > 2s(F^2)$ is used only for calculating R-factors(gt) etc. and is not relevant to the choice of reflections for refinement. R-factors based on F^2 are statistically about twice as large as those based on F , and R-factors based on ALL data will be even larger.

All esds (except the esd in the dihedral angle between two l.s. planes) are estimated using the full covariance matrix. The cell esds are taken into account individually in the estimation of esds in distances, angles and torsion angles; correlations between esds in cell parameters are only used when they are defined by crystal symmetry. An approximate (isotropic) treatment of cell esds is used for estimating esds involving l.s. planes.





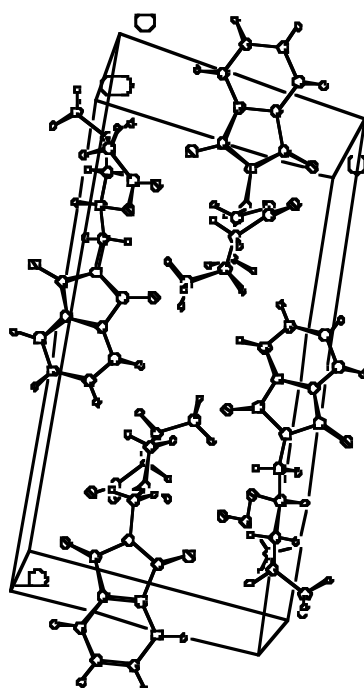
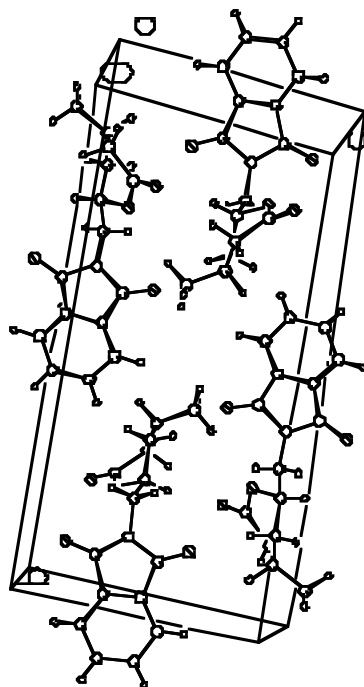


Table 2. Atomic coordinates ($\times 10^4$) and equivalent isotropic displacement parameters ($\text{\AA}^2 \times 10^3$) for JTB01 (CCDC 181862). $U(\text{eq})$ is defined as the trace of the orthogonalized U^{ij} tensor.

	x	y	z	U_{eq}
O(1)	8436(1)	2407(1)	2404(1)	32(1)
O(2)	5191(1)	2656(1)	1692(1)	27(1)
O(3)	3360(1)	3947(1)	3345(1)	33(1)
O(4)	1021(1)	3763(1)	-1307(1)	33(1)
N	2145(2)	3677(1)	1039(1)	24(1)
C(1)	6761(2)	2271(1)	1623(1)	26(1)
C(2)	6257(2)	1726(1)	544(2)	34(1)
C(3)	4416(2)	1280(1)	485(2)	34(1)
C(4)	3661(3)	892(1)	-851(2)	43(1)
C(5)	2781(2)	1731(1)	758(2)	32(1)
C(6)	3201(2)	2493(1)	708(2)	27(1)
C(7)	1738(2)	2943(1)	1113(2)	28(1)
C(8)	2953(2)	4115(1)	2163(1)	25(1)
C(9)	3146(2)	4805(1)	1580(1)	24(1)
C(10)	3904(2)	5421(1)	2214(2)	30(1)
C(11)	3914(2)	5986(1)	1383(2)	34(1)
C(12)	3170(2)	5931(1)	-26(2)	32(1)
C(13)	2400(2)	5310(1)	-662(2)	29(1)
C(14)	2416(2)	4750(1)	168(1)	23(1)
C(15)	1753(2)	4027(1)	-194(1)	24(1)

Table 3. Bond lengths [Å] and angles [°] for JTB01 (CCDC 181862).

O(1)-C(1)	1.2131(16)	C(4)-C(3)-C(5)	113.28(14)
O(2)-C(1)	1.3515(15)	C(2)-C(3)-C(5)	110.22(12)
O(2)-C(6)	1.4634(16)	C(4)-C(3)-H(3)	108.4(7)
O(3)-C(8)	1.2081(14)	C(2)-C(3)-H(3)	106.2(7)
O(4)-C(15)	1.2093(15)	C(5)-C(3)-H(3)	108.2(7)
N-C(15)	1.3913(16)	C(3)-C(4)-H(4A)	110.1(8)
N-C(8)	1.3973(16)	C(3)-C(4)-H(4B)	107.8(7)
N-C(7)	1.4525(17)	H(4A)-C(4)-H(4B)	108.8(11)
C(1)-C(2)	1.4899(19)	C(3)-C(4)-H(4C)	108.8(9)
C(2)-C(3)	1.537(2)	H(4A)-C(4)-H(4C)	109.4(12)
C(2)-H(2A)	0.976(14)	H(4B)-C(4)-H(4C)	111.9(12)
C(2)-H(2B)	0.995(14)	C(6)-C(5)-C(3)	112.23(12)
C(3)-C(4)	1.509(2)	C(6)-C(5)-H(5A)	107.5(8)
C(3)-C(5)	1.541(2)	C(3)-C(5)-H(5A)	111.4(7)
C(3)-H(3)	1.036(13)	C(6)-C(5)-H(5B)	106.7(7)
C(4)-H(4A)	1.057(16)	C(3)-C(5)-H(5B)	111.0(7)
C(4)-H(4B)	1.060(14)	H(5A)-C(5)-H(5B)	107.7(11)
C(4)-H(4C)	1.026(17)	O(2)-C(6)-C(5)	109.82(11)
C(5)-C(6)	1.5024(19)	O(2)-C(6)-C(7)	105.13(11)
C(5)-H(5A)	1.037(15)	C(5)-C(6)-C(7)	113.12(12)
C(5)-H(5B)	1.052(13)	O(2)-C(6)-H(6)	108.5(7)
C(6)-C(7)	1.5088(19)	C(5)-C(6)-H(6)	106.2(7)
C(6)-H(6)	1.018(12)	C(7)-C(6)-H(6)	114.0(7)
C(7)-H(7A)	0.943(13)	N-C(7)-C(6)	112.46(11)
C(7)-H(7B)	0.984(13)	N-C(7)-H(7A)	107.1(8)
C(8)-C(9)	1.4882(18)	C(6)-C(7)-H(7A)	110.3(8)
C(9)-C(10)	1.3757(19)	N-C(7)-H(7B)	108.1(7)
C(9)-C(14)	1.3866(18)	C(6)-C(7)-H(7B)	109.0(7)
C(10)-C(11)	1.391(2)	H(7A)-C(7)-H(7B)	109.9(11)
C(10)-H(10)	0.952(13)	O(3)-C(8)-N	125.45(12)
C(11)-C(12)	1.384(2)	O(3)-C(8)-C(9)	129.04(13)
C(11)-H(11)	0.959(13)	N-C(8)-C(9)	105.50(11)
C(12)-C(13)	1.387(2)	C(10)-C(9)-C(14)	121.29(13)
C(12)-H(12)	0.960(13)	C(10)-C(9)-C(8)	130.66(13)
C(13)-C(14)	1.3795(18)	C(14)-C(9)-C(8)	108.04(12)
C(13)-H(13)	0.975(12)	C(9)-C(10)-C(11)	117.42(14)
C(14)-C(15)	1.4788(18)	C(9)-C(10)-H(10)	121.0(8)
C(1)-O(2)-C(6)	116.71(10)	C(11)-C(10)-H(10)	121.5(8)
C(15)-N-C(8)	112.13(11)	C(12)-C(11)-C(10)	121.18(15)
C(15)-N-C(7)	122.64(12)	C(12)-C(11)-H(11)	119.5(8)
C(8)-N-C(7)	125.22(11)	C(10)-C(11)-H(11)	119.4(8)
O(1)-C(1)-O(2)	118.14(12)	C(11)-C(12)-C(13)	121.26(14)
O(1)-C(1)-C(2)	126.02(13)	C(11)-C(12)-H(12)	119.4(8)
O(2)-C(1)-C(2)	115.82(13)	C(13)-C(12)-H(12)	119.3(8)
C(1)-C(2)-C(3)	114.18(12)	C(14)-C(13)-C(12)	117.24(14)
C(1)-C(2)-H(2A)	108.5(8)	C(14)-C(13)-H(13)	121.7(7)
C(3)-C(2)-H(2A)	111.5(8)	C(12)-C(13)-H(13)	121.0(7)
C(1)-C(2)-H(2B)	108.7(8)	C(13)-C(14)-C(9)	121.60(13)
C(3)-C(2)-H(2B)	104.4(9)	C(13)-C(14)-C(15)	130.02(13)
H(2A)-C(2)-H(2B)	109.3(11)	C(9)-C(14)-C(15)	108.37(12)
C(4)-C(3)-C(2)	110.27(13)	O(4)-C(15)-N	124.54(12)

O(4)-C(15)-C(14)	129.54(13)
------------------	------------

N-C(15)-C(14)

105.92(11)

Table 4. Anisotropic displacement parameters ($\text{\AA}^2 \times 10^4$) for JTB01 (CCDC 181862). The anisotropic displacement factor exponent takes the form: $-2\pi^2 [h^2 a^{*2} U^{11} + \dots + 2 h k a^* b^* U^{12}]$

	U^{11}	U^{22}	U^{33}	U^{23}	U^{13}	U^{12}
O(1)	274(6)	301(6)	372(6)	0(5)	108(5)	-30(5)
O(2)	247(5)	231(5)	327(6)	-18(4)	110(5)	-13(4)
O(3)	397(6)	350(6)	256(6)	42(5)	142(5)	51(5)
O(4)	305(6)	376(6)	264(6)	-5(5)	49(5)	1(5)
N	238(6)	239(6)	253(6)	23(5)	105(5)	11(5)
C(1)	314(9)	227(8)	272(8)	59(6)	135(7)	3(7)
C(2)	357(10)	350(9)	318(9)	-33(7)	139(8)	68(7)
C(3)	407(10)	279(8)	295(9)	-32(7)	87(7)	23(7)
C(4)	496(12)	372(10)	376(11)	-71(8)	92(9)	19(9)
C(5)	340(10)	286(9)	315(9)	-21(7)	91(8)	-36(7)
C(6)	257(8)	290(8)	271(8)	0(7)	81(7)	0(6)
C(7)	275(9)	268(8)	313(9)	22(7)	120(7)	-29(7)
C(8)	217(8)	285(8)	267(8)	21(6)	118(6)	56(6)
C(9)	194(7)	256(8)	293(8)	29(6)	121(6)	52(6)
C(10)	280(8)	285(8)	355(9)	-38(7)	136(7)	40(7)
C(11)	293(9)	245(8)	537(11)	-35(8)	210(8)	13(7)
C(12)	290(9)	260(8)	493(11)	125(8)	225(8)	79(7)
C(13)	235(8)	337(9)	319(9)	85(7)	141(7)	69(7)
C(14)	158(7)	270(8)	295(8)	34(6)	107(6)	49(6)
C(15)	157(7)	307(8)	266(8)	30(7)	79(6)	36(6)

Table 5. Hydrogen coordinates ($\times 10^4$) and isotropic displacement parameters ($\text{\AA}^2 \times 10^3$) for JTB01 (CCDC 181862).

	x	y	z	U_{iso}
H(2A)	7460(20)	1442(7)	672(13)	36(4)
H(2B)	5870(20)	1955(8)	-365(15)	46(5)
H(3)	4920(20)	922(7)	1269(13)	38(4)
H(4A)	4850(20)	602(8)	-998(14)	54(5)
H(4B)	2520(20)	546(7)	-800(13)	41(4)
H(4C)	3130(20)	1243(9)	-1632(16)	64(5)
H(5A)	1360(20)	1636(7)	47(14)	42(4)
H(5B)	2700(20)	1631(7)	1732(14)	37(4)
H(6)	3229(18)	2588(6)	-250(13)	22(3)
H(7A)	1826(19)	2848(6)	2021(14)	29(4)
H(7B)	360(20)	2850(6)	493(13)	27(4)
H(10)	4410(20)	5457(6)	3184(14)	29(4)
H(11)	4470(20)	6418(7)	1795(13)	31(4)
H(12)	3220(20)	6327(7)	-574(13)	33(4)
H(13)	1905(18)	5270(6)	-1655(13)	24(4)

Chapter 2

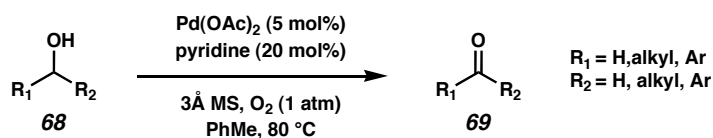
Development and Application of the Oxidative Kinetic Resolution of 2°-Alcohols by Catalytic Palladium

Introduction

Enantioselective Oxidation Background

In the last few decades, the field of organic chemistry has benefited tremendously from the development of a number of catalytic enantioselective oxidation processes including epoxidation,¹ dihydroxylation² and aziridination.³ In light of the continued success of these methods, it is surprising that there are relatively few catalytic enantioselective examples of the pervasive alcohol oxidation.⁴ Among the many hundred known processes for alcohol oxidation,⁵ comparatively few metal-catalyzed methods have been developed. Of notable exception are catalytic palladium(II) systems, which often provide efficient oxidation of 2°-alcohol to ketones in high yields.⁶ A particularly exciting example is given by Uemura,⁷ where a number of 2°-alcohols **68** are readily oxidized to ketones **69** by a catalytic palladium(II) complex in the presence of pyridine ligand, using oxygen as the sole stoichiometric oxidant (Scheme 1).

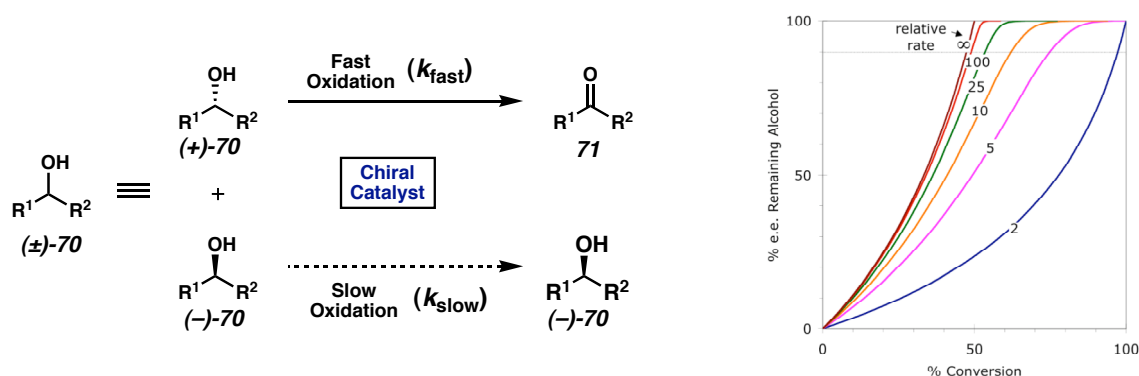
Scheme 1. Uemura's protocol for the oxidation of alcohols



We were particularly interested in Uemura's system because the inclusion of the pyridine ligand, and the non-coordinating nature of the reaction solvent are features which promote the possibility of introducing enantioselectivity. As an added bonus, the reaction employs an atmosphere of oxygen as the sole stoichiometric oxidant, making this an atom economical (with respect to the oxidant), environmentally attractive transformation.

In an enantioselective oxidation reaction, the genesis of an enantiomeric excess from a racemic mixture of alcohols (\pm)-**70** relies on the catalyst's ability to oxidize one member of the racemate (+)-**70** faster than the other member (-)-**70** (Figure 1). As conversion develops, the fast-reacting alcohol will be converted to ketone **71**, while the slow-reacting enantiomer (-)-**70** will persist. The graph in Figure 1 expresses how ee evolves over conversion for given values of selectivity (*s*), an integer value equal to the ratio of k_{fast} to k_{slow} .^{8,9} Considering a selectivity factor of 2, it is possible to attain high levels of ee (>95%) for a recovered alcohol. However, under these circumstances, a high conversion will be attained, relating to a low recovery of enantioenriched alcohol. A more desirable scenario is a resolution that proceeds with a selectivity greater than 10. Under these circumstances, >95% ee is possible for a conversion of approximately 50%. In this scenario, synthetically useful quantities of enantioenriched alcohol are accessible.

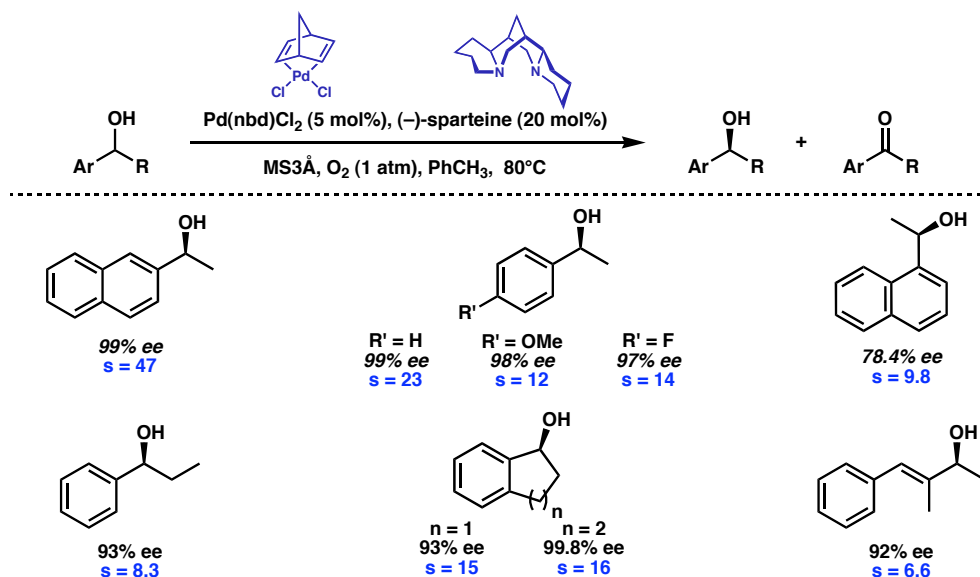
Figure 1. Principles of an oxidative kinetic resolution



The Original Oxidative Kinetic Resolution (OKR)

As part of a general program dedicated to the development of enantioselective oxidation reactions we explored the possibility of conducting enantioselective alcohol oxidation with a catalytic palladium(II) complex. As a result of our early investigations, we reported the oxidative kinetic resolution of secondary alcohols.¹⁰ Our operationally facile system employs a commercially available palladium precatalyst $[\text{Pd}(\text{nbd})\text{Cl}_2]$, inexpensive (–)-sparteine as chiral inducer, and molecular oxygen as the stoichiometric oxidant. Using our conditions as a platform, a variety of secondary alcohols, shown in Table 1, were oxidized to high enantiomeric excess with good selectivity.

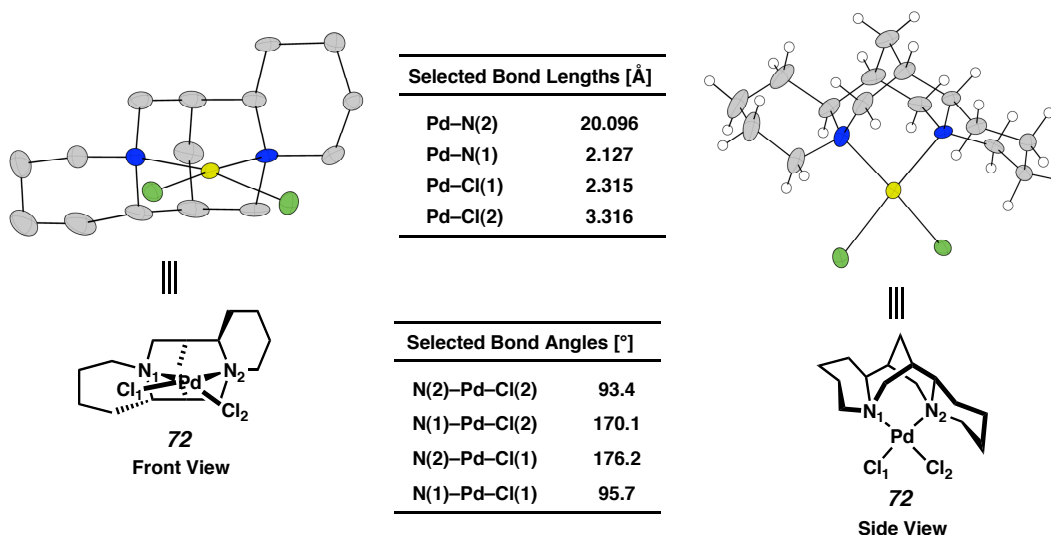
Table 1. The original oxidative kinetic resolution (OKR) of secondary alcohols



While the reported resolution protocol involves the *in situ* formation of the catalytic species, more commonly, the preformed and isolated $\text{Pd}(\text{sp})\text{Cl}_2$ complex **72** is employed directly in the resolution protocol. Crystals of the metal complex are readily

precipitated and the X-ray structure of this complex has been obtained (Figure 2). The key features of the complex are a distorted square-planar palladium center, reflecting the C_1 -symmetry of the sparteine ligand. The distortion in the square-planar geometry of palladium is particularly evident by visual inspection from the “front” view; Cl(2) resides 9.9° below the square-planar configuration.

Figure 2.



Although our originally described system was applied to a range of benzylic and allylic alcohols, the reaction times required to advance the resolutions to high conversion, consequently high enantiomeric excess, were often prohibitively long. For example, a typical reaction time was approximately 4 days. In several instances, reaction times of up to 8 days were required to attain desirable levels of resolution. While this aspect of the reaction profile was problematic, the required high operating temperatures (typically 80°C) highlight the relatively low activity of our original catalyst system. Additionally, several practical considerations must be noted. Specifically, the reaction conditions require heated mixtures of the flammable solvent toluene under an atmosphere of pure

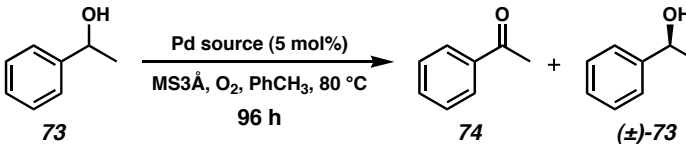
oxygen, creating a potential flame hazard. While the conditions provide a viable resolution, an underlying goal remained: to develop more general and selective catalyst systems.

II. Results and Discussion

The Role of Exogenous Base and Alcohol Additives

During the course of our investigations into the enantioselective oxidation of secondary alcohols, we prepared a number of Pd(II)-sparteine complexes and studied their activity. As a general observation, we found that the reactivity of these discrete complexes for asymmetric oxidation of alcohol **73** to ketone **74**, providing resolved alcohol (–)-**73** was greatly reduced when compared to the optimized method, wherein a 4-fold excess of (–)-sparteine relative to the Pd(II) precatalyst was used (Table 2).¹¹

Table 2. *In situ* catalyst formation with excess sparteine vs. discrete Pd(sp)Cl₂

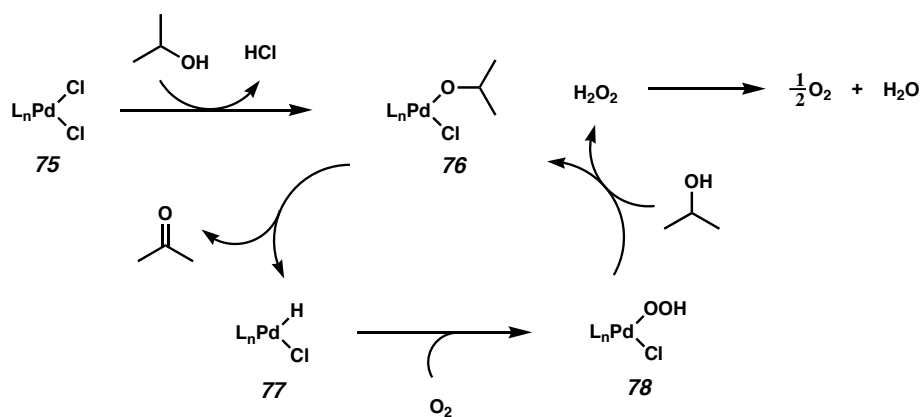
				
entry	catalyst	conversion ^a	ee ^b	s
1.	Pd(nbd)Cl ₂ (–)-sparteine (20 mol%)	59.9%	98.7%	23.1
2.	Pd(sparteine)Cl ₂	4.6%	3.4%	6.0
3.	Pd(sparteine)Cl ₂ (–)-sparteine (15 mol%)	60.6%	99.2%	23.8

^aMeasured by GC using a DB-WAX column. ^bMeasured by chiral HPLC

Interestingly, the reactivity of the system could be restored upon introduction of 3 equivalents of sparteine relative to the Pd(sp)Cl₂ complex (entry 3). Intrigued by this

finding, we hypothesized that the excess sparteine was serving as a general base for the ultimate neutralization of HCl liberated from the system upon initiation of the catalytic cycle (Figure 3), and thus investigated the effect of other bases on the reaction. The hypothesis that (–)-sparteine serves as both a ligand and a base has been confirmed by kinetic analysis.¹² According to the general mechanism for oxidation (Figure 3), ligand substitution of a chloride on complex **75** with an alcohol provides the palladium-alkoxide **76** that β-hydride eliminates, and liberates the ketone product. The resulting palladium(0)-hydride can reoxidize to Pd(II) by combining with molecular oxygen to provide palladium-hydroperoxide **78**, which is prone to a second ligand substitution event, generating the initial palladium(II)-alkoxide **76**. The liberated hydrogen peroxide disproportionates to O₂ and H₂O under the reaction conditions.

Figure 3. Plausible mechanism for Pd catalyzed oxidation with stoichiometric O₂



Our initial studies were focused on supplanting the role of (–)-sparteine as a base. Consequently, exogenous (–)-sparteine was excluded from the reaction conditions while a variety of other bases were included. As shown in Table 3, we surveyed the effect of a variety of external bases on the oxidative kinetic resolution of alcohol (±)-**79**, providing

ketone **80** and resolved alcohol (–)-**79**. We compared the results with a control reaction with excess (–)-sparteine (entry 1) as well as a control reaction deprived of any base (entry 2).

Table 3. Additive effects on the OKR

entry	additive	time	conversion ^b	ee ROH ^c	s ^d
1.	sparteine (0.3 equiv)	13 h	29%	34%	15
2.	none	13 h	2%	<2%	--
3.	Et ₃ N (0.4 equiv)	13 h	26%	31%	22
4.	Et ₃ N (2.0 equiv)	13 h	19%	19%	11
5.	Et ₃ N (4.0 equiv)	13 h	14%	11%	6
6.	DABCO (0.4 equiv)	13 h	7%	8%	20
7.	Na ₂ CO ₃ (1.0 equiv)	13 h	27%	31%	15
8.	K ₂ CO ₃ (1.0 equiv)	13 h	56%	84%	13
9.	Cs ₂ CO ₃ (1.0 equiv)	13 h	68%	99%	13

^a10 mol% Pd(nbd)Cl₂, 10 mol% (–)-sparteine, 1 atm O₂, 0.1 M substrate concentration in PhCH₃.

^bMeasured by ¹H NMR. ^cMeasured by chiral HPLC. ^dSee footnote 10.

As expected, the catalyst system was inactive without excess (–)-sparteine base. However, the catalytic activity was initially restored upon inclusion of the achiral base triethylamine (entry 3). Although addition of TEA provided a high level of selectivity, resolutions performed under these conditions failed to proceed beyond low conversion. Ultimately, the system with triethylamine exhibits a greatly reduced catalytic activity beyond 13 hours, with no further activity beyond 24 hours. Increasing the concentration of triethylamine could not compensate for the observed decreasing activity (entries 4-5). On the contrary, increasing the triethylamine concentration adversely impacted the

activity of the system. These observations are consistent with decomposition of the active $\text{Pd}(\text{sparteine})\text{Cl}_2$ catalyst to an inactive $\text{Pd}(\text{TEA})_x\text{Cl}_2$ system.¹³ While it is surprising that triethylamine could competitively displace bidentate sparteine from the complex, a general observation reveals that monodentate palladium(II)chloride-amine complexes provide inactive catalyst systems.¹⁴ Consistent with this observation, employing the much more nucleophilic, better binding base DABCO, further erodes reactivity (entry 6). In obtaining these data, it became apparent that exogenous amine bases are not likely to provide a benefit to the resolution. Consequently, a variety of inorganic bases were screened. The most dramatic effect was observed upon addition of carbonate salts. Specifically, inclusion of 1.0 equiv of powdered anhydrous Cs_2CO_3 resolved benzylic alcohol **3** in just 13 h, with comparable selectivity to our previously reported conditions. The role of Cs_2CO_3 appears to be a heterogeneous base. Several observations support this hypothesis: a) finely milled Cs_2CO_3 performs much better than the granular base of lower surface area, and b) the solubility of Cs_2CO_3 in the organic solvent toluene is very low (<2 mg/ml), even at elevated temperatures.

Having observed a marked additive effect, we attempted to further improve the system by optimizing the catalyst loading, Pd:sparteine ratio, and by continuing to study the effects of additives. As shown in Table 4, increased amounts of sparteine still have a positive effect on the selectivity and the overall rate of the reaction (entries 1-3). By simply increasing the total amount of (–)-sparteine to that previously employed (4:1 sparteine: Pd), we observed alcohol resolution to high enantiopurity in only 5 h (entry 5).

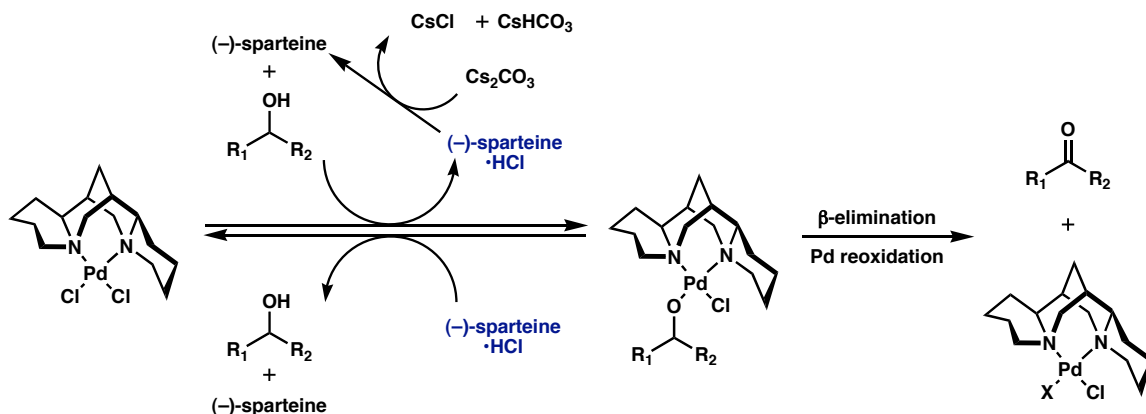
Table 4. Effect of excess (–)-sparteine

entry	additive	time	conversion ^c	ee ROH ^d	s
1.	none	5 h	31%	35%	12
2.	sparteine (5 mol%)	5 h	45%	60%	12
3.	sparteine (10 mol%)	5 h	56%	83%	12
4.	sparteine (20 mol%)	5 h	59%	90%	13
5.	sparteine (30 mol%)	5 h	61%	96%	15

^aPalladium precatalyst and (–)-sparteine are maintained at 80 °C for 10 min before introduction of alcohol. 1 atm O₂, 0.1 M substrate concentration in PhCH₃. ^bFinely milled anhydrous (1.0 equiv). ^c Measured by ¹H NMR. ^dMeasured by chiral HPLC.

That a combination of the exogenous bases sparteine and Cs₂CO₃ provides the optimal reaction rate and selectivity is interesting. The excess sparteine may be a better kinetic base for neutralizing HCl (Figure 4) than the heterogeneous base Cs₂CO₃.¹⁵ It is interesting to note that the pK_a of sparteine•HCl and CsHCO₃ are very similar (both are ~10.5).¹⁶ In the absence of a clear driving force (pK_a) to neutralize sparteine•HCl generated in the system with Cs₂CO₃, the inorganic base may ultimately remove sparteine•HCl from the system by establishing an acid/base equilibrium favoring the formation of insoluble CsCl. Since sparteine•HCl inhibits the oxidation¹² by disfavoring formation of the palladium-alkoxide according to the equilibrium in Figure 4, removal of the protonated amine from solution favors palladium-alkoxide formation.

Figure 4. The potential role of Cs_2CO_3

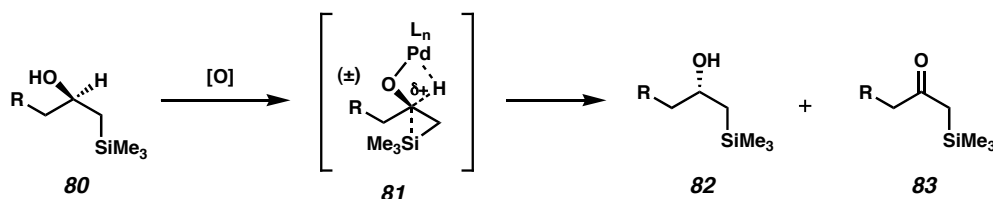


Concurrent to our studies involving the role of exogenous bases on the activity of our catalyst system was an ongoing effort to explore the substrate scope of this reaction. An early observation about our known substrate scope was that all viable resolution substrates could benefit from a π -stabilization at the carbon bearing the hydrogen participating in β -H elimination. In the evolving transition state, this carbon will presumably develop a cationic charge, which may be stabilized by the adjacent aromatic group. Indeed, Hammett studies conducted by Sigman's group confirm that electron donating substituents on the arene portion of the oxidation substrate enhance oxidation through both induction and resonance.¹⁷

Beginning from the assumption that cation stabilization lowers the energy barrier for alcohol oxidation, we speculated that β -silyl alcohol **80** (Scheme 2) may represent a reasonable substrate for resolution, providing resolved alcohol **82** and ketone **83** as products. Alcohol **80** may benefit from β -silicon stabilization (via intermediate **81**), of the cationic intermediate generated during the β -hydride elimination event. Accordingly,

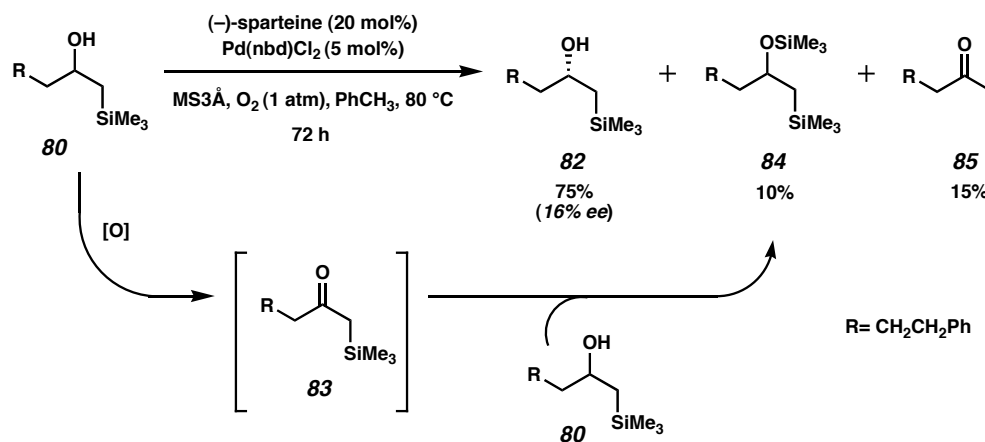
we synthesized and tested β -silyl alcohol **80** in the OKR using our published conditions without exogenous base.

Scheme 2. β -Silicon effect in cation stabilization



As seen in Scheme 3, β -silyl alcohol **80** proved to be a marginally active substrate for oxidative kinetic resolution, providing partially resolved alcohol **82** in 16% ee. Furthermore, a problematic side reaction complicated analysis. Specifically, formation of silyl ether **84** and ketone **85** occurs presumably *via* intermolecular silyl transfer between ketone **83** and a second equivalent of the starting alcohol. Based on the observed product distribution, it may be proposed that after the oxidation event, the C-Si bond present in **83** becomes weakened due to the increased bond polarization.¹⁸

Scheme 3. Tandem oxidation/intermolecular Si-transfer



In the presence of excess of secondary alcohol, silyl transfer between alcohol **80** and intermediate ketone **83** provides silyl ether **84** and ketone **85**, which were observed along with the partially resolved alcohol **82**. Since the oxidatively stable silyl ether **84** is formed continuously during the resolution process, this resolution will not provide a high ee product, since this ether is oxidatively inert to our conditions. Consequently, suppression of side-product **84** was required before the reaction could be further evaluated.

Undeterred by the unexpected side reaction, we speculated that the formation of silyl ether **84** could be suppressed by inclusion of a primary alcohol. A primary alcohol does not meet the requirements for oxidation under our resolution conditions (i.e., it's nonstabilized), however, we expected that a primary alcohol would behave as a sacrificial TMS-cation sponge, competitively removing TMS from the α -silyl ketone in the presence of a secondary alcohol. In this manner, the secondary alcohol would be available for further resolution. Titration of the exogenous non-stabilized alcohol *n*-BuOH into the reaction (Table 5) appears to suppress the formation of TMS ether **84** (entries 2-4). What was even more significant, conversion to ketone increased with increasing *n*-BuOH concentration. In the range of 0-4.2 equivalents of *n*-BuOH, the conversion of alcohol **80** to ketone **85** increased by a factor of 5.

Table 5. Effect of an oxidatively inert alcohol on the OKR of a β -silyl alcohol

$\text{R} = \text{CH}_2\text{CH}_2\text{Ph}$
80

$\xrightarrow[\text{MS3A, O}_2 (1 \text{ atm}), \text{PhCH}_3, 80^\circ\text{C}, 72 \text{ h}]{(-)\text{-sparteine (20 mol\%)}, \text{Pd(nbd)Cl}_2 (5 \text{ mol\%})^a}$

$\text{R}-\text{CH}_2-\text{CH}(\text{OH})-\text{CH}_2-\text{SiMe}_3$ (**82**) + $\text{R}-\text{CH}_2-\text{CH}(\text{OSiMe}_3)-\text{CH}_2-\text{SiMe}_3$ (**84**) + $\text{R}-\text{CH}_2-\text{C}(=\text{O})-\text{CH}_3$ (**85**)

entry	<i>n</i> -BuOH (equiv)	% Alcohol (ee) ^b 82	% Silyl Ether ^c 84	% ketone ^c 85
1.	0.0	75 (16 %)	15	10
2.	0.7	60 (34 %)	10	30
3.	2.1	35 (81 %)	5	60
4.	4.2	45 (61 %)	<5	50

^aPalladium precatalyst and (–)-sparteine are maintained at 80 °C for 10 min before introduction of alcohol, 1 atm O₂, 0.25 M substrate concentration in PhCH₃. ^bMeasured by chiral HPLC. ^cMeasured by ¹H NMR.

Having observed a dramatic dependence on the rate of the oxidative kinetic resolution with the inclusion of the primary alcohol *n*-BuOH, a wide variety of alcohol additives were evaluated for their ability to enhance catalysis. Particular attention was given to alcohols that are considered oxidatively inert to our reaction conditions. As seen in Table 6, the alcohol additives *n*-BuOH, trifluoroethanol, and *t*-BuOH were titrated into the reaction. As before, the oxidation of alcohol (\pm)-**79** to ketone **80** and recovered alcohol (–)-**79** was used as the test reaction.

Table 6. Effect of oxidatively inert alcohols on the OKR

entry	additive	time	conversion ^c	ee ROH ^d	s
1.	<i>none</i>	5.5 h	31%	35%	12
2.	<i>n</i> -BuOH (1.0 equiv)	5.5 h	66%	98%	12
3.	<i>n</i> -BuOH (2.0 equiv)	5.5 h	67%	95%	10
4.	<i>n</i> -BuOH (8.0 equiv)	19 h	48%	56%	7
5.	CF ₃ CH ₂ OH (1.0 equiv)	5.5 h	60%	89%	11
6.	CF ₃ CH ₂ OH (2.0 equiv)	5.5 h	42%	48%	8
7.	CF ₃ CH ₂ OH (8.0 equiv)	19 h	19%	16%	6
8.	<i>t</i> -BuOH (1.0 equiv)	22.5 h ^d	57%	90%	16
9.	<i>t</i> -BuOH (4.0 equiv)	11.5 h ^d	57%	94%	20
10.	<i>t</i> -BuOH (8.0 equiv)	19 h ^e	57%	90%	16

^aThe palladium precatalyst (10 mol%) and (–)-sparteine (10 mol%) are maintained at 80 °C for 10 min before introduction of the alcohol. 1 atm O₂, 0.1 M substrate concentration in PhCH₃. ^bFinely milled anhydrous 10 mol% (1.0 equiv). ^cMeasured by ¹H NMR. ^dMeasured by chiral HPLC.

In all cases, inclusion of 1.0 equiv of the exogenous alcohol additive imparts enhanced reactivity relative to the deprived system (entry 1). In the case of *n*-BuOH, inclusion of 2.0 equiv results in a decreased overall selectivity (entry 3), while increasing to 8.0 equiv appears to adversely impact both the selectivity and the reactivity of the system (entry 4). Both selectivity and conversion are negatively impacted. Likewise, the trifluoroethanol additive appears to initially increase the reaction rate relative to the additive deprived system (entry 5). However, both the catalytic turnover and the overall selectivity of the resolution process suffer at higher additive concentrations (entries 6, 7). The apparent trend of initial rate acceleration, followed by rate inhibition and selectivity

erosion at high additive concentrations applies to a wide variety of primary alcohols. Interestingly, inclusion of *t*-BuOH proved to be an excellent exogenous alcohol additive. While *t*-BuOH did not impart the highest levels of rate acceleration at one equiv, its use in the resolution results in the highest and most dependable levels of selectivity across a wide range of concentrations (entries 8-10). Consequently, we found *t*-BuOH to be the most reliable additive for this reaction.

Armed with the observed benefits of *t*-BuOH and Cs₂CO₃ additives, all reaction parameters were optimized to maximize the rate and selectivity of our oxidative kinetic resolution. After a systematic study, it was found that inclusion of 1.2 equiv of Cs₂CO₃ and 4.0 equiv of *t*-BuOH provided the optimal additive quantities. To directly compare the effect of these additives on the overall rate to that of our previous conditions, we carried out a parallel analysis at 80 °C using the oxidation of alcohol (**±**)-**86** to ketone **87** and resolved alcohol (**–**)-**86**. As shown in Table 7, there is a clear overall rate acceleration imparted to the resolution when including Cs₂CO₃ and *t*-BuOH as additives. Under these conditions, resolution of alcohol (**±**)-**86** to 98.0% ee is observed in a mere 4.5 h, as compared to 93.1% ee in 192 h for the additive-deprived conditions.

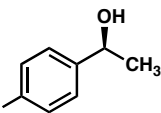
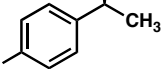

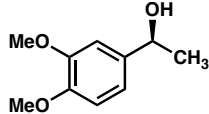
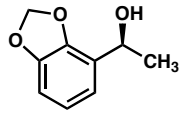
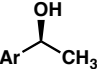
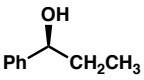
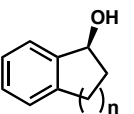
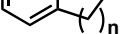
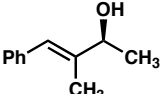
Table 7. Cesium carbonate and *t*-BuOH dramatically increase the rate of the oxidative kinetic resolution

$ \begin{array}{c} \text{OH} \\ \\ \text{Ph}-\text{CH}-\text{CH}_2\text{CH}_3 \\ (\pm)\text{-86} \end{array} \xrightarrow[\text{MS3A, O}_2, \text{PhCH}_3, 80\text{ }^\circ\text{C}]{\text{Pd(nbd)Cl}_2 (5\text{ mol}\%), \text{(-)-sparteine (20 mol}\% \text{)}^a} \begin{array}{c} \text{O} \\ \\ \text{Ph}-\text{CH}-\text{CH}_2\text{CH}_3 \\ \text{87} \end{array} + \begin{array}{c} \text{OH} \\ \\ \text{Ph}-\text{CH}-\text{CH}_2\text{CH}_3 \\ (-)\text{-86} \end{array} $				
additives	time	conversion ^b	ee ^c	s
none	192 h	59.3%	93.1%	14.8
CS ₂ CO ₃ (1.2 equiv) <i>t</i> -BuOH (4.0 equiv)	4.5 h	62.8%	98.0%	16.1

^aThe palladium precatalyst and (–)-sparteine are maintained at 80 °C for 10 min before introduction of the alcohol. 1 atm O₂, 0.1 M substrate concentration in PhCH₃. ^b Measured by GC using a DB-WAX column. ^c Measured by chiral HPLC.

When applied to our known substrate scope, the more reactive conditions were found to be broadly applicable. Most all of the activated alcohols that were previously good substrates serve as excellent substrates under the new conditions (Table 8). A range of electron-rich and electron-poor benzylic alcohols can be resolved to high enantiopurity and good selectivity by oxidative kinetic resolution in well under 24 hours.¹⁹

Table 8. Cs₂CO₃/*t*-BuOH-modified OKR

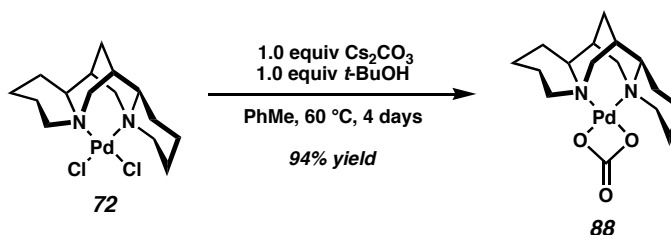
$ \begin{array}{c} \text{Pd(nbd)Cl}_2, (-)\text{-sparteine} \\ \text{Cs}_2\text{CO}_3, t\text{-BuOH}^a \\ \text{MS3\AA, O}_2, \text{PhCH}_3, 60\text{ }^\circ\text{C} \end{array} \longrightarrow \begin{array}{c} \text{O} \\ \parallel \\ \text{R}-\text{C}-\text{R}' \end{array} + \begin{array}{c} \text{OH} \\ \\ \text{R}-\text{CH}-\text{R}' \end{array} $						
entry	unreacted alcohol, major enantiomer	time	conversion ^b	ee ROH ^c	s	
1.	 R = H	12.5 h	63.9%	99.6%	20.0	
2.	 R = OMe	9.5 h	67.4%	99.5%	14.9	
3.	 R = F	12.5 h	65.7%	97.4%	12.1	
4.		18 h ^d	63.8%	98.3%	15.4	
5.		15 h	56.5%	99.7%	47.4	
6.	 Ar = 2-Naphthyl	12 h	66.1%	99.4%	15.8	
7.		4.5 h ^e	62.8%	98.0%	16.1	
8.	 n = 1	12 h ^d	74.0%	99.5%	10.1	
9.	 n = 2	12 h ^d	61.5%	99.0%	20.9	
10.		12 h	65.1%	87.9%	7.5	

^a5 mol % Pd(nbd)Cl₂, 20 mol % (–)-sparteine, 0.5 equiv of Cs₂CO₃, 1.5 equiv of *t*-BuOH, 1 atm of O₂, 0.25 M substrate concentration in PhCH₃. ^bMeasured by GC relative to an internal standard (tridecane). The total GC yield (alcohol + ketone) was >95% in all cases. ^cMeasured by chiral HPLC. ^dConducted at 40 °C. ^eConducted at 80 °C.

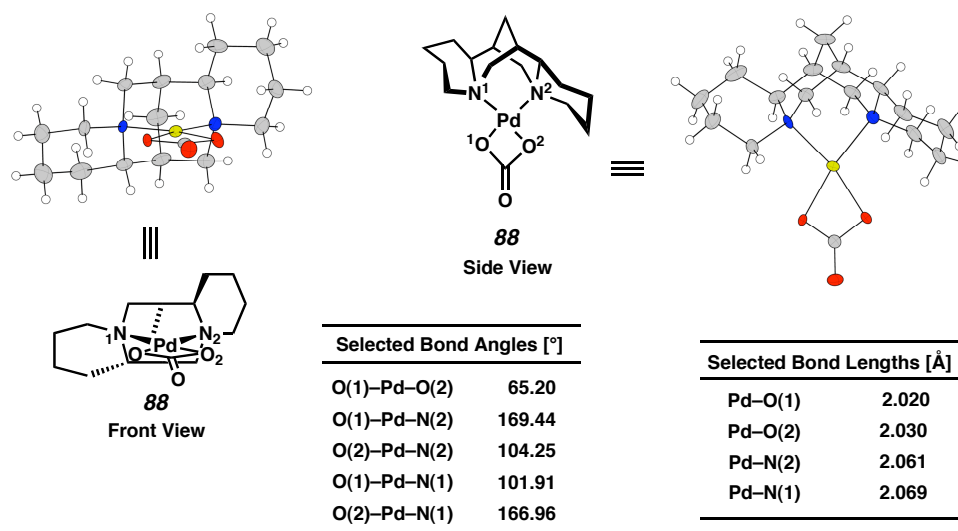
*The Mechanistic Role of *t*-BuOH as a Potential H-Bond Donor*

While the purpose of the carbonate base fit well with our mechanistic model for the oxidative kinetic resolution, the effect of *t*-BuOH remained more subtle. An initial hypothesis was that the modified reaction conditions initiated the conversion of our catalytic palladium complex Pd(sp)Cl₂ into a more reactive catalyst. To test this hypothesis, the preformed complex was subjected to conditions designed to model the reaction conditions employed in the oxidative kinetic resolution. Accordingly, treatment of complex **72** with 1.0 equiv of *t*-BuOH and 1.0 equiv of Cs₂CO₃ produced, after 4 d at 60 °C, the carbonate salt complex **88** in nearly quantitative yield (Scheme 4).

Scheme 4. Formation of a (sp)Pd(II)carbonate complex

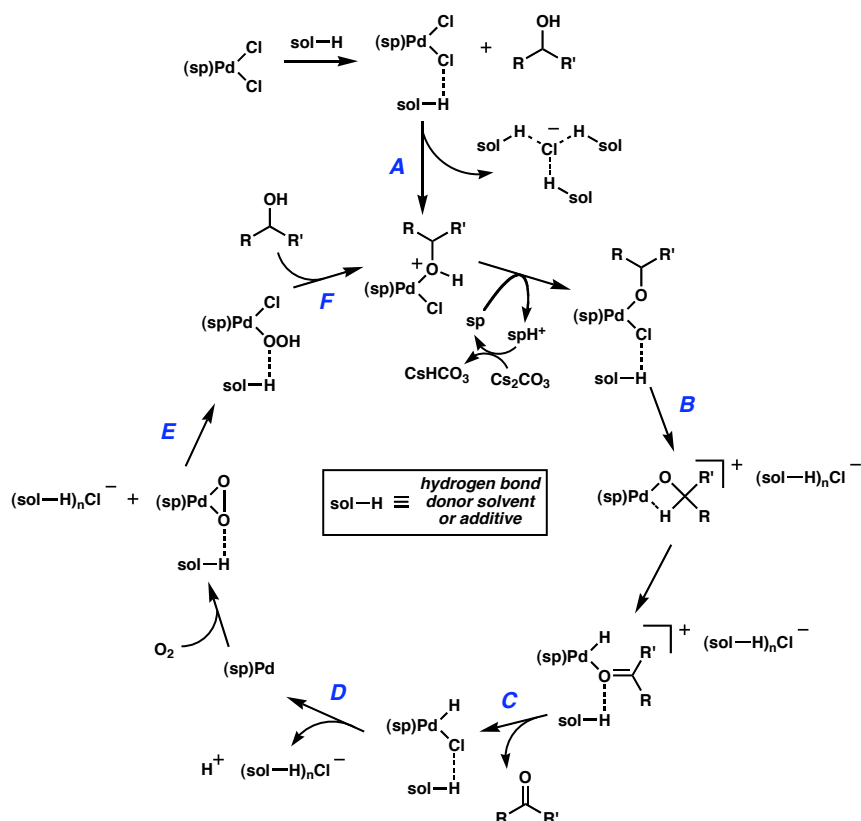


Furthermore, the structure of **88** was proven by single-crystal X-ray diffraction (Figure 5). Analogous to the crystal structure for Pd(sp)Cl₂, the palladium center in (sp)Pd^{II}(CO₃) **88** displays a distorted square-planar geometry, reflecting the C₁-symmetry of the (–)-sparteine ligand. Both N–Pd–O bond angles are more than 10° below a square-planar configuration.

Figure 5. Crystal structure of (sp)Pd(CO₃)

While this was an initially exciting discovery, the newly formed carbonate salt displayed neither catalytic, nor even stoichiometric, activity when applied to our reaction. Instead of finding a more active catalytic system, we had, in fact, discovered a catalyst deactivation pathway. Interestingly, this result suggests that Cs₂CO₃ may not be the optimal base additive.²⁰ Our base screen was designed to test for an initial rate acceleration and no particular attention was paid to catalyst longevity. To date, no better, broadly applicable base additive has been identified.

While we had identified a competitive catalyst decomposition pathway in our reaction, the precise role of *t*-BuOH as an accelerant remained elusive. At this point, we hypothesized that the exogenous alcohol was affecting reaction rates by forming hydrogen bonds to a number of plausible intermediates along the catalytic reaction manifold and/or by aiding in the solvation of pervasive chloride ions. The possible mechanistic implications of an H-bonding species are summarized in Figure 6.

Figure 6. Plausible mechanism involving H-bonding species

A number of possible H-bond/catalyst and H-bond/halide interactions are outlined in Figure 6 and include A) hydrogen bonding to, or solvation of, a chlorine substituent on the $[\text{Pd}(\text{sparteine})\text{Cl}_2]$ complex activating the complex toward alcoholysis, B) subsequently aiding in the solvation of another chloride, thereby opening a coordination site for β -hydride elimination to occur, C) facilitating product release, D) provoking reductive elimination of HCl, generating a palladium(0) species, and enhancing reoxidation to palladium(II) by E) aiding in the opening of a peroxo-palladium species to a palladium hydroperoxide, and F) participating in the turnover exchange of the palladium hydroperoxide to the palladium alkoxide complex.

In the interest of developing even more mild, active, selective, and generally useful catalyst systems for oxidative kinetic resolution, a better additive than *t*-BuOH was sought. Starting from the assumption that H-bond donation was the critical feature of the additive, a number of other H-bond donating additives (phosphates, sulfates, etc.) were explored with little success. This is not surprising as such additives are also acidic, and therefore readily neutralized under the mildly basic reaction conditions.

Another possibility for further improving the reaction's efficiency is to discover an additive that our reaction will tolerate in solvent quantities, thereby increasing the effective concentration of the additive. With this hypothesis in mind, a rigorous solvent screen was undertaken (Table 9), with particular attention given to solvents capable of donating an H-bond and/or solvating chlorine anions. Importantly, as part of our screen, we examined solvents that have the capacity to do both, that is, less traditional H-bond donating halohydrocarbon solvents such as CHCl₃. To simplify the analysis, enantiopure (R)-(+)-1-phenylethanol **(+)-89** (the fast-reacting enantiomer) was used as the substrate, generating the ketone **90**.²¹

Using preformed Pd(sp)Cl₂ with excess sparteine under an atmosphere of molecular oxygen and in the presence of 3Å molecular sieves, the reaction rate and catalytic efficiency was found to be very sensitive to the nature of the solvent. Traditional H-bond donating solvents (entries 7-10, 14) failed to provide a productive reaction, in many cases yielding a dark mixture that was presumed to indicate the presence of palladium black. However, the nonflammable solvent chloroform quickly emerged as an excellent solvent for the reaction, supporting rapid reaction rates, even at room temperature.

Table 9. Impact of solvent on reaction rate at room temperature

Pd(sparteine)Cl_2
 $(-)\text{-sparteine}^a$
 $\text{MS3A, O}_2, \text{solvent}$
 $23\text{ }^\circ\text{C, 21 h}$

$(+)\text{-89}$
 90

entry	solvent	dielectric constant	conversion (%) ^b
1.	CHCl ₃	4.8	74
2.	CHBr ₃	4.1	68
3.	ClCH ₂ CH ₂ Cl	5.7	46
4.	CCl ₄	2.2	2
5.	PhMe	2.4	23
6.	PhMe/1 equiv <i>t</i> -BuOH	2.4/1.77	39
7.	CHCl ₃ /1 equiv <i>t</i> -BuOH	4.8/1.77	72
8.	2-propanol	18.3	7
9.	PhCH ₃ / <i>t</i> -BuOH (1:1)	2.4/1.77	29
10.	<i>t</i> -amyl alcohol	26.2	21
11.	THF	7.58	14
12.	MeCN	37.5	3
13.	pinacolone	12.5	21
14.	H ₂ O/2-propanol	78.5/19.9	3
15.	EtOAc	6.0	8
16.	MeNO ₂	35.9	2

^a5 mol % Pd(sparteine)Cl₂, 7 mol % (–)-sparteine, 1 atm of O₂, all reactions conducted at 0.1 M substrate concentration in solvent. ^bMeasured by GC relative to an internal standard (tridecane). The total GC yield (alcohol + ketone) was >95% in all cases.

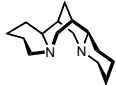
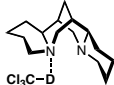
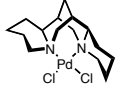
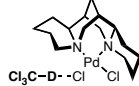
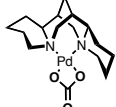
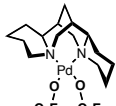
Comparison of the trihalomethanes (entries 1 and 2) reveals a tendency for more electron deficient, thus better hydrogen-bonding halocarbons, to accelerate conversion. Furthermore, when CCl₄ is substituted for a protic member of the halogenated hydrocarbon series, conversion is severely impacted (entry 4). In accord with our mechanistic hypothesis (i.e., Figure 6), this trend suggests the importance of weak potential hydrogen bond donors as a parameter for achieving an efficient resolution.

It is worth pointing out that the solubility of O₂ is not a likely factor in the observed disparate reactivity, particularly between toluene and CHCl₃, in which O₂ is

equally soluble.²² Furthermore, no correlation between conversion and solvent dielectric constant (an estimate of solvent polarity) is apparent.²³ Interestingly, when the weakly H-bond donating solvent CHCl_3 was used in concert with the *t*-BuOH additive, no further enhancement to the reaction rate was observed (entry 7). We rationalized this finding in terms of H-bonding: An H-bond from CHCl_3 may have supplanted one from *t*-BuOH, obviating its benefits. The carbonate base, however, still enhanced the reaction rate.

Evidence for the H-bond donating capacity of CHCl_3 to our $\text{Pd}(\text{sp})\text{Cl}_2$ catalytic complex is found in the IR spectrum of CDCl_3 (Table 10). A significant shift in the C–D stretching frequency of CDCl_3 ²⁴ (entry 1) occurs in the presence of H-bond acceptors (–)–sparteine (entry 2) and $\text{Pd}(\text{sp})\text{Cl}_2$ (entry 3). The observed decrease in λ_{max} corresponds to a longer C–D stretching frequency related to a weaker C–D bond in the associated CDCl_3 over the free CDCl_3 .

Table 10. C–D stretch of CDCl_3 in the presence of potential H-bond acceptors

Entry	Concentration ^a	CDCl_3 Solution ^b	λ_{max} (cm^{-1})	Predicted D–X Bond
1	—	neat	2258	none
2	0.25 M		2175	
3	0.25 M		2230	
4	0.10 M ^a		2258	none
5	0.25 M		2258	none

^aNear saturation concentration at room temperature. Sample prepared by sonication of analyte in solvent prior to analysis. ^b CDCl_3 purchased from Aldrich without TMS.

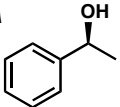
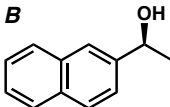
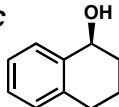
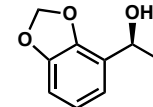
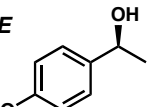
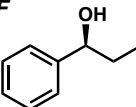
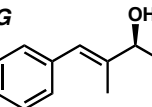
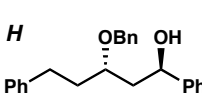
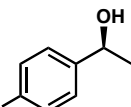
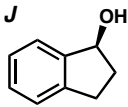
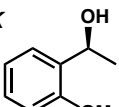
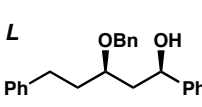
The decrease in bond energy may be accounted for by an H-bonding event between CDCl_3 and the H-bond accepting analyte. However, no such interaction is observed by IR for the $\text{Pd}(\text{sp})\text{CO}_3$ (entry 4) or the $\text{Pd}(\text{sp})(\text{OC}_6\text{F}_5)_2$ (entry 5) complexes. That no $\Delta\lambda_{\text{max}}$ is observed for these latter complexes indicates that the H-bonding event in $\text{Pd}(\text{sp})\text{Cl}_2$ (entry 2) is probably occurring at chloride, rather than at nitrogen.

Having observed a dramatic impact on conversion rate by simply changing the solvent from toluene to chloroform, it became clear that all other parameters would require reinvestigation. A study of the sparteine ligand loading revealed that 12 mol% sparteine was an optimal concentration for the reaction, compared to 20 mol% as previously reported in both toluene and dichloroethane.⁹ Evaluation of Cs_2CO_3 stoichiometry revealed that no further benefit to conversion rate was observed beyond 40 mol%. The reaction may practically be warmed to 40 °C, but higher temperatures poorly impacted catalysis.

With the essential parameters optimized, we explored the generality of our modified catalyst system (Table 11).²⁵ Importantly, all previously reported alcohol substrates (entries **A-G**, **I-K**)⁹ were resolved to high enantiomeric excess when subjected to the new conditions. These resolutions were performed at mild operating temperatures (usually room temperature), while the selectivities for the process were also increased, often by a factor of 2. Particularly striking is the enhancement in selectivity of the non-benzylic alcohol shown in entry **G**. Previously, this substrate proved difficult to resolve to high ee, displaying a low selectivity in the oxidative kinetic resolution process ($s=6.6$). *Using our chloroform conditions, the resolution proceeds at room temperature to provide the resolved alcohol in 99.0% ee with a selectivity factor of 18.* The allylic alcohol

depicted in entry **G** may be readily converted into more useful functionality and represents a segue into highly enantioselective resolutions of less activated secondary alcohols.

Table 11. Scope of the CHCl_3 conditions

$ \begin{array}{c} \text{R}-\text{CH}(\text{OH})-\text{R}' \\ \xrightarrow[\text{CHCl}_3, 23^\circ\text{C}]{\text{Pd}(\text{nbd})\text{Cl}_2 (5 \text{ mol}\%), (-)\text{-sparteine} (12 \text{ mol}\%), \text{MS3}\text{\AA}, \text{O}_2 (1 \text{ atm}), \text{Cs}_2\text{CO}_3 (0.4 \text{ equiv})} \\ \text{R}-\text{C}(=\text{O})-\text{R}' + \text{R}-\text{CH}(\text{OH})-\text{R}' \end{array} $			
A  48 h 80% yield* 99% ee s = 31	B  48 h 81% yield 99% ee s = 31	C  24 h 85% yield 98% ee s = 28	D  12 h@40 °C 90% yield 95% ee s = 29
E  45 h 75% yield 99% ee s = 27	F  72 h 83% yield 98% ee s = 25	G  48 h 75% yield 99% ee s = 18	H  72 h@40 °C 94% yield 88% ee s = 24
I  48 h 82% yield 98% ee s = 23	J  23 h 60% yield 98% ee s = 10	K  164 h 80% yield 89% ee s = 12	L  72 h@40 °C 85% yield 99% ee s = 32

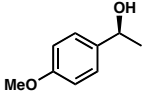
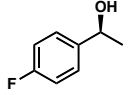
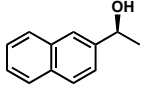
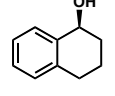
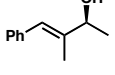
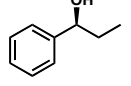
[*] Yields are based on a theoretical maximum of 50%. Conversion monitored by GC using a DB-wax column. Total isolated yield is greater than 95% in all cases. The ee determined by chiral HPLC.

Encouraged by the success of our modified reaction conditions, but curious whether the solvent could influence the post-resolution portion of the proposed mechanism, the reoxidation of $\text{Pd}(0)$ (Figure 6, C-F), we attempted to resolve secondary alcohols using the most abundant and inexpensive stoichiometric oxidant conceivable: ambient air.²⁶ By simply performing the experiments in a reaction vessel equipped with a

drying tube open to the air, a variety of secondary alcohols were resolved to high ee, and with high associated selectivity factors (Table 12). Curiously, the time required to conduct resolutions to high ee was often significantly reduced. The mechanistic implication of this observation is that an O₂ concentration above what is necessary for Pd(0) reoxidation inhibits some aspect of catalysis. The subtleties of this effect are currently under investigation.²⁷

Table 12. Comparison of oxidation performance in air vs. pure O₂

$\text{R}-\text{CH}(\text{OH})-\text{R}' \xrightarrow[\text{ambient air (1 atm),}^b \text{CHCl}_3, 23^\circ\text{C}]{\text{Pd(nbd)Cl}_2 (5 \text{ mol\%}), (-)\text{-sparteine (12 mol\%)}, \text{MS3A}, \text{Cs}_2\text{CO}_3 (0.4 \text{ equiv})} \text{R}-\text{C}(=\text{O})-\text{R}' + \text{R}-\text{CH}(\text{OH})-\text{R}'$

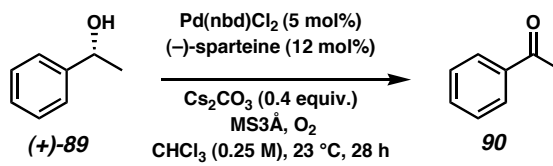
entry	unreacted alcohol major enantiomer	time	conversion (%) ^a	ee ROH (%) ^c	s
1	 <div style="display: inline-block; vertical-align: middle; margin-left: 10px;"> Black = O₂ Blue = air^b </div>	48 h 24 h	62.6 62.3	99.9 99.8	27.1 25.4
2		48 h 24 h	59.3 56.7	98.0 93.0	23.0 19.5
3		48 h 24h	59.3 55.5	99.6 98.0	31.1 37.3
4		24 h 16 h	57.5 60.2	98.0 99.6	27.6 28.0
5		48 h 44 h	62.6 64.7	98.7 98.9	17.9 15.7
6		72 h 48 h	62.6 56.8	98.2 94.9	24.4 21.7

^aConversion was measured by GC using a DB-wax column. ^bReaction performed open to the atmosphere under a short drying tube. Reactions were performed under a cylinder of air purchased from Aldrich gave identical results. ^cThe ee was determined by chiral HPLC.

Prompted by concerns over the reproducibility of our results under variable atmospheric concentrations of molecular oxygen, we sought to ascertain the lower limit

required for effective resolution. After preparing mixed volumes of nitrogen and oxygen, we found that robust oxidation was consistently supported by as little as 5% O₂. In experiments conducted on enantiopure (*R*)-(+)-1-phenyl ethanol (+)-**89**, it was observed that oxygen concentrations in the range of 5-100% had little impact on rates of conversion to ketone **90** (Table 13). For this reason, it is expected that local environmental variability in ambient oxygen concentration will not adversely affect the oxidative kinetic resolution under these conditions.²⁸ That no decrease in reaction efficiency is observed down to 5% oxygen underscores the power of molecular oxygen to reoxidize palladium(0).

Table 13. Effect of O₂ concentration in the oxidation of 2°-alcohols

		
entry	vol% O ₂ in N ₂	conversion (%) ^a
1.	100	75.4
2.	25	77.5
3.	20	80.3
4.	15	76.4
5.	10	78.9
6.	5	76.9
7.	2.5	54.3
8.	0	5.3

^aMeasured by GC using a DB-wax column.

By investigating the role of solvents capable of H-bond donation and chloride ion solvation, we have discovered the most mild and selective conditions for the oxidative

kinetic resolution of secondary alcohols by catalytic palladium to date. The features of this catalyst system suggest some interesting mechanistic variations involving H-bonded intermediates: specifically, the activation of the Pd(sparteine)Cl₂ salt toward attack by an alcohol and activation of intermediates along the reoxidation pathway. The practical consequences of this system include room temperature reactivity in nonflammable solvents and a significant increase in the resolution selectivity. This improvement brings previously poorly resolving, yet synthetically important substrates, such as allylic alcohols, into the synthetically useful range. Furthermore, we have demonstrated the first efficient palladium-catalyzed oxidative kinetic resolution process employing ambient air as the stoichiometric oxidant. These advances further establish our ability to apply this enantioselective oxidation reaction to more challenging substrates.²⁹

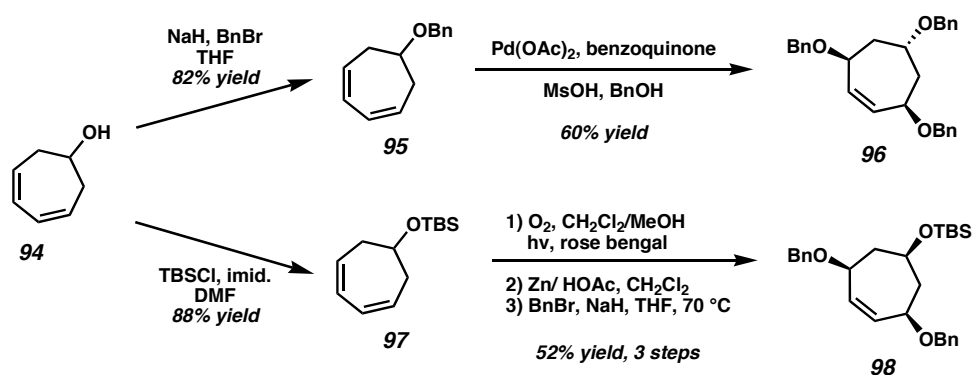
Application to the Desymmetrization of Complex Meso-Diols

Although the enantioselective oxidative kinetic resolution developed in our laboratories provides one of the most convenient methods for obtaining a secondary benzylic alcohol in very high enantiomeric excess (>95% ee), a potential disadvantage with a resolution is the limited theoretical yield. As described in Figure 1, an enantioselective oxidative kinetic resolution has a 50% theoretical yield for a resolved alcohol recovered in ee > 99%. However, this limitation in theoretical yield is removed in a desymmetrization reaction, as both enantiomeric alcohol centers are tethered to the same C₂-symmetric substrate (Figure 7).

Often complex, these *pseudo*-symmetrical stereochemical arrays are excellent targets for bidirectional synthesis followed by enantioselective desymmetrization.^{31,32} A general approach toward isotactic polymethoxydiene **91** could involve a late stage oxidative desymmetrization of *meso*-diol **92**. In turn, **92** could evolve by a bidirectional chain synthesis of a simple achiral starting material of type **93**.

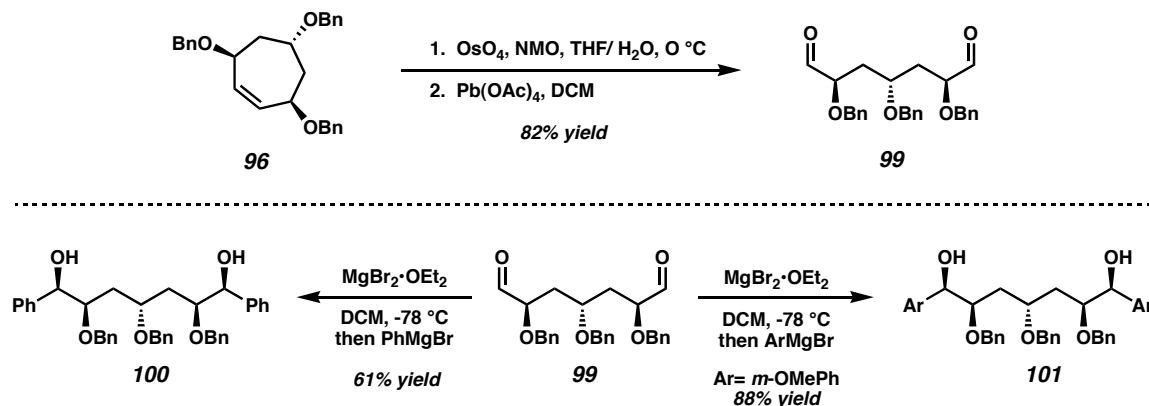
To demonstrate our technique in the desymmetrization arena, we developed a synthetic approach that allows access to a variety of *meso*-diol stereochemical arrays from a common synthetic intermediate. As shown in Scheme 6, the readily available alcohol **94**³³ may be differentially protected as either the TBS ether **97**, or the benzyl ether **95**. Palladium-catalyzed oxidative addition across the diene moiety with 2 equiv of benzyl alcohol across the diene functionality directly provides the *anti*-tris-ether **96** as a single observed diastereomer. Alternatively, the *syn*-tris-ether array **98** is obtained according to known preparations³⁴ by formal Diels-Alder addition of singlet oxygen across the diene **97**, followed by reduction of the peroxy-ether and benzylation of the intermediate diol.

Scheme 6. Variable ether arrays from a common source

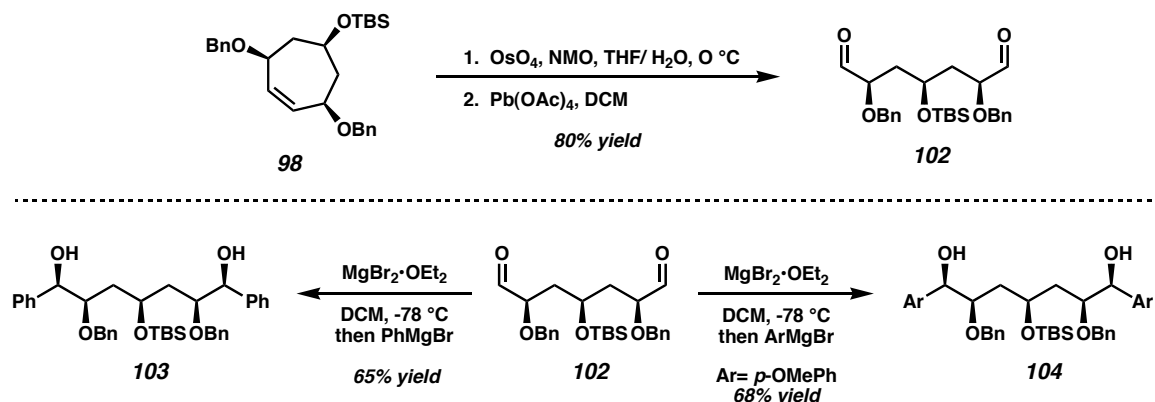


Further development of the *anti*-tris-ether **96** continues in Scheme 7 with dihydroxylation and oxidative cleavage of the intermediate diol with $\text{Pb}(\text{OAc})_4$, to generate the *meso*-dialdehyde **99**. Importantly, no epimerization of the sensitive α -benzyloxy stereocenter is observed when using this two-step oxidation protocol. *Meso*-dialdehyde **99** is converted into a variety of *meso*-diols by a diastereoselective, chelate controlled addition of an aryl nucleophile to give either **100** or **101** as a single observed diastereomer.

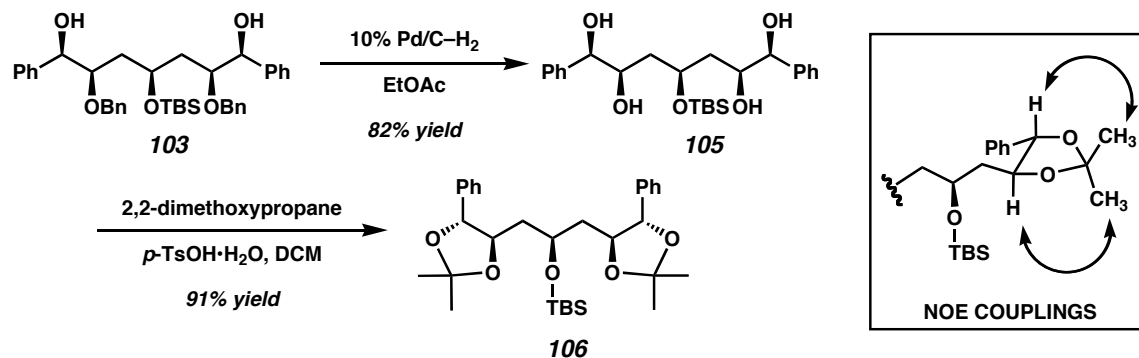
Scheme 7. Advancing the *anti*-ether array



A similar sequence of transformations develops a different array of relative ether stereochemistry, when applied to cycloheptene **98** (Scheme 8). As before, a dihydroxylation and oxidative cleavage of the intermediate diol with $\text{Pb}(\text{OAc})_4$ generates *meso*-dialdehyde **102**. Again, no epimerization of the sensitive α -benzyloxy stereocenter is observed. *Meso*-dialdehyde **102** is converted into a variety of *meso*-diols by a diastereoselective, chelate controlled addition of an aryl nucleophile to give either **103** or **104** as a single observed diastereomer.

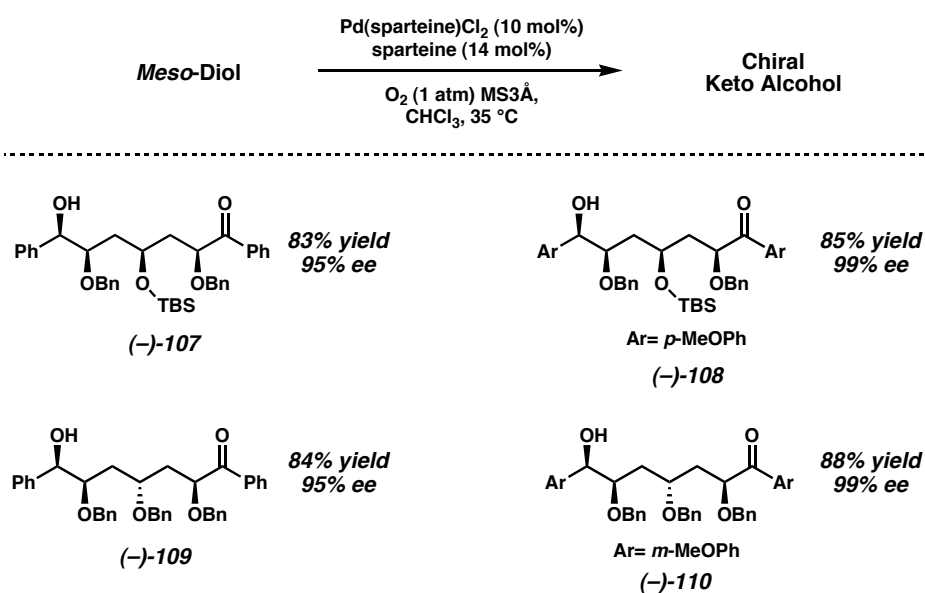
Scheme 8. Advancing the *syn*-ether array

The relative stereochemistry set during the diastereoselective Grignard addition was proven by NOE after derivatization of **103**. Hydrogenolysis of the benzyl ethers was selective in the presence of the benzylic alcohol functionality to give tetraol **105** (Scheme 9). The system of 1,2-diols was protected as the cyclic acetonides to give **106**. NOE analysis confirms that the α -hydrogens of the acetonides are coupled to different methyl groups, establishing the *trans*-stereochemistry unambiguously. The remaining stereochemical relationships for *meso*-diols **100**, **101**, **103** and **104** follow from the known relative stereochemistries of substituted cycloheptenes **96** and **98**.^{35,36}

Scheme 9. Establishing relative stereochemistry

Having established the relative stereochemistry of our *meso*-diols, we set out to apply our reaction methodology. Oxidative desymmetrization of the complex *meso*-diols **100**, **101**, **103**, and **104** was accomplished with a catalytic quantity of Pd(sparteine)Cl₂ in the presence of excess (–)-sparteine under an atmosphere of oxygen (Scheme 10). Following desymmetrization, the chiral keto alcohols (–)-**107**, (–)-**108**, (–)-**109**, and (–)-**110** were all obtained in high ee, and with good yields. Importantly, four stereocenters were defined in a single enantioselective reaction.

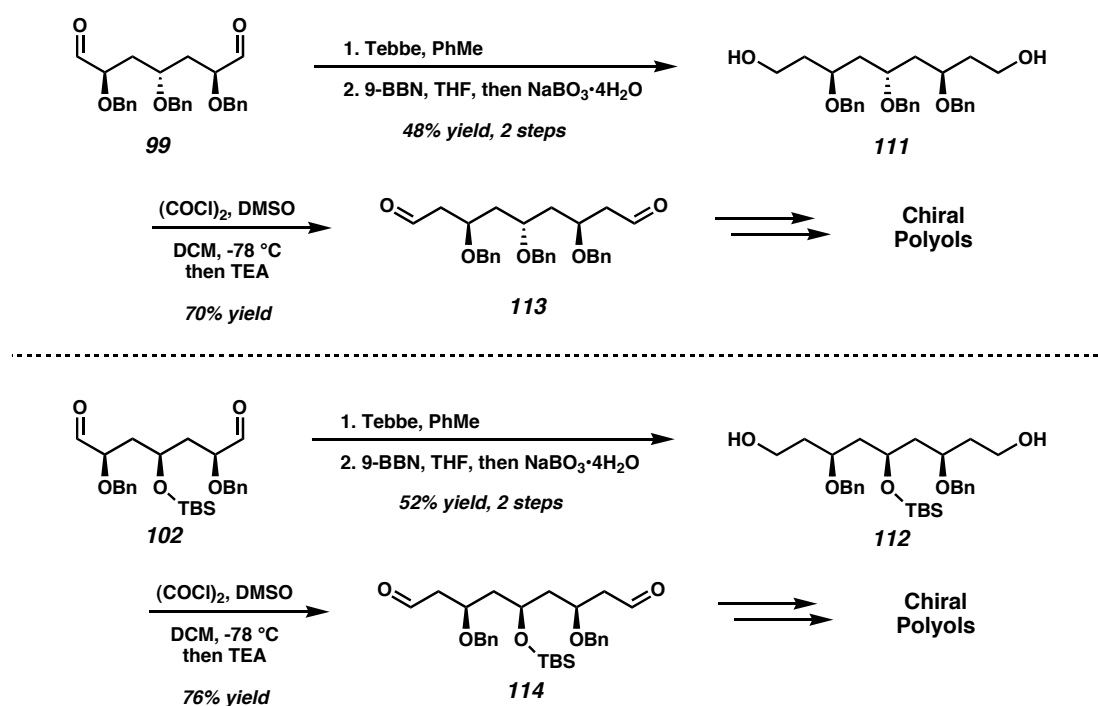
Scheme 10. Enantioselective oxidative *meso*-diol desymmetrization



Even more complex *meso*-substrate may arise from the one-carbon homologation of *meso*-aldehydes **99** and **102** (Scheme 11). This is accomplished by the treatment of either of these aldehydes with Tebbe's reagent, followed by hydroboration/oxidation of the intermediate olefin, to provide the symmetrical primary diols **111** and **112**, which are ultimately oxidized by the Swern protocol to give the *meso*-dialdehydes **113** and **114**,

respectively. These aldehydes are excellent starting materials for the genesis of complex arrays *meso*-polyols by known methods.³⁷ Subsequent oxidative desymmetrization of *meso*-diol products generated from aldehydes **113** and **114** will provide elaborate chiral keto-alcohol motifs.

Scheme 11. Homologation to the skipped framework

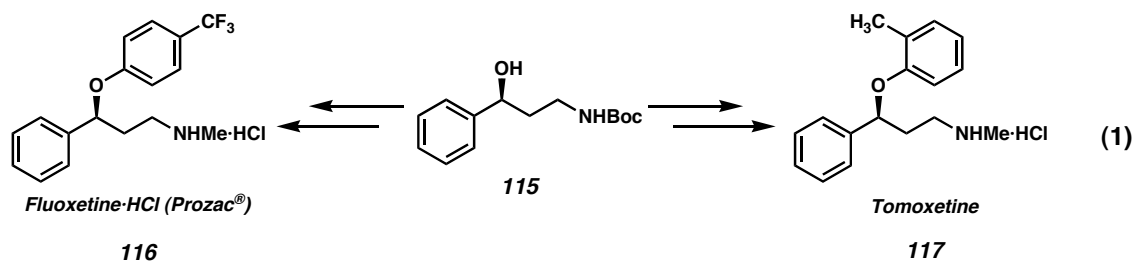


In summary, armed with increasingly reactive and selective reaction conditions for conducting enantioselective oxidations, we set out to demonstrate our technique in the synthesis of complex chiral keto-alcohols. We designed a divergent synthetic route that permitted access to a number of complex *meso*-diol substrates. All of the *meso*-diols we synthesized were excellent substrates for oxidative desymmetrization, providing the chiral keto-alcohols in good yields and high enantiomeric excesses. As a testament to the

power of our oxidation when applied to complex *meso*-diols, we defined the absolute stereochemistry of four asymmetric stereocenters in a single catalytic asymmetric transformation for all of our substrates. Furthermore, we demonstrated that key synthetic intermediates *en route* to the *meso*-diols presented may be parlayed into even more intricate *meso* substrates by one-carbon homologation and known diastereoselective methods.

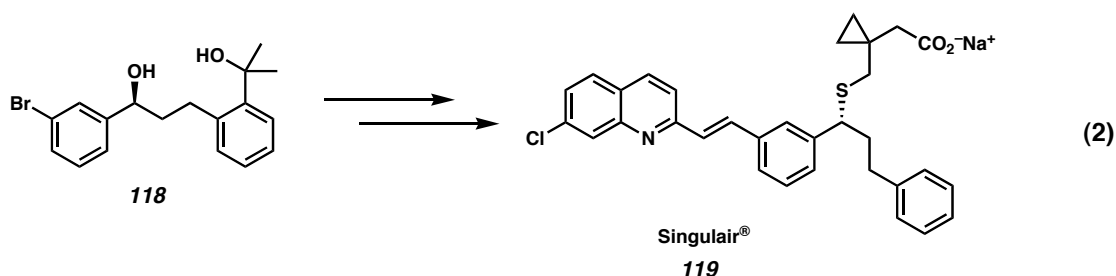
Application to Pharmaceutical Intermediates

While an oxidative desymmetrization may be a useful method for constructing complex chiral polyols, a common motif in natural products, the OKR of secondary benzylic alcohols is a useful method for accessing chiral pharmaceutical intermediates. To date, we have synthesized a number of relevant benzylic alcohols.²⁹ For example, the protected amino-alcohol **115** is an intermediate used in the synthesis of the antidepressants fluoxetine·HCl (Prozac[®]) **116** and tomoxetine **117** (eq 1).^{38,39}

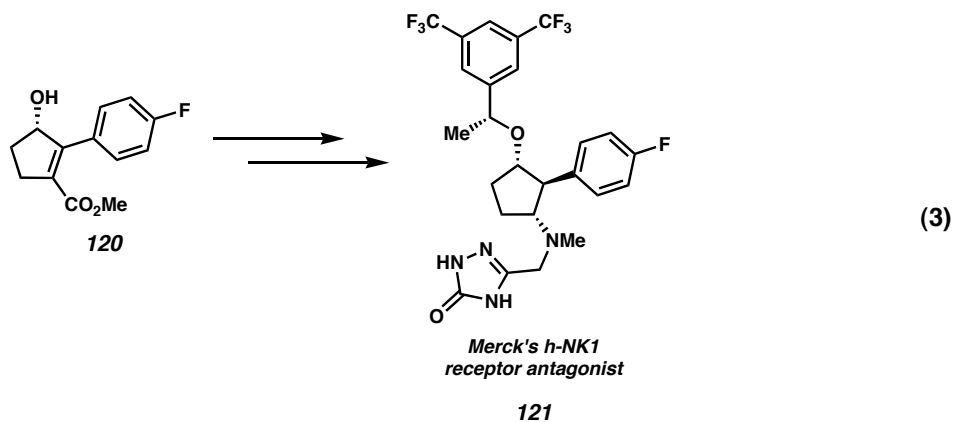


Likewise, the enantiopure benzylic alcohol **118** is established by the palladium-catalyzed OKR. In contrast to the reactivity of aryl halides in palladium-catalyzed cross-coupling processes, the aryl bromide is not affected. The enantiopure alcohol **118** is a

synthetic intermediate used in the synthesis of the leukotriene receptor agonist Singulair[®] **119** (eq 2).⁴⁰



In one of the most selective palladium-catalyzed oxidative kinetic resolutions observed to date, the enantiopure allylic alcohol **120** was synthesized (eq 3). This pharmaceutical intermediate is used in Merck's promising human neurokinin (h-NK1) receptor antagonist candidate **121**.⁴¹



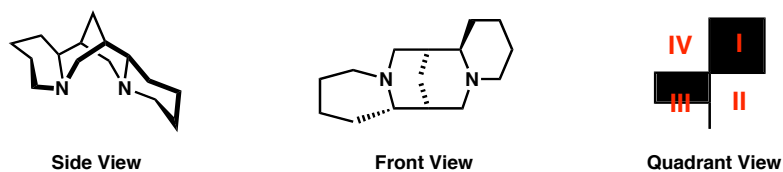
L-Type Ligand Studies

Despite our gradual success with this methodology, we believed that the key to further refinements resided in the chiral inducer for this reaction: (–)-sparteine. Specifically, the commercial availability of sparteine in only one chiral enantiomer⁴² restricts the application of our method to a single enantiomer of a chiral product. A

further restriction on our method is the low opportunity for chemical modification of sparteine since few functional groups are present.⁴³ While an efficient enantioselective synthesis of (–)-sparteine that is readily adaptable to the synthesis of (+)-sparteine has been reported,⁴⁴ laboratory-scale preparation by this route is impractical for our purposes. We require a brief, inexpensive, and scalable synthesis of a sparteine equivalent in either enantiomeric series.

Inspection of (–)-sparteine reveals an extremely rigid, conformationally restricted 3°-diamine whose nitrogen lone pairs are directed towards a single point in space, making this ligand well-suited for bidentate chelation (Figure 8). From the side view, it is easy to mistake (–)-sparteine for a C_2 -symmetric ligand. It is, in fact, a C_1 -symmetric ligand that quaternizes space into two equivalent, open quadrants and two non-equivalent obstructed quadrants. One of the obstructed quadrants is effectively “closed” and the other is “half-closed.”

Figure 8. The chirality of (–)-sparteine

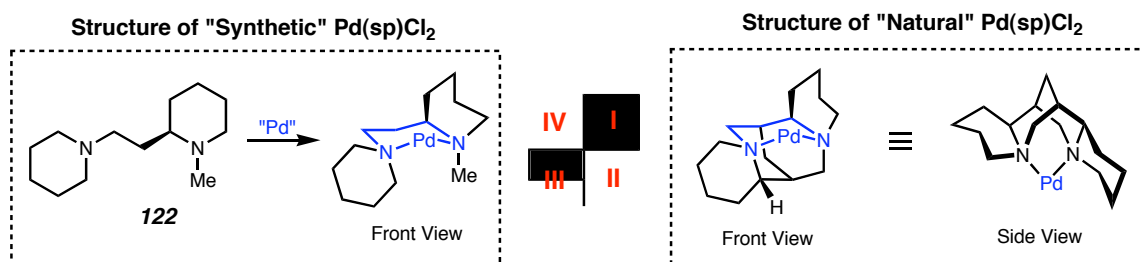


Early on in the development of the oxidative kinetic resolution, it was determined that, among the chiral liands we surveyed, (–)-sparteine was the only truly competent ligand for the reaction, despite the investigation into dozens of commercially available mono and bidentate phosphines and amines.⁴⁵ For this reason, we believed that the design of new ligands should incorporate several of the structural features of natural

sparteine. At the same time, the scaffold for any new ligand should provide a platform for derivatization, so that a number of structural variants may be synthesized and tested, should an encouraging result occur.

With these factors in mind, we synthesized the enantiopure diamine **122** according to known methods.⁴⁶ While diamine **122** may not closely resemble (–)-sparteine as the free diamine, we hypothesized that when ligated, the metal center would enforce a (–)-sparteine-like chiral geometry (Figure 9), with the key structural differences isolated primarily outside of the chiral pocket.

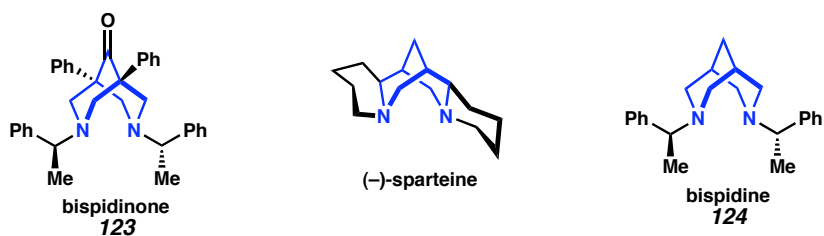
Figure 9. Synthetic diamine vs. natural (–)-sparteine chiral pocket



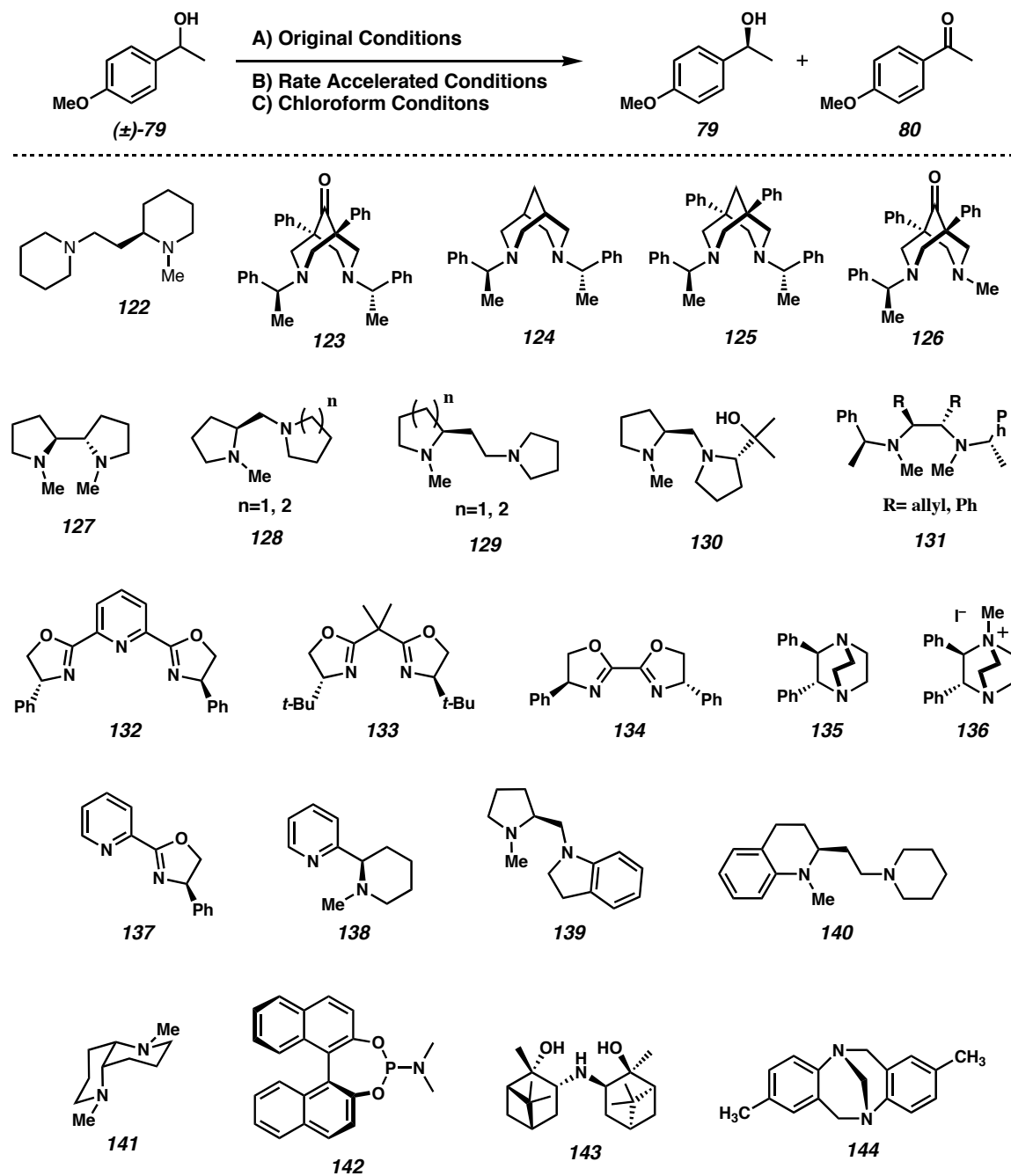
While we were excited about the prospect of diamine **122** as a chiral ligand for our enantioselective oxidation method, we were at the same time concerned that its increased flexibility might compromise strong chelation with palladium, yielding an inactive or non-selective oxidation catalyst. To address these concerns, other sparteine-like diamines were synthesized. In particular, the relatively rigid bispidinone **123**⁴⁷ and bispidine **124**⁴⁸ were synthesized according to known methods (Figure 10). While bispidinone **123** and bispidinone **124** more closely approximate the rigid [3.3.1] bridged

bicycle that defines the core of natural sparteine, the chirality at the periphery differs substantially.

Figure 10. Bispidinones, bispidinines, and (–)-sparteine



In addition to these diamine ligands, which were rationally designed to incorporate sparteine-like qualities, an arsenal of other diamines and monoamines were synthesized by known methods, and their activity in the oxidative kinetic resolution investigated across a variety of reaction conditions (Table 14).

Table 14. Monoamine and diamine ligands tested in the OKR

A) Pd(nbd)Cl₂ (10 mol%), ligand (40 mol%), 3ÅMS, PhMe, O₂ (1atm), 80 °C. **B)** Pd(nbd)Cl₂ (10 mol%), ligand (40 mol%), Cs₂CO₃ (0.5 equiv), *t*-BuOH (1.5 equiv), 3ÅMS, PhMe, O₂ (1atm), 80 °C. **C)** Pd(nbd)Cl₂ (10 mol%), ligand (25 mol%), 3ÅMS, O₂ (1 atm), Cs₂CO₃ (0.5 equiv), CHCl₃, 23 °C.

Unfortunately, the results of this study may be summarized succinctly: All amines surveyed were poor ligands for the palladium-catalyzed oxidative kinetic resolution under all established reaction conditions. The sparteine-like diamines **122-126** provided only a marginally active catalyst for the test reaction on racemic alcohol (**±**)-**79** (conversion <5%, s <3). Likewise, a host of related diamines **127-130** were found to be poor ligands for this reaction. A number of other ligands were obtained by known methods and tested, including the C₂-symmetric Py-BOX ligand **132**,⁴⁹ oxazolines **133-134** the C₁-symmetric pyridyl-oxazoline ligand **137**,⁵⁰ the chiral monodentate quinuclidine ligands **135** and **136**,⁵¹ the stilbene diamine derived ligand **131**,⁵² the indolene derived diamine **139**,⁵³ the tetrahydroquinoline derived diamine **140**,⁵⁴ the Kozlowski ligand **141**,⁵⁵ the phosphoramidite **142**,⁵⁶ the pinene derived ligand **143**,⁵⁷ and enantiopure (–)-Troger’s base **144**.⁵⁸ All of these nitrogen containing compounds were found to be uniformly poor ligands; only trace conversion was observed across a range of test reactions.

In the course of ligand screening, we were disappointed by the consistently low levels of conversion observed across our ligand scope. For this reason, we elected to focus on the ligand design elements that impart reactivity to palladium separately from those that confer transfer chirality. Specifically, our analysis focused on diamine chain length, hybridization, and flexibility, bearing in mind the features of the parent ligand, (–)-sparteine. Table 15 details the impact ligand structure has on the activity of the aerobic palladium-catalyzed oxidation of enantiopure (*R*)-1-phenylethanol.⁵⁹

Table 15. Impact of ligand structure on conversion

Reaction scheme showing the conversion of (+)-89 to 90 using a diamine catalyst.

Entry	Diamine ^b	Conversion (%) ^c	Entry	Diamine ^b	Conversion (%) ^c
1	(-)-sparteine	94.2	6		2.6
2		0.7	7		2.2
3		8.8	8		1.5
4		3.8	9		48.2
5		3.0	10		3.3

^aThe diamine and Pd(nbd)Cl₂ were maintained at 80 °C in toluene for 15 minutes prior to introduction of starting alcohol. ^bThe diamines used were purified by standard methods prior to use. ^cConversion was monitored by GC using a DB-wax column.

^dConducted on racemic 1-phenylethanol.

While several of the diamines surveyed gave only a very low conversion, some trends on the impact of ligand structure on reaction productivity may be viewed. A three carbon linker (entry 3) between diamines is optimal, with the two carbon linker (entry 2) and the four carbon linker (entry 4) conferring less reactivity in the investigated reaction.

Sparteine itself displays a three carbon linker between diamines. Furthermore, the conformationally restricted 1,4-dimethylpiperazine (entry 6) diamine provides enhances reactivity relative to the unconstrained tetramethylethane-1,2-diamine ligand (entry 2). Also, conjugated and sp^2 nitrogen centers were less active as ligands (entries 5, 7-8). While there are some apparent trends in this diamine series, (–)-sparteine was the most active ligand for the palladium catalyzed-oxidation by far.

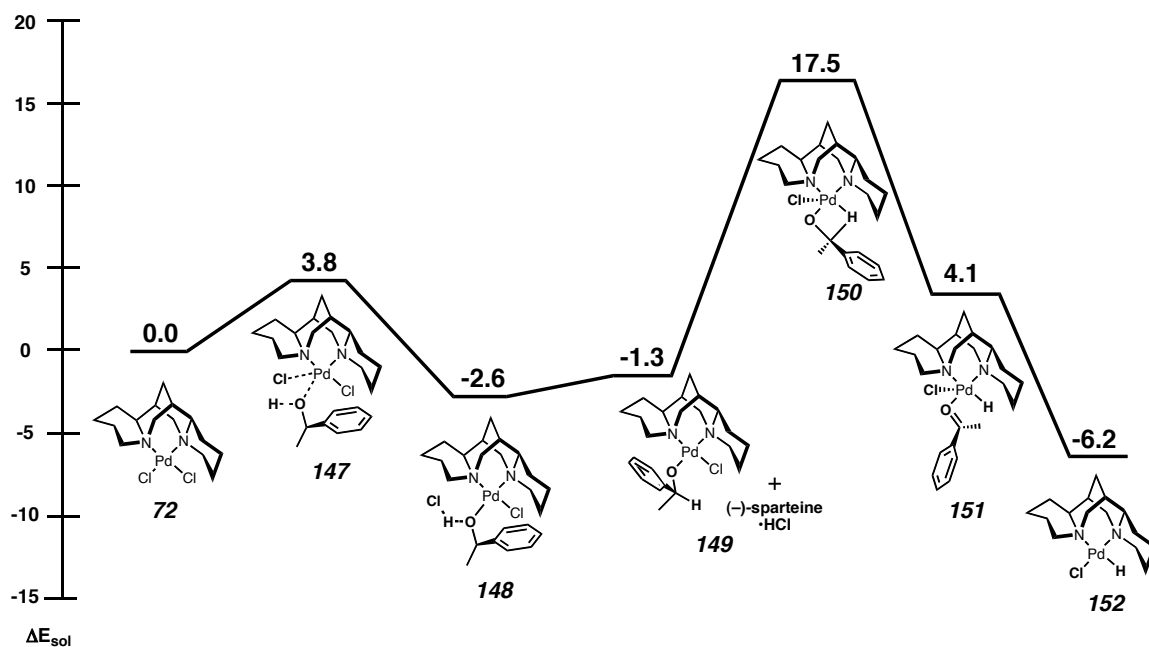
Taking as desirable ligand design elements 1) a three carbon linker between diamines 2) a well-defined, sparteine-like diamine conformation, and 3) an sp^3 -hybridized diamine, the methoxybispidine **145**⁶⁰ was synthesized. When applied to the alcohol oxidation we observed a significant amount of conversion (48.2% at 22 h), in fact, the highest levels of conversion observed for a non-sparteine diamine ligand under these conditions. We explored the possibility of introducing chirality into the bispidine motif. A direct chiral analogue was synthetically intractable, however, the relatively rigid chiral bispidine **146** was synthesized and tested. Unfortunately, no significant activity was observed.

In summary, a non-sparteine diamine capable of conducting the palladium catalyzed enantioselective oxidation by our method remains elusive. A vast number of chiral monodentate and bidentate diamines were investigated, and none of them imparted significant activity or selectivity in the oxidation. Even diamines designed to incorporate several of the unique features of sparteine proved ineffective. It should be noted that the facile synthesis of effective sparteine mimics has been a challenge to the wider community.⁶¹ In the course of these studies, however, we have delineated some of the structural requirements for a competent diamine ligand for the palladium-catalyzed OKR.

X-Type Ligand Studies

Undeterred by the difficulties encountered in the development of new chiral diamine ligands for conducting palladium-catalyzed asymmetric oxidation, we began considering other means of affecting, and eventually improving, the scope and efficiency of our methodology. We took inspiration from collaborative efforts with members of the Goddard group, who have investigated the mechanism using high level calculations (B3LYP DFT). Several possible reaction pathways were considered. As a result of their analysis, a computational model predicting the lowest energy pathway for the enantioselective oxidation event conducted by our Pd(sp)Cl₂ catalyst was elucidated (Figure 11).⁶²

Figure 11. Calculated lowest energy pathway for Pd-catalyzed enantioselective oxidation of *sec*-phenylethanol



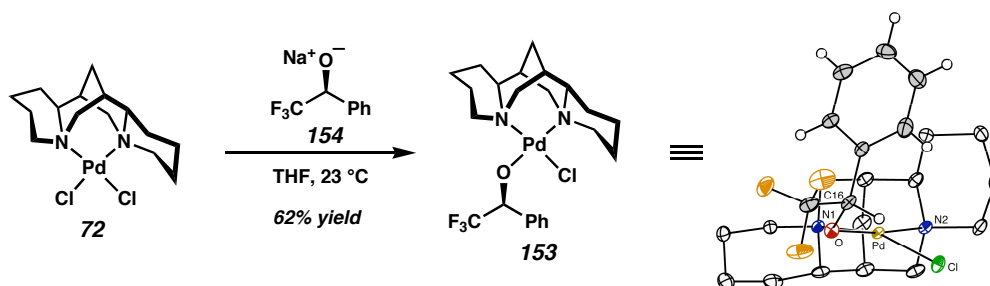
Starting from the parent Pd(sp)Cl₂ catalyst **72** as the zero point energy, the alcohol enters the coordination sphere by associative substitution of a Cl⁻ ion, providing

transition structure **147**. The predicted barrier for the displacement is lowered by the $\text{Cl}^- \cdots \text{H}-\text{OR}$ bond that forms as the substrate approaches, as in structure **148**. Since the forming Cl^- anion is not basic enough to deprotonate the bound alcohol alone, assistance in the deprotonation is found with an equivalent of exogenous sparteine. Deprotonation of the coordinated alcohol by free sparteine provides palladium alkoxide **149** and $(-)$ -sparteine $\cdot\text{HCl}$. The alkoxide **149** undergoes β -hydride elimination through the four-coordinate transition structure **150**. In this structure, the remaining Cl atom is displaced into an axial, outer-sphere position (3.00 Å from Pd). In this scenario, the anion is still associated with the metal by an electrostatic interaction. After β -hydride elimination, the ketone produced initially remains associated with the metal center, as in intermediate **151**, but disassociates as the axial Cl atom migrates back into the coordination sphere of palladium, providing the Pd-hydride complex **152**. A key insight extracted from this investigation concerns the role of the X-type ligand, chloride, on the stereochemical course of the enantioselective oxidation. The calculations have shown that the sterics of the counterion dramatically impact the selectivity of the OKR, with smaller counterions providing reduced selectivities. Experimental evidence supports this prediction.⁶³

Experimental evidence for the intermediacy of calculated structure **150** is found in the crystal structure of Pd-alkoxide **153**, prepared from $\text{Pd}(\text{sp})\text{Cl}_2$ **72** and the enantiopure alkoxide **154** (Scheme 12).⁶⁴ Importantly, substitution on palladium with the alkoxide occurred exclusively at Cl(1), reflecting the C_1 -symmetry of the sparteine ligand. The enantiopure alkoxide **154** used in this transformation corresponds to the fast-reacting enantiomer in the oxidative kinetic resolution. However, the presence of the strongly

electron-withdrawing $-\text{CF}_3$ moiety prohibits a β -hydride elimination event. In this way, the Pd-alkoxide diastereomer **153** was isolated in good yield.

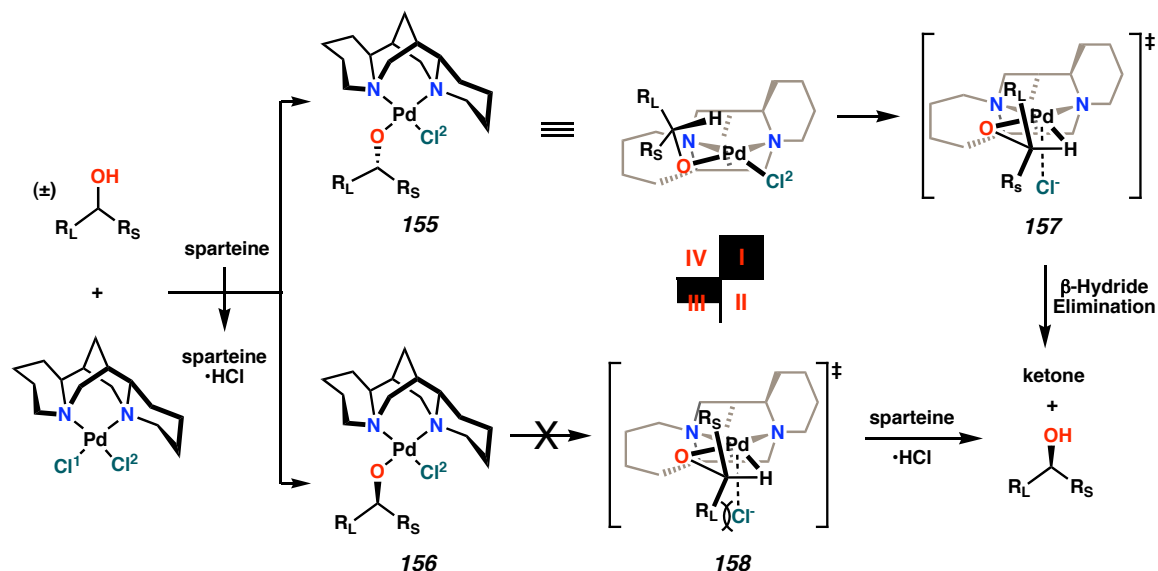
Scheme 12. Regioselective formation of a palladium-alkoxide



Upon inspection of the crystal structure, it is noteworthy that the β -hydrogen of the bound alkoxide is directed towards the distorted square-planar Pd center. Meanwhile, the remaining chloride is displaced towards the open quadrant (15.4° out of plane). Since the transition state for β -hydride elimination is expected to involve a cationic Pd species with four-coordinate square-planar geometry,⁶⁵ the intermediacy of calculated transition structure **150**, in which the Cl^- has migrated to the axial position, is reasonable based upon this analysis.

From these data, a model that accurately predicts the fast-reacting alcohol enantiomer in the palladium-catalyzed enantioselective oxidation is proposed (Figure 12). (–)-Sparteine is a C_1 -symmetric ligand, and this symmetry element is reflected in the manner in which it quaternizes space about the metal center: quadrants II and IV are considered “open,” quadrant I is considered “closed,” while quadrant III is “half-open.” In agreement with the observed regiochemistry of isolated Pd-alkoxide **153**, selective ligand substitution of $\text{Cl}(1)$ with the incoming alcohol liberates HCl to provide the diastereomeric Pd-alkoxides **155** and **156**.

Figure 12. A model for asymmetric induction in the Pd-catalyzed oxidative kinetic resolution of racemic secondary alcohols

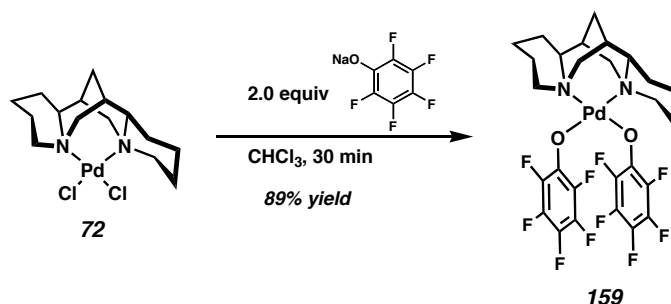


Dissection of the subsequent steric interactions involved for β -hydride elimination of the diastereomeric Pd-alkoxides **155** and **156** provides a basis for a predictive model. In this manner, Pd-alkoxide **155** may achieve a low-energy reactive conformation for β -hydride elimination by placing the R_S group in a minimized eclipsing interaction with the Cl^- group, which has now migrated into the open quadrant II as shown in transition structure **157**. In the absence of a significant destabilizing steric interaction, β -hydride elimination proceeds to generate the ketone. In contrast, Pd-alkoxide **156** experiences a severe steric interaction between the R_L group and the axial Cl^- group, thereby destabilizing a reactive conformation for β -hydride elimination, as shown in the disfavored transition structure **158**. Confronted with the significant steric interaction, the alcohol may dissociate from the metal center in the presence of HCl (sparteine•HCl), to provide the enantioenriched (*S*)-alcohol, the alcohol enantiomer observed experimentally.

Our experimentally derived model, and the calculated lowest energy pathway for oxidation suggest the importance of the chloride ligand in the enantiodetermining event. The structures in Figure 12 illustrate that there is little direct interaction between substrate and ligand. Instead, the temporarily displaced X-group lies between the two, and chiral relay occurs from the diamine ligand and alcohol substrate *via* the X-type ligand on Pd. We attempted to modulate the sterics of the X-type ligand by preparing (sp)Pd(II)Br and (sp)Pd(II) variants by a several of methods. However, our attempted preparations provided intractable mixtures with the observed precipitation of Pd-black.

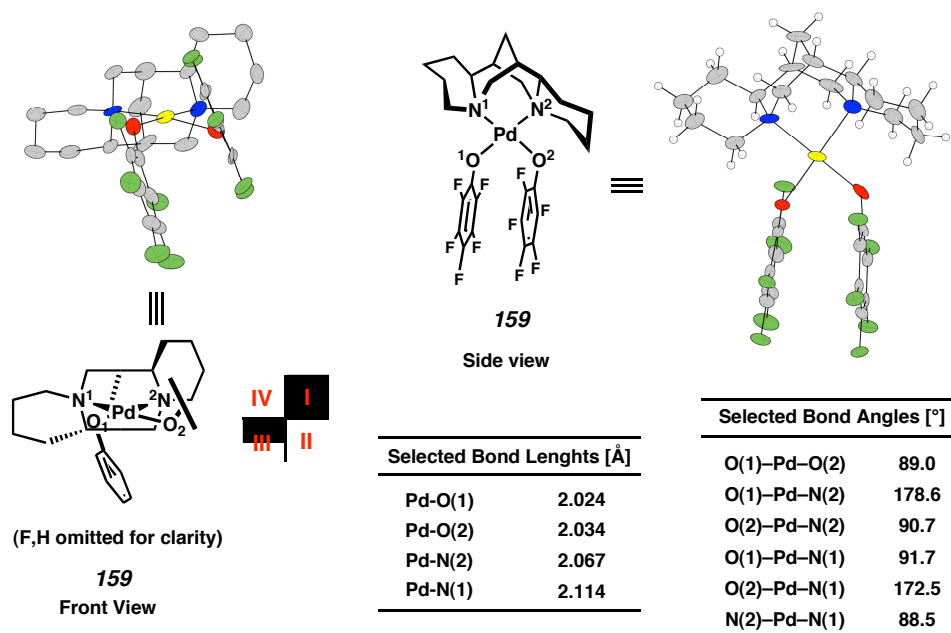
While our initial attempts aimed at modulating the X-type ligand by halide substitution met with failure, a more productive method was ultimately realized. While the palladium carbonate salt **88** formed from Pd(sp)Cl₂ and Cs₂CO₃ (Scheme 4) was catalytically inactive, it was remarkably easy to form. Taking inspiration from this result, we attempted ligand metathesis with various sodium-alkoxide salts. Treatment of Pd(sp)Cl₂ **72** with 2.0 equivalents sodium pentafluorophenoxide (Scheme 13) provided the (sp)Pd(II)phenoxide **159**.

Scheme 13. A palladium phenoxide



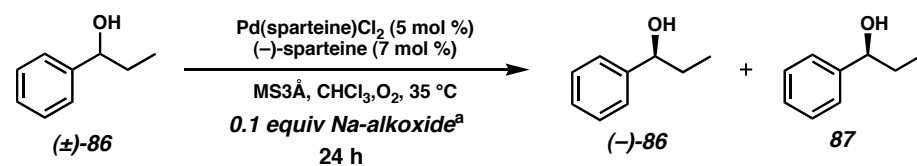
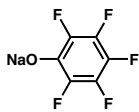
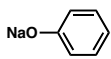
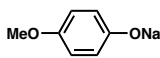
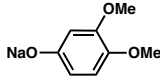
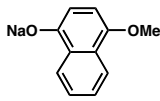
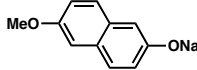
Complex **159** was readily recrystallized, and provided crystals sufficient for X-ray analysis. The crystal structure, shown in Figure 13, confirmed that displacement of both chloride ligands had occurred, to give a distorted square-planar palladium-bisphenoxide (O2-Pd-N1 is 7.5° out of plane). Inspection of the crystal structure reveals that the aromatic portion of the phenoxide ligands do not fully occupy the open quadrants defined by the environment of (–)-sparteine. However, the planar aromatic rings are oriented along the diagonal defined by the open quadrants. The phenoxide X-type ligand bears striking differences to chloride (Figure 2) with regard to the manner in which it impacts the steric environment of the metal complex, a quality that may improve the selectivity of the OKR.

Figure 13. Crystal structure of (sp)Pd^{II}(pentafluorophenoxide) **159**



In light of our struggles to isolate Pd(II) complexes bearing a non-sparteine diamine ligand, we were very pleased to have finally isolated a new Pd(II) complex, and immediately evaluated its catalytic activity. Unfortunately, the bisphenoxide **159** was only marginally active as a catalyst. However, since many alcohols and phenols are commercially available, we investigated the effect of a variety of easily prepared alkoxide salts on the resolution (Table 16).

Table 16. Effect of sodium phenoxide salts on the OKR

				
Entry	Alkoxide ^b	Conversion (%) ^c	ee ROH (%) ^d	s
1	none	36.5	53.1	27.0
2	NaO—CH ₂ CF ₃	1.2	0.0	—
3		3.1	1.8	—
4		22.8	25.1	15.7
5		40.9	59.2	23.3
6		56.4	97.3	29.5
7		48.2	83.6	49.1
8		58.8	99.8	36.6

^aPd(sparteine)Cl₂ and Na-phenoxide were reacted 1 h prior to introduction of racemic alcohol. ¹H NMR analysis of catalyst confirms formation of a new Pd-complex. ^bSodium alkoxide prepared from Na metal and the phenol. ^cConversion was monitored by GC with a DB-WAX column. ^dEnantiomeric excess determined by chiral HPLC.

For these studies, the resolution of racemic alcohol (\pm)-**86** to ketone **87** and resolved alcohol (–)-**86** was selected as a test reaction. Typically, the Pd-phenoxide was prepared in advance by the general protocol described in Scheme 13. Insoluble NaCl byproduct and excess insoluble Na-phenoxide salts were filtered from the reaction prior to introduction of the test alcohol.

Sodium trifluoroethoxide (entry 2) and the electron-deficient sodium pentafluorophenoxide salt (entry 3) dramatically inhibited reaction rates relative to the parent catalyst (entry 1). However, much of this reactivity was restored upon application of the neutral sodium phenoxide (entry 4). In fact, a trend toward increasing reactivity is apparent with increasing electron density on the aromatic portion of the phenoxide (entries 3-6). Upon increasing the conjugation of the arene portion of the phenoxide, a dramatic increase in the activity (entry 8) and selectivity (entry 7) of the reaction is observed.

While a more thorough investigation into the generality of these results across a range of substrates will be required before informed conclusions can be reliably drawn, it is interesting to note that the more sterically encumbered sodium 4-methoxynaphthalen-1-olate (entry 7) imparts a greater selectivity to the resolution, than does the relatively unhindered sodium 6-methoxynaphthalen-2-olate (entry 8). These preliminary results support the prediction that a larger counterion for palladium will impart a greater selectivity to the resolution. Further investigation into the effect of steric and electronic factors on the phenoxide ligand on the OKR is ongoing.

III. Conclusion

The first palladium-catalyzed oxidative kinetic resolution of secondary alcohols by catalytic palladium was developed in our laboratories. The key features of this enantioselective oxidation reaction are the use of the diamine (–)-sparteine as the chiral ligand for the catalytic Pd(II) metal center in a process that utilizes molecular oxygen as the sole stoichiometric oxidant. While the original system was competent at resolving a number of benzylic and allylic alcohols to very high ee, a number of factors detracted from the usefulness of the technique. Specifically, the reaction required high reaction temperatures in flammable mixtures of toluene and oxygen, very long reaction times (in most cases 4-8 days), and a somewhat limited substrate scope. By systematically investigating the role of exogenous base and H-bond donating additives/solvents, we developed increasingly mild, reactive, and selective reaction conditions for conducting the palladium-catalyzed OKR. Armed with these more reactive conditions, we applied the method towards the enantioselective oxidative desymmetrization of complex, hindered *meso*-diols. As a result, we demonstrated the synthesis of complex chiral keto-alcohols possessing multiple stereocenters.

Seeking further improvements to the method, we endeavored to supplant the chiral ligand (–)-sparteine with a readily modified ligand scaffold that would be available in either enantiomer. As a testament to how uniquely adapted the features of (–)-sparteine are to our method (i.e., highly rigid, oxidatively stable, C_1 -symmetric), we have yet to find a more competent ligand for palladium in the OKR. Preliminary results indicate that a more successful method for modulating the steric environment about palladium lies not in L-type ligand, but in the X-type ligand. Salt metathesis of the parent

Pd(sp)Cl_2 with an electron-rich phenoxide appears to dramatically improve the rate and selectivity of the resolution. Studies in this area are ongoing.

Experimental Section

Materials and Methods

Unless stated otherwise, reactions were conducted in flame-dried glassware under an atmosphere of nitrogen using anhydrous solvents (either freshly distilled or passed through activated alumina columns). All reactions were conducted under an inert atmosphere of dry nitrogen or argon, unless otherwise stated. All commercially obtained reagents were used as received. When required, commercial reagents were purified following the guidelines of Perrin and Armarego.⁶⁶ Reaction temperatures were controlled using an IKAmag temperature modulator. Thin-layer chromatography (TLC) was conducted with E. Merck silica gel 60 F254 pre-coated plates (0.25 mm) and visualized using a combination of UV, anisaldehyde, ceric ammonium molybdate, and potassium permanganate staining. ICN silica gel (particle size 0.032-0.063 mm) was used for flash chromatography using the method described by Still.⁶⁷

¹H NMR spectra were recorded on a Varian Mercury 300 (at 300 MHz), a Varian Inova 500 (at 500 MHz), and were reported relative to residual protio solvent signals. Data for ¹H NMR spectra were reported as follows: chemical shift (δ ppm), multiplicity (s = singlet, d = doublet, t = triplet, q = quartet, m = multiplet), coupling constant (Hz), and integration. ¹³C NMR spectra were recorded on a Varian Mercury 300 (at 75 MHz) and are reported relative to residual protio solvent signals. Data for ¹³C NMR spectra were reported in terms of chemical shift. IR spectra were recorded on a Perkin Elmer Paragon 1000 spectrometer and were reported in frequency of absorption (cm^{-1}). Optical rotations were measured with a Jasco P-1010 polarimeter (Na lamp, 589 nm). HPLC analysis was performed on a Hewlett-Packard 1100 Series HPLC (UV detector at 245 nm)

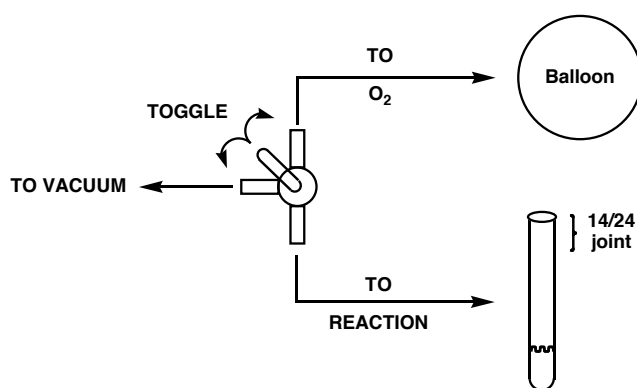
equipped with the following Chiralcel columns: OD-H (25 cm), OD guard (5 cm), AD (25 cm), OJ (25 cm) and OB-H (25 cm). High resolution mass spectra were obtained from the California Institute of Technology Mass Spectral Facility.

General Procedures

General Protocol for Oxidative Kinetic Resolution: Original Conditions

An oven-dried reaction tube (outer diameter 16 mm, length 120 mm) equipped with a magnetic stir bar was charged with oven-dried powdered molecular sieves (MS3Å, 0.5 g). After cooling, Pd(nbd)Cl₂ complex (0.02 mmol, 0.02 equiv) was added followed by toluene (2.0 mL), and (–)-sparteine (0.08 mmol, 0.08 equiv). The flask was equipped with a 14/24 joint connected to a switchable vacuum/O₂ balloon system (Figure 14) cooled to -78 °C, iteratively vacuum-evacuated and filled with O₂ (3x, balloon), then stirred at 80 °C for 15 min.

Figure 14. Experimental setup



A toluene solution (2.0 mL) of the racemic alcohol (0.4 mmol, 0.4 equiv) was introduced and the reaction mixture was heated to 80 °C. The reaction was monitored by standard analytical techniques (TLC, GC, ¹H-NMR, and HPLC) for % conversion and enantiomeric excess values. Aliquots of the reaction mixture (0.2 mL) were collected after 12h, 24h, 48h, 96h, and 178 h depending on the course of the reaction (typically three aliquots per run). Each aliquot was filtered through a small plug of silica gel (Et₂O eluent), evaporated, and analyzed. Isolated yields were obtained after filtration of the

reaction mixture through Celite, concentration of the solvent under reduced pressure, and flash chromatography over silica gel.

General Protocol for Oxidative Kinetic Resolution: $\text{Cs}_2\text{CO}_3/t\text{-BuOH}$ Conditions

An oven-dried reaction tube (outer diameter 16 mm, length 120 mm) equipped with a magnetic stir bar was charged with oven-dried powdered molecular sieves (MS3Å, 0.5 g). After cooling, Pd(sparteine) Cl_2 complex (0.05 mmol, 0.05 equiv) was added, followed by toluene (2.0 mL), and (–)-sparteine (0.15 mmol, 0.15 equiv). The flask was equipped with a 14/24 joint connected to a switchable vacuum/ O_2 balloon system (see Figure 14) cooled to $-78\text{ }^\circ\text{C}$, iteratively vacuum-evacuated and filled with O_2 (3x, balloon), then warmed to room temperature. Powdered anhydrous Cs_2CO_3 (0.5 mmol, 0.5 equiv.), anhydrous *t*-BuOH (1.5 mmol, 1.5 equiv) and a toluene solution (2.0 mL) of the racemic alcohol (1.0 mmol, 1.0 equiv) were introduced into the slurry and the reaction mixture was stirred at $60\text{ }^\circ\text{C}$. The reaction was monitored by standard analytical techniques (TLC, GC, ^1H -NMR, and HPLC) for % conversion and enantiomeric excess values. Aliquots of the reaction mixture (0.2 mL) were collected after 4h, 8h, 12h, 24h, and 48h depending on the course of the reaction (typically three aliquots per run). Each aliquot was filtered through a small plug of silica gel (Et_2O eluent), evaporated and analyzed. Isolated yields were obtained after filtration of the reaction mixture through Celite, concentration of the solvent under reduced pressure, and flash chromatography over silica gel.

General Protocol for Oxidative Kinetic Resolution: CHCl_3/O_2 Conditions

An oven-dried reaction tube (outer diameter 16 mm, length 120 mm) equipped with a magnetic stir bar was charged with oven-dried powdered molecular sieves (MS3Å, 0.5 g). After cooling, $\text{Pd}(\text{sparteine})\text{Cl}_2$ complex (0.05 mmol, 0.05 equiv) was added followed by chloroform (2.0 mL), and (–)-sparteine (0.07 mmol, 0.07 equiv). The flask was equipped with a 14/24 joint connected to a switchable vacuum/ O_2 balloon system (see Figure 14) cooled to $-78\text{ }^\circ\text{C}$, iteratively vacuum-evacuated and filled with O_2 (3x, balloon), then warmed room temperature. Powdered anhydrous Cs_2CO_3 (0.4 mmol, 0.4 equiv.) and a chloroform solution (2.0 mL) of the racemic alcohol (1.0 mmol, 1.0 equiv) were introduced and the reaction mixture was maintained at room temperature. The reaction was monitored by standard analytical techniques (TLC, GC, ^1H -NMR, and HPLC) for % conversion and enantiomeric excess values. Aliquots of the reaction mixture (0.2 mL) were collected after 4h, 8h, 12h, 24h, and 48h depending on the course of the reaction (typically three aliquots per run). Each aliquot was filtered through a small plug of silica gel (Et_2O eluent), evaporated and analyzed. Isolated yields were obtained after filtration of the reaction mixture through Celite, concentration of the solvent under reduced pressure, and flash chromatography over silica gel.

General Protocol for Oxidative Kinetic Resolution: CHCl_3/Air Conditions

An oven-dried reaction tube (outer diameter 16 mm, length 120 mm) equipped with a magnetic stir bar was charged with oven-dried powdered molecular sieves (MS3Å, 0.5 g). Do not flush reaction tube with inert gas! After cooling, $\text{Pd}(\text{sparteine})\text{Cl}_2$

complex (0.05 mmol, 0.05 equiv) was added followed by chloroform (2.0 mL), and (–)-sparteine (0.07 mmol, 0.07 equiv). The reaction flask was sealed with a septum and the contents were stirred at room temperature for 5 minutes before the consecutive addition of powdered anhydrous Cs_2CO_3 (0.4 mmol, 0.4 equiv.) and a chloroform solution (2.0 mL) of the alcohol (1.0 mmol, 1.0 equiv). The reaction was fitted with a short drying tube packed with Drierite (1.0 X 7.5 cm plug) and maintained at room temperature and was monitored by standard analytical techniques (TLC, GC, ^1H -NMR, and HPLC) for % conversion and enantiomeric excess values. Aliquots of the reaction mixture (0.2 mL) were collected after 4h, 8h, 12h, 24h, and 48h depending on the course of the reaction (typically three aliquots per run). Each aliquot was filtered through a small plug of silica gel (Et_2O eluent), evaporated and analyzed. Isolated yields were obtained after filtration of the reaction mixture through Celite, concentration of the solvent under reduced pressure, and flash chromatography over silica gel.

General Protocol for Oxidative Kinetic Resolution: Palladium Phenoxide Conditions

An oven-dried reaction tube (outer diameter 16 mm, length 120 mm) equipped with a magnetic stir bar was charged with oven-dried powdered molecular sieves (MS3\AA , 0.5 g). Meanwhile, a solution was prepared from $\text{Pd}(\text{sparteine})\text{Cl}_2$ complex (0.05 mmol, 0.05 equiv), (–)-sparteine (0.07 mmol, 0.07 equiv), a sodium phenoxide (0.1 mmol, 0.1 equiv) and chloroform (2 mL). After sonicating for 5 min, then stirring vigorously for 1 h, the solution was transferred into the reaction tube. The flask was equipped with a 14/24 joint connected to a switchable vacuum/ O_2 balloon system (see Figure 14) cooled

to -78 °C, and iteratively vacuum-evacuated and filled with O₂ (3x, balloon), then warmed to room temperature. Powdered anhydrous Cs₂CO₃ (0.4 mmol, 0.4 equiv.) and a chloroform solution (2.0 mL) of the alcohol (1.0 mmol, 1.0 equiv) were introduced and the reaction mixture was maintained at room temperature. The reaction was monitored by standard analytical techniques (TLC, GC, ¹H-NMR, and HPLC) for % conversion and enantiomeric excess values. Aliquots of the reaction mixture (0.2 mL) were collected after 4h, 8h, 12h, 24h, and 48h depending on the course of the reaction (typically three aliquots per run). Each aliquot was filtered through a small plug of silica gel (Et₂O eluent), evaporated and analyzed. Isolated yields were obtained after filtration of the reaction mixture through Celite, concentration of the solvent under reduced pressure, and flash chromatography over silica gel.

General Protocol for Oxidative Kinetic Resolution: *Meso*-Diol Desymmetrization

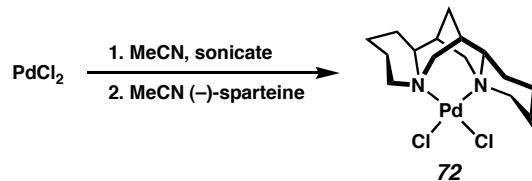
An oven-dried reaction tube (outer diameter 16 mm, length 120 mm) equipped with a magnetic stir bar was charged with oven-dried powdered molecular sieves (MS3Å, 0.5 g). After cooling, Pd(sparteine)Cl₂ complex (0.10 mmol, 0.10 equiv) was added followed by chloroform (2.0 mL), and (–)-sparteine (0.14 mmol, 0.14 equiv). The flask was equipped with a 14/24 joint connected to a switchable vacuum/O₂ balloon system (see Figure 14) cooled to -78 °C, iteratively vacuum-evacuated and filled with O₂ (3x, balloon), then warmed room temperature. Powdered anhydrous Cs₂CO₃ (0.4 mmol, 0.4 equiv.) and a chloroform solution (2.0 mL) of the meso-diol (0.5 mmol, 0.5 equiv) were introduced and the reaction mixture was maintained at 35 °C. The reaction was monitored by standard analytical techniques (TLC, GC, ¹H-NMR, and HPLC) for % conversion and

enantiomeric excess values. Isolated yields were obtained after filtration of the reaction mixture through Celite, concentration of the solvent under reduced pressure, and flash chromatography over silica gel.

General Procedure for the Oxygen Uptake Experiments for Room Temperature Oxidative Kinetic Resolution of Secondary Alcohols Under Ambient Air and Pure Oxygen.

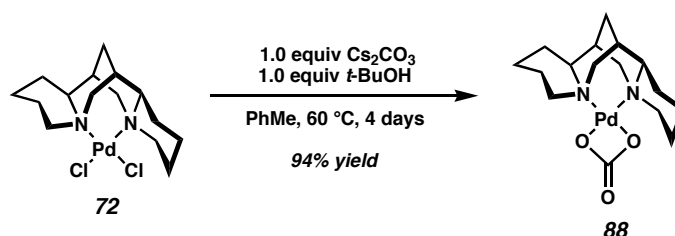
An oven-dried 25 ml round bottom flask equipped with a magnetic stir bar was charged with oven-dried powdered molecular sieves (MS3Å, 1.5 g). After cooling, Pd(nbd)Cl₂ complex (0.15 mmol, 0.05 equiv) was added followed by chloroform (6.0 mL), and (–)-sparteine (0.6 mmol, 0.20 equiv). The contents were stirred at room temperature for 15 minutes before the consecutive addition of powdered anhydrous Cs₂CO₃ (1.2 mmol, 0.4 equiv.) and a chloroform solution (6.0 mL) of the alcohol (3.0 mmol, 1.0 equiv). The reaction vessel was fitted with a gas inlet tube attached consecutively to a short drying tube then a water-filled buret tube (charged with either pure oxygen, or air, as appropriate). The water-filled buret was equipped with a side reservoir to permit pressure equilibration for accurate gas measurements. Aliquots were taken at 4h, 8h and 12h, noting the gas consumption and measuring conversion by GC analysis as before.

Preparative Procedures



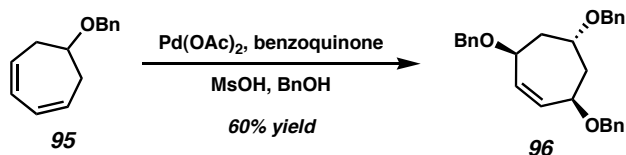
Pd(sp)Cl₂ (72). To a flask charged with PdCl₂ (355 mg, 2.00 mmol) was added MeCN (20 mL). The vessel was sonicated for 4 h to deposit a fine yellow powder, which was filtered. The powder was dried by suction filtration, then high vacuum overnight.

To a flask charged with (MeCN)₂PdCl₂ (503 mg, 1.95 mmol) was added MeCN (20 mL). To the stirred slurry was added (–)-sparteine (603 μL, 1.99 mmol) and the mixture was maintained at room temperature for 8 h with stirring. The reddish-brown slurry was then placed in a -20 °C refrigerator for 30 min, then filtered, rinsing with MeCN (10 mL). The reddish-brown powder was dried by suction filtration, then high vacuum overnight to yield the pure complex **72** (724 mg, 88% yield, 2 steps, TLC baseline).



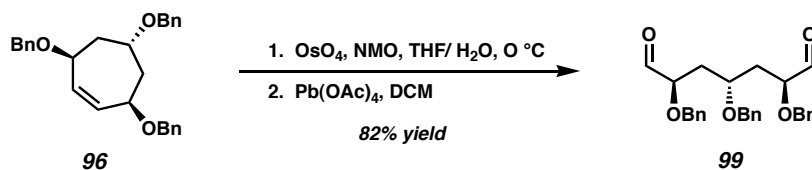
(sp)PdCO₃ (88). To a vial charged with Pd(sp)Cl₂ **72** (103 mg, 0.25 mmol), 3 Å MS (500 mg), and CHCl₃ (5 mL) was added *t*-BuOH (95 μL, 1.00 mmol). To the stirred mixture was added finely milled anhydrous Cs₂CO₃ (326 mg, 1.00 mmol) and the slurry was stirred vigorously for 4 d, then filtered. The crude mixture was placed in a vapor diffusion chamber filled with hexane to precipitate **88** as a yellow powder: ¹H NMR (300 MHz, CDCl₃) δ 4.18 (d, *J*=11.7 Hz, 1H), 4.04 (d, *J*=12.6 Hz, 1H), 3.32 (ddd, *J*=3.0, 14.1

Hz, 1H), 3.25-2.89 (comp. m, 6H), 2.62 (dd, $J=3.3, 12.8$ Hz, 1H), 2.44-1.19 (comp. m, 16H); ^{13}C NMR (300 MHz, CDCl_3) δ 167.0, 68.7, 66.2, 65.9, 63.0, 61.0, 49.2, 34.8, 34.7, 30.3, 27.6, 25.4, 23.9, 23.9, 23.7, 20.2; IR (film) 2939, 1624 cm^{-1} ; HRMS (FAB^+) calc'd for $[\text{C}_{16}\text{H}_{27}\text{N}_2\text{O}_3\text{Pd}]$: m/z 401.1057, found 401.1072; $[\alpha]_{\text{D}}^{20}$ 148.1° ($c=1$, CDCl_3).



tris(benzyloxy)cycloheptene (96). To a stirred slurry of $\text{Pd}(\text{OAc})_2$ (35.2 mg, 0.16 mmol) in benzyl alcohol (11 mL) was added methanesulfonic acid (20 μL , 0.32 mmol) and benzoquinone (432 mg, 4.00 mmol). To the stirred solution was added a solution of the cycloheptatriene **95** (400 mg, 2.00 mmol) in benzyl alcohol (3 mL) by syringe pump over 4 h. Once the addition was complete, stirring was continued for 3 h more before the addition of more benzoquinone (216 mg, 2.00 mmol). The reaction was warmed to 40 °C for 5 h, then cooled to room temperature. The reaction mixture was diluted with water (100 mL) and extracted into (2:1) Et_2O :pentane (4 x 100 mL). The combined organics were washed with 10% aqueous NaOH solution (3 x 100 mL). During the final wash, portions of NaBH_4 were added to the biphasic mixture to remove color. The organics were dried over MgO_4 and concentrated under reduced pressure. Excess benzyl alcohol was removed by Kugelrohr distillation (2 torr, pot temperature 95 °C). The crude oil was purified by flash chromatography over silica gel (10% Et_2O :pentane eluent) to provide the tris(benzyloxy)cycloheptene **96** (547 mg, 66% yield, $R_{\text{F}}=0.84$ in 50% Et_2O :pentane) as a colorless oil: ^1H NMR (300 MHz, CDCl_3) δ 7.51-7.32 (comp. m, 15H), 6.06 (d, $J=1.2$ Hz, 2H), 4.75-4.53 (comp. m, 8H), 4.08-3.99 (m,

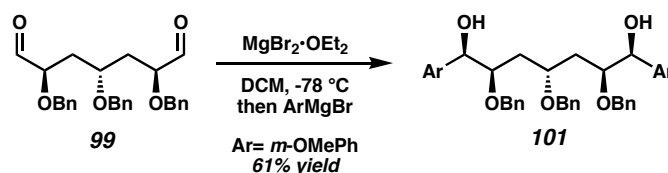
¹H), 2.37 (ddd, $J=2.1, 5.3, 13.5$ Hz, 2H), 1.90 (ddd, $J=2.4, 11.0, 13.5$ Hz, 2H); ¹³C NMR (300 MHz, CDCl₃) δ 139.2, 138.9, 138.5, 135.4, 134.5, 128.8, 128.7, 128.7, 128.5, 128.0, 128.0, 127.9, 127.8, 127.7, 73.7, 73.0, 71.0, 71.0, 70.5, 39.5, 37.4; IR (film) 2860, 1453, 1069 cm⁻¹; HRMS (EI⁺) calc'd for [C₂₈H₃₁O₃]⁺: m/z 415.2273, found 415.2280.



2,4,6-tris(benzyloxy)heptanedial (99). To a solution of cycloheptene **96** (698 mg, 1.59 mmol) in THF (18 mL) and water (6 mL) was added OsO₄ (28 mg, 0.13 mmol) and NMO (410 mg, 3.5 mmol). At 8 h, a saturated aq solution of Na₂S₂O₃ (10 mL) was added to the reaction and the biphasic mixture was stirred vigorously for 15 min. Et₂O was added (10 mL) and the layers were separated. The aqueous layer was extracted with Et₂O (3 x 10 mL) and the combined organics were washed with brine, dried over MgO₄ and concentrated under reduced pressure. The crude material was purified by flash chromatography over silica gel (15% EtOAc:hexane eluent) to yield a white waxy solid that was used in the next step without further purification.

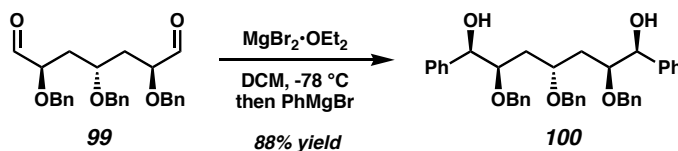
To a solution of the intermediate diol (400 mg, 0.89 mmol) in DCM (10 mL) was added Pb(OAc)₄ (435 mg, 0.98 mmol). After 15 min, the cloudy mixture was diluted with heptane (10 mL) and filtered over a pad of Celite. The liquor was concentrated under reduced pressure, then the resulting oil was purified by flash chromatography over silica gel (20% EtOAc:hexane eluent) to provide 2,4,6-tris(benzyloxy)heptanedial **99** (385 mg, 82% yield for 2 steps, R_F = 0.24-0.38 in 50% Et₂O:pentane) as a clear oil: ¹H NMR (300 MHz, CDCl₃) δ 9.63 (d, $J=1.8$ Hz, 2H), 7.48-7.16 (comp. m, 10H), 4.65 (d,

$J=11.4$ Hz, 2H), 4.40 (d, $J=11.7$ Hz, 2H), 4.29 (s, 2H), 3.96 (dq, $J=1.5, 8.9$ Hz, 2H), 3.89 (ddd, $J=4.2, 7.7, 11.6$ Hz, 1H), 2.14-1.82 (comp. m, 4H); ^{13}C NMR (300 MHz, CDCl_3) δ 203.1, 138.2, 137.4, 128.8, 128.7, 128.4, 128.4, 128.1, 128.0, 81.2, 72.8, 72.4, 71.7, 36.0; IR (film) 2866, 1732, 1117 cm^{-1} ; HRMS (EI^+) calc'd for $[\text{C}_{20}\text{H}_{30}\text{O}_5]$: m/z 446.2093, found 446.2093.

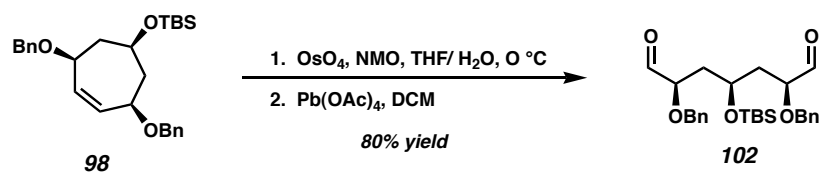


Meso-diol (101). To a 0 °C solution of 2,4,6-tris(benzyloxy)heptanedial **99** (310 mg, 0.69 mmol) in DCM (10 mL) was added anhydrous $\text{MgBr} \cdot \text{OEt}_2$ (427 mg, 1.66 mmol). The milky solution was stirred at 0 °C for 30 min, then cooled to -78 °C before the addition of a 1.0 M Et_2O solution (freshly prepared) of (3-methoxyphenyl)magnesium bromide (1.74 mL, 1.74 mmol). The reaction was stirred for 3 h, then allowed to warm to room temperature for 30 min before quenching with saturated aq NH_4Cl solution (5 mL) and diluted with water (5 mL). The layers were separated and the aqueous layer was washed with DCM (2 x 10 mL). The combined organics were washed with water (2 x 10 mL) and brine (10 mL), then dried over MgO_4 and concentrated under reduced pressure to give a crude oil, which was purified by flash chromatography over silica gel (25% EtOAc :hexane eluent) to provide *meso*-diol **101** (281 mg, 61% yield, $R_F = 0.10$ in 30% EtOAc :hexane) as a yellow oil: ^1H NMR (300 MHz, CDCl_3) δ 7.40-7.16 (comp. m, 17H), 6.96-6.79 (comp. m, 6H), 4.58 (dd, $J=5.1, 5.0$ Hz, 2H), 4.45 (d, $J=11.1$ Hz, 2H), 4.38 (d, $J=11.4$ Hz, 2H), 4.21 (s, 2H), 3.83-3.68 (comp. m, 7H), 2.87 (d, $J=4.5$ Hz, 2H), 1.80 (ddd, $J=4.5, 8.1, 14.6$ Hz, 2H), 1.68. ddd (4.5, $J=8.4, 14.2$ Hz, 2H); ^{13}C NMR (300 MHz,

CDCl₃) δ 159.7, 143.2, 138.5, 138.2, 129.4, 128.4, 128.1, 127.9, 127.8, 127.6, 127.6, 119.1, 113.4, 112.1, 80.6, 76.3, 72.9, 69.0, 55.2, 36.9; IR (film) 3436, 2920, 1047 cm⁻¹; HRMS (FAB⁺) calc'd for [C₄₂H₄₇O₇]⁺: m/z 663.3322, found 663.3342.

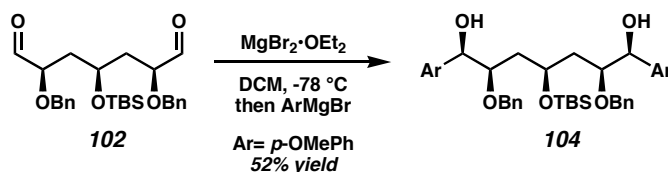


Meso-diol (100). To a 0 °C solution of 2,4,6-tris(benzyloxy)heptanedial **99** (310 mg, 0.69 mmol) in DCM (10 mL) was added anhydrous MgBr•OEt₂ (427 mg, 1.66 mmol). The milky solution was stirred at 0 °C for 30 min, then cooled to –78 °C before the addition of a 1.0 M Et₂O solution of phenylmagnesium bromide (1.74 mL, 1.74 mmol). The reaction was stirred for 3 h, then allowed to warm to room temperature for 30 min before quenching with saturated aq NH₄Cl solution (5 mL) and diluted with water (5 mL). The layers were separated and the aqueous layer was washed with DCM (2 x 10 mL). The combined organics were washed with water (2 x 10 mL) and brine (10 mL), then dried over MgO₄ and concentrated under reduced pressure to give a crude oil, which was purified by flash chromatography over silica gel (15% EtOAc:hexane eluent) to provide *meso*-diol **100** (321 mg, 88% yield, R_F=0.37 in 30% EtOAc:hexane) as a clear oil: ¹H NMR (300 MHz, CDCl₃) δ 7.49–7.20 (comp. m, 25H), 4.64 (dd, J =4.2, 3.9 Hz, 2H), 4.46 (s, 4H), 4.25 (s, 2H), 3.90–3.71 (m, 3H), 3.09 (2.4, 2H), 1.93–1.77 (m, 2H), 1.76–1.60 (m, 2H); ¹³C NMR (300 MHz, CDCl₃) δ 141.8, 138.9, 138.5, 128.8, 128.7, 128.7, 128.2, 128.1, 128.0, 128.0, 127.9, 127.1, 80.8, 76.5, 73.6, 73.2, 69.3, 37.1; IR (film) 3430, 1454, 1057 cm⁻¹; HRMS (FAB⁺) calc'd for [C₄₀H₄₃O₅]⁺: m/z 603.3110, found 603.3124.

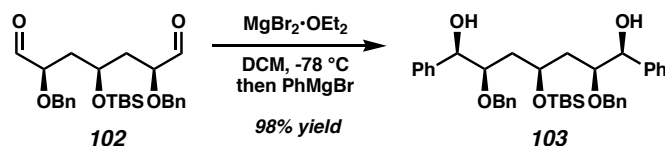


Heptanedial (102). To a solution of cycloheptene **98** (2.6 g, 5.92 mmol) in THF (26 mL) and water (6 mL) was added OsO₄ (103 mg, 0.41 mmol) and NMO (1.73 mg, 14.81 mmol). At 8 h, a saturated aq solution of Na₂S₂O₃ (50 mL) was added to the reaction and the biphasic mixture was stirred vigorously for 15 min. Et₂O was added (50 mL) and the layers were separated. The aqueous layer was extracted with Et₂O (3 x 500 mL) and the combined organics were washed with brine, dried over MgO₄ and concentrated under reduced pressure. The crude material was purified by flash chromatography over silica gel (15% EtOAc:hexane eluent) to yield a white waxy solid that was used without further purification

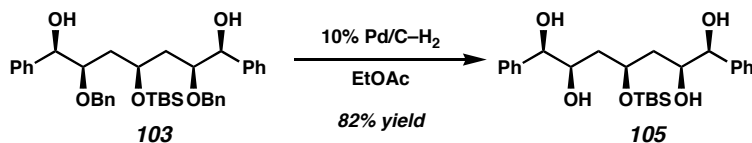
To a solution of the intermediate diol (415 mg, 0.88 mmol) in DCM (10 mL) was added Pb(OAc)₄ (429 mg, 0.97 mmol). After 15 min, a cloudy mixture was diluted with heptane (10 mL) and filtered over a pad of Celite. The liquor was concentrated under reduced pressure, then the resulting oil was purified by flash chromatography over silica gel (20% EtOAc:hexane eluent) to provide heptanedial **102** (395 mg, 80% yield for 2 steps, R_F= 0.18 in 10% EtOAc:hexane) as a clear oil: ¹H NMR (300 MHz, CDCl₃) δ 9.60 (dd, *J*=1.5 Hz, 2H), 7.51-7.22 (comp. m, 10H), 4.68 (d, *J*=11.7 Hz, 2H), 4.51 (d, *J*=11.7, 2H), 4.19 (ddd, *J*=6.0, 5.9, 11.6 Hz, 1H), 3.95 (dd, *J*=2.1, 6.6 Hz, 2H), 1.98- 1.75 (m, 4H), 0.88 (s, 9H), 0.75 (s, 6H); ¹³C NMR (300 MHz, CDCl₃) δ 203.1, 137.4, 128.8, 128.4, 80.5, 72.8, 65.4, 37.0, 26.1, 18.2, -4.2; IR (film) 2930, 1732, 1101 cm⁻¹; HRMS (FAB⁺) calc'd for [C₂₅H₃₉O₅Si]⁺: *m/z* 471.2567, found 471.2581.



Meso-diol (104). To a 0 °C solution of heptanedial **102** (393 mg, 0.84 mmol) in DCM (20 mL) was added anhydrous $\text{MgBr} \cdot \text{OEt}_2$ (521 mg, 2.02 mmol). The milky solution was stirred at 0 °C for 30 min, then cooled to -78°C before the addition of a 1.0 M DCM solution (freshly prepared in Et_2O , then concentrated and redissolved in DCM) of (4-methoxyphenyl)magnesium bromide (2.1 mL, 2.10 mmol). The reaction was stirred for 3 h, then allowed to warm to room temperature for 30 min before quenching with saturated aq NH_4Cl solution (10 mL) and diluted with water (10 mL). The layers were separated and the aqueous layer was washed with DCM (2 x 20 mL). The combined organics were washed with water (2 x 20 mL) and brine (20 mL), then dried over MgO_4 and concentrated under reduced pressure to give a crude oil, which was purified by flash chromatography over silica gel (15% EtOAc :hexane eluent) to provide *meso*-diol **104** (302 mg, 52% yield, R_F = 0.10 in 30% EtOAc :hexane) as a clear oil: ^1H NMR (300 MHz, CDCl_3) δ 7.42-7.17 (comp. m, 14H), 6.90 (d, J =8.1 Hz, 4H), 4.52 (d, J =5.7 Hz, 2H), 4.47 (d, J =11.4 Hz, 2H), 3.39 (d, J =11.7 Hz, 2H), 3.78 (s, 6H), 3.71-3.54 (m, 1H), 2.99 (br s, 2H), 1.85-1.57 (comp. m, 4H), 0.92 (s, 9H), 0.02 (s, 6H); ^{13}C NMR (300 MHz, CDCl_3) δ 159.4, 138.5, 133.6, 128.7, 128.4, 128.0, 128.0, 114.0, 81.0, 75.9, 72.8, 67.6, 55.5, 38.9, 26.3, 18.3, -4.0; IR (film) 3453, 2931, 1102 cm^{-1} ; HRMS (FAB^+) calc'd for $[\text{C}_{26}\text{H}_{36}\text{NO}_4]^+$: m/z 426.2644, found 426.2651.

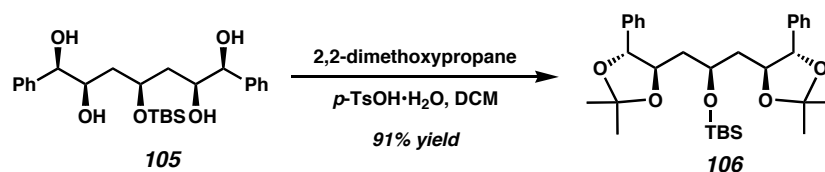


Meso-diol (103). To a 0 °C solution of heptanedial **102** (393 mg, 0.84 mmol) in DCM (20 mL) was added anhydrous $\text{MgBr} \cdot \text{OEt}_2$ (518 mg, 2.40 mmol). The milky solution was stirred at 0 °C for 30 min, then cooled to $-78\text{ }^{\circ}\text{C}$ before the addition of a 3.0 M Et_2O solution of magnesium bromide (700 μL , 2.10 mmol). The reaction was stirred for 3 h, then allowed to warm to room temperature for 30 min before quenching with saturated aq NH_4Cl solution (10 mL) and diluted with water (10 mL). The layers were separated and the aqueous layer was washed with DCM (2 x 20 mL). The combined organics were washed with water (2 x 20 mL) and brine (20 mL), then dried over MgO_4 and concentrated under reduced pressure to give a crude oil, which was purified by flash chromatography over silica gel (15% EtOAc :hexane eluent) to provide *meso*-diol **103** (435 mg, 98% yield, R_F = 0.32 in 30% EtOAc :hexane) as a clear oil: ^1H NMR (300 MHz, CDCl_3) δ 7.54–7.06 (comp. m, 20H), 4.57 (dd, J =4.8, 5.2 Hz, 2H), 4.43 (d, J =11.4 Hz, 2H), 4.32 (d, J =11.1 Hz, 2H), 3.76–3.60 (comp. m, 3H), 2.98 (d, J =4.8 Hz, 2H), 1.92–1.59 (comp. m, 4H), 0.89 (s, 9H), 0.01 (s, 6H); ^{13}C NMR (300 MHz, CDCl_3) δ 141.6, 138.4, 128.7, 128.6, 128.0, 128.0, 127.0, 80.8, 79.9, 76.2, 72.9, 67.5, 38.9, 26.2, 18.3, -4.1 ; IR (film) 3445, 2928, 1454, 1048 cm^{-1} ; HRMS (FAB^+) calc'd for $[\text{C}_{39}\text{H}_{51}\text{O}_5\text{Si}]^+$: m/z 627.3506, found 627.3503.



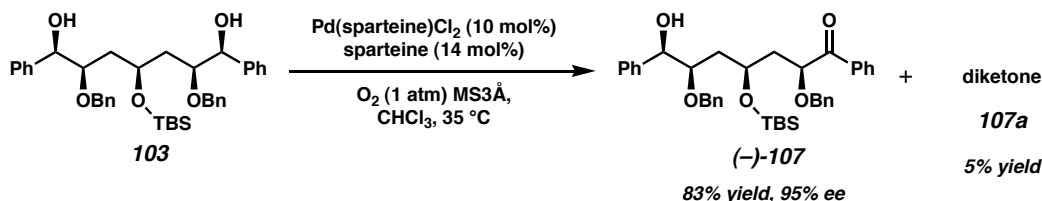
Tetraol (105). A solution of diol **103** (55 mg, 0.09 mmol) in EtOAc (2.0 mL) was purged with a stream of dry nitrogen. Then, 10% palladium on carbon (20 mg) was

added to the stirred solution and the vessel was flushed thoroughly with a stream of hydrogen. The reaction was maintained at room temperature for 24 h, then purged with a stream of nitrogen and filtered over a plug of Celite, rinsing with EtOAc. The combined organics were concentrated under reduced pressure and purified by flash chromatography over silica (60% EtOAc:hexane eluent) to provide tetraol **105** (32 mg, 82% yield, R_F = 0.12 in 50% EtOAc:hexane) as a white solid: ^1H NMR (300 MHz, CDCl_3) δ 7.44-7.21 (comp. m, 10H), 4.35 (d, J =6.6 Hz, 2H), 4.06 (dd, J =6.3, 6.3 Hz, 2H), 3.77 (dt, J =3.6 Hz, 11.1H), 3.30 (br s, 2H), 3.09 (br s, 2H), 1.68-1.42 (comp. m, 4H), 0.83 (s, 9H), -0.02 (s, 6H); ^{13}C NMR (300 MHz, CDCl_3) δ 141.0, 128.7, 128.3, 127.2, 78.1, 73.7, 70.1, 39.5, 26.1, 18.1, -4.3; IR (film) 3409, 2928, 1086 cm^{-1} ; HRMS (FAB $^+$) calc'd for $[\text{C}_{25}\text{H}_{39}\text{O}_5\text{Si}]^+$: m/z 447.2567, found 447.2550.



Acetonide (106). To a solution of tetraol **105** (16.0 mg, 0.025 mmol) in DCM (1.0 mL) was added TsOH (1.7 mg, 0.01 mmol) and 2,2-dimethoxypropane (52 mg, 0.5 mmol). The reaction was maintained at room temperature for 1 h, then quenched by the addition of saturated aq NaHCO_3 . The layers were separated and the aqueous layer was washed with DCM (1 mL). The combined organics were dried over a plug of Na_2SO_4 and concentrated under reduced pressure. The crude material was purified by flash chromatography over silica gel (20% EtOAc:hexane eluent) to provide the acetonide **106** (12 mg, 91% yield, R_F = 0.23 in 20% EtOAc:hexane) as a clear oil: ^1H NMR (300 MHz, CDCl_3) δ 7.41-7.24 (comp. m, 10H), 4.46 (d, J =7.8 Hz, 2H), 4.07-3.96 (m, 1H), 3.92

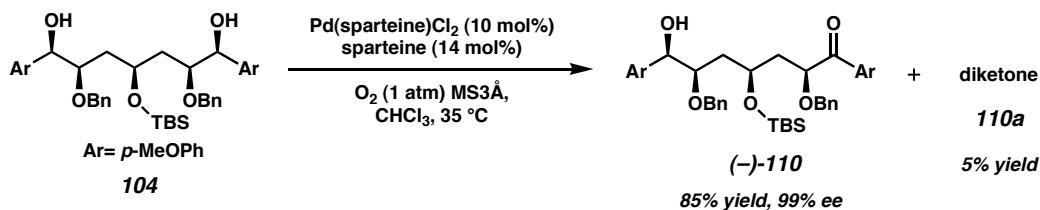
(ddd, $J=2.4, 8.6, 8.7$ Hz, 2H), 1.88-1.66 (m, 4H), 1.41 (s, 6H), 1.33 (s, 6H), 0.68 (s, 9H), -0.21 (s, 6H); ^{13}C NMR (300 MHz, CDCl_3) δ 138.0, 128.6, 128.3, 127.0, 108.9, 84.0, 79.6, 67.4, 37.9, 27.4, 27.1, 25.9, 18.1, -4.8; IR (film) 2856, 1378, 1239 cm^{-1} ; HRMS (FAB $^+$) calc'd for $[\text{C}_{31}\text{H}_{47}\text{O}_5\text{Si}]^+$: m/z 527.3139, found 527.3200.



Keto-Alcohol [(-)-107]. For preparation from *meso*-diol **103**, see the general protocol for *meso*-diol desymmetrization, chloroform conditions. Keto-alcohol **(-)-107** (83% yield, 95% ee, $R_F=0.34$ in 30% EtOAc:hexane) was obtained as an oil: ^1H NMR (300 MHz, CDCl_3) δ 8.03 (d, $J=8.1$ Hz, 2H), 7.57 (dd, $J=7.8, 7.5$ Hz, 1H), 7.43 (dd, $J=6.6, 7.4$ Hz, 2H), 7.39-7.10 (comp. m, 20H), 4.93 (dd, $J=4.5, 7.7$ Hz, 1H), 4.63-4.52 (comp. m, 2H), 4.40-4.20 (comp. m, 4H), 2.84 (br s, 1H), 2.07-1.79 (comp. m, 4H), 0.89 (s, 9H), 0.14 (s, 3H), -0.17 (s, 3H); ^{13}C NMR (300 MHz, CDCl_3) δ 200.3, 142.0, 138.4, 137.7, 135.2, 133.7, 129.1, 128.9, 128.8, 128.7, 128.6, 128.5, 128.3, 128.1, 127.9, 127.8, 127.8, 81.0, 78.5, 76.1, 73.2, 72.1, 67.3, 39.3, 38.8, 26.2, 18.3, -4.3; IR (film) 3478, 2929, 1692, 1094 cm^{-1} ; HRMS (FAB $^+$) calc'd for $[\text{C}_{39}\text{H}_{49}\text{O}_5\text{Si}]$: m/z 625.3349, found 625.3345; $[\alpha]_{\text{D}}^{20}$ -64.1° ($c=1$, CHCl_3).

The diketone **107a** (5% yield, $R_F=0.39$ in 30% EtOAc:hexane) was also recovered as an oil: ^1H NMR (300 MHz, CDCl_3) δ 8.03 (d, $J=7.5$ Hz, 4H), 7.56 (dd, $J=7.2, 7.5$ Hz, 2H), 7.40 (8.1, $J=7.8$ Hz, 4H), 7.33-7.12 (comp. m, 10H), 5.03 (dd, $J=3.6, 9.0$ Hz, 2H), 4.59 (d, $J=11.7$ Hz, 2H), 4.34 (d, $J=11.7$ Hz, 2H), 4.24 (m, 1H), 2.20-1.90

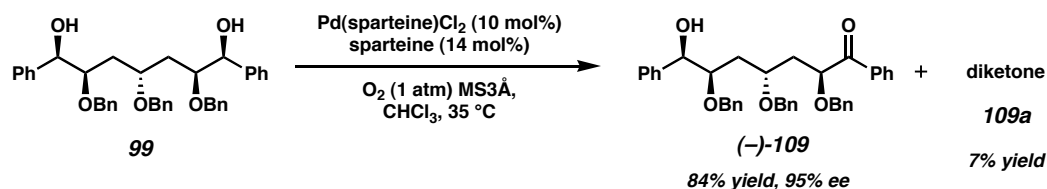
(comp. m, 4H), 0.83 (s, 9H), -0.18 (s, 6H); ^{13}C NMR (300 MHz, CDCl_3) δ 200.5, 137.6, 135.4, 133.6, 129.0, 128.8, 128.6, 128.5, 128.1, 100.2, 77.9, 71.6, 66.9, 38.4, 26.1, 18.2, -4.5; IR (film) 2930, 1692, 1256 cm^{-1} ; HRMS (FAB^+) calc'd for $[\text{C}_{39}\text{H}_{47}\text{O}_5\text{Si}]^+$: m/z 623.3193, found 623.3210.



Keto-Alcohol [(-)-108]. For preparation from *meso*-diol **104**, see the general protocol for *meso*-diol desymmetrization, chloroform conditions. Keto-alcohol **(-)-108** (85% yield, 99% ee, R_F = 0.12 in 30% EtOAc:hexane) was obtained as a slightly yellow oil: ^1H NMR (300 MHz, CDCl_3) δ 8.02 (7.9, 2H), 7.34-7.12 (comp. m, 10H), 6.87 (d, J =9.3 Hz, 2H), 6.83 (d, J =8.7 Hz, 2H), 4.81 (dd, J =4.5, 7.8 Hz, 1H), 4.57-4.22 (comp. m, 4H), 3.98-3.61 (comp. m, 9H), 2.05-1.67 (comp. m, 4H), 0.86 (s, 9H), 0.02 (d, J =6.3 Hz, 6H); ^{13}C NMR (300 MHz, CDCl_3) δ 198.7, 163.9, 159.3, 138.4, 137.8, 133.9, 131.4, 128.6, 128.6, 128.6, 128.1, 128.0, 127.9, 114.0, 113.9, 81.1, 78.6, 75.9, 73.1, 71.9, 67.3, 55.7, 55.5, 39.7, 38.7, 26.2, 18.2, -4.3; IR (film) 3492, 2929, 1680, 1600, 1251 cm^{-1} ; HRMS (FAB^+) calc'd for $[\text{C}_{41}\text{H}_{51}\text{O}_7\text{Si}]^+$: m/z 683.3404, found 683.3383; $[\alpha]_D^{20}$ -74.9° (c=1, CDCl_3).

The diketone **108a** (5% yield, R_F = 0.18 in 30% EtOAc:hexane) was also recovered as a slightly yellow oil: ^1H NMR (300 MHz, CDCl_3) δ 8.02 (d, J =8.4 Hz, 4H), 7.34-7.12 (comp. m, 10H), 6.87 (d, J =8.4 Hz, 4H), 4.98 (dd, J =3.6, 9.0 Hz, 2H), 4.57 (d, J =11.7 Hz, 2H), 4.32 (d, J =11.4 Hz, 2H), 4.29-4.22 (m, 1H), 3.84 (s, 6H), 2.19-1.90

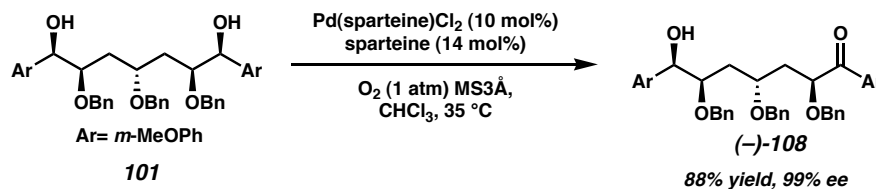
(comp. m, 4H), 0.84 (s, 9H), 0.01 (s, 6H); ^{13}C NMR (300 MHz, CDCl_3) δ 198.9, 163.9, 137.7, 131.4, 128.5, 128.4, 128.3, 128.0, 114.0, 77.8, 71.7, 67.0, 55.7, 38.7, 26.0, 18.2, -4.4; IR (film) 2930, 1681, 1599, 1257 cm^{-1} ; HRMS (FAB^+) calc'd for $[\text{C}_{41}\text{H}_{51}\text{O}_7\text{Si}]^+$: m/z 683.3404, found 683.3433.



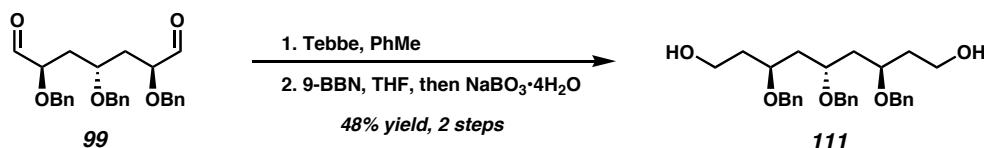
Keto-Alcohol [(-)-109]. For preparation from *meso*-diol **99**, see the general protocol for *meso*-diol desymmetrization, chloroform conditions. The keto-alcohol (-)-**109** (84% yield, 95% ee, R_F = 0.49 in 30% EtOAc:hexane) was obtained as a clear oil: ^1H NMR (300 MHz, CDCl_3) δ 8.01 (d, J =7.8 Hz, 2H), 7.57 (dd, J =6.9, 6.9 Hz, 1H), 4.42 (dd, J =6.9, 7.1 Hz, 2H), 7.38-7.14 (comp. m, 20H), 4.92 (d, J =7.8 Hz, 1H), 4.69-4.57 (comp. m, 2H), 4.53-4.34 (comp. m, 3H), 4.26-1.13 (comp. m, 2H), 3.91-3.68 (comp. m, 2H), 2.90 (br s, 1H), 2.05-1.62 (comp. m, 4H); ^{13}C NMR (300 MHz, CDCl_3) δ 200.3, 141.4, 138.8, 138.3, 137.8, 135.1, 133.7, 129.0, 128.7, 128.7, 128.6, 128.2, 128.1, 128.0, 128.0, 127.9, 127.0, 80.9, 78.9, 76.6, 73.6, 73.0, 72.1, 71.3, 39.5, 37.1; IR (film) 3467, 2874, 1692, 1454, 1095 cm^{-1} ; HRMS (FAB^+) calc'd for $[\text{C}_{40}\text{H}_{41}\text{O}_5]^+$: m/z 601.2954, found 601.2953; $[\alpha]_D^{20}$ -78.1° (c =1, CHCl_3).

The diketone **109a** (7% yield, R_F = 0.62 in 30% EtOAc:hexane) was also recovered as a clear oil: ^1H NMR (300 MHz, CDCl_3) δ 8.00 (d, J =7.2 Hz, 4H), 7.56 (dd, J =7.2, 7.5 Hz, 2H), 7.41 (dd, J =7.5, 7.5 Hz, 4H), 7.38-7.14 (comp. m, 15H), 4.88 (dd, J =4.2, 8.3 Hz, 2H), 4.62 (d, J =11.1 Hz, 2H), 4.34 (s, 2H), 4.22 (d, J =11.4 Hz, 2H), 4.15-

4.02 (m, 1H), 2.06-1.74 (comp. m, 4H); ^{13}C NMR (300 MHz, CDCl_3) δ 200.0, 138.5, 137.5, 134.8, 133.4, 128.7, 128.7, 128.4, 128.3, 127.9, 127.7, 127.6, 78.9, 77.2, 73.6, 72.6, 71.1, 39.5; IR (film) 2924, 1692, 1451 cm^{-1} ; HRMS (FAB^+) calc'd for $[\text{C}_{40}\text{H}_{39}\text{O}_5]^+$: m/z 599.2797, found 599.2826.



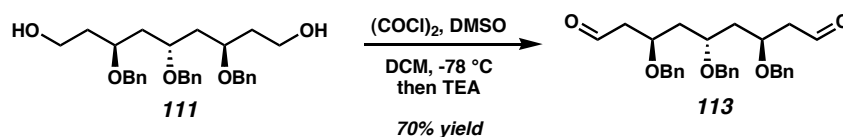
Keto-Alcohol [(-)-108]. For preparation from *meso*-diol **101**, see the general protocol for *meso*-diol desymmetrization, chloroform conditions. The keto-alcohol (-)-**108** (88% yield, 99% ee, $R_F = 0.18$ in 40% EtOAc:hexane) was obtained as a slightly yellow oil: ^1H NMR (300 MHz, CDCl_3) δ 7.58 (d, $J = 6.3$ Hz, 1H), 7.51 (dd, $J = 2.9, 2.0$ Hz, 1H), 7.38-7.06 (comp. m, 18H), 6.97-6.87 (comp. m, 2H), 6.86-6.78 (m, 1H), 4.91 (dd, $J = 2.4, 9.5$ Hz, 1H), 4.68-4.55 (comp. m, 2H), 4.47 (d, $J = 11.4$ Hz, 1H), 4.38 (d, $J = 11.4$ Hz, 1H), 4.21 (11.4, 1H), 4.14 (d, $J = 11.1$ Hz, 1H), 3.86-3.66 (comp. m, 8H), 2.83 (d, $J = 4.5$ Hz, 1H), 2.09-1.59 (comp. m, 4H); ^{13}C NMR (300 MHz, CDCl_3) δ 200.0, 160.1, 160.0, 143.0, 138.7, 138.2, 137.8, 136.4, 129.9, 129.7, 128.7, 128.6, 128.6, 128.6, 128.2, 128.1, 128.0, 128.0, 127.9, 121.5, 120.6, 119.3, 113.8, 112.7, 112.3, 80.6, 78.6, 76.5, 73.6, 73.0, 72.1, 71.3, 55.6, 55.4, 39.6, 37.0; IR (film) 3473, 2934, 1692, 1597, 1095 cm^{-1} ; HRMS (FAB^+) calc'd for $[\text{C}_{42}\text{H}_{45}\text{O}_7]^+$: m/z 661.3165, found 661.3157; $[\alpha]_{\text{D}}^{20} -56.8^\circ$ ($c = 1$, CDCl_3).



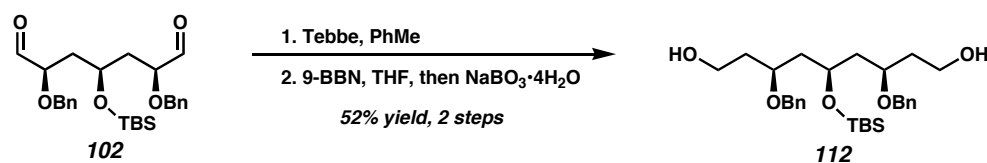
Diol (111). To a $-42\text{ }^{\circ}\text{C}$ solution of heptanedial **99** (2.40 g, 5.38 mmol) in THF (20 mL) and toluene (60 mL) was added a 0.5 M toluene solution of Tebbe reagent (24.70 mL, 12.35 mmol). After 1 h, the solution was warmed to room temperature for 1 h, then recooled to $0\text{ }^{\circ}\text{C}$ and quenched by the slow addition of ice (-10 mL). The solution was diluted with EtOAc (50 mL) and the biphasic mixture was washed with saturated aq NaHCO_3 (1 x 50 mL) then water (3 x 50 mL) and finally brine (1 x 50 mL). The organics were dried over MgO_4 and concentrated under reduced pressure to provide an oil which was purified by flash chromatography on silica gel (5-10% Et_2O :pentane). The resulting oil was used in the next step without further purification.

To a $-10\text{ }^{\circ}\text{C}$ solution of the intermediate olefin (760 mg, 1.72 mmol) in THF (25 mL) was added a 0.5 M THF solution of 9-BBN (7.6 mL, 3.8 mmol). The reaction was warmed to room temperature and maintained overnight. Then, the solution was recooled to $-10\text{ }^{\circ}\text{C}$ and solid sodium perborate tetrahydrate (1.32 g, 8.60 mmol) was added slowly. The reaction was warmed to room temperature for 2 h, then diluted with Et_2O (30 mL) and washed with water (2 x 20 mL). The aqueous layer was washed with Et_2O (2 x 20 mL) and the combined organics were washed with brine (30 mL). The organics were dried over MgO_4 then concentrated under reduced pressure. The resulting oil was purified by flash chromatography (30% EtOAc:hexane eluent) over silica gel to provide diol **111** (695 mg, 48% yield for 2 steps, $R_F = 0.26$ in 30% EtOAc:hexane) as a clear oil: ^1H NMR (300 MHz, CDCl_3) δ 7.50-7.18 (comp. m, 15H), 4.54 (d, $J=11.1$ Hz, 2H), 4.49-4.34 (m, 4H), 3.94-3.61 (comp. m, 7H), 2.37 (dd, $J=4.8, 4.8$ Hz, 2H), 2.02-1.64 (comp.

m, 8H); ^{13}C NMR (300 MHz, CDCl_3) δ 138.7, 138.5, 128.7, 128.7, 128.2, 128.0, 128.0, 75.3, 73.7, 71.4, 71.3, 60.2, 40.2, 36.4; IR (film) 3401, 2942, 1063 cm^{-1} ; HRMS (FAB^+) calc'd for $[\text{C}_{30}\text{H}_{39}\text{O}_5]^+$: m/z 479.2797, found 479.2787.



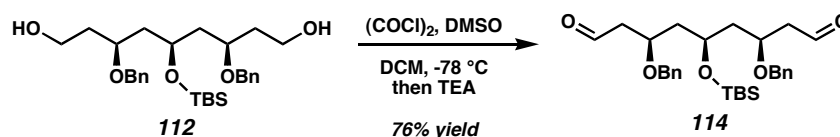
Nonanedial (113). Oxalyl chloride (380 μl , 4.36 mmol) was added to a $-79\text{ }^\circ\text{C}$ solution of DMSO (412 μl , 5.81 mmol) in DCM (25 mL). After 10 min, a solution of diol **111** (695 mg, 1.45 mmol) in DCM (12 mL) was slowly added to the cooled solution. After 30 min, triethylamine (1.62 mL, 11.62 mmol) was added and the vessel was maintained at $-78\text{ }^\circ\text{C}$ for 1 h, then warmed to room temperature for 1 h. Toluene (30 mL) was added and the reaction contents were filtered. The organics were evaporated under reduced pressure, then redissolved in toluene (20 mL) and filtered again. After concentrating under reduced pressure, the crude oil was purified by flash chromatography over silica gel (20% EtOAc:hexane eluent) to provide nonanedial **113** (483 mg, 70% yield, R_F = 0.31 in 20% EtOAc:hexane) as a clear oil: ^1H NMR (300 MHz, CDCl_3) δ 9.79 (dd, J = 1.2 Hz, 2H), 7.62-7.04 (comp. m, 15H), 4.65-4.51 (comp. m, 6H), 4.13 (m, 2H), 3.85 (m, 1H), 2.79-2.58 (comp. m, 4H), 1.00-1.73 (comp. m, 4H); ^{13}C NMR (300 MHz, CDCl_3) δ 201.3, 138.6, 138.2, 128.7, 128.1, 128.1, 128.0, 73.3, 72.0, 71.6, 71.2, 48.8, 41.1; IR (film) 2858, 1716, 1357, 1060 cm^{-1} ; HRMS (FAB^+) calc'd for $[\text{C}_{30}\text{H}_{35}\text{O}_5]^+$: m/z 475.2484, found 475.2490.



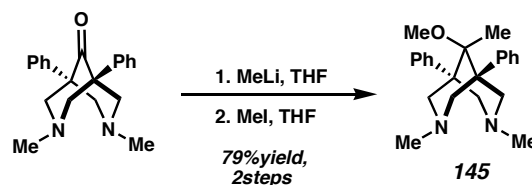
Diol (112). To a $-42\text{ }^{\circ}\text{C}$ solution of heptanedial **102** (1.08 g, 2.30 mmol) in THF (15 mL) and toluene (43 mL) was added a 0.5 M toluene solution of Tebbe reagent (10.5 mL, 5.5 mmol). After 1 h, the solution was warmed to room temperature for 1 h, then recooled to $0\text{ }^{\circ}\text{C}$ and quenched by the slow addition of ice (-10 mL). The solution was diluted with EtOAc (50 mL) and the biphasic mixture was washed with saturated aq NaHCO_3 (1 x 50 mL) then water (3 x 50 mL) and finally brine (1 x 50 mL). The organics were dried over MgO_4 and concentrated under reduced pressure to provide an oil which was purified by flash chromatography on silica gel (5-10% Et_2O :pentane). The resulting oil was used in the next step without further purification.

To a $-10\text{ }^{\circ}\text{C}$ solution of the intermediate olefin (659 mg, 1.41 mmol) in THF (20 mL) was added a 0.5 M THF solution of 9-BBN (6.20 mL, 3.1 mmol). The reaction was warmed to room temperature and maintained overnight. Then, the solution was recooled to $-10\text{ }^{\circ}\text{C}$ and solid sodium perborate tetrahydrate (1.08 g, 7.05 mmol) was added slowly. The reaction was warmed to room temperature for 2 h, then diluted with Et_2O (30 mL) and washed with water (2 x 20 mL). The aqueous layer was washed with Et_2O (2 x 20 mL) and the combined organics were washed with brine (30 mL). The organics were dried over MgO_4 then concentrated under reduced pressure. The resulting oil was purified by flash chromatography (30% EtOAc:hexane eluent) over silica gel to provide diol **110** (600 mg, 52% yield for 2 steps, $R_F = 0.21$ in 30% EtOAc:hexane) as a clear oil: ^1H NMR (300 MHz, CDCl_3) δ 7.39-7.23 (comp. m, 10H), 4.51 (s, 4H), 3.92-3.61 (comp. m, 7H), 2.43 (br s, 2H), 2.00-1.77 (comp. m, 4H), 1.77-1.40 (comp. m, 4H), 0.88 (s, 9H),

0.04 (s, 6H); ^{13}C NMR (300 MHz, CDCl_3) δ 138.4, 128.7, 128.1, 128.0, 75.6, 71.0, 67.6, 60.6, 41.8, 36.2, 26.1, 18.2, -4.1; IR (film) 3401, 2929, 1056 cm^{-1} ; HRMS (FAB^+) calc'd for $[\text{C}_{25}\text{H}_{51}\text{O}_6\text{Si}]$: m/z 503.3193, found 503.3208.



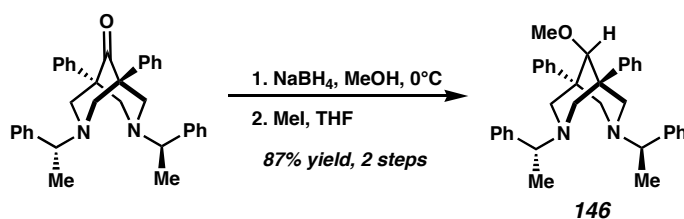
Nonanedial (114). Oxalyl chloride (240 μl , 2.75 mmol) was added to a -79 $^\circ\text{C}$ solution of DMSO (260 μl , 3.66 mmol) in DCM (20 mL). After 10 min, a solution of diol **112** (466 mg, 0.92 mmol) in DCM (10 mL) was slowly added to the cooled solution. After 30 min, triethylamine (1.05 mL, 7.32 mmol) was added and the vessel was maintained at -78 $^\circ\text{C}$ for 1 h, then warmed to room temperature for 1 h. Toluene (20 mL) was added and the reaction contents were filtered. The organics were evaporated under reduced pressure, then redissolved in toluene (15 mL) and filtered again. After concentrating under reduced pressure, the crude oil was purified by flash chromatography over silica gel (10% EtOAc:hexane eluent) to provide nonanedial **114** (380 mg, 76% yield, R_F = 0.27 in 10% EtOAc:hexane) as a clear oil: ^1H NMR (300 MHz, CDCl_3) δ 9.75 (dd, J = 1.2, 0.9 Hz, 2H), 7.42-7.21 (comp. m, 10H), 4.58 (d, J = 11.7 Hz, 2H), 4.46 (d, J = 11.7 Hz, 2H), 4.06 (ddd, J = 6.0, 18.0 Hz, 2H), 3.91 (ddd, J = 6.0, 18.0 Hz, 1H), 2.57 (dd, J = 2.1, 5.6 Hz, 4H), 1.99-1.83 (comp. m, 2H), 1.75-1.60 (comp. m, 2H), 0.88 (s, 9H), 0.38 (s, 6H); ^{13}C NMR (300 MHz, CDCl_3) δ 201.4, 138.2, 128.7, 128.0, 71.5, 71.3, 66.6, 48.6, 41.9, 26.1, 18.2, -4.2; IR (film) 2857, 1725, 1108 cm^{-1} ; HRMS (FAB^+) calc'd for $[\text{C}_{29}\text{H}_{41}\text{O}_5\text{Si}]^+$: m/z 497.2723, found 497.2728.



Methoxy Bispinidine (145). To a room temperature solution of the starting bispinidone (640 mg, 2.00 mmol) in Et₂O (10 mL) and THF (5 mL) was added a 1.6 M THF solution of MeLi (1.9 mL, 3.00 mmol). The reaction was maintained at room temperature for 3 h, then quenched by the addition of saturated aq NH₄Cl (5 mL), then diluted with water (5 mL). The layers were separated and the aqueous layer was washed with Et₂O (2 x 10 mL). The combined organics were washed with saturated aq NaHCO₃, then brine (10 mL) and dried over MgO₄. After filtering, the organics were concentrated under reduced pressure. The resulting oil was purified by flash chromatography over silica gel (4% MeOH:DCM eluent) and used directly in the next step.

To a room temperature solution of the diamino alcohol (580 mg, 1.43 mmol) in THF (15 mL) was added a 60 wt% dispersion of NaH in mineral oil (172 mg, 4.28 mmol). After 15 min, MeI (446 μ l, 7.13 mmol) was added to the stirred solution and the reaction was heated to 70 °C for 12 h. The vessel was then cooled to room temperature and quenched by the addition of saturated aq NH₄Cl (5 mL), then diluted with water (5 mL). The layers were separated and the aqueous layer was washed with Et₂O (2 x 10 mL). The combined organics were washed with saturated aq NaHCO₃, then brine (10 mL) and dried over MgO₄. After filtering, the organics were concentrated under reduced pressure. The resulting oil was purified by flash chromatography over silica gel (4% MeOH:DCM eluent) to provide methoxy bispinidine **145** (551 mg, 79% yield, 2 steps, R_F= 0.26 in 4% MeOH:DCM) as a white solid: ¹H NMR (300 MHz, CDCl₃) δ 7.44 (d,

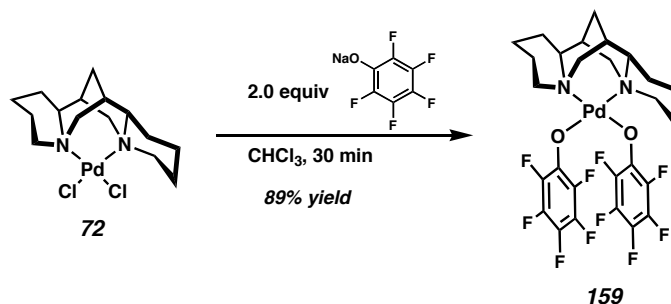
$J=7.2$ Hz, 4H), 7.37-7.19 (comp. m, 6H), 4.50 (d, $J=13.8$ Hz, 2H), 3.99 (s, 2H), 3.81 (s, 2H), 3.64 (d, $J=13.2$ Hz, 2H), 3.02 (s, 3H), 3.01 (s, 3H), 2.50 (s, 3H), 0.72 (s, 3H); ^{13}C NMR (300 MHz, CDCl_3) δ 138.1, 128.9, 128.6, 128.6, 128.1, 73.9, 65.5, 63.3, 62.3, 54.8, 48.8, 45.8, 12.3; IR (film) 2181, 1444 cm^{-1} ; HRMS (EI^+) calc'd for $[\text{C}_{23}\text{H}_{30}\text{N}_2\text{O}]^+$: m/z 350.2358, found 350.2367.



Methoxy-bispinidine. (146) To a 0 °C solution of the starting bispinidone (500 mg, 1.00 mmol) in MeOH (15 mL) was added NaBH_4 (114 mg, 3.00 mmol) in several portions. After 1 h, the reaction was warmed to room temperature for 1 h, then concentrated under reduced pressure. The resulting paste was redissolved in DCM (30 mL) and washed with saturated aq NH_4Cl (10 mL), water (10 mL), and brine (10 mL). The organic layer was dried over Na_2SO_4 then concentrated under reduced pressure and placed under a high vacuum for several hours to provide a white solid that was used without further purification.

To a room temperature solution of the diamino alcohol (500 mg, 1.00 mmol) in THF (10 mL) was added a 60 wt% dispersion of NaH in mineral oil (120 mg, 3.00 mmol). After 15 min, MeI (500 μl , 4.00 mmol) was added to the stirred solution and the reaction was heated to 70 °C for 12 h. The vessel was then cooled to room temperature and quenched by the addition of saturated aq NH_4Cl (5 mL), then diluted with water (5 mL). The layers were separated and the aqueous layer was washed with Et_2O (2 x 10

mL). The combined organics were washed with saturated aq NaHCO₃, then brine (10 mL), and dried over Na₂SO₄. After filtering, the organics were concentrated under reduced pressure. The resulting white solid was purified by flash chromatography over silica gel (4% MeOH:DCM eluent) to provide methoxy-bispinidine **146** (450 mg, 87% yield, 2 steps, R_F= 0.31 in 4% MeOH:DCM) as an oil: ¹H NMR (300 MHz, CDCl₃) δ 7.70-7.14 (comp. m, 20H), 2.42 (s, 1H), 3.78 (dd, *J*=6.6, 13.2 Hz, 1H), 3.65 (dd, *J*=6.6, 13.2 Hz, 1H), 3.34 (comp. m, 7H), 2.75 (d, *J*=10.2 Hz, 1H), 2.40 (s, 3H), 1.59 (d, *J*=6.6 Hz, 6H); ¹³C NMR (300 MHz, CDCl₃) δ 148.6, 148.3, 145.8, 144.3, 128.6, 128.4, 128.3, 128.2, 128.1, 128.1, 127.2, 127.0, 126.4, 126.1, 126.1, 87.2, 64.9, 64.4, 62.8, 62.2, 61.2, 53.9, 50.1, 43.2, 43.1, 20.1, 19.7; IR (film) 2971, 1451, 1102 cm⁻¹; HRMS (EI⁺) calc'd for [C₃₆H₄₀N₂O]⁺: *m/z* 516.3141, found 516.3161; [α]_D²⁰ +9.6° (c=1, CDCl₃).



(sp)Pd(OC₆F₆)₂ (159) In a dry box, a vial was charged with Pd(sp)Cl₂ (103 mg, 0.25 mmol) and sodium pentafluorophenoxide (105 mg, 0.51 mmol). The vial was removed from the box and dissolved in CHCl₃ (2 mL, amylene stabilized), sonicated for 5 min, then stirred vigorously for 1 h. The solution was filtered over a pad of Celite, then concentrated to 1 mL total volume under a stream of nitrogen in a vial. The vial was transferred to a vapor deposition chamber filled with hexanes. After a few days, analytically pure red crystals of **159** (157 mg, 89% yield) were deposited: m.p.

(decomposition) 122 °C ^1H NMR (300 MHz, CDCl_3) δ 4.43 (d, $J=12.0$ Hz, 1H), 4.26 (d, $J=12.6$ Hz, 1H), 3.54-3.29 (comp. m, 2H), 3.25 (10.8, 1H), 3.02 (d, $J=12.9$ Hz, 1H), 2.87 (dd, $J=3.3, 13.4$ Hz, 1H), 2.62 (d, $J=14.4$ Hz, 1H), 2.45 (dd, $J=2.7, 12.6$ Hz, 2H), 2.26-1.16 (comp. m, 16H); ^{13}C NMR (300 MHz, CDCl_3) δ 144.1-128.0, 70.01, 66.1, 65.2, 62.6, 58.5, 48.9, 35.0, 34.8, 30.1, 27.7, 26.4, 24.3, 23.7, 23.4, 19.9; IR (film) 2949, 1504, 998 cm^{-1} ; HRMS (FAB $^+$) calc'd for $[\text{C}_{27}\text{H}_{25}\text{N}_2\text{O}_2\text{F}_{10}\text{Pd}]^+$: m/z 705.0791, found 705.0772; $[\alpha]_{\text{D}}^{20}$ 165.2° ($c=1$, CDCl_3).

Table 16. HPLC methods for determination of ee

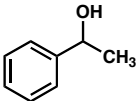
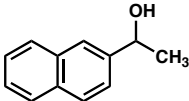
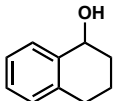
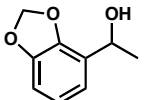
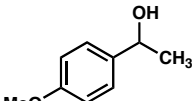
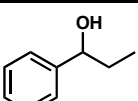
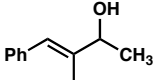
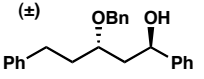
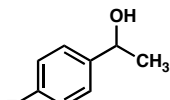
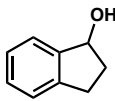
entry	Substrate	ee Assay	Conditions	Retention Time of (<i>R</i>) isomer (min)	Retention Time of (<i>S</i>) isomer (min)
A.		HPLC Chiralcel OD-H	3% EtOH/hexane 1.0 mL/min	10.69	13.37
B.		HPLC Chiralcel OJ	4% 2-propanol/hexane 1.0 mL/min	38.69	31.32
C.		HPLC Chiralcel AS	2% EtOH/hexane 1.0 mL/min	15.55	12.68
D.		HPLC Chiralcel OBH	2% IPA/hexane 1.0 mL/min	18.65	32.20
E.		HPLC Chiralcel OD-H	3% EtOH/hexane 1.0 mL/min	14.60	16.52
F.		HPLC Chiralcel OD-H	3% EtOH/hexane 1.0 mL/min	11.15	13.23
G.		HPLC Chiralcel OD-H	4% 2-propanol/hexane 1.0 mL/min	13.44	15.44
H.		HPLC Chiracel AD	4% IPA/hexane 1.0 ml/min	25.90	30.61
I.		HPLC Chiracel AS	2% EtOH/hexane 1.0 ml/min	15.10	17.35
J.		HPLC Chiralcel OJ	3% EtOH/hexane 1.0 mL/min	17.35	14.76

Table 16 (cont'd). HPLC methods for determination of ee

entry	Substrate	ee Assay	Conditions	Retention Time of (<i>R</i>) isomer (min)	Retention Time of (<i>S</i>) isomer (min)
K.		HPLC Chiralcel OBH	4% IPA/hexane 1.0 mL/min	8.67	9.67
L.		HPLC Chiralcel OJ	10% EtOH/hexane 1.0 ml/min	19.54	25.18
Product H and L ^[6]		HPLC Chiralcel OJ	4% IPA/hexane 1.0 ml/min	47.98	57.82
		HPLC Chiralcel OJ	2% IPA/hexane 1.0 ml/min	20.06	22.74
		HPLC Chiralcel OJ	6% IPA/hexane 1.0 ml/min	29.86	39.31
		HPLC Chiralcel OBH	6% EtOH/hexane 1.0 ml/min	24.52	29.91
		HPLC Chiralcel OBH	4% IPA/hexane 1.0 ml/min	20.06	22.74

Notes and References

- (1) (a) Johnson, R. A.; Sharpless, K. B. In *Catalytic Asymmetric Synthesis*; Ojima, I., Ed.; Wiley & Sons: New York, 2000; pp 231-280. (b) Katsuki, T. In *Catalytic Asymmetric Synthesis*; Ojima, I.; Ed.; Wiley & Sons: New York, 2000; pp 287-325.
- (2) Bolm, C.; Hildebrand, J. P.; Muniz, K. In *Catalytic Asymmetric Synthesis*; Ojima, I., Ed.; Wiley & Sons: New York, 2000; pp 399-428.
- (3) Muller, P. In *Advances in Catalytic Processes*; JAI Press Inc.: Greenwich, CT, 1997; Vol. 2, pp 113-151.
- (4) (a) Ohkubo, K.; Hirata, K.; Yoshinaga, K.; Okada, M. *Chem Lett.* **1976**, 183. (b) Berti, C.; Perkind, M. J. *Angew. Chem., Int. Ed. Engl.* **1979**, 18, 864. (c) Ishii, Y.; Suzuki, K.; Ikarira, T.; Saburi, M.; Yoshikawa, S. *J. Org. Chem.* **1986**, 51, 2822. (d) Ma, Z.; Huang, Q.; Bobbitt, J. M. *J. Org. Chem.* **1993**, 58, 4837. (e) Hashiguchi, S.; Fujii, A.; Haack, K.-J.; Matsumura, K.; Ikariya, T.; Noyori, R. *Angew. Chem., Int. Ed. Engl.* **1997**, 36, 288. (f) Nishibayashi, Y., Y.; Takei, I.; Uemura, S.; Hidai, M. *Organometallics* **1999**, 18, 2291. (g) Masutani, K.; Uchida, T.; Irie, R.; Katsuki, T. *Tetrahedron Lett.* **2000**, 41, 5119. (h) Kuroboshi, M.; Yoshihisa, H.; Cortona, M. N.; Kawakami, Y.; Gao, Z.; Tanaka, H. *Tetrahedron Lett.* **2000**, 41, 8131.
- (5) Larock, R. C. *Comprehensive Organic Transformations*; Wiley & Sons: New York, 1999; pp 1234-1248.
- (6) (a) Blackburny, T. F.; Schwartz, J. J. *Chem. Soc., Chem. Commun.* **1977**, 157. (b) Tamaru, Y.; Yamamoto, Y.; Yamada, Y.; Yoshida, Z. *Tetrahedron Lett.* **1979**, 20, 1401. (c) Nagashima, H.; Tsuji, J. *Chem. Lett.* **1995**, 36, 2473. (e) Peterson, K. P.; Larock, R. C. *J. Org. Chem.* **1998**, 63, 3185.
- (7) Nishimura, T.; Onoue, T.; Ohe, K.; Uemura, S. *J. Org. Chem.* **1999**, 64, 6750.
- (8) The selectivity factor (s) was determined from the equation (where C=conversion): $s = k_{\text{rel}}(\text{fast/slow}) = \ln[(1-C)(1-ee)]/\ln[(1-C)(1+ee)]$.
- (9) For discussions on kinetic resolution, see: a) Martin, V. S.; Woodard, S. S.; Katsuki, T.; Yamada, Y.; Ikeda, M.; Sharpless, K. B. *J. Am. Chem. Soc.* **1981**, 103, 6237. b) Chen, C.-S.; Fujimoto, Y.; Girdaukis, G.; Sih, C. J. *J. Am. Chem Soc.* **1982**, 104, 7294. c) Kagan, H. B.; Fiaud, J. C. In *Topics in Stereochemistry*; E. L. Eliel, Ed.; Wiley: New York, 1988; pp. 249-330.

-
- (10) (a) Ferreira, E. M.; Stoltz, B. M. *J. Am. Chem. Soc.* **2001**, *123*, 7725. (b) concurrent with our publication, a closely related system was reported: Jensen, D. R.; Pugsley, J. S.; Sigman, M. S. *J. Am. Chem. Soc.* **2001**, *123*, 7475.
- (11) Recently, Stahl has studied the mechanistic details of related, non-asymmetric systems; see: (a) Steinhoff, B. A.; Stahl, S. S. *Org. Lett.* **2002**, *4*, 4179. (b) Steinhoff, B. A.; Fix, S. R.; Stahl, S. S. *J. Am. Chem. Soc.* **2002**, *124*, 766. (c) Stahl, S. S.; Thorman, J. L.; Nelson, R. C.; Kozee, M. A. *J. Am. Chem. Soc.* **2001**, *123*, 7188.
- (12) Mueller, J. A.; Jensen, D. R.; Sigman, M. S. *J. Am. Chem. Soc.* **2002**, *124*, 8202.
- (13) A variety of $(R_3N)_2PdCl_2$ provide inactive catalysts for oxidation.
- (14) This contrasts the reactivity of Pd(II)OAc complexes of monodentate amines, which provide active catalysts for racemic oxidation. For an example, see: Schultz, M. J.; Park, C. C.; Sigman, M. S. *Chem. Commun.* **2002**, *24*, 3034.
- (15) The effect of Cs_2CO_3 particle size on palladium catalyzed processes in toluene has been studied, and shown to be significant. This results are consistent with a heterogenous process. For details, see: Meyers, C.; Maes, B. U. W.; Loones, K. T. J.; Bal, G.; Lemiere, G. L. F.; Dommisse, R. A. *J. Org. Chem.* **2004**, *69*, 6010.
- (16) Extrapolated from values listed in: March, J. *Advanced Organic Chemistry*; Wiley & Sons, 4th Ed.: New York, 1992; pp 251-252.
- (17) Mueller, J. A.; Sigman, M. S. *J. Am. Chem. Soc.* **2003**, *125*, 7005.
- (18) Heterolysis of the α -silylketone, provides a stabilized enolate and the stabilized cation R_3Si^+ .
- (19) Bagdanoff, J. T.; Ferreira, E. M.; Stoltz B. M. *Org. Lett.* **2003**, *5*, 835.
- (20) For very select substrate powdered, anhydrous NaOH is a superior exogenous base. No catalyst activation is observed for alcohol substrate that tolerates these conditions. To date, no better, generally applicable base additive has been found.
- (21) Reaction rates in the OKR are relatively fast at low conversion (<20%), then gradually decrease as the k_{fast} alcohol enantiomer is consumed. This behavior complicates detailed rate analysis on racemic material.
- (22) For relevant tables, see: F. Fisher, G. Pfeleiderer, *Z. Anorg. Allg. Chem.* **1922**, *124*, 61.

-
- (23) For relevant tables, see: E. W. Flick in *Industrial Solvents Handbook*; E. W. Flick, Ed.; Noyes Data Corp.: New Jersey, 1985, 3rd Ed., pp. 637-647.
- (24) The IR spectrum of CHCl_3 was investigated. However, the C-H stretch was not well resolved. CDCl_3 performs identically to CHCl_3 as a reaction solvent.
- (25) Bagdanoff, J. T.; Stoltz, B. M. *Angew. Chem. Int. Ed.* **2004**, 43, 353.
- (26) For an example of a non-asymmetric alcohol oxidation catalyzed by palladium using air as the stoichiometric oxidant, see: Hallman, K.; Moberg, C. *Adv. Synth. Catal.* **2001**, 343, 260.
- (27) Spectroscopic-grade chloroform (Aldrich) or chloroform stabilized by amylenes was used without further purification. While a drying tube was employed in the reaction setup, no marked effect was observed when wet air was used. Addition of trace concentrated HCl during the resolution had little effect. Additionally, freshly distilled CHCl_3 (washed with H_2O , dried over CaCl_2 , and distillation from CaCl_2) gives identical results. Chloroform stabilized by EtOH must be distilled prior to use to remove the alcohol additive.
- (28) Oxygen uptake experiments confirm a 2:1 stoichiometry for substrate: O_2 , indicating that CHCl_3 is not involved as an oxidant.
- (29) For the resolution of pharmaceutically relevant molecules, see: Caspi, D. D.; Ebner, D. C.; Bagdanoff, J. T.; Stoltz, B. M. *Adv. Synth. Catal.* **2004**, 346, 185.
- (30) Rao, M. R.; Faulkner, J. D. *J. Nat. Prod.* **2002**, 65, 1201.
- (31) For examples of bidirectional synthesis/terminus differentiation in natural products synthesis, see (a) Harada, T.; Kagamihara, Y. Tanaka, S.; Sakamoto, K.; Akira Oku *J. Org. Chem.* **1992**, 57, 1637. (b) Poss C. S.; Rychnovsky, S. D.; Schreiber, S. L. *J. Am. Chem. Soc.* **1993**, 115, 3360. (c) Schreiber, S. L.; Sammakia, T.; Uehling, D. E. *J. Org. Chem.* **1989**, 54, 15. (d) Ikemoto, N.; Schreiber, S. L. *J. Am. Chem. Soc.* **1990**, 112, 9657.
- (32) For discussions on synthetic approaches based on bidirectional chain synthesis, see: (a) Poss, C. S.; Schreiber, S. L. *Acc. Chem. Res.* **1994**, 27, 9. (b) Schreiber, S. L.; Goulet, M. T.; Schulte, G. *J. Am. Chem. Soc.* **1987**, 109, 4718.
- (33) (a) Reingold, I. D.; DiNardo, L. J. *J. Org. Chem.* **1982**, 47, 3544. (b) Reingold, I. D.; Kwong, K. S.; B.; Kahr, B. E.; Menard, M.; Cummings, G.; Kowalski, J. A. *Syn. Comm.* **1993**, 23, 1463.
- (34) Johnson, C. R.; Golebiowski, A.; McGill, T. K.; Steensma, D. H. *Tetrahedron Lett.* **1991**, 32, 2597.

-
- (35) Johnson, C. R.; Golebiowski, A.; McGill, T. K.; Steensma, D. H. *Tetrahedron Lett.* **1991**, 32, 2597.
- (36) (a) Baekvall, J.-E; Vaegberg, J. O. *J. Org. Chem.* **1988**, 53, 5695. (b) Bakval, J. E.; Bystrom, S. E.; Nordberg, R. E. *J. Org. Chem.* **1984**, 49, 4619.
- (37) (a) Reetz, M. T.; Jung, A. *J. Am. Chem. Soc.* **1983**, 105, 4833 (b) Ruck, R. T.; Jacobsen, E. N. *Angew. Chem. Int. Ed.* **2003**, 42, 4771. (c) Lucas, B. S.; Burke, S. D. *Org. Lett.* **2003**, 3915. (c) Tatsuta, K.; Takano, S.; Ikeda, Y.; Nakano, S.; Miyazaki, S. *J. Antibiot.* **1999**, 52, 1146.
- (38) Sold commercially as the racemate.
- (39) (a) Mitchell, D.; Koenig, T. M. *Synth. Commun.* **1995**, 25, 1231. (b) Kumar, A.; Ner, D. H.; Dike, S. Y. *Tetrahedron Lett.* **1991**, 32, 1901. (c) Koenig, T. M.; Mitchell, D. *Tetrahedron Lett.* **1994**, 35, 1339. (d) Ali, I. S.; Sudalai, A. *Tetrahedron Lett.* **2002**, 43, 5435.
- (40) (a) Larsen, R. D.; Corley, E. G.; King, A. O.; Carroll, J. D.; Davis, P.; Verhoeven, T. R.; Reider, P. J.; Labelle, M.; Gauthier, J. Y.; Xiang, Y. B.; Zamboni, R. J. *J. Org. Chem.* **1996**, 61, 3398. (b) King, A. O.; Corley, E. G.; Anderson, R. K.; Larsen, R. D.; Verhoeven, T. R.; Reider, P. J.; Xiang, Y. B.; Belley, M.; Leblanc, Y.; Labelle, M.; Prasat, P.; Zamboni, R. J. *J. Org. Chem.* **1993**, 58, 3731. (c) Bhupathy, M.; McNamara, J. M.; Sidler, D. R.; Volante, R. P.; Bergan, J. J. (Merck & Co., Inc.), *World Patent* 95/18107, **1995**. (d) Bhupathy, M.; McNamara, J. M.; Sidler, D. R.; Volante, R. P.; Bergan, J. J. (Merck & Co., Inc.), *US Patent* 5,614,632 **1997**.
- (41) (a) Kuethe, J. T.; Wong, A.; Wu, J.; Davies, I. W.; Dormer, P. G.; Welch, C. J.; Hillier, M. C.; Hughes, D. L.; Reider, P.J. *J. Org. Chem.* **2002**, 67, 5993. (b) Desai, R.C.; Cicalia, P.; Meurer, L.C.; Finke, P.E. *Tetrahedron Lett.* **2002**, 43, 4569
- (42) (+)-Sparteine, or pachycarpine is also naturally occurring, but far less abundant. For enantioselective synthesis of sparteine, see: a) Smith, B. T.; Wendt, J. A.; Aubé, J. *Org. Lett.* **2002**, 4, 2577. b) Hermet, J.-P. R.; McGrath, M. J.; O'Brien, P.; Porter, D. W. and Gilday, J. *Chem. Commun.* **2004**, 1830. For the first racemic synthesis, see: Leonard, N. J.; Beyler, R. E. *J. Am. Chem. Soc.* **1948**, 70, 2298.
- (43) In a rare example, (–)-sparteine can be converted into the related natural product, (–)-α-isosparteine. For a reference, see: Leonard, N. J.; Beyler, R. E. *J. Am. Chem. Soc.* **1950**, 72, 1316.

-
- (44) Hermet, J.-P. R.; McGrath, M. J.; O'Brien, P.; Porter, D. W.; Gilday, J. *Chem. Commun.* **2004**, 16, 1830.
- (45) Unpublished results. For a partial list, see reference 10.
- (46) Hermet, J.-P. R.; Porter, D. W.; Dearden, M. J.; Harrison, J. R.; Koplin, T.; O'Brien, P.; Parmene, J.; Tyurin, V.; Whitwood, A. C.; Gilday, J.; Smith, N. M. *Org. Biomol. Chem.* **2003**, 22, 3977.
- (47) (a) Black, D. S.; Deacon, G. B.; Rose, M. *Tetrahedron* **1995**, 51, 2055. (b) Black, D. S.; Horsham, M. A.; Rose, M. *Tetrahedron* **1995**, 51, 4819. For example of Pd(π -allyl)bispidinone complexes, see: Gogoll, A.; Grennberg, H.; Axen, A. *Organometallics* **1997**, 16, 1167.
- (48) (a) Gogoll, A.; Johansson, C.; Axen, A.; Grennberg, H. *Chem. Eur. J.* **2001**, 7, 396. (b) Miyahara, Y.; Goto, K.; Inazu, T. *Synthesis* **2001**, 364.
- (49) (a) Davies, I. W.; Gerena, L.; Lu, N.; Larsen, R. D.; Reider, P. J. *J. Org. Chem.* **1996**, 61, 9629. (b) Tottleben, M. J.; Prasad, J. S.; Simpson, J. A.; Chan, S. H.; Vanyo, D. J.; Kuehner, D. E.; Deshpande, R.; Kodersha, G. A. *J. Org. Chem.* **2001**, 66, 1057.
- (50) (a) Brunner, H.; Obermann, U. *Chem. Ber.* **1989**, 122, 499. (b) Meyers, A. I.; Robichaud, A. J.; McKennon, M. J. *Tetrahedron Lett.* **1992**, 33, 1181.
- (51) Oi, R.; Sharpless, K. B. *Tetrahedron Lett.* **1991**, 32, 4853.
- (52) (a) Neumann, W. L.; Rogic, M. M.; Dunn, T. J. *Tetrahedron Lett.* **1991**, 32, 5865. (b) Alvaro, G.; Grepion, F.; Savoia, D. *J. Org. Chem.* **1996**, 62, 4180.
- (53) Kobayashi, S.; Horibe, M. *Chem. Europ. J.* **1997**, 3, 1472.
- (54) Made by known preparations: Hermet, J.-P. R.; Porter, D. W.; Dearden, M. J.; Harrison, J. R.; Koplin, T.; O'Brien, P.; Parmene, J.; Tyurin, V.; Whitwood, A. C.; Gilday, J.; Smith, N. M. *Org. Biomol. Chem.* **2003**, 22, 3977.
- (55) (a) Li, X.; Schenkel, L. B.; Kozlowski, M. C. *Org. Lett.* **2000**, 2, 875. (b) Li, X.; Yang, J.; Koslowski, M. C. *Org. Lett.* **2001**, 3, 1137.
- (56) (a) Vries, A. H.; Andre, H. M.; Meetsma, A.; Feringa, B. L. *Angew. Chem.* **1996**, 108, 2526. (b) Kangying, L.; Zhenghong, Z.; Guofeng, Z.; Chuchi, T. *Heteroat. Chem.* **2003**, 14, 546.
- (57) Markowicz, S. W.; Pokzeptowicz, K.; Karolac-Wojciechowska, J.; Czylkowski, R.; Omelanczuk, J.; Sobczak, A. *Tetrahedron: Asymmetry* **2002**, 13, 1981.

-
- (58) Purchased from Aldrich and used without purification.
- (59) The fast-reacting enantiomer in the oxidative kinetic resolution is used to limit rate complications associated with a resolution process.
- (60) Bispidinone and bispidine diamines are known to rapidly interconvert: Brukwicki, T. *J. Mol. Struct.* **1998**, 446, 69. (b) Galasso, V.; Goto, K.; Miyahara, Y.; Kovac, B.; Klasinc, L. *Chem. Phys.* **2002**, 277, 229. (c) Vatsadze, Sergey Z.; Krut'ko, Dmitry P.; Zyk, Nikolai V.; Zefirov, Nikolai S.; Churakov, Andrei V.; Howard, Judith A. *Mendeleev Commun.* **1999**, 3, 5248.
- (61) The most facile synthesis of a successful sparteine mimic has been synthesized in 3 steps from natural product. For a reference, see: Dearden, M. J.; Firkin, C. R.; Hermet, J.-P. R.; O'Brien, P. *J. Am. Chem. Soc.* **2002** 124, 11870.
- (62) Nielsen, R. J.; Keith, J. M.; Stoltz, B. M.; Goddard, W. A. *J. Am. Chem. Soc.* **2004**, 126, 7967.
- (63) When the resolution is conducted with an effectively smaller X-type ligand, such as Pd^{II}(sp)OAc, a reduced selectivity is observed in the OKR.
- (64) Trend, R. M.; Stoltz, B. M. *J. Am. Chem. Soc.* **2004**, 126, 4482.
- (65) (a) Bryndza, H. E.; Tam, W. *Chem. Rev.* **1988**, 88, 1163. (b) Zhao, J.; Hesslink, H.; Hartwig, J. F. *J. Am. Chem. Soc.* **1986**, 108, 4805. (c) For an alternative with Pt, see: Bryndza, H. E.; Calabrese, J. C.; Marsi, M.; Roe, D. C.; Tam, W.; Bercaw, J. E. *J. Am. Chem. Soc.* **1986**, 108, 4805.
- (66) Perrin, D. D.; Armarego, W. L. F. *Purification of Laboratory Chemicals*; 3rd ed., Pergamon Press, Oxford, 1988.
- (67) Still, W. C.; Kahn, M.; Mitra, A. J. *J. Org. Chem.* **1978**, 43, 2923.

APPENDIX TWO

Spectra Relevant to Chapter 2:

Development and Application of the Oxidative Kinetic Resolution of 2°-Alcohols by Catalytic Palladium

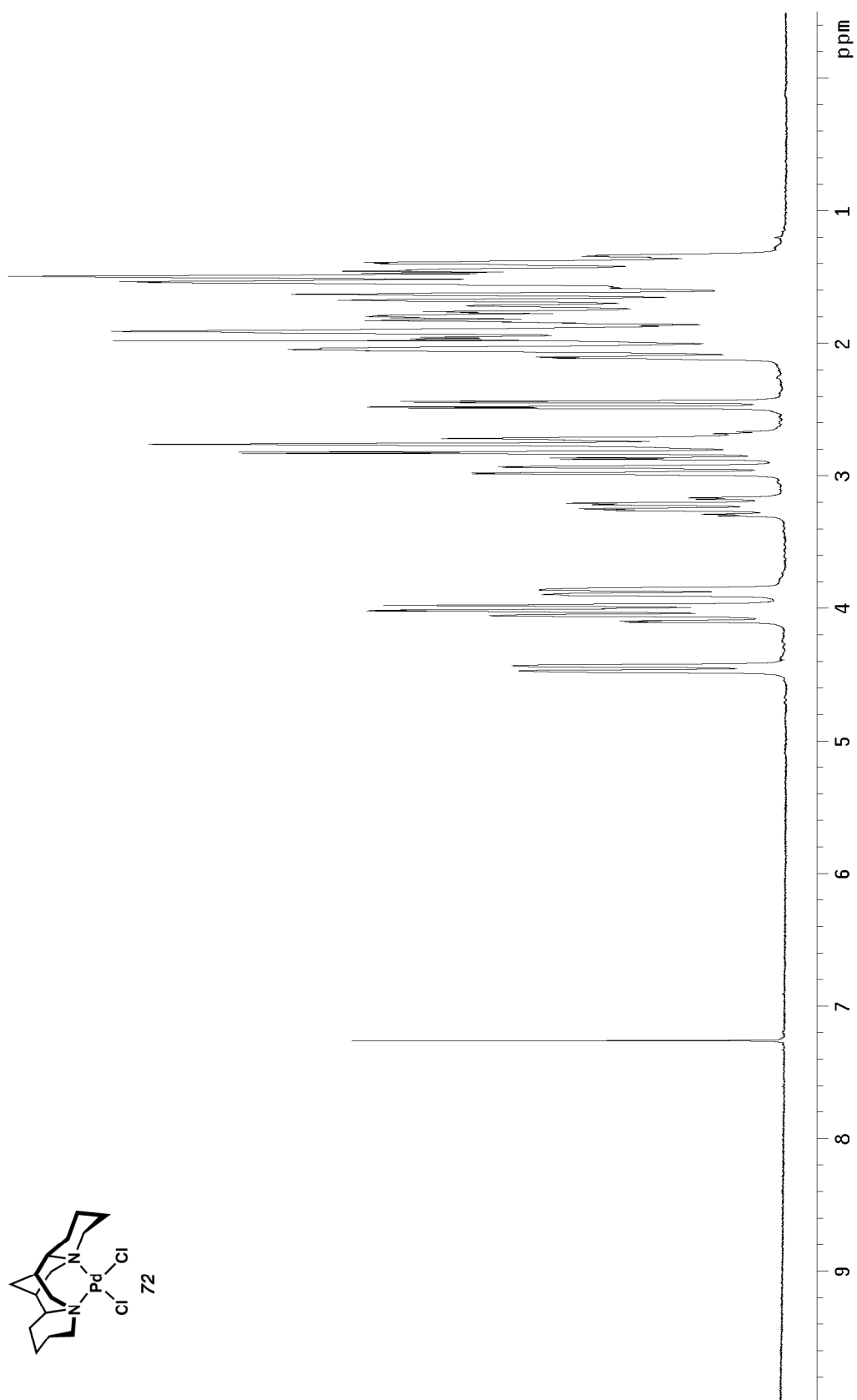


Figure A2.1 ^1H NMR (300 MHz, CDCl_3) of compound 72.

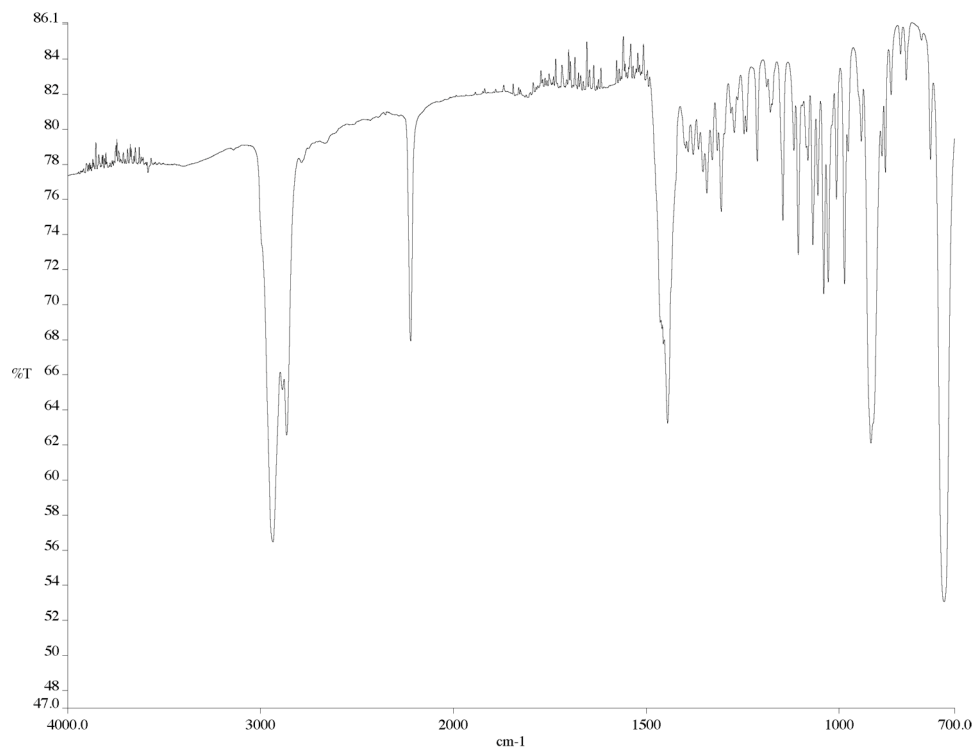


Figure A2.2 Infrared spectrum (thin film/NaCl) of compound **72**.

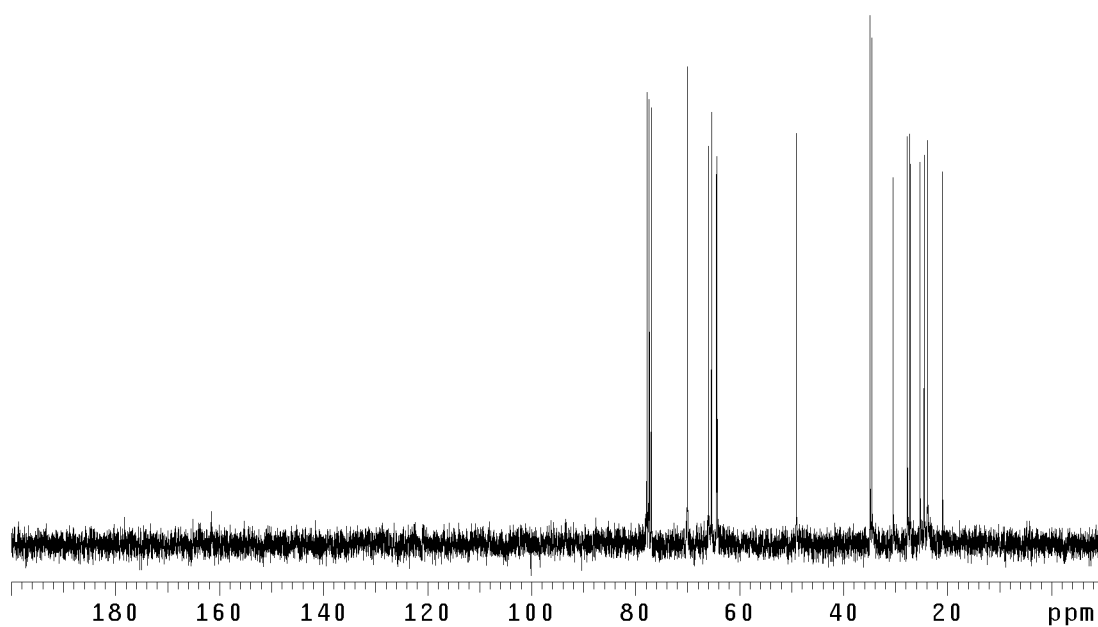


Figure A2.3 ¹³CNMR (125 MHz, CDCl₃) of compound **72**.

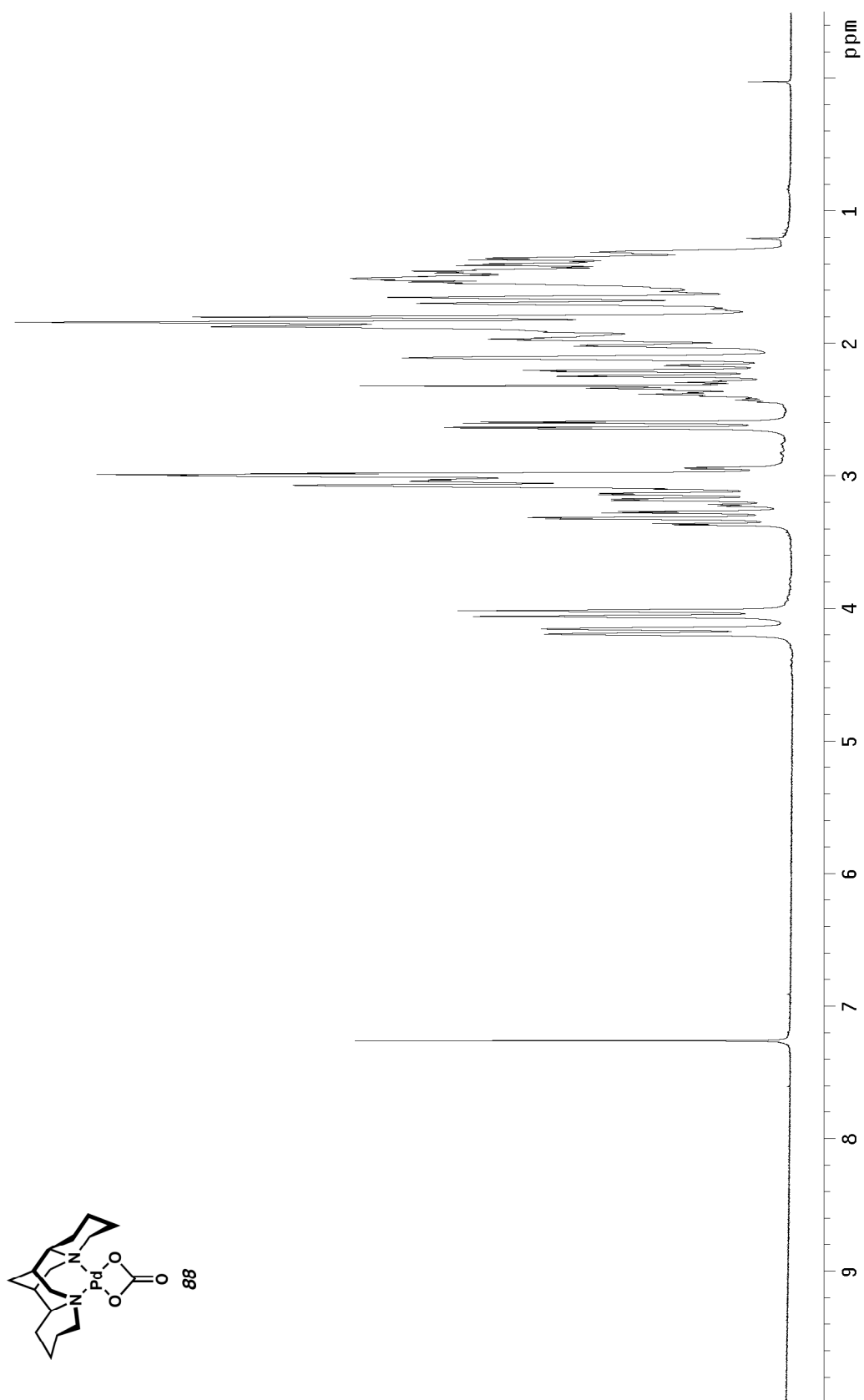


Figure A2.4 ^1H NMR (300 MHz, CDCl_3) of compound **88**.

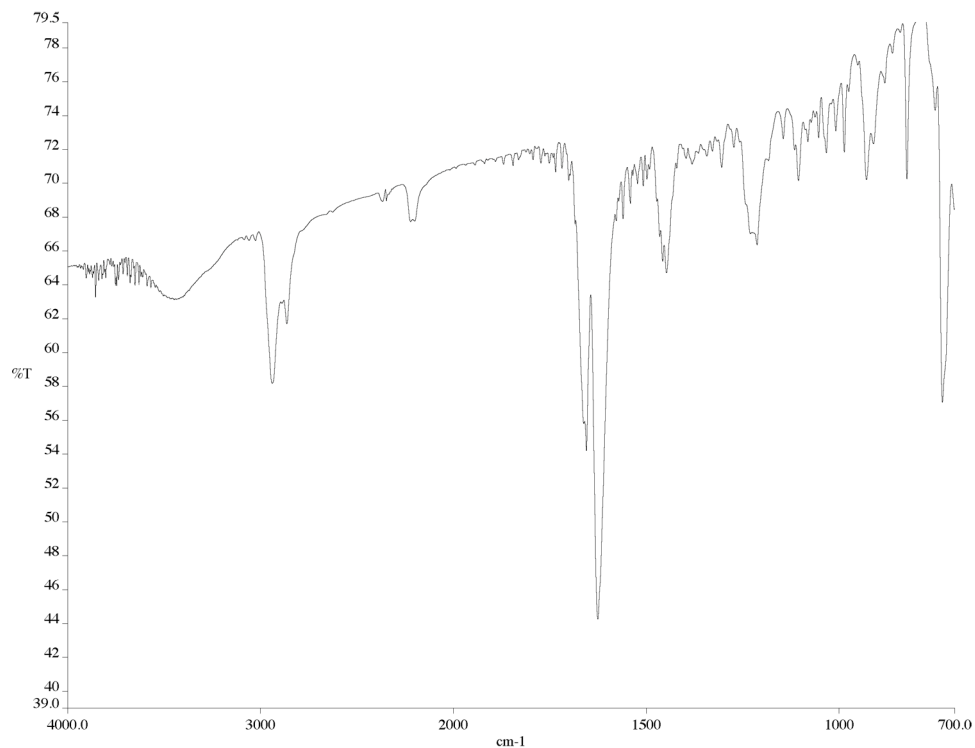


Figure A2.5 Infrared spectrum (thin film/NaCl) of compound **88**.

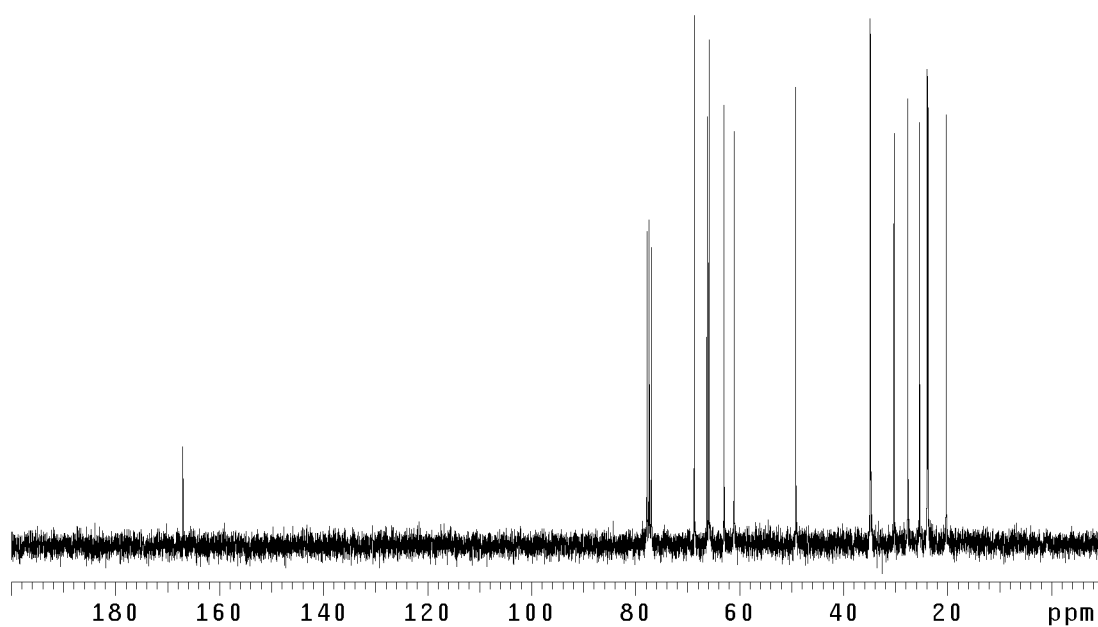


Figure A2.6 ¹³CNMR (125 MHz, CDCl₃) of compound **88**.

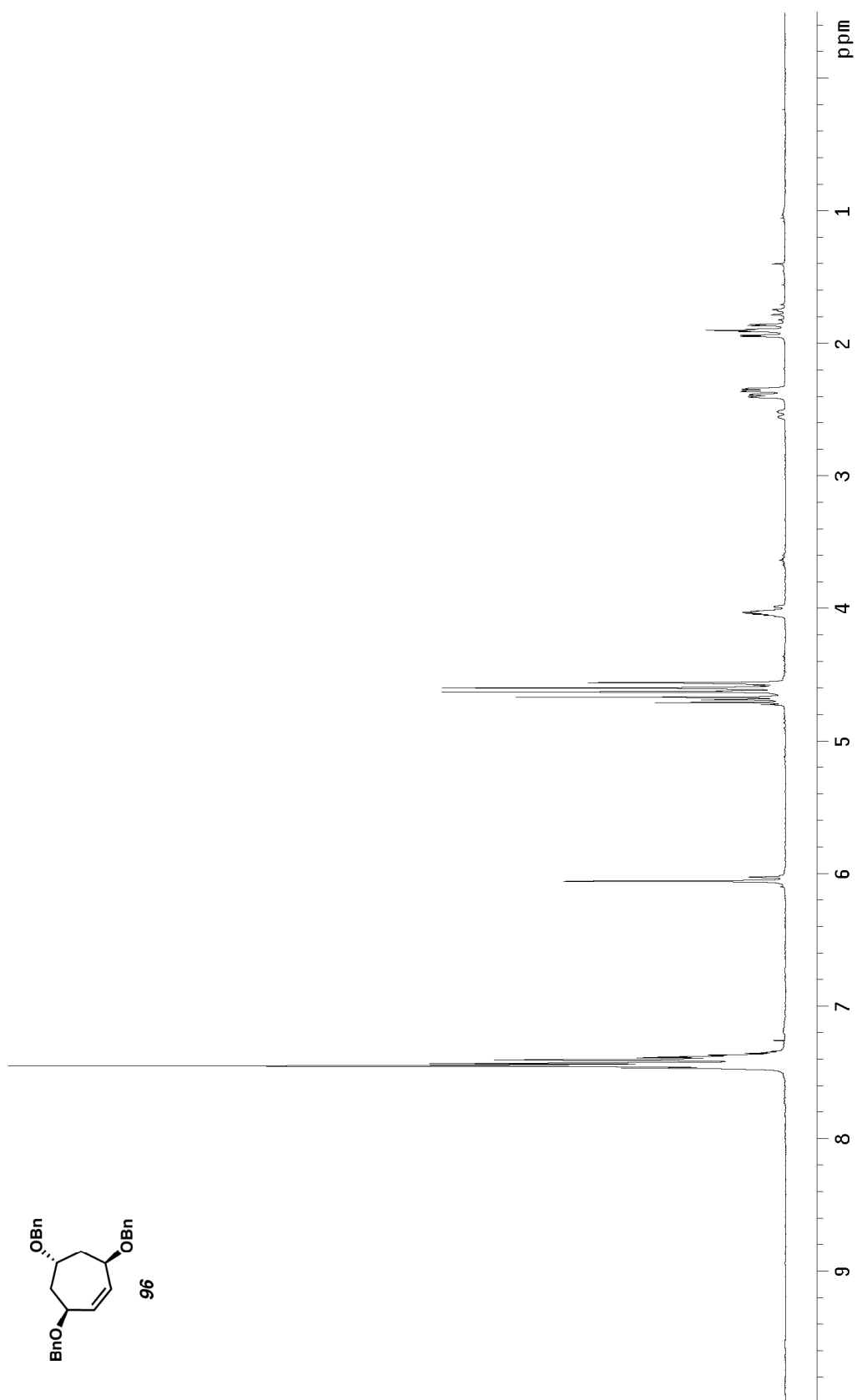


Figure A2.7 ^1H NMR (300 MHz, CDCl_3) of compound **96**.

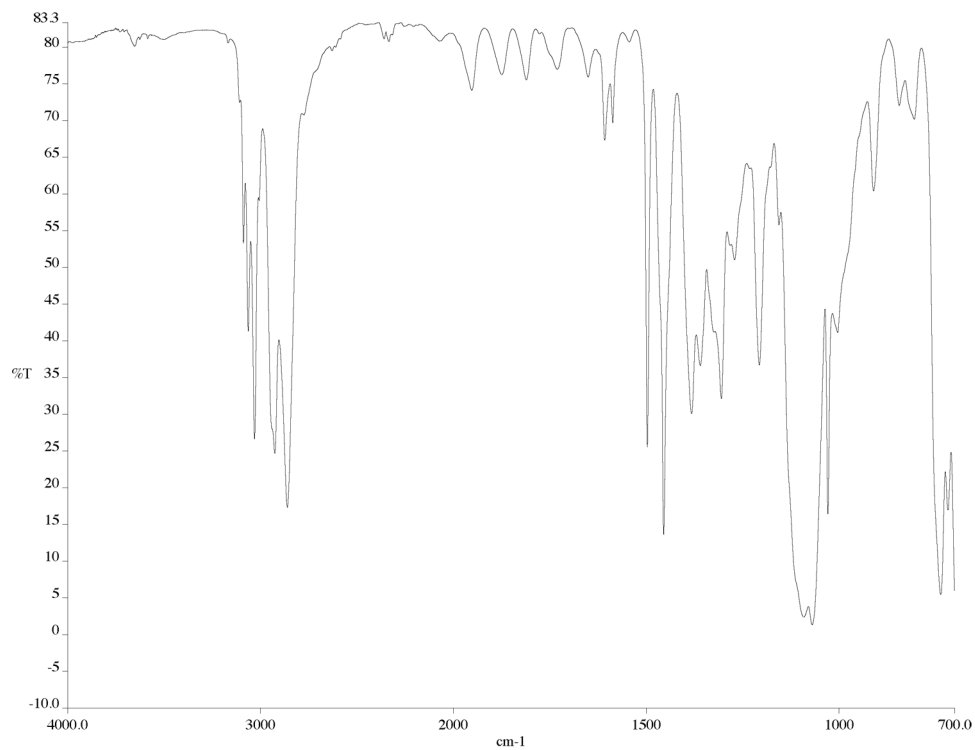


Figure A2.8 Infrared spectrum (thin film/NaCl) of compound **96**.

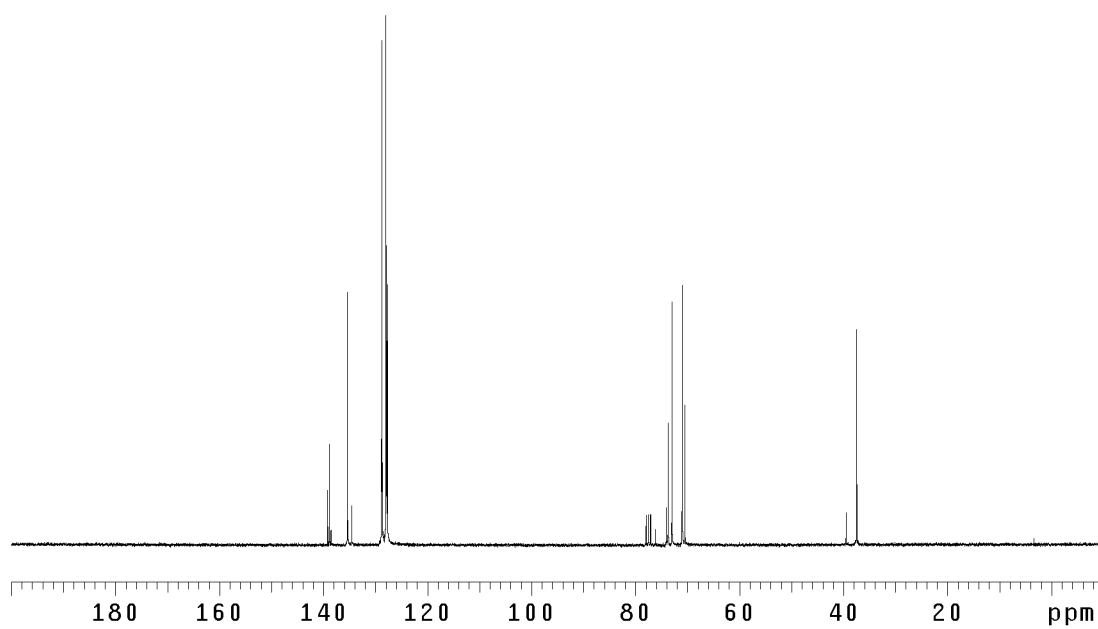


Figure A2.9 ¹³CNMR (125 MHz, CDCl₃) of compound **96**.

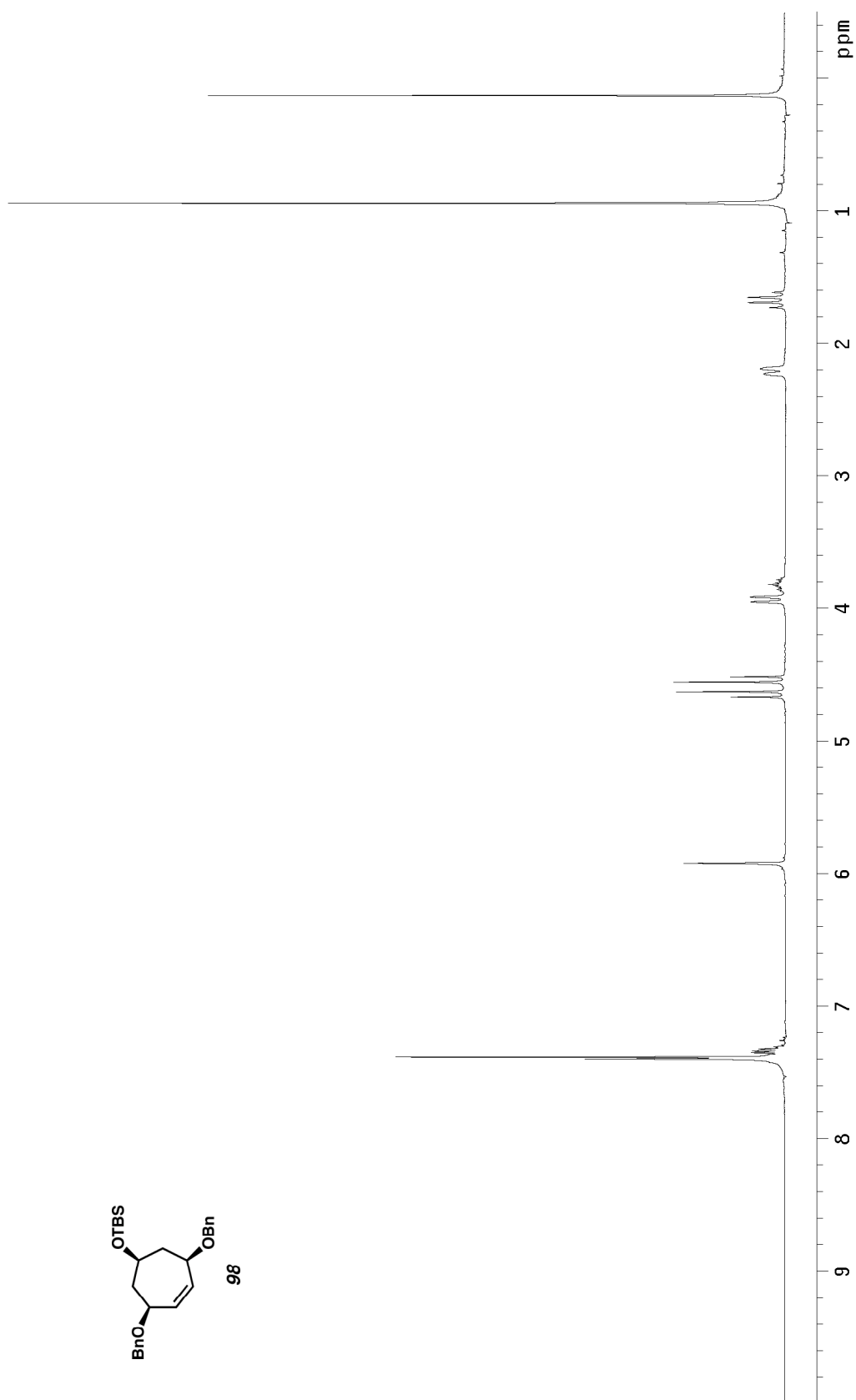
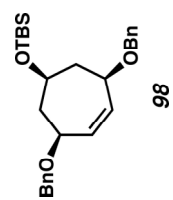


Figure A2.10 ^1H NMR (300 MHz, CDCl_3) of compound **98**.

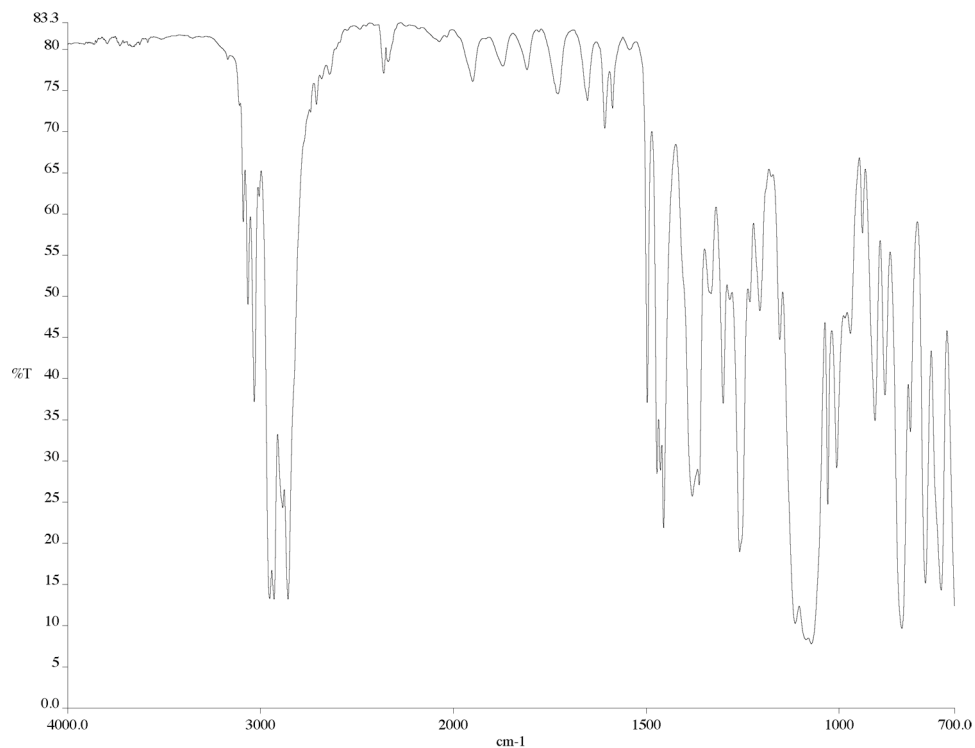


Figure A2.11 Infrared spectrum (thin film/NaCl) of compound **98**.

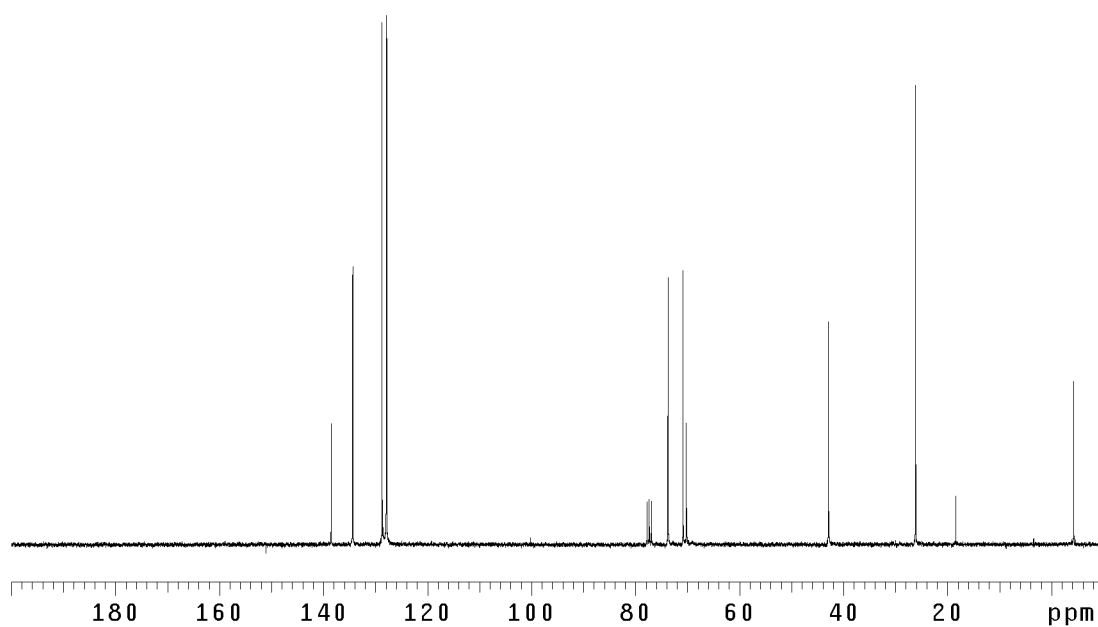


Figure A2.12 ¹³CNMR (125 MHz, CDCl₃) of compound **98**.

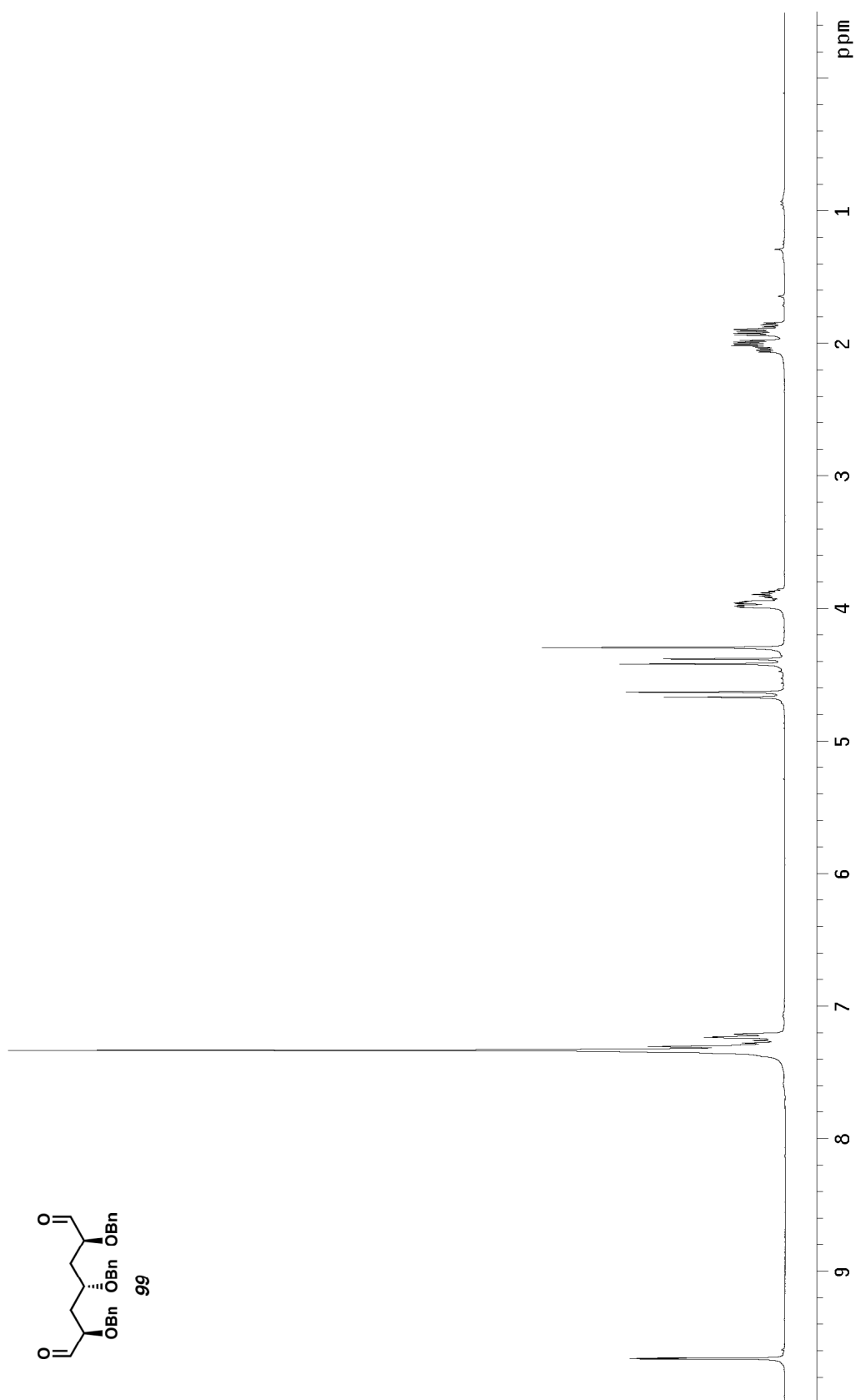


Figure A2.13 ^1H NMR (300 MHz, CDCl_3) of compound **99**.

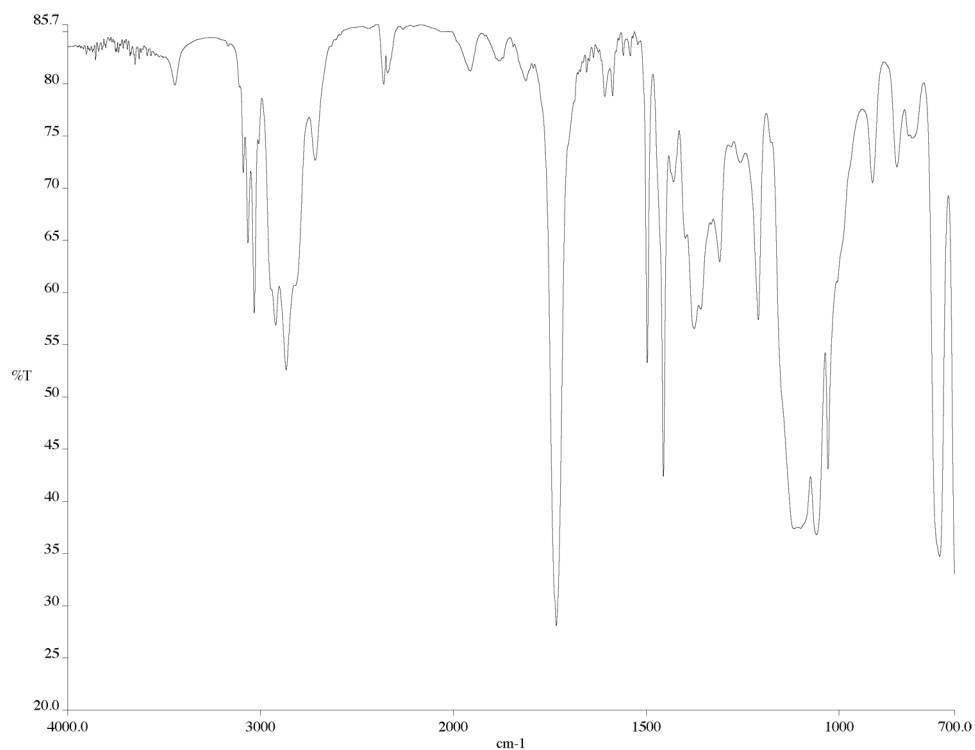


Figure A2.14 Infrared spectrum (thin film/NaCl) of compound **99**.

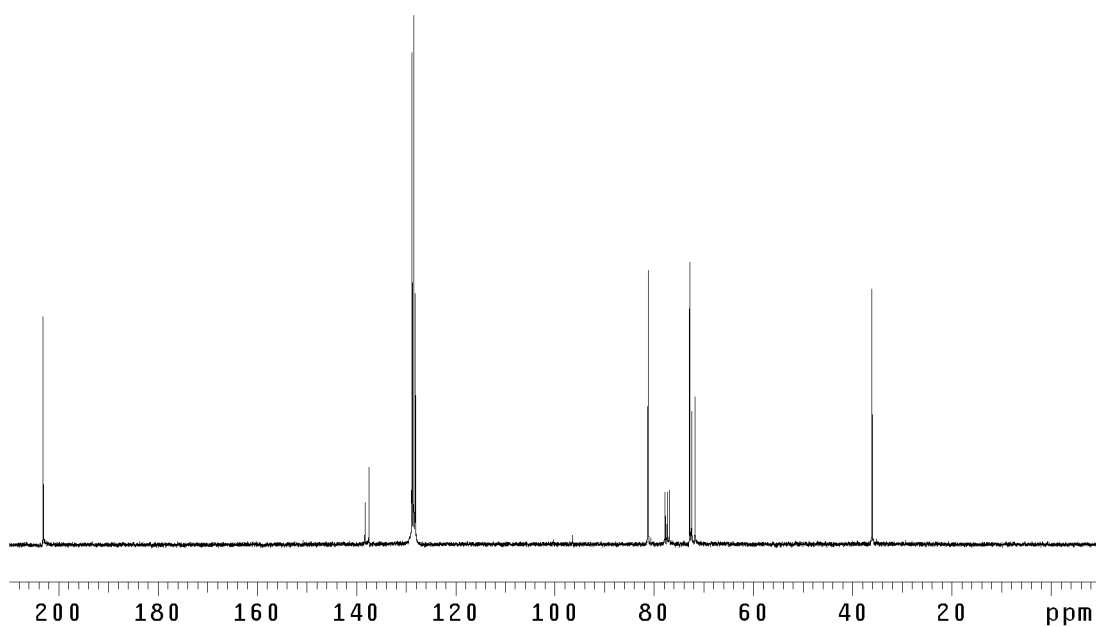


Figure A2.15 ¹³CNMR (125 MHz, CDCl₃) of compound **99**.

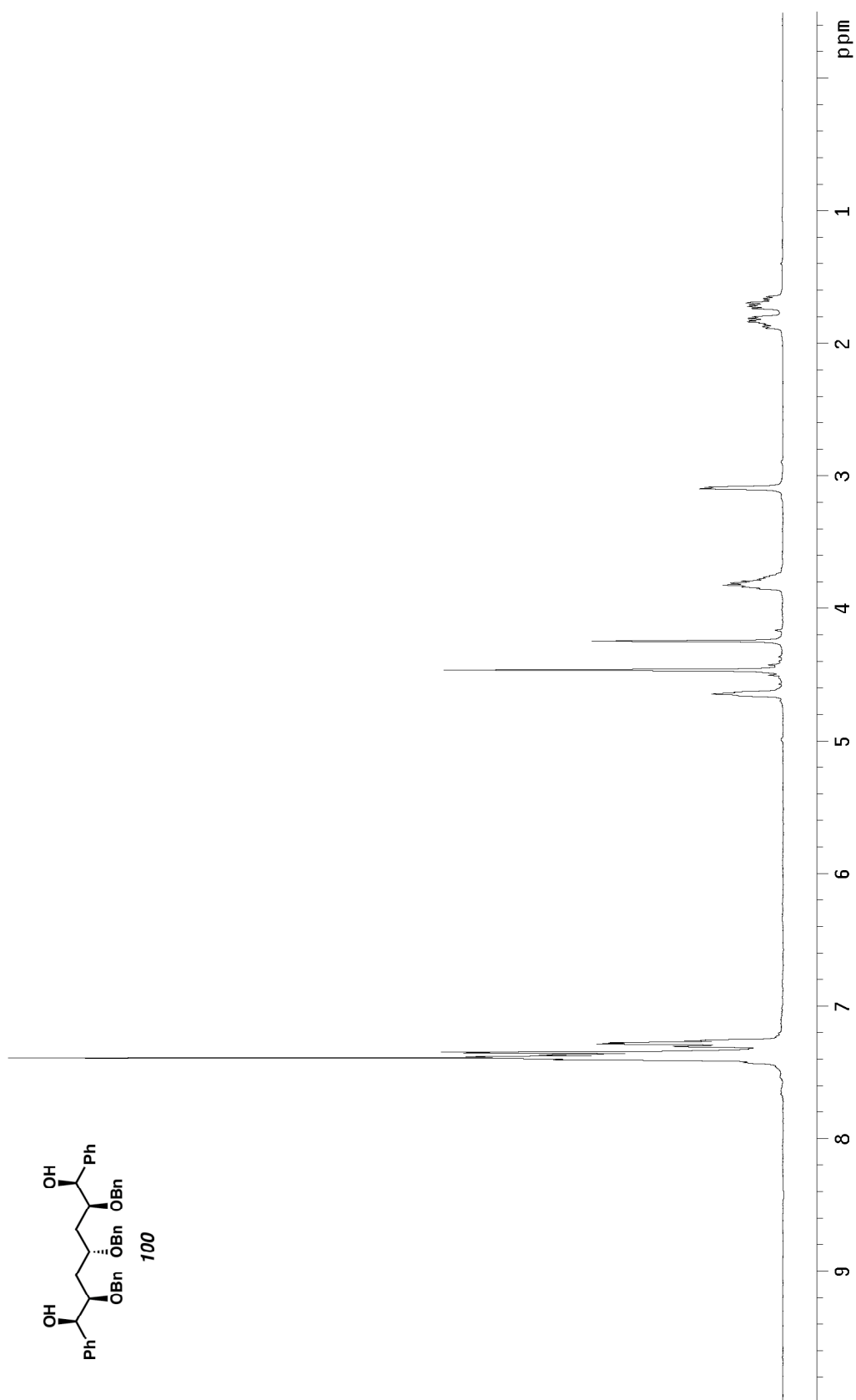


Figure A2.16 ^1H NMR (300 MHz, CDCl_3) of compound **100**.

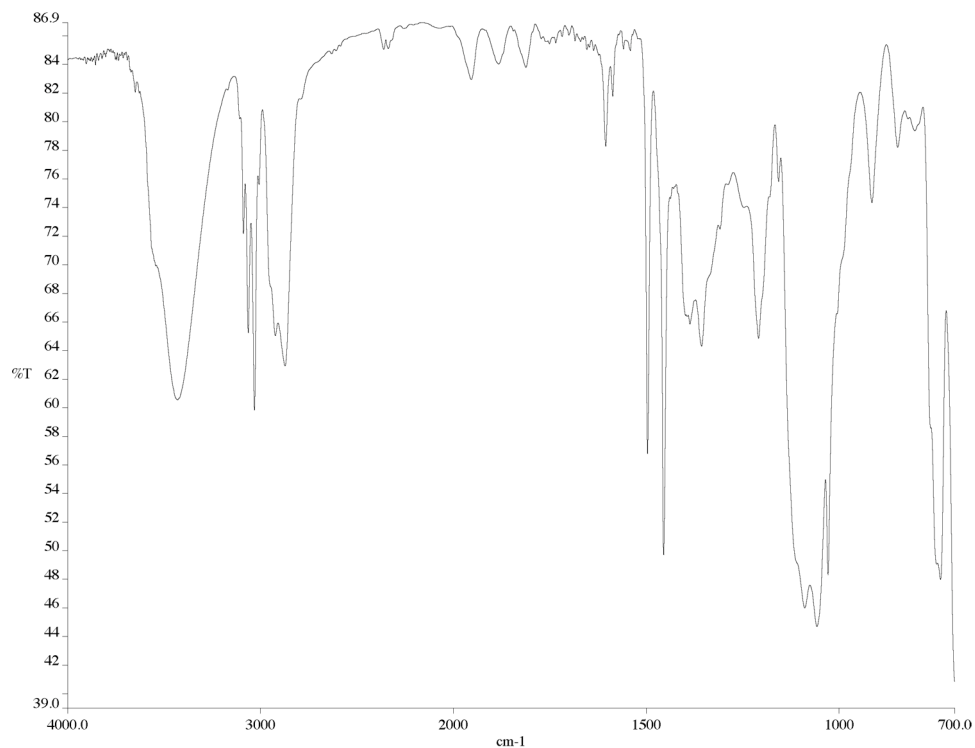


Figure A2.17 Infrared spectrum (thin film/NaCl) of compound **100**.

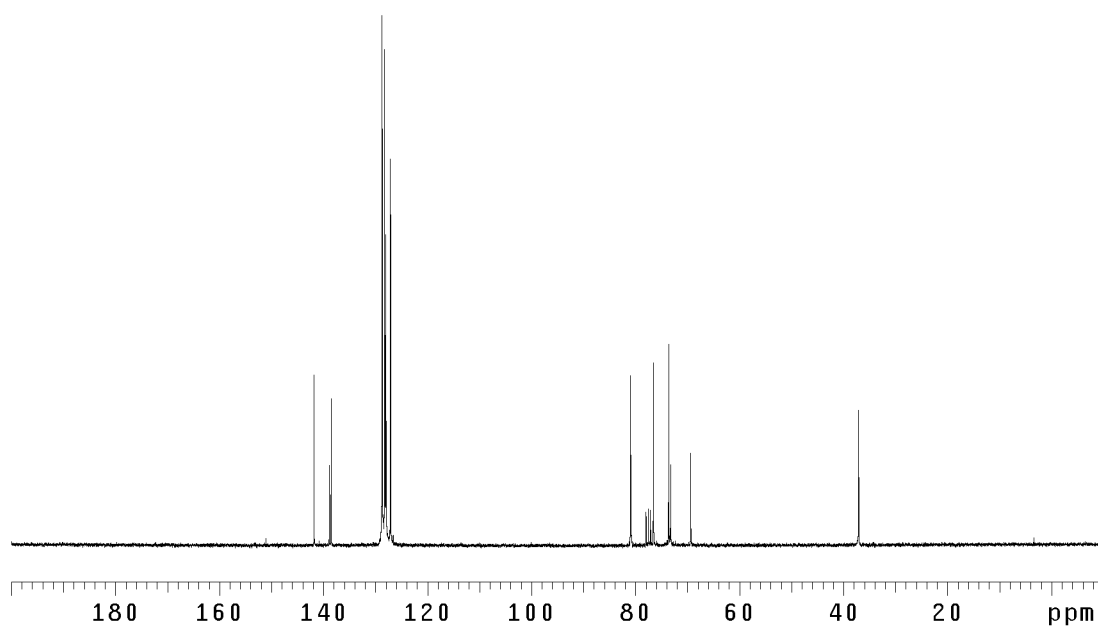


Figure A2.18 ¹³CNMR (125 MHz, CDCl₃) of compound **100**.

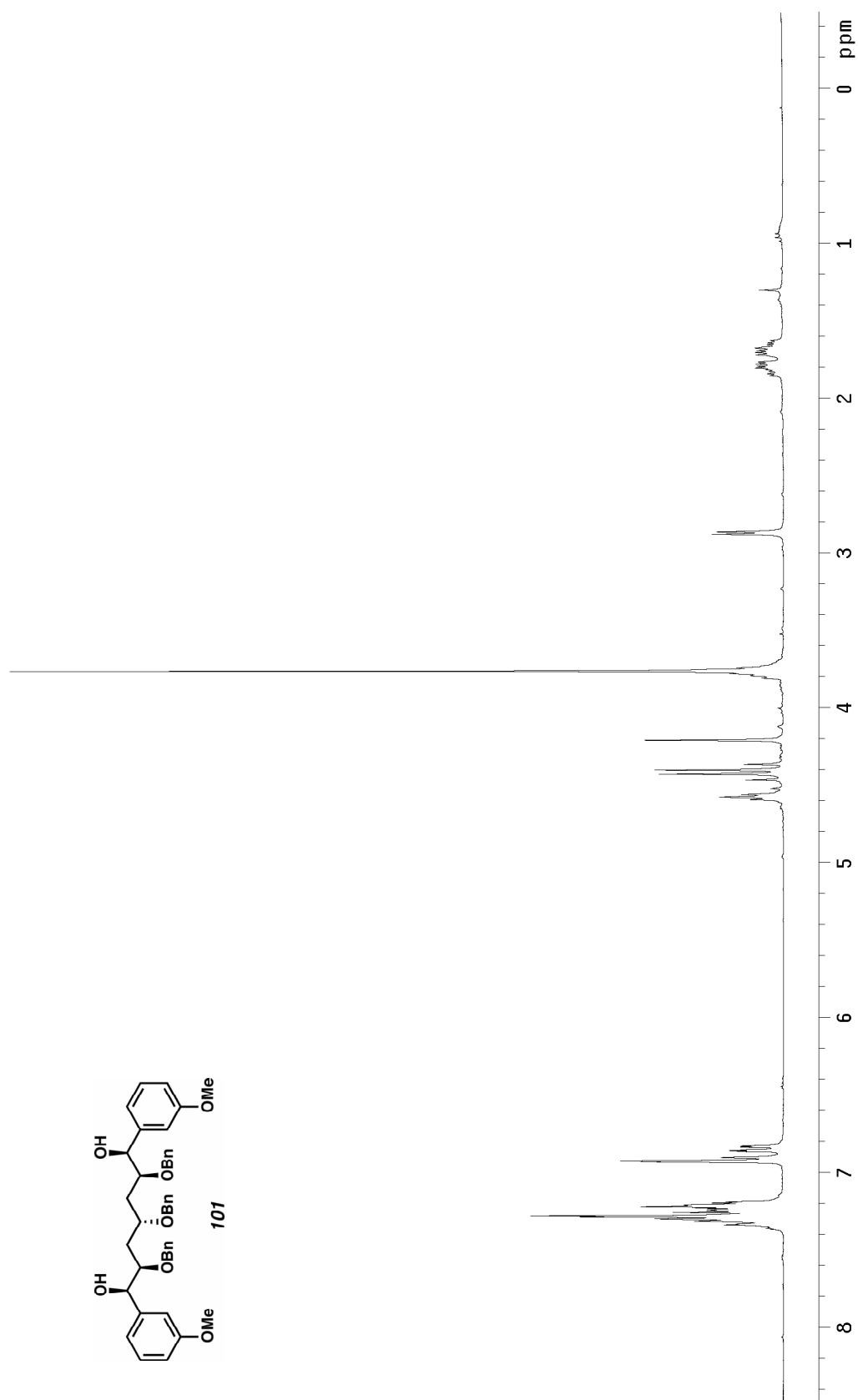


Figure A2.19 ^1H NMR (300 MHz, CDCl_3) of compound **101**.

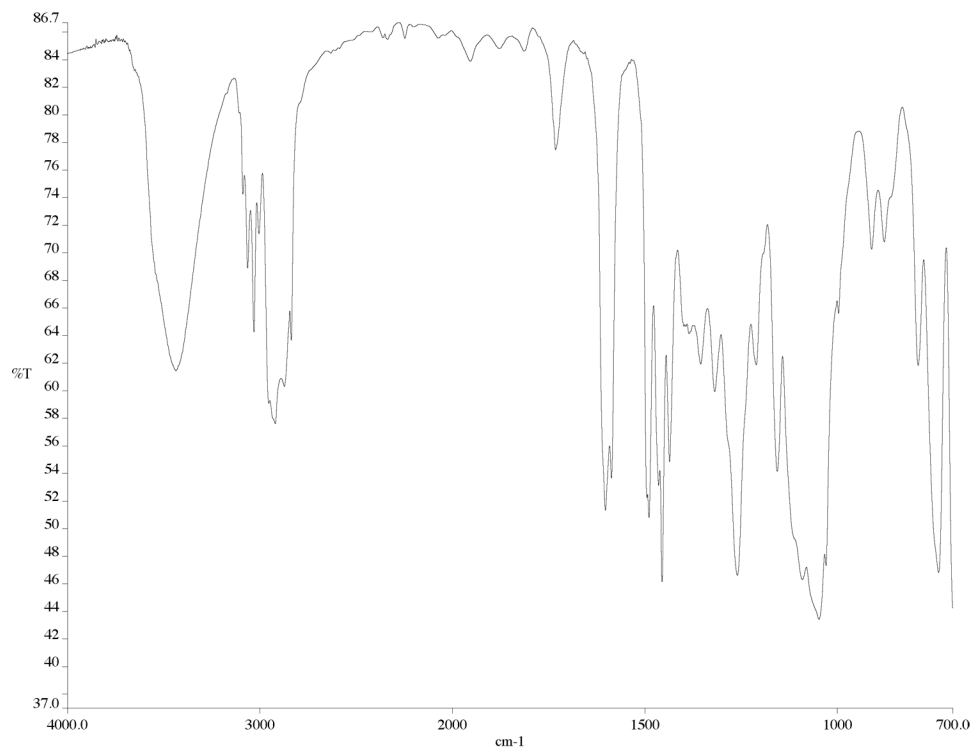


Figure A2.20 Infrared spectrum (thin film/NaCl) of compound **101**.

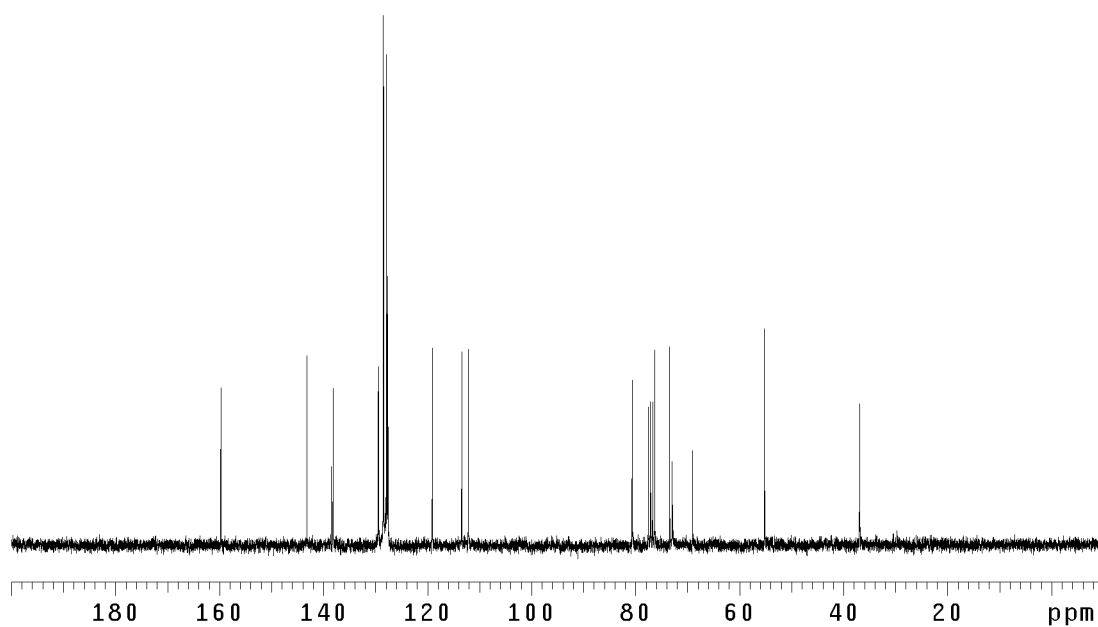


Figure A2.21 ¹³CNMR (125 MHz, CDCl₃) of compound **101**.

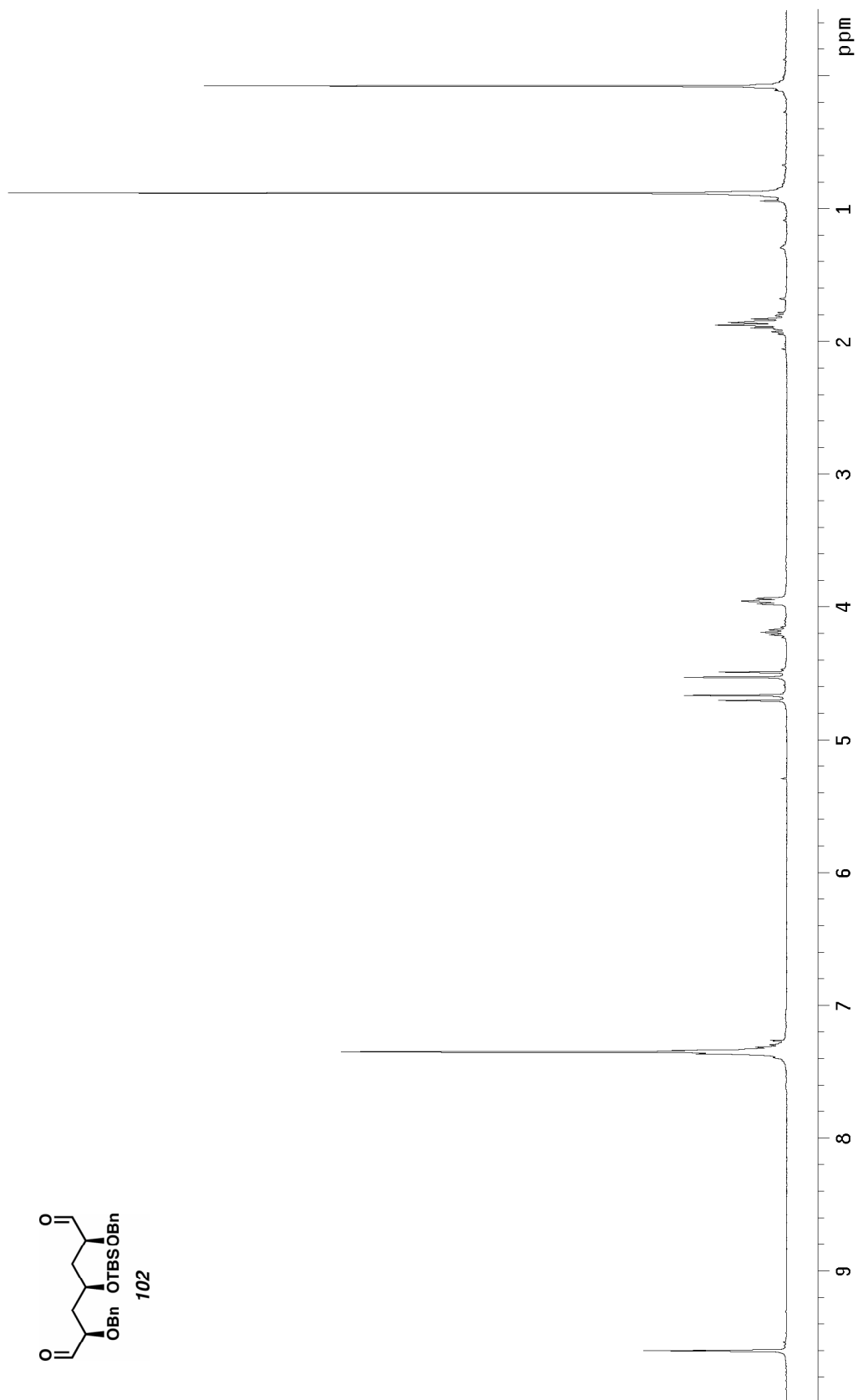
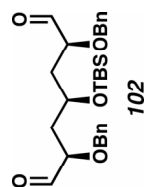


Figure A2.22 ¹H NMR (300 MHz, CDCl₃) of compound **102**.

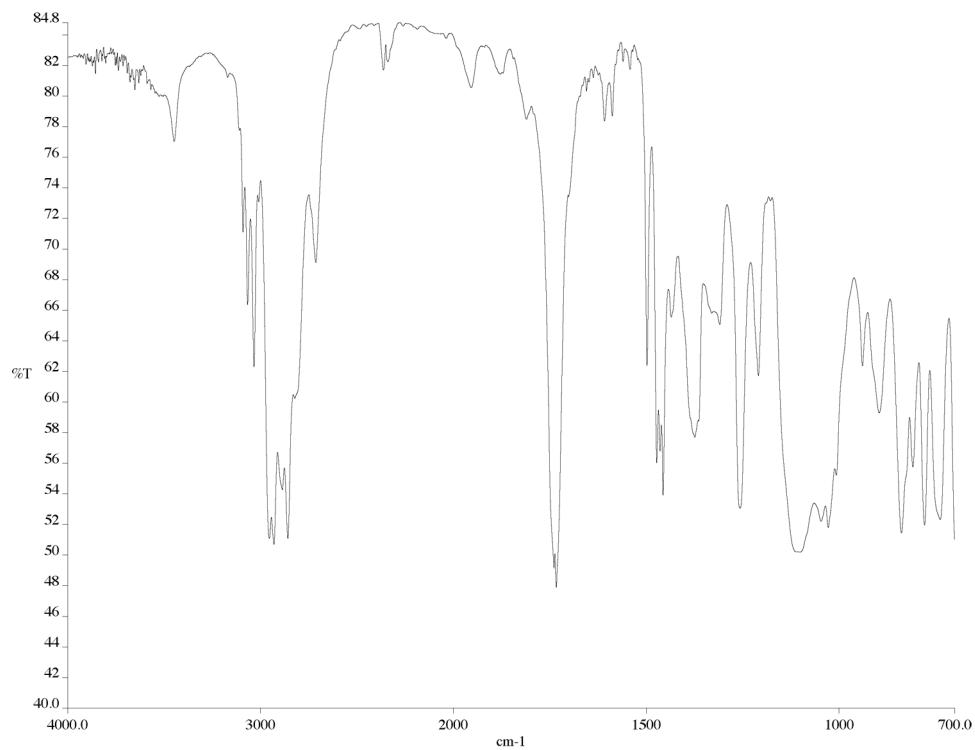


Figure A2.23 Infrared spectrum (thin film/NaCl) of compound **102**.

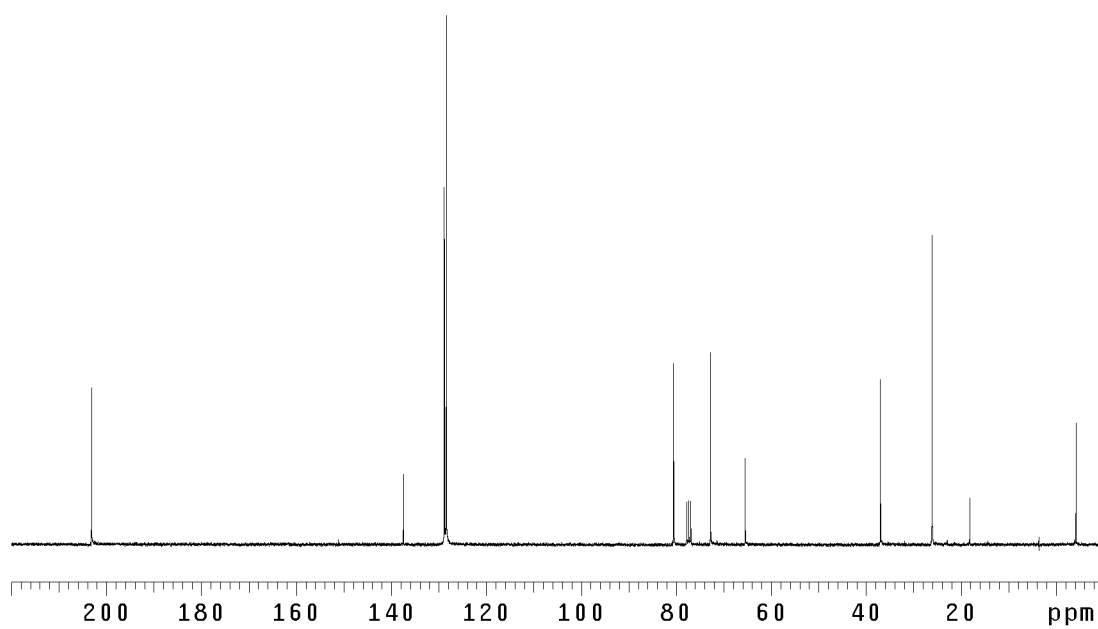
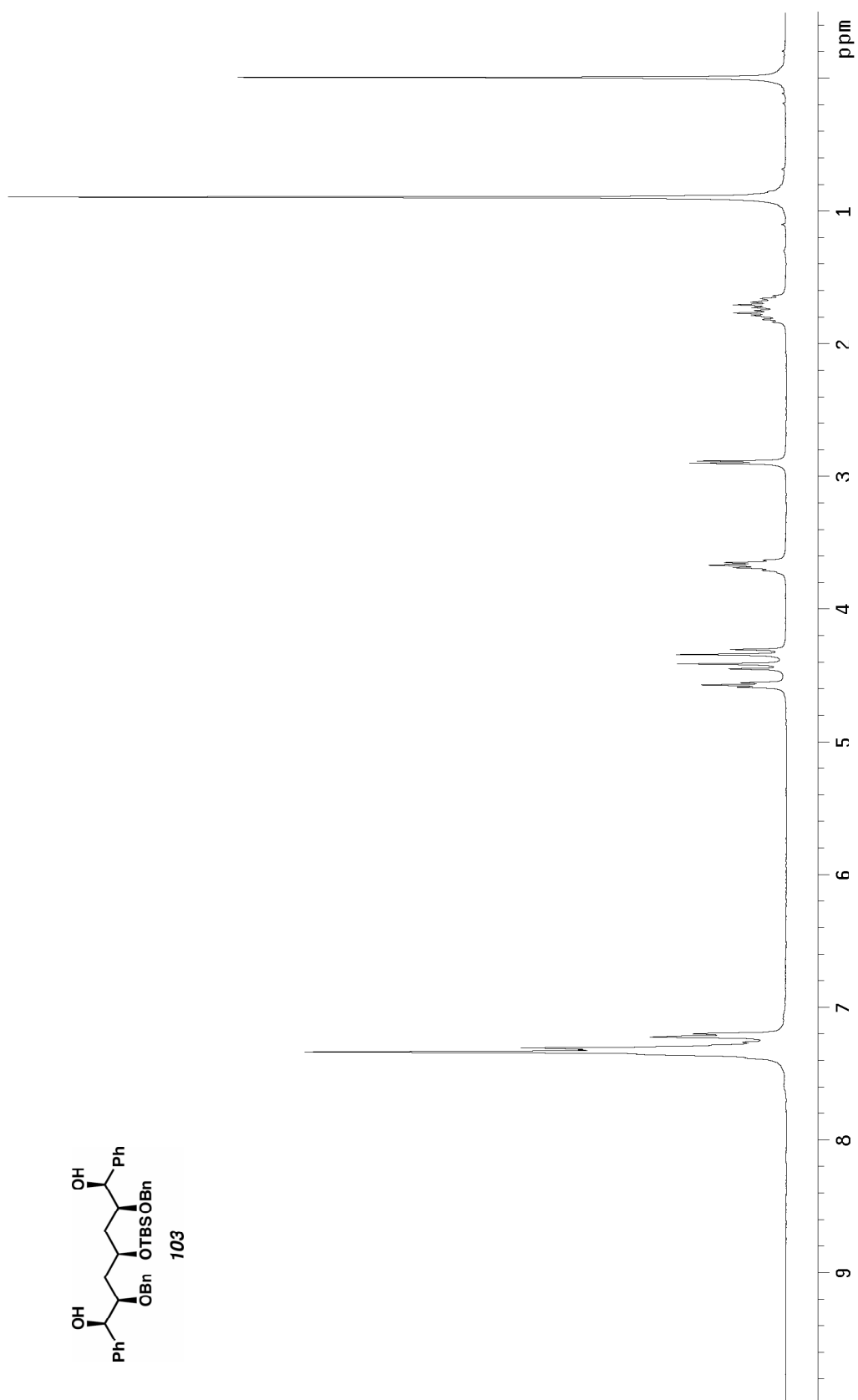


Figure A2.24 ¹³CNMR (125 MHz, CDCl₃) of compound **102**.



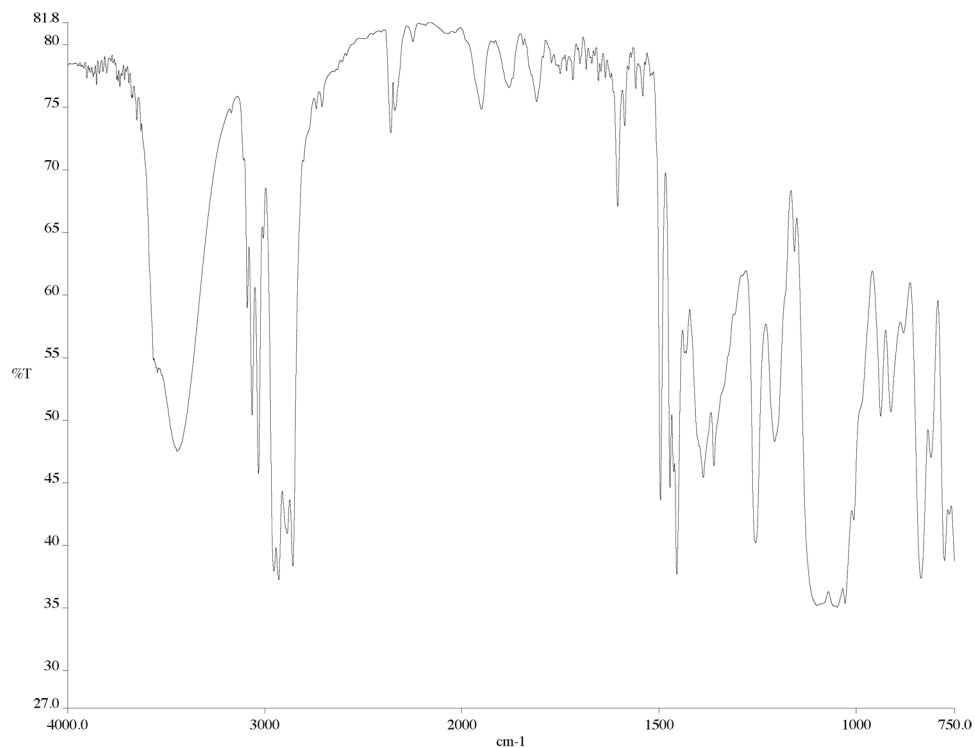


Figure A2.26 Infrared spectrum (thin film/NaCl) of compound **103**.

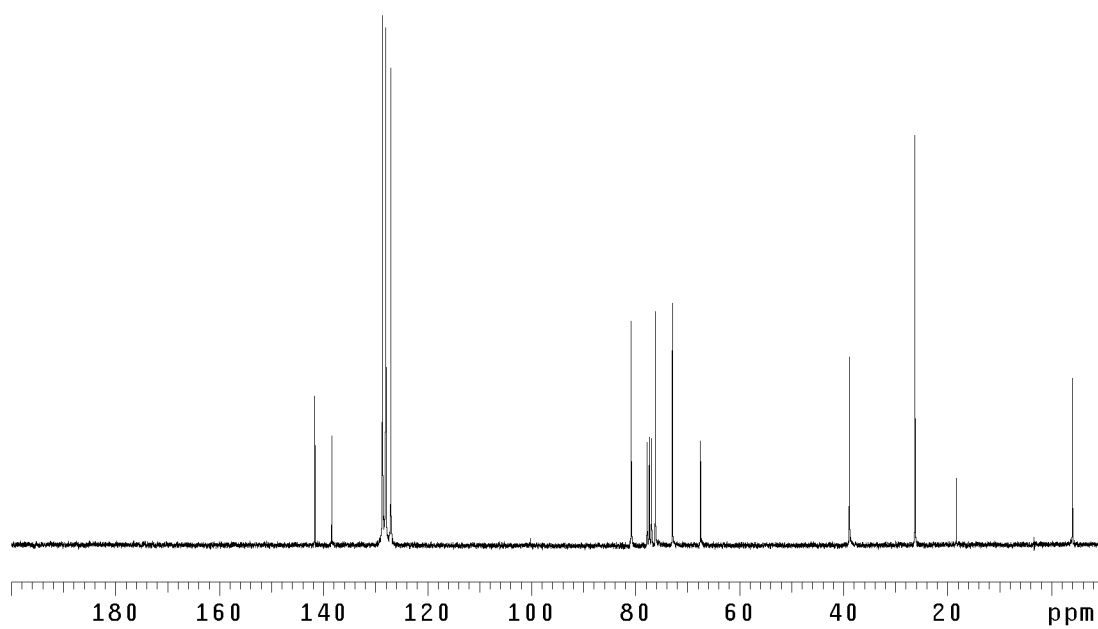


Figure A2.27 ¹³CNMR (125 MHz, CDCl₃) of compound **103**.

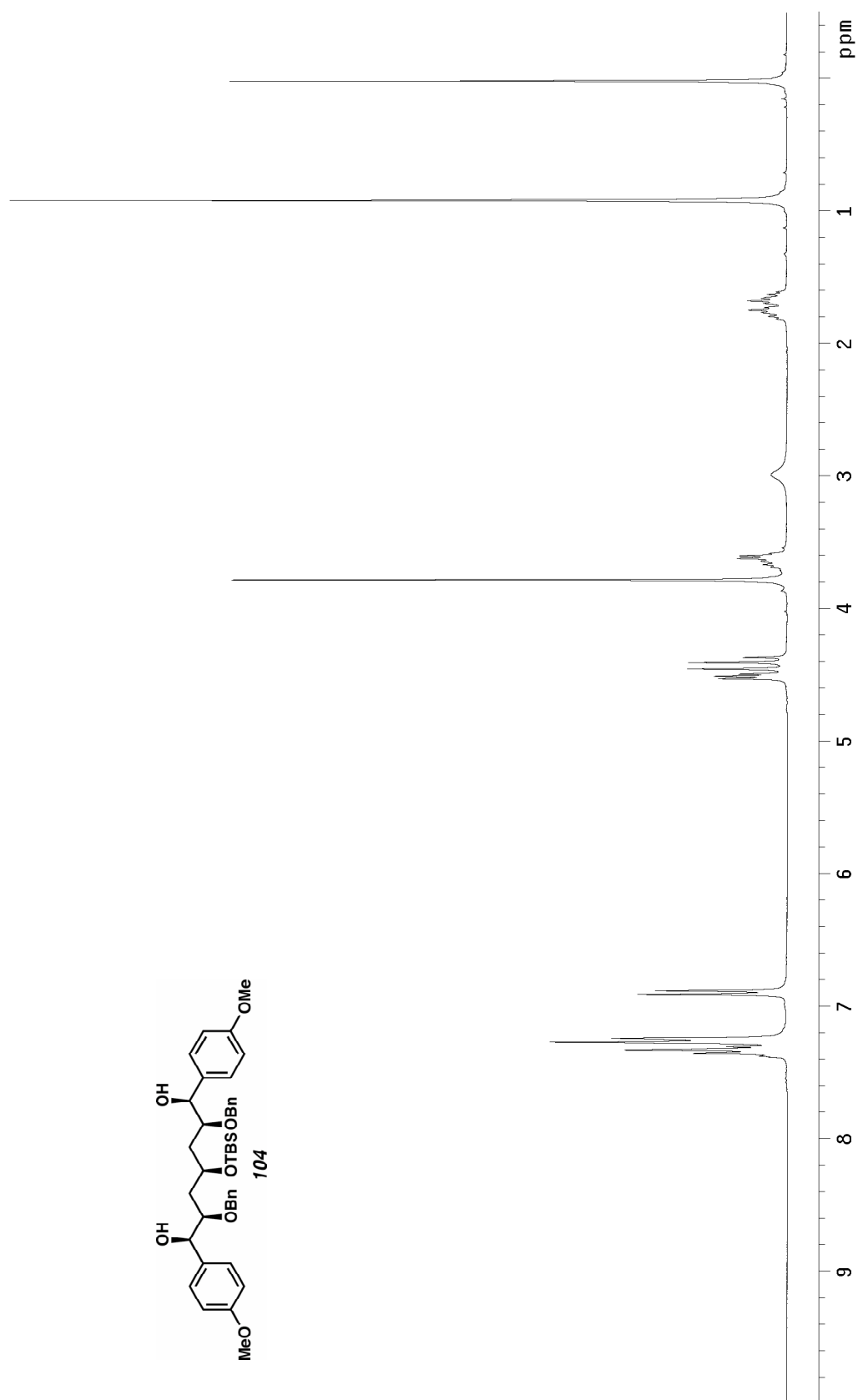


Figure A2.28 ^1H NMR (300 MHz, CDCl_3) of compound **104**.

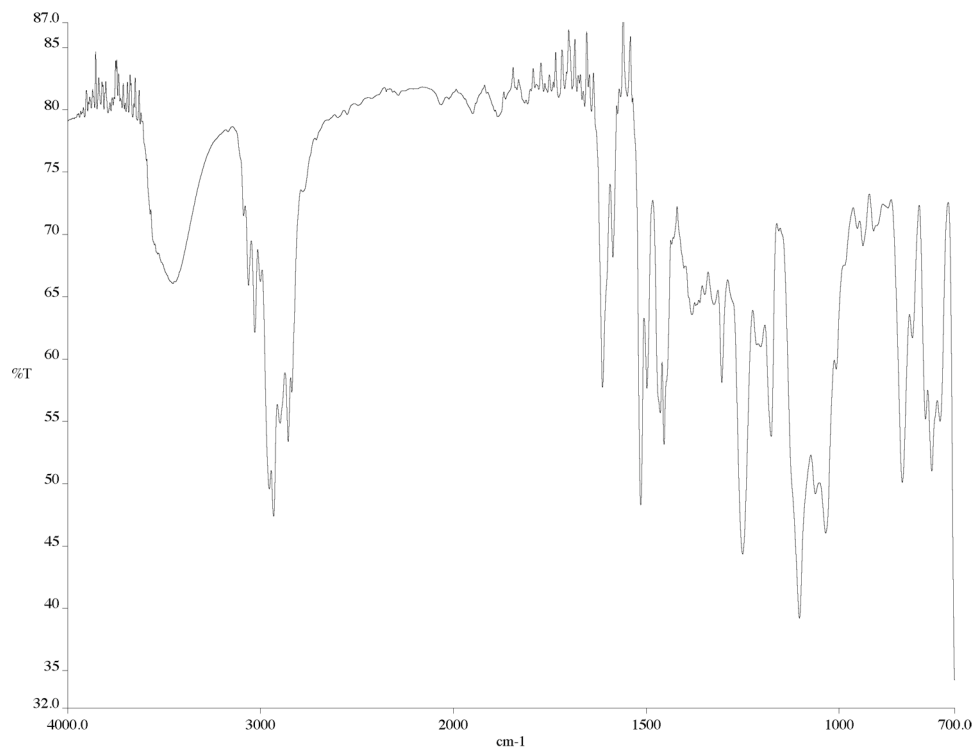


Figure A2.29 Infrared spectrum (thin film/NaCl) of compound **104**.

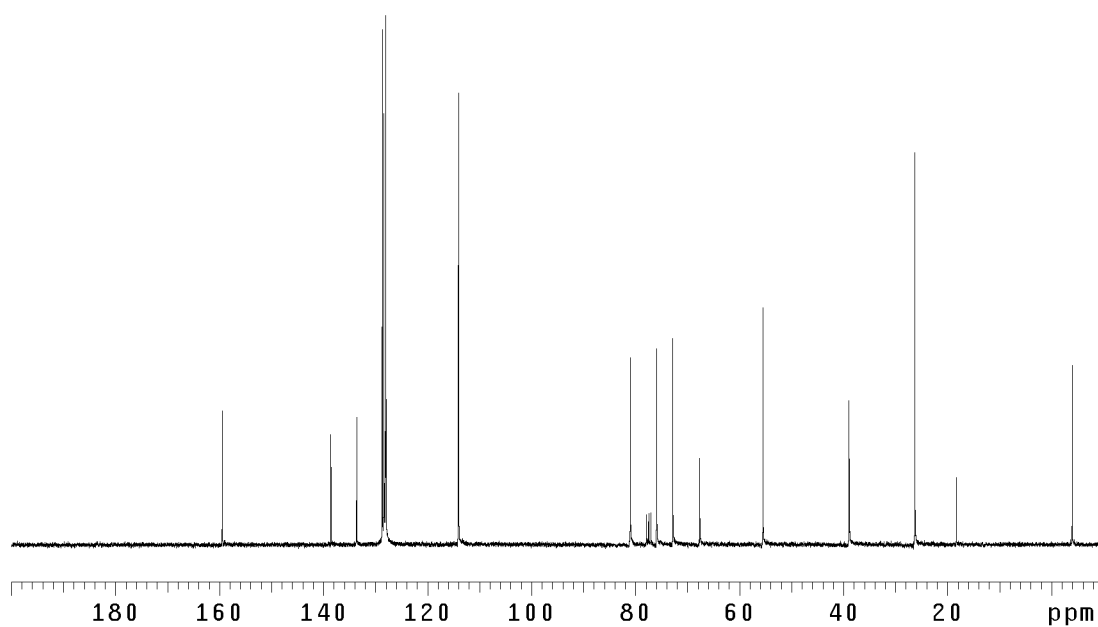


Figure A2.30 ¹³CNMR (125 MHz, CDCl₃) of compound **104**.

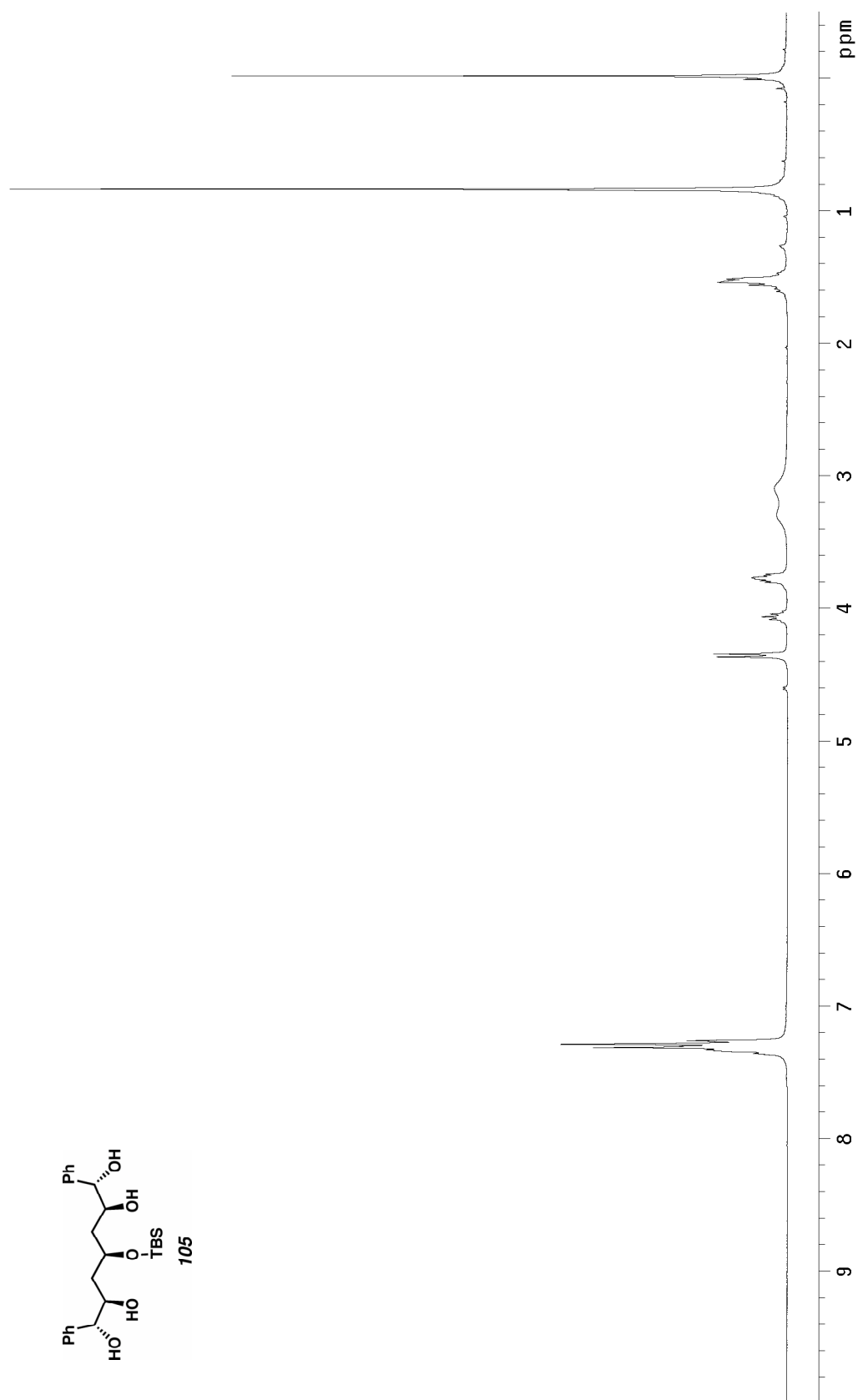


Figure A2.31 ^1H NMR (300 MHz, CDCl_3) of compound **105**.

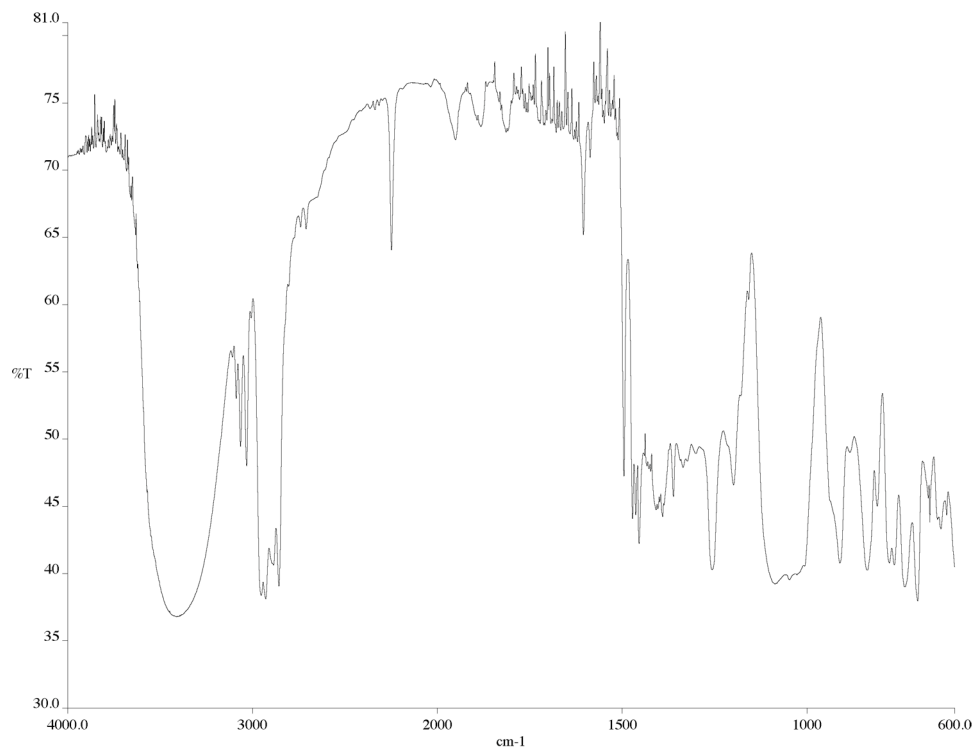


Figure A2.32 Infrared spectrum (thin film/NaCl) of compound **105**.

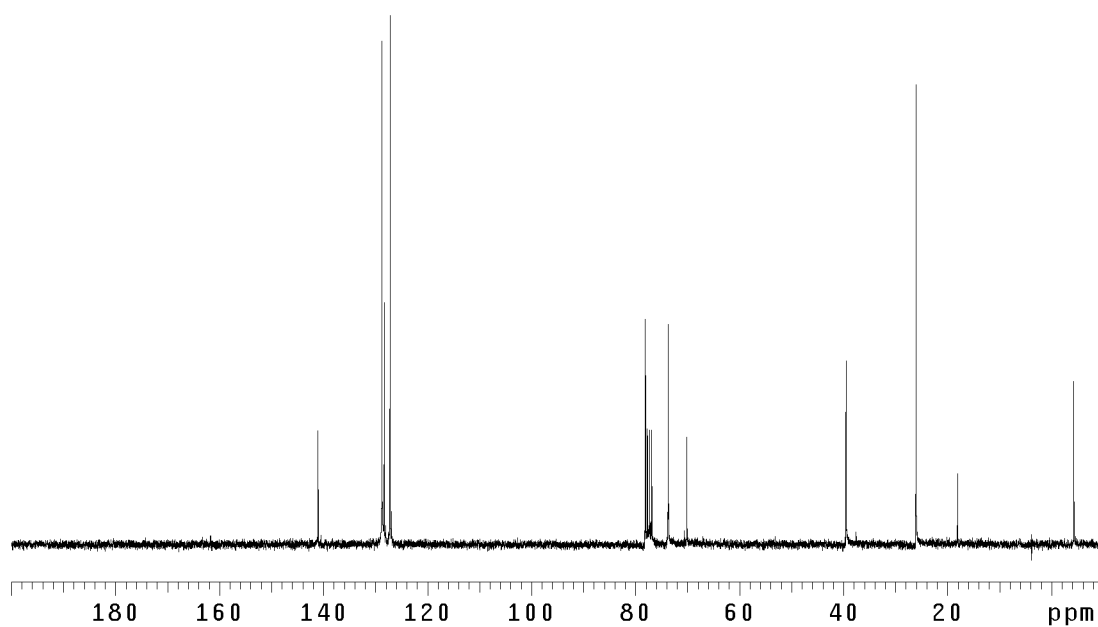


Figure A2.33 ¹³CNMR (125 MHz, CDCl₃) of compound **105**.

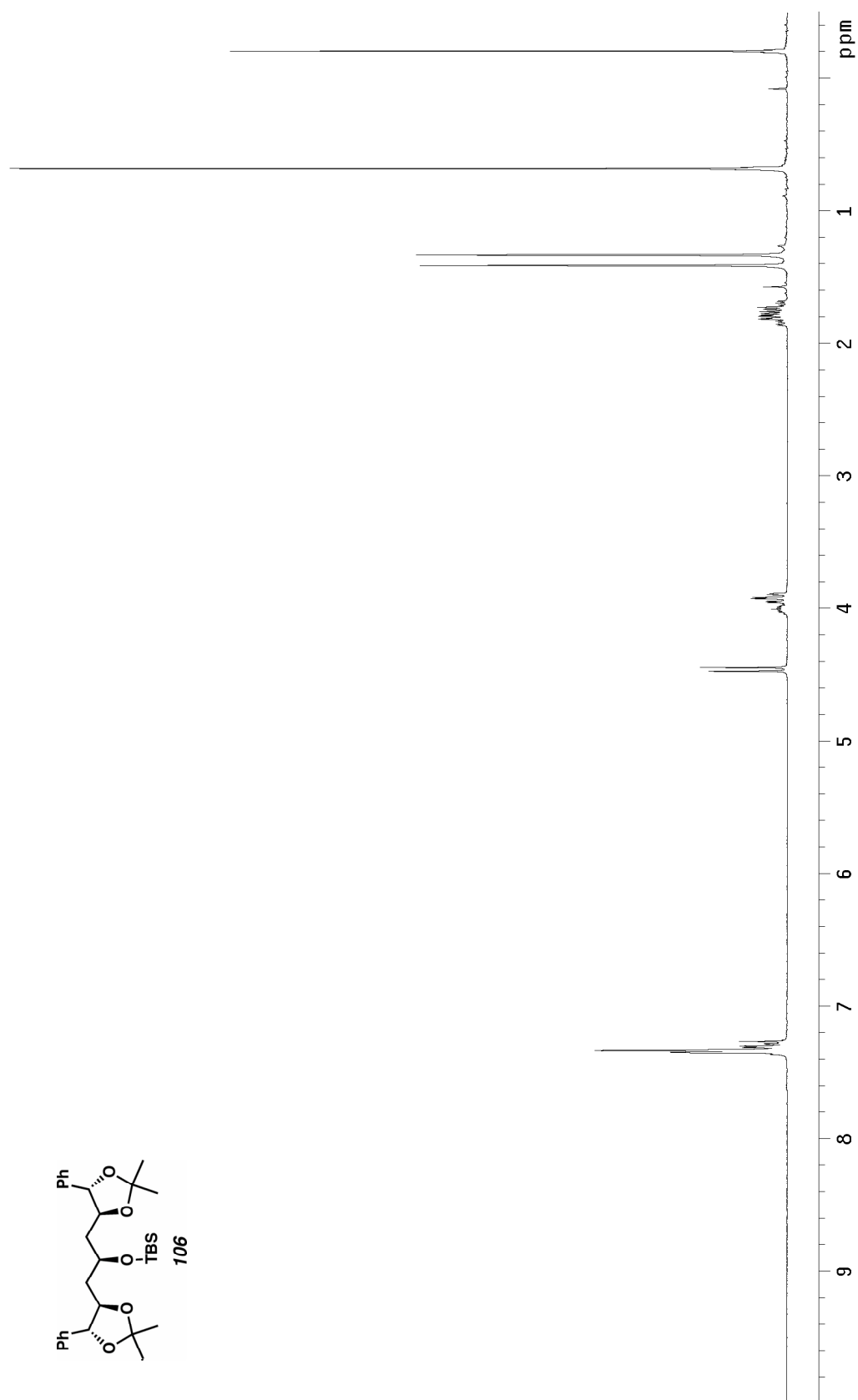


Figure A2.34 ^1H NMR (300 MHz, CDCl_3) of compound **106**.

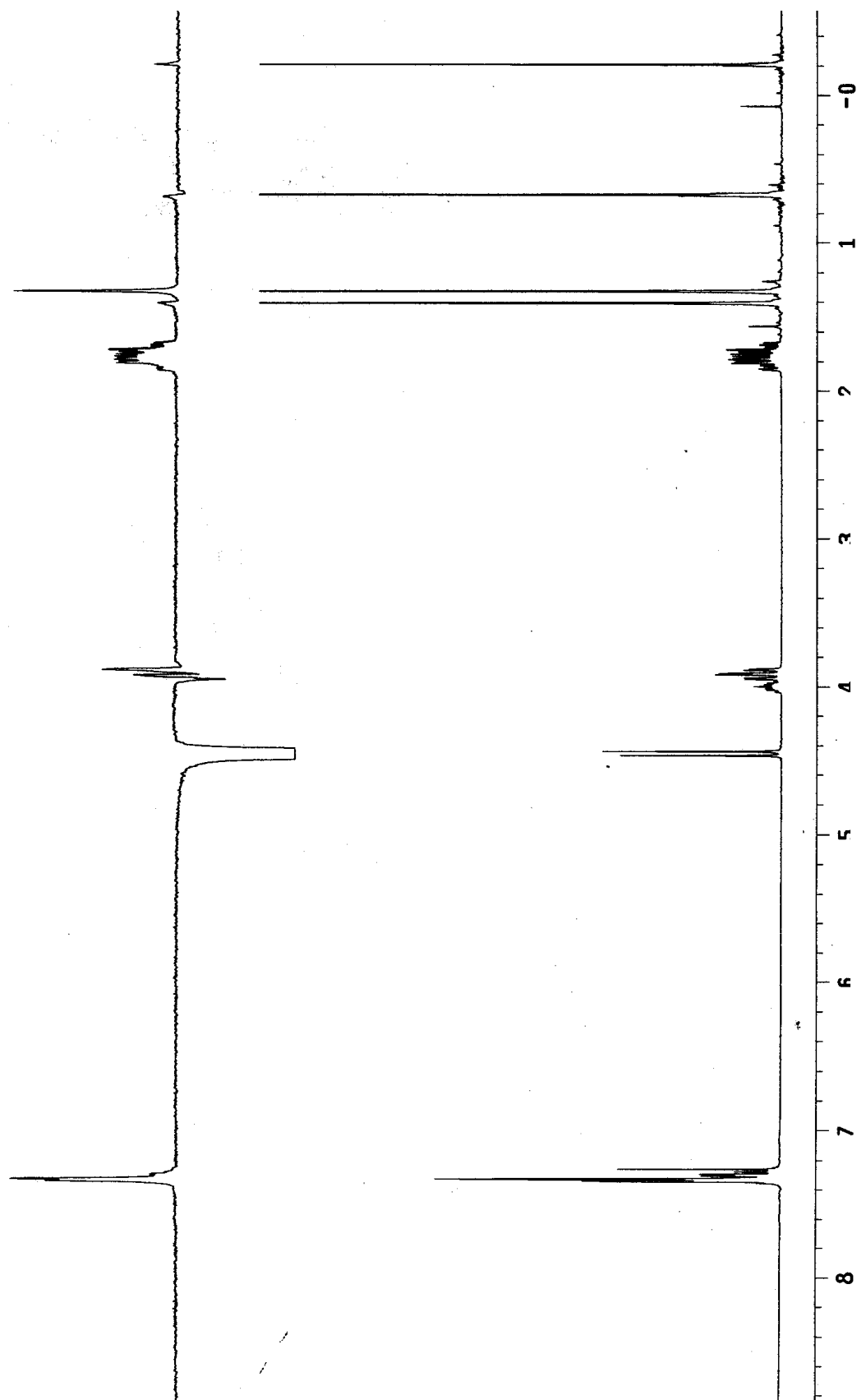


Figure A2.35 ^1H NMR (300 MHz, CDCl_3) of compound **106**.

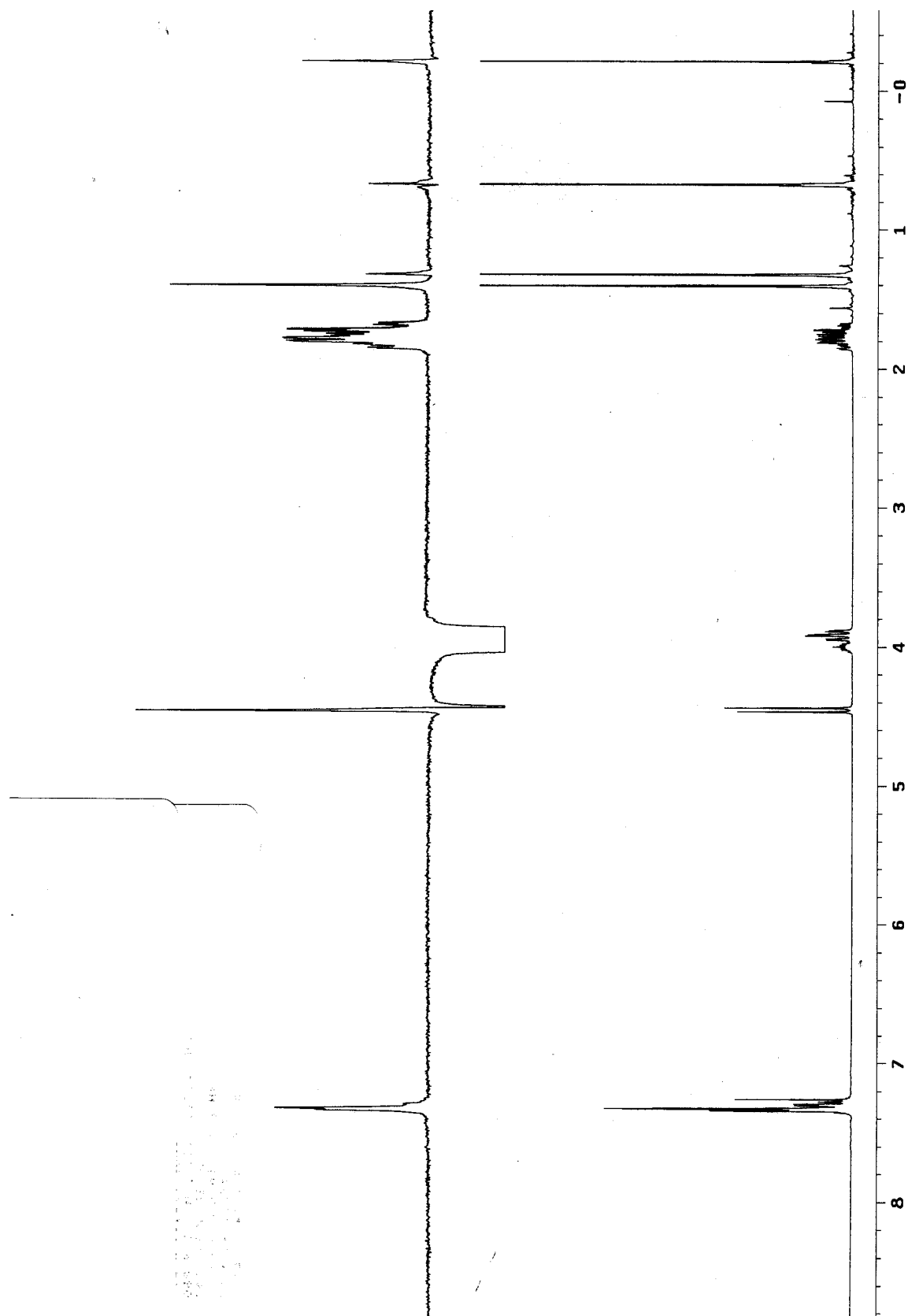


Figure A2.36 ^1H NMR (300 MHz, CDCl_3) of compound **106**.

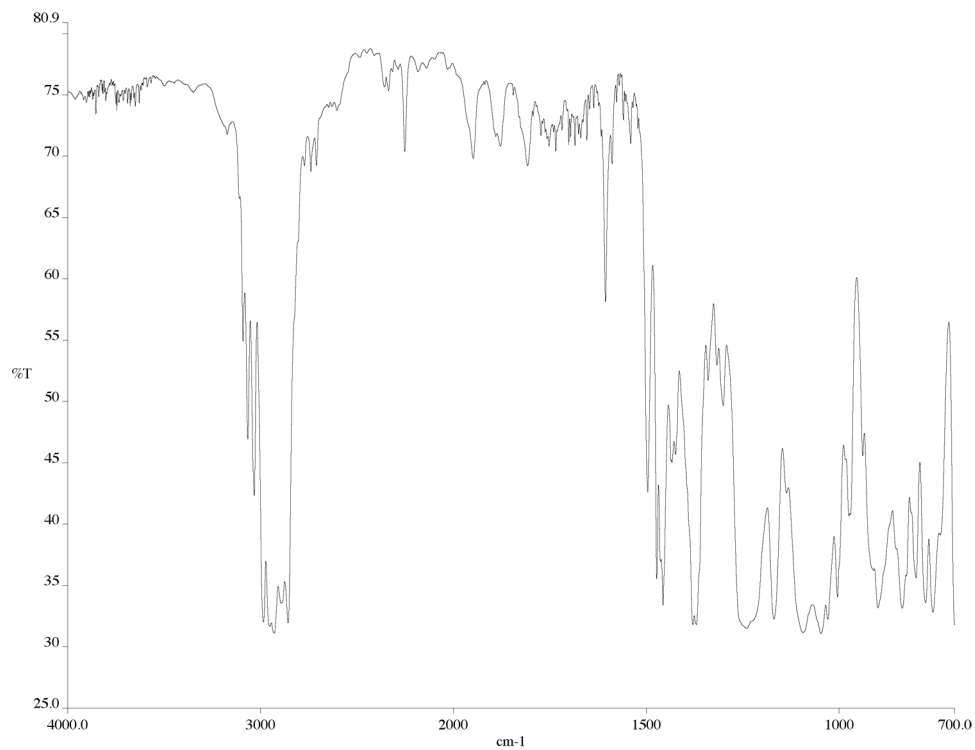


Figure A2.37 Infrared spectrum (thin film/NaCl) of compound **106**.

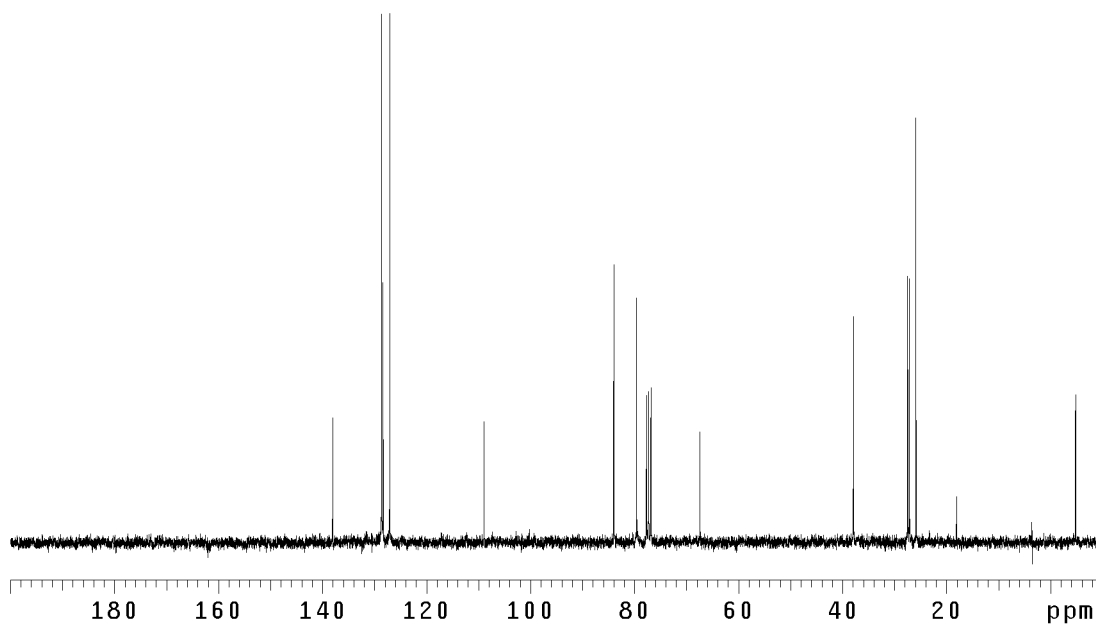


Figure A2.38 ¹³CNMR (125 MHz, CDCl₃) of compound **106**.

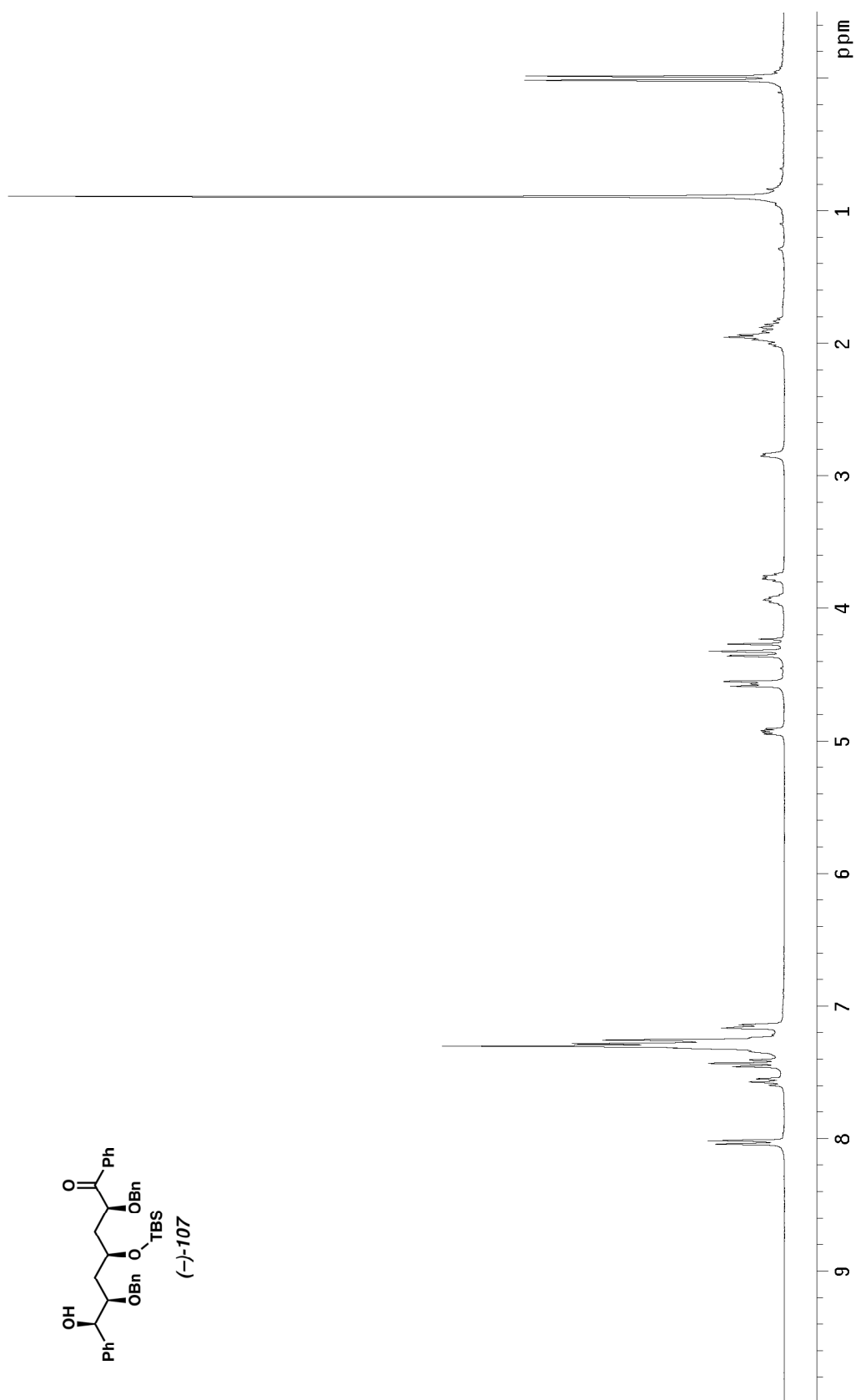


Figure A2.39 ^1H NMR (300 MHz, CDCl_3) of compound **(-)-107**.

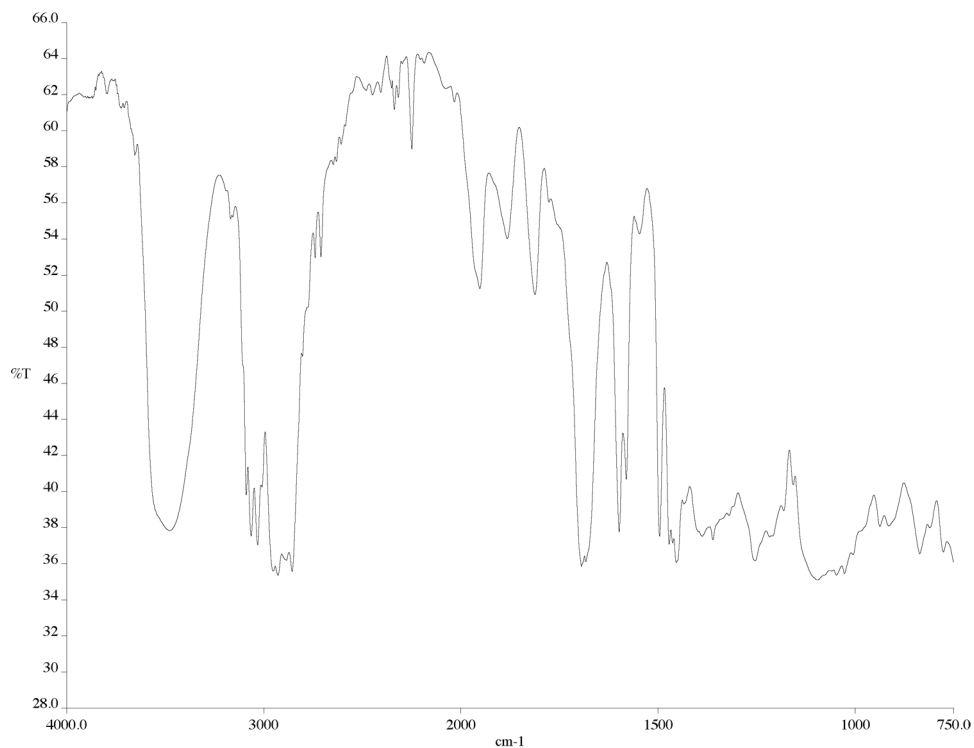


Figure A2.40 Infrared spectrum (thin film/NaCl) of compound (-)-**107**

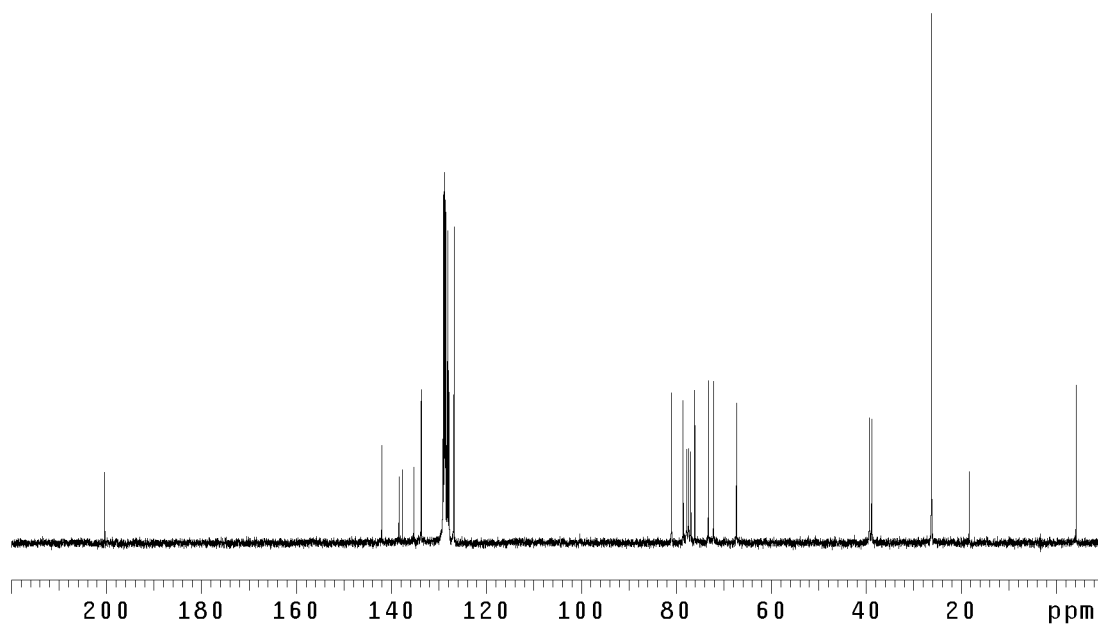


Figure A2.41 ¹³CNMR (125 MHz, CDCl₃) of compound (-)-**107**.

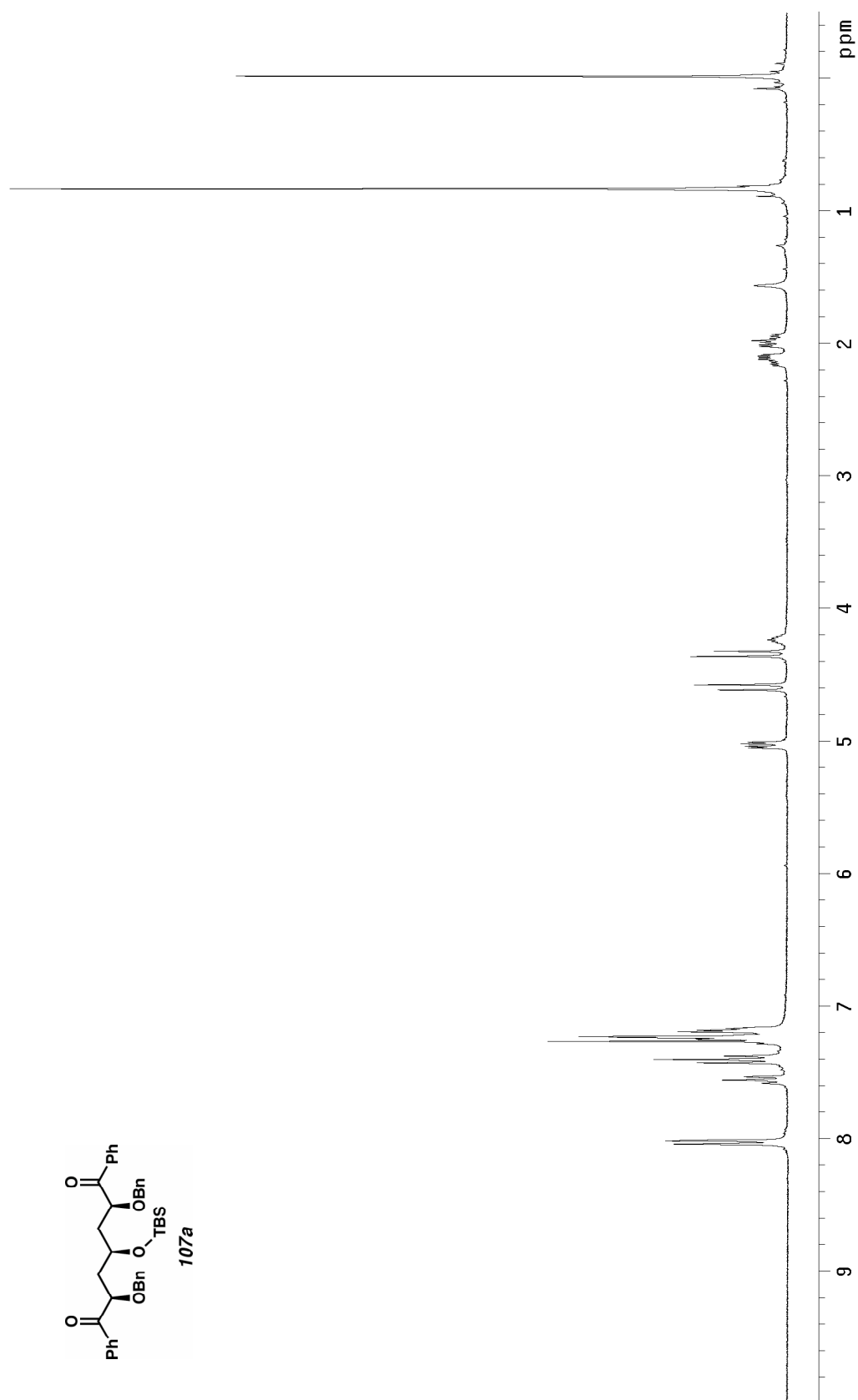


Figure A2.42 ^1H NMR (300 MHz, CDCl_3) of compound **107a**.

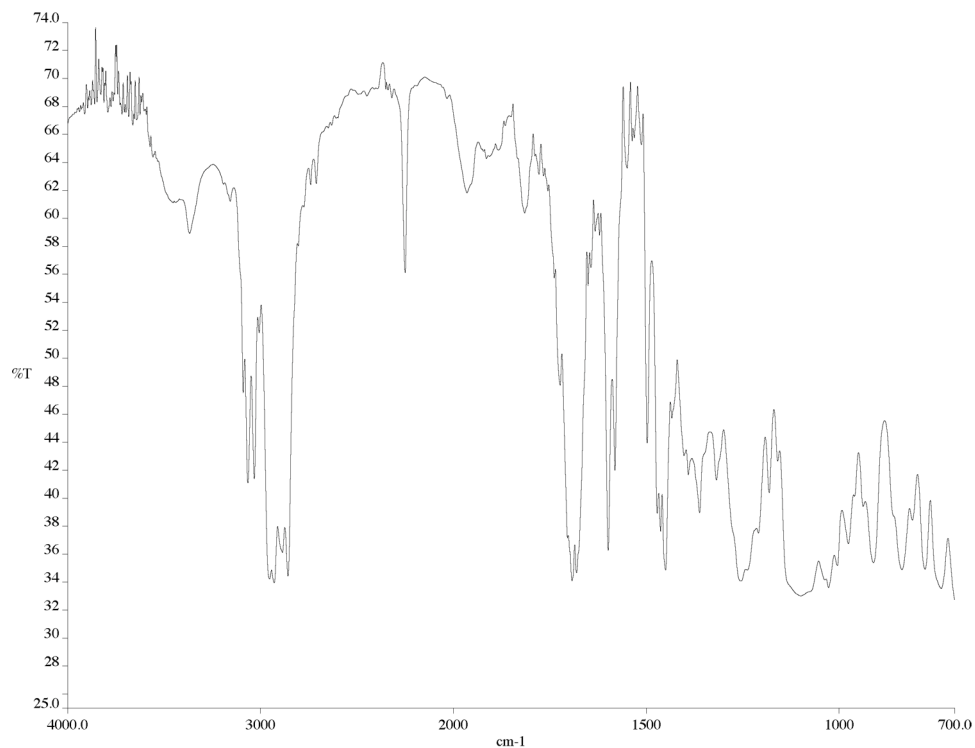


Figure A2.43 Infrared spectrum (thin film/NaCl) of compound **107a**.

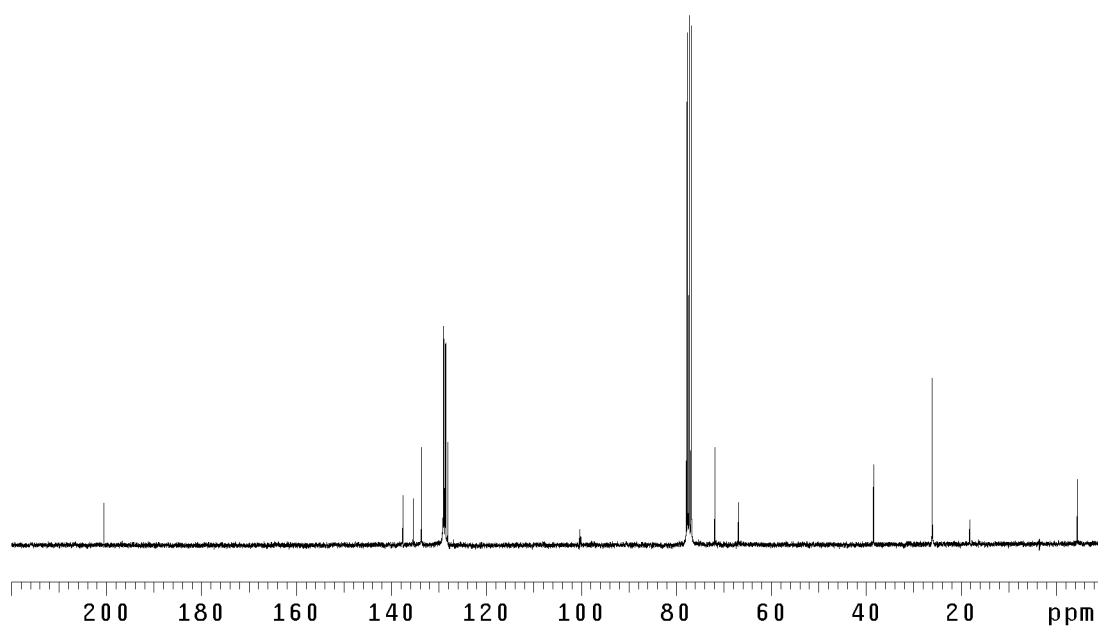


Figure A2.44 ¹³CNMR (125 MHz, CDCl₃) of compound **107a**.

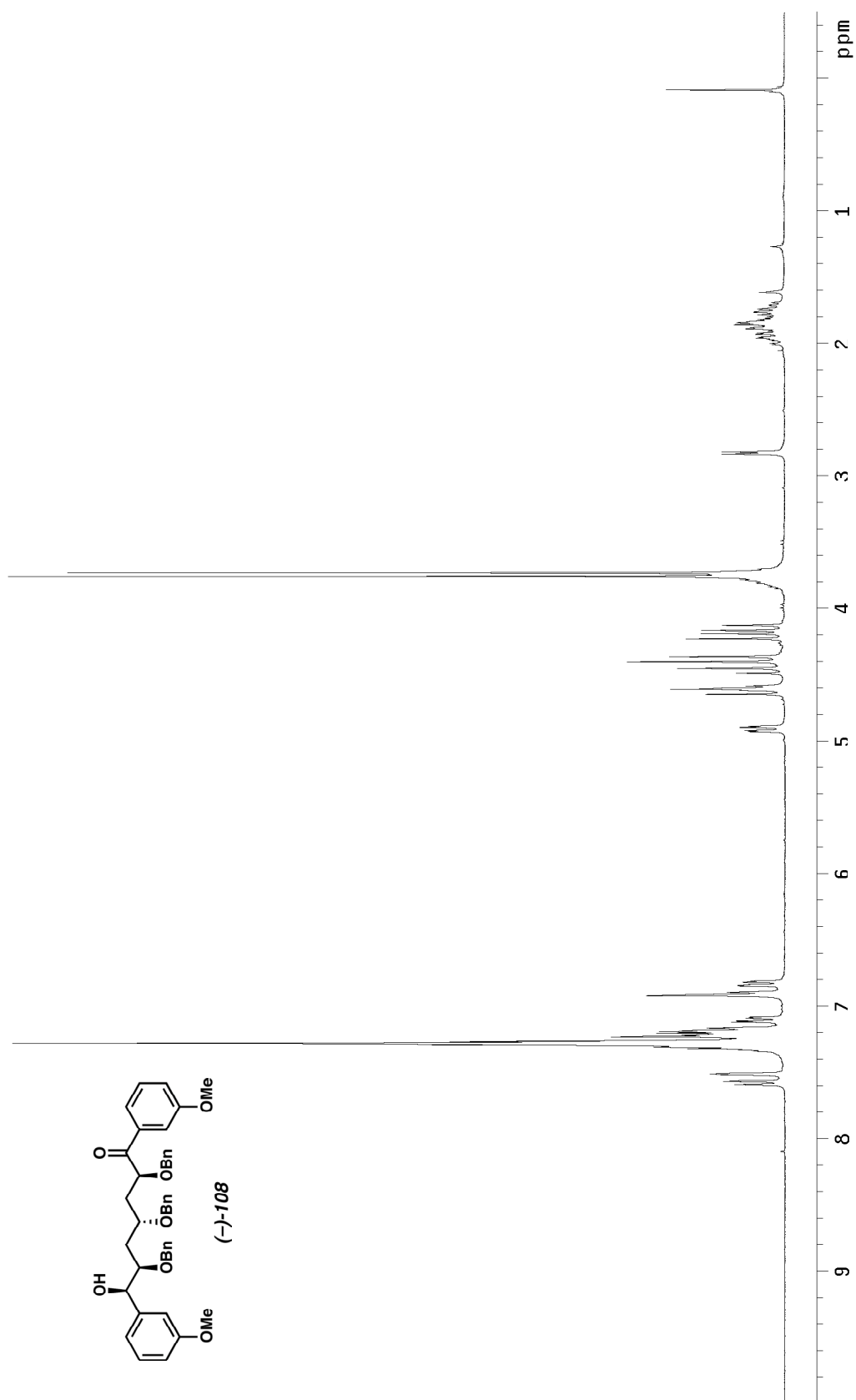


Figure A2.45 ^1H NMR (300 MHz, CDCl_3) of compound **(-)-108**.

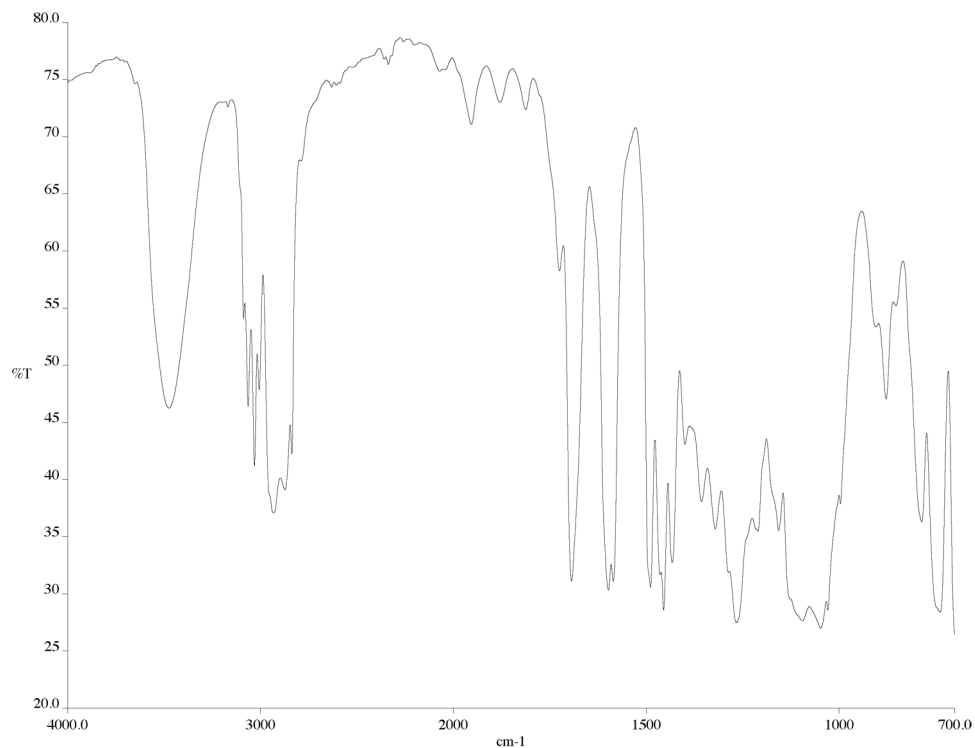


Figure A2.46 Infrared spectrum (thin film/NaCl) of compound **(-)-108**.

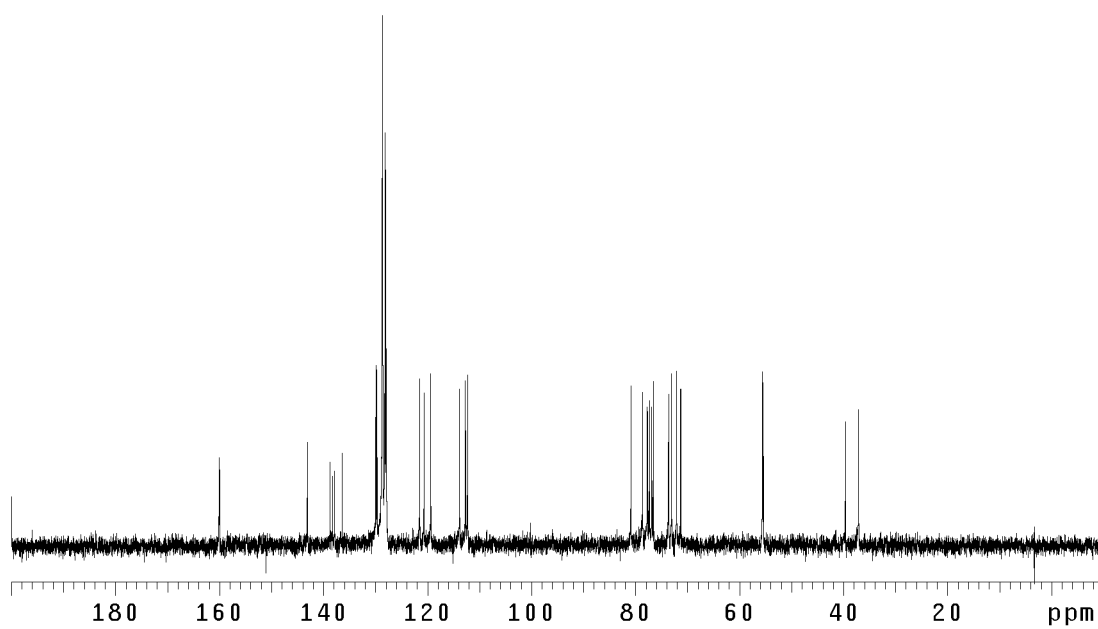


Figure A2.47 ¹³CNMR (125 MHz, CDCl₃) of compound **(-)-108**.

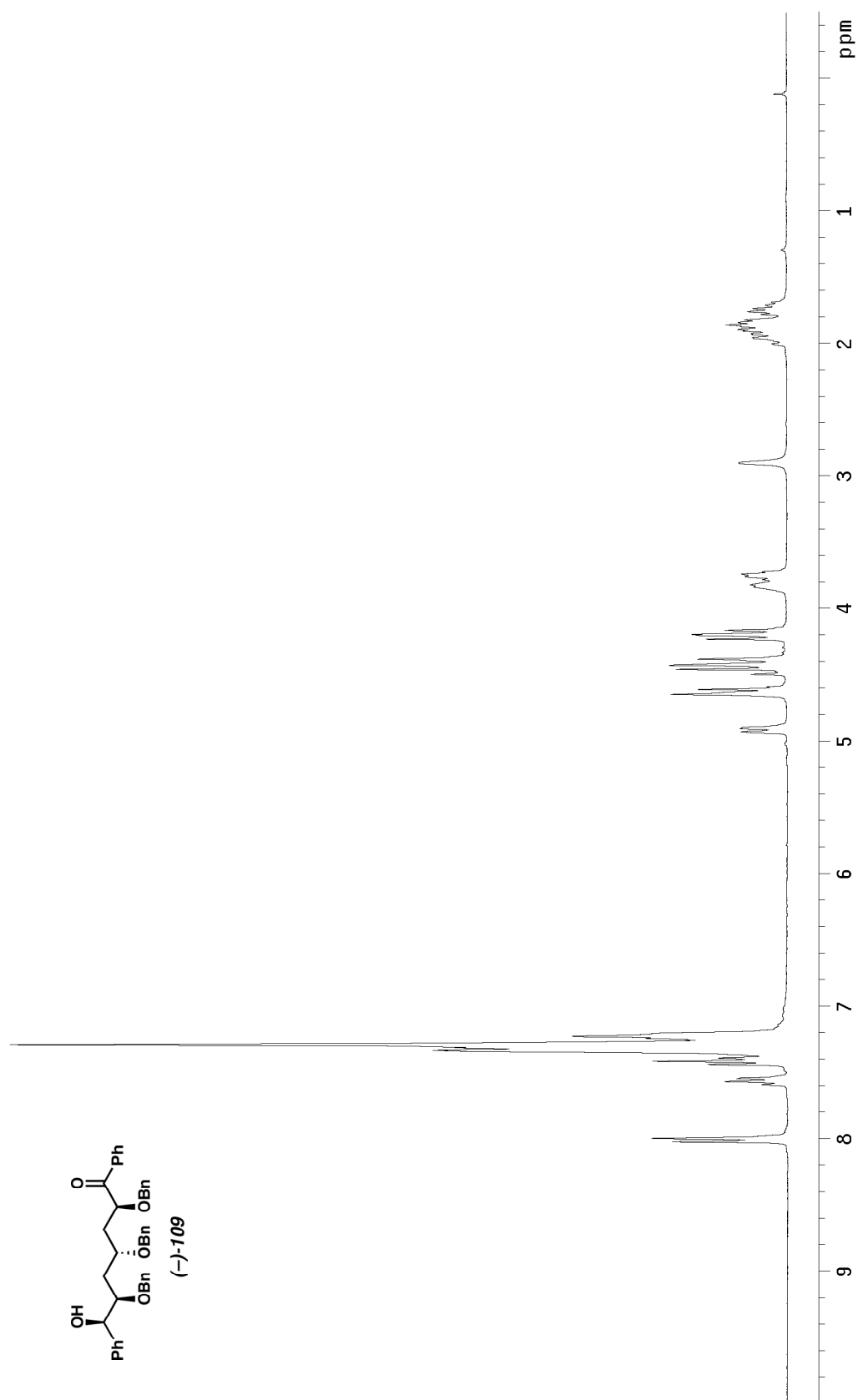


Figure A2.48 ^1H NMR (300 MHz, CDCl_3) of compound **(-)-109**.

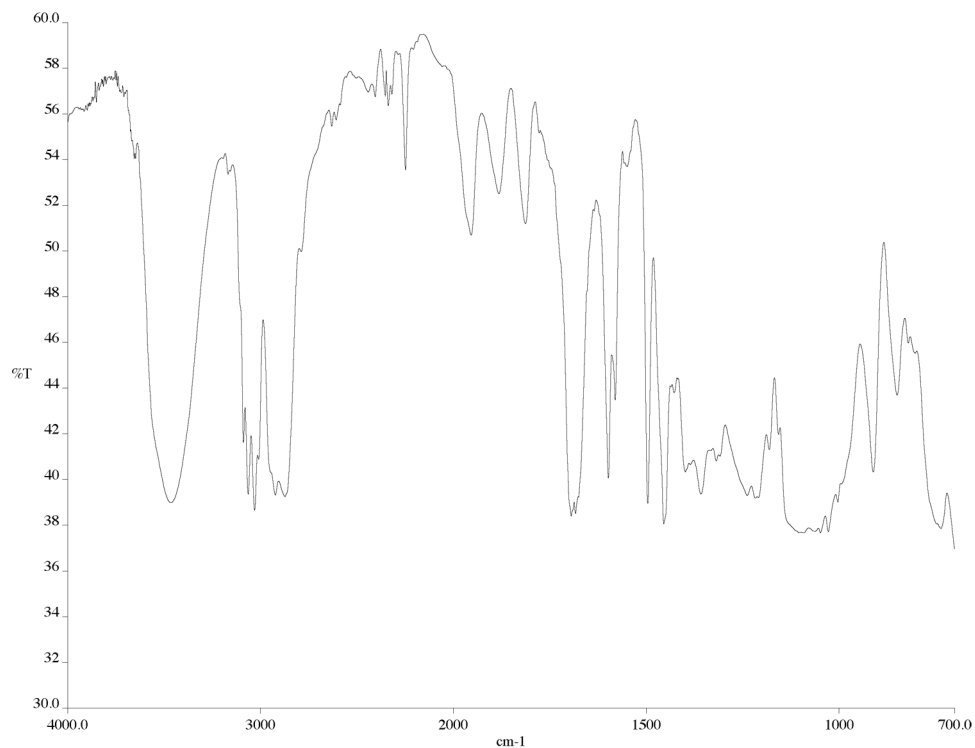


Figure A2.49 Infrared spectrum (thin film/NaCl) of compound **(-)-109**.

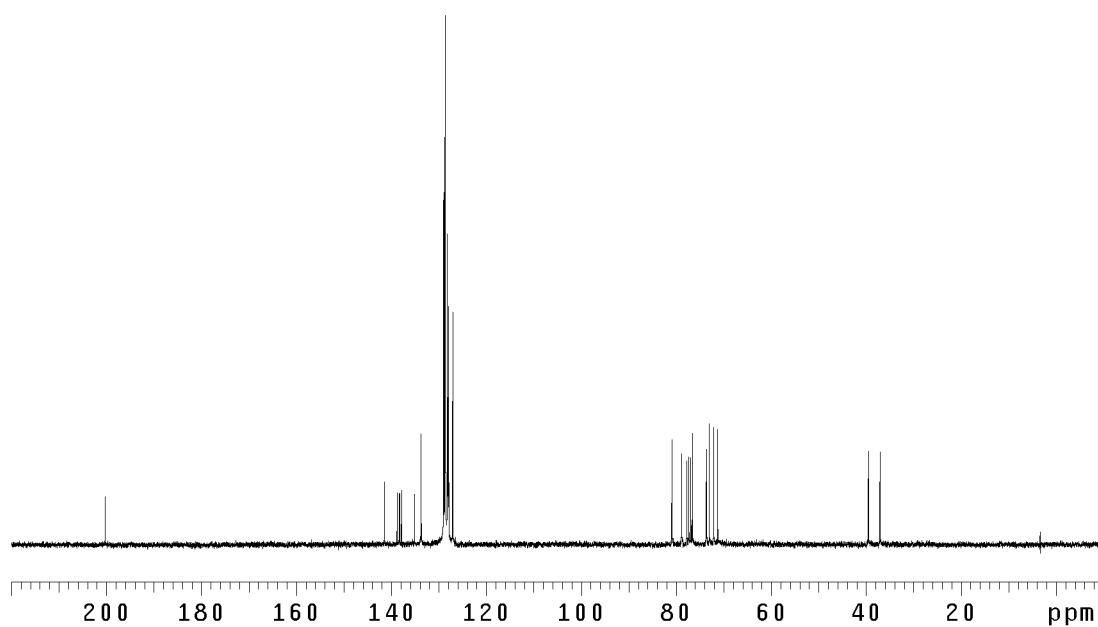


Figure A2.50 ¹³CNMR (125 MHz, CDCl₃) of compound **(-)-109**.

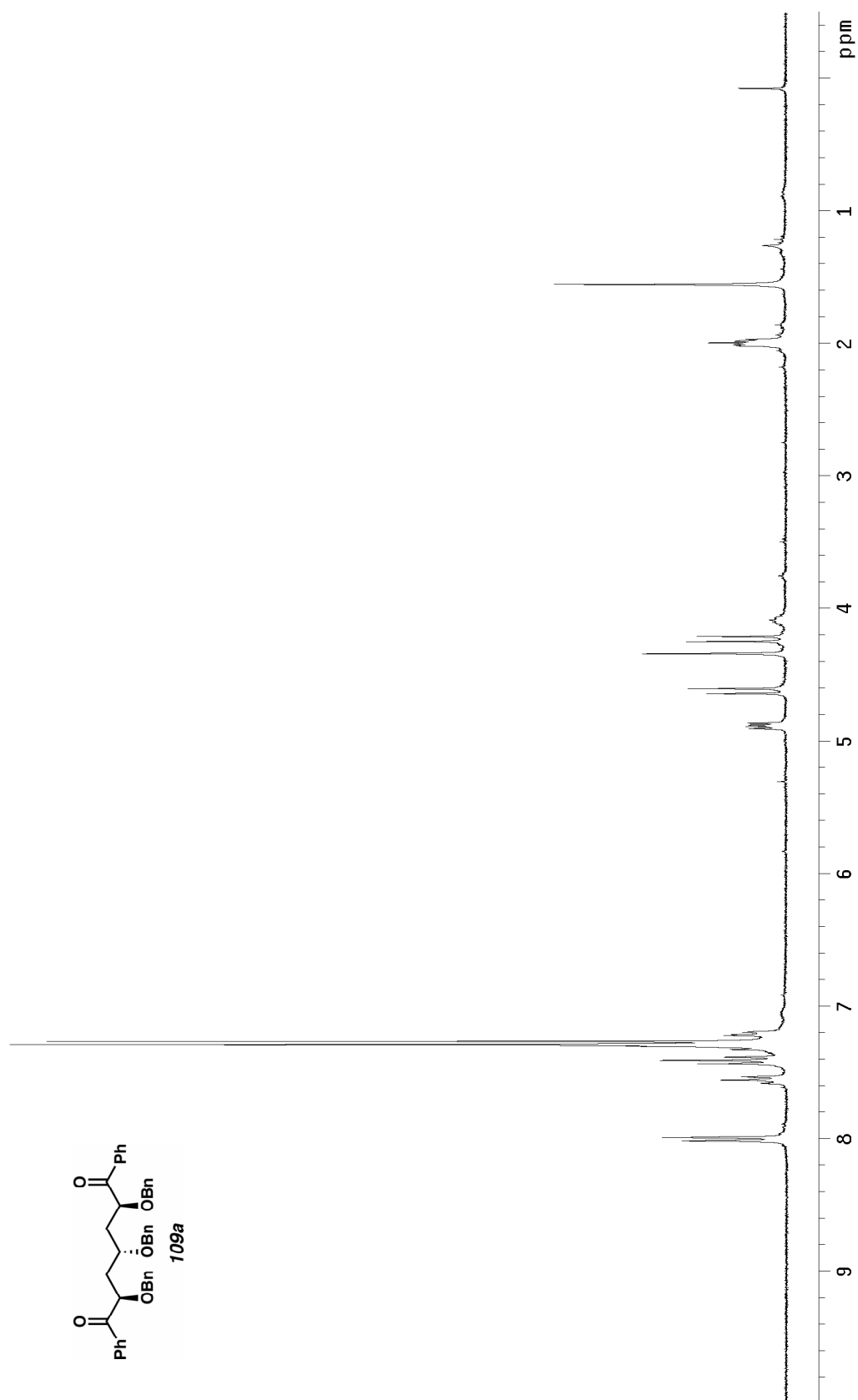


Figure A2.51 ^1H NMR (300 MHz, CDCl_3) of compound **109a**.

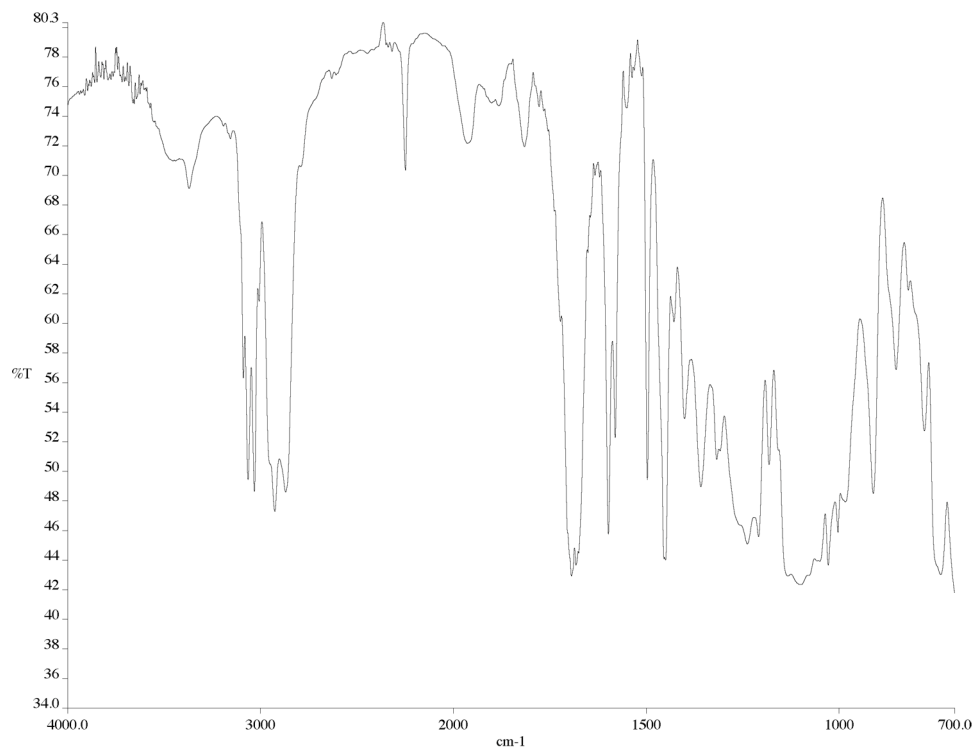


Figure A2.52 Infrared spectrum (thin film/NaCl) of compound **109a**.

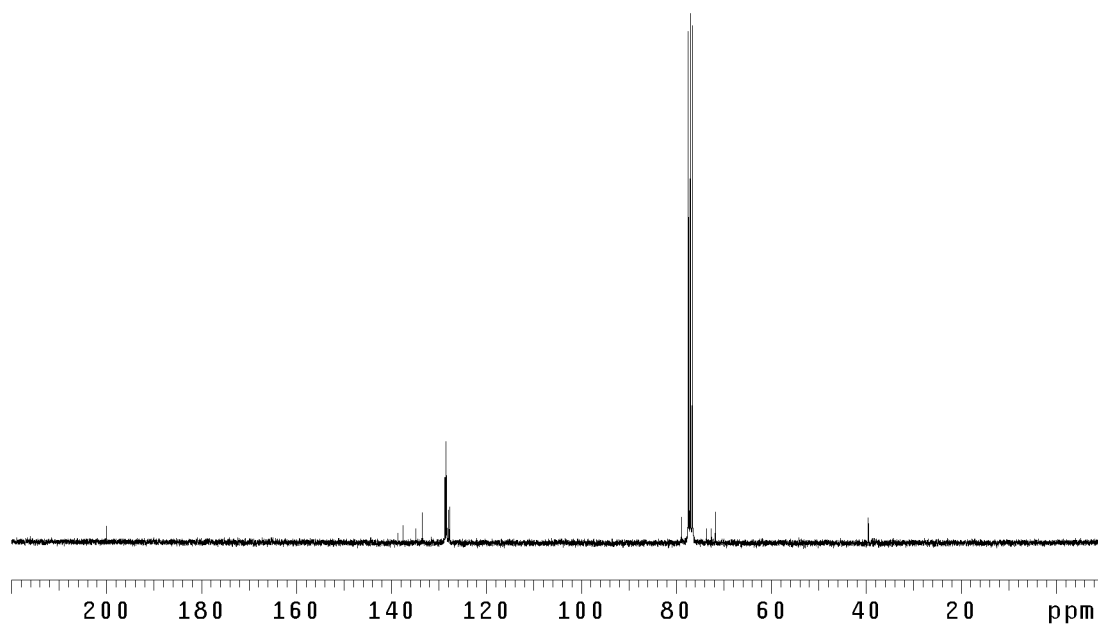


Figure A2.53 ¹³CNMR (125 MHz, CDCl₃) of compound **109a**.

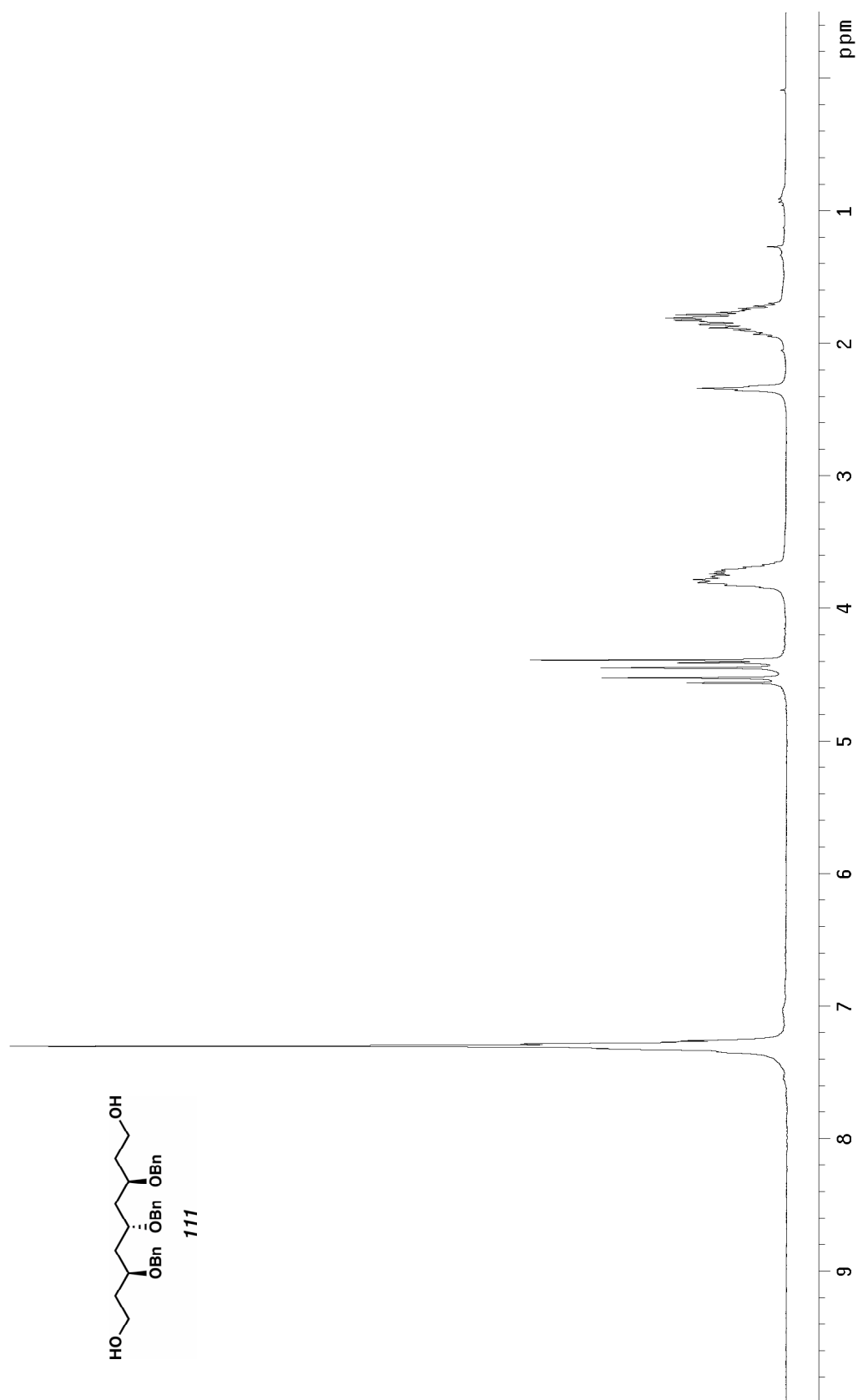


Figure A2.54 ^1H NMR (300 MHz, CDCl_3) of compound **111**.

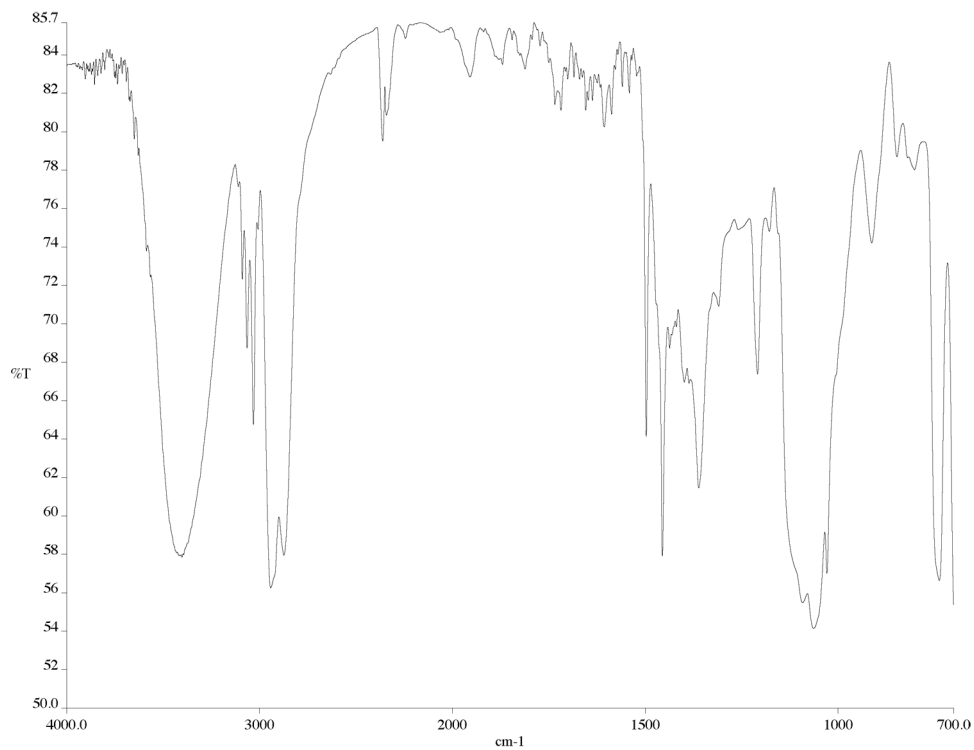


Figure A2.55 Infrared spectrum (thin film/NaCl) of compound **111**.

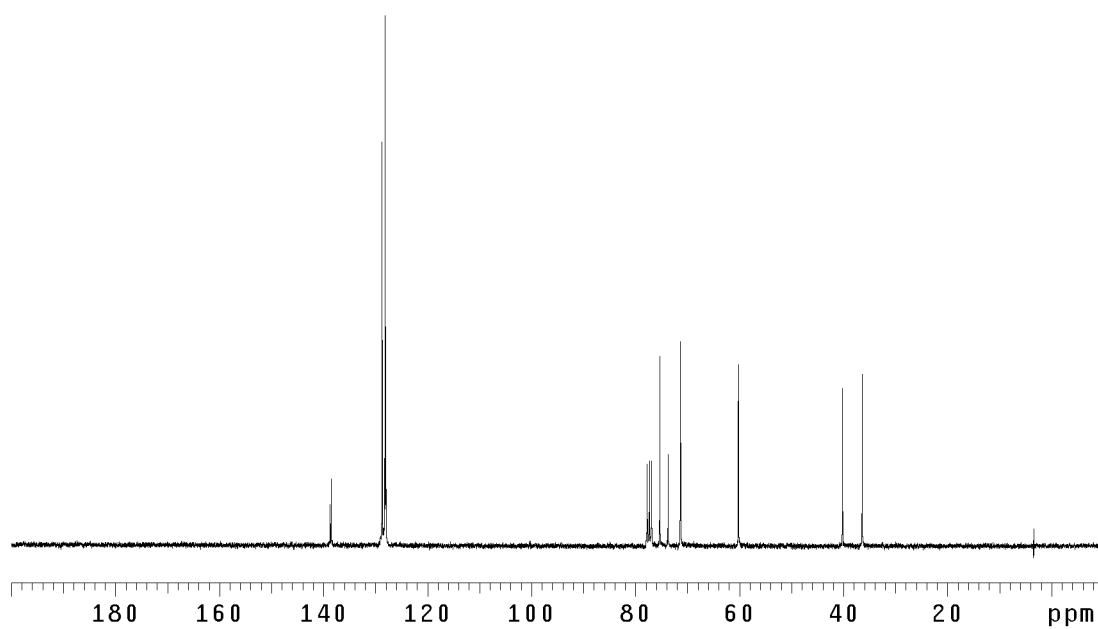


Figure A2.56 ¹³CNMR (125 MHz, CDCl₃) of compound **111**.

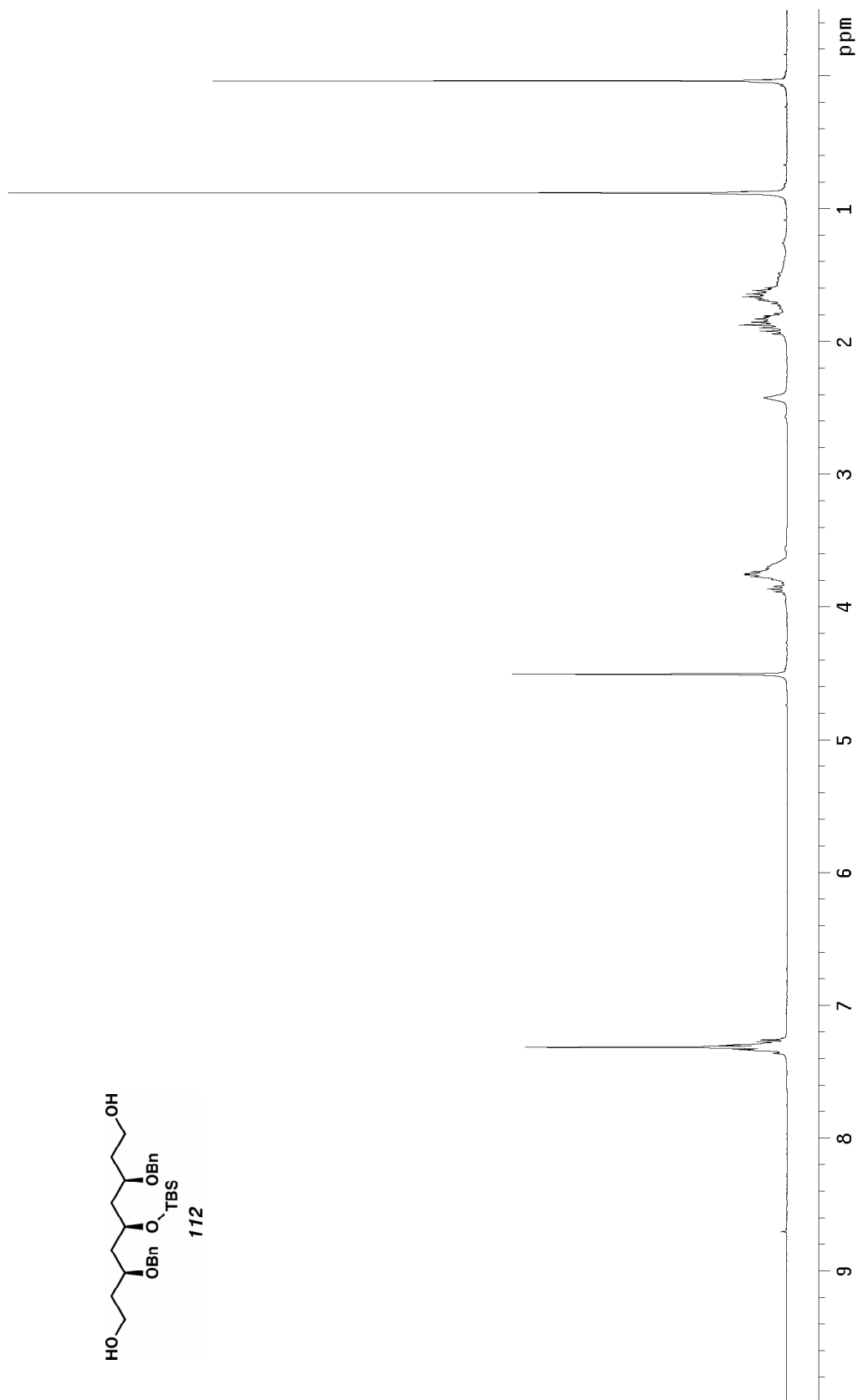
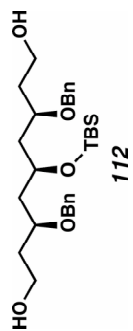


Figure A2.57 ¹H NMR (300 MHz, CDCl₃) of compound **112**.

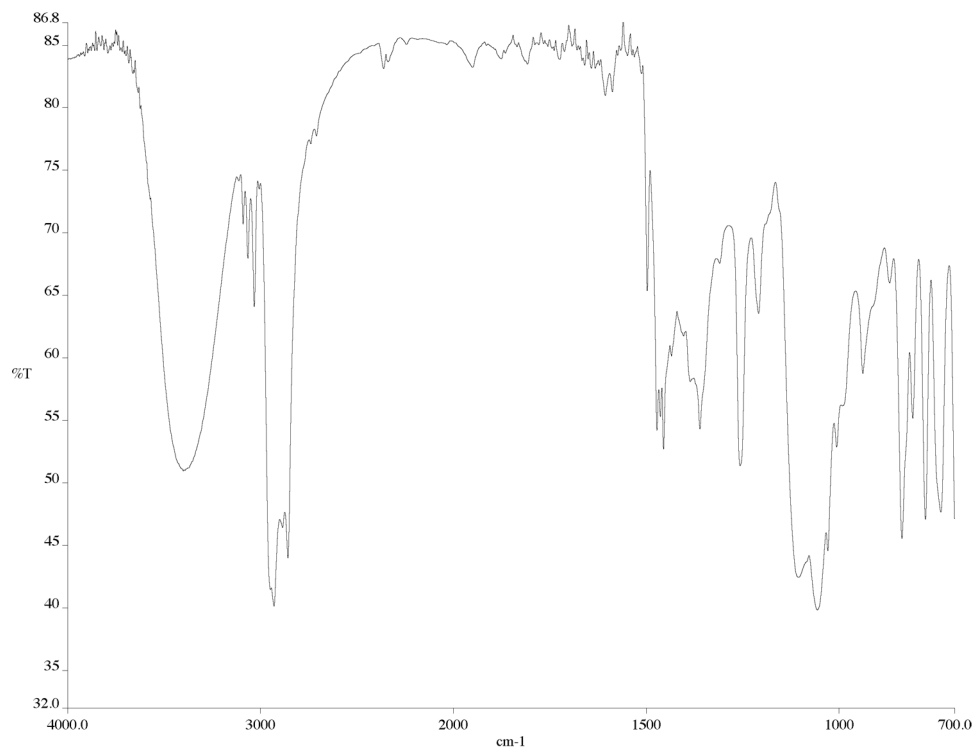


Figure A2.58 Infrared spectrum (thin film/NaCl) of compound **112**.

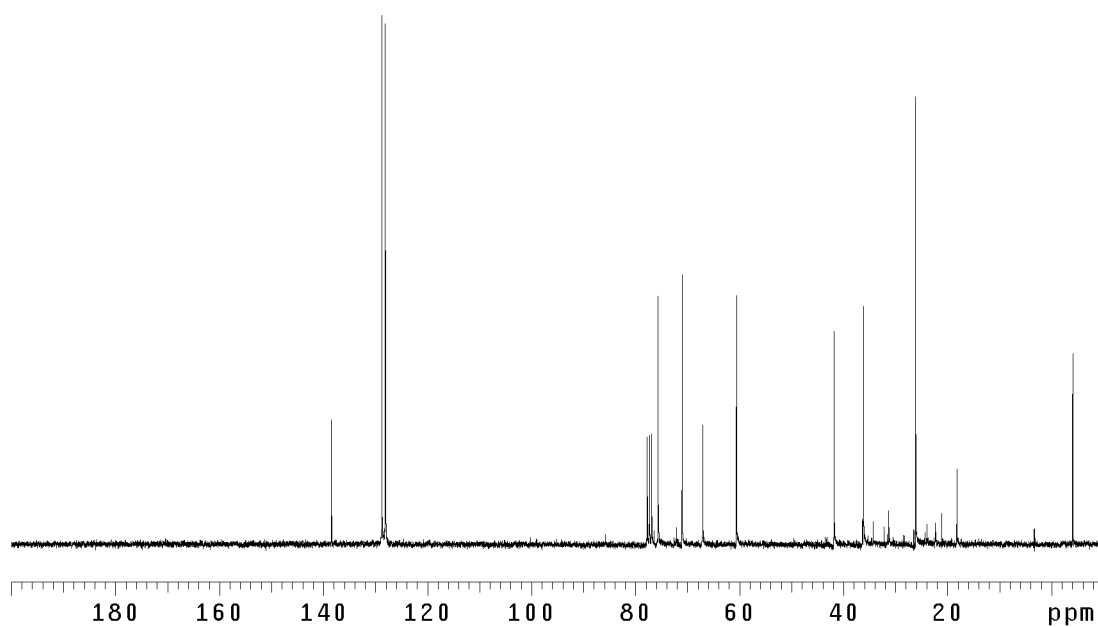


Figure A2.59 ¹³CNMR (125 MHz, CDCl₃) of compound **112**.

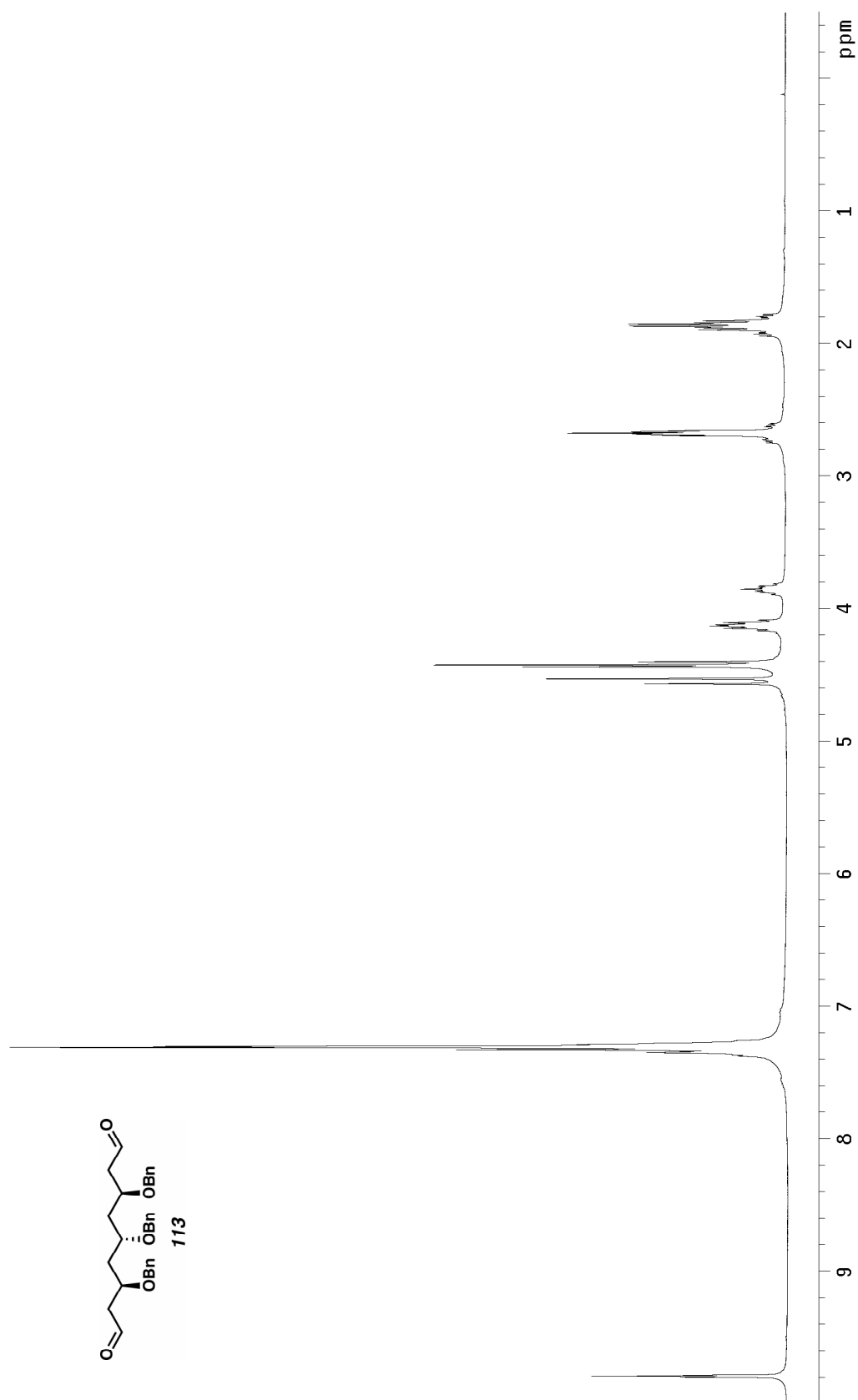


Figure A2.60 ¹H NMR (300 MHz, CDCl₃) of compound **113**.

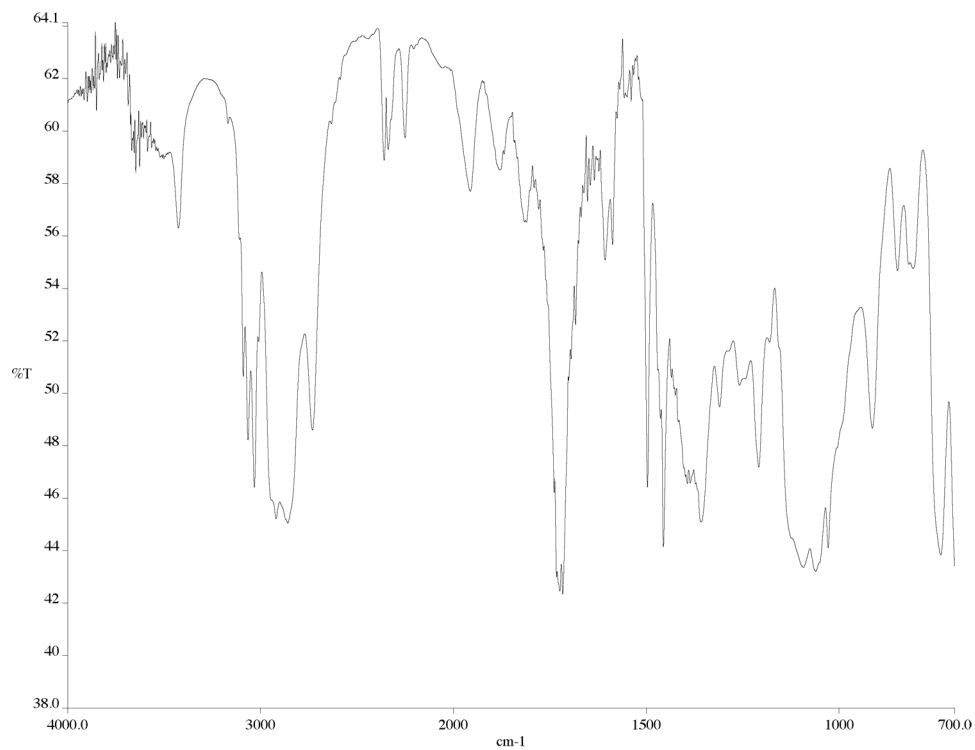


Figure A2.61 Infrared spectrum (thin film/NaCl) of compound **113**.

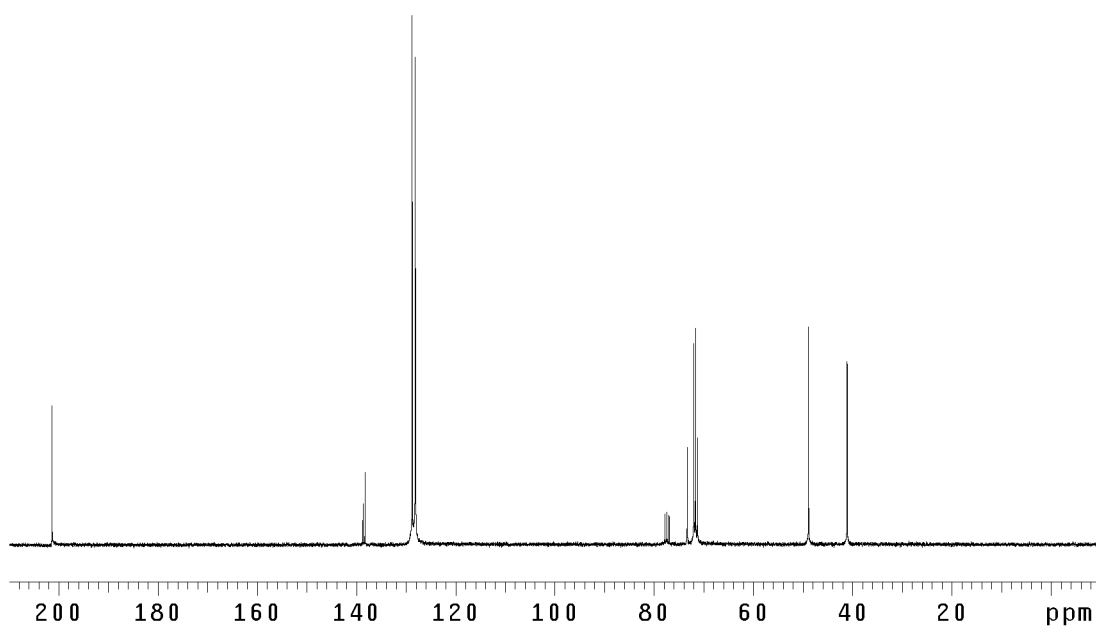


Figure A2.62 ¹³CNMR (125 MHz, CDCl₃) of compound **113**.

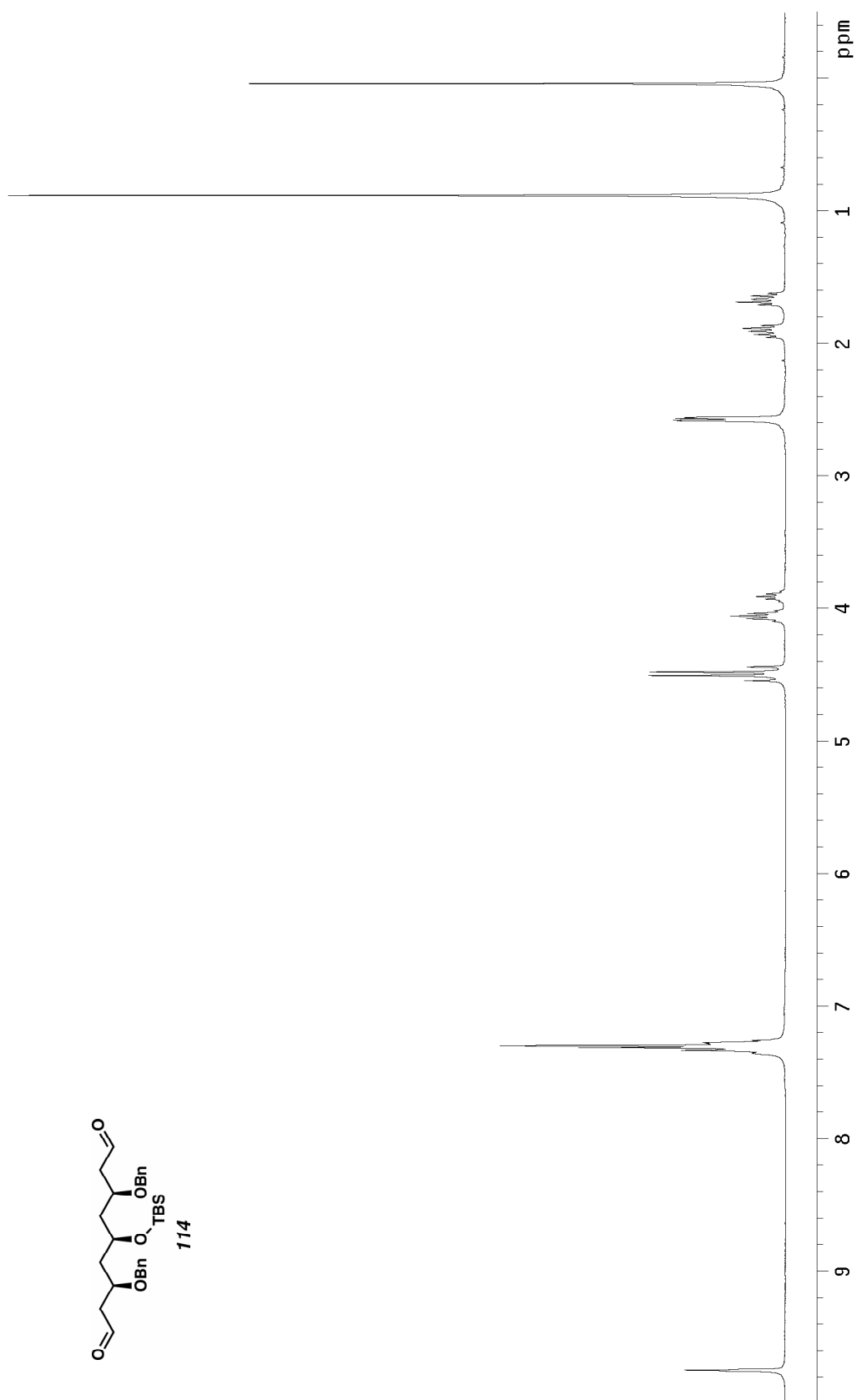
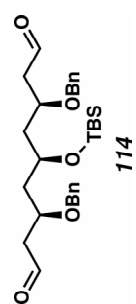


Figure A2.63 ^1H NMR (300 MHz, CDCl_3) of compound **114**.

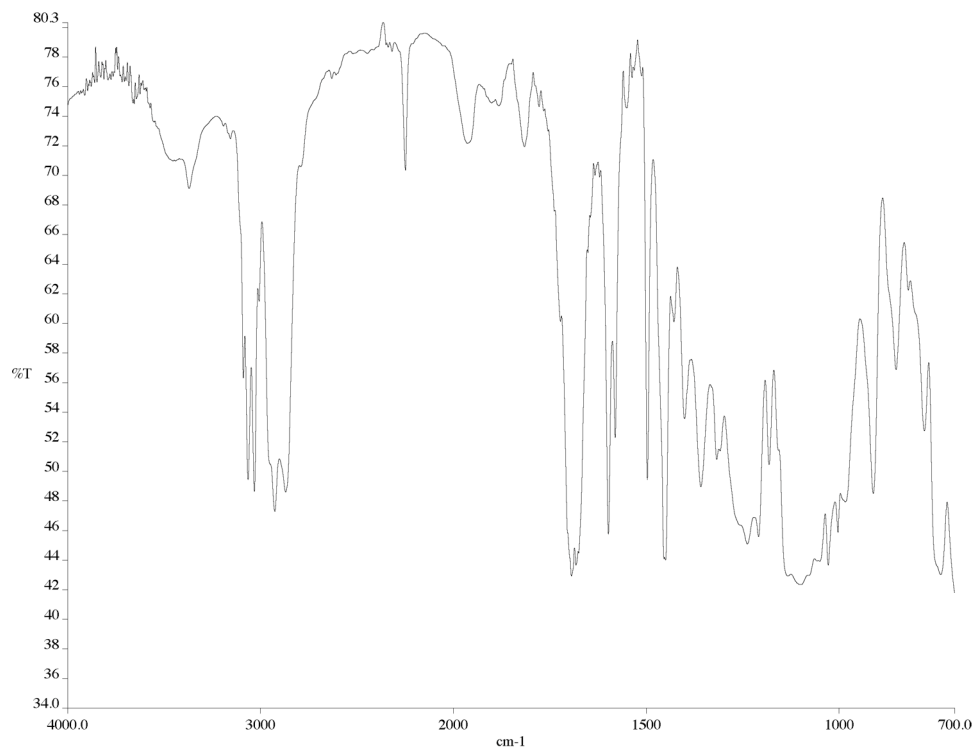


Figure A2.64 Infrared spectrum (thin film/NaCl) of compound **114**.

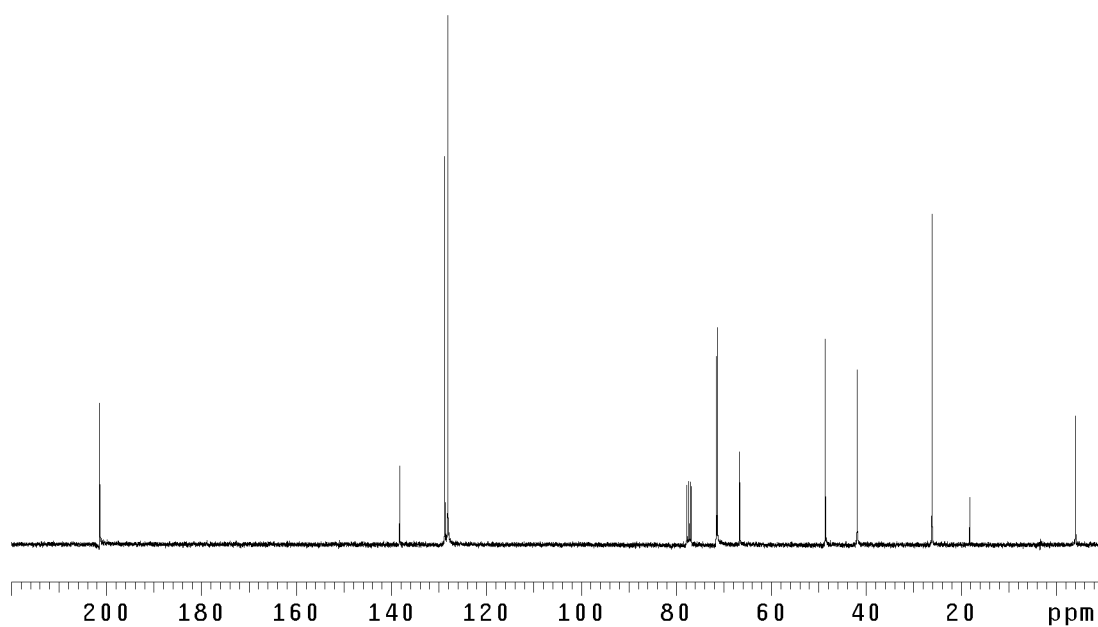


Figure A2.65 ¹³CNMR (125 MHz, CDCl₃) of compound **114**.

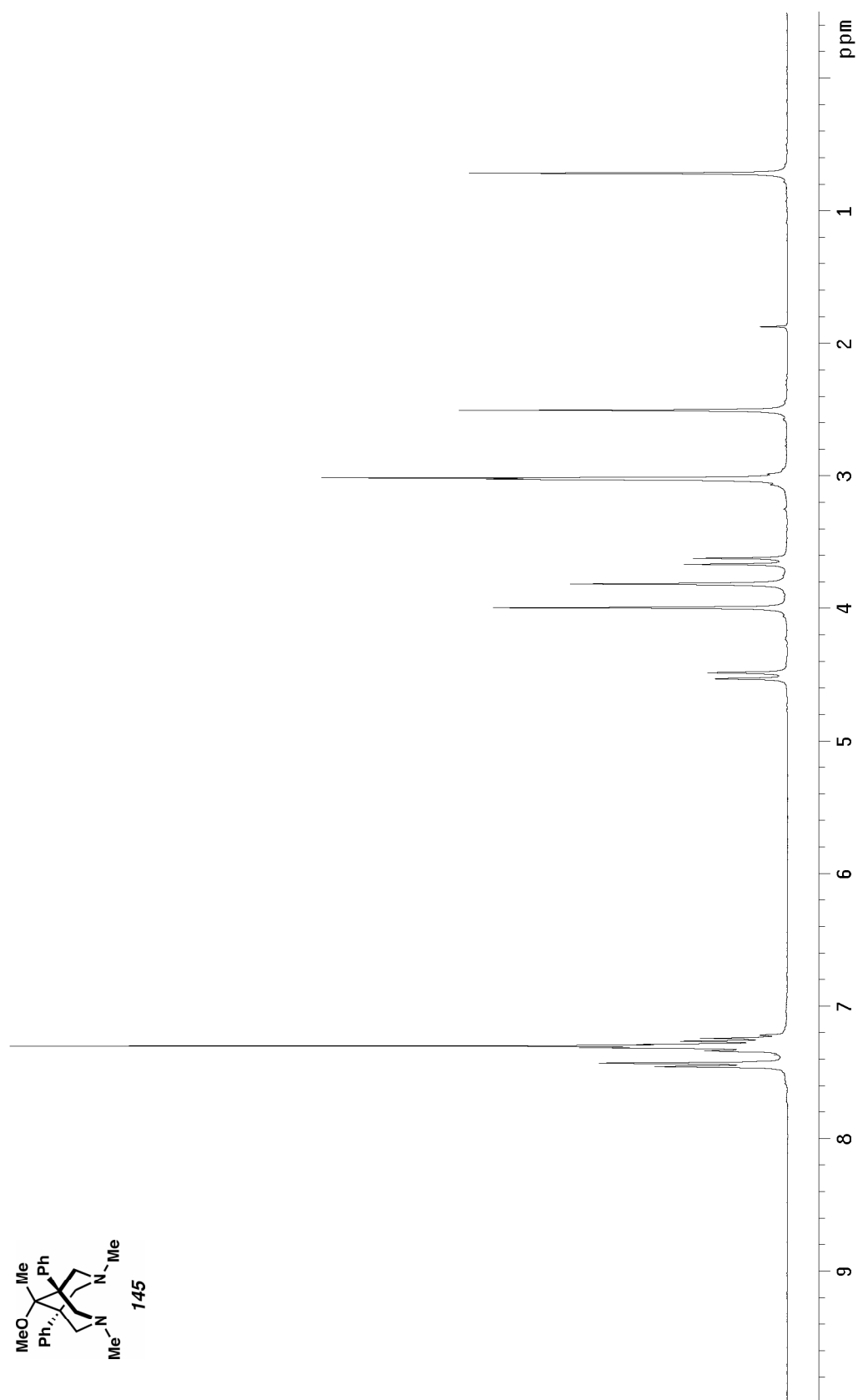


Figure A2.66 ^1H NMR (300 MHz, CDCl_3) of compound **145**.

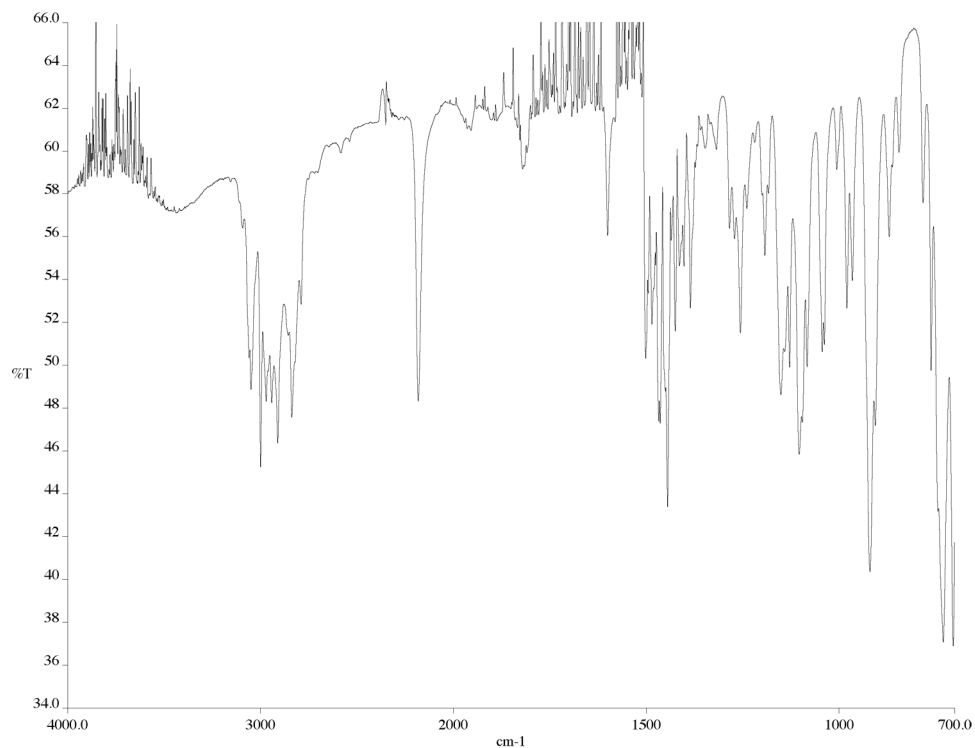


Figure A2.67 Infrared spectrum (thin film/NaCl) of compound **145**.

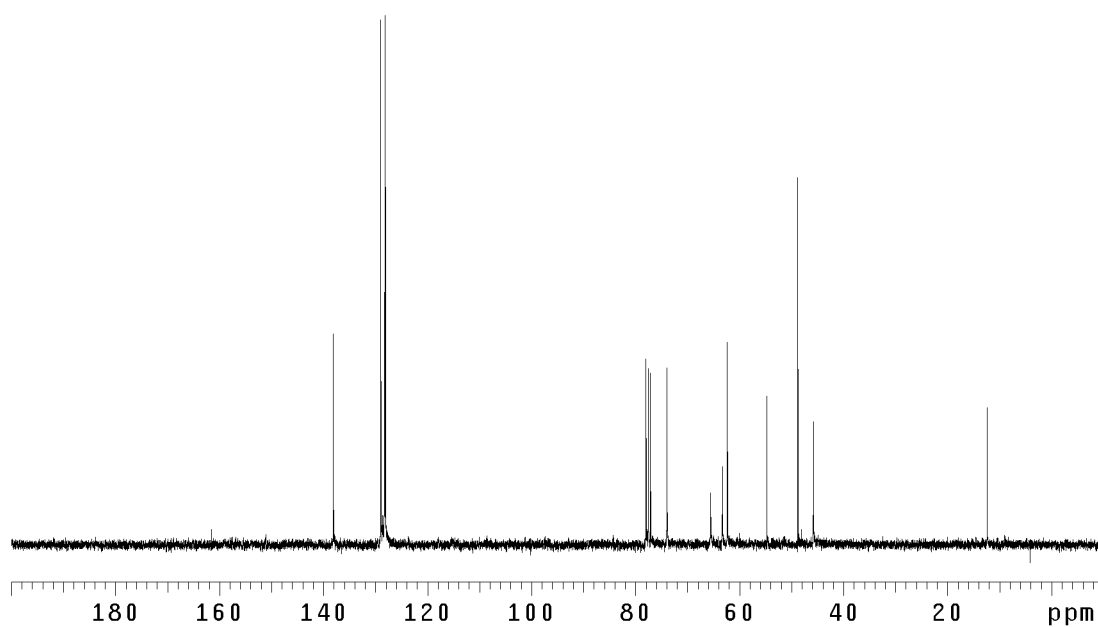


Figure A2.68 ¹³CNMR (125 MHz, CDCl₃) of compound **145**.

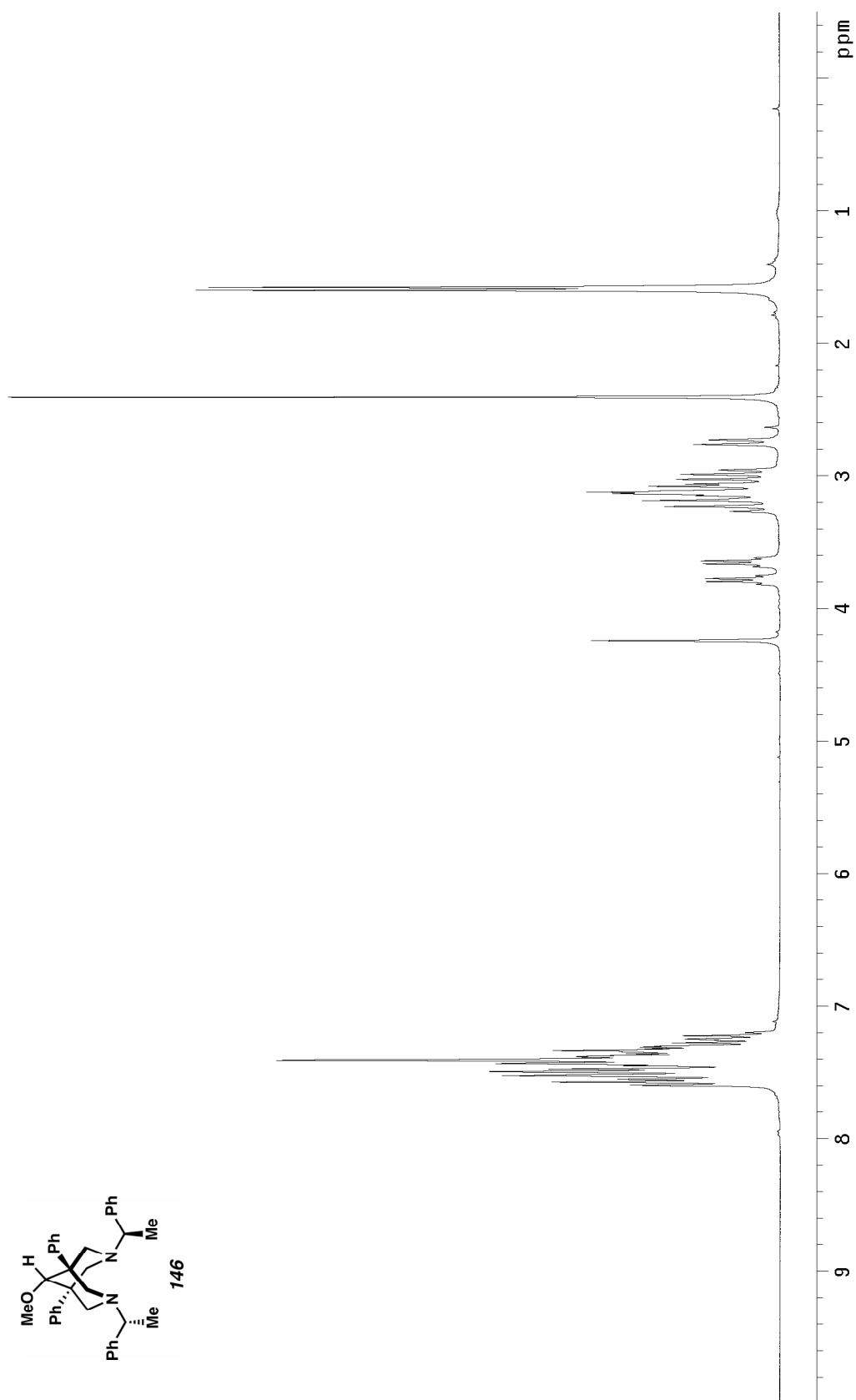


Figure A2.69 ^1H NMR (300 MHz, CDCl_3) of compound **146**.

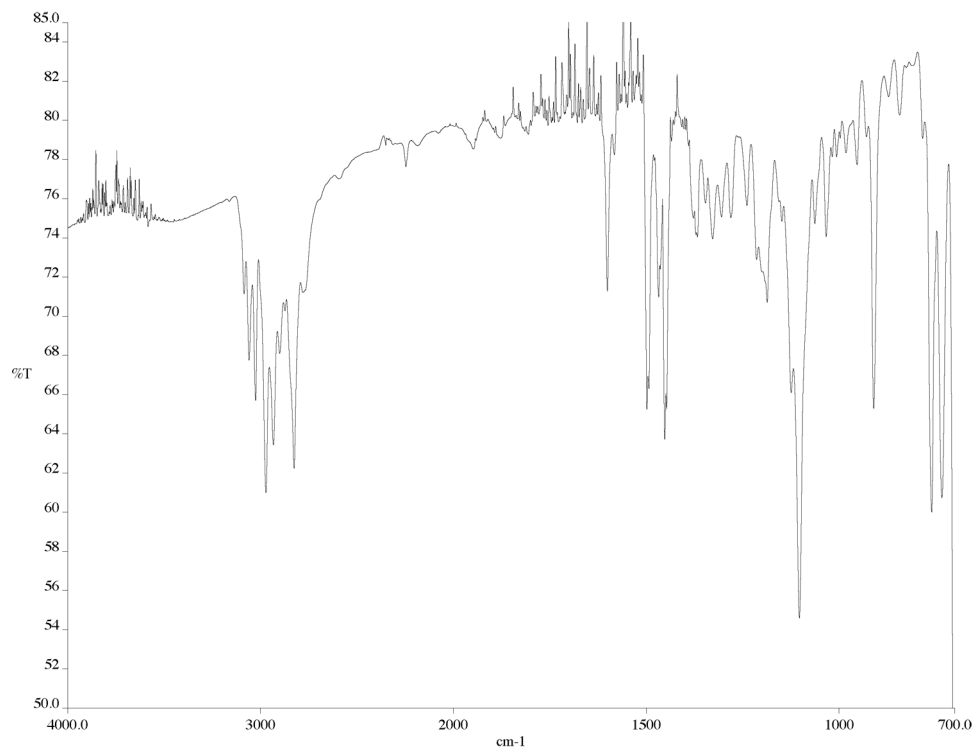


Figure A2.70 Infrared spectrum (thin film/NaCl) of compound **146**.

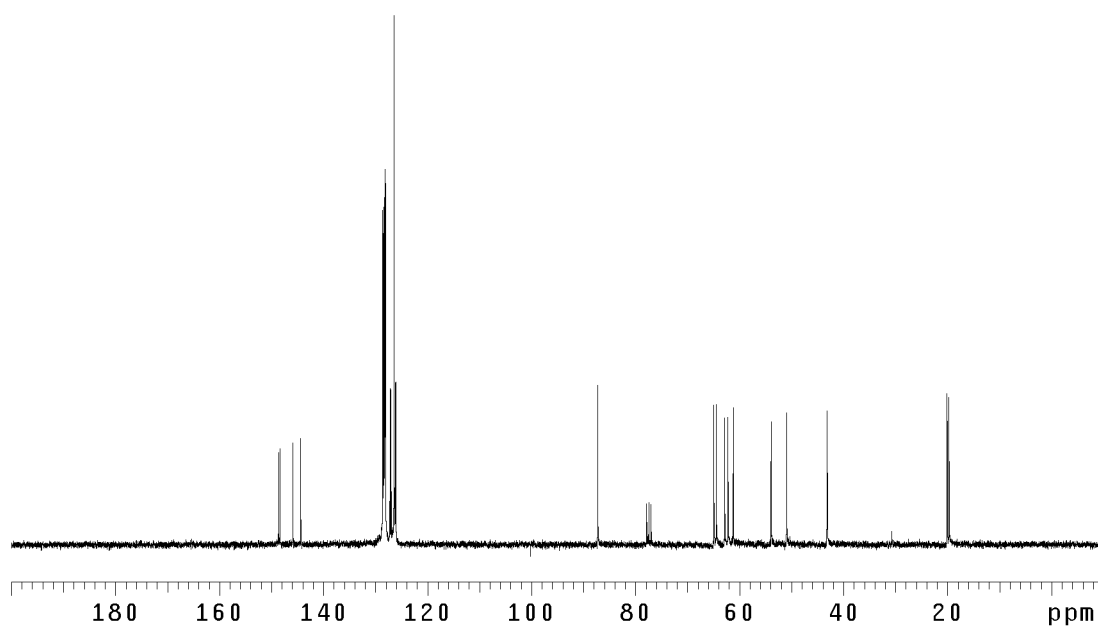


Figure A2.71 ¹³CNMR (125 MHz, CDCl₃) of compound **146**.

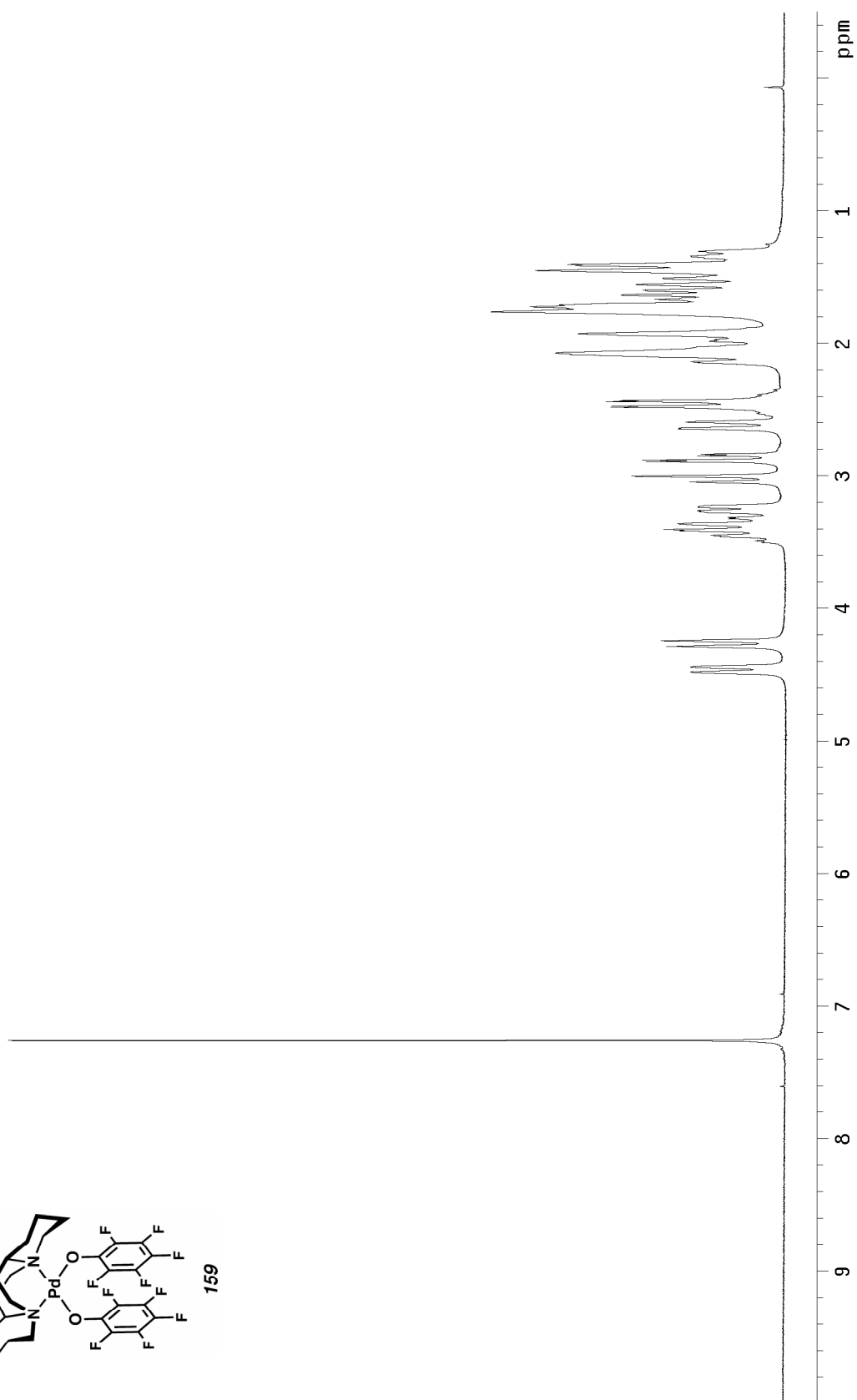
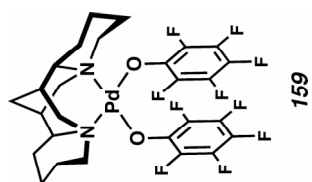


Figure A2.72 ^1H NMR (300 MHz, CDCl_3) of compound **159**.

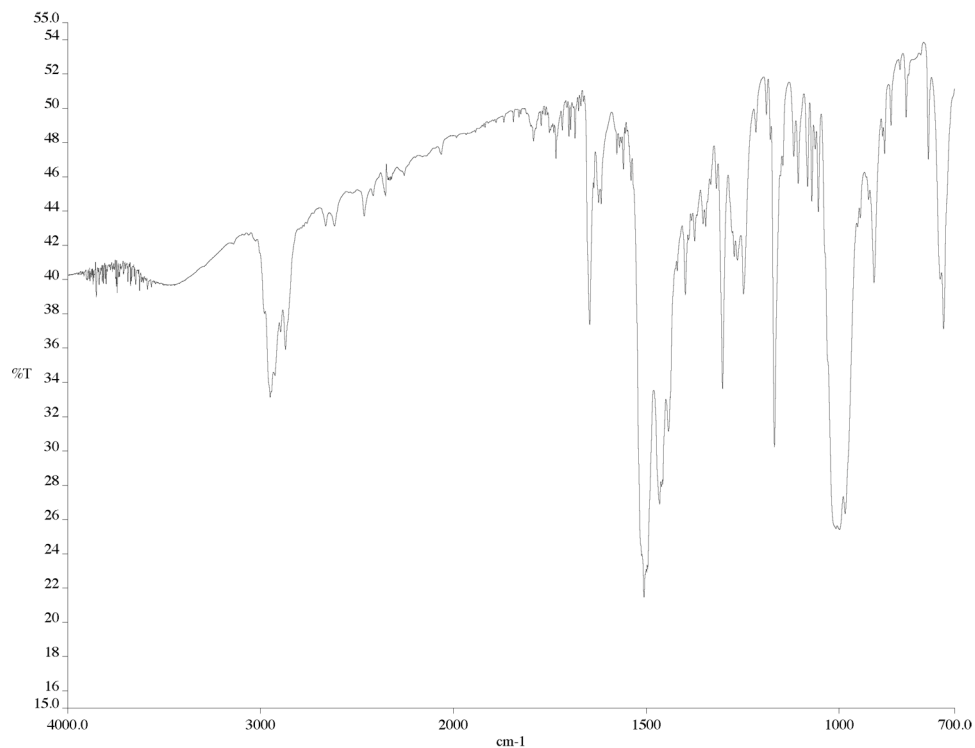


Figure A2.73 Infrared spectrum (thin film/NaCl) of compound **159**.

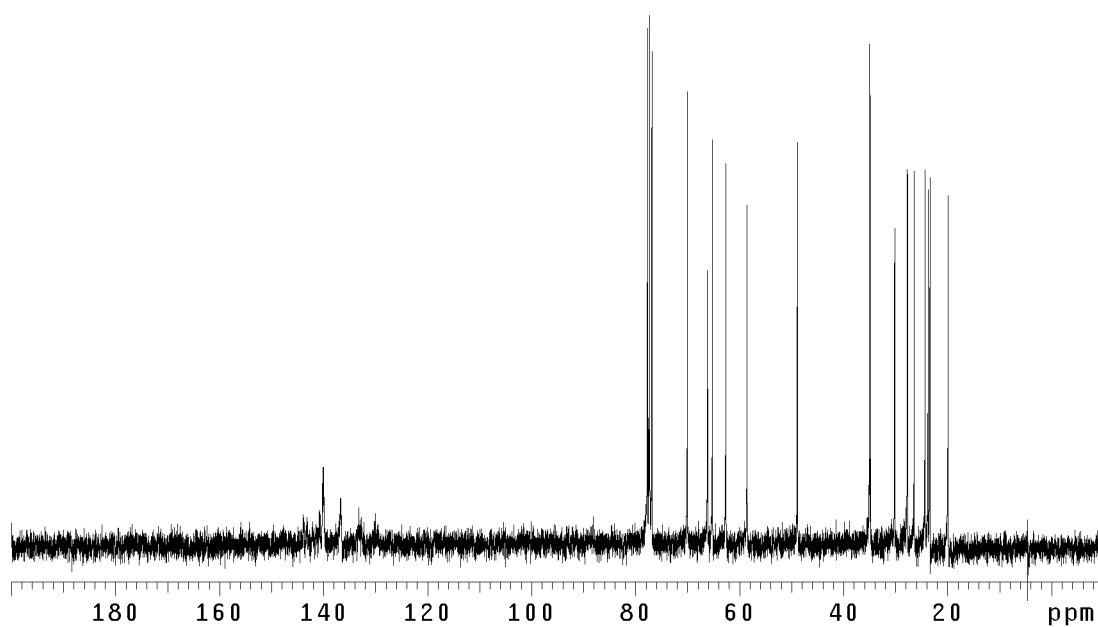


Figure A2.74 ¹³CNMR (125 MHz, CDCl₃) of compound **159**.

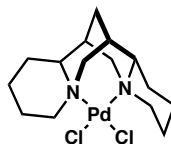
STRUCTURE 2:**Palladium[(-)-sparteine] dichloride**Contents

Table 1.	Crystal data
Figures	Figures for publication
Table 2.	Atomic coordinates
Table 3.	Selected bond distances and angles
Table 4.	Full bond distances and angles (for deposit)
Table 5.	Anisotropic displacement parameters
Table 6.	Hydrogen atomic coordinates

Table 1. Crystal data and structure refinement for EMF01 (CCDC 203513).

Empirical formula	$\text{C}_{15}\text{H}_{26}\text{Cl}_2\text{N}_2\text{Pd} \cdot 2\text{CHCl}_3$
Formula weight	650.41
Crystallization solvent	Chloroform
Crystal habit	Blade
Crystal size	0.33 x 0.15 x 0.06 mm ³
Crystal color	Orange

Data Collection

Preliminary photos	Rotation
Type of diffractometer	Bruker SMART 1000
Wavelength	0.71073 Å MoK α
Data collection temperature	98(2) K
θ range for 17268 reflections used in lattice determination	2.17 to 28.42°
Unit cell dimensions	a = 10.5805(7) Å b = 12.4401(8) Å c = 18.6906(12) Å
Volume	2460.1(3) Å ³
Z	4
Crystal system	Orthorhombic
Space group	P2 ₁ 2 ₁ 2 ₁
Density (calculated)	1.756 Mg/m ³
F(000)	1304
θ range for data collection	1.97 to 28.44°
Completeness to $\theta = 28.44^\circ$	96.7 %
Index ranges	$-13 \leq h \leq 14$, $-16 \leq k \leq 16$, $-24 \leq l \leq 24$
Data collection scan type	ω scans at 5 ϕ settings
Reflections collected	43840
Independent reflections	5883 [$R_{\text{int}} = 0.0794$]
Absorption coefficient	1.632 mm ⁻¹
Absorption correction	None
Max. and min. transmission	0.9084 and 0.6150

Table 1 (cont.)**Structure solution and Refinement**

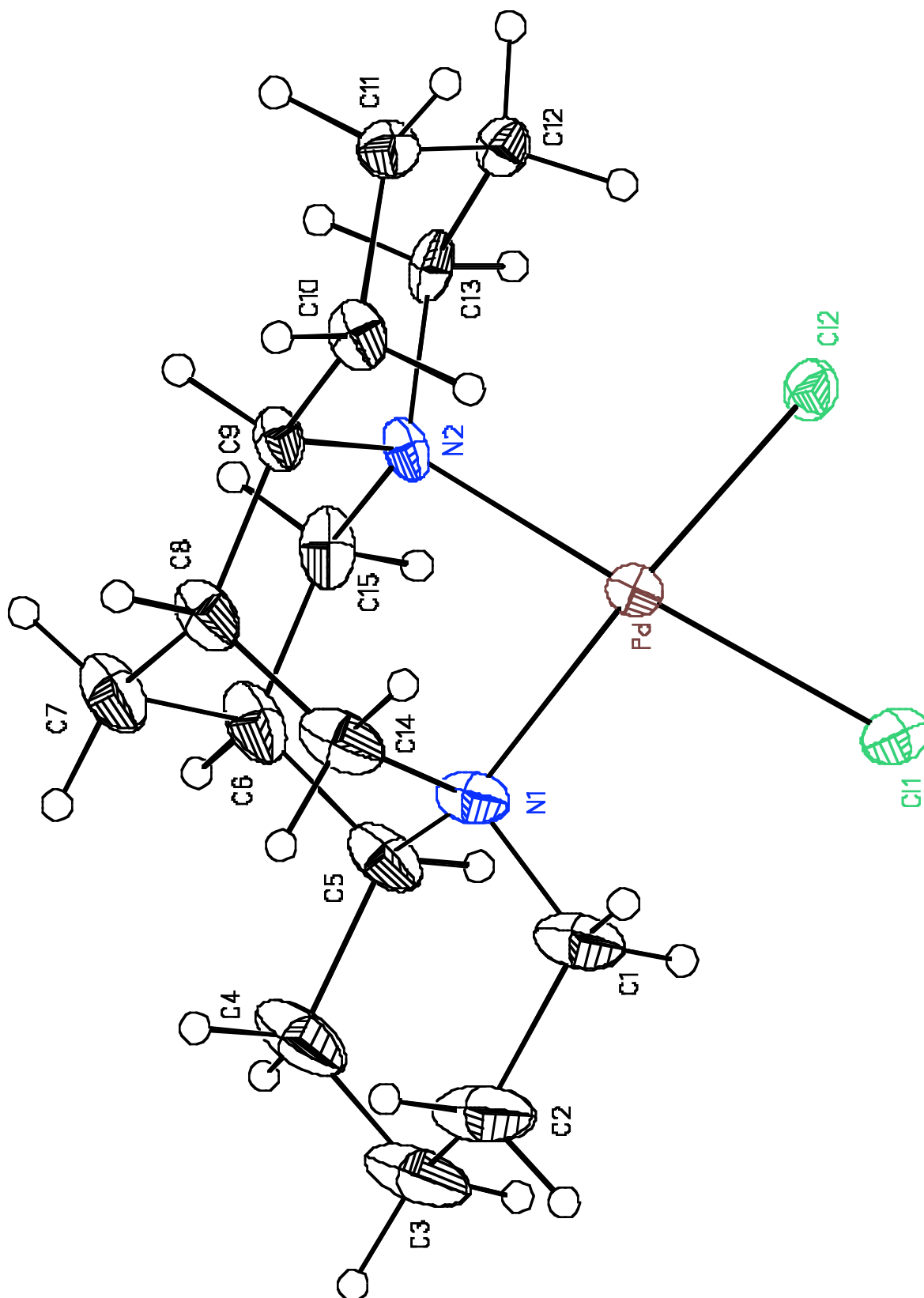
Structure solution program	SHELXS-97 (Sheldrick, 1990)
Primary solution method	Patterson method
Secondary solution method	Difference Fourier map
Hydrogen placement	Difference Fourier map
Structure refinement program	SHELXL-97 (Sheldrick, 1997)
Refinement method	Full matrix least-squares on F^2
Data / restraints / parameters	5883 / 24 / 329
Treatment of hydrogen atoms	Riding
Goodness-of-fit on F^2	1.367
Final R indices [$I > 2\sigma(I)$, 5041 reflections]	$R1 = 0.0332$, $wR2 = 0.0526$
R indices (all data)	$R1 = 0.0436$, $wR2 = 0.0538$
Type of weighting scheme used	Sigma
Weighting scheme used	$w = 1/\sigma^2(F_o^2)$
Max shift/error	0.002
Average shift/error	0.000
Absolute structure parameter	-0.04(2)
Largest diff. peak and hole	0.984 and -0.639 e.Å ⁻³

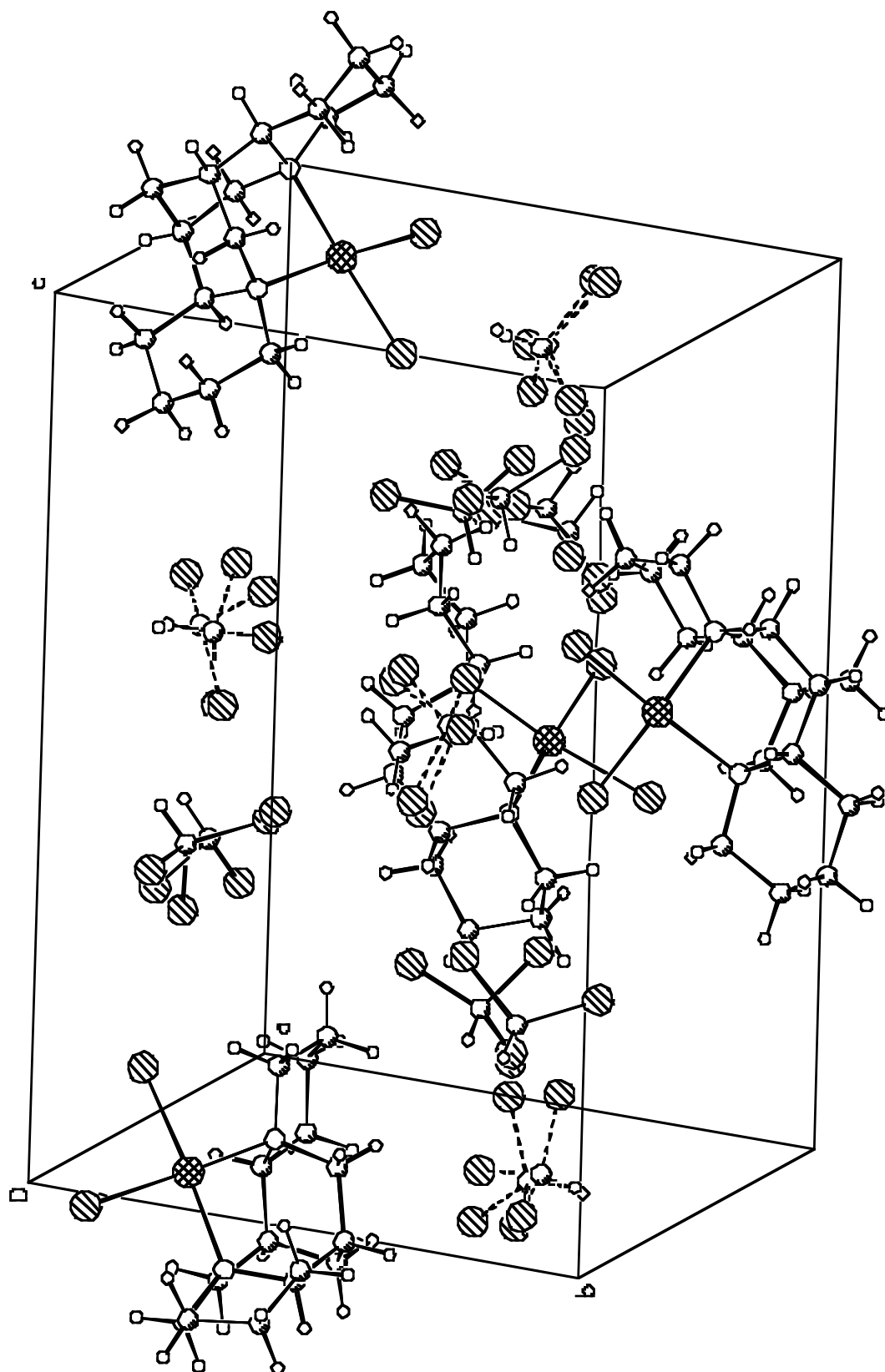
Special Refinement Details

The crystals contain chloroform as a solvent of co-crystallization. Each asymmetric unit contains two molecules of disordered chloroform. The disorder was successfully modeled and all solvent atoms were refined anisotropically. However, the 1,2 and 1,3 distances within the solvents were restrained to be similar and each distance was assigned a free variable so as to not place artificial values in the geometry. All hydrogen atoms were constrained to ride on the corresponding carbon.

Refinement of F^2 against ALL reflections. The weighted R-factor (wR) and goodness of fit (S) are based on F^2 , conventional R-factors (R) are based on F , with F set to zero for negative F^2 . The threshold expression of $F^2 > 2s(F^2)$ is used only for calculating R-factors(gt), etc., and is not relevant to the choice of reflections for refinement. R-factors based on F^2 are statistically about twice as large as those based on F , and R-factors based on ALL data will be even larger.

All esds (except the esd in the dihedral angle between two l.s. planes) are estimated using the full covariance matrix. The cell esds are taken into account individually in the estimation of esds in distances, angles and torsion angles; correlations between esds in cell parameters are only used when they are defined by crystal symmetry. An approximate (isotropic) treatment of cell esds is used for estimating esds involving l.s. planes.





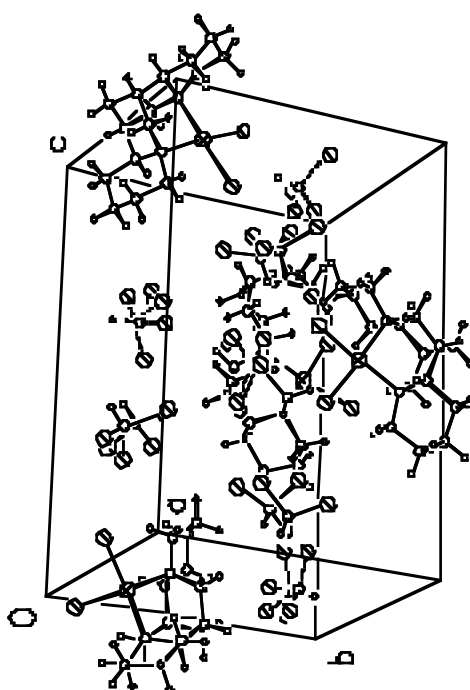
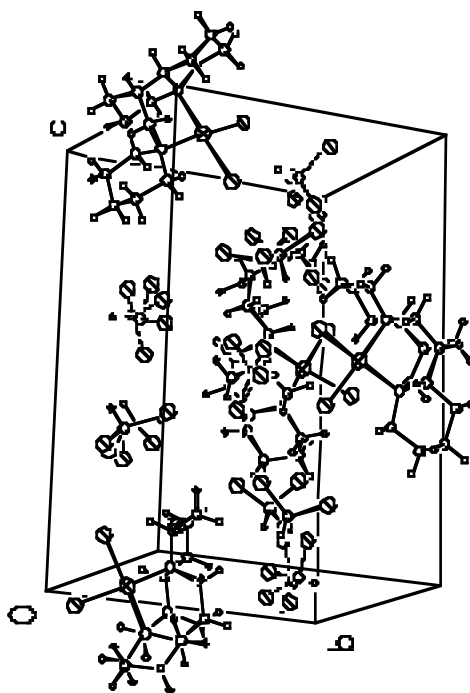


Table 2. Atomic coordinates ($\times 10^4$) and equivalent isotropic displacement parameters ($\text{\AA}^2 \times 10^3$) for EMF01 (CCDC 203513). U_{eq} is defined as the trace of the orthogonalized U_{ij} tensor.

	x	y	z	U_{eq}	Occ
Pd	6127(1)	2578(1)	9793(1)	16(1)	1
Cl(1)	6430(1)	3588(1)	8766(1)	23(1)	1
Cl(2)	5727(1)	4241(1)	10300(1)	22(1)	1
N(1)	6161(3)	1060(2)	9270(1)	23(1)	1
N(2)	5780(2)	1746(2)	10748(1)	16(1)	1
C(1)	6534(4)	1183(3)	8504(2)	33(1)	1
C(2)	6261(4)	209(3)	8033(2)	44(1)	1
C(3)	4861(4)	-33(3)	8050(2)	48(1)	1
C(4)	4454(4)	-225(3)	8811(2)	42(1)	1
C(5)	4780(3)	695(3)	9325(2)	28(1)	1
C(6)	4439(3)	404(3)	10093(2)	30(1)	1
C(7)	5283(3)	-507(3)	10358(2)	33(1)	1
C(8)	6628(3)	-48(3)	10367(2)	27(1)	1
C(9)	6689(3)	846(3)	10911(2)	19(1)	1
C(10)	8007(3)	1299(3)	11044(2)	22(1)	1
C(11)	7993(3)	2003(3)	11704(2)	22(1)	1
C(12)	7010(3)	2882(2)	11618(2)	19(1)	1
C(13)	5727(3)	2418(3)	11409(2)	20(1)	1
C(14)	7034(3)	276(3)	9620(2)	31(1)	1
C(15)	4482(3)	1304(3)	10634(2)	25(1)	1
C(16A)	516(5)	9209(5)	8232(3)	39(2)	0.669(4)
Cl(3A)	-534(4)	8190(4)	8468(3)	68(1)	0.669(4)
Cl(4A)	1767(1)	8715(2)	7721(1)	64(1)	0.669(4)
Cl(5A)	-307(2)	10180(2)	7716(1)	52(1)	0.669(4)
C(16B)	821(9)	8675(8)	8396(6)	36(4)	0.331(4)
Cl(3B)	-688(5)	8128(5)	8540(5)	31(2)	0.331(4)
Cl(4B)	1883(3)	7660(4)	8165(2)	80(2)	0.331(4)
Cl(5B)	763(7)	9641(4)	7725(2)	114(4)	0.331(4)
C(17A)	6072(7)	6401(10)	9225(4)	27(3)	0.523(5)
Cl(6A)	6365(4)	6902(2)	8365(1)	55(1)	0.523(5)
Cl(7A)	4516(2)	6717(2)	9484(2)	38(1)	0.523(5)
Cl(8A)	7155(6)	6948(9)	9833(3)	32(1)	0.523(5)
C(17B)	6234(7)	6229(12)	9150(4)	27(4)	0.477(5)
Cl(6B)	4728(3)	6713(2)	8939(3)	64(1)	0.477(5)
Cl(7B)	7253(4)	6374(4)	8420(1)	64(1)	0.477(5)
Cl(8B)	6842(6)	6923(10)	9897(4)	42(2)	0.477(5)

Table 3. Selected bond lengths [\AA] and angles [$^\circ$] for EMF01 (CCDC 203513).

Pd-N(2)	2.096(3)	N(2)-Pd-N(1)	87.51(10)
Pd-N(1)	2.127(2)	N(2)-Pd-Cl(2)	93.44(7)
Pd-Cl(2)	2.3150(8)	N(1)-Pd-Cl(2)	170.06(8)
Pd-Cl(1)	2.3161(9)	N(2)-Pd-Cl(1)	176.24(7)
		N(1)-Pd-Cl(1)	95.65(8)
		Cl(2)-Pd-Cl(1)	83.09(3)

Table 4. Bond lengths [Å] and angles [°] for EMF01 (CCDC 203513).

Pd-N(2)	2.096(3)	C(16A)-Cl(4A)	1.743(6)
Pd-N(1)	2.127(2)	C(16A)-Cl(5A)	1.773(6)
Pd-Cl(2)	2.3150(8)	C(16A)-H(16A)	1.0000
Pd-Cl(1)	2.3161(9)	C(16B)-Cl(5B)	1.739(8)
N(1)-C(1)	1.492(4)	C(16B)-Cl(4B)	1.744(9)
N(1)-C(14)	1.494(4)	C(16B)-Cl(3B)	1.756(8)
N(1)-C(5)	1.534(4)	C(16B)-H(16B)	1.0000
N(2)-C(13)	1.493(4)	C(17A)-Cl(8A)	1.751(8)
N(2)-C(15)	1.495(4)	C(17A)-Cl(6A)	1.752(8)
N(2)-C(9)	1.507(4)	C(17A)-Cl(7A)	1.761(8)
C(1)-C(2)	1.524(5)	C(17A)-H(17A)	1.0000
C(1)-H(1A)	0.9900	C(17B)-Cl(7B)	1.747(8)
C(1)-H(1B)	0.9900	C(17B)-Cl(6B)	1.749(8)
C(2)-C(3)	1.512(6)	C(17B)-Cl(8B)	1.763(8)
C(2)-H(2A)	0.9900	C(17B)-H(17B)	1.0000
C(2)-H(2B)	0.9900		
C(3)-C(4)	1.506(6)	N(2)-Pd-N(1)	87.51(10)
C(3)-H(3A)	0.9900	N(2)-Pd-Cl(2)	93.44(7)
C(3)-H(3B)	0.9900	N(1)-Pd-Cl(2)	170.06(8)
C(4)-C(5)	1.534(5)	N(2)-Pd-Cl(1)	176.24(7)
C(4)-H(4A)	0.9900	N(1)-Pd-Cl(1)	95.65(8)
C(4)-H(4B)	0.9900	Cl(2)-Pd-Cl(1)	83.09(3)
C(5)-C(6)	1.523(5)	C(1)-N(1)-C(14)	108.9(3)
C(5)-H(5)	1.0000	C(1)-N(1)-C(5)	110.3(3)
C(6)-C(15)	1.508(5)	C(14)-N(1)-C(5)	111.4(3)
C(6)-C(7)	1.526(4)	C(1)-N(1)-Pd	110.8(2)
C(6)-H(6)	1.0000	C(14)-N(1)-Pd	112.87(19)
C(7)-C(8)	1.533(4)	C(5)-N(1)-Pd	102.44(19)
C(7)-H(7A)	0.9900	C(13)-N(2)-C(15)	106.9(2)
C(7)-H(7B)	0.9900	C(13)-N(2)-C(9)	105.8(2)
C(8)-C(9)	1.509(5)	C(15)-N(2)-C(9)	110.0(2)
C(8)-C(14)	1.515(5)	C(13)-N(2)-Pd	115.78(18)
C(8)-H(8)	1.0000	C(15)-N(2)-Pd	102.76(19)
C(9)-C(10)	1.525(4)	C(9)-N(2)-Pd	115.25(18)
C(9)-H(9)	1.0000	N(1)-C(1)-C(2)	115.0(3)
C(10)-C(11)	1.513(4)	N(1)-C(1)-H(1A)	108.5
C(10)-H(10A)	0.9900	C(2)-C(1)-H(1A)	108.5
C(10)-H(10B)	0.9900	N(1)-C(1)-H(1B)	108.5
C(11)-C(12)	1.517(4)	C(2)-C(1)-H(1B)	108.5
C(11)-H(11A)	0.9900	H(1A)-C(1)-H(1B)	107.5
C(11)-H(11B)	0.9900	C(3)-C(2)-C(1)	109.4(3)
C(12)-C(13)	1.526(4)	C(3)-C(2)-H(2A)	109.8
C(12)-H(12A)	0.9900	C(1)-C(2)-H(2A)	109.8
C(12)-H(12B)	0.9900	C(3)-C(2)-H(2B)	109.8
C(13)-H(13A)	0.9900	C(1)-C(2)-H(2B)	109.8
C(13)-H(13B)	0.9900	H(2A)-C(2)-H(2B)	108.2
C(14)-H(14A)	0.9900	C(4)-C(3)-C(2)	109.4(3)
C(14)-H(14B)	0.9900	C(4)-C(3)-H(3A)	109.8
C(15)-H(15A)	0.9900	C(2)-C(3)-H(3A)	109.8
C(15)-H(15B)	0.9900	C(4)-C(3)-H(3B)	109.8
C(16A)-Cl(3A)	1.742(6)	C(2)-C(3)-H(3B)	109.8

H(3A)-C(3)-H(3B)	108.2	H(12A)-C(12)-H(12B)	108.0
C(3)-C(4)-C(5)	114.1(3)	N(2)-C(13)-C(12)	113.0(2)
C(3)-C(4)-H(4A)	108.7	N(2)-C(13)-H(13A)	109.0
C(5)-C(4)-H(4A)	108.7	C(12)-C(13)-H(13A)	109.0
C(3)-C(4)-H(4B)	108.7	N(2)-C(13)-H(13B)	109.0
C(5)-C(4)-H(4B)	108.7	C(12)-C(13)-H(13B)	109.0
H(4A)-C(4)-H(4B)	107.6	H(13A)-C(13)-H(13B)	107.8
C(6)-C(5)-C(4)	111.1(3)	N(1)-C(14)-C(8)	113.7(3)
C(6)-C(5)-N(1)	111.1(3)	N(1)-C(14)-H(14A)	108.8
C(4)-C(5)-N(1)	113.1(3)	C(8)-C(14)-H(14A)	108.8
C(6)-C(5)-H(5)	107.0	N(1)-C(14)-H(14B)	108.8
C(4)-C(5)-H(5)	107.0	C(8)-C(14)-H(14B)	108.8
N(1)-C(5)-H(5)	107.0	H(14A)-C(14)-H(14B)	107.7
C(15)-C(6)-C(5)	116.6(3)	N(2)-C(15)-C(6)	113.4(3)
C(15)-C(6)-C(7)	108.4(3)	N(2)-C(15)-H(15A)	108.9
C(5)-C(6)-C(7)	110.1(3)	C(6)-C(15)-H(15A)	108.9
C(15)-C(6)-H(6)	107.1	N(2)-C(15)-H(15B)	108.9
C(5)-C(6)-H(6)	107.1	C(6)-C(15)-H(15B)	108.9
C(7)-C(6)-H(6)	107.1	H(15A)-C(15)-H(15B)	107.7
C(6)-C(7)-C(8)	105.7(3)	Cl(3A)-C(16A)-Cl(4A)	111.5(4)
C(6)-C(7)-H(7A)	110.6	Cl(3A)-C(16A)-Cl(5A)	108.7(3)
C(8)-C(7)-H(7A)	110.6	Cl(4A)-C(16A)-Cl(5A)	108.4(3)
C(6)-C(7)-H(7B)	110.6	Cl(3A)-C(16A)-H(16A)	109.4
C(8)-C(7)-H(7B)	110.6	Cl(4A)-C(16A)-H(16A)	109.4
H(7A)-C(7)-H(7B)	108.7	Cl(5A)-C(16A)-H(16A)	109.4
C(9)-C(8)-C(14)	114.3(3)	Cl(5B)-C(16B)-Cl(4B)	110.1(6)
C(9)-C(8)-C(7)	108.7(3)	Cl(5B)-C(16B)-Cl(3B)	110.2(6)
C(14)-C(8)-C(7)	110.7(3)	Cl(4B)-C(16B)-Cl(3B)	110.1(6)
C(9)-C(8)-H(8)	107.6	Cl(5B)-C(16B)-H(16B)	108.8
C(14)-C(8)-H(8)	107.6	Cl(4B)-C(16B)-H(16B)	108.8
C(7)-C(8)-H(8)	107.6	Cl(3B)-C(16B)-H(16B)	108.8
N(2)-C(9)-C(8)	112.6(3)	Cl(8A)-C(17A)-Cl(6A)	110.0(6)
N(2)-C(9)-C(10)	110.0(3)	Cl(8A)-C(17A)-Cl(7A)	110.3(5)
C(8)-C(9)-C(10)	115.0(3)	Cl(6A)-C(17A)-Cl(7A)	109.7(5)
N(2)-C(9)-H(9)	106.2	Cl(8A)-C(17A)-H(17A)	108.9
C(8)-C(9)-H(9)	106.2	Cl(6A)-C(17A)-H(17A)	108.9
C(10)-C(9)-H(9)	106.2	Cl(7A)-C(17A)-H(17A)	108.9
C(11)-C(10)-C(9)	109.7(3)	Cl(7B)-C(17B)-Cl(6B)	110.5(5)
C(11)-C(10)-H(10A)	109.7	Cl(7B)-C(17B)-Cl(8B)	110.0(6)
C(9)-C(10)-H(10A)	109.7	Cl(6B)-C(17B)-Cl(8B)	110.0(6)
C(11)-C(10)-H(10B)	109.7	Cl(7B)-C(17B)-H(17B)	108.7
C(9)-C(10)-H(10B)	109.7	Cl(6B)-C(17B)-H(17B)	108.7
H(10A)-C(10)-H(10B)	108.2	Cl(8B)-C(17B)-H(17B)	108.7
C(10)-C(11)-C(12)	109.8(3)		
C(10)-C(11)-H(11A)	109.7		
C(12)-C(11)-H(11A)	109.7		
C(10)-C(11)-H(11B)	109.7		
C(12)-C(11)-H(11B)	109.7		
H(11A)-C(11)-H(11B)	108.2		
C(11)-C(12)-C(13)	111.3(3)		
C(11)-C(12)-H(12A)	109.4		
C(13)-C(12)-H(12A)	109.4		
C(11)-C(12)-H(12B)	109.4		
C(13)-C(12)-H(12B)	109.4		

Table 5. Anisotropic displacement parameters ($\text{\AA}^2 \times 10^4$) for EMF01 (CCDC 203513). The anisotropic displacement factor exponent takes the form: $-2\pi^2 [h^2 a^{*2} U^{11} + \dots + 2 h k a^* b^* U^{12}]$

	U^{11}	U^{22}	U^{33}	U^{23}	U^{13}	U^{12}
Pd	112(1)	179(1)	185(1)	-17(1)	-1(1)	14(1)
Cl(1)	180(5)	329(5)	183(4)	4(4)	0(3)	-41(4)
Cl(2)	306(5)	164(4)	199(4)	12(4)	24(4)	57(3)
N(1)	207(15)	246(15)	245(15)	-83(12)	-63(15)	64(14)
N(2)	90(13)	120(14)	271(15)	14(12)	-4(11)	-8(10)
C(1)	310(20)	360(20)	320(20)	-164(18)	-75(18)	79(18)
C(2)	510(30)	460(30)	340(20)	-199(19)	-150(20)	160(20)
C(3)	520(30)	360(30)	570(30)	-260(20)	-310(20)	160(20)
C(4)	360(20)	260(20)	650(30)	-160(20)	-270(20)	46(18)
C(5)	182(19)	200(19)	460(20)	-70(18)	-157(17)	30(15)
C(6)	166(17)	205(19)	530(30)	31(18)	-119(18)	-44(14)
C(7)	310(20)	188(19)	500(30)	-12(18)	-107(19)	-1(15)
C(8)	209(18)	163(17)	420(30)	-16(16)	-116(17)	51(14)
C(9)	152(18)	149(17)	282(19)	35(15)	-42(15)	0(14)
C(10)	129(17)	178(18)	340(20)	21(15)	-41(15)	53(14)
C(11)	189(18)	238(19)	224(19)	-6(14)	-9(15)	-7(14)
C(12)	185(18)	184(18)	195(17)	16(13)	9(14)	35(13)
C(13)	189(15)	191(17)	222(16)	91(17)	81(12)	47(16)
C(14)	221(19)	260(20)	430(30)	-141(18)	-107(18)	110(15)
C(15)	90(16)	239(19)	410(20)	110(17)	-28(16)	-8(14)
C(16A)	300(40)	670(60)	190(40)	-150(40)	10(30)	-110(40)
Cl(3A)	650(20)	950(30)	439(18)	-150(16)	120(15)	-307(16)
Cl(4A)	212(9)	1160(30)	538(12)	-531(14)	8(8)	-41(10)
Cl(5A)	515(13)	557(13)	495(11)	-251(9)	-13(9)	-160(9)
C(16B)	260(80)	670(110)	160(60)	130(70)	-10(50)	-100(70)
Cl(3B)	130(20)	320(30)	470(40)	80(20)	42(19)	138(17)
Cl(4B)	440(20)	1110(50)	860(30)	-640(40)	60(20)	-50(30)
Cl(5B)	2510(110)	600(30)	330(20)	-10(20)	-120(40)	-940(60)
C(17A)	400(70)	100(50)	310(60)	60(40)	220(50)	60(40)
Cl(6A)	960(30)	385(13)	302(11)	32(9)	123(14)	-188(16)
Cl(7A)	203(10)	208(10)	730(20)	3(11)	-16(11)	-13(7)
Cl(8A)	210(20)	310(15)	450(20)	-24(16)	-90(17)	-6(18)
C(17B)	230(60)	300(80)	280(60)	-90(50)	-130(50)	-50(50)
Cl(6B)	388(16)	308(14)	1230(40)	58(18)	-280(20)	-3(12)
Cl(7B)	700(30)	860(30)	345(14)	54(15)	159(14)	-420(20)
Cl(8B)	450(40)	279(17)	520(20)	-144(16)	-10(20)	-30(30)

Table 6. Hydrogen coordinates ($\times 10^4$) and isotropic displacement parameters ($\text{\AA}^2 \times 10^3$) for EMF01 (CCDC 203513).

	x	y	z	U_{iso}
H(1A)	7451	1339	8482	40
H(1B)	6084	1812	8303	40
H(2A)	6530	358	7536	52
H(2B)	6742	-420	8210	52
H(3A)	4384	580	7847	58
H(3B)	4681	-678	7757	58
H(4A)	4859	-892	8986	51
H(4B)	3528	-340	8819	51
H(5)	4242	1323	9188	34
H(6)	3552	125	10087	36
H(7A)	5229	-1134	10033	40
H(7B)	5027	-736	10845	40
H(8)	7208	-633	10531	32
H(9)	6406	527	11375	23
H(10A)	8615	702	11111	26
H(10B)	8282	1726	10625	26
H(11A)	8837	2329	11775	26
H(11B)	7792	1562	12130	26
H(12A)	7293	3394	11245	23
H(12B)	6928	3282	12073	23
H(13A)	5404	1975	11809	24
H(13B)	5125	3016	11333	24
H(14A)	7889	597	9645	37
H(14B)	7089	-376	9318	37
H(15A)	3920	1891	10471	30
H(15B)	4151	1036	11096	30
H(16A)	855	9555	8675	46
H(16B)	1115	9023	8849	44
H(17A)	6173	5602	9219	32
H(17B)	6168	5448	9271	33

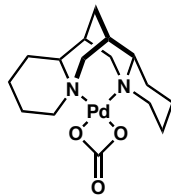
STRUCTURE 3:**Palladium(II)[(-)-sparteine] carbonate**Contents

Table 1.	Crystal data
Figures	for publication
Table 2.	Atomic coordinates
Table 3.	Selected bond distances and angles
Table 4.	Full bond distances and angles (for deposit)
Table 5.	Anisotropic displacement parameters
Table 6.	Observed and calculated structure factors (for deposit)

Table 1. Crystal data and structure refinement for JTB02 (CCDC 218105).

Empirical formula	C ₁₆ H ₂₆ N ₂ O ₃ Pd
Formula weight	400.79
Crystallization Solvent	Chloroform/heptane
Crystal Habit	Plate
Crystal size	0.26 x 0.22 x 0.07 mm ³
Crystal color	Pale yellow

Data Collection

Preliminary Photos	Rotation
Type of diffractometer	Bruker SMART 1000
Wavelength	0.71073 Å MoK α
Data Collection Temperature	100(2) K
θ range for 15498 reflections used in lattice determination	2.23 to 28.38°
Unit cell dimensions	a = 9.1237(6) Å b = 11.0293(8) Å c = 15.6088(11) Å
Volume	1570.68(19) Å ³
Z	4
Crystal system	Orthorhombic
Space group	P2 ₁ 2 ₁ 2 ₁
Density (calculated)	1.695 Mg/m ³
F(000)	824
Data collection program	Bruker SMART v5.054
θ range for data collection	2.26 to 28.39°
Completeness to $\theta = 28.39^\circ$	96.2 %
Index ranges	-11 \leq h \leq 12, -14 \leq k \leq 14, -20 \leq l \leq 20
Data collection scan type	ω scans at 5 ϕ settings
Data reduction program	Bruker SAINT v6.022
Reflections collected	23359
Independent reflections	3727 [R _{int} = 0.0728]
Absorption coefficient	1.196 mm ⁻¹
Absorption correction	None
Max. and min. transmission	0.9209 and 0.7462

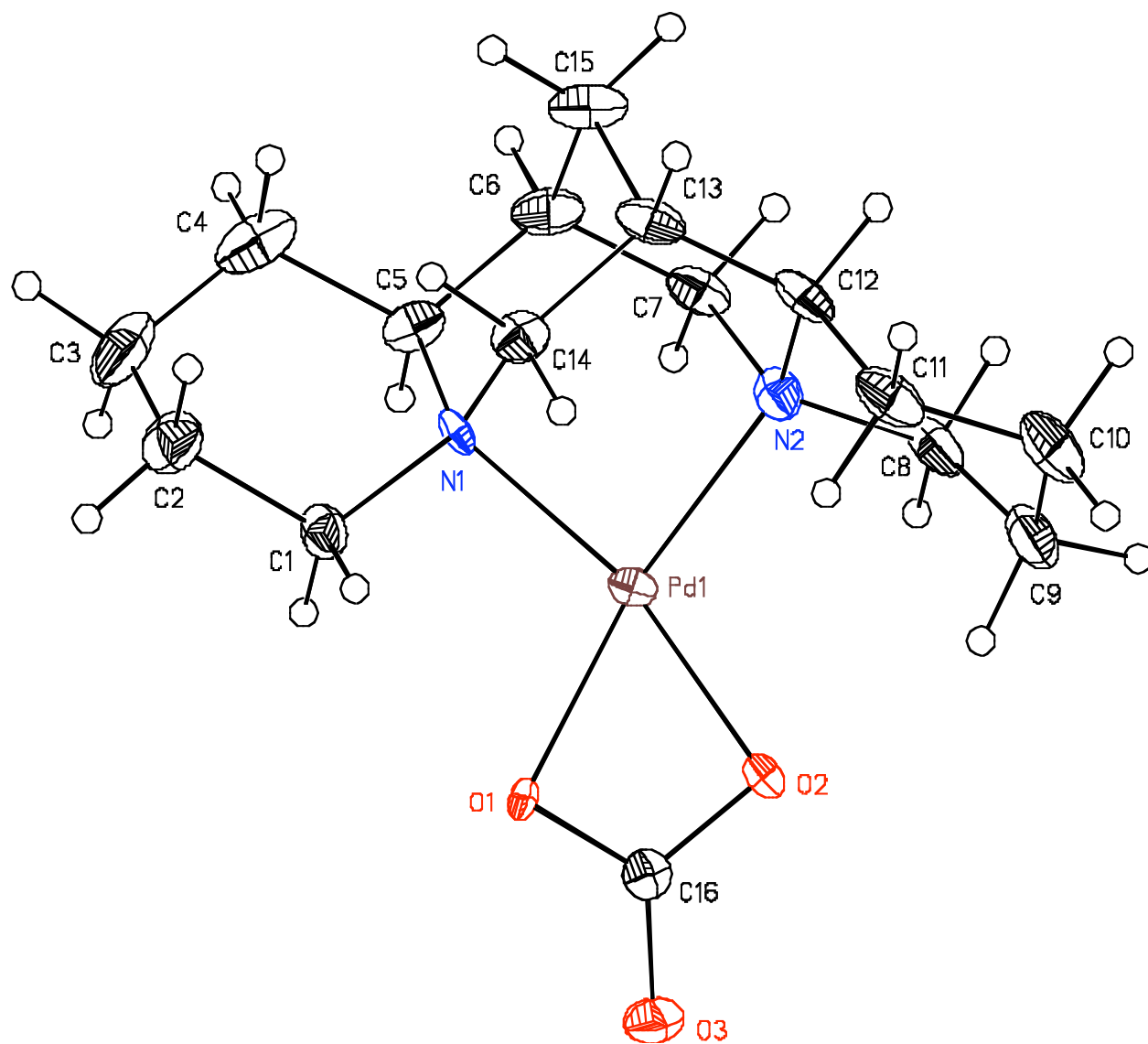
Table 1 (cont.)**Structure solution and Refinement**

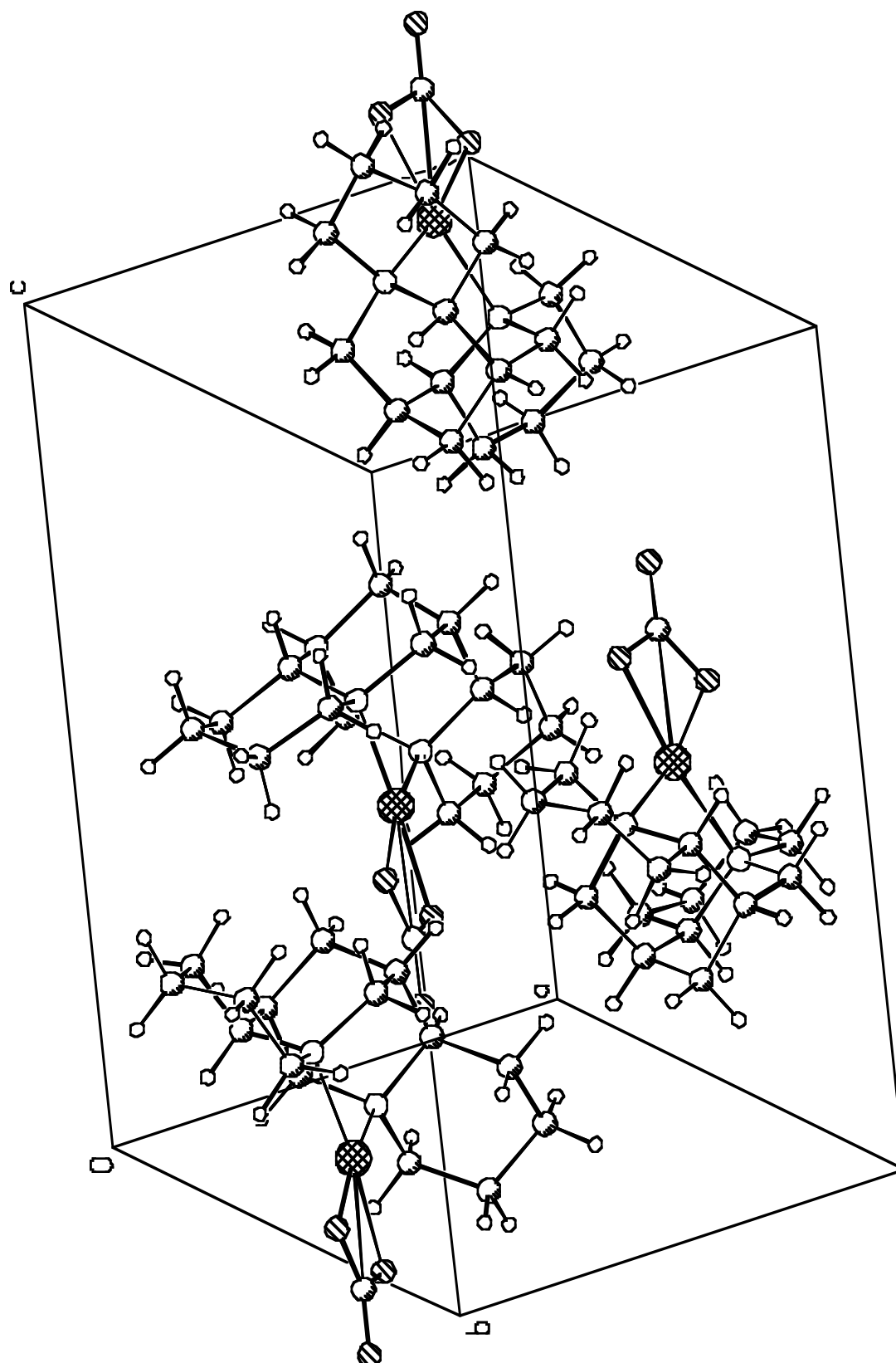
Structure solution program	SHELXS-97 (Sheldrick, 1990)
Primary solution method	Direct methods
Secondary solution method	Difference Fourier map
Hydrogen placement	Geometric positions
Structure refinement program	SHELXL-97 (Sheldrick, 1997)
Refinement method	Full matrix least-squares on F^2
Data / restraints / parameters	3727 / 0 / 199
Treatment of hydrogen atoms	Riding
Goodness-of-fit on F^2	1.833
Final R indices [$I > 2\sigma(I)$, 3515 reflections]	$R1 = 0.0333$, $wR2 = 0.0594$
R indices (all data)	$R1 = 0.0365$, $wR2 = 0.0600$
Type of weighting scheme used	Sigma
Weighting scheme used	$w = 1/\sigma^2(F_o^2)$
Max shift/error	0.000
Average shift/error	0.000
Absolute structure parameter	0.02(3)
Largest diff. peak and hole	1.309 and -0.502 e.Å ⁻³

Special Refinement Details

Refinement of F^2 against ALL reflections. The weighted R-factor (wR) and goodness of fit (S) are based on F^2 , conventional R-factors (R) are based on F , with F set to zero for negative F^2 . The threshold expression of $F^2 > 2s(F^2)$ is used only for calculating R-factors(gt), etc., and is not relevant to the choice of reflections for refinement. R-factors based on F^2 are statistically about twice as large as those based on F , and R-factors based on ALL data will be even larger.

All esds (except the esd in the dihedral angle between two l.s. planes) are estimated using the full covariance matrix. The cell esds are taken into account individually in the estimation of esds in distances, angles and torsion angles; correlations between esds in cell parameters are only used when they are defined by crystal symmetry. An approximate (isotropic) treatment of cell esds is used for estimating esds involving l.s. planes.





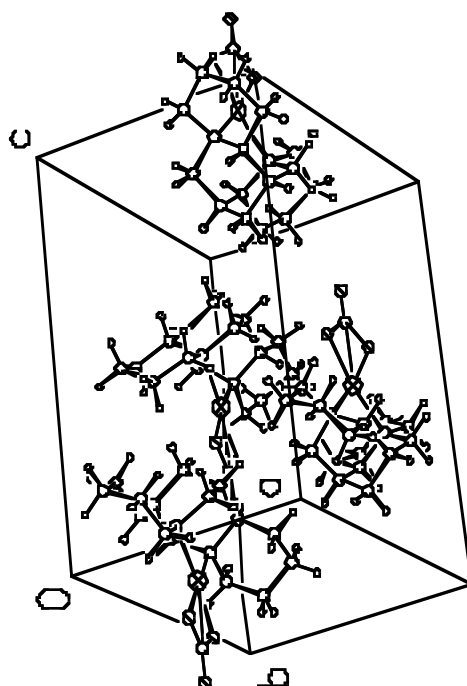
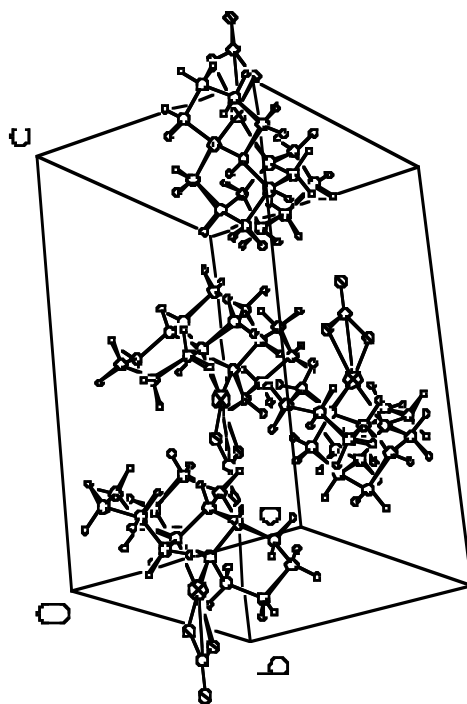


Table 2. Atomic coordinates ($\times 10^4$) and equivalent isotropic displacement parameters ($\text{\AA}^2 \times 10^3$) for JTB02 (CCDC 218105). $U(\text{eq})$ is defined as the trace of the orthogonalized U^{ij} tensor.

	x	y	z	U_{eq}
Pd(1)	2868(1)	3270(1)	23(1)	14(1)
O(1)	3077(3)	2262(2)	-1050(2)	13(1)
O(2)	2600(3)	4200(2)	-1089(2)	18(1)
O(3)	2842(3)	3158(3)	-2327(2)	24(1)
N(1)	3133(3)	1982(3)	974(2)	13(1)
N(2)	2568(4)	4555(3)	965(2)	18(1)
C(1)	3478(4)	839(3)	530(2)	20(1)
C(2)	3435(4)	-269(3)	1093(3)	31(1)
C(3)	1945(5)	-383(4)	1525(3)	38(1)
C(4)	1621(4)	753(4)	2011(3)	35(1)
C(5)	1706(4)	1910(3)	1473(2)	21(1)
C(6)	1461(4)	3044(3)	2001(2)	24(1)
C(7)	1240(4)	4188(3)	1479(2)	23(1)
C(8)	2279(4)	5777(3)	581(2)	27(1)
C(9)	3580(4)	6289(3)	122(3)	28(1)
C(10)	4941(4)	6319(3)	683(3)	35(1)
C(11)	5201(4)	5057(4)	1059(2)	28(1)
C(12)	3879(4)	4643(3)	1565(2)	23(1)
C(13)	4081(4)	3480(3)	2066(2)	22(1)
C(14)	4393(4)	2359(3)	1534(2)	20(1)
C(15)	2726(5)	3253(5)	2628(2)	30(1)
C(16)	2846(3)	3199(3)	-1539(2)	16(1)

Table 3. Selected bond lengths [\AA] and angles [$^\circ$] for JTB02 (CCDC 218105).

Pd(1)-O(1)	2.020(3)	O(1)-Pd(1)-O(2)	65.20(10)
Pd(1)-O(2)	2.030(3)	O(1)-Pd(1)-N(2)	169.44(11)
Pd(1)-N(2)	2.061(3)	O(2)-Pd(1)-N(2)	104.25(12)
Pd(1)-N(1)	2.069(3)	O(1)-Pd(1)-N(1)	101.91(10)
Pd(1)-C(16)	2.439(3)	O(2)-Pd(1)-N(1)	166.96(10)
		N(2)-Pd(1)-N(1)	88.61(12)
		O(1)-Pd(1)-C(16)	32.23(10)
		O(2)-Pd(1)-C(16)	32.97(10)
		N(2)-Pd(1)-C(16)	137.22(12)
		N(1)-Pd(1)-C(16)	134.13(12)

Table 4. Bond lengths [Å] and angles [°] for JTB02 (CCDC 218105).

Pd(1)-O(1)	2.020(3)	C(7)-N(2)-Pd(1)	107.5(2)
Pd(1)-O(2)	2.030(3)	C(12)-N(2)-Pd(1)	112.2(2)
Pd(1)-N(2)	2.061(3)	N(1)-C(1)-C(2)	114.5(3)
Pd(1)-N(1)	2.069(3)	C(1)-C(2)-C(3)	110.4(3)
Pd(1)-C(16)	2.439(3)	C(4)-C(3)-C(2)	109.4(3)
O(1)-C(16)	1.302(4)	C(3)-C(4)-C(5)	114.2(3)
O(2)-C(16)	1.328(4)	C(6)-C(5)-N(1)	111.2(3)
O(3)-C(16)	1.231(4)	C(6)-C(5)-C(4)	112.5(3)
N(1)-C(1)	1.473(4)	N(1)-C(5)-C(4)	111.6(3)
N(1)-C(14)	1.503(4)	C(5)-C(6)-C(7)	114.5(3)
N(1)-C(5)	1.519(4)	C(5)-C(6)-C(15)	111.1(3)
N(2)-C(8)	1.499(4)	C(7)-C(6)-C(15)	108.6(3)
N(2)-C(7)	1.508(5)	N(2)-C(7)-C(6)	113.8(3)
N(2)-C(12)	1.522(4)	C(9)-C(8)-N(2)	113.0(3)
C(1)-C(2)	1.505(4)	C(8)-C(9)-C(10)	112.4(3)
C(2)-C(3)	1.523(6)	C(9)-C(10)-C(11)	109.2(3)
C(3)-C(4)	1.494(6)	C(12)-C(11)-C(10)	110.6(3)
C(4)-C(5)	1.530(5)	C(11)-C(12)-C(13)	115.4(3)
C(5)-C(6)	1.515(5)	C(11)-C(12)-N(2)	109.0(3)
C(6)-C(7)	1.515(5)	C(13)-C(12)-N(2)	111.1(3)
C(6)-C(15)	1.531(5)	C(12)-C(13)-C(14)	115.5(3)
C(8)-C(9)	1.497(5)	C(12)-C(13)-C(15)	109.6(3)
C(9)-C(10)	1.519(5)	C(14)-C(13)-C(15)	109.3(3)
C(10)-C(11)	1.529(5)	N(1)-C(14)-C(13)	113.6(3)
C(11)-C(12)	1.512(5)	C(6)-C(15)-C(13)	105.4(3)
C(12)-C(13)	1.513(5)	O(3)-C(16)-O(1)	123.8(3)
C(13)-C(14)	1.516(5)	O(3)-C(16)-O(2)	124.0(3)
C(13)-C(15)	1.537(5)	O(1)-C(16)-O(2)	112.2(3)
		O(3)-C(16)-Pd(1)	179.6(3)
O(1)-Pd(1)-O(2)	65.20(10)	O(1)-C(16)-Pd(1)	55.85(17)
O(1)-Pd(1)-N(2)	169.44(11)	O(2)-C(16)-Pd(1)	56.34(16)
O(2)-Pd(1)-N(2)	104.25(12)		
O(1)-Pd(1)-N(1)	101.91(10)		
O(2)-Pd(1)-N(1)	166.96(10)		
N(2)-Pd(1)-N(1)	88.61(12)		
O(1)-Pd(1)-C(16)	32.23(10)		
O(2)-Pd(1)-C(16)	32.97(10)		
N(2)-Pd(1)-C(16)	137.22(12)		
N(1)-Pd(1)-C(16)	134.13(12)		
C(16)-O(1)-Pd(1)	91.92(19)		
C(16)-O(2)-Pd(1)	90.69(19)		
C(1)-N(1)-C(14)	110.3(3)		
C(1)-N(1)-C(5)	112.3(3)		
C(14)-N(1)-C(5)	111.9(3)		
C(1)-N(1)-Pd(1)	105.9(2)		
C(14)-N(1)-Pd(1)	108.5(2)		
C(5)-N(1)-Pd(1)	107.7(2)		
C(8)-N(2)-C(7)	108.2(3)		
C(8)-N(2)-C(12)	109.1(3)		
C(7)-N(2)-C(12)	108.7(3)		
C(8)-N(2)-Pd(1)	110.9(2)		

Table 5. Anisotropic displacement parameters ($\text{\AA}^2 \times 10^4$) for JTB02 (CCDC 218105). The anisotropic displacement factor exponent takes the form: $-2\pi^2 [h^2 a^{*2} U^{11} + \dots + 2 h k a^* b^* U^{12}]$

	U^{11}	U^{22}	U^{33}	U^{23}	U^{13}	U^{12}
Pd(1)	134(1)	171(1)	112(1)	-22(2)	-10(2)	4(1)
O(1)	162(13)	81(12)	132(11)	29(10)	-4(11)	1(9)
O(2)	266(16)	127(13)	146(11)	-41(11)	-12(11)	-39(10)
O(3)	297(14)	274(14)	137(11)	13(12)	-40(12)	13(14)
N(1)	124(16)	75(15)	179(14)	-63(12)	13(11)	43(11)
N(2)	193(18)	159(16)	198(15)	-9(13)	-39(12)	20(12)
C(1)	229(17)	135(16)	223(17)	-19(14)	-34(15)	43(13)
C(2)	380(20)	260(19)	279(19)	75(18)	-79(18)	-4(17)
C(3)	440(30)	350(20)	350(20)	194(19)	-70(20)	-89(19)
C(4)	260(20)	520(30)	260(20)	160(20)	30(17)	-12(18)
C(5)	151(16)	290(20)	181(16)	34(16)	15(13)	19(13)
C(6)	162(16)	400(20)	156(16)	8(16)	26(14)	28(15)
C(7)	211(18)	278(19)	203(17)	-100(16)	39(15)	12(15)
C(8)	310(20)	213(17)	276(19)	-109(15)	-71(17)	70(15)
C(9)	361(18)	182(14)	310(20)	-90(18)	-40(20)	-29(13)
C(10)	360(20)	280(20)	410(20)	-158(19)	-70(20)	-63(17)
C(11)	203(18)	350(20)	285(19)	-160(18)	-46(16)	-50(15)
C(12)	230(18)	247(19)	220(18)	-129(15)	-69(15)	-7(14)
C(13)	170(16)	340(20)	153(15)	-81(16)	-67(13)	42(14)
C(14)	167(17)	235(18)	185(18)	25(15)	-66(14)	9(14)
C(15)	280(20)	460(30)	142(16)	-20(20)	-1(16)	0(20)
C(16)	117(14)	178(15)	181(15)	-10(14)	-13(13)	-4(15)

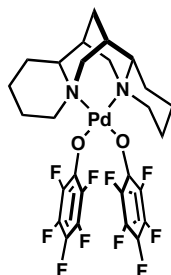
STURCTURE 4:**Palladium(II)[(-)-sparteine]pentafluorophenoxide**Contents

Table 1. Crystal data
Figures for Publication
Table 2. Atomic coordinates
Table 3. Selected bond distances and angles
Table 4. Full bond distances and angles
Table 5. Anisotropic displacement parameters
Table 6. Observed and calculated structure factors (available upon request)

Table 1. Crystal data and structure refinement for JTB05 (CCDC 272190).

Empirical formula	C ₂₇ H ₂₆ F ₁₀ N ₂ O ₂ Pd
Formula weight	706.90
Crystallization solvent	Dichloromethane/pentane
Crystal habit	Block
Crystal size	0.31 x 0.22 x 0.21 mm ³
Crystal color	Orange

Data Collection

Type of diffractometer	Bruker SMART 1000
Wavelength	0.71073 Å MoK α
Data collection temperature	100(2) K
θ range for 10228 reflections used in lattice determination	2.19 to 27.71°
Unit cell dimensions	a = 10.9581(10) Å b = 12.8577(12) Å c = 18.6047(18) Å
Volume	2621.3(4) Å ³
Z	4
Crystal system	Orthorhombic
Space group	P2 ₁ 2 ₁ 2 ₁
Density (calculated)	1.791 Mg/m ³
F(000)	1416
Data collection program	Bruker SMART v5.630
θ range for data collection	1.93 to 28.13°
Completeness to $\theta = 28.13^\circ$	95.9 %
Index ranges	-14 \leq h \leq 14, -17 \leq k \leq 16, -23 \leq l \leq 23
Data collection scan type	ω scans at 3 ϕ settings
Data reduction program	Bruker SAINT v6.45A
Reflections collected	22971
Independent reflections	5989 [R _{int} = 0.0584]
Absorption coefficient	0.810 mm ⁻¹
Absorption correction	None
Max. and min. transmission	0.8484 and 0.7874

Table 1 (cont.)**Structure solution and Refinement**

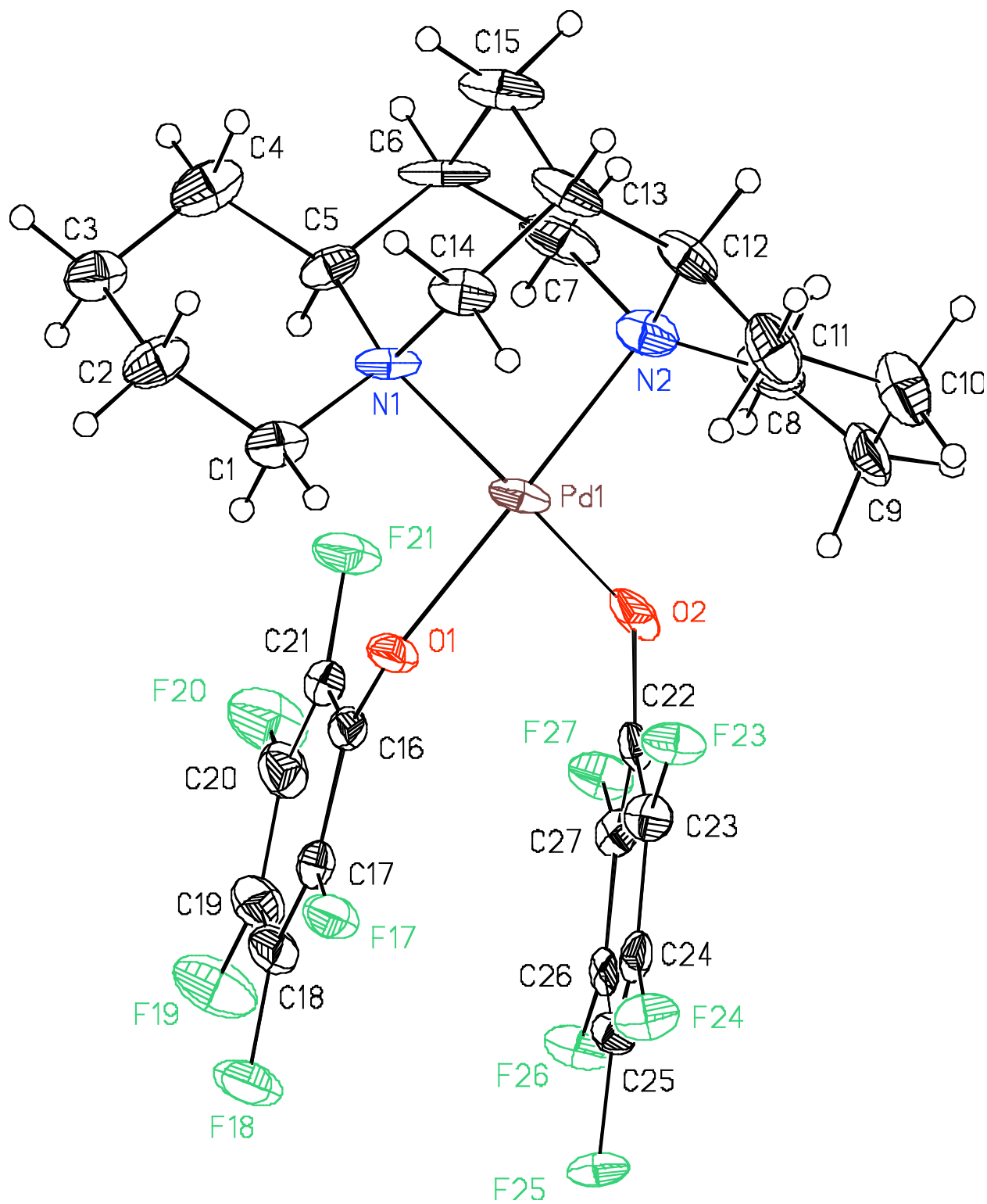
Structure solution program	Bruker XS v6.12
Primary solution method	Direct methods
Secondary solution method	Difference Fourier map
Hydrogen placement	Geometric positions
Structure refinement program	Bruker XL v6.12
Refinement method	Full matrix least-squares on F^2
Data / restraints / parameters	5989 / 0 / 379
Treatment of hydrogen atoms	Riding
Goodness-of-fit on F^2	2.387
Final R indices [$I > 2\sigma(I)$, 5016 reflections]	$R1 = 0.0642$, $wR2 = 0.1049$
R indices (all data)	$R1 = 0.0784$, $wR2 = 0.1061$
Type of weighting scheme used	Sigma
Weighting scheme used	$w = 1/\sigma^2(F_o^2)$
Max shift/error	0.000
Average shift/error	0.000
Absolute structure parameter	-0.04(4)
Largest diff. peak and hole	5.273 and -2.809 e.Å ⁻³

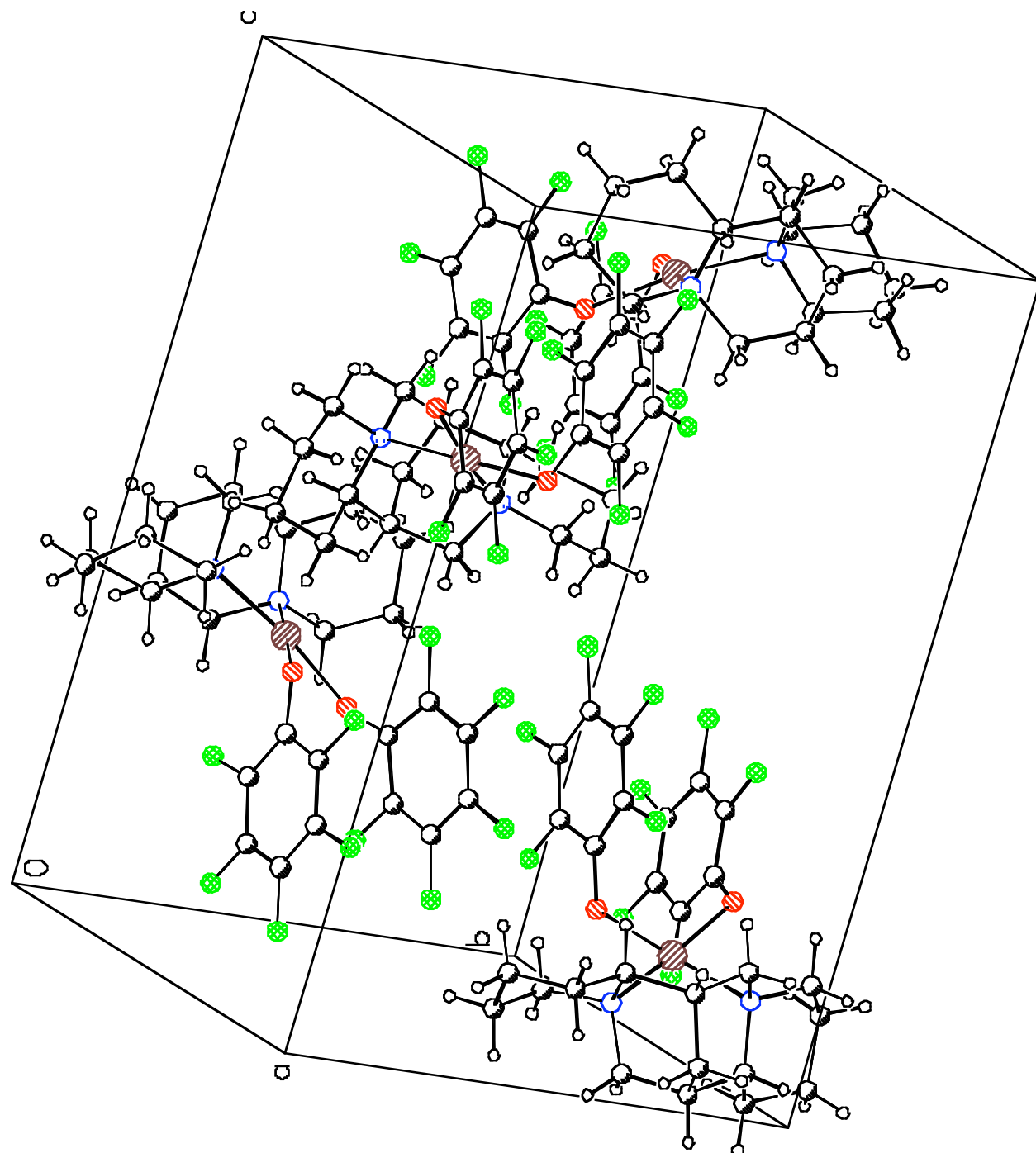
Special Refinement Details

Features in the final difference electron density Fourier map representing more than one electron lie near the Pd atom.

Refinement of F^2 against ALL reflections. The weighted R-factor (wR) and goodness of fit (S) are based on F^2 , conventional R-factors (R) are based on F , with F set to zero for negative F^2 . The threshold expression of $F^2 > 2\sigma(F^2)$ is used only for calculating R-factors(gt), etc., and is not relevant to the choice of reflections for refinement. R-factors based on F^2 are statistically about twice as large as those based on F , and R-factors based on ALL data will be even larger.

All esds (except the esd in the dihedral angle between two l.s. planes) are estimated using the full covariance matrix. The cell esds are taken into account individually in the estimation of esds in distances, angles and torsion angles; correlations between esds in cell parameters are only used when they are defined by crystal symmetry. An approximate (isotropic) treatment of cell esds is used for estimating esds involving l.s. planes.





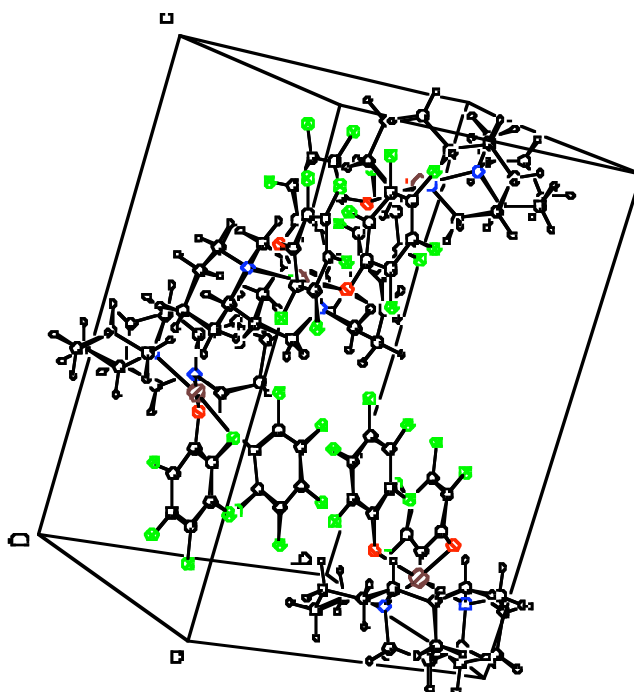
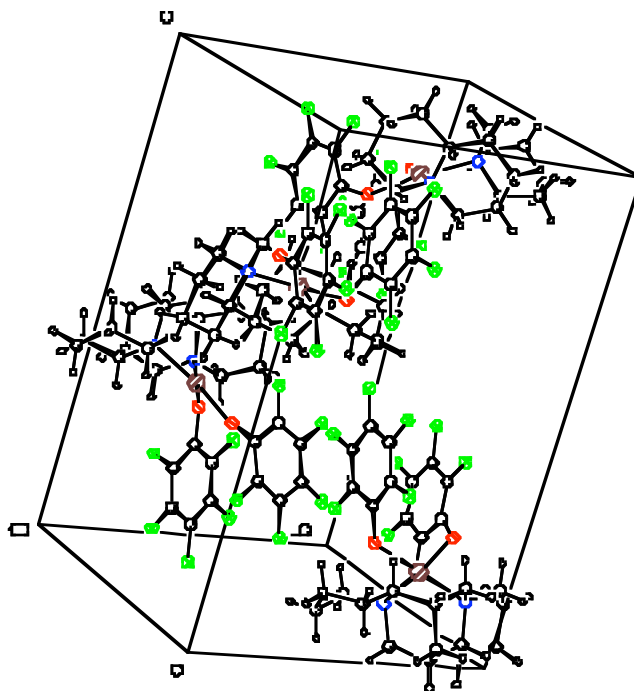


Table 2. Atomic coordinates ($\times 10^4$) and equivalent isotropic displacement parameters ($\text{\AA}^2 \times 10^3$) for JTB05 (CCDC 272190). U_{eq} is defined as the trace of the orthogonalized U^{ij} tensor.

	x	y	z	U_{eq}
Pd(1)	3386(1)	7161(1)	8487(1)	22(1)
F(17)	-713(3)	7912(3)	8241(2)	29(1)
F(18)	-1856(3)	7990(3)	6964(2)	41(1)
F(19)	-543(4)	8086(4)	5712(2)	51(1)
F(20)	1932(3)	8097(4)	5777(2)	49(1)
F(21)	3093(3)	8048(3)	7043(2)	35(1)
F(23)	1246(3)	5748(3)	9031(2)	25(1)
F(24)	-1182(3)	5495(3)	8825(2)	25(1)
F(25)	-2106(3)	5316(3)	7479(2)	24(1)
F(26)	-576(3)	5370(3)	6331(2)	28(1)
F(27)	1843(3)	5650(3)	6514(2)	28(1)
O(1)	1748(3)	7855(4)	8333(2)	25(1)
O(2)	2816(4)	5959(3)	7860(3)	29(1)
N(1)	4083(4)	8490(4)	9015(3)	21(1)
N(2)	5070(5)	6462(5)	8619(3)	28(2)
C(1)	3067(5)	9246(5)	9135(3)	27(2)
C(2)	3455(7)	10346(5)	9372(3)	33(2)
C(3)	4329(6)	10801(6)	8820(4)	32(2)
C(4)	5396(7)	10062(5)	8723(4)	36(2)
C(5)	5023(5)	8960(5)	8521(4)	24(2)
C(6)	6134(5)	8218(6)	8472(4)	37(2)
C(7)	5900(5)	7166(7)	8177(3)	38(2)
C(8)	5103(6)	5403(6)	8350(4)	40(2)
C(9)	4387(7)	4637(6)	8768(4)	36(2)
C(10)	4710(8)	4660(6)	9588(4)	42(2)
C(11)	4699(7)	5774(6)	9842(4)	38(2)
C(12)	5523(6)	6454(6)	9390(4)	28(2)
C(13)	5730(6)	7536(6)	9682(4)	36(2)
C(14)	4589(6)	8202(5)	9731(4)	28(2)
C(15)	6701(6)	8084(6)	9220(3)	42(2)
C(16)	1241(5)	7932(5)	7690(3)	22(2)
C(17)	-31(5)	7962(6)	7637(3)	21(2)
C(18)	-614(6)	7998(6)	6979(4)	31(2)
C(19)	36(6)	8036(6)	6353(4)	31(2)
C(20)	1270(6)	8048(5)	6383(4)	29(2)
C(21)	1866(5)	8022(5)	7046(4)	28(2)
C(22)	1654(6)	5739(5)	7779(3)	18(1)
C(23)	808(5)	5666(5)	8354(3)	21(2)
C(24)	-427(6)	5528(5)	8250(3)	20(2)
C(25)	-892(5)	5423(5)	7576(4)	19(2)
C(26)	-115(6)	5447(5)	6993(3)	17(1)
C(27)	1120(5)	5583(5)	7097(4)	19(2)

Table 3. Selected bond lengths [\AA] and angles [$^\circ$] for JTB05 (CCDC 272190).

Pd(1)-O(1)	2.024(4)	O(1)-Pd(1)-O(2)	88.96(16)
Pd(1)-O(2)	2.034(5)	O(1)-Pd(1)-N(2)	178.6(2)
Pd(1)-N(2)	2.067(5)	O(2)-Pd(1)-N(2)	90.7(2)
Pd(1)-N(1)	2.114(5)	O(1)-Pd(1)-N(1)	91.72(18)
		O(2)-Pd(1)-N(1)	172.50(19)
		N(2)-Pd(1)-N(1)	88.5(2)

Table 4. Bond lengths [Å] and angles [°] for JTB05 (CCDC 272190).

Pd(1)-O(1)	2.024(4)	O(2)-Pd(1)-N(2)	90.7(2)
Pd(1)-O(2)	2.034(5)	O(1)-Pd(1)-N(1)	91.72(18)
Pd(1)-N(2)	2.067(5)	O(2)-Pd(1)-N(1)	172.50(19)
Pd(1)-N(1)	2.114(5)	N(2)-Pd(1)-N(1)	88.5(2)
F(17)-C(17)	1.351(7)	C(16)-O(1)-Pd(1)	122.2(4)
F(18)-C(18)	1.361(7)	C(22)-O(2)-Pd(1)	121.8(4)
F(19)-C(19)	1.351(7)	C(14)-N(1)-C(1)	107.8(5)
F(20)-C(20)	1.342(7)	C(14)-N(1)-C(5)	113.0(5)
F(21)-C(21)	1.345(7)	C(1)-N(1)-C(5)	109.9(5)
F(23)-C(23)	1.353(7)	C(14)-N(1)-Pd(1)	110.5(4)
F(24)-C(24)	1.352(6)	C(1)-N(1)-Pd(1)	109.0(3)
F(25)-C(25)	1.350(6)	C(5)-N(1)-Pd(1)	106.7(4)
F(26)-C(26)	1.335(7)	C(8)-N(2)-C(12)	108.2(6)
F(27)-C(27)	1.346(7)	C(8)-N(2)-C(7)	110.8(6)
O(1)-C(16)	1.324(7)	C(12)-N(2)-C(7)	108.6(5)
O(2)-C(22)	1.313(8)	C(8)-N(2)-Pd(1)	112.9(4)
N(1)-C(14)	1.490(8)	C(12)-N(2)-Pd(1)	114.0(4)
N(1)-C(1)	1.494(8)	C(7)-N(2)-Pd(1)	102.1(4)
N(1)-C(5)	1.507(8)	N(1)-C(1)-C(2)	115.7(5)
N(2)-C(8)	1.452(9)	C(3)-C(2)-C(1)	109.5(5)
N(2)-C(12)	1.518(8)	C(4)-C(3)-C(2)	108.9(6)
N(2)-C(7)	1.525(9)	C(3)-C(4)-C(5)	113.9(6)
C(1)-C(2)	1.542(9)	N(1)-C(5)-C(4)	114.0(6)
C(2)-C(3)	1.521(9)	N(1)-C(5)-C(6)	109.1(6)
C(3)-C(4)	1.517(10)	C(4)-C(5)-C(6)	112.1(5)
C(4)-C(5)	1.523(9)	C(7)-C(6)-C(15)	107.7(6)
C(5)-C(6)	1.550(9)	C(7)-C(6)-C(5)	116.6(5)
C(6)-C(7)	1.482(10)	C(15)-C(6)-C(5)	109.4(6)
C(6)-C(15)	1.534(9)	C(6)-C(7)-N(2)	116.5(6)
C(8)-C(9)	1.480(10)	N(2)-C(8)-C(9)	115.4(6)
C(9)-C(10)	1.566(10)	C(8)-C(9)-C(10)	112.4(7)
C(10)-C(11)	1.508(10)	C(11)-C(10)-C(9)	108.7(6)
C(11)-C(12)	1.512(10)	C(10)-C(11)-C(12)	111.7(6)
C(12)-C(13)	1.511(10)	C(13)-C(12)-C(11)	115.0(6)
C(13)-C(14)	1.519(9)	C(13)-C(12)-N(2)	112.5(6)
C(13)-C(15)	1.539(10)	C(11)-C(12)-N(2)	109.5(6)
C(16)-C(21)	1.384(9)	C(12)-C(13)-C(14)	114.6(6)
C(16)-C(17)	1.398(8)	C(12)-C(13)-C(15)	109.0(6)
C(17)-C(18)	1.382(9)	C(14)-C(13)-C(15)	110.1(6)
C(18)-C(19)	1.367(9)	N(1)-C(14)-C(13)	113.1(5)
C(19)-C(20)	1.353(8)	C(6)-C(15)-C(13)	106.2(5)
C(20)-C(21)	1.397(9)	O(1)-C(16)-C(21)	125.5(5)
C(22)-C(27)	1.412(8)	O(1)-C(16)-C(17)	119.0(6)
C(22)-C(23)	1.419(8)	C(21)-C(16)-C(17)	115.5(6)
C(23)-C(24)	1.378(9)	F(17)-C(17)-C(18)	118.8(5)
C(24)-C(25)	1.361(8)	F(17)-C(17)-C(16)	119.5(5)
C(25)-C(26)	1.378(8)	C(18)-C(17)-C(16)	121.6(6)
C(26)-C(27)	1.378(8)	F(18)-C(18)-C(19)	120.2(6)
		F(18)-C(18)-C(17)	118.7(6)
O(1)-Pd(1)-O(2)	88.96(16)	C(19)-C(18)-C(17)	121.1(6)
O(1)-Pd(1)-N(2)	178.6(2)	F(19)-C(19)-C(20)	120.3(6)

F(19)-C(19)-C(18)	120.6(6)
C(20)-C(19)-C(18)	119.0(6)
F(20)-C(20)-C(19)	120.4(6)
F(20)-C(20)-C(21)	119.4(5)
C(19)-C(20)-C(21)	120.2(6)
F(21)-C(21)-C(16)	120.1(6)
F(21)-C(21)-C(20)	117.6(6)
C(16)-C(21)-C(20)	122.3(5)
O(2)-C(22)-C(27)	122.5(6)
O(2)-C(22)-C(23)	124.1(6)
C(27)-C(22)-C(23)	113.4(6)
F(23)-C(23)-C(24)	119.3(5)
F(23)-C(23)-C(22)	117.7(5)
C(24)-C(23)-C(22)	123.0(6)
F(24)-C(24)-C(25)	119.8(5)
F(24)-C(24)-C(23)	119.6(6)
C(25)-C(24)-C(23)	120.6(6)
F(25)-C(25)-C(24)	120.2(6)
F(25)-C(25)-C(26)	120.4(6)
C(24)-C(25)-C(26)	119.5(6)
F(26)-C(26)-C(25)	119.4(5)
F(26)-C(26)-C(27)	120.6(6)
C(25)-C(26)-C(27)	119.9(6)
F(27)-C(27)-C(26)	118.2(6)
F(27)-C(27)-C(22)	118.1(5)
C(26)-C(27)-C(22)	123.5(6)

Table 5. Anisotropic displacement parameters ($\text{\AA}^2 \times 10^4$) for JTB05 (CCDC 272190). The anisotropic displacement factor exponent takes the form: $-2\pi^2 [h^2 a^{*2} U^{11} + \dots + 2 h k a^* b^* U^{12}]$

	U^{11}	U^{22}	U^{33}	U^{23}	U^{13}	U^{12}
Pd(1)	97(2)	413(3)	155(2)	2(3)	-3(2)	12(3)
F(17)	184(16)	340(20)	330(20)	20(20)	-27(15)	27(19)
F(18)	200(20)	510(30)	520(30)	-10(20)	-103(18)	60(20)
F(19)	400(30)	810(40)	310(20)	40(30)	-180(20)	110(30)
F(20)	370(30)	790(40)	310(20)	210(20)	-5(19)	40(20)
F(21)	146(19)	540(30)	370(20)	90(20)	-14(16)	-26(18)
F(23)	165(19)	440(30)	150(20)	22(18)	27(15)	-29(17)
F(24)	211(19)	380(30)	160(20)	-59(18)	84(16)	-52(17)
F(25)	122(17)	350(30)	240(20)	-75(19)	23(16)	-68(16)
F(26)	173(18)	480(30)	190(20)	-119(19)	-4(16)	46(18)
F(27)	170(18)	440(20)	217(18)	-40(20)	79(19)	39(16)
O(1)	170(19)	270(20)	310(30)	-30(30)	-93(19)	10(20)
O(2)	160(20)	340(30)	360(30)	100(20)	110(20)	150(20)
N(1)	110(30)	430(40)	90(30)	-20(30)	10(20)	-70(30)
N(2)	200(30)	390(40)	250(40)	-70(30)	-10(30)	40(30)
C(1)	250(40)	400(50)	150(40)	50(30)	-10(30)	-90(30)
C(2)	320(40)	390(50)	260(40)	0(30)	50(40)	-150(40)
C(3)	300(40)	410(50)	250(40)	120(40)	-50(30)	-110(40)
C(4)	400(40)	470(60)	190(40)	20(40)	40(30)	-200(40)
C(5)	230(30)	290(40)	200(40)	-80(40)	30(40)	-90(30)
C(6)	90(30)	780(60)	230(40)	-220(50)	20(30)	-120(30)
C(7)	150(30)	730(60)	240(40)	60(50)	50(30)	110(40)
C(8)	270(40)	480(50)	460(60)	-130(50)	-20(40)	130(40)
C(9)	350(40)	260(50)	470(50)	-30(40)	-40(40)	190(40)
C(10)	520(50)	380(50)	360(50)	30(40)	-70(40)	160(40)
C(11)	450(50)	420(50)	280(50)	110(40)	-20(40)	140(40)
C(12)	220(40)	410(50)	220(40)	-50(40)	-20(30)	150(40)
C(13)	200(30)	580(60)	300(40)	-20(40)	-110(30)	120(30)
C(14)	230(40)	430(50)	160(40)	-70(30)	-10(30)	-10(30)
C(15)	170(30)	730(60)	350(40)	-140(40)	-60(40)	-10(40)
C(16)	240(30)	140(40)	280(40)	-10(40)	-110(30)	-10(30)
C(17)	240(30)	120(40)	280(40)	-40(40)	-10(30)	10(30)
C(18)	280(40)	270(50)	370(40)	30(40)	-160(30)	20(40)
C(19)	290(40)	340(50)	290(40)	80(40)	-90(30)	30(30)
C(20)	310(40)	290(50)	270(40)	90(40)	-10(30)	40(30)
C(21)	220(40)	190(40)	420(40)	90(40)	-40(30)	-30(30)
C(22)	210(30)	140(40)	190(30)	60(30)	20(30)	60(30)
C(23)	210(30)	210(40)	190(40)	-90(30)	10(30)	20(30)
C(24)	230(30)	90(40)	290(40)	-10(30)	90(30)	20(30)
C(25)	160(30)	200(40)	200(40)	-20(30)	0(30)	40(30)
C(26)	230(30)	60(40)	210(40)	-70(30)	0(30)	60(30)
C(27)	200(30)	150(40)	210(40)	-70(30)	80(30)	20(30)

Chapter 3

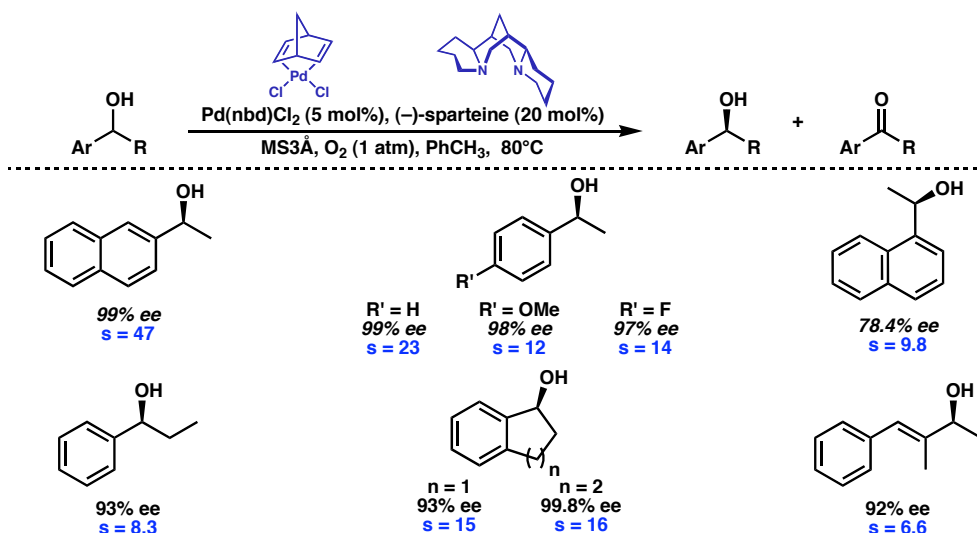
Enantioselective Oxidation of *Meso*-Diols by Catalytic Palladium: Total Synthesis of (–)-Lobeline and (–)-Sedamine

I. Introduction

Enantioselective Oxidation

The application of new reaction methodology remains an enduring strategy in the synthesis of complex natural products. In a complementary manner, the demonstration of new reaction methodology in the synthesis of complex natural products provides a powerful indication of that method's generality. Recently, our laboratories reported the first oxidative kinetic resolution (OKR) of racemic 2°-alcohols catalyzed by a palladium(II) complex with (–)-sparteine as the source of asymmetric induction.^{1,2} Using a catalyst system employing molecular oxygen as the terminal oxidant, a variety of secondary alcohols, including electron-rich and electron-deficient aromatics, were oxidized to high enantiomeric excess and with good overall selectivity (Table 1).

Table 1. Scope of the original palladium catalyzed OKR



Subsequent to our initial discovery, a number of mechanistic hypotheses regarding the role of exogenous bases and H-bond-donating additives in the oxidative kinetic resolution guided further development.^{3,4,5} The gradual improvements to the reaction profile are exemplified by the resolution of allylic alcohol (\pm)-**160** to alcohol (–)-**160**, and ketone **161** (Table 2). In the course of our studies, we evolved dramatically more reactive reaction conditions, relative to the original protocol (entry 1), by employing Cs₂CO₃ as an exogenous base, and conducting the reaction in the presence of an H-bonding additive *t*-BuOH (entry 2).

Table 2. Evolution of the palladium-catalyzed OKR

Entry	Conditions	Time (h)	Conversion (%)	ee ROH (%)	s
1	A	120	70	92.0	6.6
2	B	12	65	88.0	7.5
3	C	48	63	98.7	18.0
4	D	44	65	98.9	16.0
5	E	32	61	98.3	19.5

(A) **ORIGINAL**: Pd(nbd)Cl₂ (5 mol%), (–)-sparteine (20 mol%), O₂ (1 atm), 3Å MS, PhMe (B) **RATE ACCELERATED**: Pd(sp)Cl₂ (5 mol %), (–)-sparteine (15 mol%), Cs₂CO₃ (1.2 equiv), *t*-BuOH (4.0 equiv), O₂, (1 atm), 3Å MS, PhMe (C) **CHLOROFORM**: Pd(sp)Cl₂ (5 mol %), (–)-sparteine (7 mol%), Cs₂CO₃ (0.4 equiv), O₂ (1.1 atm), 3Å MS, CHCl₃ (D) **CHLOROFORM/AIR**: Pd(sp)Cl₂ (5 mol %), (–)-sparteine (7 mol%), Cs₂CO₃ (0.4 equiv), ambient air, 3Å MS, CHCl₃ (E) **PALLADIUM-ALKOXIDE**: Pd(sp)Cl₂ (5 mol %), (–)-sparteine (7 mol %), sodium 6-methoxynaphthalen-2-olate (0.1 equiv), O₂ (1 atm), 3Å MS, CHCl₃

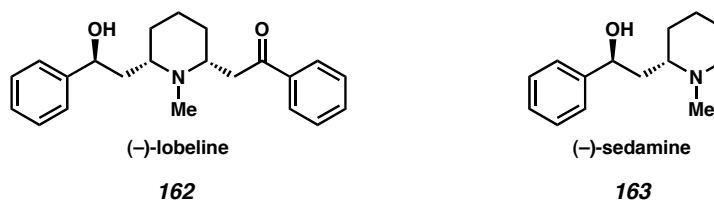
Furthermore, we discovered that when the *t*-BuOH additive was substituted with the weakly H-bond donating solvent chloroform, we could conduct the resolution at room temperature while maintaining reactivity (entry 3). At the reduced reaction temperatures,

superior selectivities were observed. As an added bonus, it was found that ambient air was sufficient as a stoichiometric oxidant (entry 4). Later, we found that the X-type chloride ligands on palladium could be substituted with a phenoxide to generate an even more reactive and selective catalyst system (entry 5).⁶

Piperidine Natural Products

With an arsenal of increasingly reactive and selective catalyst systems for enantioselective alcohol oxidation in hand, we set out to demonstrate our technique in the context of natural products synthesis. Our enantioselective oxidation method has resolved a variety of 2°-alcohols, and is particularly well-suited for discriminating between racemic benzylic alcohols. With this in mind, the natural products (–)-lobeline **162** and (–)-sedamine **163** attracted our interest (Figure 1). Though the structure of **162** has been known for decades, the few known enantioselective total syntheses are very long, are complicated by poorly diastereoselective transformations, and do not employ any new synthetic methodology.⁷

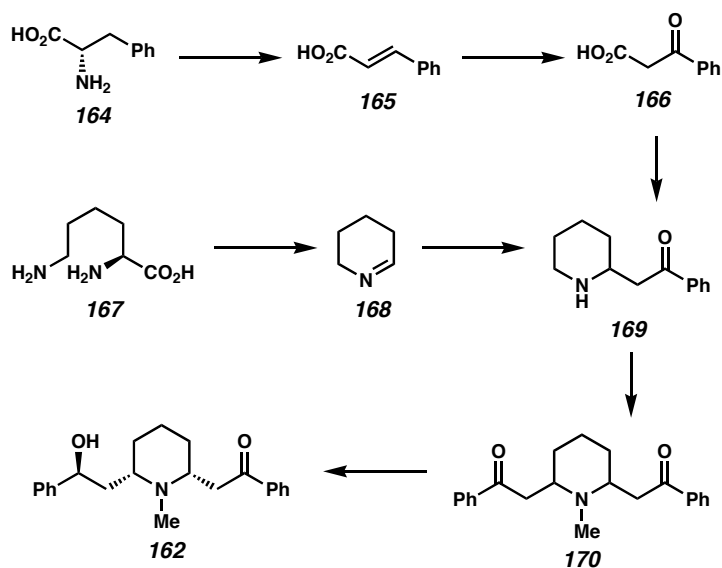
Figure 1. Structures of piperidine natural products



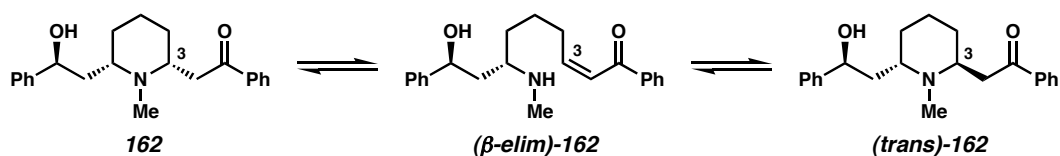
(-)-Lobeline **162**⁸ is a primary alkaloid constituent of *Lobelia inflata*, a plant commonly known as “Indian tobacco” because it was previously used by North American Indians as a tobacco substitute. (-)-Lobeline **162** itself mildly mimics the effect of nicotine, and thus has been applied as a smoking cessation agent. As a respiratory stimulant, the plant’s crude extracts have been widely used for the treatment of respiratory illnesses, including asthma, bronchitis, pneumonia, and whooping cough. Although generally accepted that (-)-lobeline **162** acts as a nicotinic receptor agonist, recent studies suggest it has a more complex pharmacological role.⁹ Lobeline has been shown to inhibit dopamine uptake and promote dopamine release from storage vesicles within dopaminergic presynaptic terminals.

Proposed Biogenesis

Feeding experiments establish that administration of isotopically labeled lysine and phenylalanine to *Lobelia inflata* produce radiolabeled lobeline.¹⁰ The sequence of biosynthetic events is believed to involve β -elimination of phenylalanine **164** to provide cinnamic acid **165**, which subsequently undergoes hydration and oxidation to generate benzoylacetic acid **166** (Figure 2). Meanwhile, lysine **167** may undergo several transformations *in vivo* to provide tetrahydropyridine **168**.¹⁰ Subsequent decarboxylative condensation between components **166** and **168** provides the ketone **169**, which upon condensation with another molecule of benzoylacetic acid **166** yields norlobelanine **170**. Enzymatic reduction of diketone **170** provides (-)-lobeline **162**.

Figure 2. Proposed biogenesis of (-)-lobeline

While it may be isolated from the natural source as a single isomer in salt form, in the solution state the free base of **162** is known to exist as a 1:1 mixture of the **162** and (*trans*)-**162** configurations at C-3, resulting from the base-catalyzed equilibration via enone (β -elim)-**162**, shown in Scheme 1. The equilibration is also promoted by H-bond donating solvents.¹¹

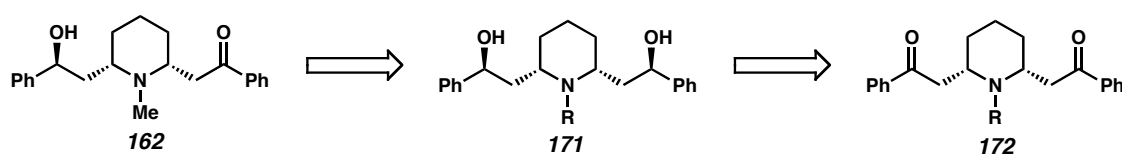
Scheme 1. Epimerization pathway

Because of this well-established equilibrium,¹² synthesis by Lebreton¹³ and Marzano¹⁴ detail the synthesis of lobeline as the (1:1) *cis:trans* mixture of **162**. In order to obtain the natural isolate in pure form, this equilibrium will need to be addressed. Furthermore, the known syntheses of (–)-lobeline **162** require several synthetic steps and rely on stoichiometric chiral auxiliaries and poorly diastereoselective transformations. With an enantioselective method for discriminating between enantiotopic alcohols developed in-house, we initiated synthetic studies on **162** with the intent of taking advantage of the symmetry of advanced lobeline intermediates.

Retrosynthesis

Inspection of (–)-lobeline **162** reveals a pseudo C_2 -symmetric *cis*-2,6-disubstituted piperidine, which may arise from the strictly C_2 -symmetric diol **171** (Figure 3). Since the *meso*-diol **171** is well-disposed for an enantioselective oxidation reaction of the type developed in our laboratories, early on we identified it as an excellent prospective intermediate for the total synthesis of **162**. The requisite *meso*-diol **171** may, in turn, be obtained by a diastereoselective reduction of diketone **172**. With this general synthetic plan in mind, we began by exploring routes to the diketone **172**.

Figure 3. Lobeline derived from a *meso*-diol



II. Results and Discussion

Preliminary Results

Initially, our synthetic design focused on intermediates which would carry a carbamate protecting group on the nitrogen functionality, since the functional group tolerance of the oxidative kinetic resolution (OKR) was previously shown to favor carbamates over other types of nitrogen functionality. For example, as shown in Table 3, OKR of carbamate protected β -amino alcohol **173** (entry 1) was more productive than either the amide protected β -amido alcohol **174** (entry 2) or the free β -amino alcohol **175** (entry 3), both in terms of reactivity and selectivity. Considering these substrates as crude models for the C_2 -symmetric β -amido diol **171**, we initially believed that a carbamate protecting group on nitrogen would provide an optimal oxidative desymmetrization as the key step in our synthesis.

Table 3. Impact of *N*-protecting groups on the OKR

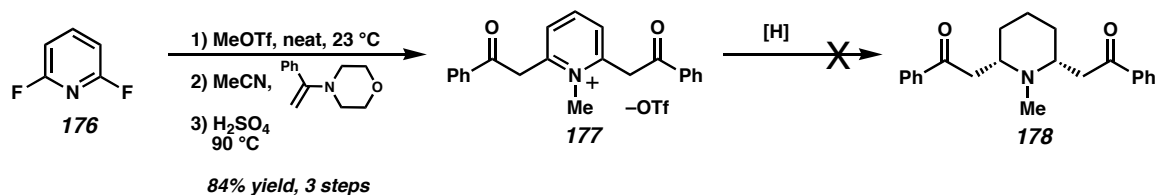
entry	Unreacted Alcohol Major Enantiomer	Time	Conversion [%] ^a	ee ROH [%] ^b	s ^c
1	 173	24 h	57.5	95.1	20.7
2	 174	24 h	52.3	82.1	17.5
3	 175	24 h	18.9	15.7	6.0

^aConversion determined by GC using a DB-wax column ^bEnantiomeric excess (ee) determined by HPLC. Total mass recovery is greater than 90%. ^cSelectivity was calculated from the equation $s = \ln[(1-c)(1-ee)] / \ln[(1-c)(1+ee)]$.

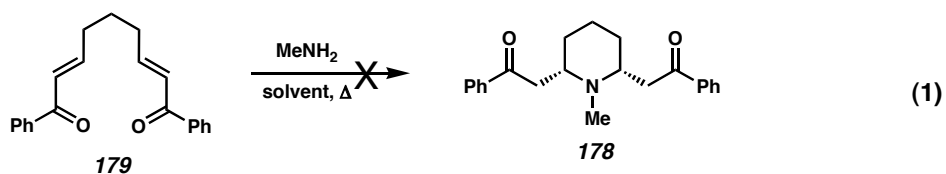
With the *meso*-diol of type **171** in mind as our key intermediate, and an understanding of the optimal protecting group on nitrogen, we pursued a number of synthetic routes. Our early synthetic approaches sought to take advantage of the inherent C_2 -symmetry of advanced lobeline intermediates. Accordingly, we initially favored methods that would provide a *meso*-diol of type **171** from a bidirectional synthetic approach.

In an initially exciting development, the pyridinium salt **177** could be synthesized in a one pot procedure from commercially available 2,6-difluoropyridine **176**. After formation of the pyridinium salt **177**, alkylation with the morpholine enamine of acetophenone directly constructs the lobeline C–C framework **177** directly (Scheme 2). However, an extensive screen of reaction conditions¹⁵ failed to provide a method of accomplishing the required ring hydrogenation.

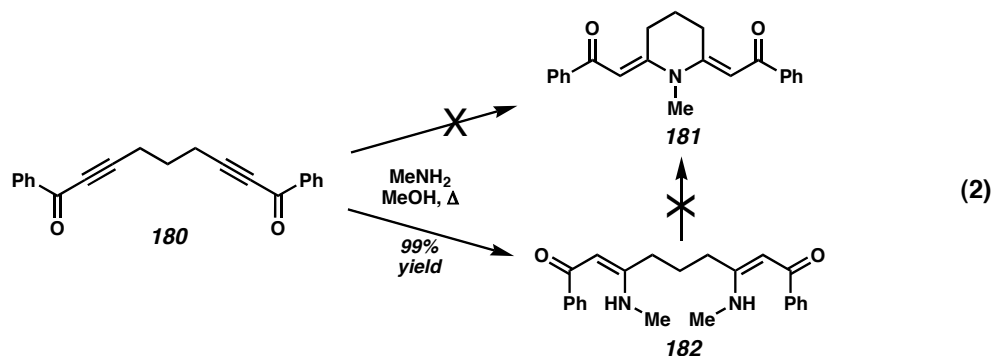
Scheme 2. Attempted ring hydrogenation route



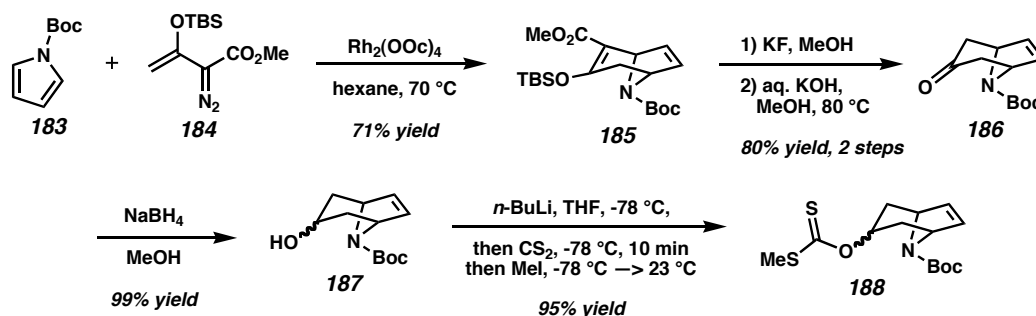
In an attempt to circumvent a ring hydrogenation event *en route* to intermediate **178**, we attempted a conjugate addition of methylamine into the symmetrical enone **179** (eq 1). However, the system proved either unreactive or unstable to all surveyed reaction conditions.



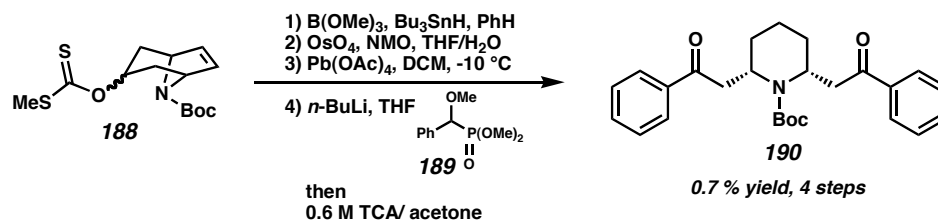
Likewise, the attempted conjugate addition of methylamine into yne-one **180** met with failure, providing the bis-enamineone **182**, rather than the desired cyclic enamineone **181** (eq 2). A systematic effort to favor the desired product, or convert **182** into the cyclic enamineone **181** proved unsuccessful.



Confronted with difficulties in directly obtaining a *meso*-2,6-disubstituted piperidine **178** directly, we investigated a more stepwise construction of this key intermediate. A new synthesis was initiated by treating diazo compound **184** with a rhodium dimer in the presence of *N*-Boc-pyrrole **183**, to provide the decorated tropene analogue **185** (Scheme 3). Desilylation with methanolic KF, followed by decarboxylation provided tropenone **186**, which was reduced with sodium borohydride to generate tropenol **187** as a mixture of diastereomers. Formation of the xanthate **188** proceeded by deprotonation of the alcohol followed by iterative anion trapping with CS₂, then MeI.

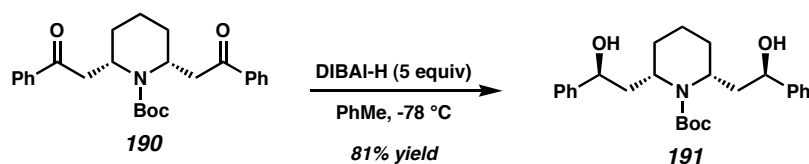
Scheme 3. Attempted tropenone rout

While the initial steps of this synthesis proceeded smoothly and in good yield, complications immediately followed upon evolution of the xanthate **188**. In the sequence detailed in Scheme 4, radical deoxygenation of **188** is followed by two-step olefin oxidation. The resulting intermediate bis-aldehyde ultimately undergoes the bi-directional Horner-Emmons-type reaction with ylide precursor **189**, followed by *in situ* hydrolysis of the bis-methyl enol-ether to furnish diketone **190**. Given the overall transformation, the procedure was concise, however, only a small fraction of the theoretical yield (0.7% yield, 4 steps) was observed for this sequence.

Scheme 4. Small quantities of a key intermediate

While material throughput was a clear drawback to the sequence given in Scheme 4, we took advantage of the small quantities diketone **190** obtained and explored the efficiency of a diastereoselective bidirectional ketone reduction. To our delight, subjection of diketone **190** to an excess of DIBAL-H in the non-coordinating solvent toluene provided exclusively the *meso*-diol **191** in good yield. A stereochemical model for the observed stereoinduction will be presented in the next section.

Scheme 5. Diastereoselective reduction



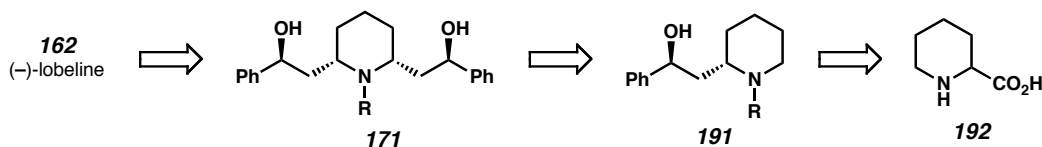
While demonstration of a bidirectional diastereoselective ketone reduction was a long-standing goal in this project, ultimately, the low material throughput deprioritized the synthetic route given in Schemes 3 through 5 in favor of a higher yielding method. Confronted with the difficulties of constructing the lobeline framework in a bidirectional fashion, we revisited our retrosynthetic plan.

Revised Retrosynthesis

A key design element in the attempted synthesis of (–)-lobeline discussed up to this point is the utility of symmetrical intermediates. While the concept of bidirectional synthesis in the pursuit of *meso*-diols served us well for efficiently synthesizing chiral polyol arrays (Chapter 2), restricting our attention to symmetrical intermediates in the pursuit of (–)-lobeline ultimately hampered our efforts. For this reason, a new synthetic route was investigated.

In the revised retrosynthesis (Scheme 6), the 2,6-disubstituted piperidine (–)-lobeline **162** is obtained via a late stage enantioselective oxidative desymmetrization of *meso*-diol **171**, just as previously planned. However, we chose to construct **171** using a C-C bond disconnection to provide the amino-alcohol **191**, which may arise from commercially available, inexpensive pipecolic acid **192**.

Scheme 6. Retrosynthesis of (–)-lobeline

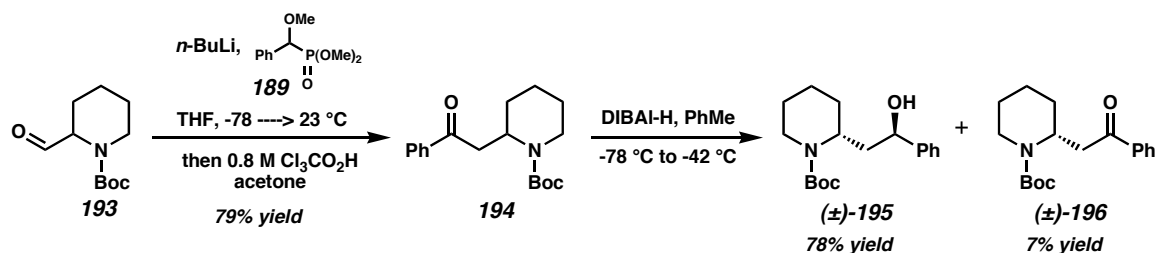


Total Synthesis of (–)-Lobeline

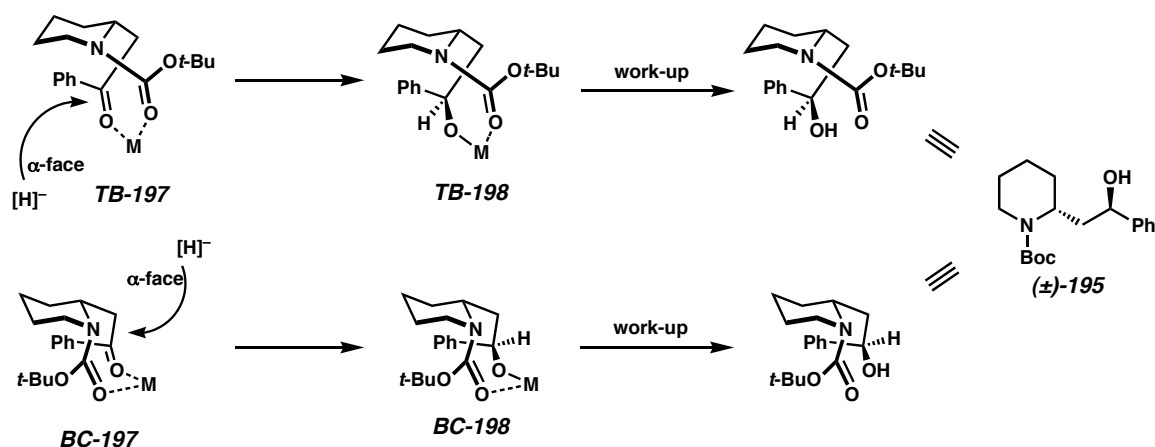
Synthesis begins by treatment of aldehyde **193** (obtained from **192** in three steps) with the activated Horner-Emmons reagent **189**, followed by *in situ* hydrolysis of the resulting methyl-enol ether to provide ketone **194** in good overall yield (Scheme 7). A screen of reducing conditions reveals that treatment of **194** with DIBAL-H in cold toluene

provides *anti* amino-alcohol (\pm)-**195** as the major diastereomer and the *syn* amino-alcohol (\pm)-**196** as the minor diastereomer ($dr=11:1$).

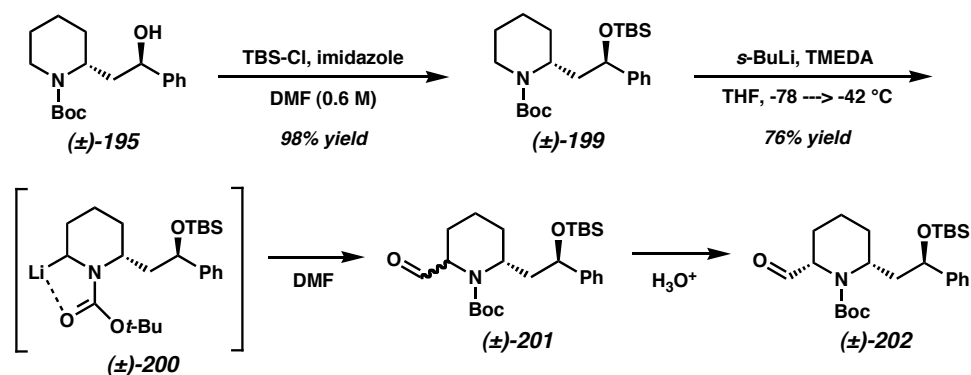
Scheme 7. Advancing the piperidine



A plausible stereochemical rationale for the observed diastereoselectivity may be proposed based on existing models for known diastereoselective transformations involving medium rings.¹⁶ For this discussion, the reduction substrate **194**, once chelated to a Lewis acid, may be approximated by *cis,cis*-1,4-cyclooctadiene. Computational studies find that the lowest energy conformations of *cis,cis*-1,4-cyclooctadiene are twist-boat and boat-chair.¹⁷ These competing conformations were found to be of equal energy within the limits of the computational method. X-ray crystal structures of substituted medium rings bearing the same unsaturation pattern depict solid state conformations that are in good agreement with these calculations.¹⁸ Taking *cis,cis*-1,4-cyclooctadiene as a model for our ketone substrate **194** after chelation to a metal, we may consider two transition states: the twist-boat structure **TB-197** and the boat-chair structure **BC-197** (Figure 4). The sterics of the system demand delivery of the bulky hydride source be directed from the α -face of the molecule, to provide **TB-198** and/or **BC-198**, respectively. In either event, aqueous workup provides the alcohol diastereomer preferred experimentally.

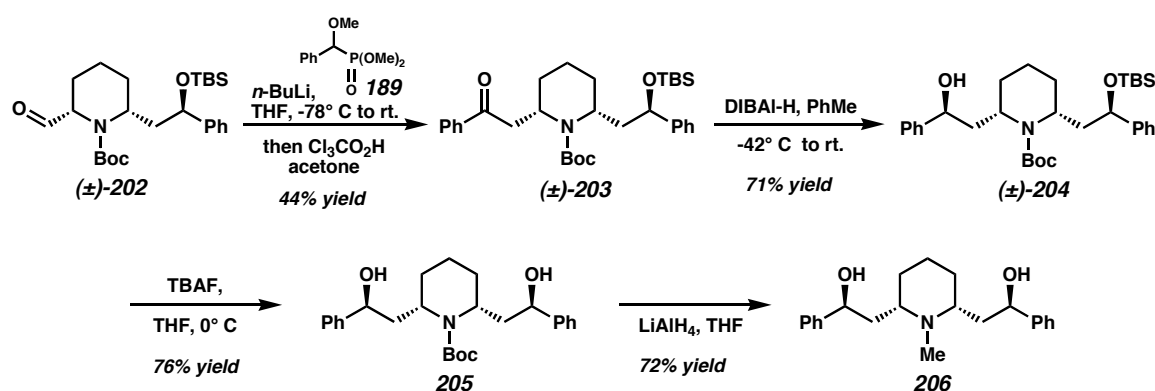
Figure 4. Stereochemical rationale for hydride addition

After separation of the diastereomers on silica, alcohol (±)-**195** is protected as TBS ether (±)-**199** in DMF at high concentration (Scheme 8). Formylation proceeds by deprotonation of (±)-**199** with *s*-BuLi in the presence of TMEDA to give the stabilized organo-lithium species (±)-**200**. Subsequent trapping of the anion with an excess of DMF is used to initially generate the diastereomeric mixture (±)-**201**, which quickly equilibrates exclusively to the thermodynamically favored *cis* diastereomer (±)-**202** upon treatment with mild acid.¹⁹

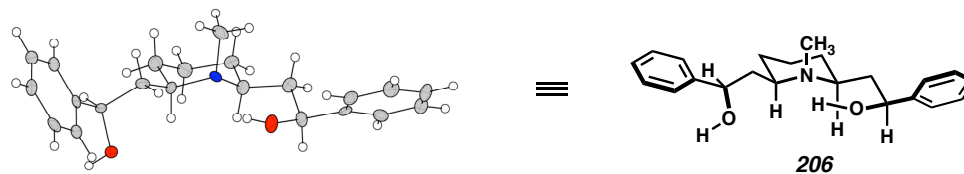
Scheme 8. Functionalizing the piperidine ring

After functionalizing the piperidine ring, the final C-C bond event occurs (Scheme 9) when aldehyde (\pm)-**202** is treated with the activated Horner-Emmons reagent **189**, then hydrolyzed *in situ* under mildly acidic conditions to provide the ketone (\pm)-**203**.²⁰ The ketone (\pm)-**203** is reduced by DIBAL-H in cold toluene to give exclusively the *anti*-alcohol diastereomer (\pm)-**204** before TBAF mediated desilylation of the alcohol, giving rise to *meso*-diol **205**. The natural product lobelanidine **206** is released after exhaustive reduction of the carbamate, revealing the latent *N*-methyl functionality.

Scheme 9. Completion of the *meso*-diol

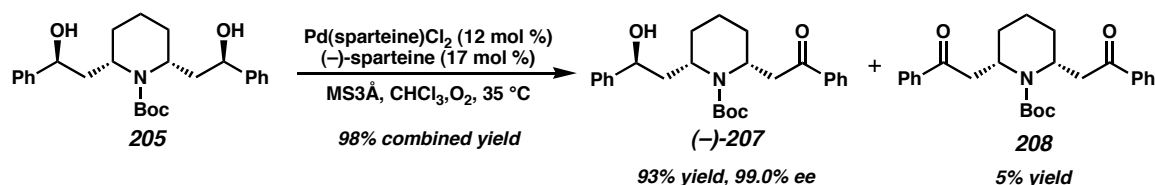


The chemical shift of the benzylic position *meso*-diol **206** was in good agreement with that of the natural keto-alcohol (–)-lobeline, indicating that we had obtained the correct intermediate. However, at this stage we sought to establish more rigorously the relative stereochemistry. To that end, quality crystals of **206** were produced in a vapor deposition chamber and an X-ray crystal structure was obtained (Figure 5). The crystal structure confirmed our relative stereochemical assignment.

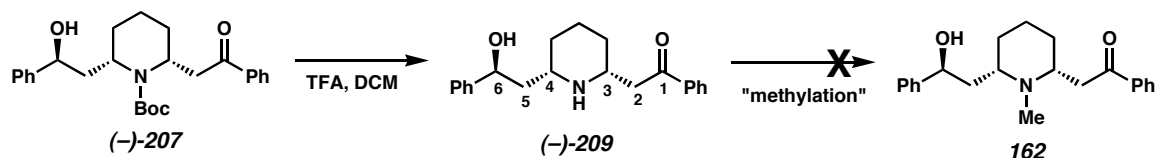
Figure 5. X-ray crystal structure of diol **206** (lobelanine)

From inspection of the crystal structure, it is clear that the methyl group on nitrogen occupies an axial position relative the piperidine ring, while the alkyl arms extending outward from the ring occupy an equatorial position. Consistent with known crystal structures for (–)-lobeline•HBr, there is an H-bond between one of the vicinal hydroxyl groups and the piperidine nitrogen. In the case of lobelanine **206**, the hydrogen of the remaining hydroxyl group is oriented away from the nitrogen.

Having demonstrated unambiguously the relative stereochemistry of lobelanidine **206**, we were poised to execute the key step in this synthesis: the palladium-catalyzed aerobic enantioselective oxidation developed in our lab as a *meso*-diol desymmetrization. In accord with our assumption that the *N*-Boc-protected lobeline intermediate **205** would provide the optimal oxidative desymmetrization substrate (Table 3), we applied our palladium-catalyzed enantioselective oxidation method. We were pleased to find that **205** was indeed an excellent substrate, providing *N*-Boc keto-alcohol (–)-**207** in 93% yield and 99.0% ee (Scheme 10). The doubly oxidized product diketone **208** accounted for nearly the balance of the material and was obtained in 5% yield, making the overall yield for this transformation 98%.

Scheme 10. OKR on an advanced lobeline intermediate

The late-stage intermediate **(-)-207** was deprotected under acidic conditions to generate norlobeline **(-)-209** (Scheme 11). Interestingly, no epimerization at C-3 was observed either to the free base or the TFA salt, indicating that, unlike **(-)-lobeline**, norlobeline **(-)-209** is not prone to epimerization. At this stage, we were encouraged that the configurational stability of **(-)-209** would facilitate our total synthesis of diastereomerically pure **(-)-lobeline**.

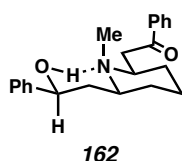
Scheme 11. Attempted methylation

Unfortunately, amine **(-)-209** proved resistant to a wide variety of methylation conditions; extensive screening of *N*-alkylation reactions and reductive amination reactions consistently provided either starting material, extensive starting material decomposition, or overmethylation of the amine and/or alcohol.

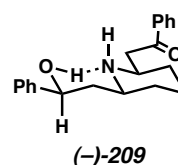
The difficulty in engaging this methylation is perhaps not surprising considering the conformational stress induced upon alkylation of piperidine (–)-**209**. Inspection of the crystal structure of (–)-lobeline²¹ reveals that the 2,6-disubstitution about the piperidine ring occupies the equatorial positions, while the methyl group on nitrogen is forced into an axial arrangement, presumably to avoid eclipsing interactions with the flanking alkyl arms. Solution NMR studies and molecular mechanics predict that, in the solution phase, the piperidine nitrogen is further congested by participating in an intramolecular H-bond with the tethered alcohol. From these data, and our own crystal structure of lobelanidine **206** (Figure 5), it can be inferred that the solution phase conformations of (–)-lobeline **162** and (–)-norlobeline (–)-**209** might be given in Figure 6.

Figure 6. Predicted solution phase conformations of (–)-lobeline and (–)-norlobeline

**Predicted Solution Phase Conformation:
(–)-Lobeline**



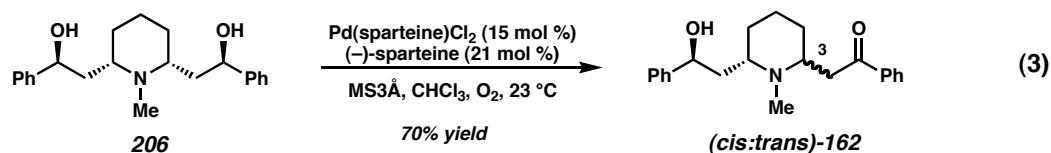
**Predicted Solution Phase Conformation:
(–)-Norlobeline**



By inspection of (–)-norlobeline (–)-**209**, it is apparent that alkylation on nitrogen will place the incoming group in an axial position relative to the ring. Furthermore, the nucleophilicity of the nitrogen will be reduced because of its participation in an H-bond. Nucleophilic methylation may be further complicated by other nucleophilic sites present in β -amino keto-alcohol (–)-**209**, and by the known natural product equilibrium (Scheme 1). Several undesirable reaction pathways involving the overmethylation of (–)-**209** are reasonable.

In any event, it became apparent that some reworking of the endgame *en route* to (–)-lobeline would be required. With ample quantities of enantioenriched (–)-*N*-Boc keto-alcohol (–)-**207** in hand, we were tempted to bridge the gap between our intermediate and (–)-lobeline via a protecting group strategy. However, in the face of a complicated and inefficient end-game, we opted to first attempt the resolution directly on lobelanidine **206**, bearing the unprotected basic 3°-nitrogen functionality.

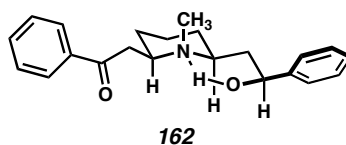
We were pleasantly surprised to find that despite the early observation that an unprotected nitrogen functionality was incompatible with our reaction conditions (Table 3), the *meso*-diol **206** was in fact a suitable substrate for the enantioselective oxidative desymmetrization. Using our optimized reaction conditions with catalytic Pd(sp)Cl₂ in chloroform, a productive enantioselective oxidation of *meso*-diol **206** was observed at room temperature, providing (–)-lobeline (*cis:trans*)-**162** as a 1:1 mixture of *cis:trans* epimers (eq 3) in 70% yield as a preliminary result. A comparison of natural equilibrated (1:1) *cis:trans*-(–)-lobeline with the synthetic material showed that the ¹H NMR, ¹³C NMR, IR, optical rotation, and mass spectral data were in agreement with literature values.



This provides the first example of a palladium-catalyzed oxidative reaction performed on a substrate containing an unprotected amine. The success of this transformation may be attributed to the strong preference of Pd(II) salts to bind rigid

bidentate ligands over a monodentate, highly hindered mobile amine. In this manner, the amine present in lobelanidine **206** is not suited to displace the (–)-sparteine ligand from the metal center. Inspection of the steric environment about the 3° amine centrality present in (–)-lobeline gives further insight into the success of *meso*-diol **206** as a oxidative desymmetrization substrate. Inspection of (–)-lobeline **162** in the solid and solution state indicates that the inherently sterically congested 2,6-disubstituted piperidine is further occupied by participation in an intramolecular H-bond with the vicinal hydroxyl group to form a six-membered hydrogen bridge (Figure 7).

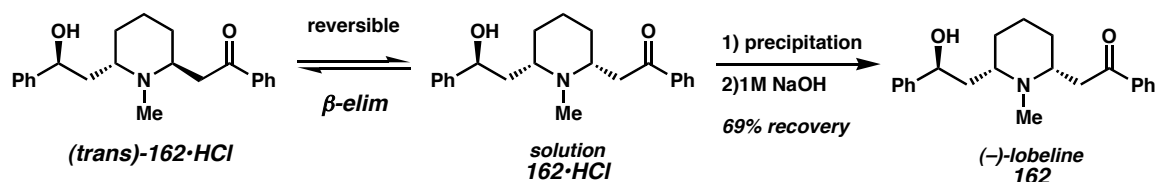
Figure 7. Steric congestion about the 3°-amine in (–)-lobeline



While we had completed an efficient synthesis of (*cis:trans*)-**162** featuring a late-stage palladium-catalyzed enantioselective oxidation as the key step, we remained interested in the epimerization at C-3, and how we might leverage this feature in obtaining diastereomerically pure (–)-lobeline **162**. Observation of natural lobeline in a number of solvents reveals some trends in the rate of epimerization: 1) rate of epimerization increases with increasing exogenous stoichiometric base strength, and 2) the rate of epimerization increases dramatically in protic solvents. Furthermore, the HCl salt of (*cis:trans*)-**162** can be equilibrated in protic solvent to a 3:1 mixture (*cis:trans*). Prompted by these observations, we developed a dynamic crystallization method allowing for the selective precipitation of the *cis* isomer **162**. Heating (*cis:trans*)-

162·HCl in isopropanol for 8 h, followed by slow recrystallization in a vapor diffusion chamber (heptane) permitted a 69% recovery of (–)-lobeline **162** after treatment of 1 M NaOH exclusively in the natural *cis* configuration (Scheme 12). That (–)-lobeline **162** is obtained in greater than 50% yield from the recrystallization when a *cis:trans* (1:1) mixture is present in the initial liquor, indicates that the recrystallization is a dynamic process favoring the *cis* configuration.

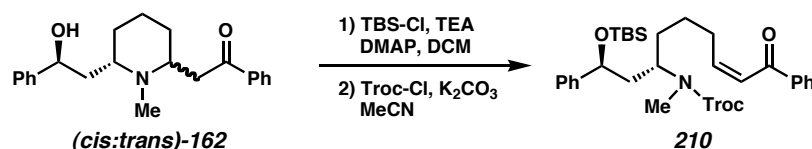
Scheme 12. Dynamic precipitation of (–)-lobeline



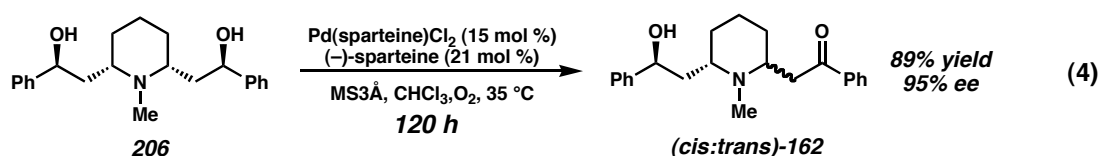
Comparison of the spectral data of synthetic **162** with an authentic sample of (–)-lobeline confirmed the identity by ^1H NMR, ^{13}C NMR, IR, HRMS, and optical rotation. What remained unclear at this point was the precise enantiomeric excess of synthetic **162**. Measuring an enantiomeric excess by chiral HPLC proved to be problematic, probably because the natural product rapidly epimerizes at C-3. Epimerization will occur much faster than chiral HPLC analysis and only a very complicated HPLC trace was observed. Confronted with this difficulty, we considered many possibilities for obtaining an enantiomeric excess for this compound. Ultimately, we elected to derivatize **162** into a compound that may more tractably be measured by chiral HPLC. This effort was facilitated with the aid of a recent report by Crooks et al.²² According to their method, the unrecrystallized desymmetrization product (*cis:trans*)-**162** was silylated with TBS-Cl

to form a TBS ether and subsequently treated with Troc chloride to form carbamate **210** exclusively as the *Z*-olefin (Scheme 13). When subjected to HPLC analysis, it was determined that the oxidative desymmetrizations detailed in Equation 3 had generated keto-alcohol (*cis:trans*)-**162** in 94% ee. When the crystalline material obtained from the dynamic recrystallization (Scheme 12) was derivatized to carbamate **210**, it was found to have an enantiomeric excess of 99%.

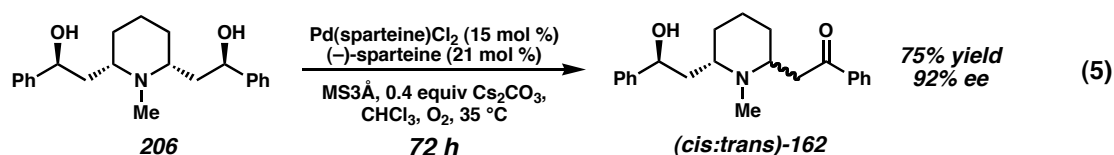
Scheme 13. Derivatization to a HPLC tractable analogue



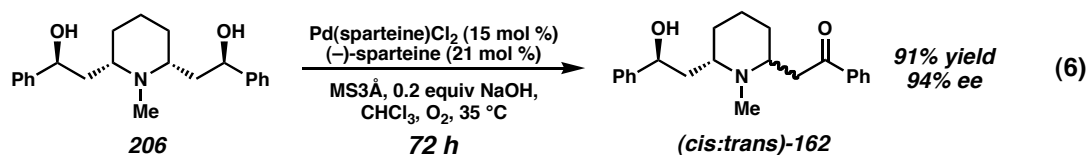
After establishing a reliable method for determining the enantiomeric excess for synthetic (–)-lobeline, we revisited a number of our conditions for enantioselective oxidation, in order to compare the reaction efficiencies for the desymmetrization complex *meso*-diol **206**. All reactions were monitored by LCMS to observe consumption of starting material. Enantiomeric excess was determined after derivatization by the method described in Scheme 13. Using the chloroform conditions without excess base, the desymmetrization required 120 h for complete reaction to provide (*cis:trans*)-**162** in 85% yield and 95% ee (eq 4).



Upon addition of the exogenous base Cs_2CO_3 , no significant improvement to reactivity was observed (eq 5). The reaction was stopped after 72 h, since the active catalytic species $\text{Pd}(\text{sp})\text{Cl}_2$ is known to not be present beyond this time (converted to inactive $\text{Pd}(\text{sp})\text{CO}_3$). Under these conditions, keto-alcohol **(cis:trans)-162** was obtained in 75% yield and 92% ee. The balance of the material was recovered as the starting *meso*-diol.

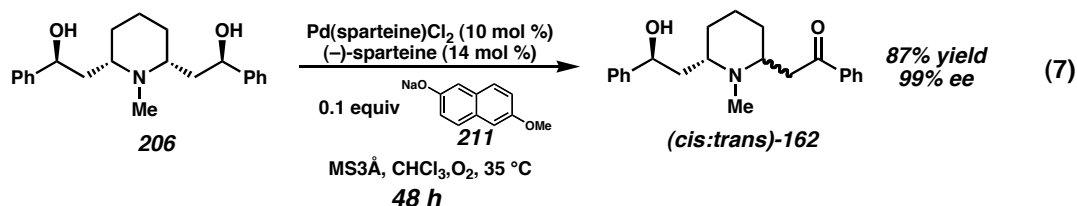


Catalyst deactivation can apparently be avoided in this reaction by employing NaOH as the exogenous base (eq 6).²³ In this way, after warming for 72 h, the reaction proceeded in 91% yield to provide keto-alcohol **(cis:trans)-162** in 94% ee.



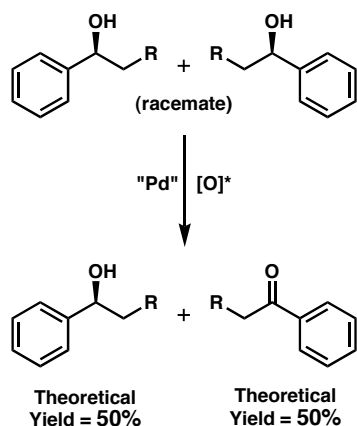
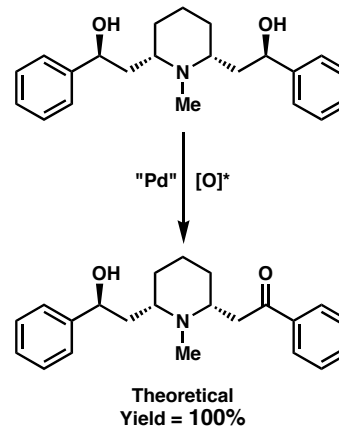
Encouraged by the success of this reaction, we attempted the desymmetrization by our newly developed protocol, involving the formation of a reactive $\text{Pd}^{\text{II-}}$ -naphthaleneoxide (eq 7). Accordingly, after stirring the starting $\text{Pd}(\text{sp})\text{Cl}_2$ catalyst with the soluble sodium naphthaleneoxide **211**, a dramatic color change was observed (orange to dark red), the

starting *meso*-diol **206** was introduced. We were pleased to find that, despite a reduction in catalyst loading (from 15% Pd to 10% Pd), keto-alcohol (*cis:trans*)-**162** was obtained in 87% yield and 99% ee in less time (48 h) than previously observed.

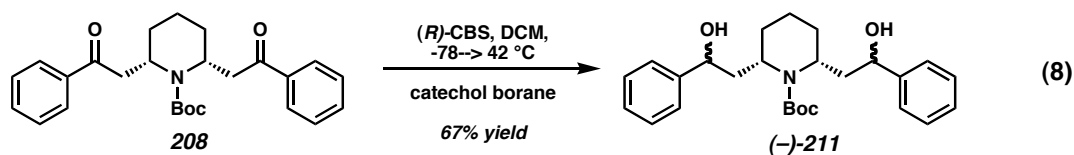


Features of the Oxidative Desymmetrization

Having demonstrated the first enantioselective synthesis of (–)-lobeline by employing an enantioselective, catalytic transformation, it is worth considering some subtleties of the palladium-catalyzed enantioselective alcohol oxidation featured as the key step. Although the enantioselective oxidative kinetic resolution developed in our laboratories provides one of the most convenient methods for obtaining a secondary benzylic alcohol in very high enantiomeric excess (>95% ee), a potential disadvantage with a resolution is the limited theoretical yield. As described in Figure 8, an enantioselective oxidative kinetic resolution has a 50% theoretical yield for a resolved alcohol recovered in ee > 99%. However, this limitation in theoretical yield is removed in a desymmetrization reaction, as either enantiomer of the alcohol is tethered to the C₂-symmetric substrate.

Figure 8. Oxidative kinetic resolution vs. oxidative desymmetrization**Enantioselective Oxidative Kinetic Resolution****Enantioselective Oxidative Desymmetrization**

An enantioselective oxidative desymmetrization reaction also provides some important benefits over other enantioselective methods that yield enantioenriched secondary alcohols. Consider, for example, the CBS reduction of *N*-Boc-dehydrolobeline **208** (eq 8). It is immediately apparent that an enantioselective method of this type is inadequate for the synthesis of (–)-lobeline. Instead of providing the desired product (–)-lobeline **162**, the product of our enantioselective oxidative desymmetrization, the pseudo- C_2 -symmetric diol (–)-**211** is obtained as a mixture of alcohol diastereomers.



While the CBS catalyst is classically adept at performing enantiofacial discrimination (though not in this particular instance), in the absence of a compelling

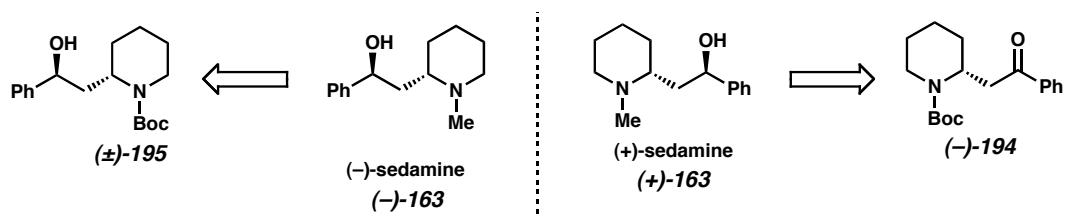
mismatched catalyst–substrate interaction, the CBS catalyst is incapable of providing functional group discrimination. In this event, both ketones are reduced. However, our $\text{Pd}^{\text{II}}(\text{sp})$ catalyst readily discriminates between alcohols, providing (–)-lobeline as the direct desymmetrization product (after equilibration) in high enantiomeric excess.

In summary, the total synthesis of (–)-lobeline was achieved in 9 synthetic transformations and features a dynamic recrystallization, making this synthesis the shortest known synthesis by far, and the only synthesis employing a catalytic, enantioselective process. Furthermore, the synthesis is not complicated by poorly diastereoselective transformations at any stage. The key steps in this sequence are a highly diastereoselective ketone reduction, a highly diastereoselective piperidine formylation reaction, and a palladium-catalyzed enantioselective oxidative alcohol desymmetrization on an advanced natural product intermediate featuring an unprotected basic nitrogen functionality. Furthermore, this synthesis constitutes the first total synthesis of a complex natural product achieved by the enantioselective oxidation methodology developed in our laboratories.

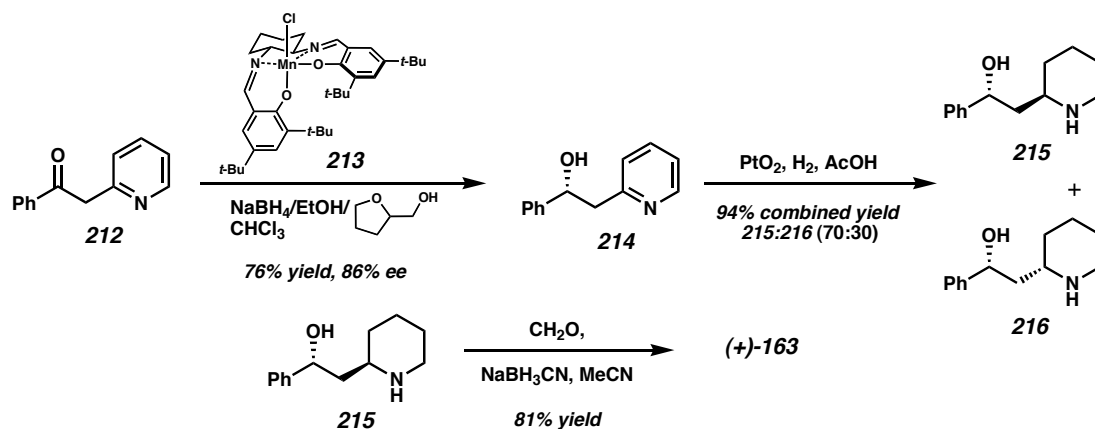
Total Synthesis of (+)-Sedamine and (–)-Sedamine

Having demonstrated a concise total synthesis of isomerically pure (–)-lobeline **162**, we explored the utility of the protected amino-alcohol (±)-**195** for the synthesis of a related *lobelia* alkaloid: (–)-sedamine (–)-**163**. Furthermore, we endeavored to utilize the resolution product ketone (+)-**194** in the synthesis of the opposite sedamine enantiomer (+)-sedamine (+)-**163** (Figure 9).

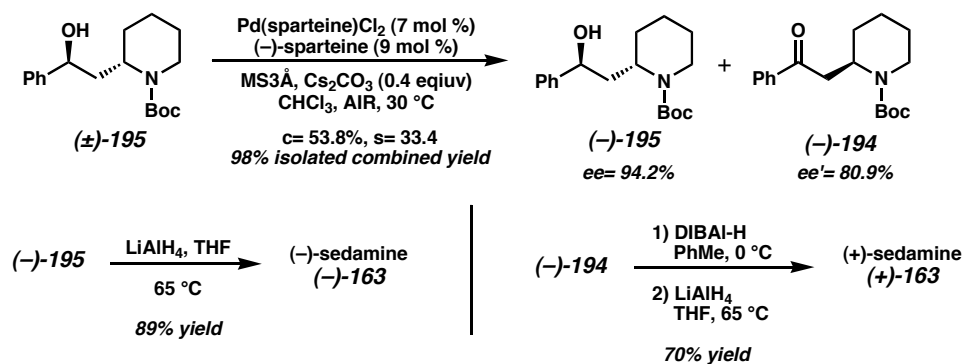
Figure 9. Retrosynthesis of sedamine alkaloids



(–)-Sedamine is one of a series of substituted piperidine derivatives found in various sedium species.²⁴ It was the first of these alkaloids to be characterized and structurally elucidated.²⁵ Many of the past syntheses of sedamine alkaloids have been restricted primarily to either racemic methods²⁶ or diastereoselective methods involving chiral auxiliaries.²⁷ One notable example²⁸ of an enantioselective synthesis employs Jacobsen's manganese catalyst²⁹ **213** as a chiral Lewis acid for the reduction of ketone **212** to homochiral alcohol **214** in 86% ee (Scheme 14). Subsequent ring hydrogenation provided a 70:30 mixture of (+)-norsedamine **215** and (+)-norallosedamine **216**. Selective *N*-methylation of **215** generated (+)-sedamine (+)-**163**.

Scheme 14. Previous enantioselective synthesis of sedum alkaloids

In the course of our total synthesis of (–)-lobeline, we generated an enantiopure intermediate immediately recognizable as a synthon for the sedum alkaloids, the diastereomerically pure protected β -amino alcohol (\pm)-195. Exposure of (\pm)-195 to our optimized Pd(II)-catalyzed enantioselective aerobic oxidation conditions produced alcohol (–)-195 (ee=94.2%), and ketone (–)-194 (ee'=80.9%) in excellent yield and selectivity (Scheme 15).³⁰

Scheme 15. OKR of a sedamine intermediate

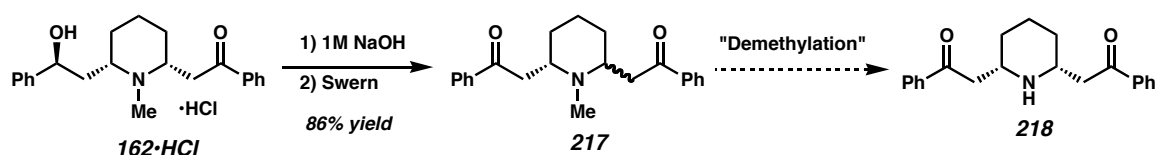
Direct reduction of (–)-**195** with LiAlH_4 provided (–)-sedamine (–)-**163**. The recovered ketone (–)-**194**, also chiral product, proved a useful intermediate as well. Reiteration of the diastereoselective DIBAL-H reduction of ketone (–)-**194** reduces the ketone, and the carbamate was fully reduced with LiAlH_4 to access the opposite sedamine enantiomer (+)-**163**. In this way, we are able to access either enantiomer of sedamine from a common synthetic intermediate.

Acidic Polonovski-Type Demethylation

In the course of our investigations into the total synthesis of (–)-lobeline **162**, a key question arose concerning the practicality of installing protecting groups at nitrogen on late stage intermediates. Since this question was formulated early in our synthetic studies, no late stage intermediates were available. However, the natural product (–)-lobeline is a modestly priced (~ \$60/g), commercial material. Taking advantage of our target's ready availability, we initiated a relay synthesis so that we might address synthetic end-game issues early on.

After free-basing commercially available (–)-lobeline•HCl with sodium hydroxide solution, the keto-alcohol was subjected to a Swern oxidation, yielding diketone **217** a mixture of diastereomers (Scheme 16). Since diketone **217** was identified as a possible late stage synthetic intermediate, we were poised to explore the possibility of a demethylation reaction to provide the dihydro-norlobeline **218**.

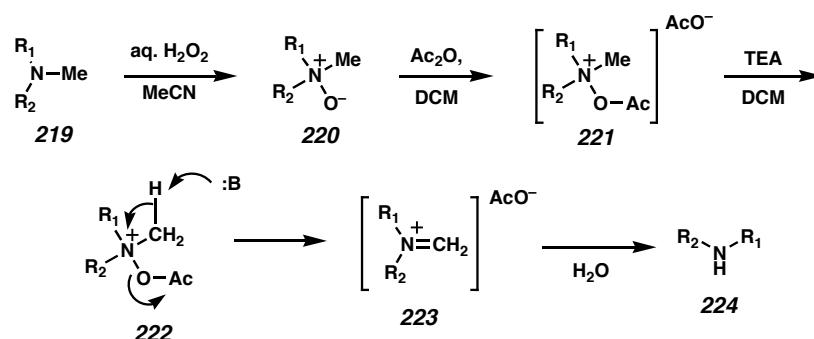
Scheme 16. Demethylation problem



In order to derive the secondary amine **218** from which protecting group installation studies would be conducted, diketone **217** required demethylation. However, few methods exist for demethylating a nitrogen. Of these, the Polonovski protocol³¹ remains the classic technique, and has been demonstrated on a number of *N*-methylpiperidines.³²

According to Polonovski's method, treatment of a 3°-methyamine **219** with hydrogen peroxide provides 3°-*N*-oxide **220** (Scheme 17). Addition of acetic anhydride to the isolated *N*-oxide provides the *N,O*-acetate salt **221**, which is treated *in situ* with triethylamine. According to the accepted mechanism, kinetic deprotonation of a hydrogen on the methyl group forms iminium ion **223** with loss of acetate anion. The iminium ion is hydrolyzed to the secondary amine **224** upon aqueous workup.

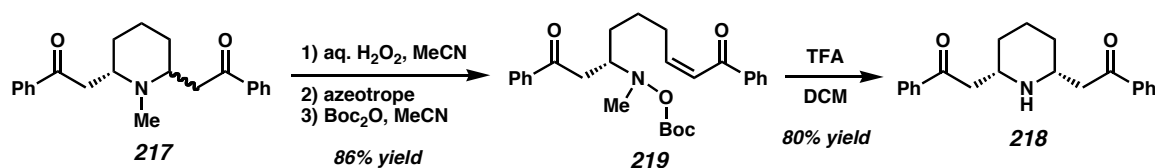
Scheme 17. Mechanism for the Polonovski demethylation



After successfully repeating the Polonovski protocol on a published substrate, we applied the method to the demethylation of diketone **217**. However, to our disappointment, no demethylated product **218** was ever obtained. After extensive screening of reaction conditions, only complex mixtures were obtained. Although we found this disappointing, we made a key observation in the course of reaction screening: *N,O*-acetate salts of diketone **217** were *generally unstable to base*. Seeking a method to initiate a Polonovski reaction independent of base, we investigated acidic variants of the demethylation.

To this end, diketone **217** was treated with hydrogen peroxide (Scheme 18). Following concentration of the reaction, and azeotroping the resulting white foam from toluene, addition of Boc-anhydride provided the hydroxylamine carbonate **219**, a readily isolable compound. At this point, we were pleased to find that exposure of **219** to an excess of TFA in DCM directly provided dihydro-norlobeline **218** as a single isomer.

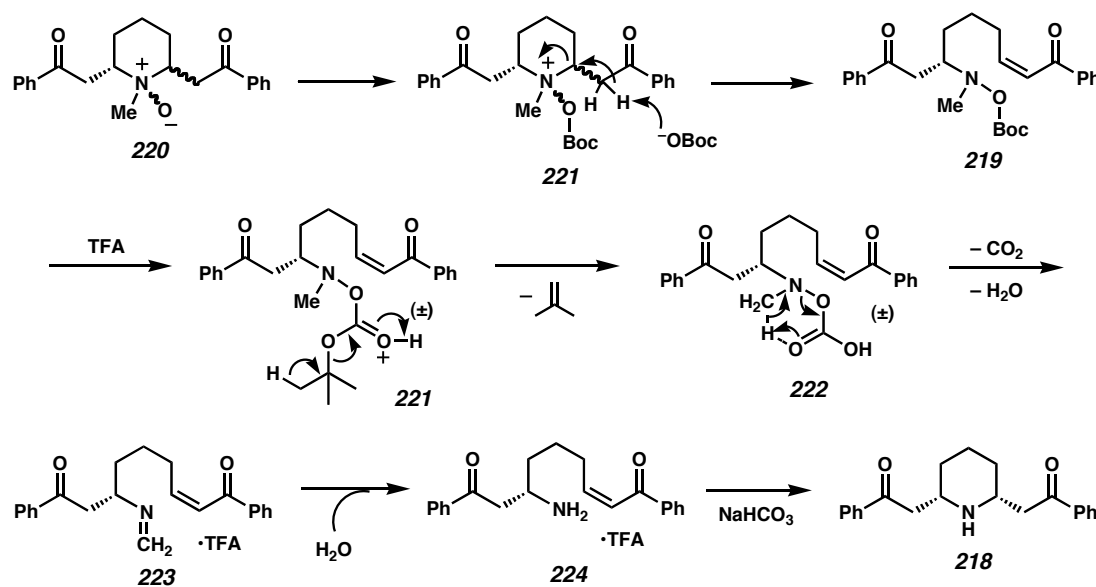
Scheme 18. Modified Polonovski demethylation



A plausible mechanism for the transformation is given in Figure 10. After treatment of the zwitterionic *N*-oxide **220** with Boc-anhydride, the resulting ammonium salt can rapidly β-eliminate from either adjacent ketone to give the neutral hydroxylamine

carbonate **219** as a single olefin isomer. After treatment of the isolated **219** with TFA, *t*-butyl carbonate decomposition is initiated (structure **221**) to form the intermediate hydroxylamine-carbonic acid **222**, liberating isobutylene. With a basic carbonyl in the vicinity of the methyl group, a concerted, intramolecular deprotonation can occur, forming the imine **223** with loss of hydrogen carbonate, which disproportionates to carbon dioxide and water. Having generated an equivalent of water as a byproduct in the previous step, the water can hydrolyze imine **223** under acidic conditions to generate the primary amine **224**, which is isolated as the conjugate addition product **218**, as a single diastereomer after quenching with weak aqueous base.

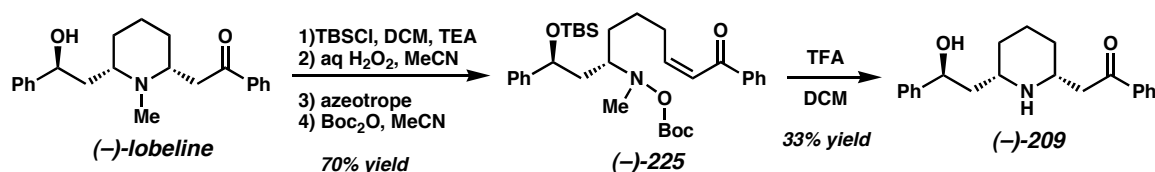
Figure 10. Proposed mechanism of the modified Polonovski demethylation



We have also applied this unique demethylation procedure directly to (–)-lobeline (Scheme 19). After protection as the silyl ether, treatment of the piperidine with hydrogen peroxide precedes thorough drying and formation of the *N,O*-carbamate (–)-

225. Exposure of (–)-**225** to excess TFA triggers the demethylation event and removes the silyl ether, to provide norlobeline (–)-**209**.

Scheme 19. Lobeline demethylation



III. Conclusion

In summary, we have demonstrated the palladium(II)-catalyzed oxidative kinetic resolution in the realm of natural product synthesis with an efficient enantioselective synthesis of both (–)-sedamine and (+)-sedamine. Furthermore, we have detailed the shortest known route to (–)-lobeline (9 steps) by employing our enantioselective oxidation methodology in the desymmetrization of a *meso*-diol. Importantly, we access the natural product directly from our key step. Some critical features of this reaction are 1) the oxidative desymmetrization of a *meso*-diol in the presence of an unprotected 3°-amine, and 2) defining three stereocenters absolutely in a single asymmetric transformation. In the course of conducting synthetic studies on advanced lobeline intermediates, we have discovered an acidic variant of the Polonovski demethylation of 3°-amines. While this work represents the first application of Pd-catalyzed aerobic asymmetric oxidation in the realm of natural product synthesis, we have demonstrated this technique as a general method for synthesizing complex keto-alcohols displaying

diverse stereochemical arrays. While working with advanced lobeline intermediates, we have developed an acidic variant of the Polonovski demethylation of cyclic β -amino ketones.

IV. Experimental Section

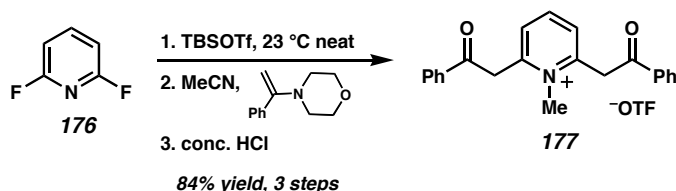
Materials and Methods

Unless stated otherwise, all reactions were conducted in flame-dried glassware using anhydrous solvents (either freshly distilled or passed through activated alumina columns). All reactions were conducted under an inert atmosphere of dry nitrogen or argon, unless otherwise stated. All commercially obtained reagents were used as received. When required, commercial reagents were purified following the guidelines of Perrin and Armarego.³³ Reaction temperatures were controlled using an IKA Mag temperature modulator. Thin-layer chromatography (TLC) was conducted with E. Merck silica gel 60 F254 pre-coated plates (0.25 mm) and visualized using a combination of UV, anisaldehyde, ceric ammonium molybdate, and potassium permanganate staining. ICN silica gel (particle size 0.032-0.063 mm) was used for flash chromatography (unless otherwise stated) using the method described by Still.³⁴

¹H NMR spectra were recorded on a Varian Mercury 300 (at 300 MHz) or a Varian Inova 500 (at 500 MHz), and were reported relative to residual protio solvent signals. Data for ¹H NMR spectra were reported as follows: chemical shift (δ ppm), multiplicity (s = singlet, d = doublet, t = triplet, q = quartet, m = multiplet), coupling constant (Hz), and integration. ¹³C NMR spectra were recorded on a Varian Mercury 300 (at 75 MHz) and were reported relative to residual protio solvent signals. Data for ¹³C NMR spectra were reported in terms of chemical shift. IR spectra were recorded on a Perkin Elmer Paragon 1000 spectrometer and were reported in frequency of absorption (cm^{-1}). Optical rotations were measured with a Jasco P-1010 polarimeter (Na lamp, 589 nm). HPLC analysis was performed on a Hewlett-Packard 1100 Series HPLC (UV

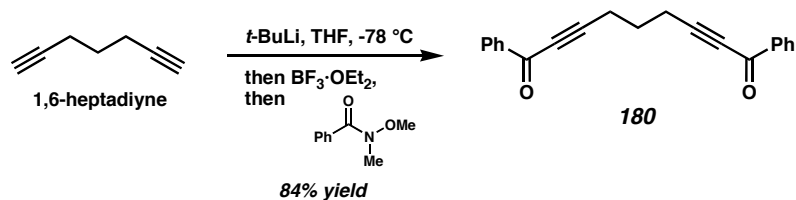
detector at 245 nm) equipped with the following Chiralcel columns: OD-H (25 cm), OD guard (5 cm), AD (25 cm), OJ (25 cm) and OB-H (25 cm). High resolution mass spectra were obtained from the California Institute of Technology Mass Spectral Facility.

Preparative Procedures

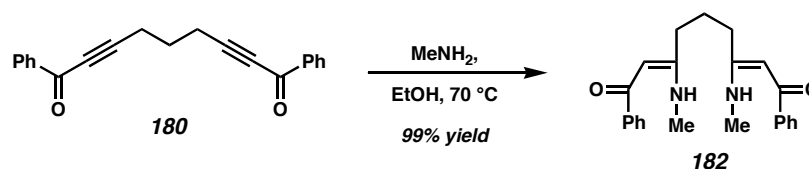


Pyridinium salt (177). To a flask charged with 2,6-difluoropyridine **176** (7.01 g, 60.94 mmol) was added MeOTf (10.00 g, 60.94 mmol). The mixture was maintained at room temperature with stirring for 8 h, at which point a white solid developed. The white solid was used without further purification.

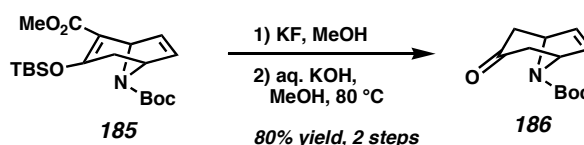
To a solution of the intermediate solid (1.47 g, 5.28 mmol) in MeCN (4 mL) was added a solution of the enamine (2.1 g, 11.09 mmol) in MeCN (4 mL). After 18 h, the reaction was concentrated under reduced pressure to a thick glassy plastic, then dissolved in concentrated HCl (12 mL) and heated to reflux in a sealed tube. After 6 h, the reaction was cooled to $-20\text{ }^\circ\text{C}$ for several hours, then filtered. The filtrate was washed with ice water (1 x 5 mL), then EtOAc (2 x 5 mL), and dried under reduced pressure overnight to provide pyridinium salt **177** (1.63 g, 84% yield, 3 steps, $R_F = 0.11$ in 4% MeOH:DCM) as a crystalline solid: m.p. 185-187 $^\circ\text{C}$; ^1H NMR (300 MHz, $\text{D}_6\text{-DMSO}$) δ 8.55 (dd, $J=7.8$, 8.0 Hz, 1H), 8.11 (d, $J=7.2$ Hz, 6H), 7.76 (dd, $J=7.2$, 7.4 Hz, 2H), 7.64 (dd, $J=7.2$ Hz, 7.2H), 5.44 (s, 4H), 4.02 (s, 3H); ^{13}C NMR (300 MHz, $\text{D}_6\text{-DMSO}$) δ 194.8, 154.8, 145.4, 136.0, 135.0, 130.5, 129.6, 129.3, 61.7, 45.5, 41.9; IR (KBr pellet) 1690, 1275 cm^{-1} ; HRMS (FAB $^+$) calc'd for $[\text{C}_{22}\text{H}_{20}\text{NO}_4]^+$: m/z 330.1494, found 330.1481.



Alkynone (180). To a -78°C solution of 1,6-heptadiyne (101 μL , 0.88 mmol) in THF (5 mL) was slowly added a solution of 1.65 M of *t*-BuLi in Et_2O (1.12 mL, 1.85 mmol). After 5 min, neat $\text{BF}_3 \cdot \text{OEt}_2$ (248 μL , 1.96 mmol) was slowly added to the stirred cooled solution. After an additional 15 min, a solution of the Weinreb amide (323 mg, 1.96 mmol) in THF (2 mL) was added dropwise. After 30 min, the reaction was warmed to room temperature, then quenched with the addition of saturated aq NH_4Cl (5 mL) and diluted with water (5 mL). The layers were separated and the aqueous layer was washed with EtOAc (2 x 10 mL). The combined organics were washed with brine (1 x 10 mL), dried over MgSO_4 , and concentrated under reduced pressure. The crude oil was purified by flash chromatography on silica gel (20% EtOAc:hexane eluent) to yield alkynone **180** (221 mgs, 84% yield, $R_F = 21\%$ in 20% EtOAc:hexane) as a yellow oil: ^1H NMR (300 MHz, CDCl_3) δ 8.14-6.06 (m, 4H), 7.60-7.52 (m, 2H), 7.50-7.39 (m, 4H), 2.69 (ddd, $J=1.8, 6.9$ Hz, 4H), 2.09-1.94 (m, 2H); ^{13}C NMR (300 MHz, CDCl_3) δ 178.2, 136.9, 134.3, 129.7, 128.8, 94.6, 80.7, 26.3, 18.7; IR (film) 2939, 2198, 1651, 1263 cm^{-1} ; HRMS (EI^+) calc'd for $[\text{C}_{21}\text{H}_{15}\text{O}_2]^+$: 299.1072, found 299.1062.



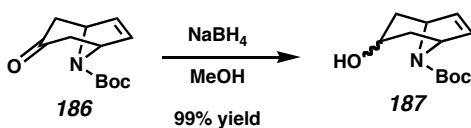
Enamineone (182). To a vial charged with alkyneone **180** (150 mgs, 0.50 mmol) was added a saturated solution of methylamine in EtOH (12 mL). The vial was sealed and heated to 70 °C for 2 h. The vial was cooled to 0 °C before opening, and the reaction was concentrated under a reduced pressure to provide **182** (179 mgs, 99% yield, R_F = 0.05 in 70% EtOAc:hexane) as a waxy solid that was used without further purification: m.p. 141-143 °C; ^1H NMR (CDCl_3) δ 7.85 (dt, J =5.4, 1.8 Hz, 4H), 7.47-7.34 (m, 6H), 5.71 (s, 2), 3.01 (d, J =5.7 Hz, 6H), 2.46 (dd, J =4.2, 7.7 Hz, 4H), 1.96 (m, 2H); ^{13}C NMR (300 MHz, CDCl_3) δ 188.3, 168.1, 140.6, 130.8, 128.4, 127.1, 91.4, 31.6, 29.7, 25.5; IR (film) 2934, 1603, 1325 cm^{-1} ; HRMS (EI^+) calc'd for $[\text{C}_{23}\text{H}_{26}\text{N}_2\text{O}_2]^+$: m/z 362.1994, found 362.1977.



Tropenone (186). To a stirred, -10 °C solution of the silyl enol ether **185** (16.61 g, 42.20 mmol) in MeOH (300 mL) was added a solution of KF (44.31 mL, 1.0 M in MeOH). The reaction was maintained at -10 °C for 15 min, then treated with solid NH_4Cl (2.37 g, 44.31 mmol) and warmed to room temperature. The reaction was stirred an additional 15 min, then concentrated under reduced pressure. The crude paste was taken up in EtOAc (300 mL) and washed with water (2 x 100 mL) and brine solution

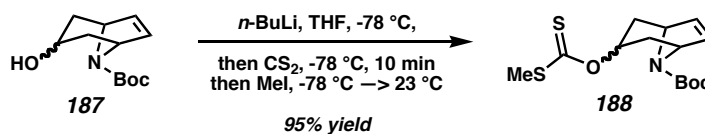
(100 mL), then dried over MgSO_4 and concentrated under reduced pressure. The resulting green oil was used in the next step without further purification.

To a solution of the crude keto-ester (7.81 g, 27.76 mmol) in MeOH (100 mL) was added 5% (w/v) aq KOH (100 mL). The reaction vessel was equipped with a reflux condenser and heated to 110 °C for 45 min, then cooled to room temperature and quenched with saturated aq NH_4Cl . The solution was extracted with DCM (3 x 150 mL) and the combined organics were washed with brine (150 mL), then dried over MgSO_4 and concentrated under a reduced pressure. The crude material was flashed over silica (20% EtOAc:hexane eluent) to provide tropenone **186** (5.00 g, 80% yield, 2 steps, $R_F=0.42$ in 50% EtOAc:hexane) as a clear oil: ^1H NMR (300 MHz, CDCl_3) δ 6.14 (s, 2H), 4.72 (s, 2H), 2.63 (br s, 2H), 2.29 (dd, $J=1.5, 17.4$ Hz, 2H), 1.43 (s, 9H); ^{13}C NMR (300 MHz, CDCl_3) δ 206.1, 152.4, 134.0, 80.7, 56.4, 56.0, 45.8, 45.4, 28.6; IR (film) 2977, 1698, 1393 cm^{-1} ; HRMS (EI^+) calc'd for $[\text{C}_{12}\text{H}_{17}\text{NO}_3]^+$: m/z 223.1208, found 223.1209.



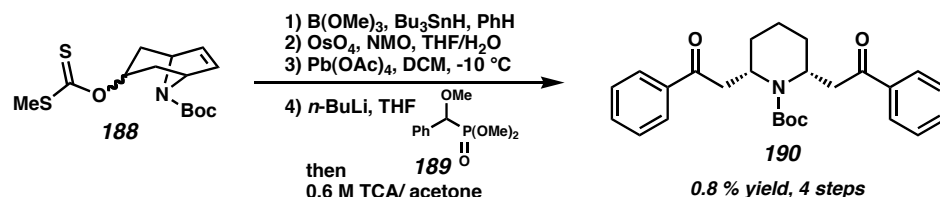
Tropenol (187) To a -10 °C solution of tropenone **186** (4.41 g, 19.77 mmol) in MeOH (150 mL) was added NaBH_4 in several portions over 10 min. The reaction was maintained at -10 °C for 1 h, then warmed to room temperature. Acetone (5 mL) was added to the stirred solution, then the reaction was concentrated under reduced pressure. The crude solid was diluted with DCM (300 mL) then washed with water (2 x 100 mL) and brine (100 mL), then dried over MgSO_4 and concentrated under reduced pressure to

yield tropenol **187** (4.35 g, 99% yield, R_F = 0.10 in 30% EtOAc:hexane) as a mixture of diastereomers. The white solid was placed under a high vacuum for several hours to provide analytically pure material that was used without further purification as a mixture of diastereomers: m.p 75-78 °C; ^1H NMR (300 MHz, CDCl_3) δ 6.36 (br s, 2H), 5.98 (d, J =4.2 Hz, 2H), 4.64-4.40 (m, 2H), 3.98-3.68 (m, 1H), 2.36-1.50 (comp m, 4H), 1.45 (s, 9H); ^{13}C NMR (300 MHz, CDCl_3) δ 152.5, 136.4, 136.0, 131.4, 131.1, 79.9, 79.8, 65.9, 34.9, 57.5, 56.8, 35.8, 35.0, 34.6, 33.9, 28.7; IR (film) 3436, 2975, 1699 cm^{-1} ; HRMS calc'd for $[\text{C}_{12}\text{H}_{19}\text{NO}_3]^+$: m/z 225.1365, found 225.1359.



Xanthate (188) To a -78 °C solution of alcohol **187** (4.47 g, 19.86 mmol) in THF (125 mL) was added slowly a 2.5 M hexanes solution of *n*-BuLi (9.53 mL, 23.83 mmol). The cooled solution was stirred for 15 min before the addition of CS_2 (2.39 mL, 39.71 mmol). After an additional 15 min, MeI (2.48 mL, 39.71 mmol) was added to the stirred solution. The reaction was maintained at -78 °C for 15 min, then warmed slowly to room temperature. The crude reaction mixture was then concentrated under reduced pressure and purified by flash chromatography of over silica gel (10% Et_2O :pentane eluent) to yield the xanthate **188** (5.93 g, 95% yield, R_F = 0.21 in 20% Et_2O :pentane) in a mixture of diastereomers as an orange oil: ^1H NMR (300 MHz, CDCl_3) δ 6.26-5.98 (m, 2H), 5.82-5.64 (m, 1H), 4.64-4.34 (m, 2H), 2.54-2.42 (m, 3H), 2.40-1.98 (m, 2H), 1.96-1.56 (m, 2H), 1.43 (br s, 9H); ^{13}C NMR (300 MHz, CDCl_3) δ 214.1, 152.4, 152.2, 134.4, 134.0,

131.7, 131.4, 80.4, 77.8, 77.5, 57.3, 56.9, 56.7, 56.1, 31.8, 31.0, 30.4, 29.5, 28.7, 19.1, 18.8; IR (film) 2974, 1699 cm^{-1} ; HRMS (EI^+) calc'd for $[\text{C}_{14}\text{H}_{21}\text{NS}_2\text{O}_3]^+$: m/z 315.0963, found 315.0957.



Diketone (190) To a room temperature solution of xanthate **188** (4.20 g, 13.30 mmol) in benzene (60 mL) was added BET_3 (1.60 mL, 16.00 mmol) and Bu_3SnH (5.30 mL, 20.00 mmol). The reaction solution was exposed to a stream of dry oxygen for 2 min, then the reaction was maintained for 30 min. At completion, the reaction was treated with solid KF (12.6 g, 46.55 mmol), then water (20 mL). The reaction was stirred vigorously for 5 min, then the layers were separated and the aqueous layer was washed with EtOAc (2 x 20 mL). The combined organics were dried over MgSO_4 and concentrated under reduced pressure. The resulting crude was purified by flash chromatography over silica gel (10% Et_2O :pentane eluent) to provide a clear oil that was used directly in the next step.

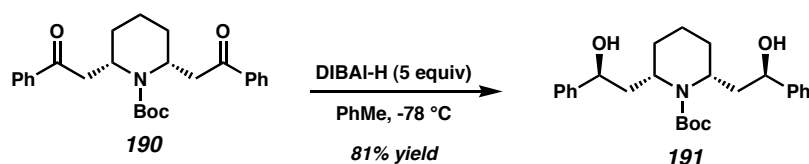
A flask containing the deoxygenated product (1.82 g, 8.70 mmol) was subsequently dissolved in THF (120 mL) and water (10 mL), then treated with *N*-methyl morpholine-*N*-oxide (5.11 g, 43.5 mmol) and OsO_4 (111 mg, 0.44 mmol). After 12 h, the reaction was warmed to 65°C for 1 h, then cooled and treated with saturated aq $\text{Na}_2\text{S}_2\text{O}_3$ solution (40 mL) and stirred vigorously for 30 min. The layers were separated and the aqueous layer was extracted into DCM (3 x 40 mL). The combined organics were

washed with brine, then dried over Na_2SO_4 and concentrated under reduced pressure. The crude material was purified by flash chromatography over silica gel (70% EtOAc:hexane eluent) to provide a white solid that was directly used in the next reaction.

A flask containing the dihydroxylated product (1.41 g, 5.1 mmol) dissolved in DCM (80 mL) and cooled to $-10\text{ }^\circ\text{C}$ before the addition of a solution of $\text{Pb}(\text{OAc})_4$ (2.37 g, 5.36 mmol) in DCM (20 mL). The reaction was maintained at $-10\text{ }^\circ\text{C}$ for 15 min, then warmed to room temperature. The crude mixture was filtered to remove solids and concentrated under a reduced pressure. The concentrate was redissolved in toluene (50 mL) and filtered again. The resulting clear oil was azeotroped with toluene (2 x 30 mL) and heptane (2 x 30 mL) to remove trace acetic acid, then used directly in the next reaction without further purification.

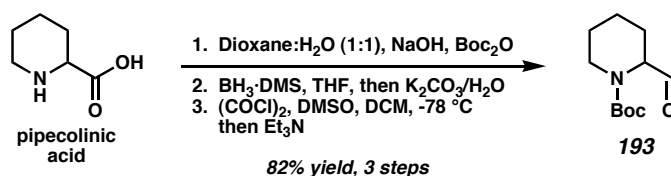
To a $-42\text{ }^\circ\text{C}$ solution of dimethyl methoxy(phenyl)methylphosphonate **189** (2.53 g, 11.00 mmol) in THF (100 mL) was added a 2.5 M solution of *n*-BuLi in hexane (4.32 mL, 10.80 mmol). After 10 min, a solution of the lead tetraacetate cleavage product (1.35 g, 5.0) mmol) in THF (30 mL) was slowly introduced into the cooled reaction vessel. The reaction was maintained at $-42\text{ }^\circ\text{C}$ with vigorous stirring for 30 min, then warmed to room temperature. The resulting gelatinous reaction vessel contents were carefully concentrated under reduced pressure to a thick plastic, then redissolved in a 0.8 M solution of trichloroacetic acid in acetone (100 mL). The reaction was maintained at room temperature for 3 h, then the acid was neutralized by the careful addition of saturated aq NaHCO_3 solution (200 mL). The mixed system was extracted with EtOAc (4 x 200 mL) and the combined organic layers were washed with brine (2 x 100 mL), dried over Na_2SO_4 , and concentrated under reduced pressure. The resulting crude oil was

purified by flash chromatography over silica gel (10% EtOAc:hexane eluent) to provide the diketone **190** (159 mg, 0.8% yield for 4 steps, R_F = 0.51 in 20% EtOAc:hexanes) as a clear oil: ^1H NMR (300 MHz, CDCl_3) δ 8.06 (d, J =7.2 Hz, 4H), 7.58 (dd, J =6.6, 7.5 Hz, 2H), 7.49 (dd, J =7.8, 7.5 Hz, 4H), 4.84 (dd, J =4.5, 5.6 Hz, 2H), 3.29 (d, J =7.2 Hz, 4H), 1.86-1.42 (comp m, 6H), 1.35 (s, 9H); ^{13}C NMR (300 MHz, CDCl_3) δ 198.6, 155.1, 137.0, 133.4, 128.9, 128.6, 80.3, 47.4, 43.5, 28.5, 28.3, 14.1; IR (film) 2938, 1680, 1371 cm^{-1} ; HRMS (EI^+) calc'd for $[\text{C}_{26}\text{H}_{31}\text{NO}_4]^+$: m/z 421.2253, found 421.2244.



***N*-Boc Piperidyl *Meso*-Diol (**191**).** To a $-78\text{ }^\circ\text{C}$ solution of diketone ketone **190** (88.0 mg, g, 0.21 mmol) in toluene (10 mL) was slowly added neat DIBAL-H (188 μL , 1.05 mmol). After 2 h, the reaction was warmed to $-42\text{ }^\circ\text{C}$ for 1 h, then warmed to room temperature for 1 h. At this time, the reaction was cooled to $0\text{ }^\circ\text{C}$ and quenched by the careful addition of saturated aq Na,K-tartrate (5 mL) and diluted with water (3 mL). The biphasic mixture was stirred vigorously for 2 h to dissipate the cloudy mixture, then the layers were separated. The aqueous layer was washed with EtOAc (3 x 10 mL) and the combined organics were washed with brine solution (20 mL) then dried over MgSO_4 and concentrated under reduced pressure. The resulting crude was purified by flash chromatography over silica (15-20% EtOAc:hexanes eluent) to yield the desired alcohol diastereomer **191** (71 mg, 81% yield, R_F = 0.34 in 20% EtOAc:hexanes) as a clear oil: ^1H NMR (300 MHz, CDCl_3) δ 7.42-7.16 (m, 10H), 4.62 (dd, J =10.2, 2.7 Hz, 2H), 4.37 (br s, 2H), 3.06 (s, 2H), 1.99-1.58 (comp m, 10H), 1.54 (s, 9H); ^{13}C NMR (300 MHz, CDCl_3) δ

156.3, 145.0, 128.7, 127.6, 126.0, 129.9, 80.9, 72.6, 48.2, 28.8, 14.0; IR (film) 3393, 2937, 1653 cm^{-1} ; HRMS (FAB^+) calc'd for $[\text{C}_{26}\text{H}_{36}\text{NO}_4]^+$: m/z 426.2644, found 426.2660.

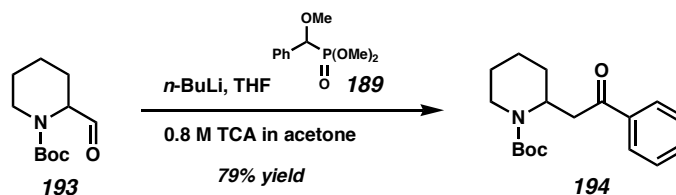


***n*-Boc 2-Formylpiperidine (193).** To a vigorously stirred, room temperature solution of pipercolinic acid (12.92 g, 100.00 mmol) in dioxane (375 mL) and H_2O (375 mL) was added Boc-anhydride (24.00 g, 110 mmol). The solution was maintained at $\text{pH}=10.5$ by the portionwise addition of 30% aq NaOH (v/w) and monitoring with indicating pH paper. After 4 h, no further addition of NaOH solution was required and the reaction was stirred an additional 2 h. At this time, the solution was acidified to $\text{pH} = 5$ by the addition of 2 M HCl. The slightly acidic solution was extracted into EtOAc (3 x 400 mL) and the combined organics were washed with brine solution (300 mL). The organics were dried over MgSO_4 , and evaporated under reduced pressure. The resulting oil was azeotroped with toluene (3 x 250 mL) and placed under a high vacuum overnight. The resulting white waxy solid (22.47 g, 98% yield) was used without further purification.

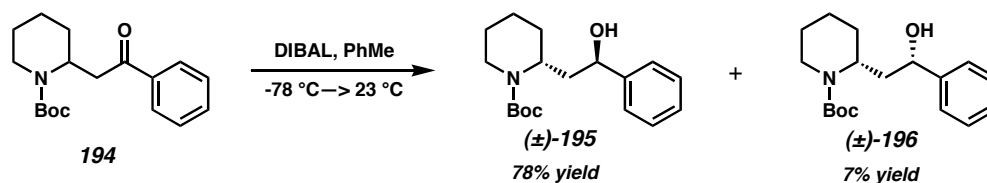
To a 0 $^\circ\text{C}$ solution of the intermediate *N*-Boc piperidine carboxylic acid (22.47 g, 98.00 mmol) in THF (400 mL) was slowly added neat $\text{BH}_3\cdot\text{DMS}$ (24.17 mL, 254.80 mmol). After 30 min, the cold bath was removed and the solution was allowed to warm to room temperature. After an additional 2 h, the reaction was cooled to 0 $^\circ\text{C}$ and quenched by the careful addition of H_2O (150 mL). Then K_2CO_3 (50 g, 36.18 mmol) was added and the mixture was stirred vigorously for 2 h. The layers were separated and the

aqueous layer was extracted into ether (3 x 200 mL). The combined organics were washed with brine (200 mL) and dried over MgSO_4 and concentrated under reduced pressure. The resulting oil was azeotroped with toluene (3 x 250 mL) and placed under high vacuum overnight to provide a white waxy solid (19.83 g, 94% yield), which was used in the next step without further purification.

To a $-78\text{ }^\circ\text{C}$ solution of DMSO (11.06 mL, 155.59 mmol) in DCM (400 mL) was slowly added oxalyl chloride (10.20 mL, 116.91 mmol). After 30 min, a solution of the intermediate alcohol (16.78 g, 77.94 mmol) in DCM (150 mL) was cannulated along the cooled inner walls of reaction vessel. The reaction was stirred for 1 h before the addition of Et_3N . Stirring was continued at $-78\text{ }^\circ\text{C}$ for 1 h, then the reaction vessel was warmed to room temperature for 2 h. At this time, the solids were filtered off and the reaction mixture was concentrated. The crude mixture was then diluted with toluene (300 mL) and solids were filtered. After concentration of the organics under reduced pressure, the crude was purified by flash chromatography over silica gel (10% EtOAc:hexane eluent) to provide aldehyde **193** (14.79 g, 89% yield, R_F = 0.22 EtOAc:hexane) as a clear oil: ^1H NMR (300 MHz, CDCl_3) δ 9.58 (s, 1H), 4.58 (br s, 1H), 3.92 (br s, 1H), 2.90 (br s, 1H), 2.26-2.08 (m, 1H), 1.74-1.52 (m, 5H), 1.46 (s, 9H), 1.34-1.12 (m, 1H); ^{13}C NMR (300 MHz, CDCl_3) δ 201.3, 80.4, 60.84, 43.2, 28.4, 27.8, 24.8, 23.7, 21.1; IR (film) 2938, 1735, 1695, 1406 cm^{-1} ; HRMS (FAB^+) calc'd for $\text{C}_{11}\text{H}_{20}\text{NO}_3$: m/z 214.1443, found 214.1440.



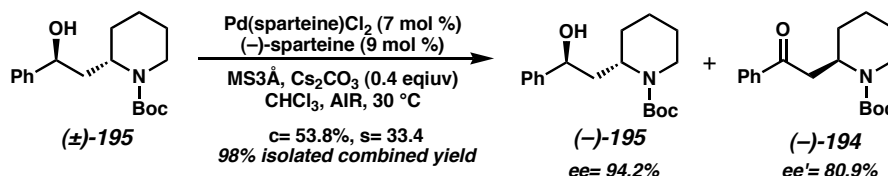
Ketone (194). To a $-78\text{ }^{\circ}\text{C}$ stirred solution of dimethyl methoxy(phenyl)methylphosphonate **189** (23.70 g, 102.95 mmol) in THF (600 mL) was slowly added *n*-BuLi (40.4 mL, 2.5 M in THF). After 15 min, a solution of aldehyde **193** (20.72 g, 97.13 mmol) in THF (150 mL) was introduced into the cooled reaction vessel, then stirred for 1 h with vigorous stirring. The reaction was then warmed to room temperature, and the resulting gel was carefully concentrated to 1/3 the original volume under reduced pressure. The crude mixture was then redissolved in a 0.8 M solution of trichloroacetic acid in acetone (650 mL) and stirred at room temperature for 6 h. The reaction was then neutralized by the addition of saturated aq NaHCO_3 until gas evolution subsided and extracted into EtOAc (3 x 1500 mL). The combined organics were washed with brine solution (500 mL) and dried over MgSO_4 , then concentrated under reduced pressure. Purification immediately followed by flash chromatography over silica gel (10-20% EtOAc:hexane eluent) to provide ketone **194** (23.29 g, 79% yield, $R_F = 0.47$ in 30% Et_2O :pentane) as a colorless oil: ^1H NMR (300 MHz, CDCl_3) δ 8.00-7.9.4 (m, 2H), 7.59-7.40 (m, 3H), 4.82 (m, 1H), 4.03 (d, $J=12.6$ Hz, 1H), 3.00-2.17 (m, 2H), 2.86 (t, $J=2.1$ Hz, 1H), 1.68-1.38 (m, 6H), 1.34 (s, 9H); ^{13}C NMR (300 MHz, CDCl_3) δ 198.6, 154.9, 137.0, 133.4, 128.9, 128.5, 79.8, 48.4, 39.4, 28.5, 25.5, 19.1; IR (film) 2938, 1688, 1411 cm^{-1} ; HRMS (FAB $^+$) calc'd for $[\text{C}_{18}\text{H}_{26}\text{NO}_3]^+$: m/z 304.1913, found 304.1916.



Alcohol [(±)-195]. To a -78 °C solution of ketone **194** (11.07 g, 36.25 mmol) in toluene (400 mL) was slowly added neat DIBAL-H (8.10 mL, 45.31 mmol). After 2 h, the reaction was warmed to -42 °C for 1 h, then warmed to room temperature for 1 h. At this time, the reaction was cooled to 0 °C and quenched by the careful addition of saturated aq Na,K-tartrate (100 mL) and diluted with water (100 mL). The mixture was stirred vigorously for 2 h to dissipate the cloudy mixture, then the layers were separated. The aqueous layer was washed with EtOAc (3 x 200 mL) and the combined organics were washed with brine solution (200 mL) then dried over MgSO₄ and concentrated under reduced pressure. The resulting crude was purified by flash chromatography over silica (10-15% EtOAc:hexanes eluent) to yield the desired alcohol diastereomer **(±)-195** (8.36 g, 78% yield, R_F = 0.34 in 30% EtOAc:hexane) as a white waxy solid: m.p. 58-59 °C; ¹H NMR (300 MHz, CDCl₃) δ 7.40-7.18 (m, 5H), 4.68 (dd, J =8.0, 5.4 Hz, 1H), 4.35 (s, 1H), 3.91 (d, J =11.4 Hz, 1H), 3.59 (bs, 1H), 2.77 (t, J =13.5 Hz, 1H), 2.15-2.0 (m, 1H), 1.92-1.80 (m, 1H), 1.67-1.47 (m, 1H), 1.43 (s, 9H); ¹³C NMR (300 MHz, CDCl₃) δ 155.7, 145.0, 128.5, 127.4, 126.1, 79.9, 72.6, 48.6, 40.3, 39.7, 29.2, 28.7, 25.7, 19.3; IR (film) 3412, 2933, 1688, 1416 cm⁻¹; HRMS (FAB⁺) calc'd for [C₁₈H₁₈NO₃]⁺: m/z 306.2069, found 306.2057.

The minor diastereomer **(±)-196** (1.50g, 14% yield, R_F = 0.51 30% EtOAc:hexane) was also isolated as a white waxy solid: m.p. 55-57 °C; ¹H NMR (300 MHz, CDCl₃) δ 7.40-7.14 (m, 5H), 4.78-4.52 (br s, 1H), 4.03 (d, J =5.7 Hz, 1H), 2.79 (m 1), 2.20 (m, 1H),

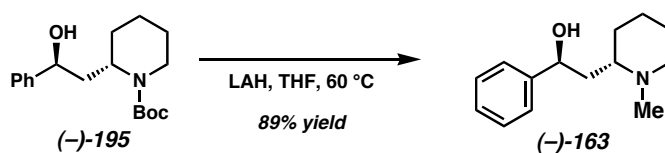
1.84-1.14 (comp m, 16H); ^{13}C NMR (300 MHz, CDCl_3) δ 144.3, 128.5, 127.2, 125.8, 80.6, 70.0, 46.9, 40.6, 39.8, 29.5, 28.7, 28.6, 25.7, 19.4; IR (film) 3423, 2938, 1688, 1658 cm^{-1} ; HRMS (FAB^+) calc'd for $[\text{C}_{18}\text{H}_{28}\text{NO}_3]^+$: m/z 306.2069, found 306.2084.



Oxidative Kinetic Resolution of Alcohol [(±)-195]. An oven-dried reaction tube was charged with alcohol (±)-**195** (142 mg, 0.465 mmol), 3 Å MS (250 mg), finely milled anhydrous Cs_2CO_3 (60 mg, 0.186 mmol), and chloroform (1.5 mL). To the slurry was added a solution of Pd(sparteine)Cl_2 (9.6 mg, 0.023 mmol) and $(-)\text{-sparteine}$ (7.5 μL , 0.033 mmol) in chloroform (0.5 mL). The reaction tube was fitted with a short drying tube and allowed to stir open to the atmosphere. After 60 h, the reaction was filtered over a short pad of silica (Et_2O eluent), and the volatiles were removed under reduced pressure. The crude mixture was then purified by flash chromatography (15-25% Et_2O :pentane eluent) to provide the resolved alcohol $(-)\text{-195}$ (75 mg, 45% yield, R_F = 0.34 in 30% EtOAc :hexane) in 94.2% ee as a white waxy solid: m.p. 58-59 °C; ^1H NMR (300 MHz, CDCl_3) δ 7.40-7.18 (m, 5H), 4.68 (dd, J =8.0, 5.4 Hz, 1H), 4.35 (s, 1H), 3.91 (d, J =11.4 Hz, 1H), 3.59 (bs, 1H), 2.77 (t, J =13.5 Hz, 1H), 2.15-2.0 (m, 1H), 1.92-1.80 (m, 1H), 1.67-1.47 (m, 1H), 1.43 (s, 9H); ^{13}C NMR (300 MHz, CDCl_3) δ 155.7, 145.0, 128.5, 127.4, 126.1, 79.9, 72.6, 48.6, 40.3, 39.7, 29.2, 28.7, 25.7, 19.3; IR (film) 3412,

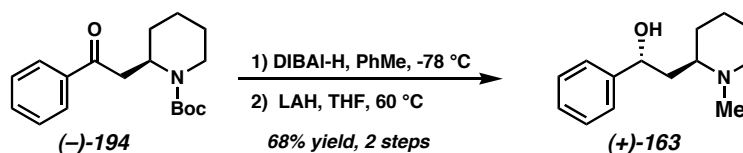
2933, 1688, 1416 cm^{-1} ; HRMS (FAB⁺) calc'd for $[\text{C}_{18}\text{H}_{18}\text{NO}_3]^+$: m/z 306.2069, found 306.2057; $[\alpha]_{\text{D}}^{20}$ -127.5° ($c=1$, CHCl_3).

The ketone (–)-**194** (64 mg, 53% yield, $R_{\text{F}}=0.47$ in 30% Et_2O :pentane) was recovered in 80.9% ee as a clear oil: ^1H NMR (300 MHz, CDCl_3) δ 8.00–7.9.4 (m, 2H), 7.59–7.40 (m, 3H), 4.82 (m, 1H), 4.03 (d, $J=12.6$ Hz, 1H), 3.00–2.17 (m, 2H), 2.86 (t, $J=2.1$ Hz, 1H), 1.68–1.38 (m, 6H), 1.34 (s, 9H); ^{13}C NMR (300 MHz, CDCl_3) δ 198.6, 154.9, 137.0, 133.4, 128.9, 128.5, 79.8, 48.4, 39.4, 28.5, 25.5, 19.1; IR (film) 2938, 1688, 1411 cm^{-1} ; HRMS (FAB⁺) calc'd for $[\text{C}_{18}\text{H}_{26}\text{NO}_3]^+$: m/z 304.1913, found 304.1916; $[\alpha]_{\text{D}}^{20}$ -9.7° ($c=1$, CHCl_3).



(–)-**Sedamine** [(–)-**163**]. To a 0 °C solution of alcohol (–)-**195** (70 mg, 0.23 mmol) in THF (3 mL) was added a solution of LiAlH_4 in THF (0.92 mL, 1.0 M). The reaction was heated to 70 °C in a sealed vial for 8 h, then cooled to 0 °C and carefully quenched by the sequential addition of water (50 μL), 15% (w/v) aq NaOH (50 μL), then water (50 μL). The resulting mixture was filtered over a pad of Celite to remove solids, rinsing with ether. The mixture was concentrated under reduced pressure and the resulting oil was purified by Kugelrohr distillation to provide (–)-sedamine (–)-**163** (45 mg, 89% yield, $R_{\text{F}}=0.33$ in 10% MeOH, 1% TEA in DCM) as a clear oil: ^1H NMR (300 MHz, CDCl_3) δ 7.42 (comp m, 5H), 5.85 (br s, 1H), 4.87 (dd, $J=2.7, 10.5$ Hz, 1H), 3.14–3.0 (m, 1H), 2.92–2.78 (m, 1H), 2.64–2.50 (m, 1H), 2.48 (s, 3H), 2.12 (ddd, $J=3.9, 9.9$ Hz, 1H), 1.84–1.22 (comp m, 7H); ^{13}C NMR (300 MHz, CDCl_3) δ 145.9, 128.5, 127.2, 125.8,

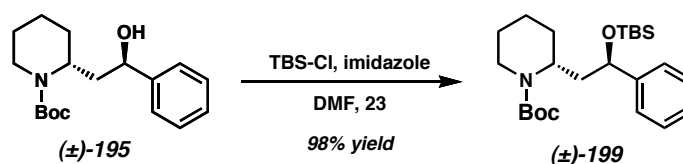
74.7, 61.1, 51.6, 40.2, 40.0, 26.1, 22.6, 20.8; IR (film) 3369, 2938, 1457 cm^{-1} ; HRMS (EI^+) calc'd for $[\text{C}_{14}\text{H}_{21}\text{NO}]^+$: m/z 219.1623, found 219.1619; $[\alpha]_{\text{D}}^{20}$ -89.2° ($c=1$, CHCl_3).



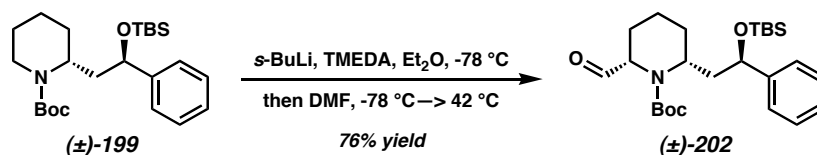
(+)-Sedamine [(+)-163]. To a -78°C solution of ketone **(-)-194** (111 mg, 0.36 mmol) in toluene (4 mL) was slowly added neat DIBAL-H (81 μL , 0.45 mmol). After 2 h, the reaction was warmed to -42°C for 1 h, then warmed to room temperature for 1 h. At this time, the reaction was cooled to 0°C and quenched by the careful addition of saturated aq Na,K-tartrate (1 mL) and diluted with water (1 mL). The mixture was stirred vigorously for 1 h to dissipate the cloudy mixture, then the layers were separated. The aqueous layer was washed with EtOAc (3 x 2 mL) and the combined organics were washed with brine solution (2 mL) then dried over MgSO_4 and concentrated under reduced pressure. The resulting crude was purified by flash chromatography over silica (10-15% EtOAc:hexanes eluent) and used directly in the next reaction.

To a 0°C solution of the reduction product (75.0 mg, 0.25 mmol) in THF (3 mL) was added a solution of LiAlH_4 in THF (0.97 mL, 1.0 M). The reaction was heated to 70°C in a sealed vial for 8 h, then cooled to 0°C and carefully quenched by the sequential addition of water (50 μL), 15% (w/v) aq NaOH (50 μL), then water (50 μL). The resulting mixture was filtered over a pad of Celite to remove solids, rinsing with ether. The mixture was concentrated under reduced pressure and the resulting oil was purified by Kugelrohr distillation to provide (+)-sedamine **(+)-163** (38.1 mg, 68% yield $R_{\text{F}}=0.33$ in 10% MeOH, 1% TEA in DCM) as a clear oil: ^1H NMR (300 MHz, CDCl_3) δ 7.42

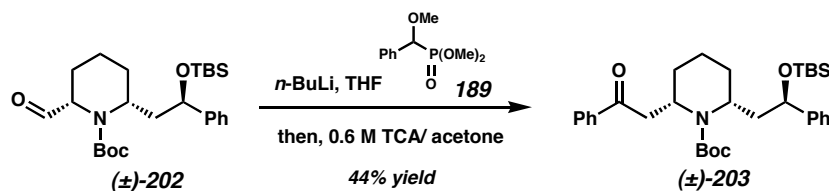
(comp m, 5H), 5.85 (br s, 1H), 4.87 (dd, $J=2.7, 10.5$ Hz, 1H), 3.14-3.0 (m, 1H), 2.92-2.78 (m, 1H), 2.64-2.50 (m, 1H), 2.48 (s, 3H), 2.12 (ddd, $J=3.9, 9.9$ Hz, 1H), 1.84-1.22 (comp m, 7H); ^{13}C NMR (300 MHz, CDCl_3) δ 145.9, 128.5, 127.2, 125.8, 74.7, 61.1, 51.6, 40.2, 40.0, 26.1, 22.6, 20.8; IR (film) 3369, 2938, 1457 cm^{-1} ; HRMS (EI^+) calc'd for $[\text{C}_{14}\text{H}_{21}\text{NO}]^+$: m/z 219.1623, found 219.1619; $[\alpha]_{\text{D}}^{20} +72.2^\circ$ ($c=1$, CHCl_3).



TBS-ether $(\pm)\text{-199}$. To a room temperature solution of alcohol $(\pm)\text{-195}$ (6.11 g, 19.88 mmol) in DMF (20 mL) was added imidazole (2.165g 31.80 mmol) in one portion. After 5 minutes, a solution of TBSCl (4.2 g, 27.83 mmol) in DMF (5 mL) was added to the stirred reaction mixture. After, 1 h the reaction was diluted with water (100 mL) and extracted into hexane (4 x 100 mL). The combined organics were washed with brine solution (80 mL), dried over MgSO_4 and concentrated under reduced pressure. The resulting crude was purified by flash chromatography (5-10% Et_2O :pentane eluent) to provide the TBS-ether $(\pm)\text{-199}$ (8.21 g, 98% yield $R_{\text{F}}=0.66$ in 20% EtOAc :hexane) as a clear oil: ^1H NMR (300 MHz, CDCl_3) δ 7.35-7.20 (m, 5H), 4.62 (t, $J=6.6$ Hz, 1H), 4.26 (m, 1H), 3.98 (d, $J=13.5$ Hz, 1H), 2.78 (t, $J=8.8$ Hz, 1H), 2.04-1.84 (m, 2H), 1.65-1.48 (m, 5H), 1.46 (s, 9H), 0.87 (s 9), 0.01 (s, 3H), -0.19 (s, 3H); ^{13}C NMR (300 MHz, CDCl_3) δ 155.26, 145.42, 128.35, 127.37, 126.46, 79.30, 73.25, 47.92, 40.93, 39.41, 28.79, 27.80, 26.10, 19.27, 18.39, -4.33, -4.75; IR (film) 2938, 1690, 1411, 1163 cm^{-1} ; HRMS (FAB^+) calc'd for $[\text{C}_{24}\text{H}_{42}\text{NO}_3]^+$: m/z 420.2934, found 420.2920.

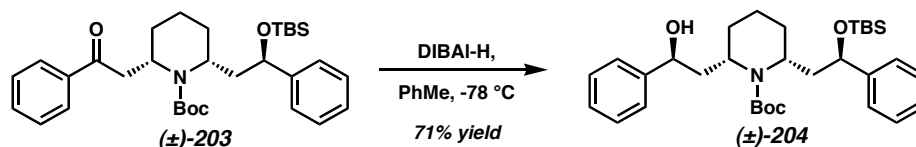


Aldehyde [(±)-202]. To a $-78\text{ }^{\circ}\text{C}$ solution of TBS-ether (±)-199 (4.10 g, 9.77 mmol) and TMEDA (2.65 mL, 17.59 mmol) in Et_2O (150 mL) was added slowly a 1.4 M cyclohexane solution of *s*-BuLi (12.2 mL, 17.1 mmol). After 15 minutes, the stirred solution was warmed to $-42\text{ }^{\circ}\text{C}$ for 45 min, then treated with DMF (1.89 mL, 24.43 mmol). The solution was maintained at $-42\text{ }^{\circ}\text{C}$ for 1 h, then warmed to room temperature for 30 min before quenching with saturated aq NH_4Cl (40 mL) and diluting with water (40 mL). The layers were separated and the aqueous layer was extracted with Et_2O (2 x 100 mL). After combining all organic layers, they were washed with brine (50 mL), dried over MgSO_4 , and concentrated under reduced pressure. The crude oil was purified by flash chromatography over silica (5-10% EtOAc :hexane eluent), to provide aldehyde (±)-202 (3.32 g, 76% yield, $R_F = 0.51$ in 20% EtOAc :hexane) as a clear oil: ^1H NMR (300 MHz, CDCl_3) δ 9.26 (d, $J=2.7$ Hz, 1H), 7.42-7.14 (m, 5H), 4.68 (t, $J=5.7$ Hz, 1H), 4.29 (br s, 1H), 3.48 (dt, $J=10.8, 3.3$ Hz, 1H), 2.02- 1.38 (m, 8H), 1.46 (s, 9H), 0.88 (s, 9H), 0.01 (s, 3H), -0.20 (s, 3H); ^{13}C NMR (300 MHz, CDCl_3) δ 196.1, 145.0, 128.5, 128.2, 127.6, 126.1, 81.5, 73.0, 60.1, 49.4, 40.8, 28.7, 28.6, 26.3, 26.1, 25.1, 18.4, 17.4, -4.3 , -4.8 ; IR (film) 2933, 1731, 1683, 1366 cm^{-1} ; HRMS (FAB^+) calc'd for $[\text{C}_{25}\text{H}_{42}\text{NO}_4\text{Si}]^+$: m/z 448.2883, found 448.2870.

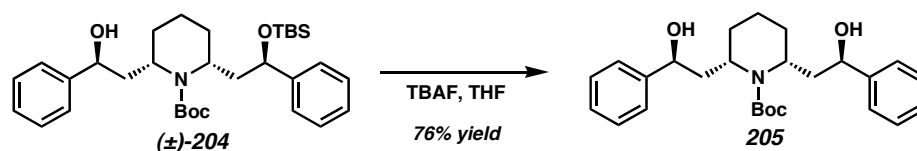


Ketone [(±)-203]. To a -78 °C stirred solution of dimethyl methoxy(phenyl)methylphosphonate **189** (1.80 g, 7.80 mmol) in THF (60 mL) was slowly added a 2.5 M solution of *n*-BuLi in THF (3.06 mL, 7.66 mmol). After 15 min, a solution of aldehyde **(±)-202** (3.31g, 7.36 mmol) in THF (15 mL) was cannulated into the cooled reaction vessel, then stirred vigorously for 1 h. At this time, the reaction was warmed to room temperature, and the resulting gel was carefully concentrated to 1/3 the original volume under reduced pressure. The crude mixture was then redissolved in a 0.6 M solution of trichloroacetic acid in acetone (75 mL) and stirred at room temperature for 6 h. The reaction was then neutralized by the addition of saturated aq NaHCO₃ until gas evolution subsided and extracted into EtOAc (3 x 150 mL). The combined organics were washed with brine solution (100 mL) and dried over MgSO₄, then concentrated under reduced pressure. The resulting crude oil was purified by flash chromatography (5-10% Et₂O:pentane eluent) with silica to furnish ketone **(±)-203** (1.75 g, 44% yield, R_F= 0.48 in 20% Et₂O:pentane) as a clear oil: ¹H NMR (300 MHz, CDCl₃) δ 8.03 (d, *J*=7.2 Hz, 2H), 7.62-7.20 (comp m, 8H), 4.86-4.66 (comp m, 1H), 4.4-3.8 (m, 1H), 3.54-3.08 (comp m, 1H), 2.36-1.84 (m, 1H), 1.78-1.56 (m, 2H), 1.56-1.40 (m, 9H), 0.90 (s, 9H), 0.04 (s, 3H), -0.16 (s, 3H); ¹³C NMR (300 MHz, CDCl₃) δ 198.9, 155.6, 155.3, 145.5, 145.3, 137.2, 137.0, 133.3, 133.2, 128.8, 128.8, 128.7, 128.5, 128.5, 128.4, 128.5, 127.4, 126.5, 126.4, 79.8, 76.6, 73.8, 73.5, 49.8, 49.0, 47.3, 45.0, 44.1, 43.7, 43.5, 28.9, 28.8, 27.9, 26.6, 26.2,

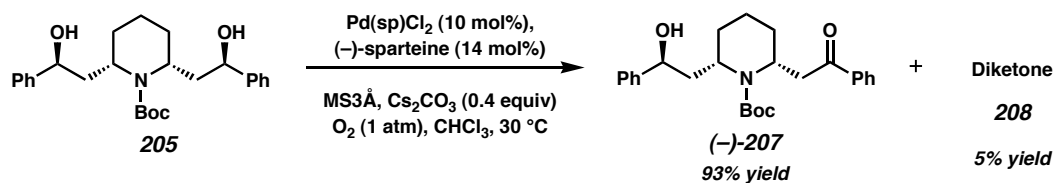
26.1, 25.9, 25.9, 25.1, 18.5, 18.4, 16.1, 14.3, -4.2, -4.3, -4.7; IR (film) 2931, 1685, 1365 cm^{-1} ; HRMS (FAB⁺) calc'd for $[\text{C}_{32}\text{H}_{48}\text{NO}_4\text{Si}]^+$: m/z 538.3353, found 538.3356.



***N*-Boc, *O*-TBS-Dihydro-Lobeline [(±)-204].** To a -78 °C solution of ketone (±)-**203** (810 mg, 1.507 mmol) in toluene (30 mL) was slowly added neat DIBAL-H (296 μL , 1.658 mmol). After 1 h, the reaction was warmed to -42 °C for 1 h, then warmed to room temperature for 30 min. At this time, the reaction was cooled to 0 °C and quenched by the careful addition of saturated aq Na,K-tartrate (10 mL) and diluted with water (10 mL). The mixture was stirred vigorously for 1 h to dissipate the cloudy mixture, then the layers were separated. The aqueous layer was washed with EtOAc (20 x 3 mL) and the combined organics were washed with brine solution (20 mL) then dried over MgSO_4 and concentrated under reduced pressure. The resulting crude was purified by flash chromatography over silica (10% EtOAc:hexanes eluent) to yield the desired alcohol diastereomer (±)-**204** (573 mg, 71% yield, R_F = 0.55 in 20% EtOAc:hexane) as a clear oil: ^1H NMR (300 MHz, CDCl_3) δ 7.48-7.14 (m, 10H), 4.98-4.60 (m, 3H), 4.52-4.30 (m, 2H), 4.16-3.92 (m, 1H), 2.34-1.62 (comp m, 10H), 1.62-1.50 (m, 9H), 0.98-0.88 (m, 9H), 0.10-0.03 (m, 3H), -0.11-0.17 (m, 3H); ^{13}C NMR (CDCl_3) δ 156.3, 145.4, 128.5, 127.6, 127.3, 126.3, 126.0, 80.4, 80.2, 73.7, 73.5, 72.8, 50.1, 49.0, 48.3, 47.8, 46.9, 44.7, 43.9, 29.0, 26.2, 25.7, 23.7, 18.5, 14.4, 14.2, -4.1, -4.7; IR (film) 3401, 2931, 1658 cm^{-1} ; HRMS (FAB⁺) calc'd for $[\text{C}_{32}\text{H}_{50}\text{NO}_4\text{Si}]^+$: m/z 540.3509, found 540.3500.



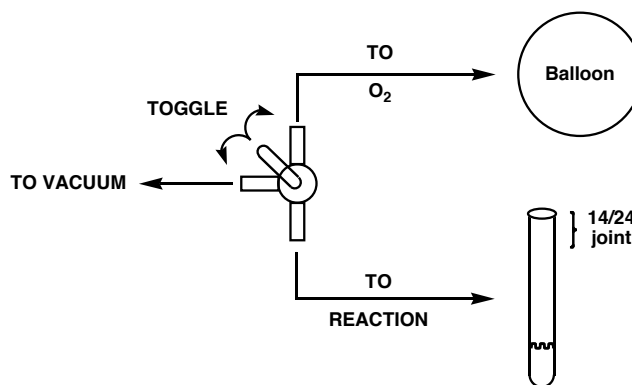
Meso-Diol (205). To a stirred, room temperature solution of ketone **(±)-204** (352 mg, 0.653 mmol) in THF (7 mL) was added a 1 M solution of TBAF in THF (1.6 mL, 1.96 mmol). After 8 h, the reaction was concentrated under reduced pressure and purified by flash chromatography with silica gel (20% EtOAc:hexane eluent) to yield the *meso*-diol **205** (210 mg, 76% yield, R_F = 0.30 in 20% EtOAc:hexane) as a clear oil: ^1H NMR (300 MHz, CDCl_3) δ 7.42-7.16 (m, 10H), 4.62 (dd, J =10.2, 2.7 Hz, 2H), 4.37 (br s, 2H), 3.06 (s, 2H), 1.99-1.58 (comp m, 10H), 1.54 (s, 9H); ^{13}C NMR (300 MHz, CDCl_3) δ 156.3, 145.0, 128.7, 127.6, 126.0, 129.9, 80.9, 72.6, 48.2, 28.8, 14.0; IR (film) 3393, 2937, 1653 cm^{-1} ; HRMS (FAB^+) calc'd for $[\text{C}_{26}\text{H}_{36}\text{NO}_4]^+$: m/z 426.2644, found 426.2660.



N-Boc-(-)-Lobeline [(-)-207] A reaction tube (ID= 1.4 cm, OD= 1.8 cm, height= 14 cm) equipped with a 14/24 female joint was charged with hot, oven-dried (oven temp = 130 °C, >2 days) 3Å molecular sieves (500 mg). After cooling to room temperature, the vessel was charged with a solution of Pd(sp)Cl_2 (20.6 mg, 0.05 mmol) and (-)-sparteine (16.1 μl , 0.07 mmol) in CHCl_3 (2 mL). The reaction tube was equipped

with a 14/24 male joint connected by vacuum quality tubing to a valve connected differentially to a high-vacuum source and a balloon of dry O₂ (Figure 11).

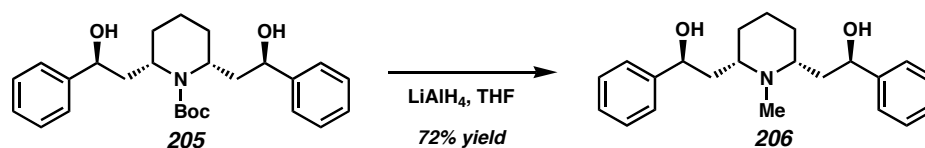
Figure 11. Experimental set-up



The reaction slurry was cooled to $-78\text{ }^{\circ}\text{C}$, then purged with dry O₂ by iteratively evacuating the reaction tube, then refilling from the balloon (3 iterations) using the toggle valve. The 14/24 joint was removed such that a stream of O₂ flowed over the reaction tube while a solution of the *meso*-diol **205** (213 mg, 0.5 mmol) in CHCl₃ (2 mL) was introduced into the frozen slurry. The 14/24 joint was replaced and the reaction tube was again purged with O₂ by 3 evacuation/refilling cycles in the manner previously described. The reaction was then removed from the cooling bath and warmed to $35\text{ }^{\circ}\text{C}$. The reaction was monitored by TLC (30% EtOAc:hexanes eluent R_f diol = 0.25; R_f keto-alcohol = 0.4; R_f diketone = 0.55). At 60 h, the reaction was filtered over a plug of Celite, rinsing with DCM, then concentrated under reduced vacuum. The crude material was purified by flash chromatography over silica gel (20% EtOAc:hexanes eluent) to yield the *N*-Boc-(-)-lobeline (-)-**207** (198 mg, 93 % yield, R_f = 0.43 in 20% EtOAc:hexanes) as a clear oil: ¹H NMR (300 MHz, CDCl₃) δ 7.97 (d, J =7.5 Hz, 2H), 7.64-7.22 (comp m, 8H), 4.79 (br s, 1H), 4.72 (dd, J =10.2, 2.7 Hz, 1H), 3.26-2.94 (m, 2H), 2.09 (ddd, J =8.3, 2.7 Hz, 1H), 1.91 (ddd, J =3.0, 10.3 Hz, 1H), 1.84-1.50 (comp m, 6H), 1.46 (s, 9H); ¹³C NMR

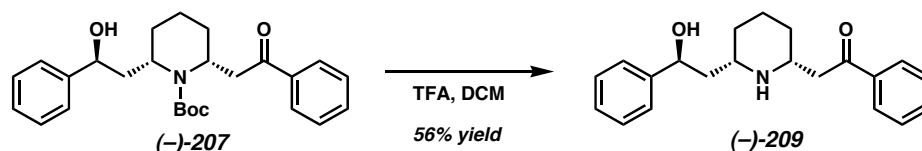
(300 MHz, CDCl₃) δ 198.5, 155.9, 145.3, 136.9, 133.5, 128.9, 128.7, 128.5, 127.5, 125.9, 80.8, 72.8, 48.1, 47.5, 46.9, 43.0, 28.7, 28.0, 14.0; IR (film) 3420, 2937, 1680, 1367 cm⁻¹; HRMS (EI⁺) calc'd for [C₂₆H₃₄NO₄]⁺: m/z 424.2488, found 424.2465; [α]_D²⁰ -202.1° (c=1, CDCl₃).

The diketone **208** (11 mg, 5 % yield, R_F= 0.51 in 20% EtOAc:hexanes) was also recovered as a clear oil: ¹H NMR (300 MHz, CDCl₃) δ 8.06 (d, J =7.2 Hz, 4H), 7.58 (dd, J =6.6, 7.5 Hz, 2H), 7.49 (dd, J =7.8, 7.5 Hz, 4H), 4.84 (dd, J =4.5, 5.6 Hz, 2H), 3.29 (d, J =7.2 Hz, 4H), 1.86-1.42 (comp m, 6H), 1.35 (s, 9H); ¹³C NMR (300 MHz, CDCl₃) δ 198.6, 155.1, 137.0, 133.4, 128.9, 128.6, 80.3, 47.4, 43.5, 28.5, 28.3, 14.1; IR (film) 2938, 1680, 1371 cm⁻¹; HRMS (EI⁺) calc'd for [C₂₆H₃₁NO₄]⁺: m/z 421.2253, found 421.2244.

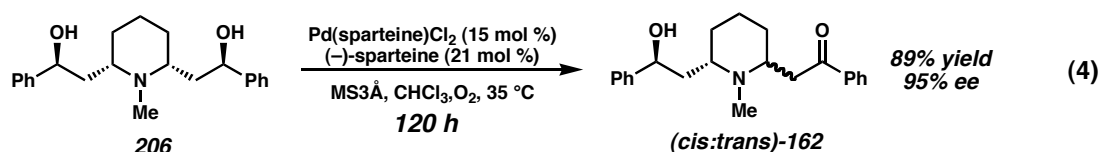


Lobelanine (206). A solution of the *N*-Boc-piperidine **205** (630 mg, 1.48 mmol) was dissolved in THF (40 mL) and cooled to 0 °C before treatment with a 1 M THF solution of LiAlH₄ (7.40 mL, 7.40 mmol). The reaction was heated to 55 °C in a sealed vial for 8 h, then cooled to 0 °C before quenching by the sequential addition of water (400 μ L), 15% (w/v) aq NaOH (400 μ L), then water (400 μ L). The crude amino diol was purified by preparatory TLC (8% MeOH/0.5% Et₃N:DCM eluent). The white solid was then recrystallized from benzene/heptane to give lobelanine **206** (360 mg, 72% yield, R_F= 0.31 in 10% MeOH:DCM) as a white solid: m.p. 178-180 °C; ¹H NMR (300 MHz, CDCl₃) δ 7.54-7.22 (m, 10H), 4.87 (dd, J =5.4, 8.6 Hz, 2H), 4.65 (br s, 2H), 2.95 (dd,

$J=15.9, 10.8$ Hz, 2H), 2.32 (s, 3H), 2.01 (ddd, $J=4.5, 9.3, 14.1$ Hz, 2H), 1.78 (br s, 1H), 1.64-1.44 (comp m, 5H), 1.22-0.8 (m, 2H); ^{13}C NMR (300 MHz, CDCl_3) δ 145.1, 128.6, 127.6, 126.1, 74.3, 62.3, 41.8, 25.9, 25.2, 23.4; IR (film) 3309, 2929, 1452 cm^{-1} ; HRMS (FAB $^+$) calc'd for $[\text{C}_{22}\text{H}_{30}\text{O}_2\text{N}]^+$: m/z 340.2277, found 340.2278.

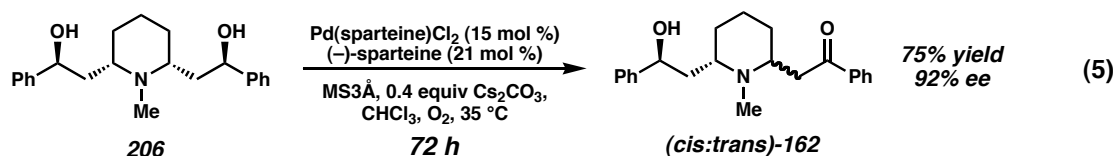


(-)-Norlobeline [(-)-209]. TFA (0.27 mL, 3.5 mmol) was added to a stirred, 35 °C solution of diol (-)-**207** in DCM. After 1 h, the reaction was cooled to 0 °C and quenched upon addition of 1 M NaOH (4 mL). The layers were separated and the aqueous layer was extracted with DCM (3 x 5 mL). After combining the organic layers, they were dried over Na_2SO_4 and concentrated under reduced pressure. The crude material was purified by flash chromatography over silica gel (8% MeOH/0.5% Et_3N : DCM eluent) to give the (-)-norlobeline (-)-**209** (29 mg, 56% yield, $R_F = 0.13$ in 10% MeOH:DCM) as a waxy solid: m.p. 72-74 °C; ^1H NMR (300 MHz, CDCl_3) δ 7.94 (d, $J=7.2$ Hz, 2H), 7.57 (dd, $J=7.5, 7.5$ Hz, 1H), 7.46 (dd, $J=8.7, 7.5$ Hz, 2H), 7.40-7.18 (comp m, 6H), 4.93 (dd, $J=4.2, 9.5$ Hz, 1H), 4.84-4.24 (br s, 2H), 3.38-3.22 (comp m, 2H), 3.20-2.96 (comp m, 2H), 1.98-1.08 (comp m, 6H); ^{13}C NMR (300 MHz, CDCl_3) δ 199.0, 144.8, 136.9, 133.7, 128.9, 128.6, 128.4, 127.6, 125.9, 75.4, 58.7, 53.6, 44.8, 44.6, 32.5, 31.5, 24.4; IR (film) 3480, 2923, 1682, 1449 cm^{-1} ; HRMS (EI $^+$) calc'd for $[\text{C}_{21}\text{H}_{25}\text{NO}_2]^+$: m/z 323.1885, found 323.1891; $[\alpha]_D^{20} -13.5^\circ$ ($c=1$, CDCl_3).



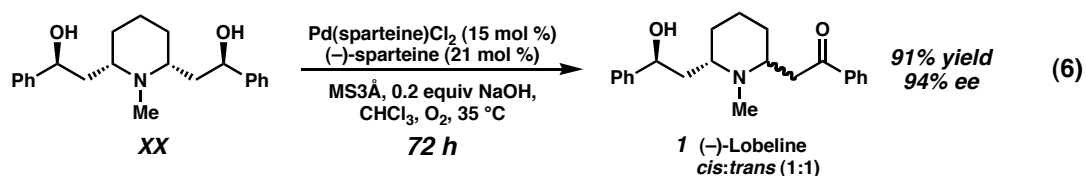
(*cis:trans*)-(-)-Lobeline [(*cis:trans*)-162]: Equation 4 Method. A reaction tube (ID=1.4 cm, OD= 1.8 cm, height=14 cm) equipped with a 14/24 female joint was charged with hot, oven-dried (oven temp = 130 °C, >2 days) 3Å molecular sieves (100 mg). After cooling to room temperature, the vessel was charged with crystalline amino diol **206** (68 mg, 0.20 mmol). The reaction tube was equipped with a 14/24 male joint connected by vacuum quality tubing to a valve connected differentially to a high-vacuum source and a balloon of dry O₂ (see Figure 11). The reaction tube was cooled to -78 °C, then purged with dry O₂ by iteratively evacuating the reaction tube, then refilling from the balloon (3 iterations) using the toggle valve. The 14/24 joint was removed such that a stream of O₂ flowed over the reaction tube while a solution of Pd(sp)Cl₂ (12.4 mg, 0.03 mmol) and (-)-sparteine (9.7 µl) in CHCl₃ (1.8 mL) was introduced into the cold reaction tube. The 14/24 joint was replaced and the reaction tube was again purged with O₂ by 3 evacuation/refilling cycles in the manner previously described. The reaction was then removed from the cooling bath and warmed to 35 °C. At 96 h, the reaction was treated with MeOH (100 µL) filtered over a plug of Celite, the pad was rinsed with DCM, then the organics were concentrated under reduced vacuum. The crude material was purified by flash chromatography over Silicycle™ (pH=6.5-7.0) Ultra Pure Silica Gel (8% MeOH:0.25% TEA:DCM eluent) to yield (-)-lobeline as **(*cis:trans*)-162** (61 mg, 89 % yield) in a 1:1 mixture of *cis:trans* isomers as a white foam: m.p. 129-130° (130); ¹H NMR (300 MHz, CDCl₃) δ 8.01-7.97 (m, 2H, *cis* isomer), 8.01-7.97 (m, 2H, *trans* isomer), 7.64-7.22 (m, 8H, *cis* isomer), 7.64-7.22 (m, 8H, *trans* isomer), 4.97 (dd, *J*=2.9,

10.8 Hz, 1H, *cis* isomer), 4.93 (dd, $J=2.6, 10.7$ Hz, 1H, *trans* isomer), 3.65-3.59 (m, 1H, *cis* isomer), 3.85-3.80 (m, 1H, *trans* isomer), 3.26 (ddm, $J=5.0, 16.0$ Hz, 2H, *cis* isomer), 3.32-3.22 (m, 2H, *trans* isomer), 3.0 (dd, $J=8.5, 16.0$ Hz, 1H, *cis* isomer), 3.1 (dd, $J=9.8, 14.9$ Hz, 1H, *trans* isomer), 2.58 (s, 3H, *trans* isomer), 2.38 (s, 3H, *cis* isomer), 2.38-2.18 (m, 1H, *trans* isomer), 2.06-1.46 (m, 7H, *cis* isomer), 1.83-1.46 (m, 6H, *trans* isomer), 1.29-1.18 (m, 1H, *cis* isomer); ^{13}C NMR (300 MHz, CDCl_3) δ 198.4, 198.3, 145.5, 145.2, 137.1, 136.7, 133.3, 133.3, 128.8, 128.8, 128.4, 128.3, 128.2, 128.2, 127.1, 127.0, 125.6, 125.6, 75.8, 75.7, 64.6, 61.1, 59.1, 51.7, 43.8, 43.2, 38.8, 40.5, 35.8, 27.4, 24.8, 23.5, 23.5, 23.4, 23.0, 20.5; IR (film) 311, 2933, 1685 cm^{-1} ; HRMS (EI^+) calc'd for $[\text{C}_{22}\text{H}_{27}\text{NO}_2]^+$: m/z 337.2042, found 337.2027; $[\alpha]_{\text{D}}^{20}$ -55.8° ($c=1$, CDCl_3). Enantiomeric excess was determined after derivatization by the method described in Scheme 13. Measurement conducted by chiral HPLC using a Chiracel OJ as described in the Material and Methods section of the experimentals; (0.6% EtOH:hexane eluent @ 1.0 mL/min) major enantiomer $T_{\text{R}}=14.6$ min; minor enantiomer $T_{\text{R}}=28.9$ min.



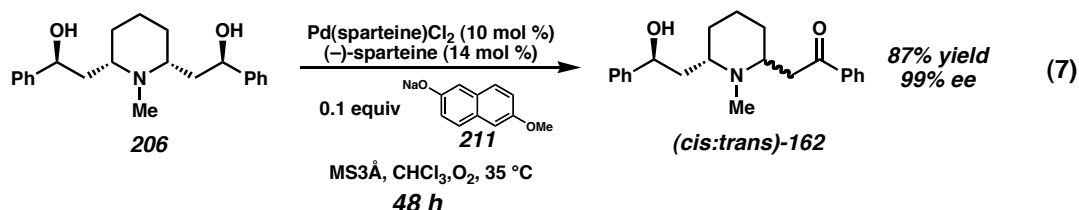
(*cis:trans*)-(-)-Lobeline [(*cis:trans*)-162]: Equation 5 Method. A reaction tube (ID=1.4 cm, OD= 1.8 cm, height=14 cm) equipped with a 14/24 female joint was charged with hot, oven-dried (oven temp = 130 °C, >2 days) 3Å molecular sieves (100 mg). After cooling to room temperature, the vessel was charged with crystalline amino diol **206** (68 mg, 0.20 mmol) and finely milled anhydrous Cs_2CO_3 (26 mg, 0.08 mmol). The reaction

tube was equipped with a 14/24 male joint connected by vacuum quality tubing to a valve connected differentially to a high-vacuum source and a balloon of dry O₂ (see Figure 11). The reaction tube was cooled to -78 °C, then purged with dry O₂ by iteratively evacuating the reaction tube, then refilling from the balloon (3 iterations) using the toggle valve. The 14/24 joint was removed such that a stream of O₂ flowed over the reaction tube while a solution of Pd(sp)Cl₂ (12.4 mg, 0.03 mmol) and (-)-sparteine (9.7 µl) in CHCl₃ (1.8 mL) was introduced into the cold reaction tube. The 14/24 joint was replaced and the reaction tube was again purged with O₂ by 3 evacuation/refilling cycles in the manner previously described. The reaction was then removed from the cooling bath and warmed to 35 °C. At 96 h, the reaction was treated with MeOH (100 µL) filtered over a plug of Celite, the pad was rinsed with DCM, then the organics were concentrated under reduced vacuum. The crude material was purified by flash chromatography over SilicycleTM (pH=6.5-7.0) Ultra Pure Silica Gel (8% MeOH:0.25% TEA:DCM eluent) to yield (-)-lobeline as (*cis:trans*)-**162** (51 mg, 75 % yield) in a 1:1 mixture of *cis:trans* isomers as a white foam: see above for analytical data.



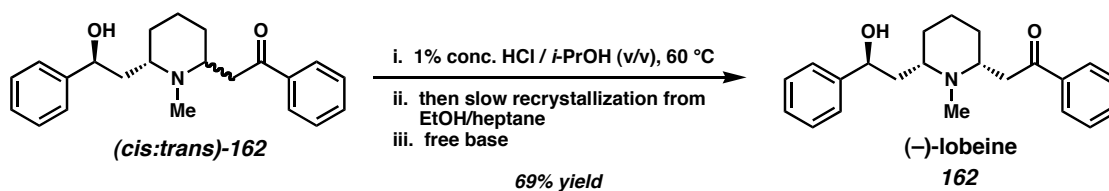
(*cis:trans*)-(-)-Lobeline [(*cis:trans*)-162**]: Equation 6 Method.** A reaction tube (ID=1.4 cm, OD= 1.8 cm, height=14 cm) equipped with a 14/24 female joint was charged with hot, oven-dried (oven temp = 130 °C, >2 days) 3Å molecular sieves (100 mg). After cooling to room temperature, the vessel was charged with crystalline amino diol **206** (68

mg, 0.20 mmol) and finely milled anhydrous NaOH (3.2 mg, 0.08 mmol). The reaction tube was equipped with a 14/24 male joint connected by vacuum quality tubing to a valve connected differentially to a high-vacuum source and a balloon of dry O₂ (see Figure 11). The reaction tube was cooled to -78 °C, then purged with dry O₂ by iteratively evacuating the reaction tube, then refilling from the balloon (3 iterations) using the toggle valve. The 14/24 joint was removed such that a stream of O₂ flowed over the reaction tube while a solution of Pd(sp)Cl₂ (12.4 mg, 0.03 mmol) and (-)-sparteine (9.7 µl) in CHCl₃ (1.8 mL) was introduced into the cold reaction tube. The 14/24 joint was replaced and the reaction tube was again purged with O₂ by 3 evacuation/refilling cycles in the manner previously described. The reaction was then removed from the cooling bath and warmed to 35 °C. At 96 h, the reaction was treated with MeOH (100 µL) filtered over a plug of Celite, the pad was rinsed with DCM, then the organics were concentrated under reduced vacuum. The crude material was purified by flash chromatography over Silicycle™ (pH=6.5-7.0) Ultra Pure Silica Gel (8% MeOH:0.25% TEA:DCM eluent) to yield (-)-lobeline as (*cis:trans*)-**162** (62 mg, 91 % yield) in a 1:1 mixture of *cis:trans* isomers as a white foam: see above for analytical data.

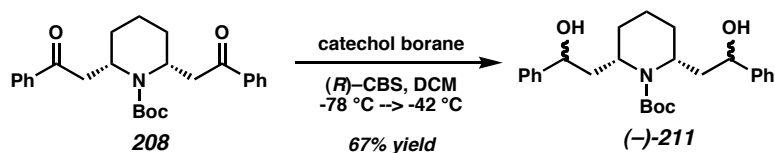


(*cis:trans*)-(-)-Lobeline [(*cis:trans*)-162]: Equation 7 Method. A reaction tube (ID=1.4 cm, OD= 1.8 cm, height=14 cm) equipped with a 14/24 female joint was charged

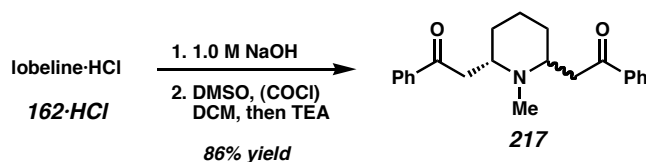
with hot, oven-dried (oven temp = 130 °C, >2 days) 3 Å molecular sieves (100 mg). After cooling to room temperature, the vessel was charged with crystalline amino diol **206** (68 mg, 0.20 mmol). In a separate flask Pd(sp)Cl₂ (8.2 mg, 0.02 mmol) and the sodium naphthaleneoxide (7.9 mg, 0.04 mmol) are combined in a dry box, then diluted with CHCl₃ (1.8 mL). The catalyst solution was stirred vigorously for 1 h prior to use. After this time, the reaction tube containing the starting diol **206** was equipped with a 14/24 male joint connected by vacuum quality tubing to a valve connected differentially to a high-vacuum source and a balloon of dry O₂ (see Figure 11). The reaction tube was cooled to -78 °C, then purged with dry O₂ by iteratively evacuating the reaction tube, then refilling from the balloon (3 iterations) using the toggle valve. The 14/24 joint was removed such that a stream of O₂ flowed over the reaction tube while a solution of the preformed (sp)Pd(naphthaleneoxide)₂ **211** and (–)-sparteine (9.7 µl) was introduced into the cold reaction tube. The 14/24 joint was replaced and the reaction tube was again purged with O₂ by 3 evacuation/refilling cycles in the manner previously described. The reaction was then removed from the cooling bath and warmed to 35 °C. At 96 h, the reaction was treated with MeOH (100 µL) filtered over a plug of Celite, the pad was rinsed with DCM, then the organics were concentrated under reduced vacuum. The crude material was purified by flash chromatography over Silicycle™ (pH=6.5-7.0) Ultra Pure Silica Gel (8% MeOH:0.25% TEA:DCM eluent) to yield (–)-lobeline as (*cis:trans*)-**162** (59 mg, 87 % yield) in a 1:1 mixture of *cis:trans* isomers as a white foam. See above for analytical data.



To a solution of (1:1) **(cis:trans)-162** (57 mg, 0.17 mmol) in *i*-PrOH (2 mL) was added conc. HCl (20 μ L). The reaction was heated to 60 °C for 8 h, then cooled to room temperature, then concentrated under a reduced pressure. ^1H NMR analysis of the free base (from saturated aq NaHCO_3) revealed a 3:1 mixture of isomers favoring the *cis* configuration at this stage. The white foam was taken up in EtOH (0.8 mL) and placed in a heptane vapor diffusion chamber. The chamber was maintained at 4 °C for several days to deposit white crystals. The crystals were dissolved in benzene and free based with saturated aq NaHCO_3 before concentrating the organics under reduced pressure, to provide **(-)-lobeline 162** (40 mg, 69% yield). The ^1H NMR spectra was recorded immediately in CDCl_3 to observe exclusively the *cis* configuration, which was identical to natural **(-)-lobeline** free base: m.p. 130° (130); ^1H NMR (300 MHz, CDCl_3) δ 7.97-8.01 (m, 2H), 7.64-7.22 (m, 8H), 4.97 (dd, $J=2.9, 10.8$ Hz, 1H), 3.65-3.59 (m, 1H), 3.26 (ddm, $J=5.0, 16.0$ Hz, 2H), 3.0 (dd, $J=8.5, 16.0$ Hz, 1H), 2.38 (s, 3H), 2.06-1.46 (m, 7H), 1.29-1.18 (m, 1H); ^{13}C NMR (300 MHz, CDCl_3) δ 198.3, 145.2, 137.1, 133.3, 128.8, 128.3, 128.2, 127.1, 125.6, 75.8, 64.6, 59.1, 43.8, 40.5, 27.4, 24.8, 23.5, 23.4; IR (film) 3111, 2933, 1685 cm^{-1} ; HRMS (EI^+) calc'd for $[\text{C}_{22}\text{H}_{27}\text{NO}_2]^+$: m/z 337.2042, found 337.2043; $[\alpha]_{\text{D}}^{20}$ -41.3° ($c=1$, CHCl_3).

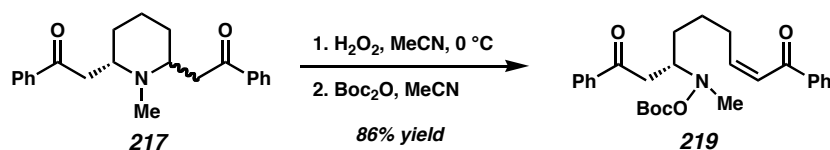


Diol mixture [(-)-211]. To a -78°C solution of diketone **208** (27.2 mg, 0.065 mmol) in DCM (3 mL) was added a 1.0 M toluene solution of (*R*)-CBS catalyst (19.4 μL , 0.019 mmol) and catechol borane (27.5 μL , 0.258 mmol). The reaction was maintained at -78°C for 2 d, then warmed to -40°C for 1 d. At completion, the reaction was quenched at -40°C by the addition of saturated aq NH_4Cl (0.5 mL), then diluted with water (1 mL). The layers were separated and the aqueous layer was extracted with DCM. The combined organics were dried over Na_2SO_4 , then concentrated under reduced pressure. The crude material was purified by flash chromatography over silica gel (20% EtOAc:hexane eluent) to yield diol mixture **(-)-211** (18.2 mg, 67% yield, $R_F = 0.31$ in 20% EtOAc:hexane) as a clear oil: ^1H NMR (300 MHz, CDCl_3) δ 7.58-7.15 (comp m, 10H), 5.09 (m, 2H), 4.88-4.22 (comp m, 4H), 2.24-1.86 (comp m, 4H), 1.85-1.20 (comp m, 15H); ^{13}C NMR (300 MHz, CDCl_3) δ 156-154, 144.7, 144.4, 136.9, 133.5, 129.5-125.2, 81.6-81.0, 73.0-72.2, 70.8-70.2, 48.4-47.9, 47.0-46.0, 45.1-44.1, 43.0, 30.2-26.9, 28.7, 28.0, 27.8-25.2, 14.5, 14.0; IR (film) 3411, 2935, 1650, 1409, 1170 cm^{-1} ; HRMS (FAB^+) calc'd for $[\text{C}_{41}\text{H}_{53}\text{O}_7\text{Si}]^+$: m/z 685.3561, found 685.3593; $[\alpha]_D^{20}$ 60.6° ($c=1$, CDCl_3).



***cis:trans*-Dehydrolobeline (217).** (–)-Lobeline·HCl (270 mg, 0.72 mmol) was dissolved in DCM (15 mL) and the solution was washed with 1 M NaOH (5 mL). The organics was dried over Na₂SO₄ and concentrated under reduced pressure.

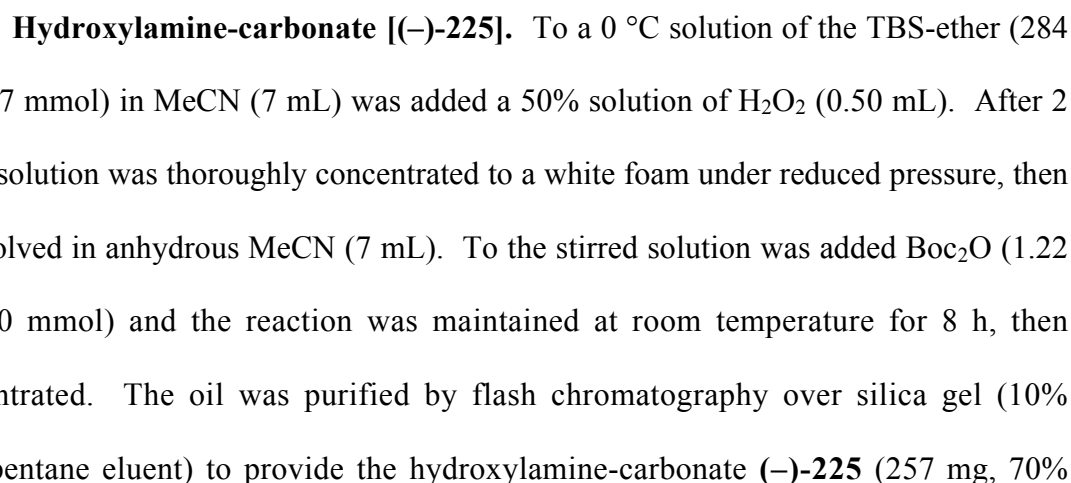
To a –78 °C solution of DMSO (198 µl, 2.78 mmol) in DCM (6 mL) was added oxalyl chloride (182 µl, 2.09 mmol) dropwise. The solution was maintained at –78 °C for 10 min before the dropwise addition of (–)-lobeline free base (235 mg, 0.70 mL). The reaction was maintained at –78 °C for 1 h before the addition of TEA (970 µl, 6.96 mmol). After 1 h, the reaction was warmed to room temperature for 2 h, then diluted with heptane and filtered. The liquor was concentrated under reduced pressure and toluene (10 mL) was added to the resulting grainy oil. The mixture was filtered again before concentrating under reduced pressure. The oil was purified by flash chromatography over silica gel (5-8% MeOH, 0.5% TEA:DCM) to provide *cis:trans*-dehydrolobeline **217** (201 mg, 86 % yield, R_F= 0.35, 10% MeOH:DCM) as a white solid: m.p. 128-130; ¹H NMR (300 MHz, CDCl₃) δ 8.06-7.18 (m, 10H), 4.95 (dd, *J*=10.6, 3.0 Hz, 1H, *cis* isomer), 4.90 (dd, *J*=10.7 Hz, 2.6 Hz, 1, *trans* isomer), 3.78 (m, 1H, *trans* isomer), 3.55 (m, 1H, *cis* isomer), 3.19-3.30 (ddm, *J*=15.9, 5.0 Hz, 2H), 3.03 (dd, *J*=15.3, 9.2 Hz, 1H, *trans* isomer), 3.01 (dd, *J*=16.0, 8.4 Hz, 1H, *cis* isomer), 2.56 (s, 3H, *trans* isomer), 2.37 (s, 3H, *cis* isomer), 2.25 (m, 1H), 1.95 (m, 1H), 1.15-1.85 (m, 7H); ¹³C NMR (CDCl₃) δ 198.4, 198.3, 145.6, 145.2, 137.1, 136.8, 133.3-125.6, 75.8, 75.8, 64.6, 61.2, 59.2, 51.6, 43.9, 43.3, 40.6, 38.9, 35.8, 27.5, 24.8, 23.5, 23.0, 20.6; HRMS (EI⁺) calc'd for [C₂₂H₂₇NO₂]⁺: *m/z* 337.2042, found 337.2032; [α]_D²⁰ -54.0 (c=1, CHCl₃).



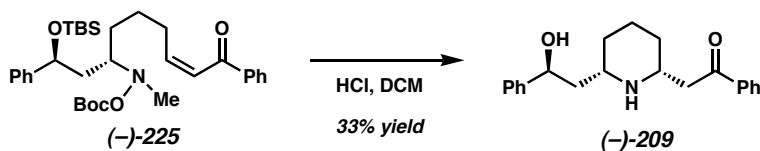
Hydroxylamine-carbonate (219). To a 0 °C solution of dehydrolobeline **217** (181 mg, 0.54 mmol) in MeCN (10 mL) was added a 50% solution of H₂O₂ (0.50 mL). After 2 h, the solution was thoroughly concentrated to a white foam under reduced pressure, then redissolved in anhydrous MeCN (8 mL). To the stirred solution was added Boc₂O (590 mg, 2.70 mmol) and the reaction was maintained at room temperature for 8 h, then concentrated. The oil was purified by flash chromatography over silica gel (30% Et₂O:pentane eluent) to provide the hydroxylamine-carbonate **219** (210 mg, 86% yield, R_F= 0.33 in 30% Et₂O:pentane) as an oil: ¹H NMR (300 MHz, CDCl₃) δ 7.95-7.83 (m, 4H), 7.54-7.33 (m, 6H), 6.98 (dt, *J*=6.6, 15.3 Hz, 1H), 6.82 (d, *J*=15.6 Hz, 1H), 3.71-3.57 (m, 1H), 3.43 (dd, *J*=4.2, 17.1 Hz, 1H), 2.91 (dd, *J*=7.2, 20.3 Hz, 1H), 2.73 (s, 3H), 2.34-2.27 (m, 2H), 1.86-1.43 (comp m., 4H), 1.40 (s, 9H); ¹³C NMR (300 MHz, CDCl₃) δ 198.6, 190.9, 153.3, 149.5, 138.2, 137.1, 133.5, 132.8, 128.9, 128.7, 128.7, 128.5, 128.3, 126.4, 83.2, 62.8, 42.7, 38.0, 32.8, 32.4, 27.9, 25.0; IR (film) 2933, 1767, 1683 cm⁻¹; HRMS (FAB⁺) calc'd for [C₂₇H₃₄NO₅]⁺: *m/z* 452.2437, found 452.2423.



Dehydro-norlobeline (218). To a solution of hydroxylamine-carbonate **219** (190 mg, 0.42 mmol) in DCM (8 mL) was added a 2.0 M solution of HCl in Et₂O (2.00 mL).



yield, $R_F = 0.52$ in 30% $\text{Et}_2\text{O}:\text{pentane}$) as a clear oil: ^1H NMR (300 MHz, CDCl_3) δ 7.90 (d, $J=7.5$ Hz, 2H), 7.56-7.37 (comp m, 3H), 7.35-7.13 (comp m, 5H), 7.09-6.94 (m, 1H), 6.83 (d, $J=15.9$ Hz, 1H), 4.87 (dd, $J=5.7, 7.7$ Hz, 1H), 2.75 (dd, $J=4.7$ Hz, 1H), 2.68 (s, 3H), 2.31-2.18 (m, 1H), 2.17-2.03 (m, 1H), 1.78-1.47 (comp m, 6H), 1.45 (s, 9H), 0.85 (s, 9H), -0.01 (s, 3H), -0.24 (s, 3H); ^{13}C NMR (300 MHz, CDCl_3) δ 190.9, 153.6, 149.7, 145.3, 138.2, 132.8, 128.7, 128.7, 128.3, 127.4, 126.4, 82.8, 72.9, 63.6, 42.0, 40.6, 33.1, 30.4, 28.7, 28.3, 28.0, 26.1, 25.2, 18.3, -4.3, -4.7; IR (film) 2931, 1766, 1250 cm^{-1} ; HRMS (FAB $^+$) calc'd for $[\text{C}_{33}\text{H}_{50}\text{NO}_5\text{Si}]^+$: m/z 568.3458, found 568.3477; $[\alpha]_D^{20}$ -33.1 $^\circ$ ($c=1$, CDCl_3).



Norlobeline [(–)-209]. To a solution of hydroxylamine-carbonate (–)-225 (238 mg, 0.42 mmol) in DCM (8 mL) was added a 2.0 M solution of HCl in Et₂O (2.00 mL). After 2 h, the reaction was slowly quenched with saturated aq NaHCO₃ (4 mL) and diluted with water (3 mL). The layers were separated and the aqueous layer was washed with DCM (2 x 5 mL). The combined organics were washed with brine (1 x 10 mL), dried over Na₂SO₄ and concentrated under reduced pressure. The resulting oil was purified by flash chromatography over Silicycle™ (pH=6.5-7.0) Ultra Pure Silica Gel (5-8% MeOH, 0.5% TEA:DCM eluent) to provide desmethyl-dehydrolobeline (–)-209 (45 mg, 33% yield, R_F= 0.11 in 10% MeOH:DCM) as a slightly yellow oil: ¹H NMR (300 MHz, CDCl₃) δ 7.94 (d, *J*=7.2 Hz, 2H), 7.57 (dd, *J*=7.5, 7.5 Hz, 1H), 7.46 (dd, *J*=8.7, 7.5

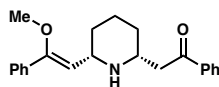
Hz, 2H), 7.40-7.18 (comp m, 6H), 4.93 (dd, $J=4.2, 9.5$ Hz, 1H), 4.84-4.24 (br s, 2H), 3.38-3.22 (comp m, 2H), 3.20-2.96 (comp m, 2H), 1.98-1.08 (comp m, 6H); ^{13}C NMR (300 MHz, CDCl_3) δ 199.0, 144.8, 136.9, 133.7, 128.9, 128.6, 128.4, 127.6, 125.9, 75.4, 58.7, 53.6, 44.8, 44.6, 32.5, 31.5, 24.4; IR (film) 3480, 2923, 1682, 1449 cm^{-1} ; HRMS (EI^+) calc'd for $[\text{C}_{21}\text{H}_{25}\text{NO}_2]^+$: m/z 323.1885, found 323.1891; $[\alpha]_{\text{D}}^{20}$ -13.5° ($c=1$, CDCl_3).

Notes and References

- (1) Ferreira, E. M.; Stoltz, B. M. *J. Am. Chem. Soc.* **2001**, *123*, 7725.
- (2) Simultaneous to our publication a related system was reported, see: Jensen., D. R.; Pugsley, J. S.; Sigman, M. S. *J. Am. Chem. Soc.* **2001**, *123*, 7475.
- (3) Bagdanoff, J. T.; Ferreira, E. M.; Stoltz, B. M. *Org. Lett.* **2003**, *5*, 835.
- (4) Bagdanoff, J. T.; Stoltz, B. M. *Angew. Chem.* **2004**, *43*, 353.
- (5) For mechanistic studies relating to Pd(II) catalyzed oxidation, see: (a) Mueller, J. A.; Sigman, M.S. *J. Am. Chem. Soc.* **2003**, *125*, 7005. (b) Mueller, J.A.; Goller, C.P.; Sigman, M.S. *J. Am. Chem. Soc.* **2004**, *126*, 9724. (c) Mueller, J.A.; Jensen, D.R.; Sigman, M.S. *J. Am. Chem. Soc.* **2002**, *124*, 8202. (d) Steinhoff, B. A.; Stahl, S. S. *Org. Lett.* **2002**, *4*, 4179. (b) Steinhoff, B. A.; Fix, S. R.; Stahl, S. S. *J. Am. Chem. Soc.* **2002**, *124*, 766. (c) Stahl, S. S.; Thorman, J. L.; Nelson, R. C.; Kozee, M. A. *J. Am. Chem. Soc.* **2001**, *123*, 7188.
- (6) Unpublished results.
- (7) (a) Compere, D.; Marzano, C.; Das, B. C. *J. Org. Chem.* **1994**, *64*, 4528. (b) Felpin, F. X.; Lebreton, J. *J. Org. Chem.* **2002**, *67*, 9192. (c) Dwoskin, L.P.; Crooks, P.A. *J. Org. Chem.* **2004**, *69*, 8514. (d) Cossy, J.; Willis, C.; Bellosta, V.; BouzBouz, S. *J. Org. Chem.* **2002**, *67*, 1982.
- (8) Wieland, H.; Koshara, W.; Dane, E.; Renz, J.; Schwarze, W.; Linde, W. *Justus Liebigs Ann. Chem.* **1939**, *540*, 103. (b) For a recent X-ray study of (-)-lobeline salts, see: Glaser, R.; Hug, P.; Drouin, M.; Michael, A. *J. Chem. Soc., Perkin Trans. 2* **1992**, 1071. (c) For a biosynthetic study of (-)-lobeline, see: Keogh, M. F.; O'Donovan, D. G. *J. Chem. Soc.* **1970**, 2470.
- (9) (a) Dwoskin, L.P.; Crooks, P.A. *Biochem. Pharmacol.* **2002**, *63*, 89. (b) Zheng, G.; Dwoskin, L.P.; Crooks, P.A. *J. Org. Chem.* **2004**, *69*, 8514.
- (10) (a) Smogrovicova, H.; Nemec, P.; Kompis, I.; Jindra, A.; Kovacs, P. *Celostanti Biochemicky Sjezed.* **1966**, *4*. (b) Beecham, A. F.; Johns, S. R.; Lamberton, J. A. *Austral. J. Chem.* **1967**, *20*, 2291. (c) Keogh, M. F.; O'Donovan, D. G. *J. Chem. Soc.* **1970**, 2470. (d) Smogrovicova, H.; Jindra, A.; Kovacs, P. *Coll. Czech. Chem. Comm.* **1968**, *33*, 1967.
- (11) Based on NMR studies on the rates of equilibration of *cis*-(-)-lobeline to a 1:1 mixture of *cis:trans* (-)-lobeline in various solvents: equilibration in C₆D₆

required 5 d; equilibration in CDCl_3 required 2 d; equilibration in CD_3OD required 2 h.

- (12) We have independently observed lobeline free base to equilibrate to a 1:1 mixture of *cis* and *trans* configuration upon standing in CDCl_3 for 48h.
- (13) Felpin, F.-X., Lebreton, J. *J. Org. Chem.* **2002**, 67, 9192.
- (14) The natural product (–)-lobeline is obtained in 18 steps: Compere, D.; Marazano, C.; Das, B.C. *J. Org. Chem.* **1999**, 64, 4528.
- (15) A number of known hydrogenations on pyridinium salts are known: (a) Yu, C.-Y.; Taylor, D. L.; Meth-Cohn, O. *Tetrahedron Lett.* **1999**, 40, 6661. (b) Yu, C.-Y.; Meth-Cohn, O. *Tetrahedron Lett.* **1999**, 40, 6665. (c) Meth-Cohn, O.; Yu, C.-Y. *J. Het. Chem.*, **1999**, 36, 1549.
- (16) For a review on diastereoselective reactions involving medium rings, see: Still, W. C. *Tetrahedron* **1981**, 37, 3981.
- (17) Anet, F. A. L.; Yavari, I. *J. Am. Chem. Soc.* **1977**, 99, 6986.
- (18) Burke, L. P.; DeBellis, A. D.; Fuhrer, H.; Meier, H.; Pastor, S. D.; Rihs, G.; Rist, G.; Rodebaugh, R. K.; Shum, S. P. *J. Am. Chem. Soc.* **1997**, 119, 8313.
- (19) (a) Neipp, C. E.; Martin, S. F. *J. Org. Chem.* **2003**, 68, 8867. (b) Paulson, H.; Todt, K. *Angew. Chem. Int. Ed.* **1966**, 5, 899. (c) Chow, Y. L.; Colon, C. J.; Tam, J. N. S. *Can. J. Chem.* **1968**, 46, 2821. (d) Johnson, F. *Chem. Rev.* **1968**, 68, 375. (e) Fraser, R. R.; Grindley, T. B. *Tetrahedron Lett.* **1974**, 15, 4169. (f) Quick, J.; Mondello, C.; Humora, M.; Brennan, T. *J. Org. Chem.* **1978**, 43, 2705.
- (20) A major byproduct was isolated from this reaction whose spectral data was consistent with enol ether shown below:



- (21) For a discussion on the solution and solid state conformation of (–)-lobeline salts, see: Glaser, R.; Hug, P.; Drouin, M.; Michel, A. *J. Chem. Soc. Perkin Trans. 2* **1992**, 1071.
- (22) Zheng, G.; Dwoskin, L. P.; Crooks, P. A. *J. Org. Chem.* **2004**, 69, 8514.
- (23) No catalyst decomposition is observed upon treatment of $\text{Pd}(\text{sparteine})\text{Cl}_2$ with excess powered anhydrous NaOH in the presence of oxidatively inert *t*-BuOH for several days.

-
- (24) Frank, B. *Chem. Ber.* **1959**, 92, 1001.
- (25) Martin, L. *Can. J. Res., B*, **1945**, 23, 165.
- (26) (a) Ghiaci, M.; Adibi, M. *Oppi Briefs*, **1996**, 4, 474. (b) Vaultier, M.; Tirel, P. J.; Carrie, R. *Tetrahedron Lett.* **1989**, 30, 1947. (c) Tufariello, J.J.; Ali, S. A. *Tetraherdron Lett.* **1978**, 47, 4674. (d) Shono, T.; Matsumura, Y.; Tsubana, K. *J. Am. Chem. Soc.* **1981**, 103, 1172. (e) Hootele, C; Ibebeke-Bomangwa, W. Drissens, F.; Sabil, S. *Bull. Soc. Chim. Belg.* **1987**, 96, 57.
- (27) (a) Pyne, S. G.; Bloem, P.; Chapman, S. L.; Dixon, C. E.; Griffith, R. *J. Org. Chem.* **1990**, 55, 1086. (b) Felpin, F.-X., Lebreton, J. *J. Org. Chem.* **2002**, 67, 9192. (c) Compere, D.; Marazano, C.; Das, B.C. *J. Org. Chem.* **1999**, 64, 4528.
- (28) Yu, C.-Y.; Meth-Cohn, O. *Tetrahedron Lett.* **1990**, 40, 6665.
- (29) Larrow, J. F.; Jacobsen, E. N. *J. Org. Chem.* **1994**, 59, 1939.
- (30) Conversion for the resolution may be calculated directly from the ee of either chiral resolution product, ee and ee' from the equation: $ee/ee' = C/(1-C)$. Selectivity is calculated in the usual way, using the equation $s = [\ln(1-c)(1-ee)]/\ln[(1-c)(1+ee)]$. For a review on resolution chemistry, and derivations of relevant equations, see: Kagan, H. B.; Fiaud, J. C. in *Topics in Stereochemistry*, Vol. 18 (Ed.: E. L. Eliel), Wiley, New York, **1988**, pp. 249-330.
- (31) For the original reference, see: Polonovski, M.; Polonovski, M. *Bull. Soc. Chim. Fr.* **1927** 41, 1190.
- (32) (a) McCamley, K.; Ripper, J. A.; Singer, R. D.; Scammells, P. *J. Org. Chem.* **2003**, 68, 9847. (b) Raucher, S.; Bray, B. L.; Lawrence, R. F. *J. Am. Chem. Soc.* **1987**, 109, 442. (c) Grierson, David. *Org. React.* **1990**, 39, 85.
- (33) Perrin, D. D.; Armarego, W. L. F. *Purification of Laboratory Chemicals*; 3rd ed., Pergamon REss, Oxford, 1988.
- (34) Still, W. C.; Kahn, M.; Mitra, A. J. *J. Org. Chem.* **1978**, 43, 2923.

APPENDIX THREE

Spectra Relevant to Chapter 3:

**Enantioselective Oxidation of *Meso*-Diols by Catalytic Palladium:
Total Synthesis of (–)-Lobeline and (–)-Sedamine**

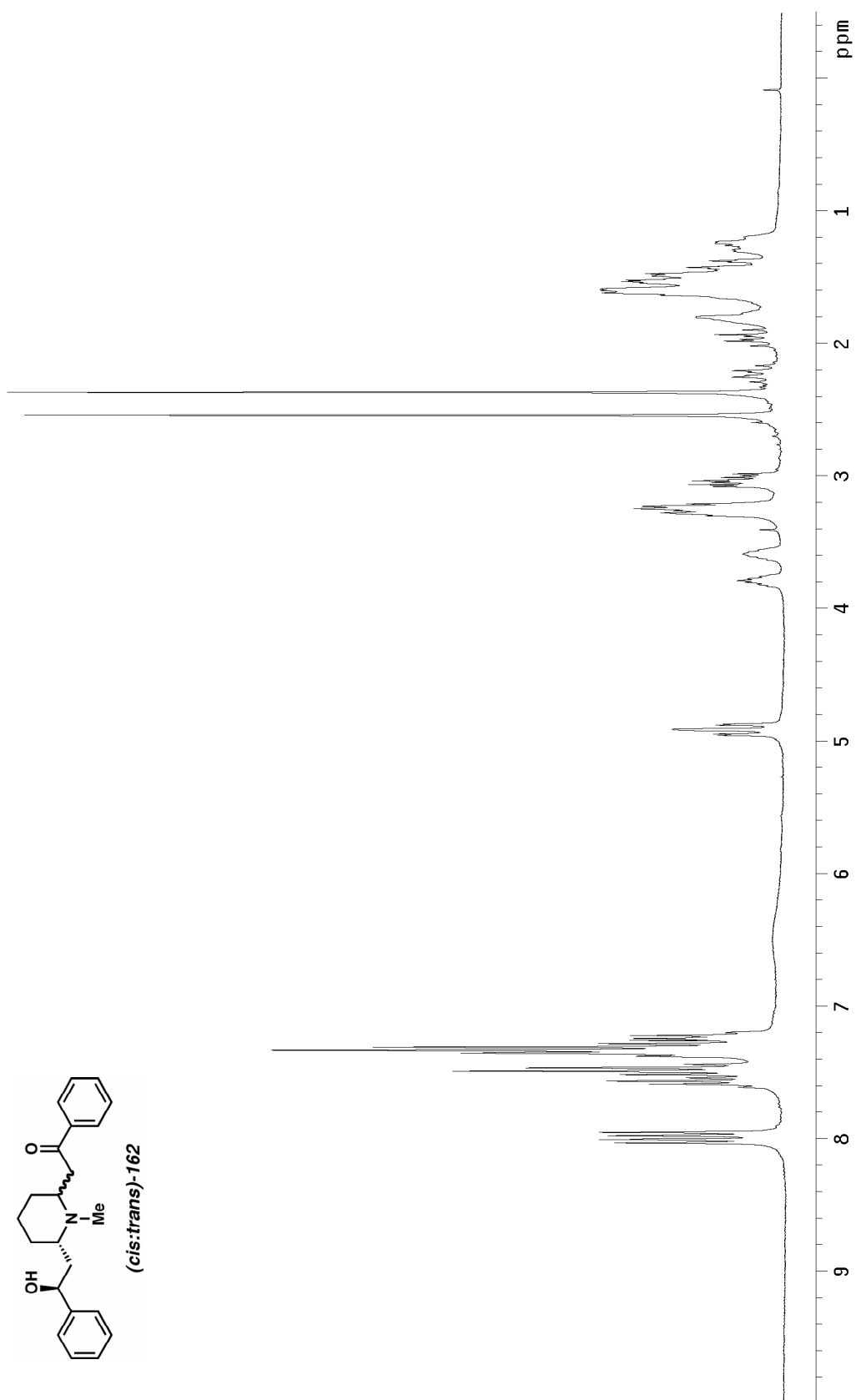


Figure A3.1 ^1H NMR (300 MHz, CDCl_3) of compound (cis:trans)-162.

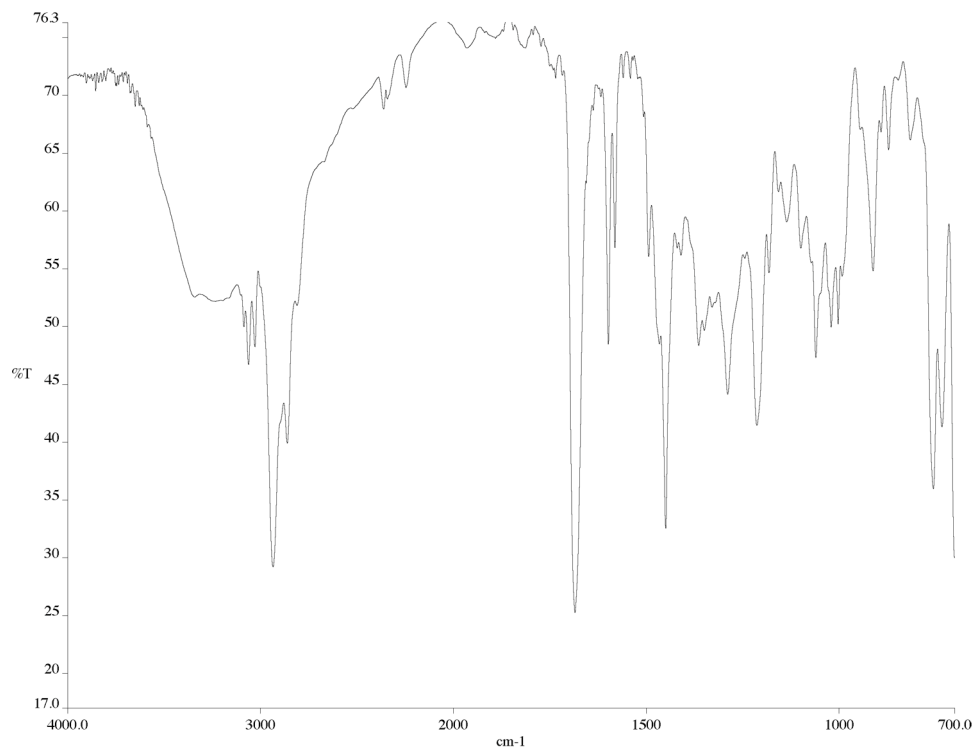


Figure A3.2 Infrared spectrum (thin film/NaCl) of compound **(cis:trans)-162**.

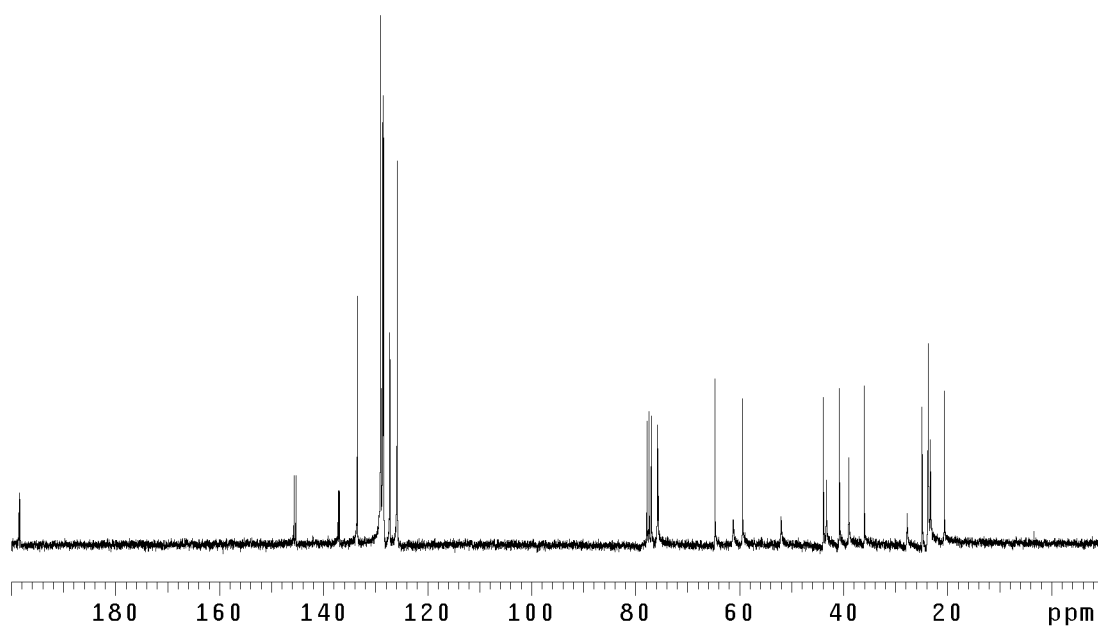


Figure A3.3 ¹³CNMR (125 MHz, CDCl₃) of compound **(cis:trans)-162**.

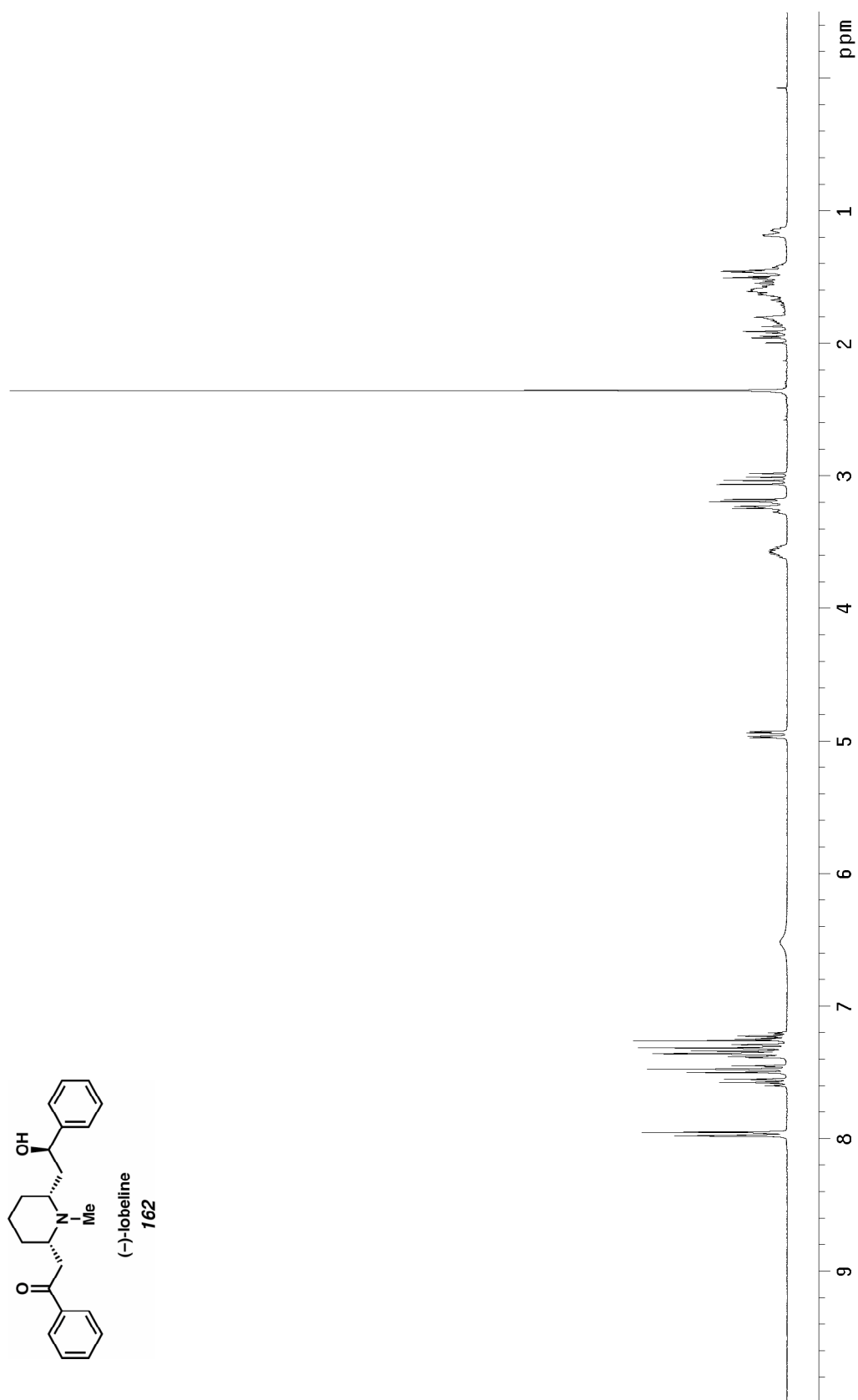


Figure A3.4 ^1H NMR (300 MHz, CDCl_3) of compound **162**.

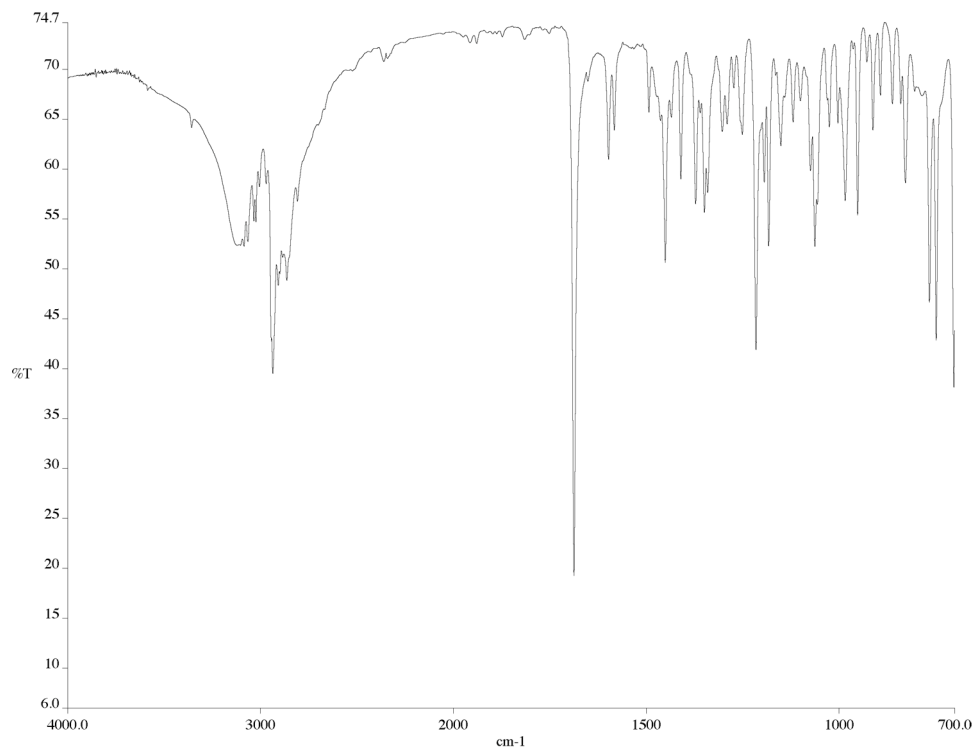


Figure A3.5 Infrared spectrum (thin film/NaCl) of compound **162**.

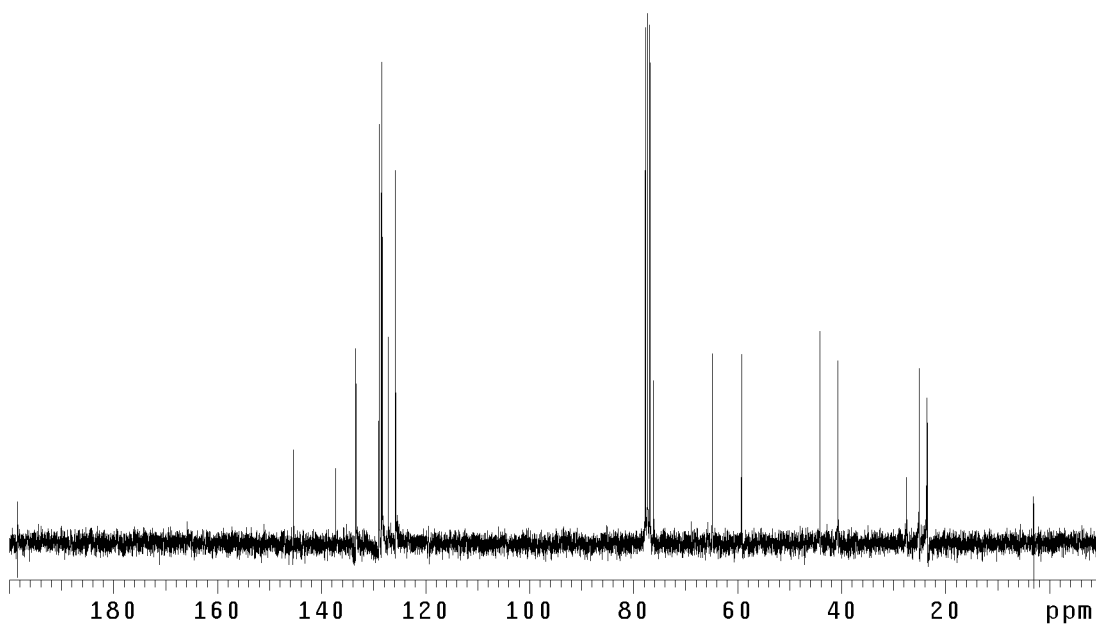


Figure A3.6 ¹³CNMR (125 MHz, CDCl₃) of compound **162**.

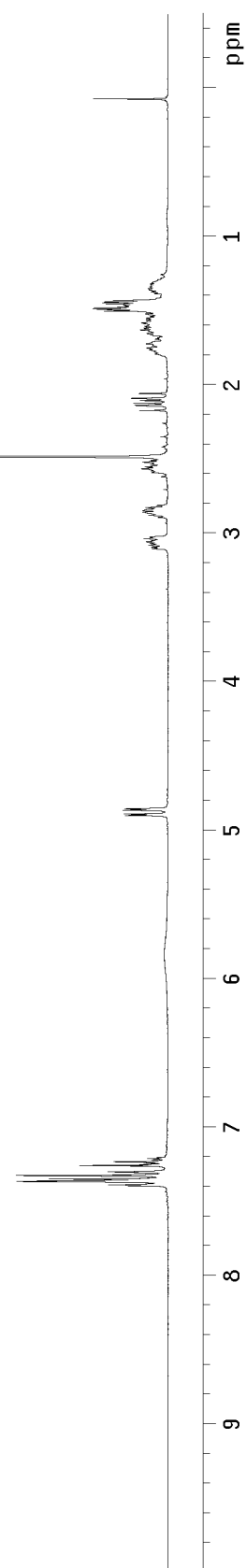
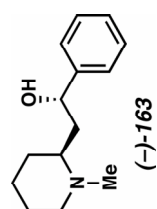


Figure A3.7 ^1H NMR (300 MHz, CDCl_3) of compound (-)-163.

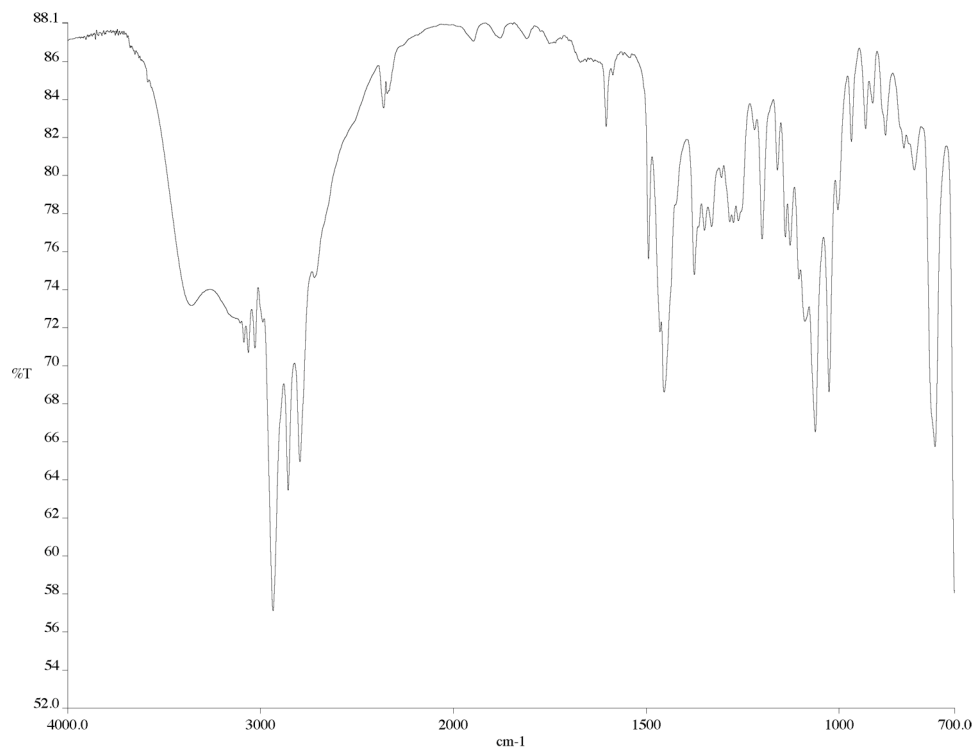


Figure A3.8 Infrared spectrum (thin film/NaCl) of compound (–)-163.

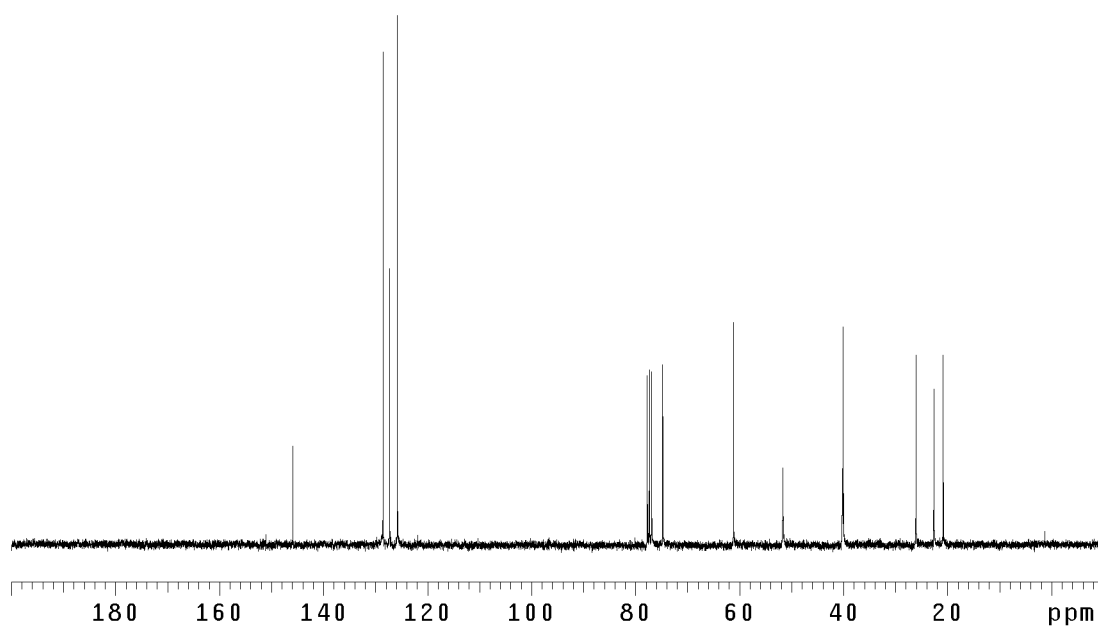


Figure A3.9 ¹³CNMR (125 MHz, CDCl₃) of compound (–)-163.

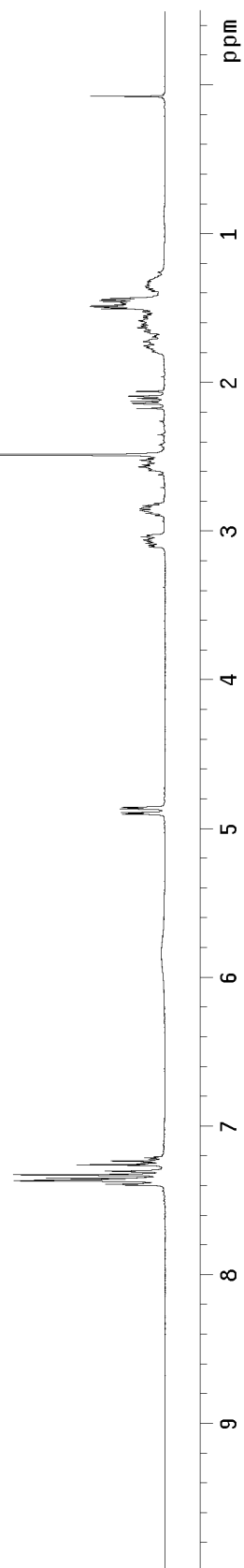
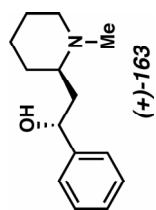


Figure A3.10 ^1H NMR (300 MHz, CDCl_3) of compound (+)-163.

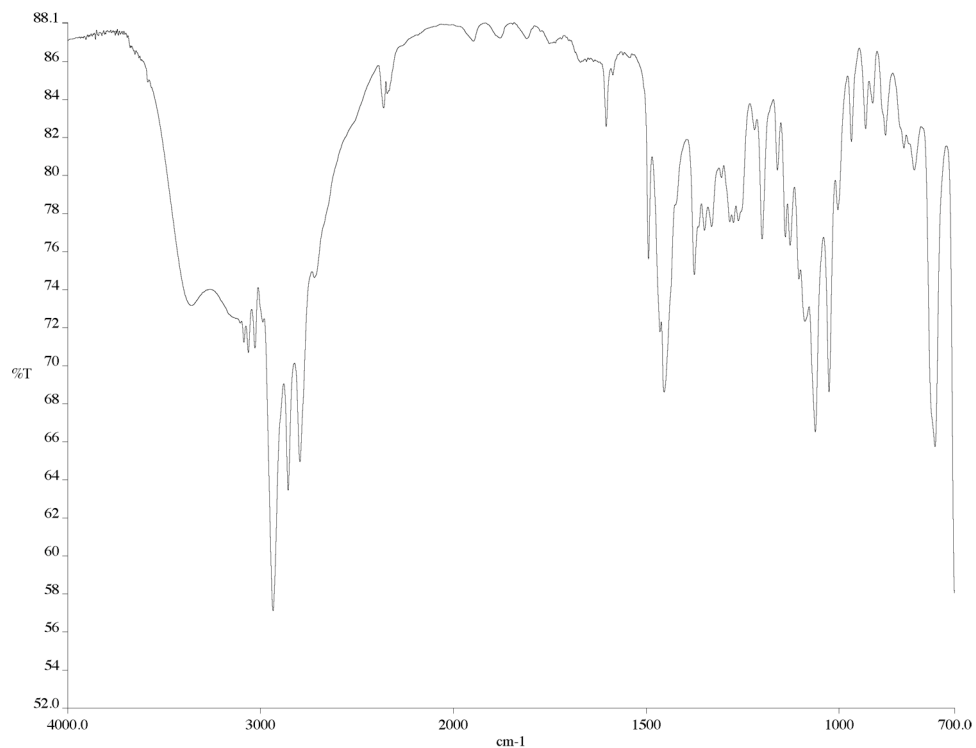


Figure A3.11 Infrared spectrum (thin film/NaCl) of compound (+)-163.

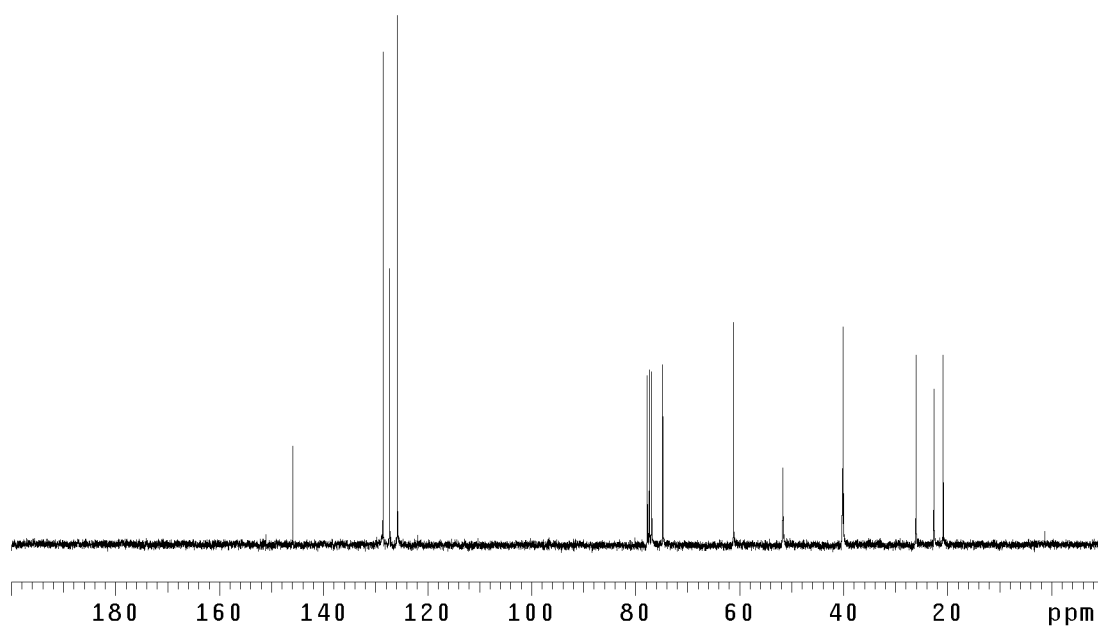


Figure A3.12 ¹³CNMR (125 MHz, CDCl₃) of compound (+)-163.

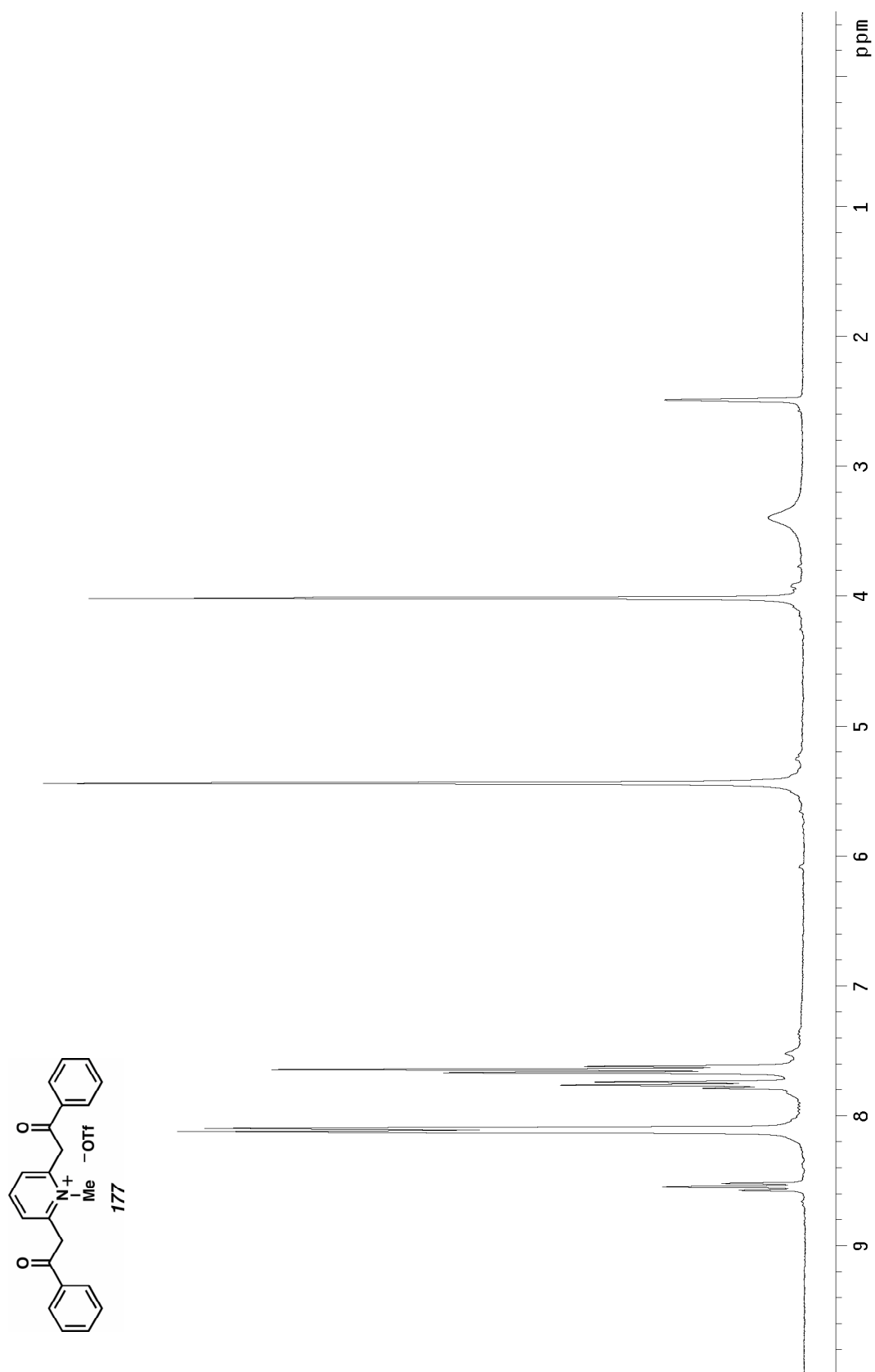


Figure A3.13 ^1H NMR (300 MHz, $\text{D}_6\text{-DMSO}$) of compound **177**.

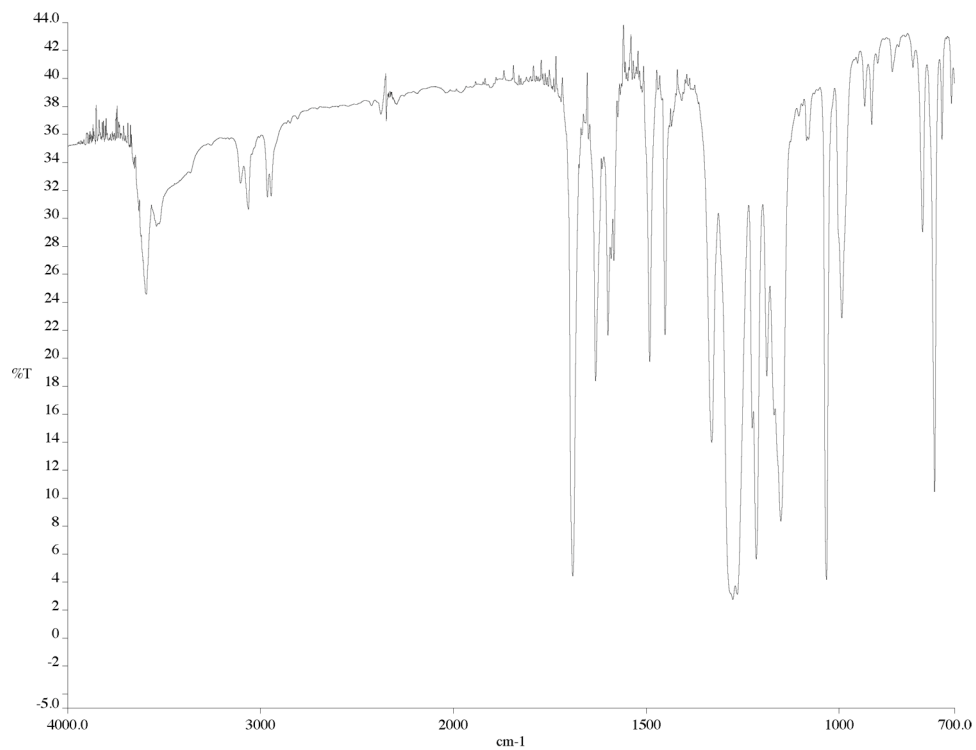


Figure A3.14 Infrared spectrum (KBr pellet) of compound **177**.

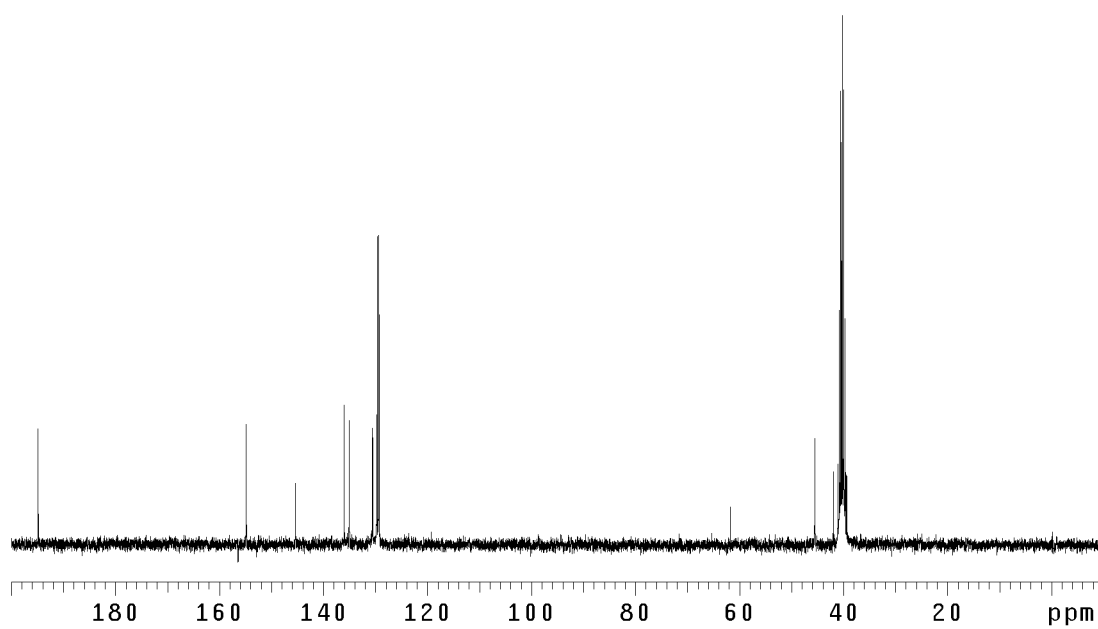


Figure A3.15 ¹³C NMR (125 MHz, D₆-DMSO) of compound **177**.

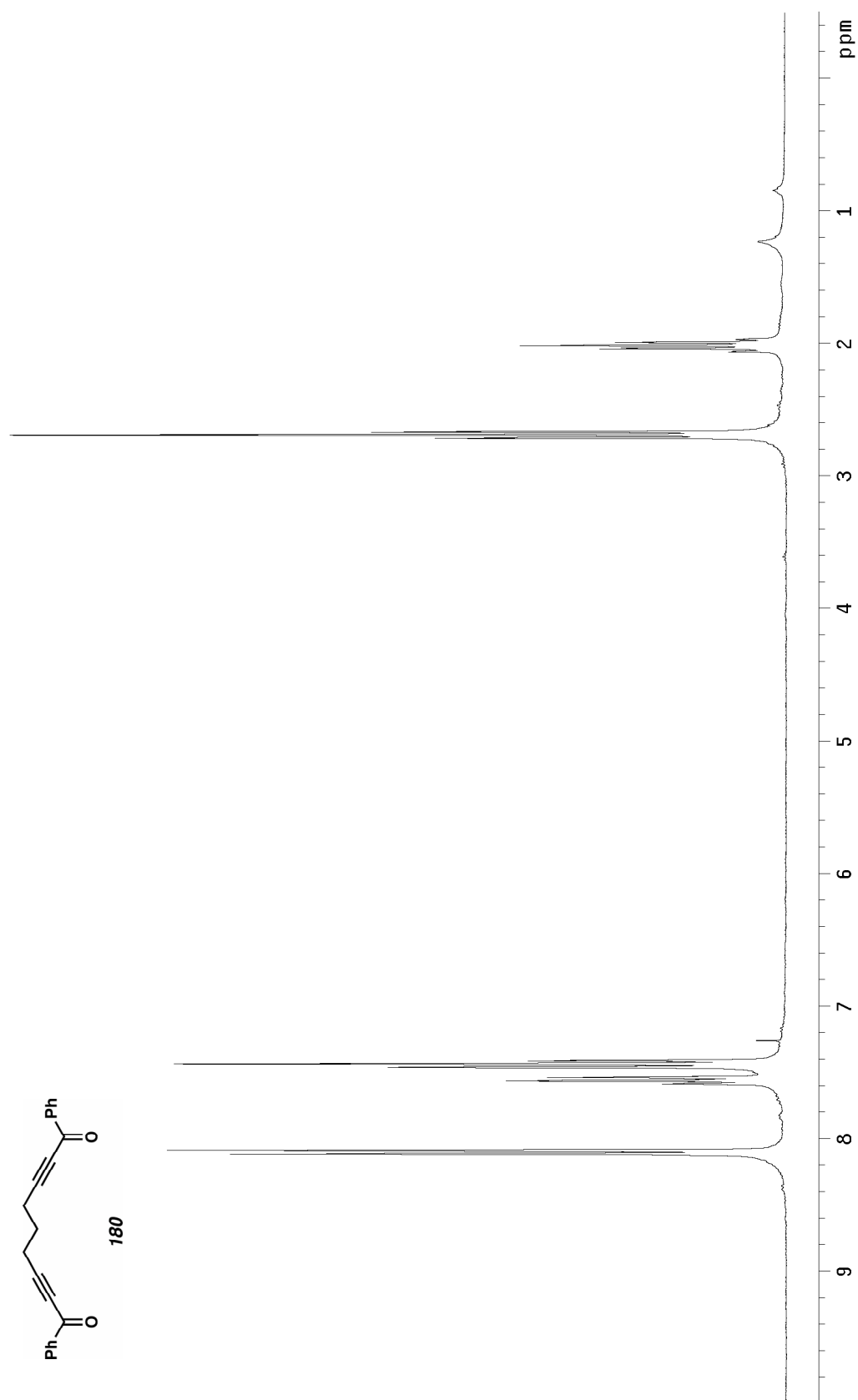


Figure A3.16 ^1H NMR (300 MHz, CDCl_3) of compound **180**.

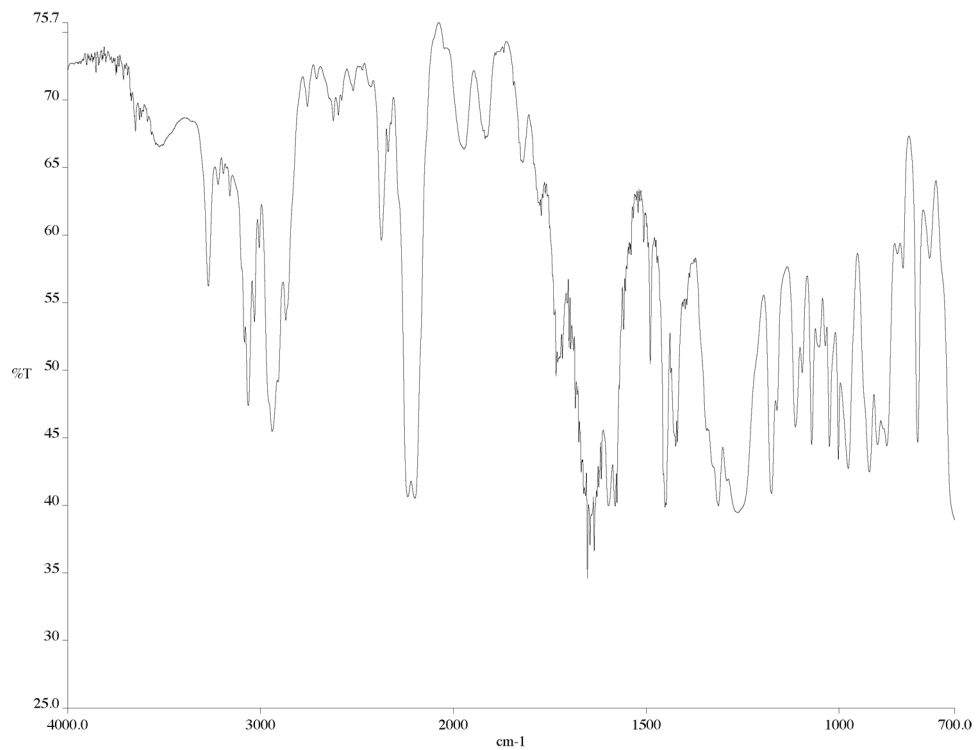


Figure A3.17 Infrared spectrum (thin film/NaCl) of compound **180**.

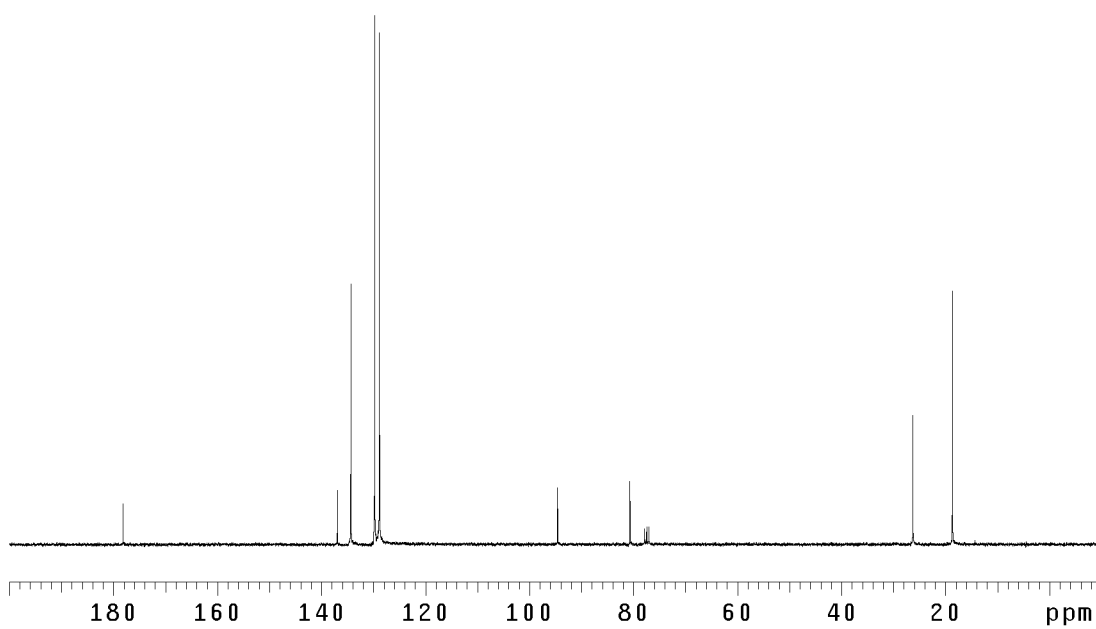


Figure A3.18 ¹³CNMR (125 MHz, CDCl₃) of compound **180**.

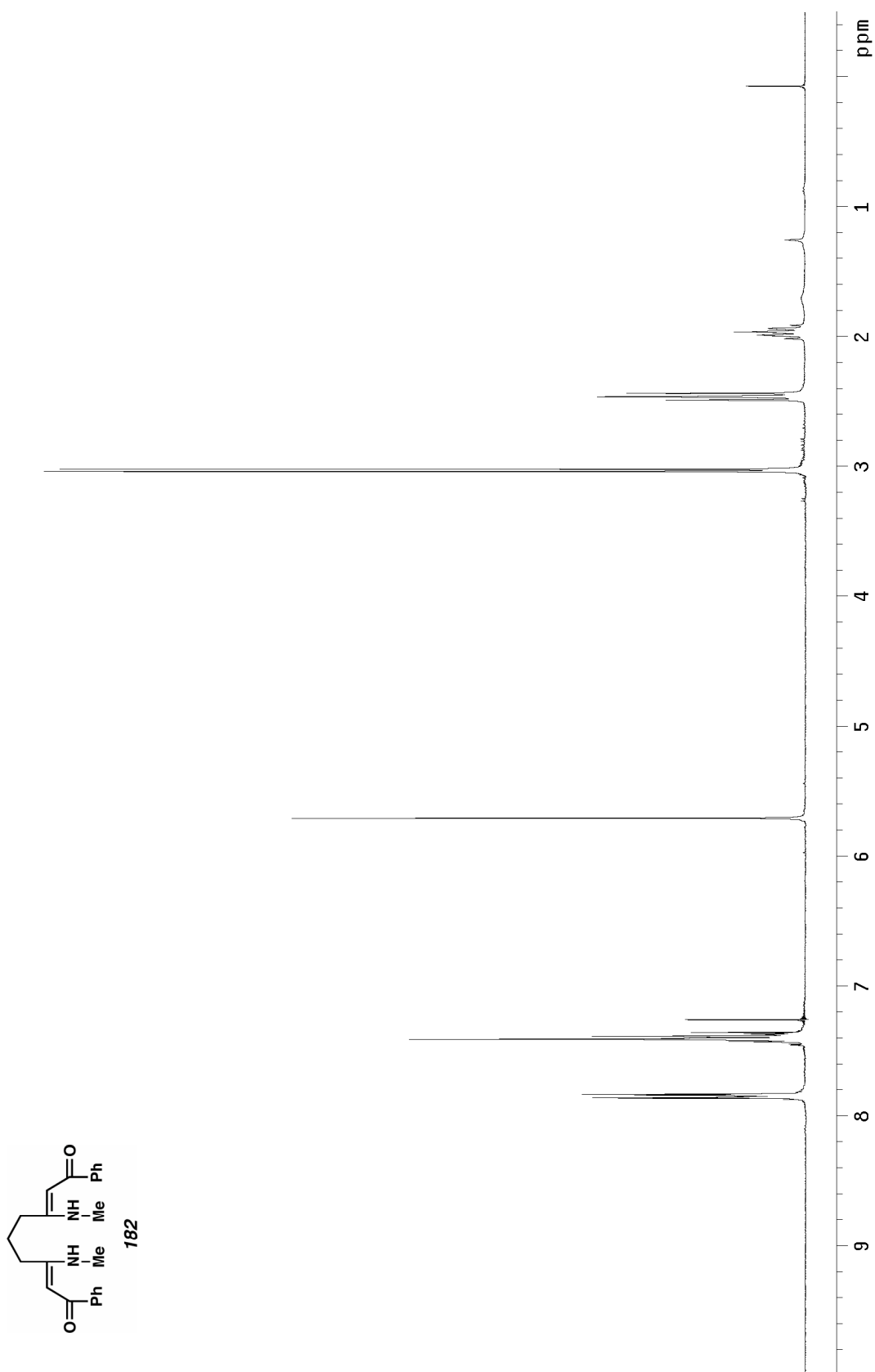


Figure A3.19 ^1H NMR (300 MHz, CDCl_3) of compound **182**.

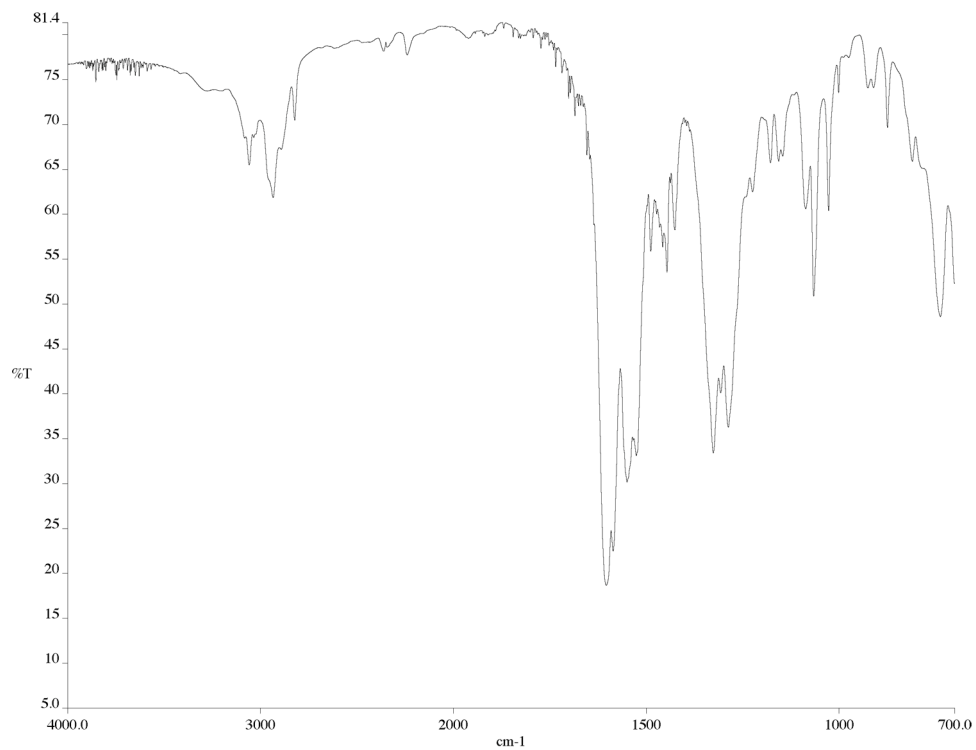


Figure A3.20 Infrared spectrum (thin film/NaCl) of compound **182**.

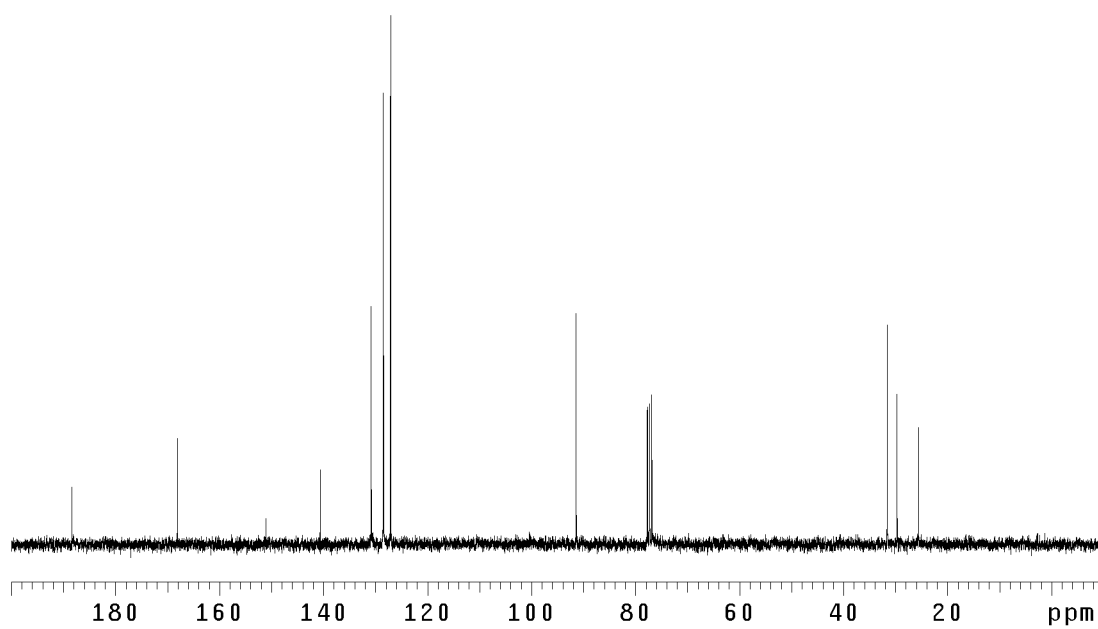


Figure A3.21 ¹³CNMR (125 MHz, CDCl₃) of compound **182**.

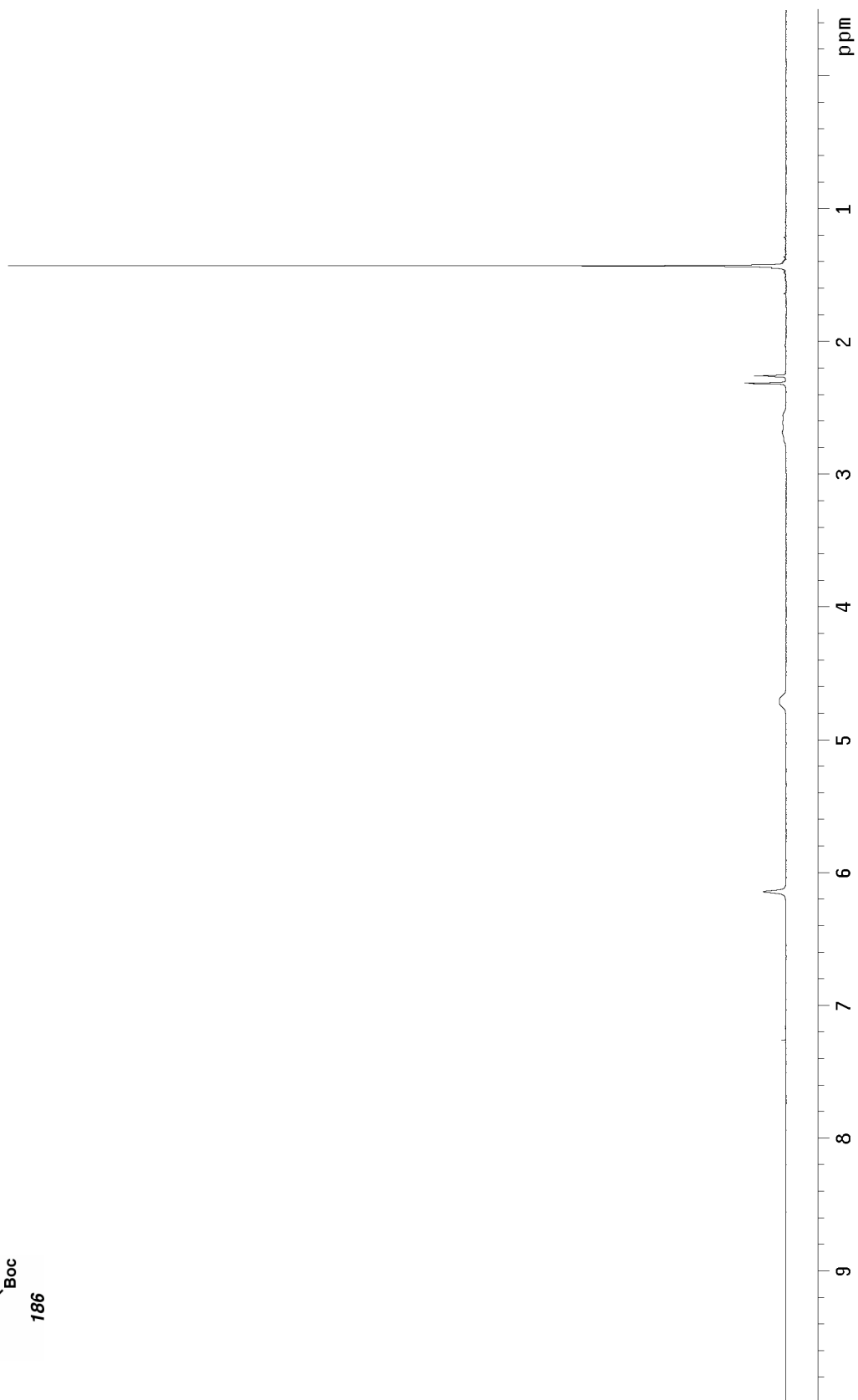
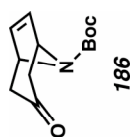


Figure A3.22 ^1H NMR (300 MHz, CDCl_3) of compound **186**.

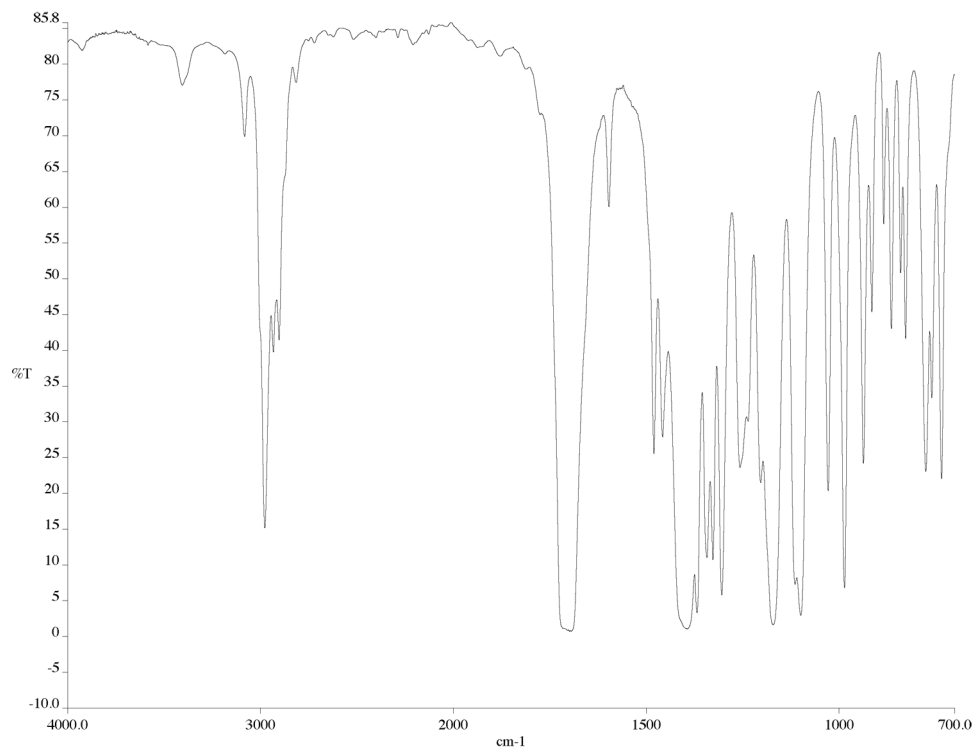


Figure A3.23 Infrared spectrum (thin film/NaCl) of compound **186**.

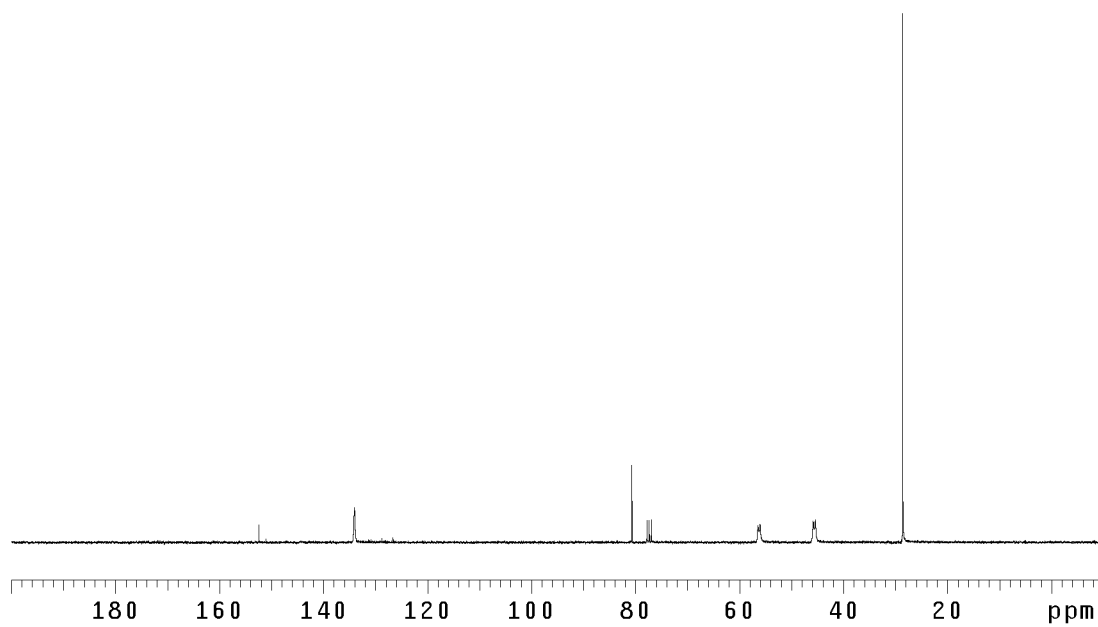


Figure A3.24 ¹³C NMR (125 MHz, CDCl₃) of compound **186**.

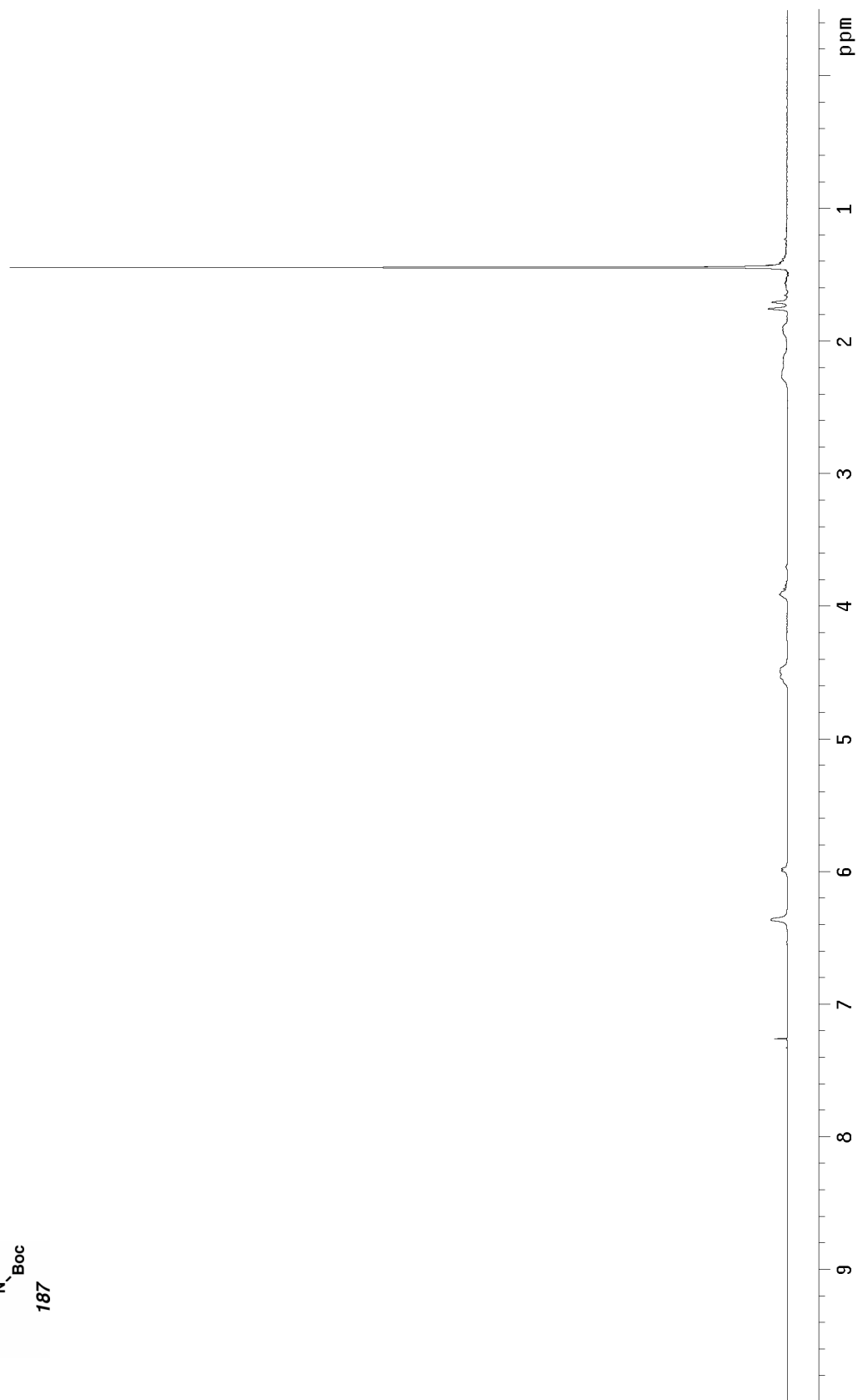
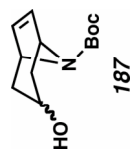


Figure A3.25 ¹H NMR (300 MHz, CDCl₃) of compound **187**.

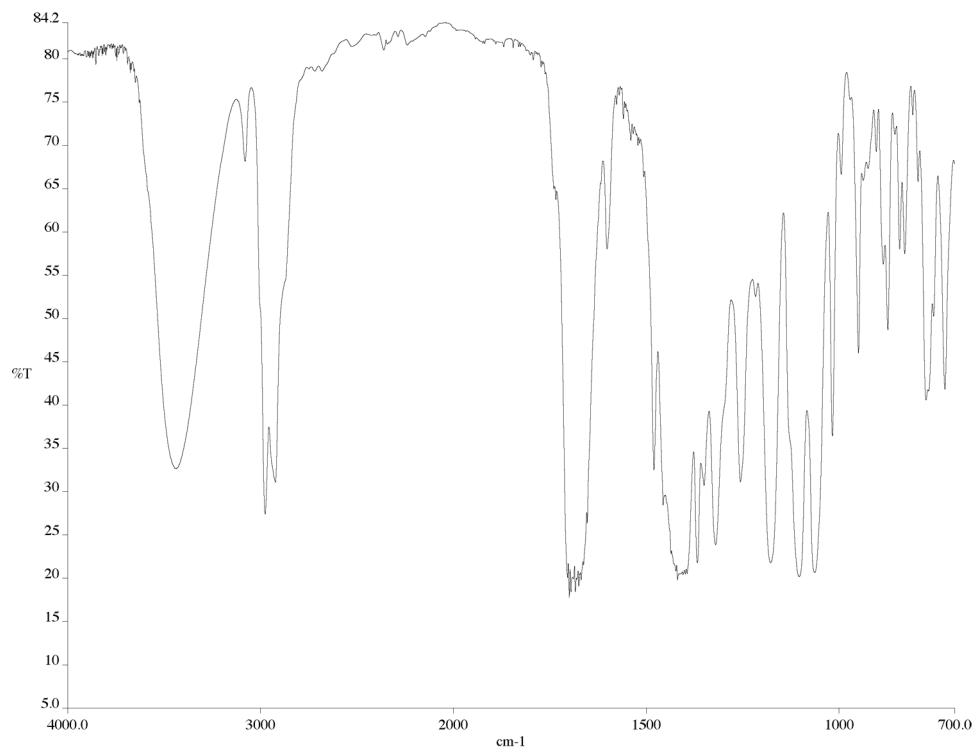


Figure A3.26 Infrared spectrum (thin film/NaCl) of compound **187**.

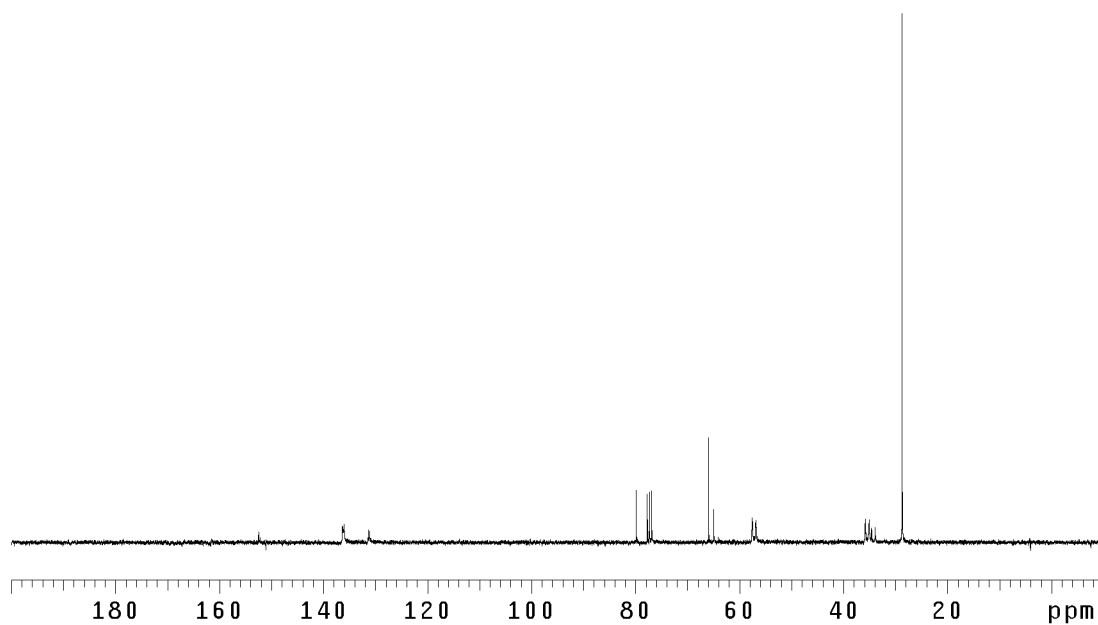


Figure A3.27 ¹³CNMR (125 MHz, CDCl₃) of compound **187**.

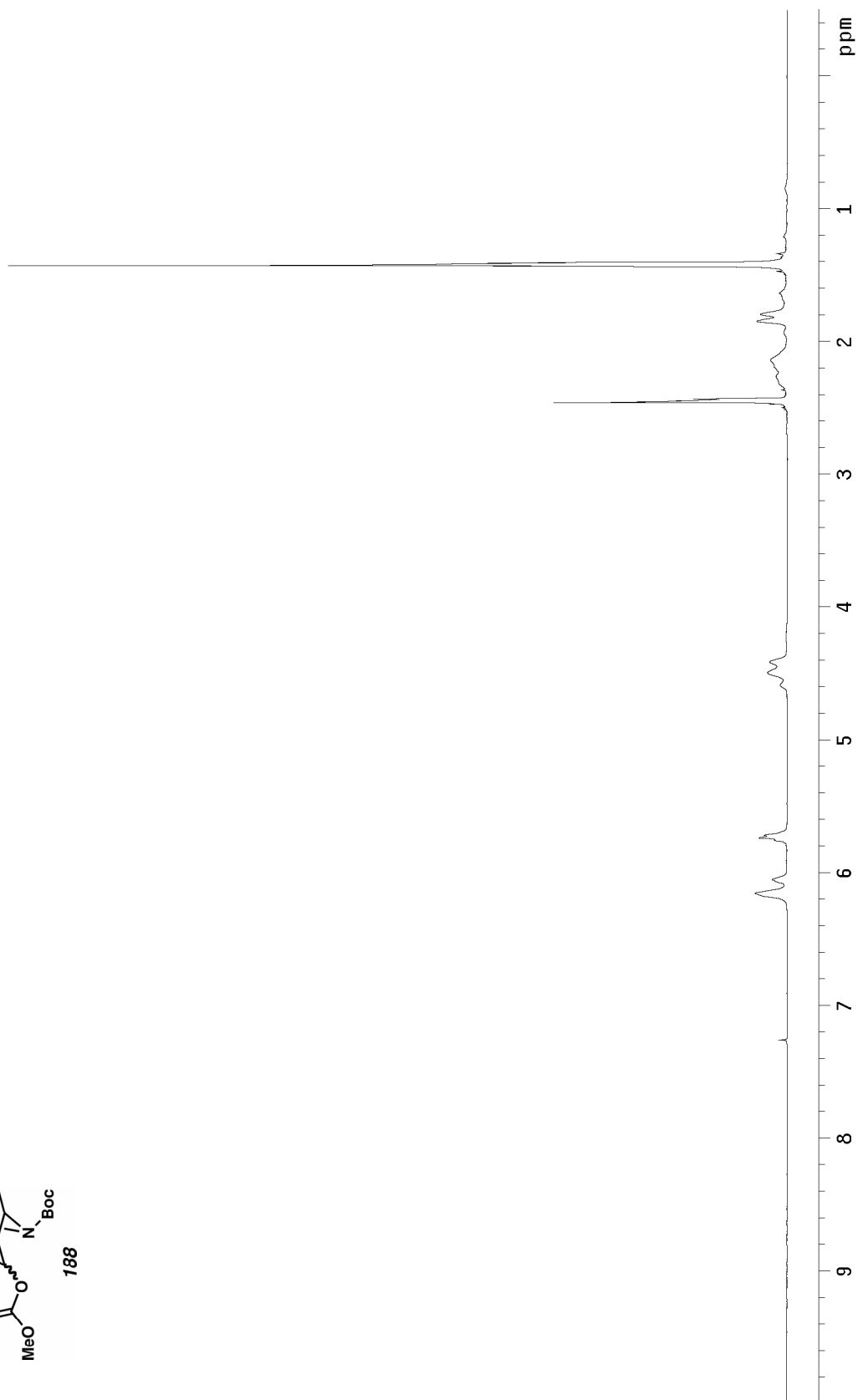
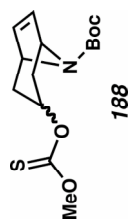


Figure A3.28 ^1H NMR (300 MHz, CDCl_3) of compound **188**.

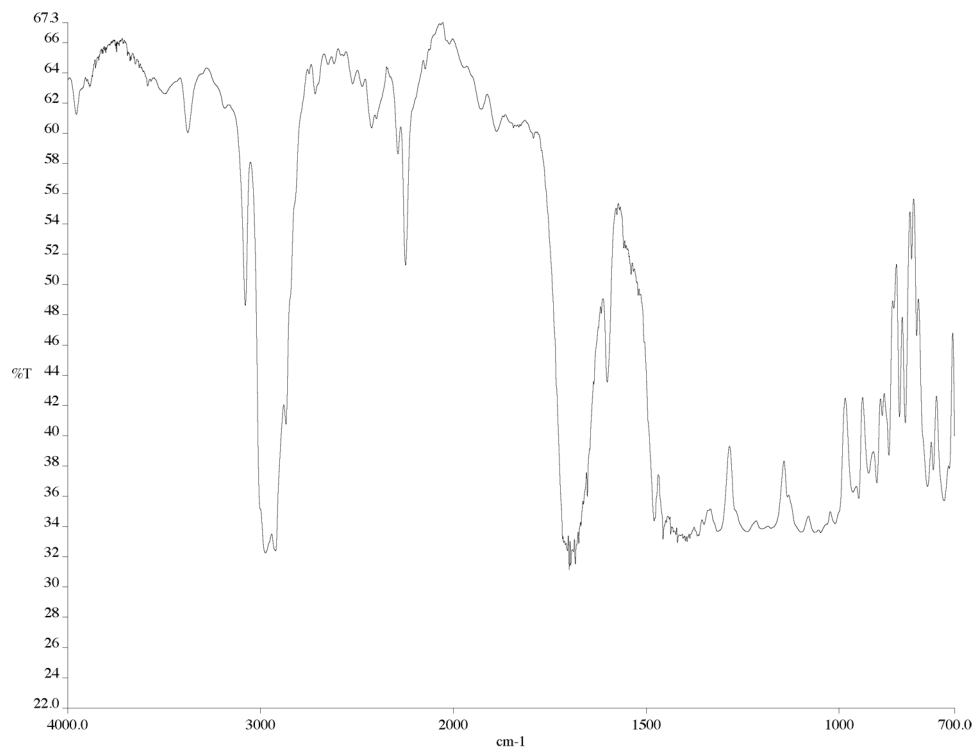


Figure A3.29 Infrared spectrum (thin film/NaCl) of compound **188**.

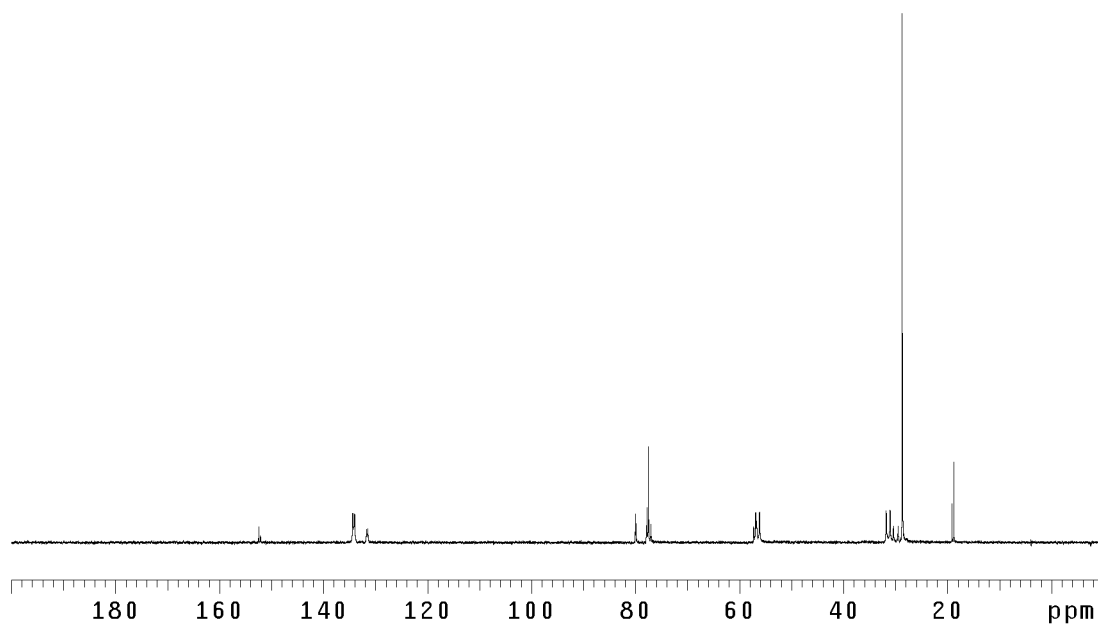


Figure A3.30 ¹³C NMR (125 MHz, CDCl₃) of compound **188**.

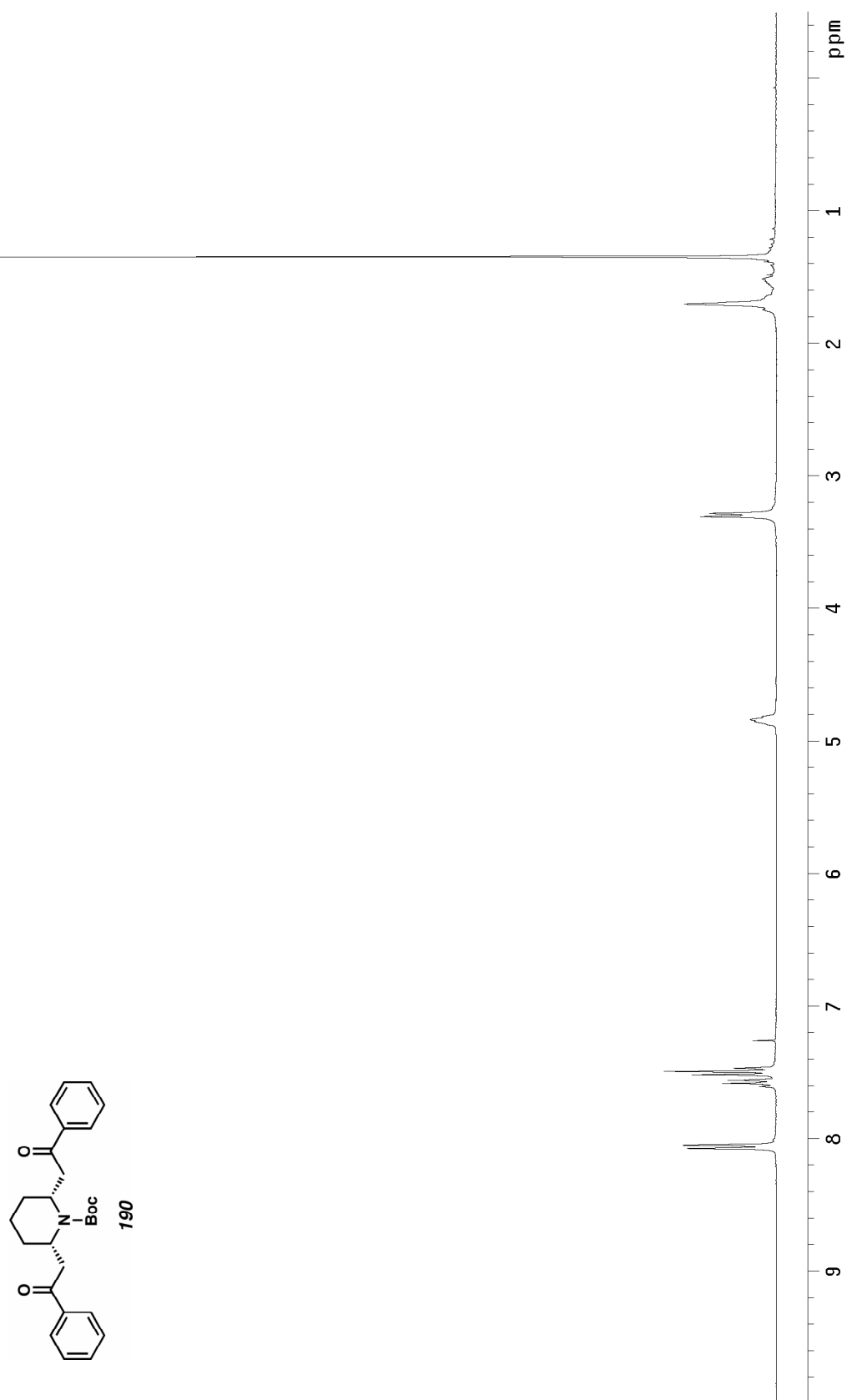


Figure A3.31 ^1H NMR (300 MHz, CDCl_3) of compound **190**.

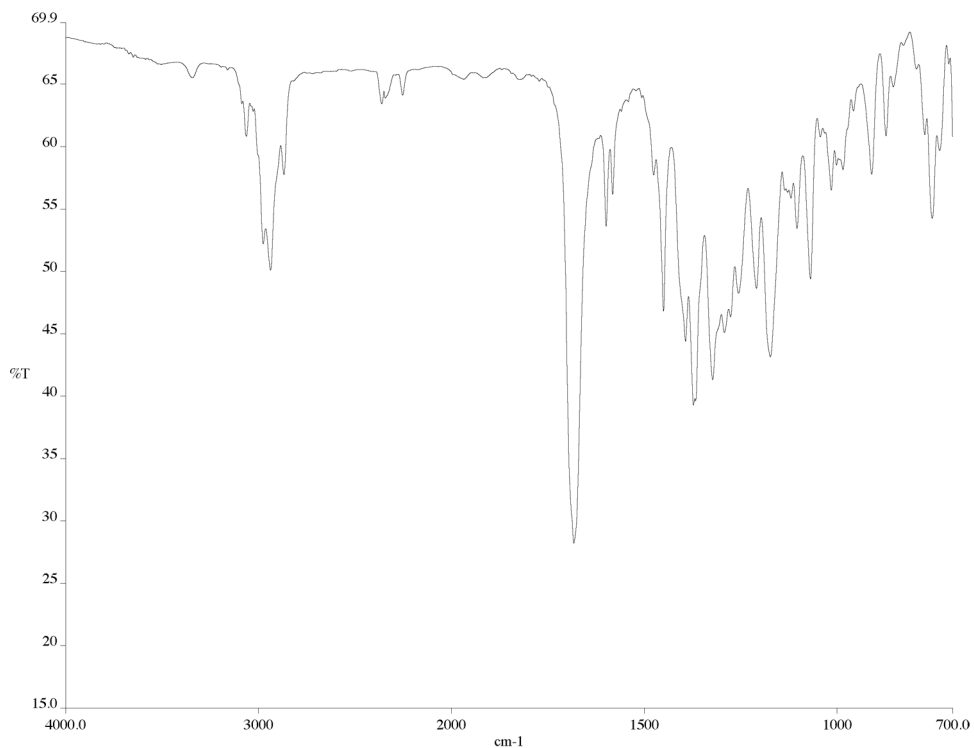


Figure A3.32 Infrared spectrum (thin film/NaCl) of compound **190**.

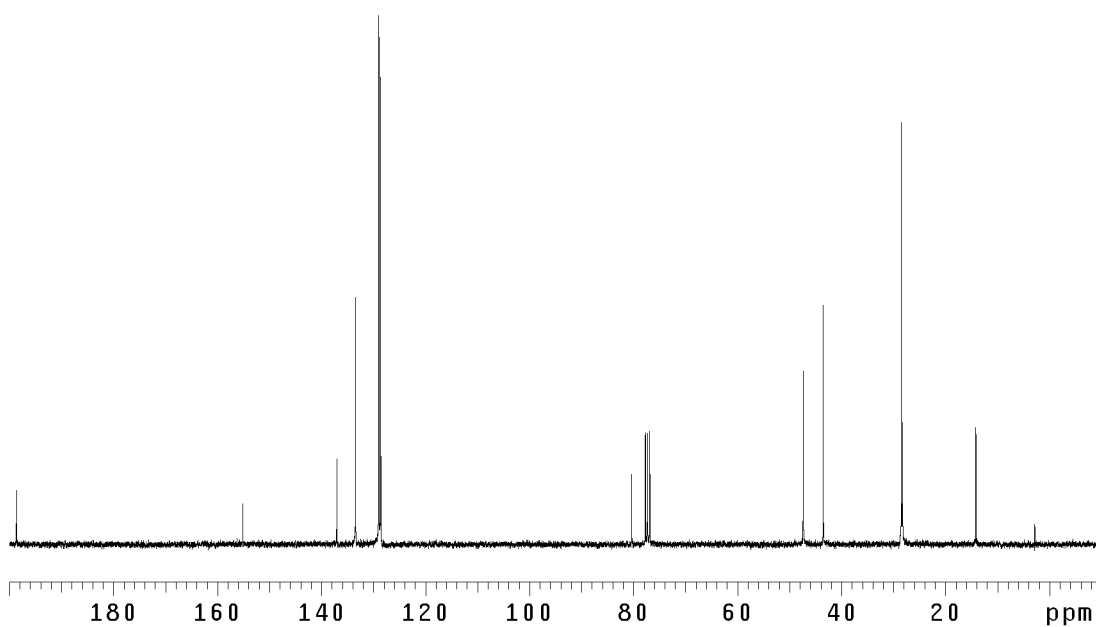


Figure A3.33 ¹³CNMR (125 MHz, CDCl₃) of compound **190**.

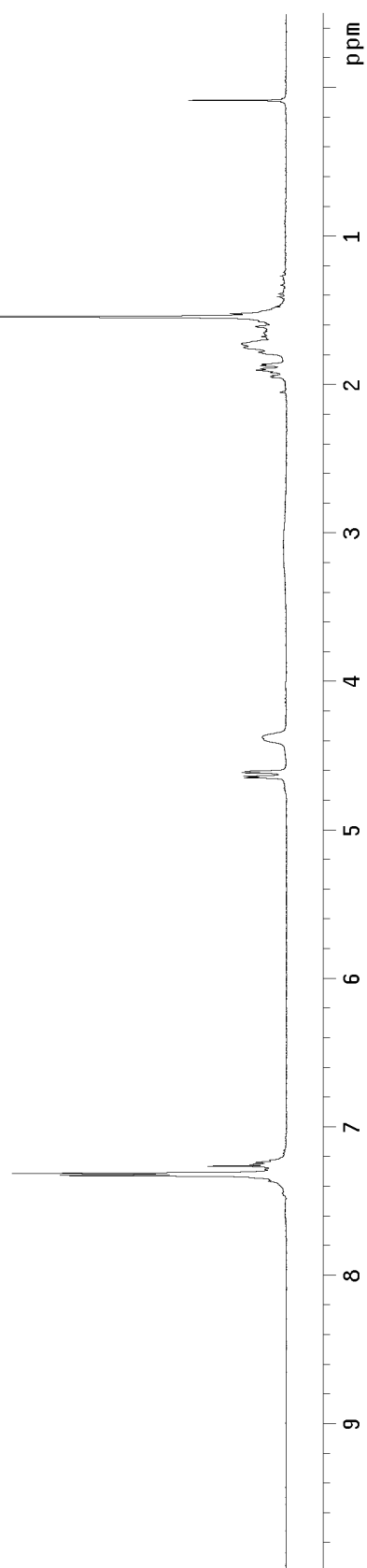
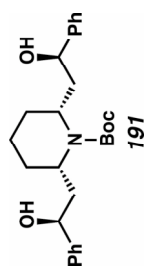


Figure A3.34 ¹H NMR (300 MHz, CDCl₃) of compound **191**.

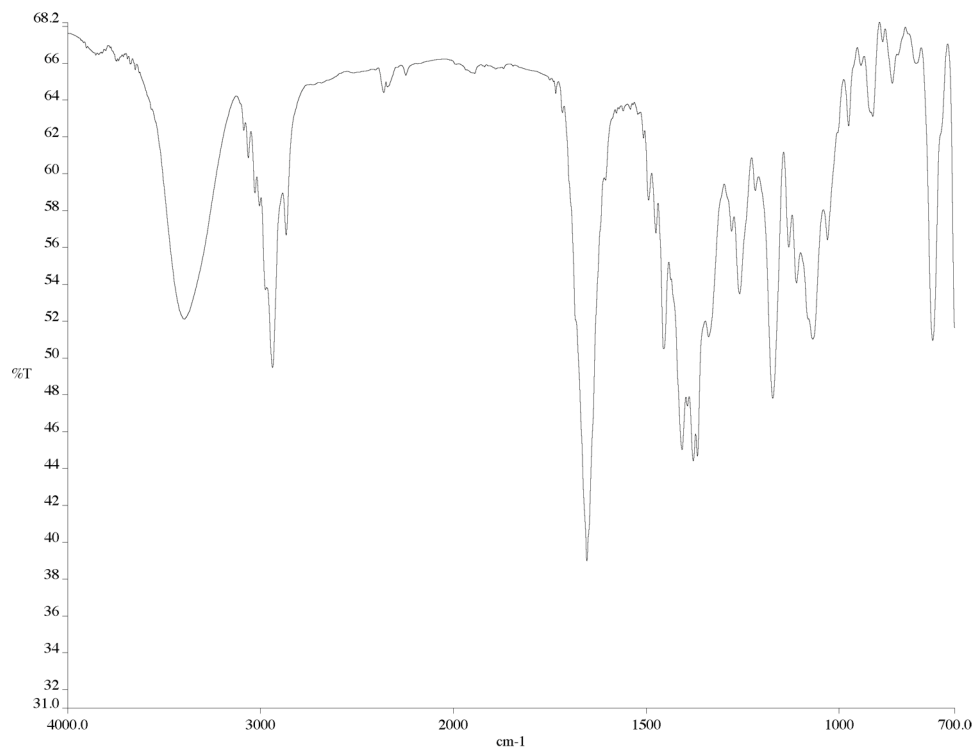


Figure A3.35 Infrared spectrum (thin film/NaCl) of compound **191**.

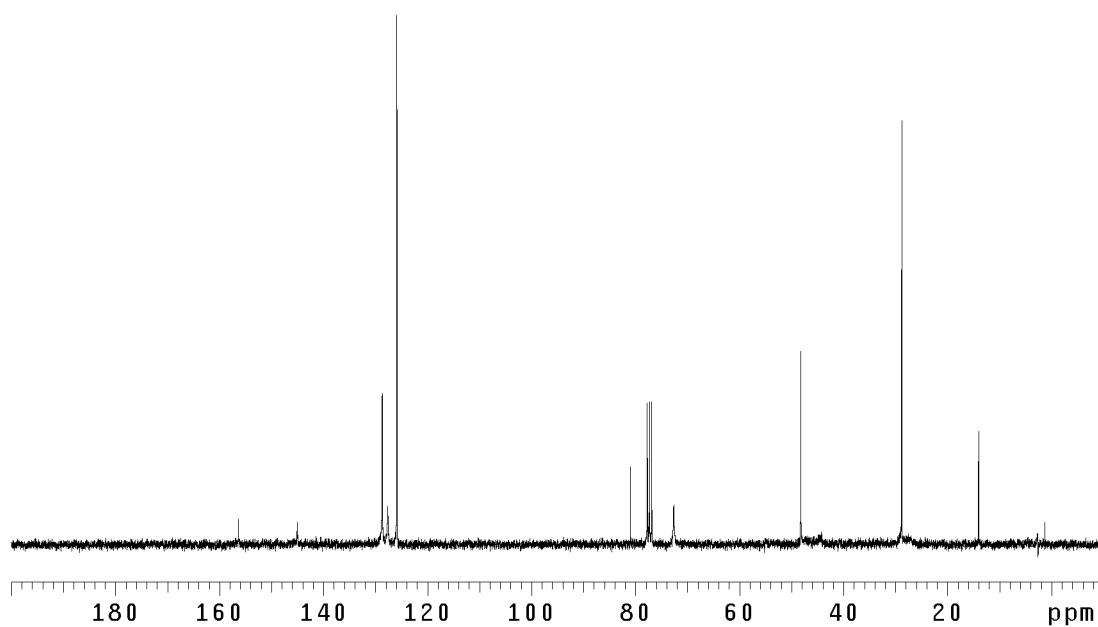


Figure A3.36 ¹³CNMR (125 MHz, CDCl₃) of compound **191**.

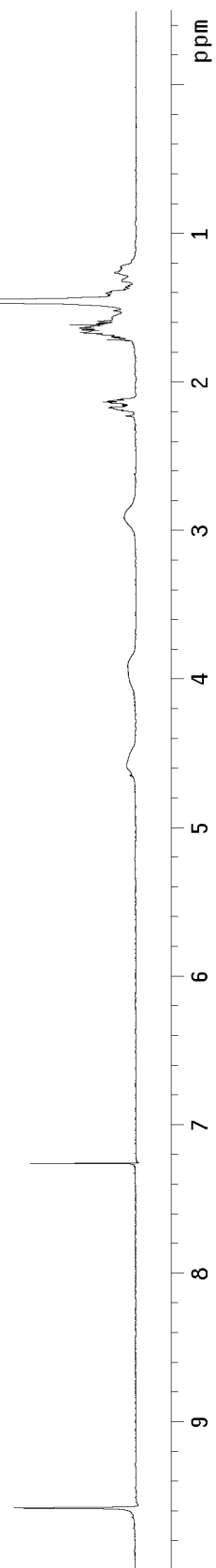
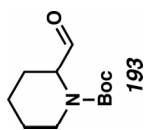


Figure A3.37 ^1H NMR (300 MHz, CDCl_3) of compound **193**.

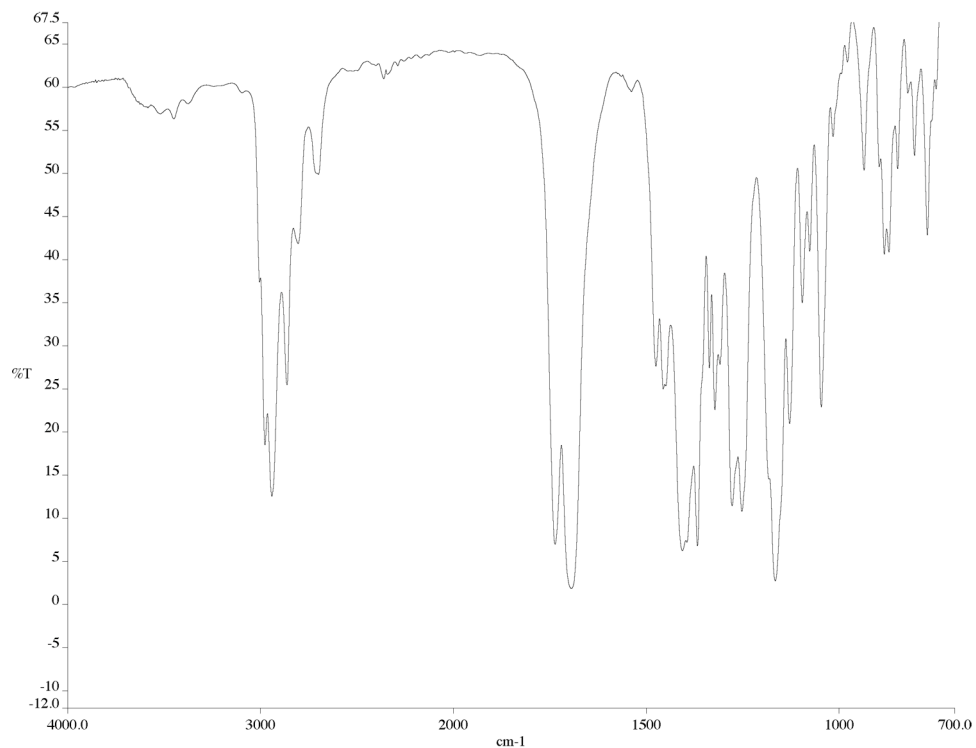


Figure A3.38 Infrared spectrum (thin film/NaCl) of compound **193**.

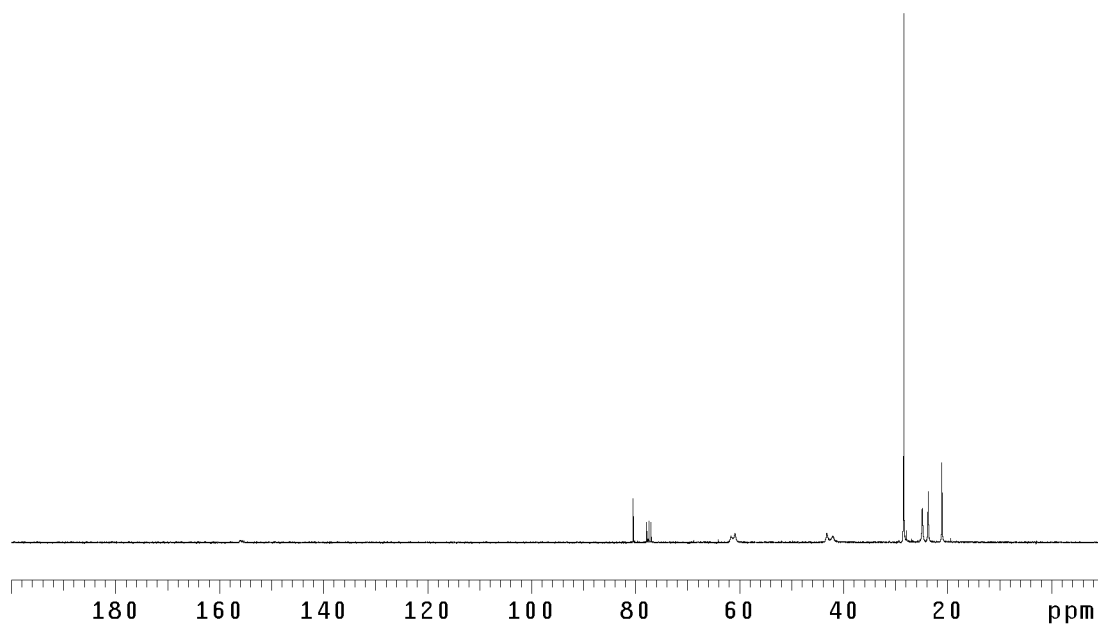


Figure A3.39 ¹³C NMR (125 MHz, CDCl₃) of compound **193**.

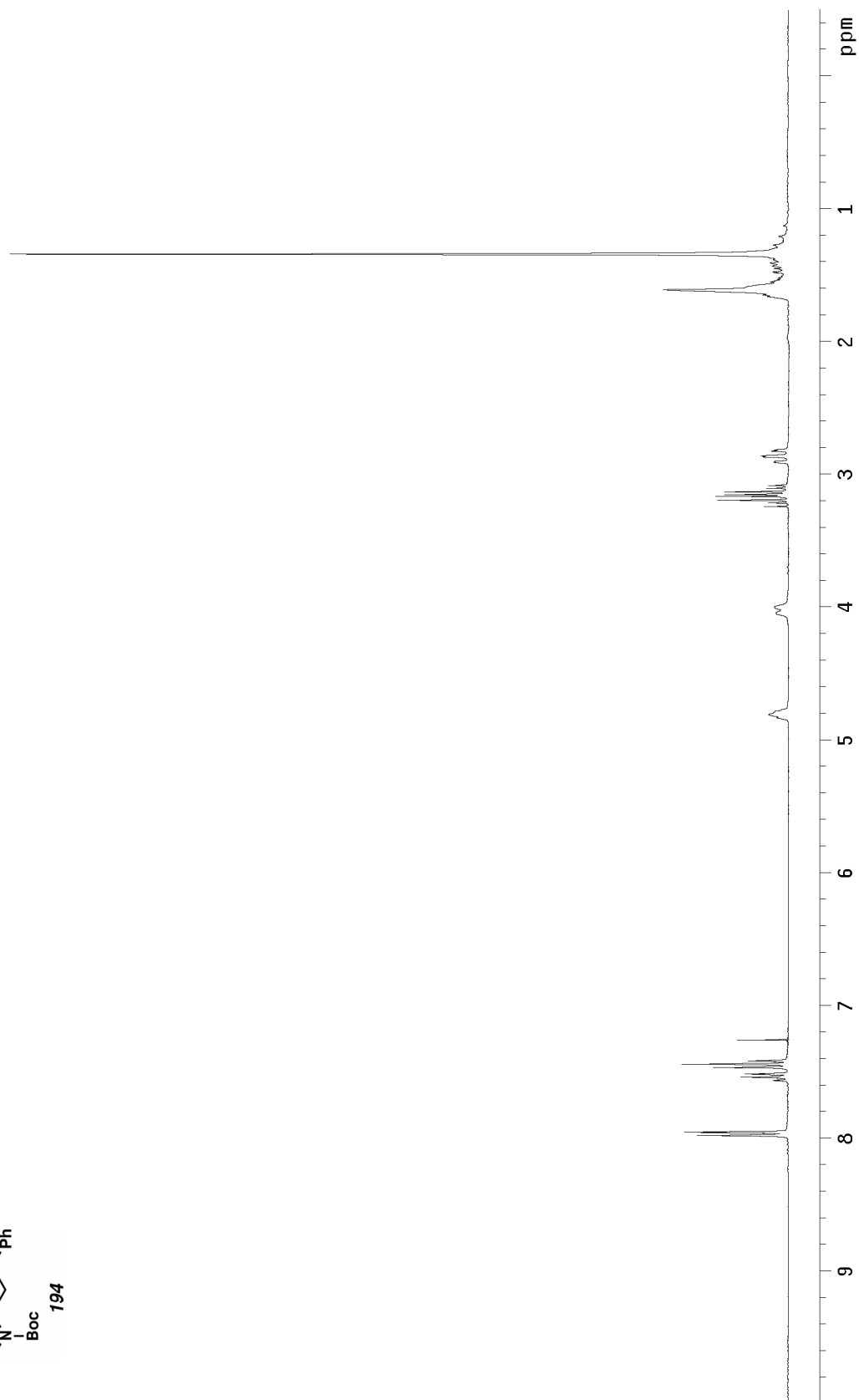
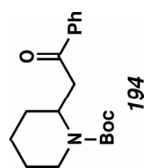


Figure A3.40 ^1H NMR (300 MHz, CDCl_3) of compound **194**.

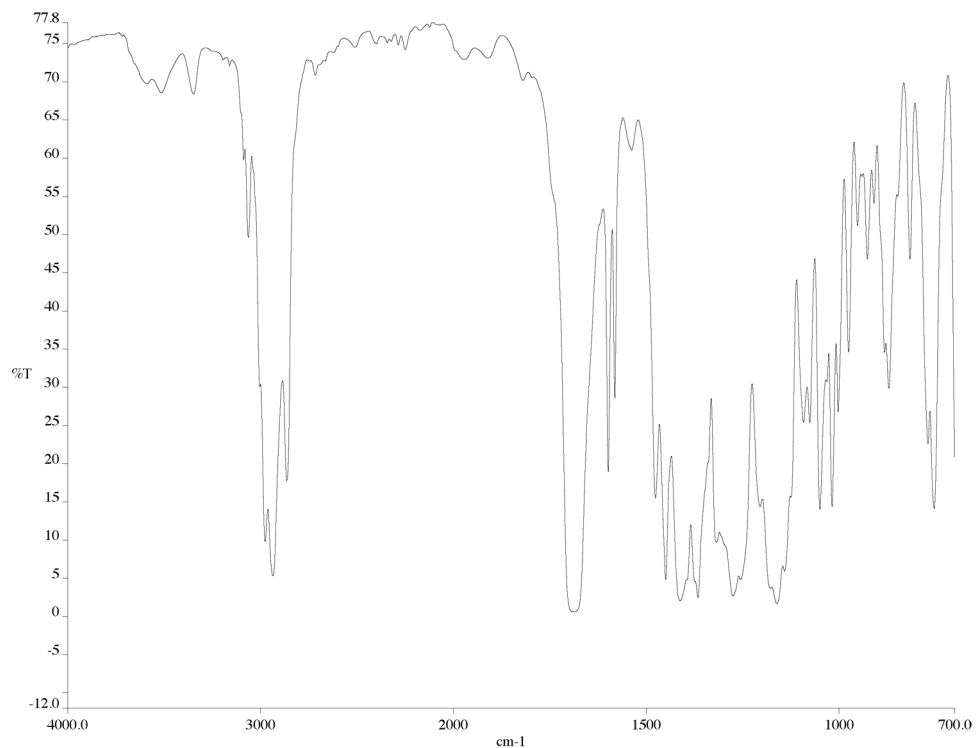


Figure A3.41 Infrared spectrum (thin film/NaCl) of compound **194**.

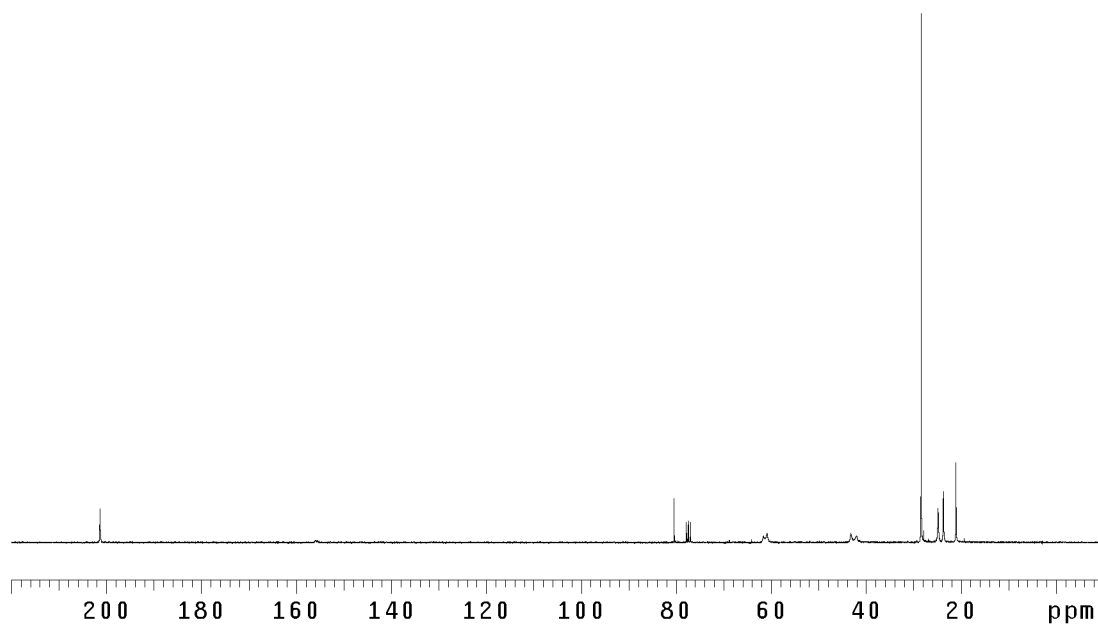


Figure A3.42 ¹³CNMR (125 MHz, CDCl₃) of compound **194**.

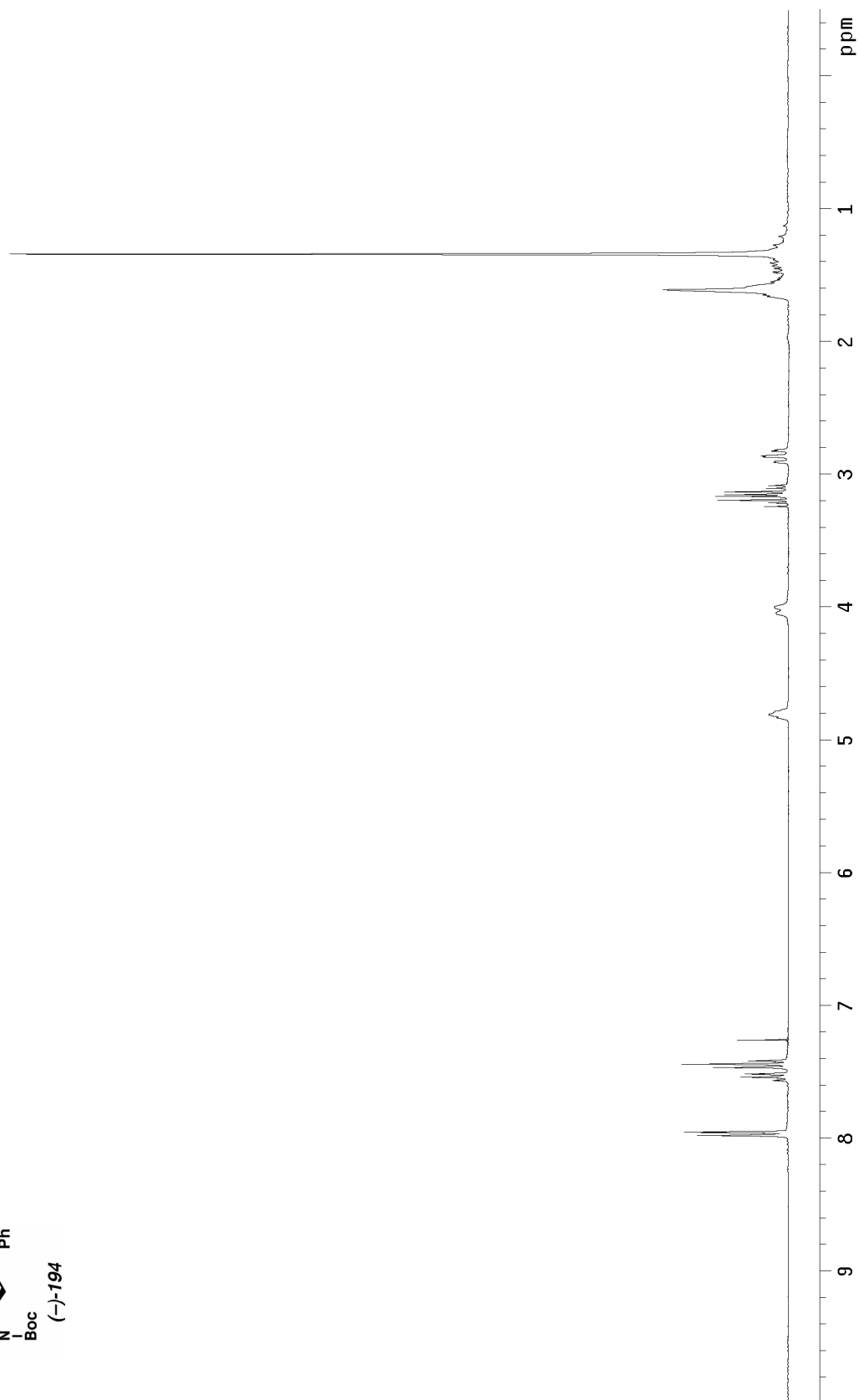
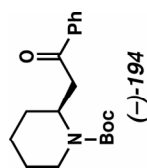


Figure A3.43 ^1H NMR (300 MHz, CDCl_3) of compound (-)-194.

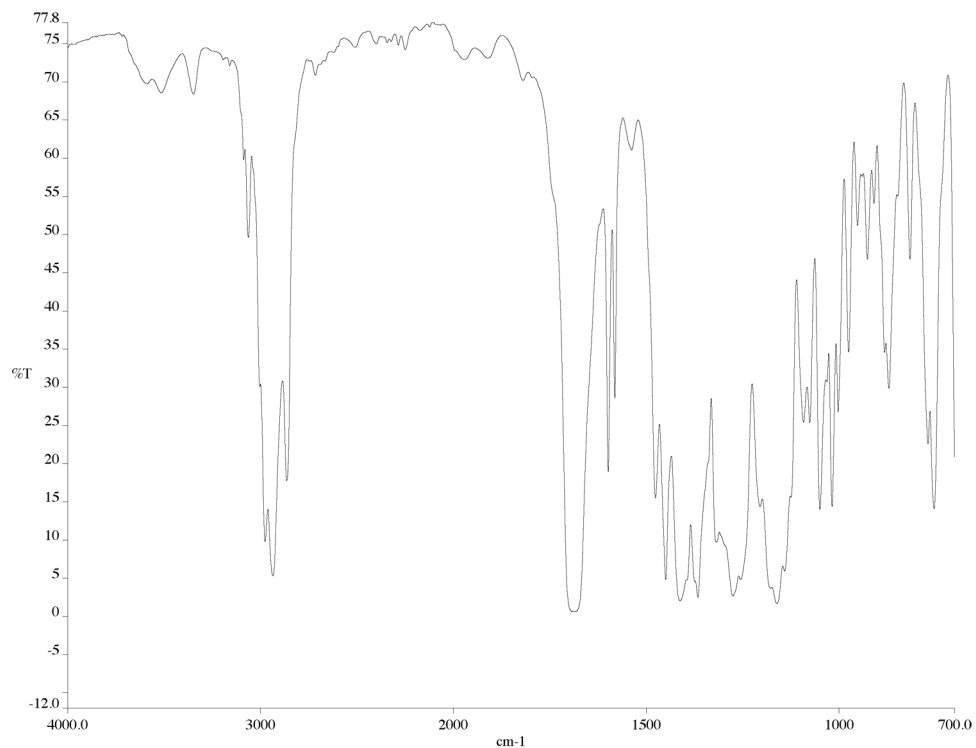


Figure A3.44 Infrared spectrum (thin film/NaCl) of compound **(-)-194**.

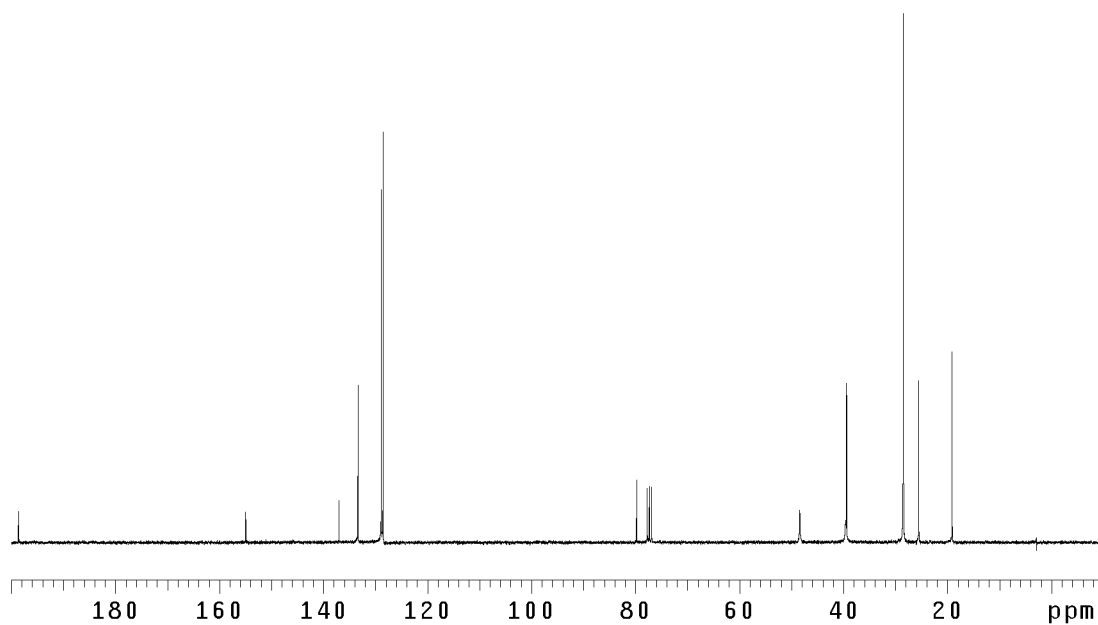


Figure A3.45 ¹³CNMR (125 MHz, CDCl₃) of compound **(-)-194**.

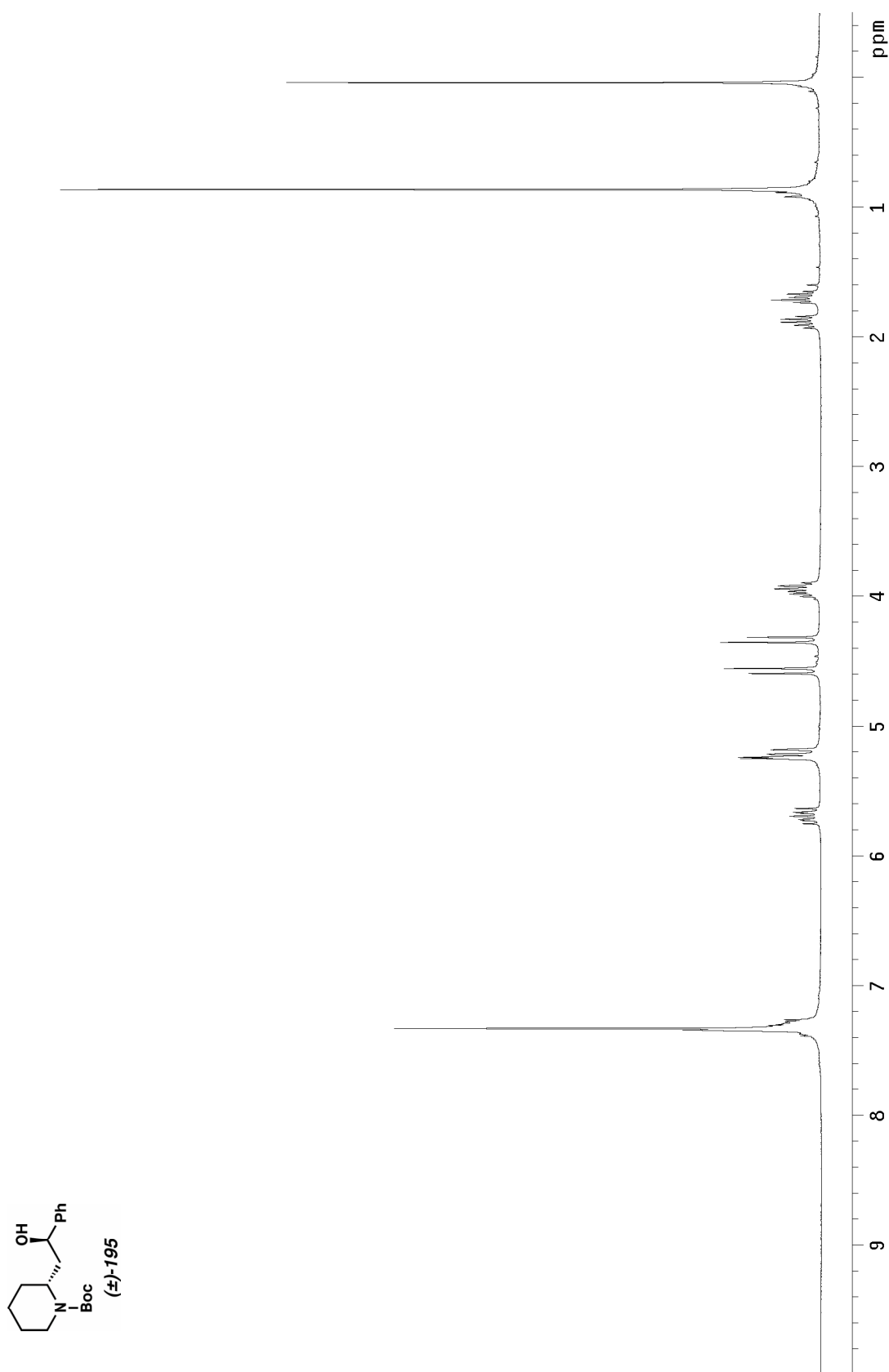


Figure A3.46 ^1H NMR (300 MHz, CDCl_3) of compound (+)-195.

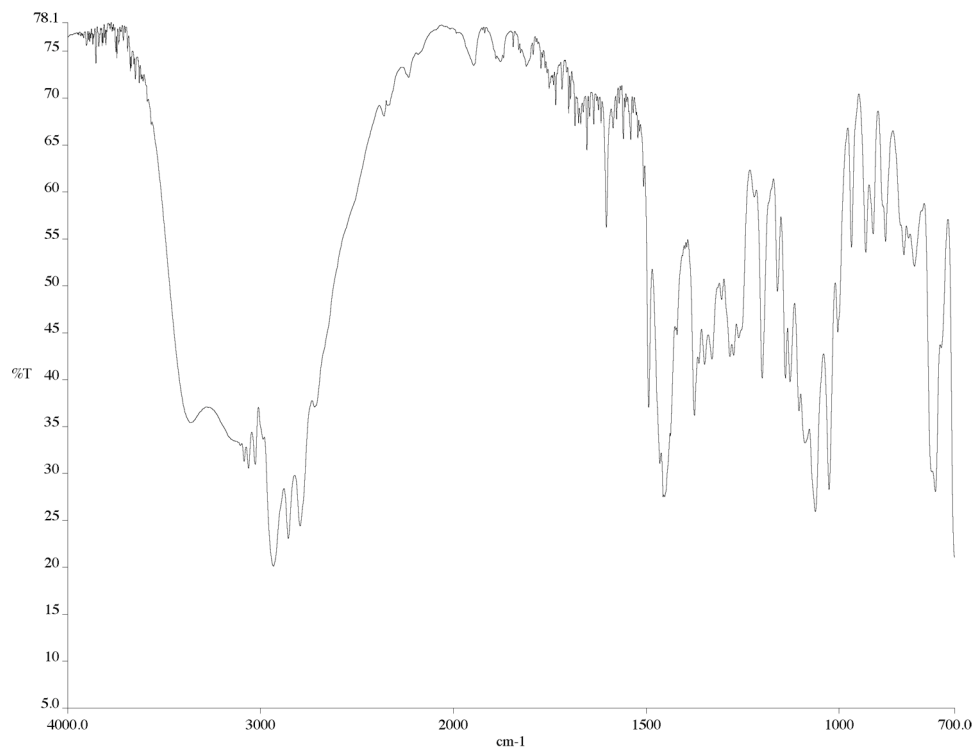


Figure A3.47 Infrared spectrum (thin film/NaCl) of compound (+)-195.

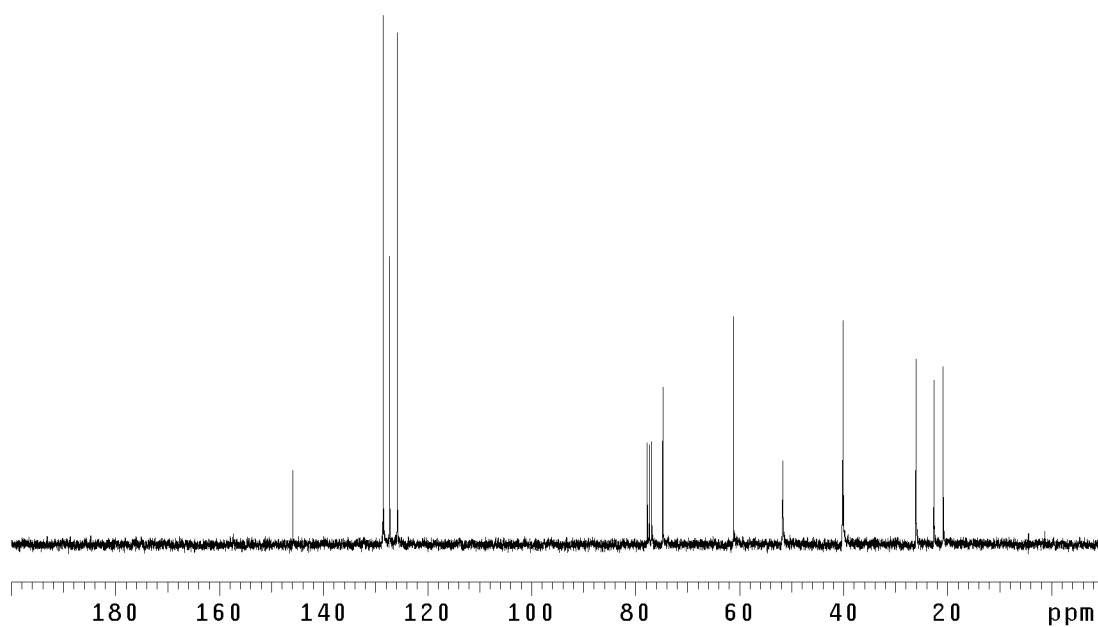


Figure A3.48 ¹³CNMR (125 MHz, CDCl₃) of compound (+)-195.

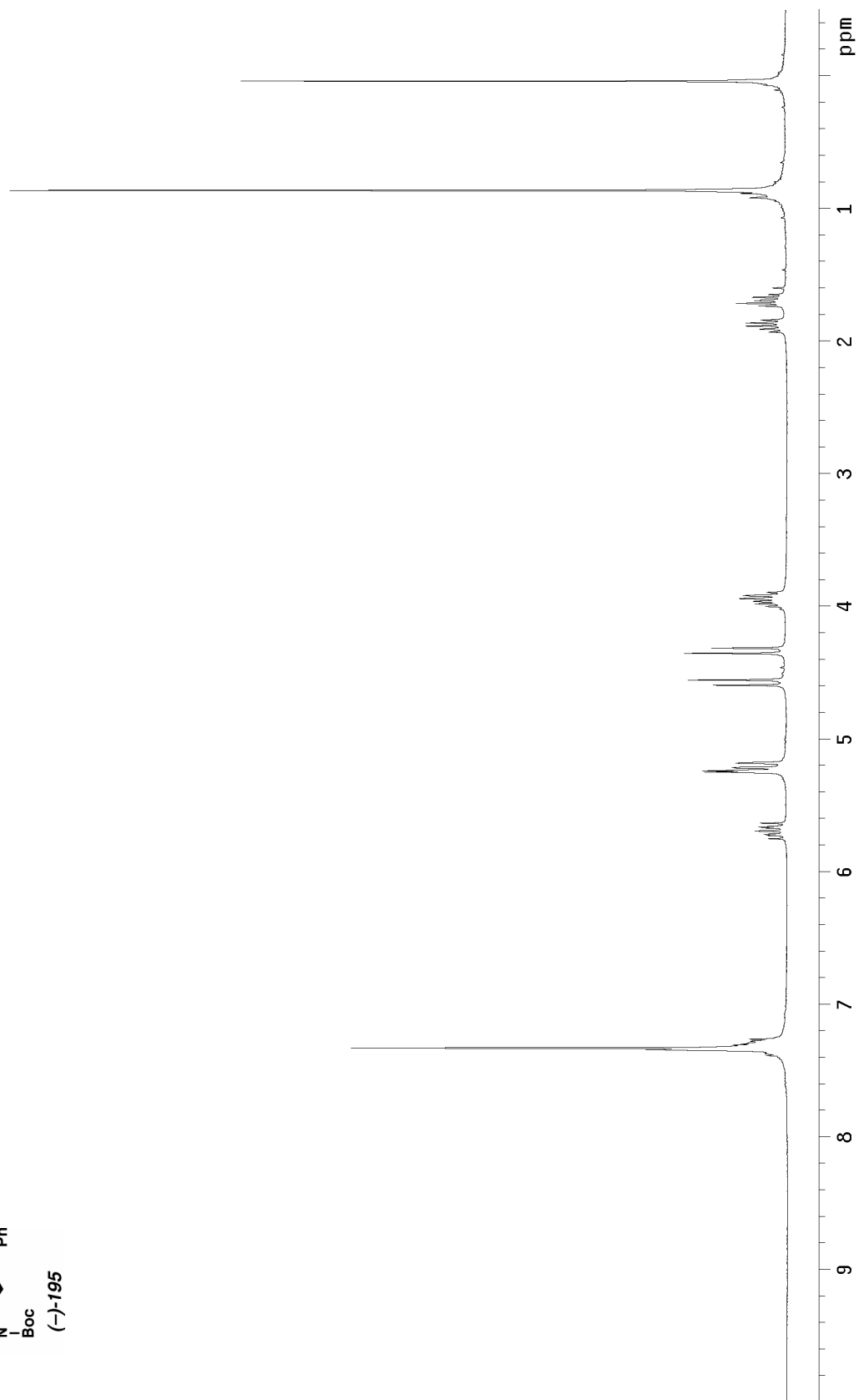
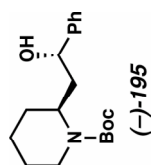


Figure A3.49 ^1H NMR (300 MHz, CDCl_3) of compound (-)-195.

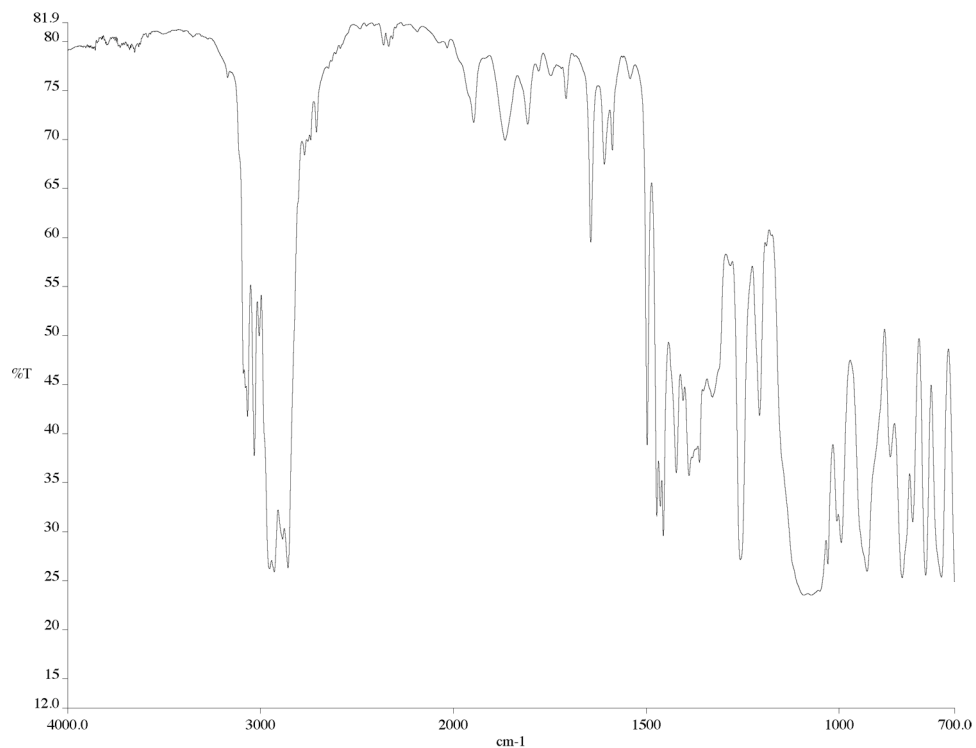


Figure A3.50 Infrared spectrum (thin film/NaCl) of compound **(-)-195**.

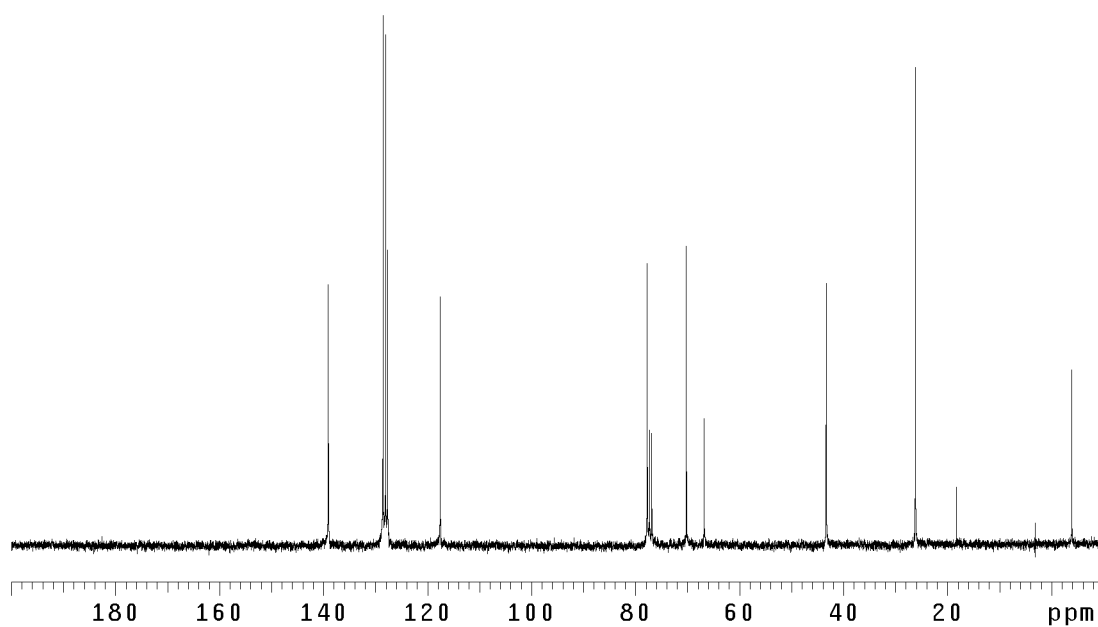


Figure A3.51 ¹³CNMR (125 MHz, CDCl₃) of compound **(-)-195**.

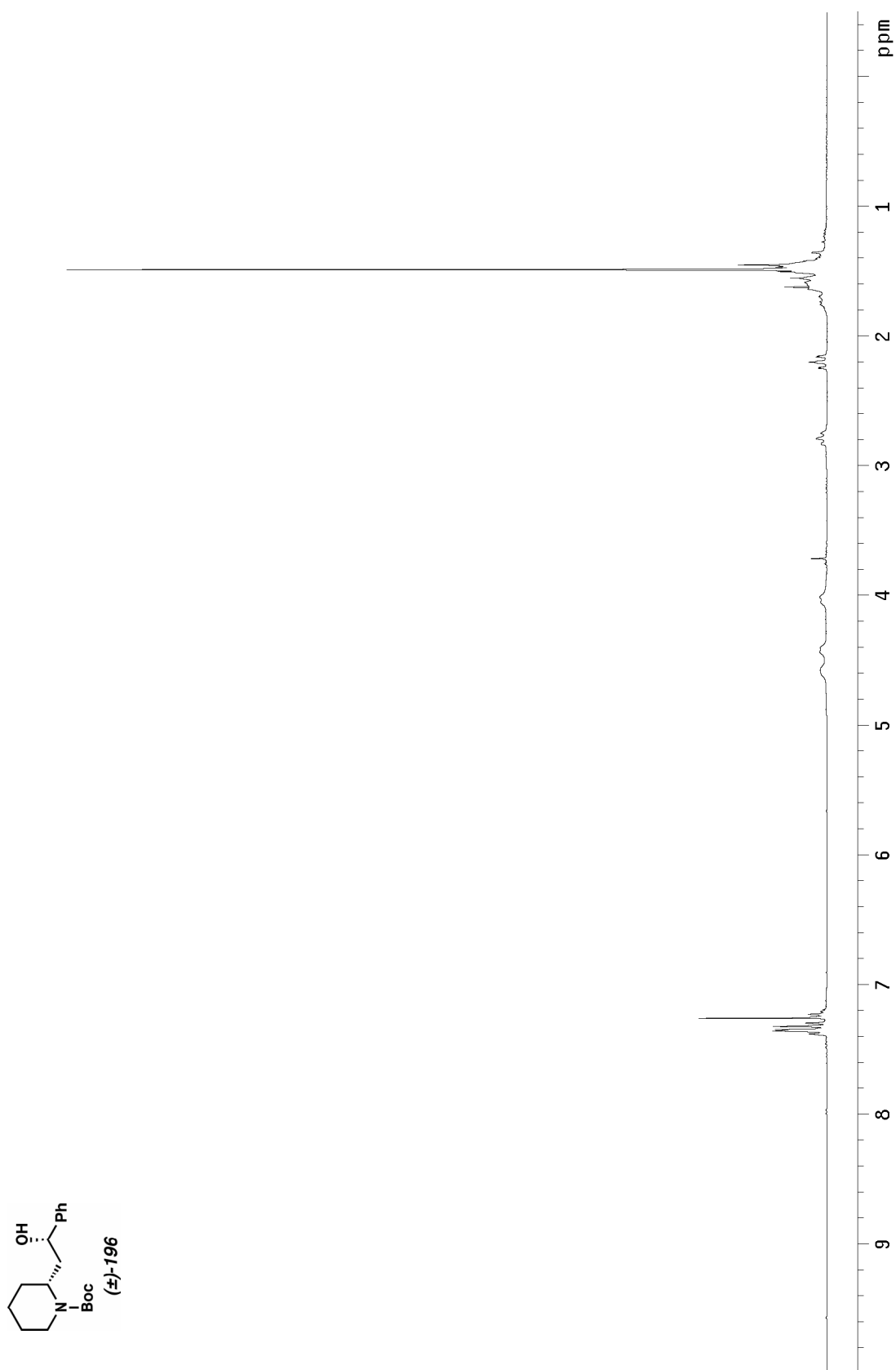


Figure A3.52 ¹H NMR (300 MHz, CDCl₃) of compound (±)-196.

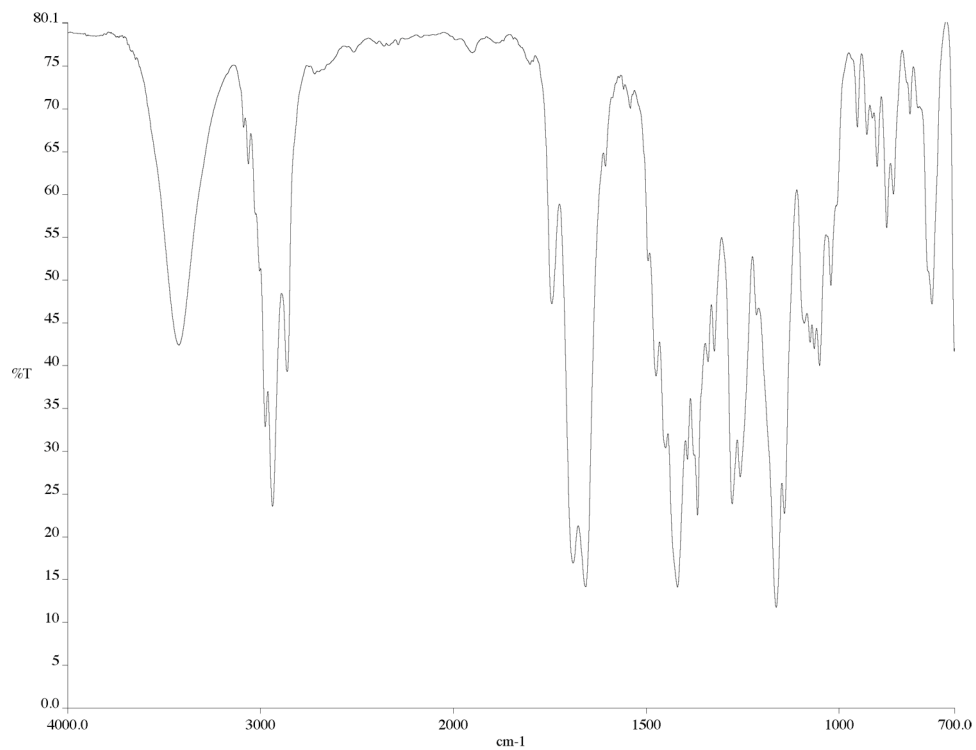


Figure A3.53 Infrared spectrum (thin film/NaCl) of compound (±)-196.

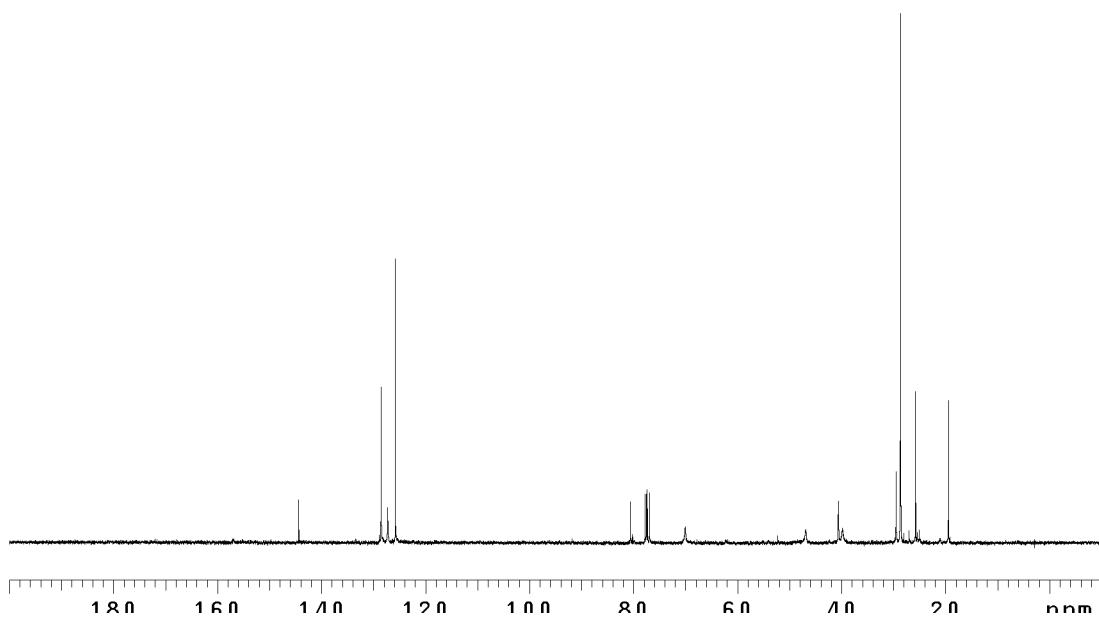


Figure A3.54 ¹³CNMR (125 MHz, CDCl₃) of compound (±)-196.

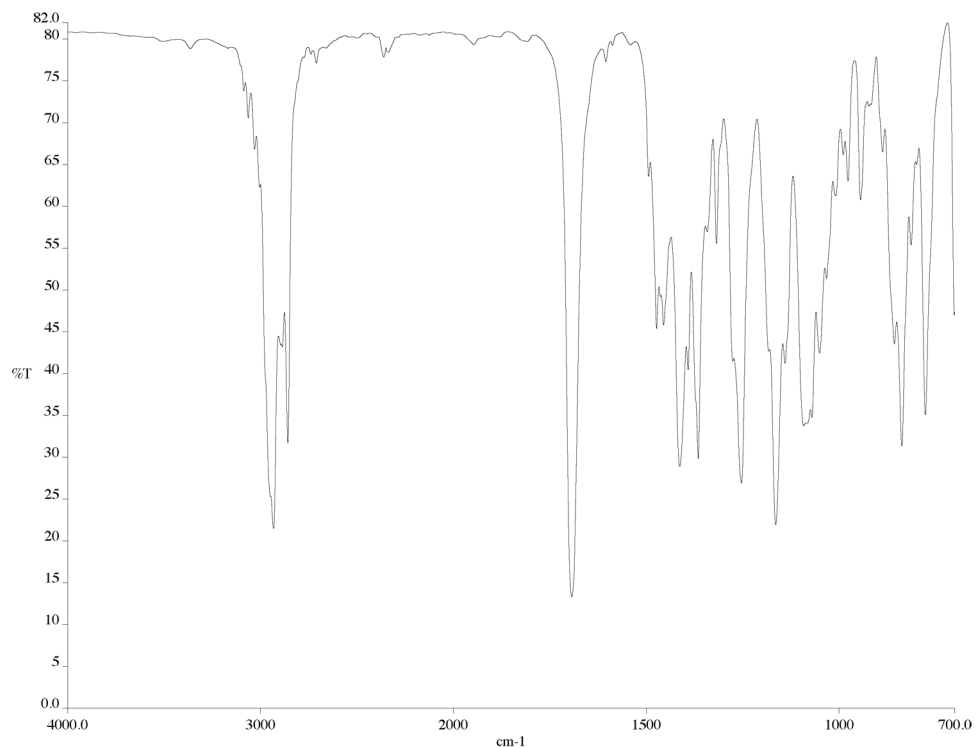


Figure A3.56 Infrared spectrum (thin film/NaCl) of compound (±)-199.

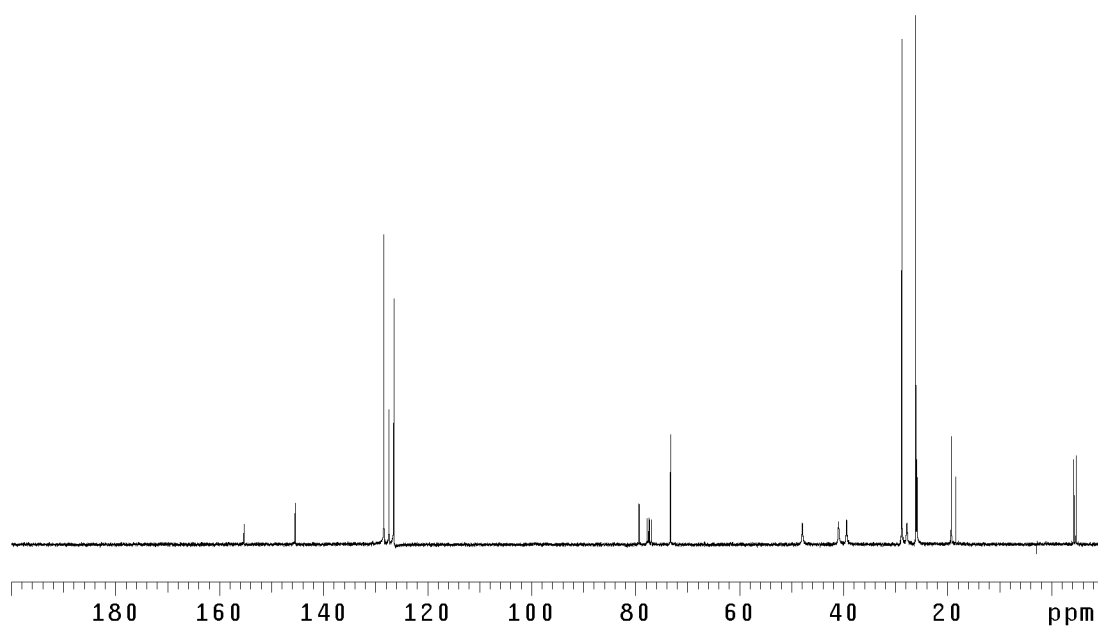


Figure A3.57 ¹³CNMR (125 MHz, CDCl₃) of compound (±)-199.

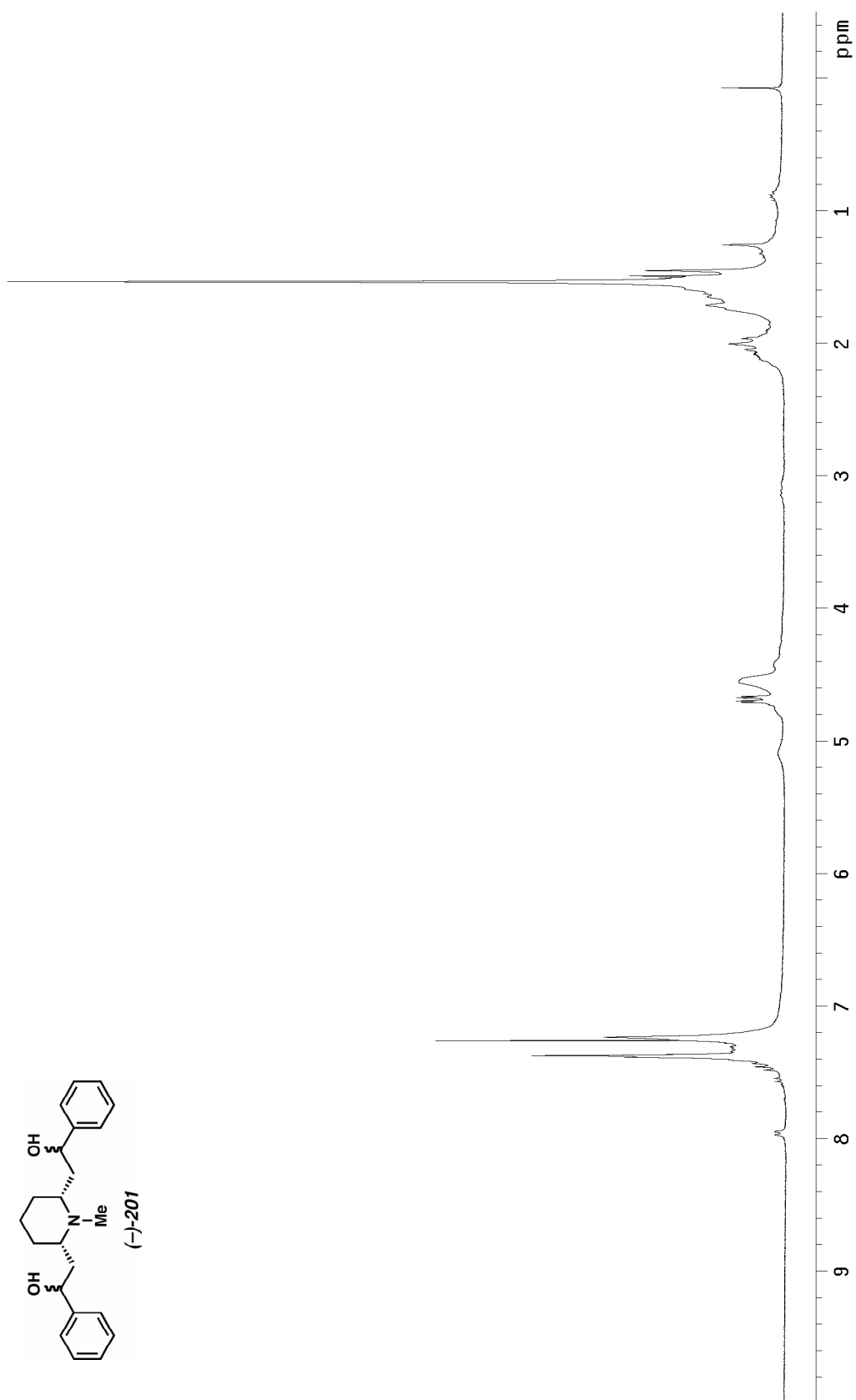


Figure A3.58 ^1H NMR (300 MHz, CDCl_3) of compound **(-)-201**.

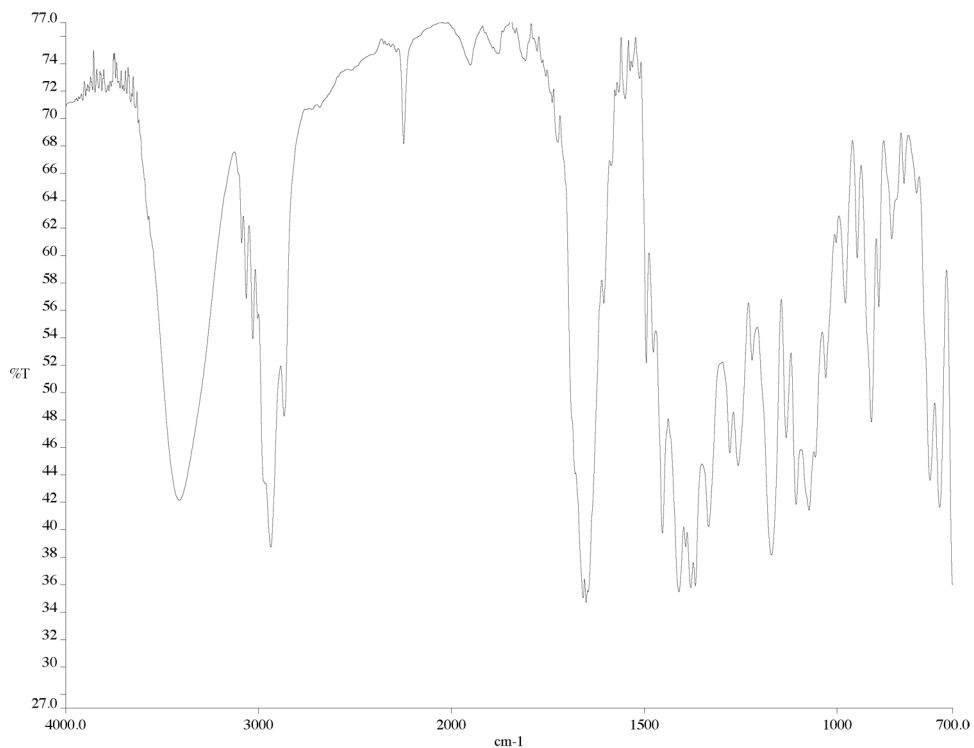


Figure A3.59 Infrared spectrum (thin film/NaCl) of compound (–)-201.

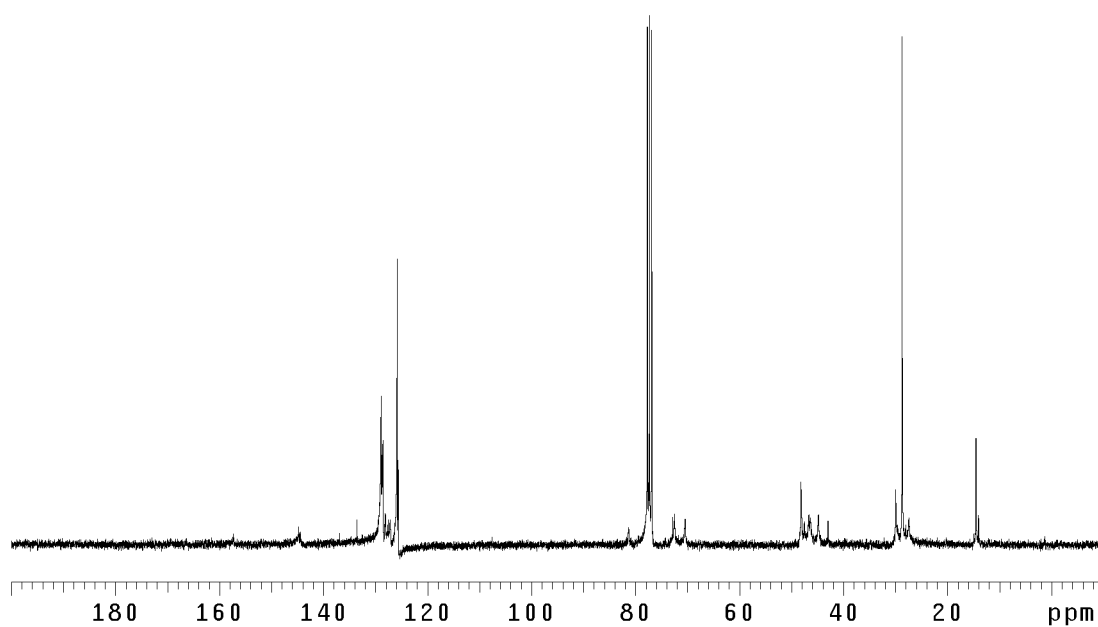


Figure A3.60 ¹³CNMR (125 MHz, CDCl₃) of compound (–)-201.

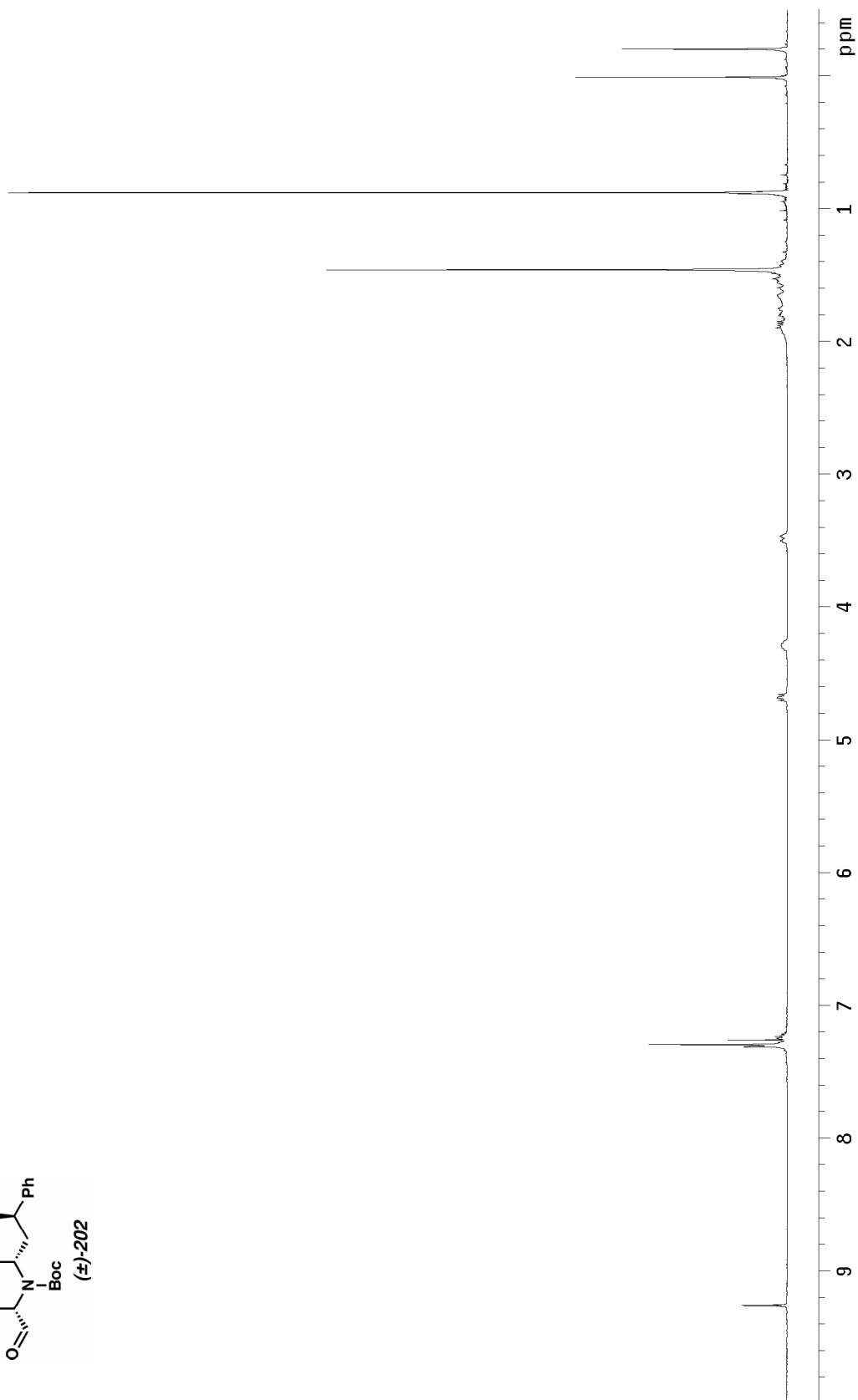
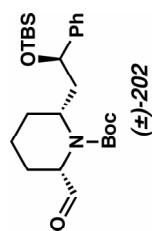


Figure A3.61 ^1H NMR (300 MHz, CDCl_3) of compound (±)-202.

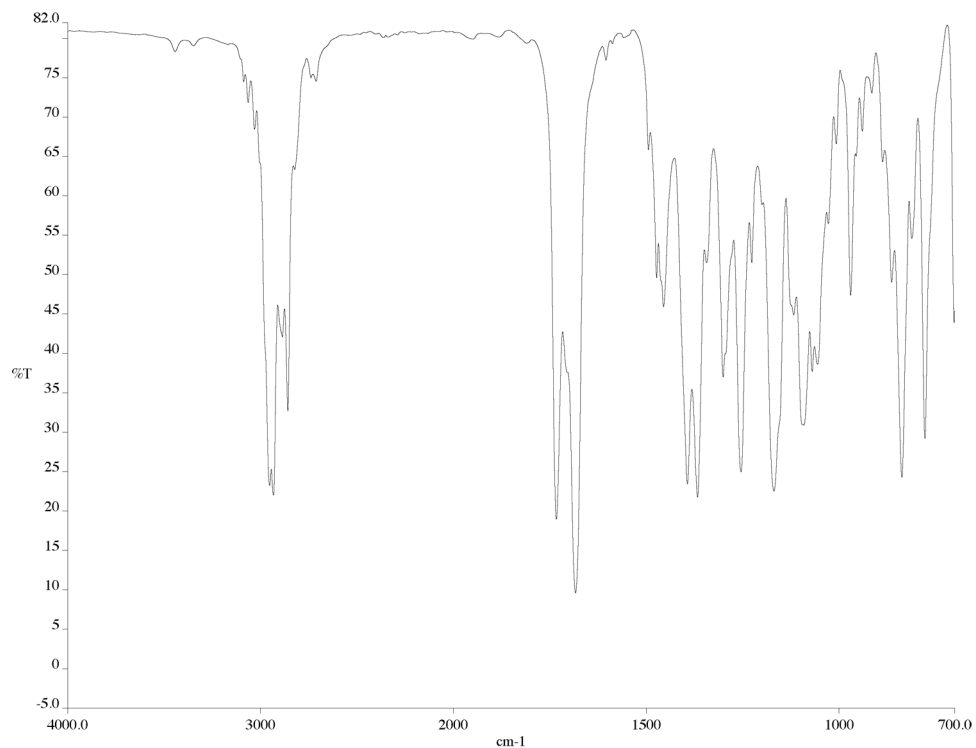


Figure A3.62 Infrared spectrum (thin film/NaCl) of compound (±)-202.

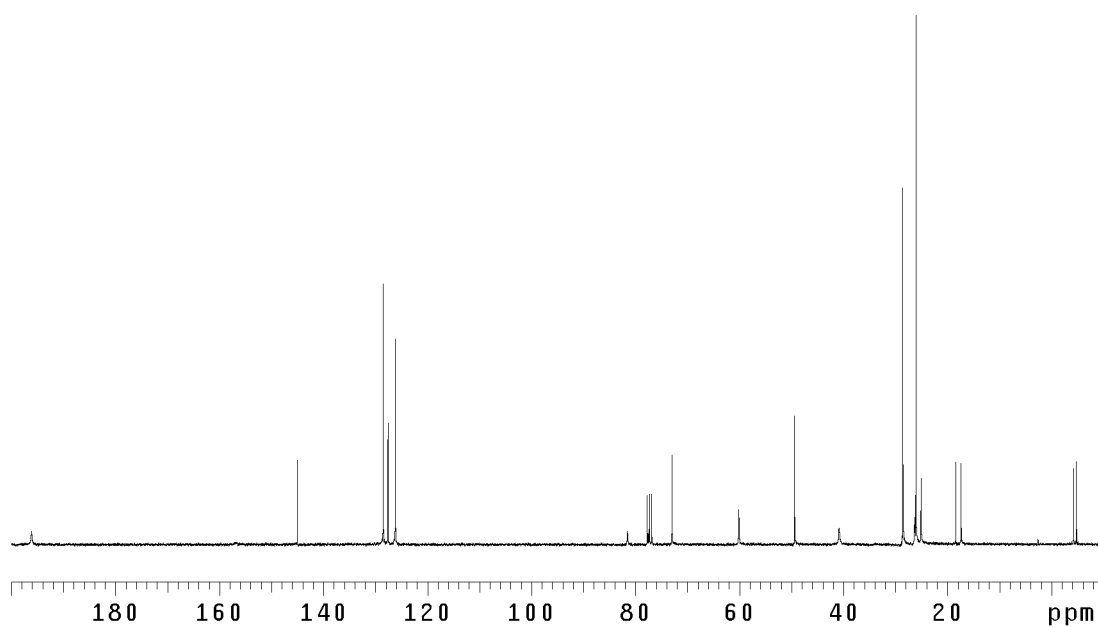


Figure A3.63 ¹³CNMR (125 MHz, CDCl₃) of compound (±)-202.

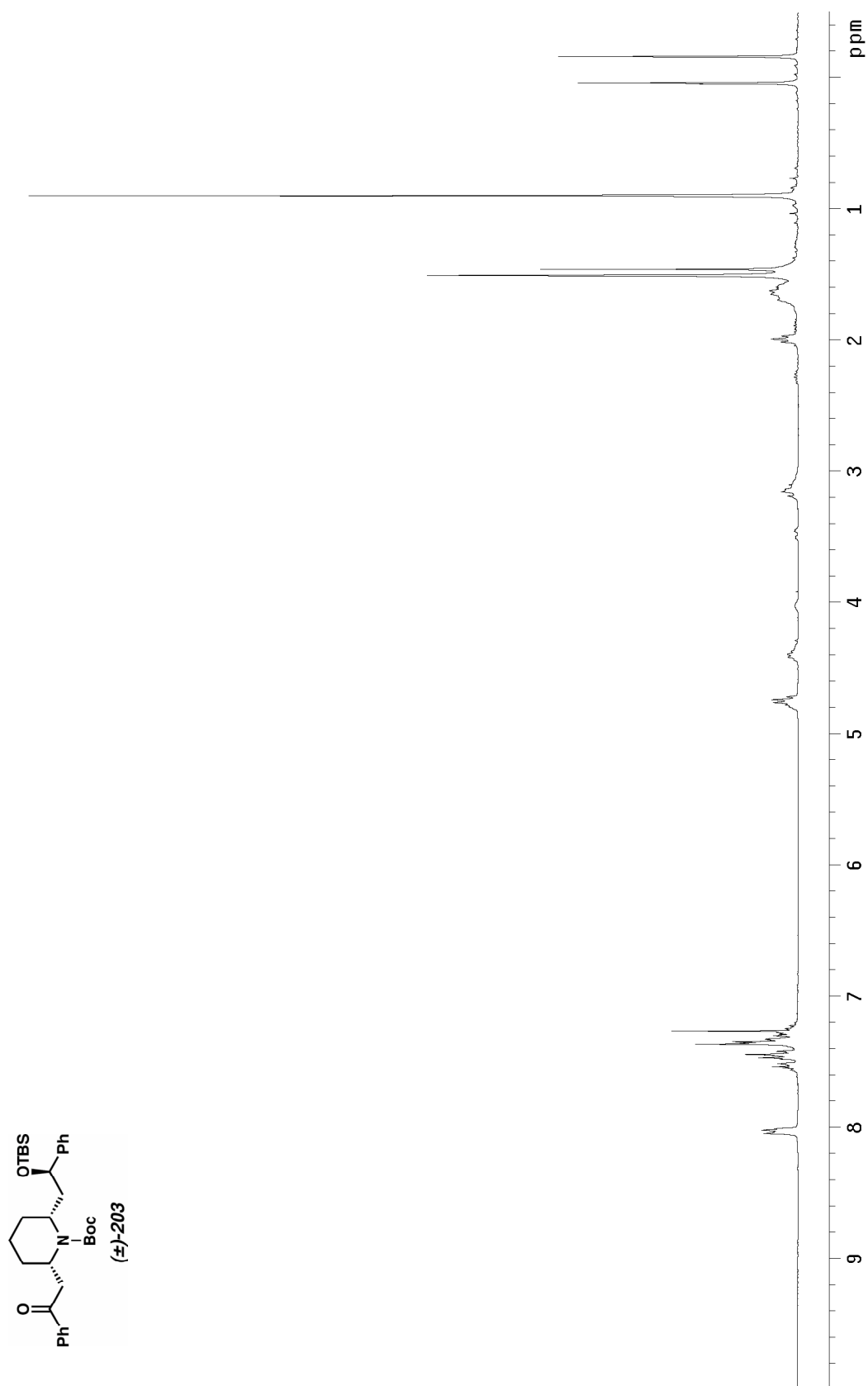


Figure A3.64 ^1H NMR (300 MHz, CDCl_3) of compound (±)-203.

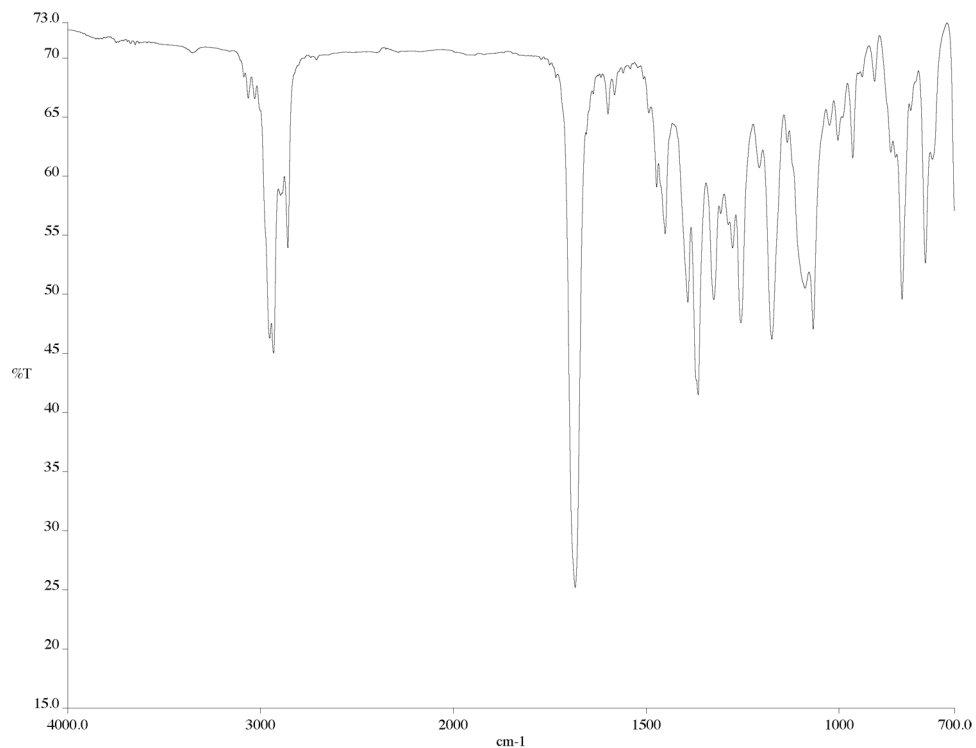


Figure A3.65 Infrared spectrum (thin film/NaCl) of compound (±)-203.

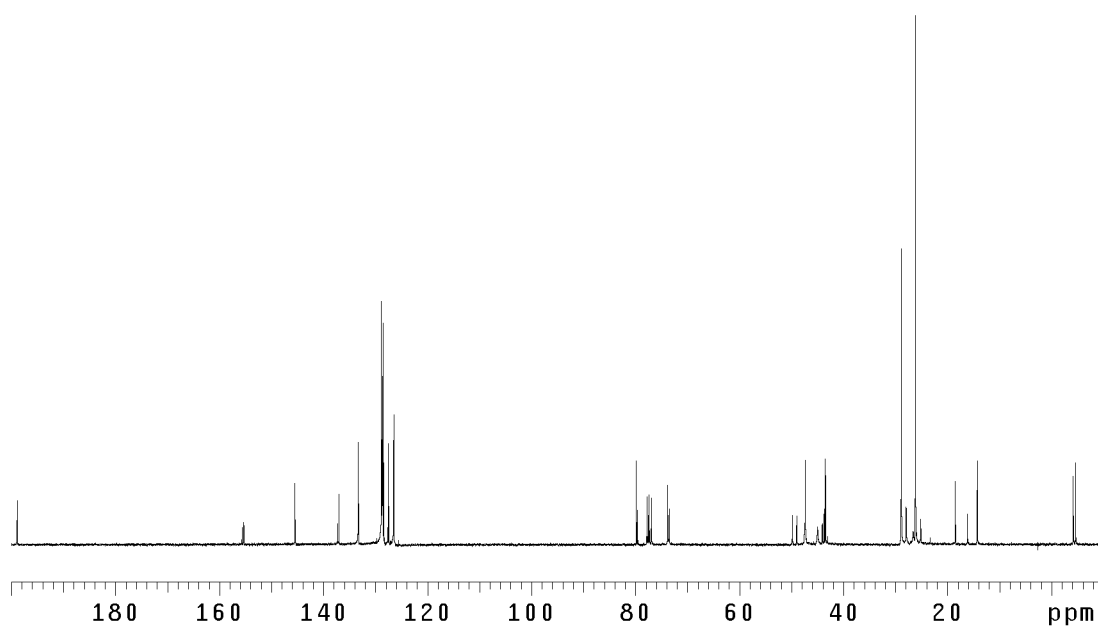
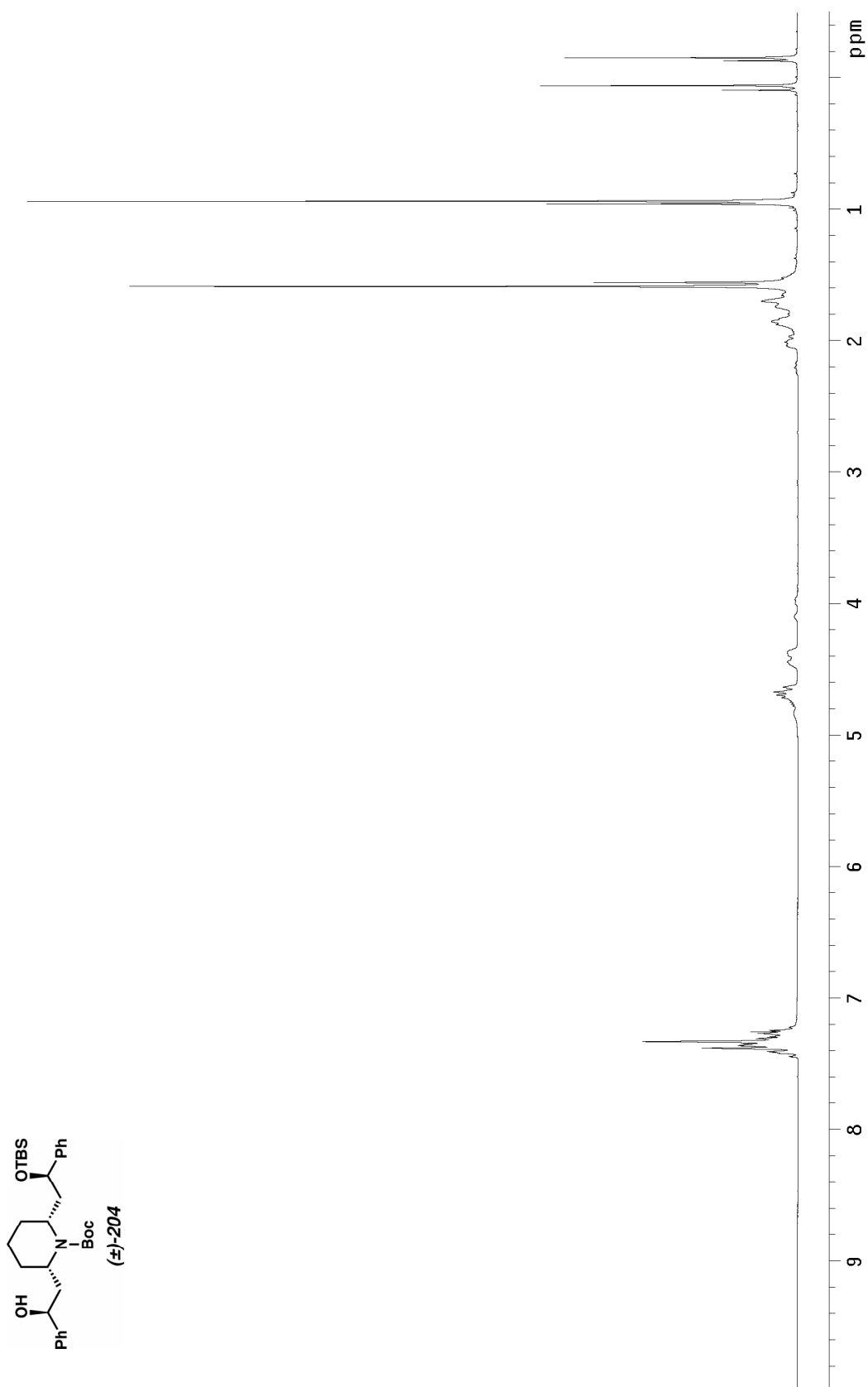


Figure A3.66 ¹³CNMR (125 MHz, CDCl₃) of compound (±)-203.



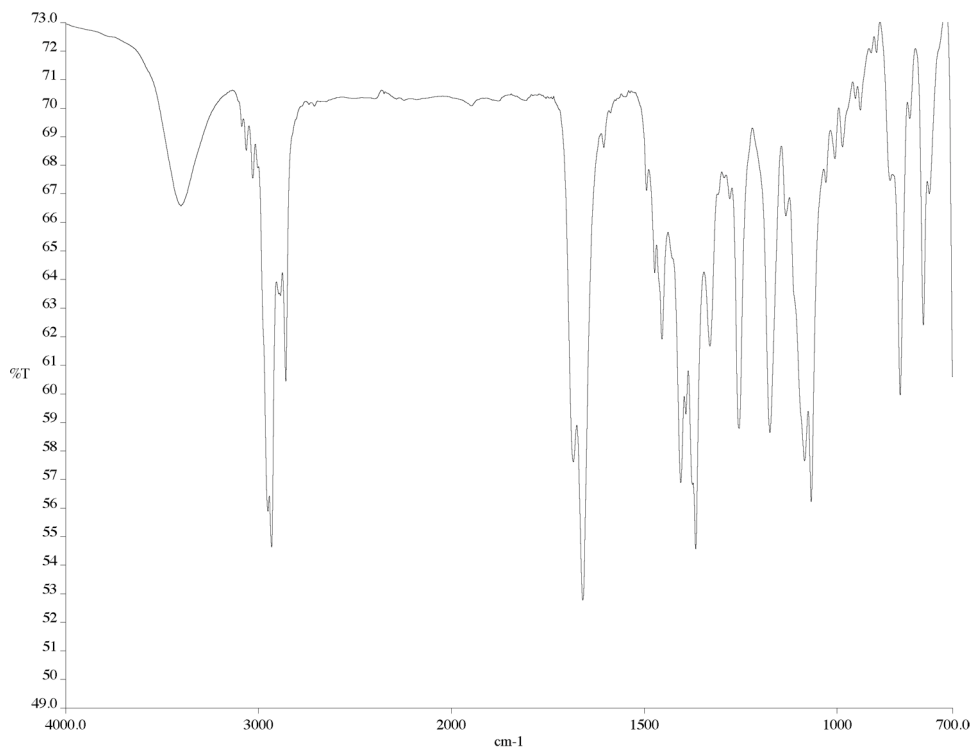


Figure A3.68 Infrared spectrum (thin film/NaCl) of compound (±)-204.

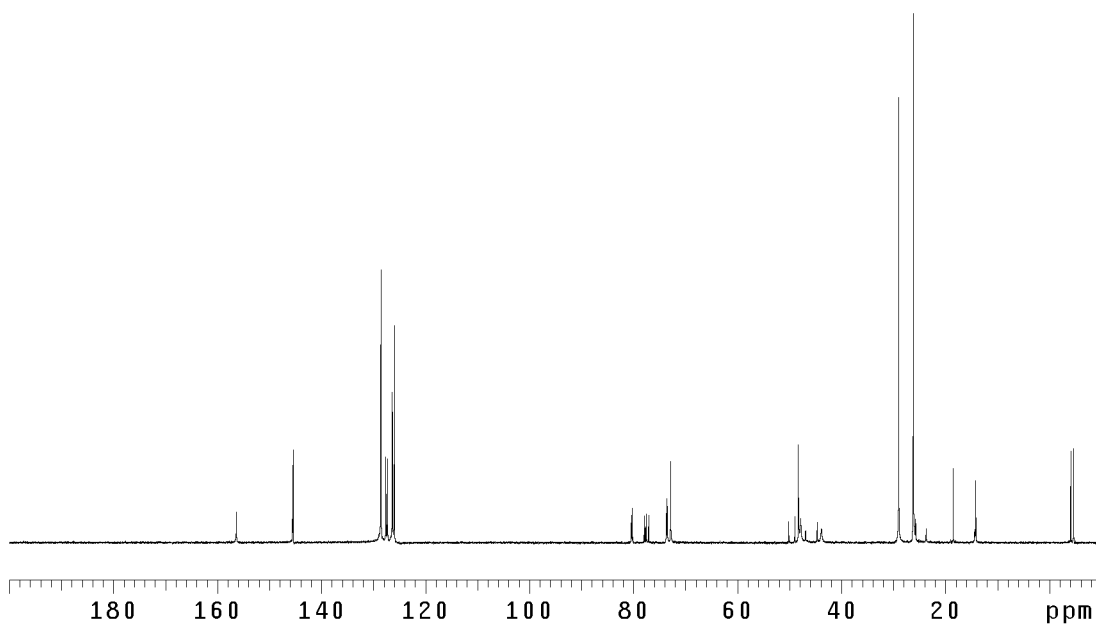


Figure A3.69 ¹³CNMR (125 MHz, CDCl₃) of compound (±)-204.

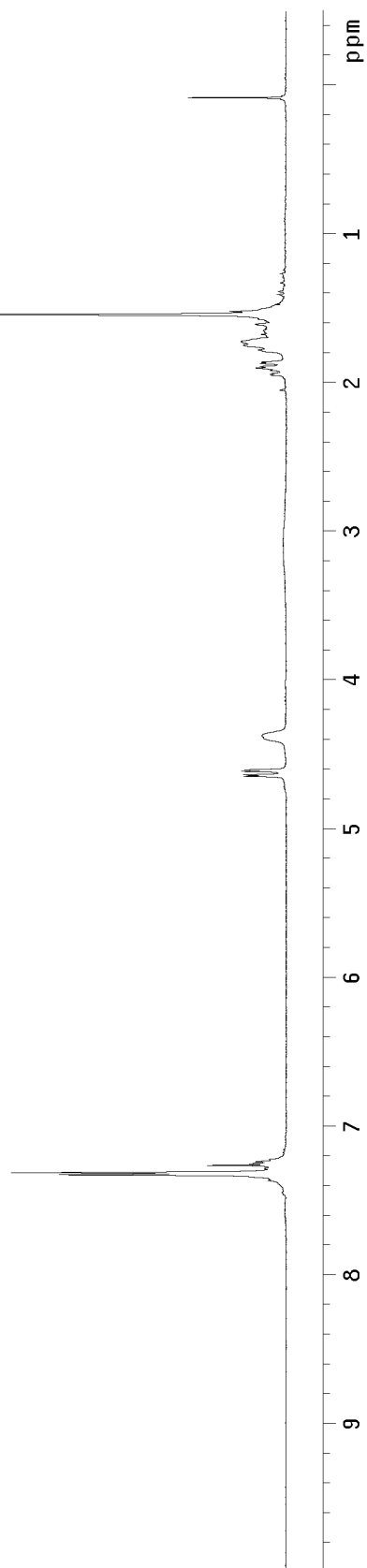
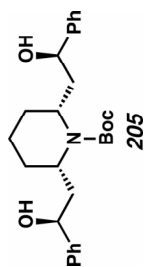


Figure A3.70 ^1H NMR (300 MHz, CDCl_3) of compound **205**.

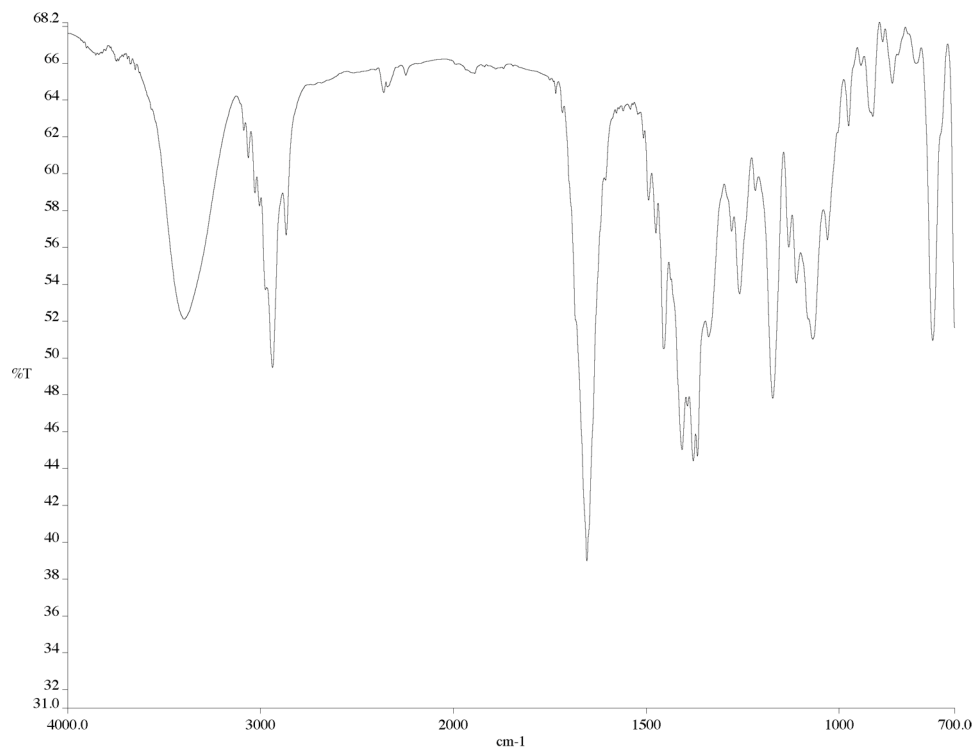


Figure A3.71 Infrared spectrum (thin film/NaCl) of compound **205**.

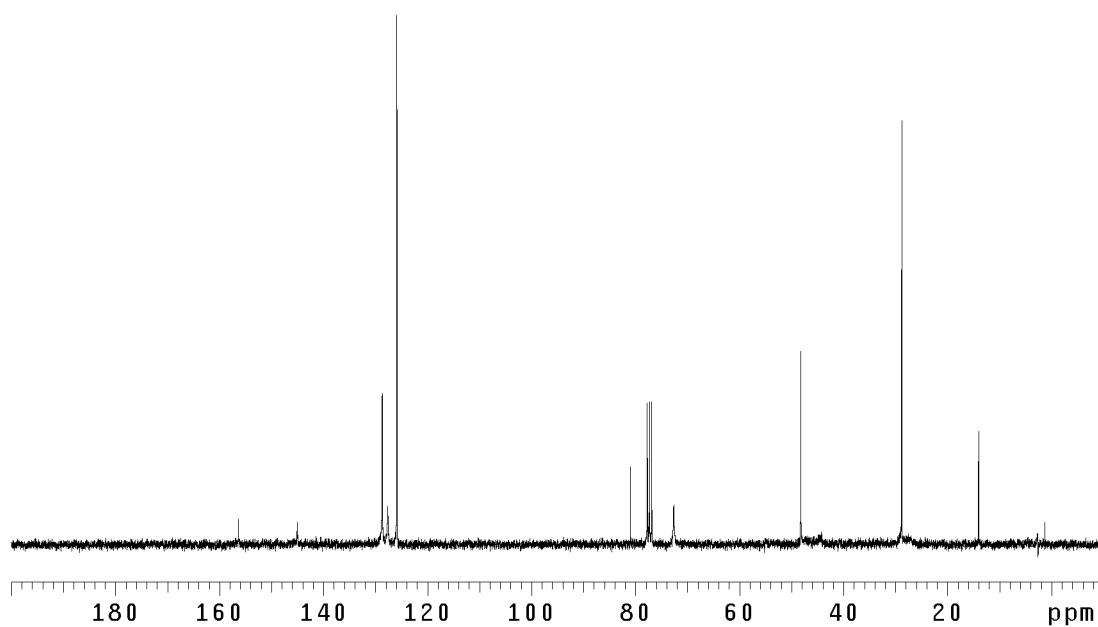


Figure A3.72 ¹³CNMR (125 MHz, CDCl₃) of compound **205**.

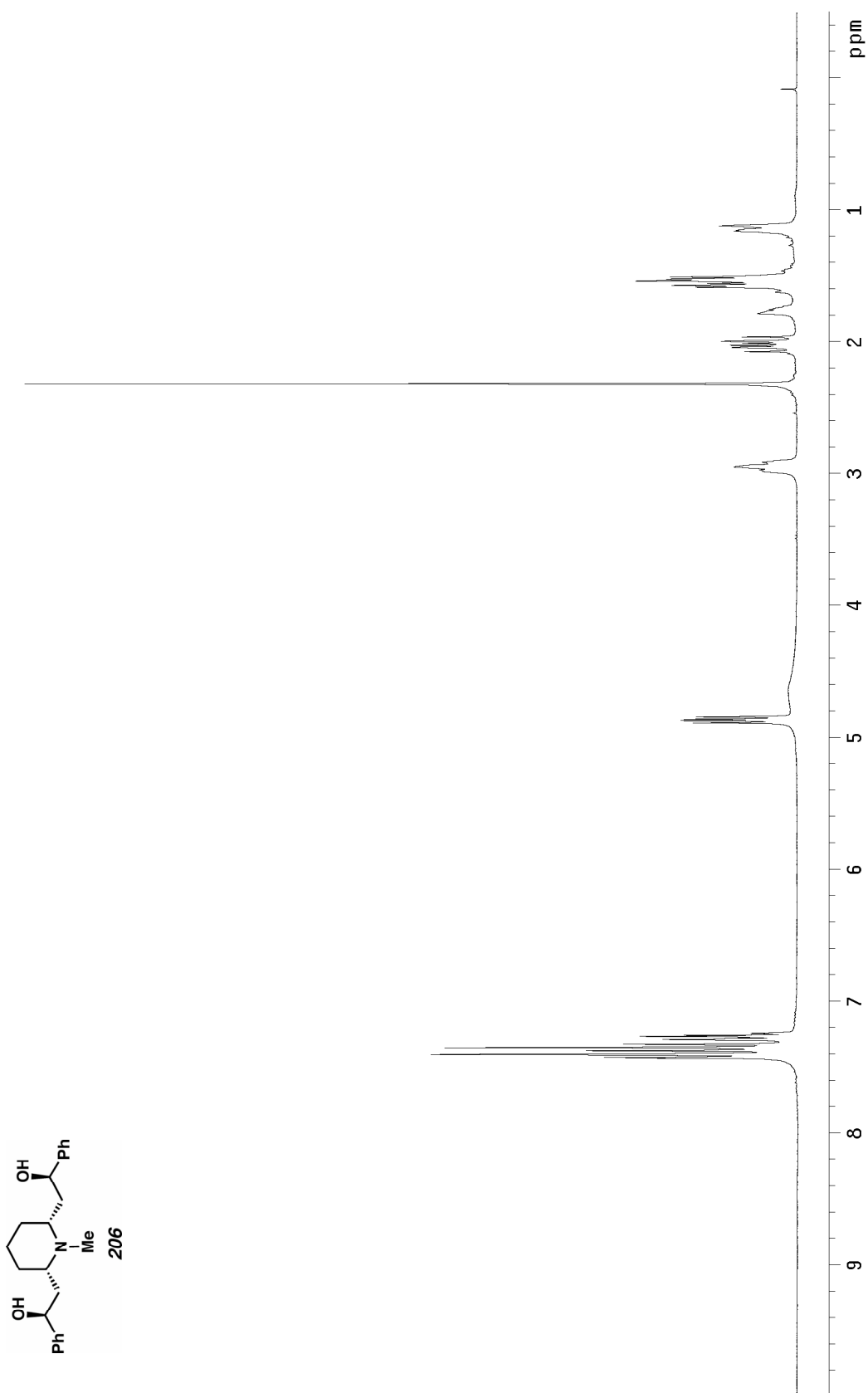


Figure A3.73 ^1H NMR (300 MHz, CDCl_3) of compound **206**.

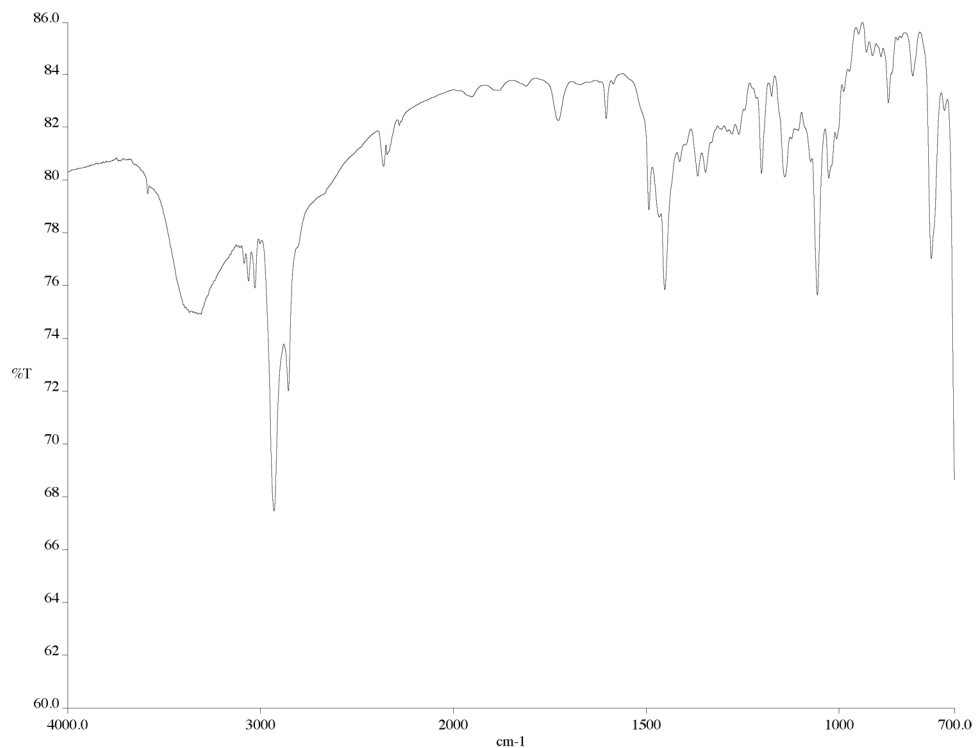


Figure A3.74 Infrared spectrum (thin film/NaCl) of compound **206**.

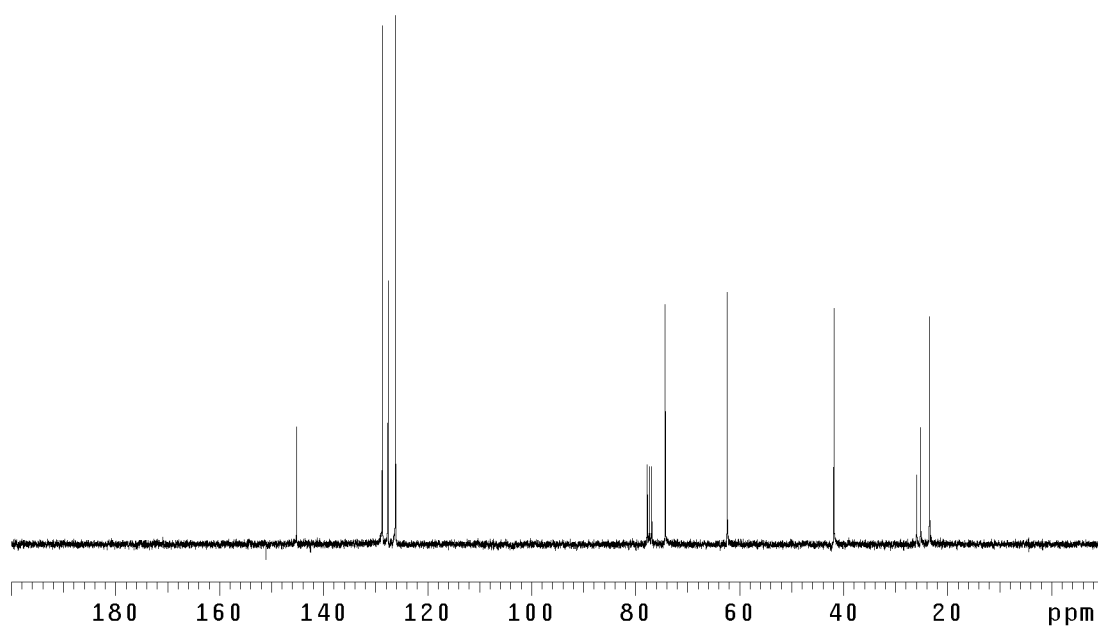


Figure A3.75 ¹³CNMR (125 MHz, CDCl₃) of compound **206**.

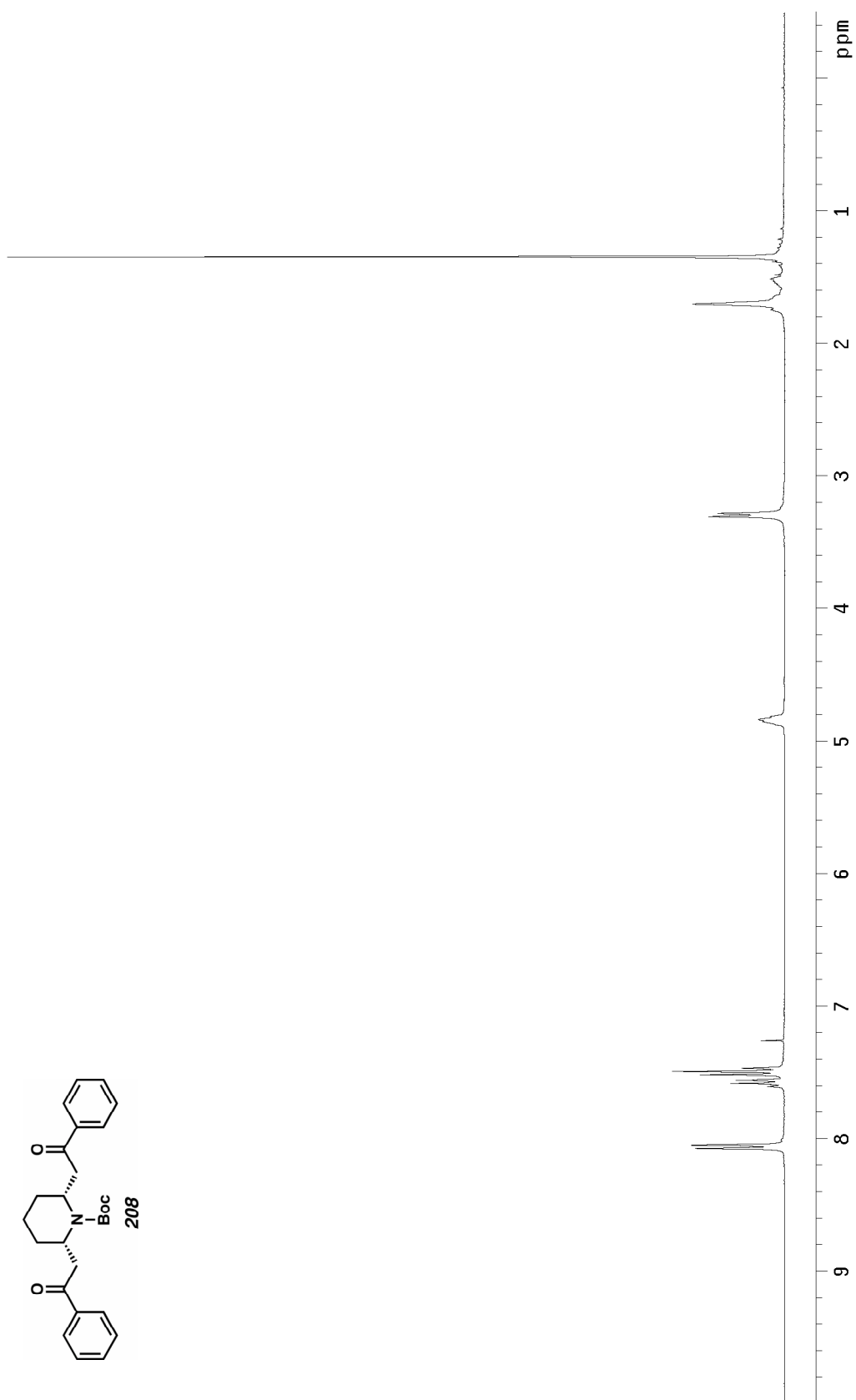


Figure A3.76 ^1H NMR (300 MHz, CDCl_3) of compound **208**.

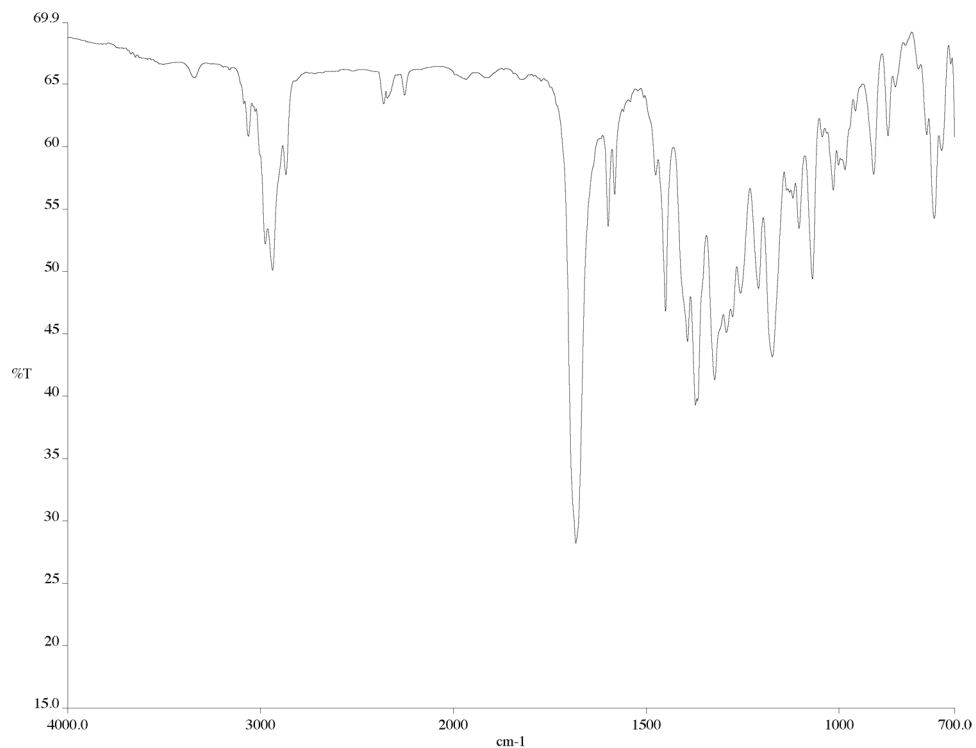


Figure A3.77 Infrared spectrum (thin film/NaCl) of compound **208**.

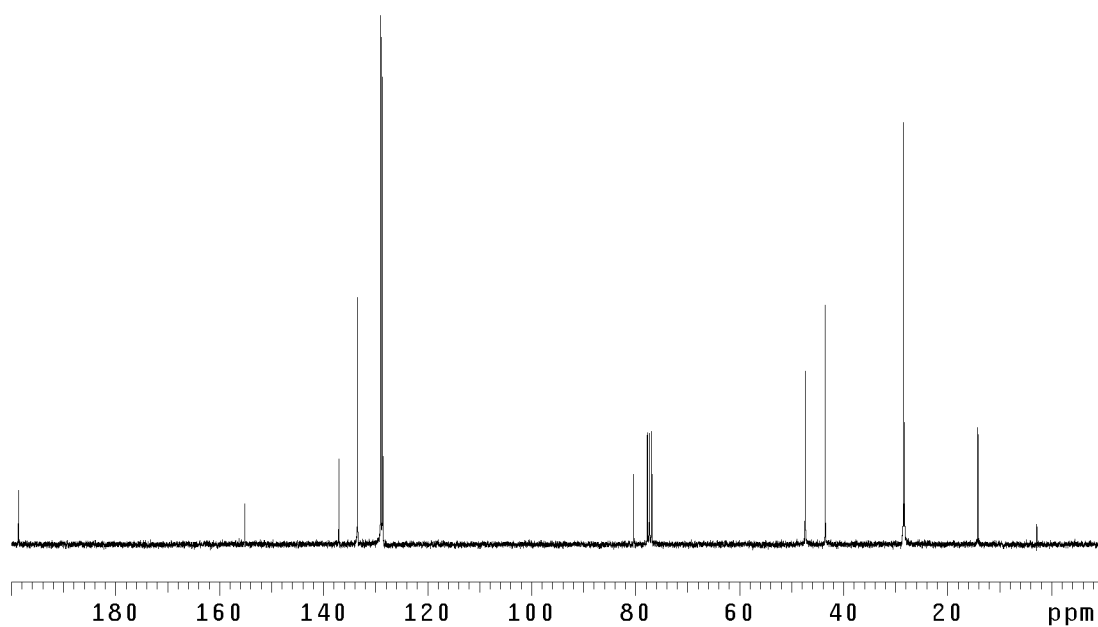


Figure A3.78 ¹³CNMR (125 MHz, CDCl₃) of compound **208**.

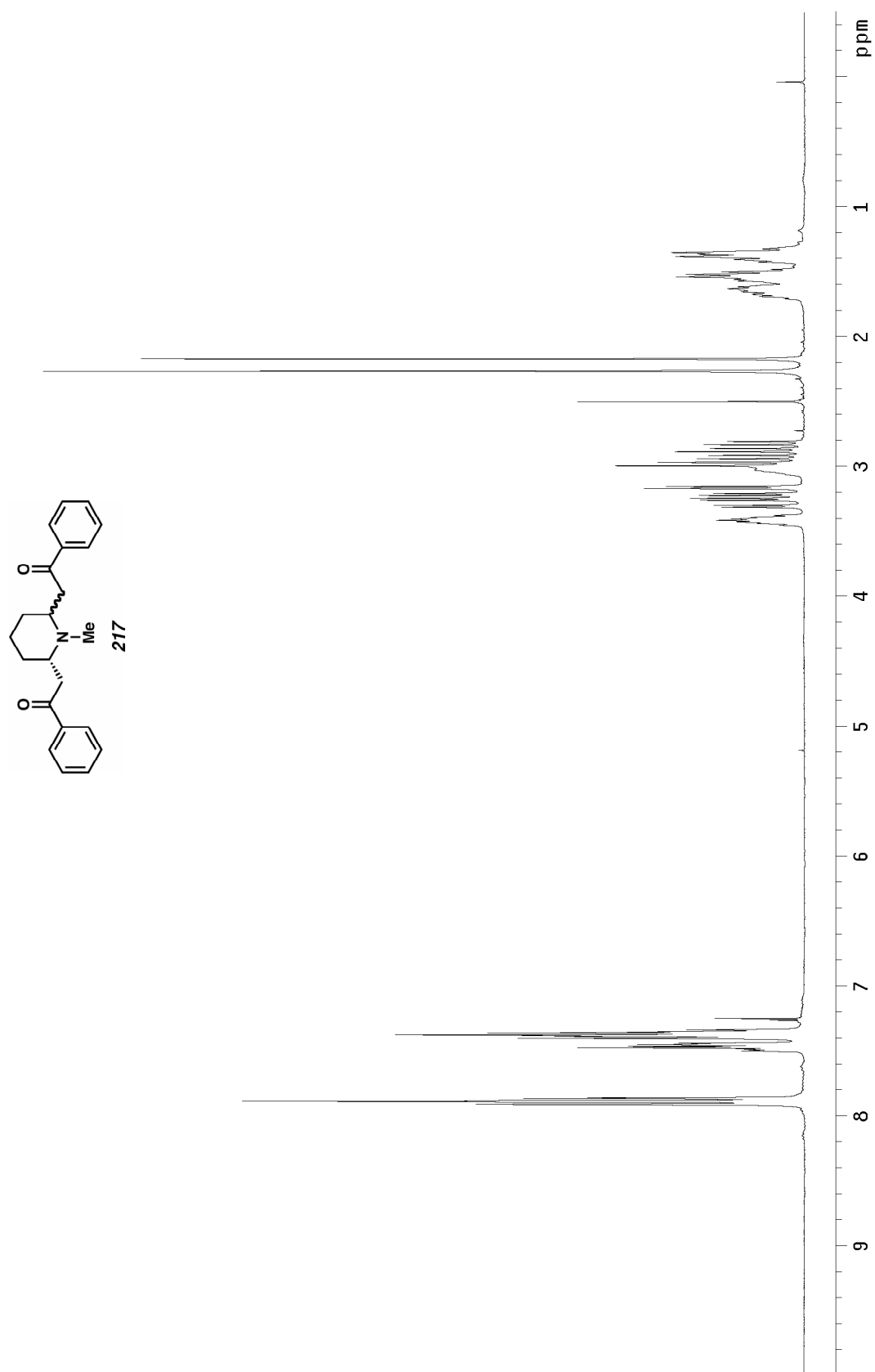


Figure A3.79 ¹H NMR (300 MHz, CDCl₃) of compound **217**.

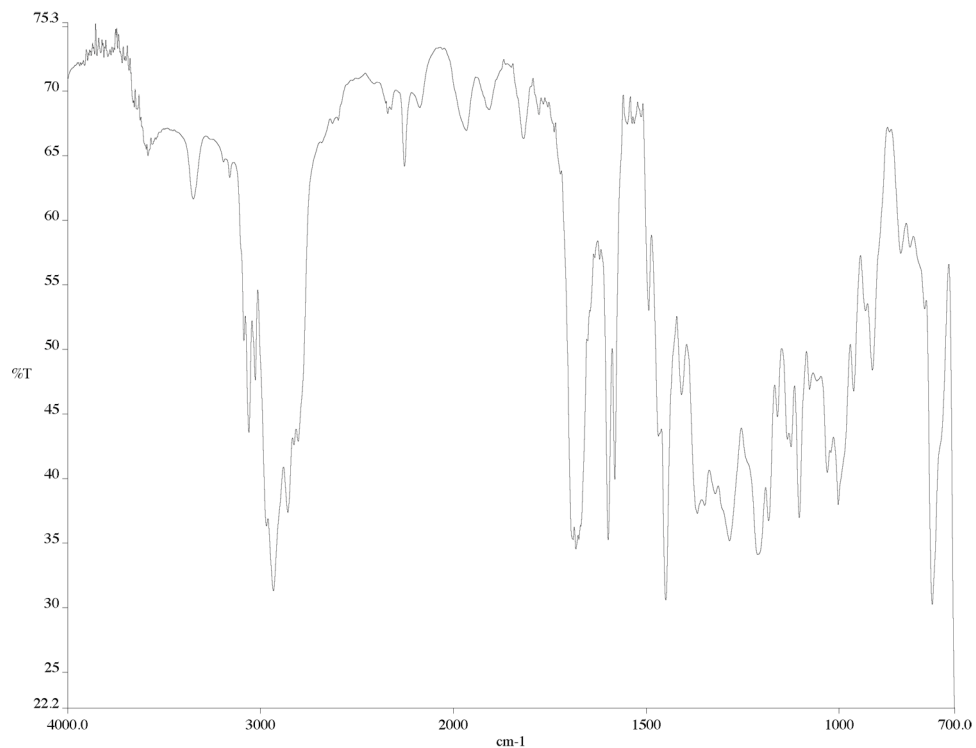


Figure A3.80 Infrared spectrum (thin film/NaCl) of compound **217**.

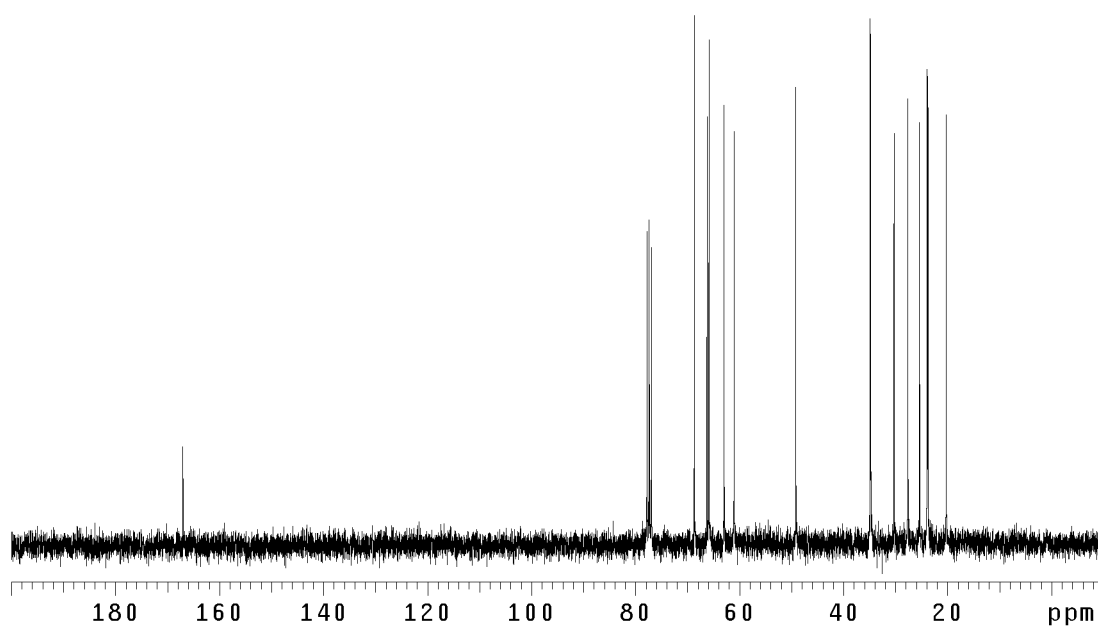


Figure A3.81 ¹³CNMR (125 MHz, CDCl₃) of compound **217**.

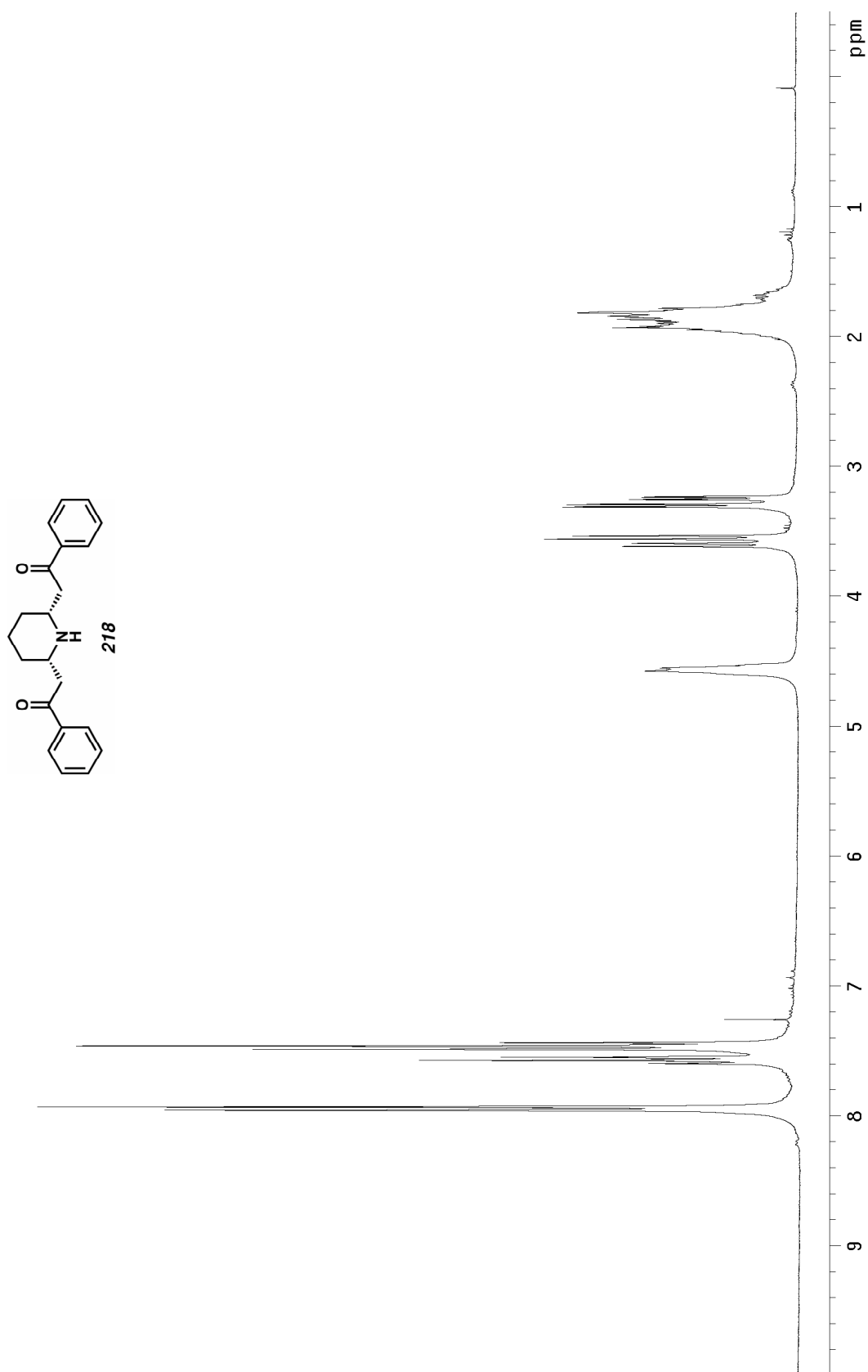


Figure A3.82 ^1H NMR (300 MHz, CDCl_3) of compound **218**.

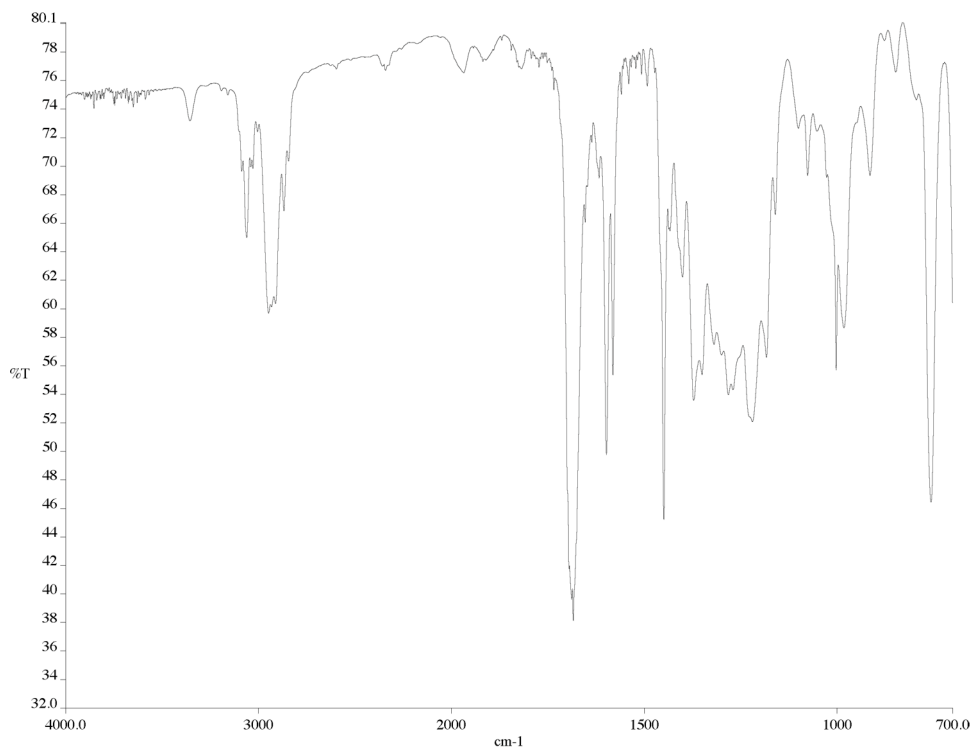


Figure A3.83 Infrared spectrum (thin film/NaCl) of compound **218**.

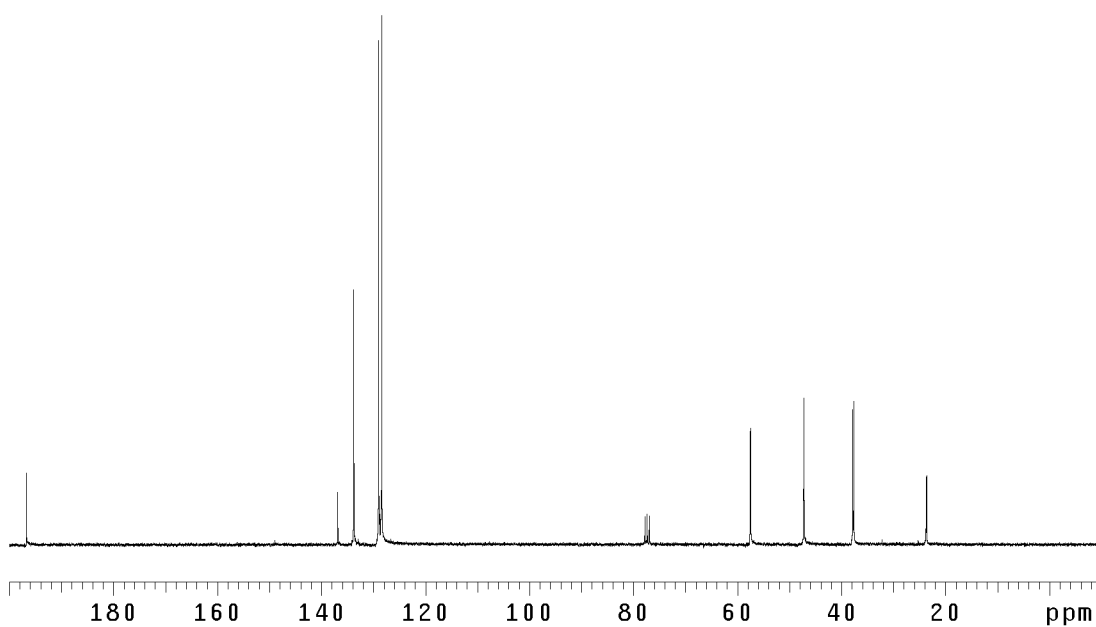


Figure A3.84 ¹³C NMR (125 MHz, CDCl₃) of compound **218**.

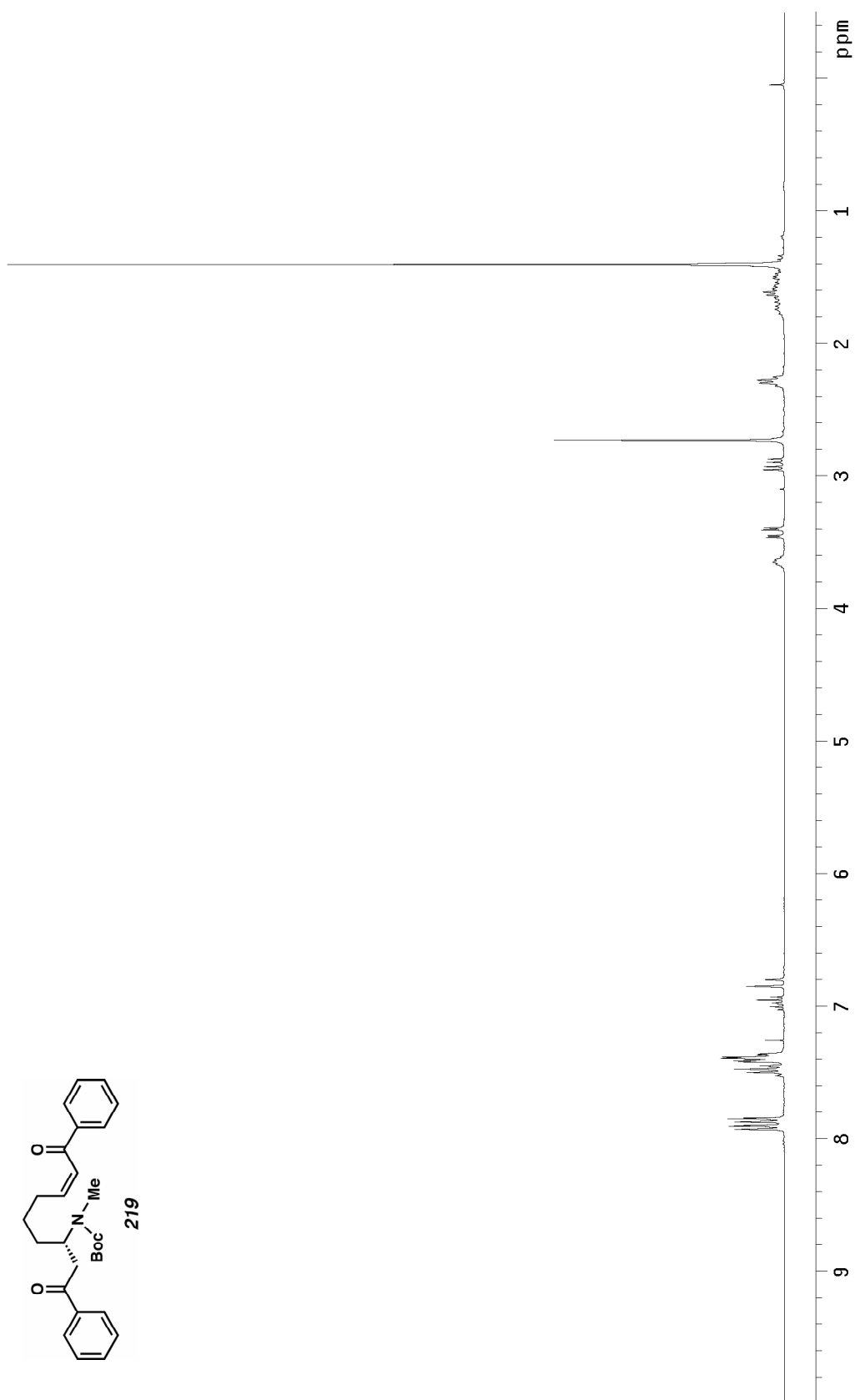


Figure A3.85 ^1H NMR (300 MHz, CDCl_3) of compound **219**.

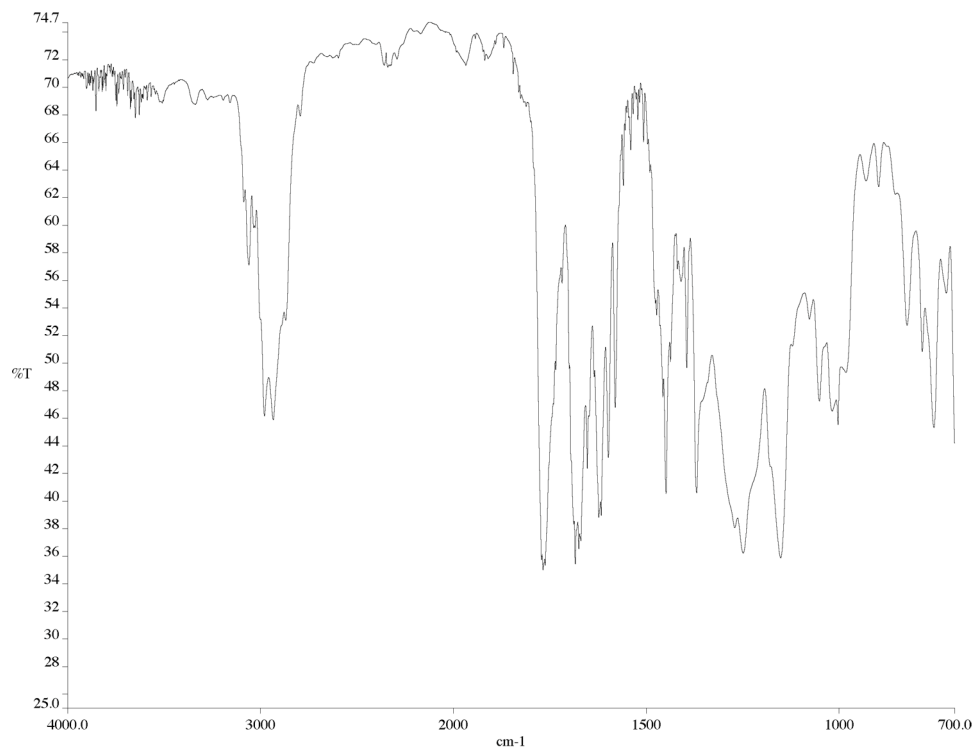


Figure A3.86 Infrared spectrum (thin film/NaCl) of compound **219**.

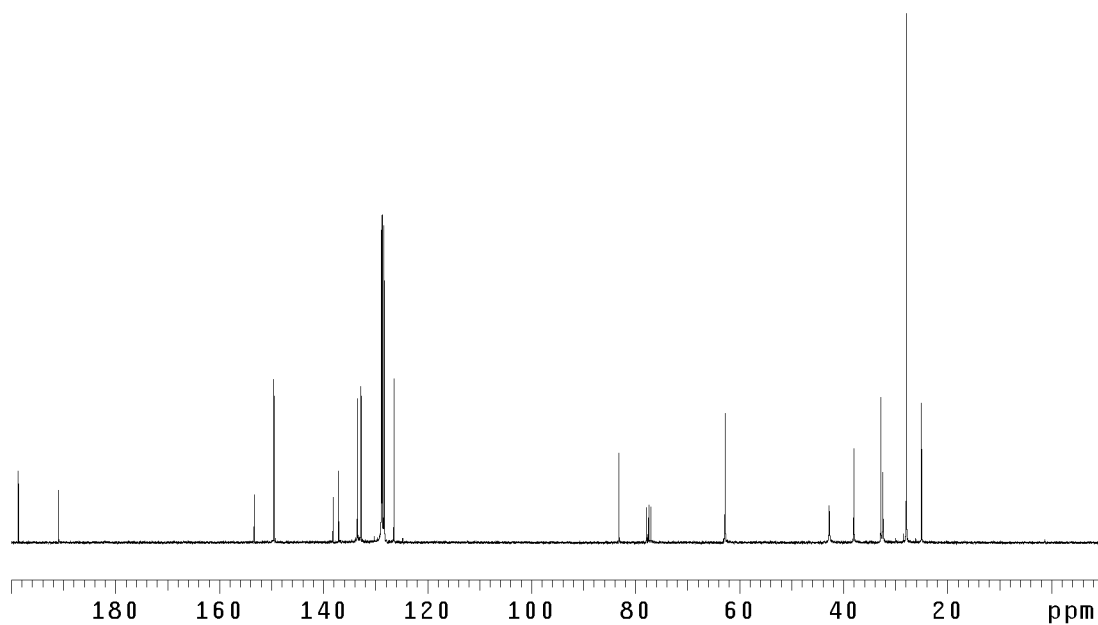


Figure A3.87 ¹³C NMR (125 MHz, CDCl₃) of compound **219**.

X-RAY CRYSTAL STRUCTURE 5:

(*R*)-2-((2*R*,6*S*)-6-((*S*)-2-hydroxy-2-phenylethyl)-1-methylpiperidin-2-yl)-1-phenylethanol:
***meso*-hydrolobeline**

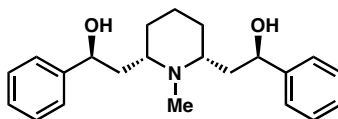
Contents

Table 1.	Crystal data
Figures	Figures
Table 2.	Atomic coordinates
Table 3.	Full bond distances and angles
Table 4.	Anisotropic displacement parameters
Table 5.	Hydrogen bond distances and angles
Table 6.	Observed and calculated structure factors (available upon request)

Table 1. Crystal data and structure refinement for JTB03 (CCDC 269741).

Empirical formula	C ₂₂ H ₂₉ NO ₂	
Formula weight	339.46	
Crystal Habit	Needle	
Crystal size	0.44 x 0.11 x 0.07 mm ³	
Crystal color	Colorless	
Data Collection		
Type of diffractometer	Bruker SMART 1000	
Wavelength	0.71073 Å MoKα	
Data Collection Temperature	100(2) K	
θ range for 4480 reflections used in lattice determination	2.35 to 25.81°	
Unit cell dimensions	a = 18.1917(12) Å b = 8.8565(6) Å c = 24.6411(17) Å	β= 107.826(3)°
Volume	3779.4(4) Å ³	
Z	8	
Crystal system	Monoclinic	
Space group	P2 ₁ /c	
Density (calculated)	1.193 Mg/m ³	
F(000)	1472	
Data collection program	Bruker SMART v5.630	
θ range for data collection	1.18 to 26.20°	
Completeness to θ = 26.20°	91.1 %	
Index ranges	-21 ≤ h ≤ 21, -10 ≤ k ≤ 10, -30 ≤ l ≤ 26	
Data collection scan type	ω scans at 3 φ settings	
Data reduction program	Bruker SAINT v6.45A	
Reflections collected	25316	
Independent reflections	6904 [R _{int} = 0.1374]	
Absorption coefficient	0.075 mm ⁻¹	
Absorption correction	None	
Max. and min. transmission	0.9947 and 0.9676	

Table 1 (cont.)**Structure solution and Refinement**

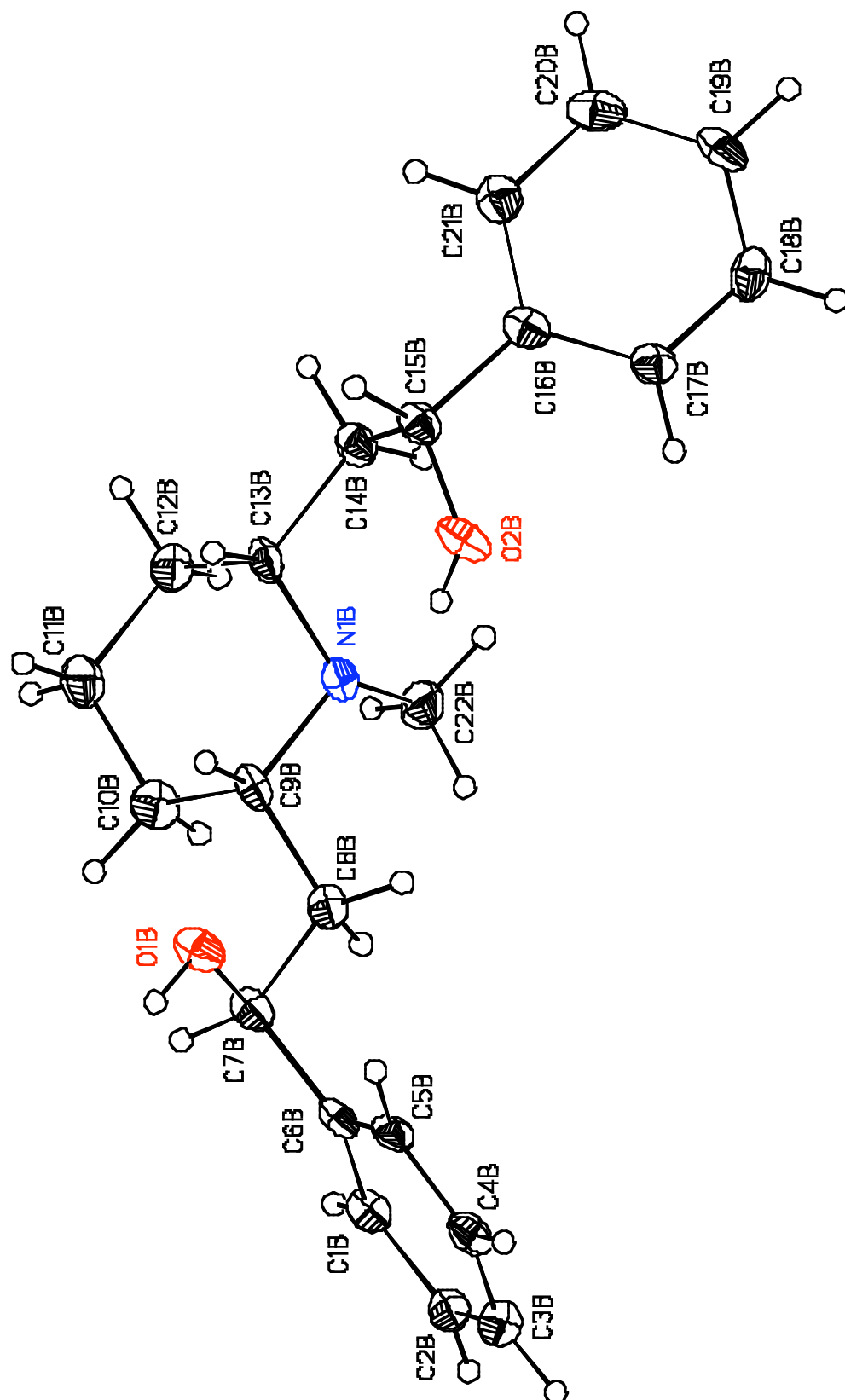
Structure solution program	Bruker XS v6.12
Primary solution method	Direct methods
Secondary solution method	Difference Fourier map
Hydrogen placement	Geometric positions
Structure refinement program	Bruker XL v6.12
Refinement method	Full matrix least-squares on F^2
Data / restraints / parameters	6904 / 0 / 453
Treatment of hydrogen atoms	Riding
Goodness-of-fit on F^2	1.429
Final R indices [$I > 2\sigma(I)$, 3276 reflections]	$R1 = 0.0814$, $wR2 = 0.1171$
R indices (all data)	$R1 = 0.1710$, $wR2 = 0.1283$
Type of weighting scheme used	Sigma
Weighting scheme used	$w = 1/\sigma^2(F_o^2)$
Max shift/error	0.000
Average shift/error	0.000
Largest diff. peak and hole	0.304 and -0.447 e. \AA^{-3}

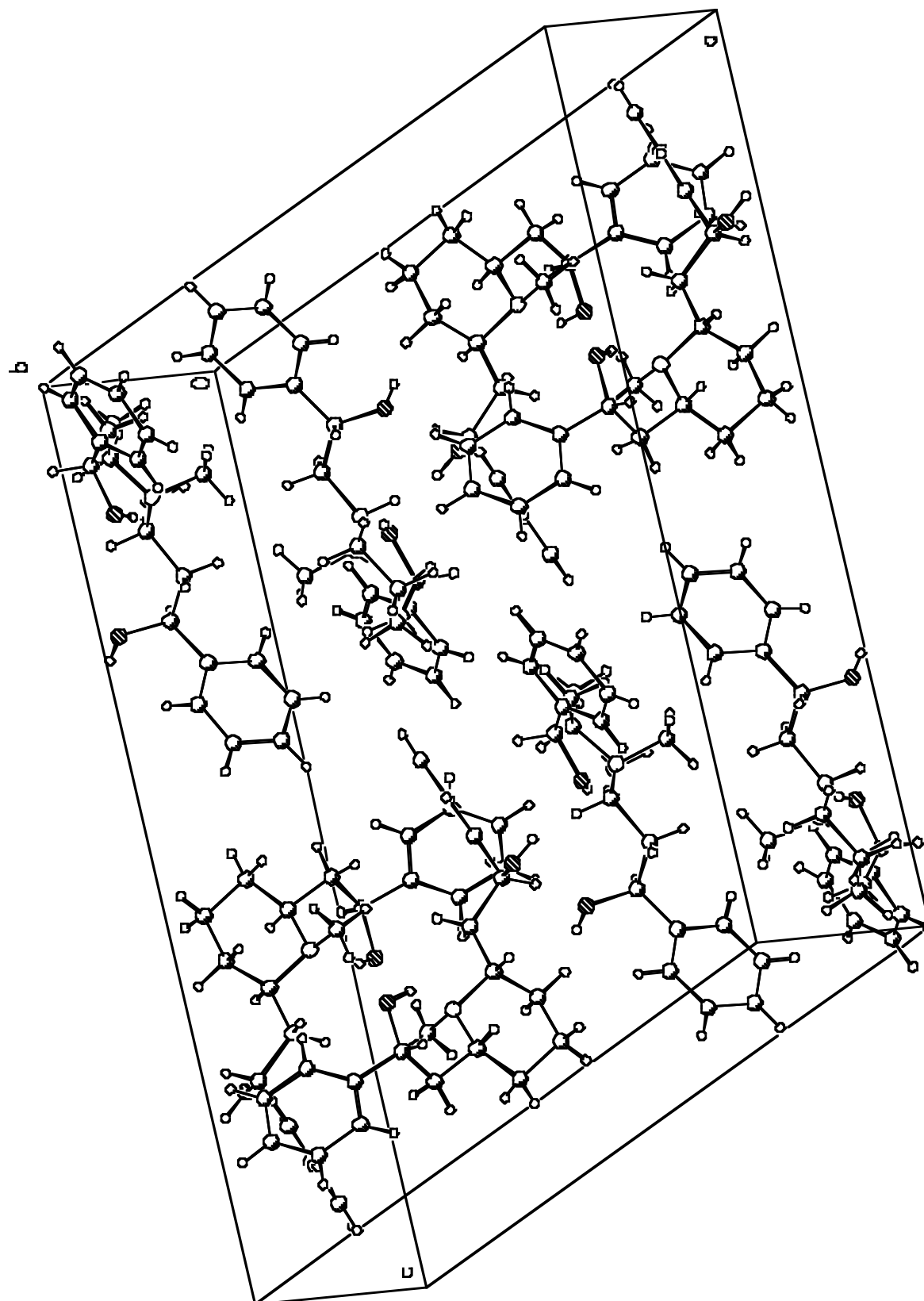
Special Refinement Details

The data for this crystal were very weak with less than 50% of the measured intensities exceeding the 2σ level. However, all hydrogen atoms appeared as the most intense features of the difference electron density map calculated with heavy atoms only. Hydrogen atoms were placed consistent with the map and refined as riding atoms (with idealized geometry) during least-squares refinement. Of particular interest is the intramolecular hydrogen bond formed between the hydrogen on O2 and N1. Formation of an intermolecular hydrogen bond at this site is inconsistent with data and produces impossibly close contacts between molecules. Therefore, O2 acts as a donor in the intramolecular hydrogen bond to N1 and an acceptor in the intermolecular hydrogen with O1 (see Table 5).

Refinement of F^2 against ALL reflections. The weighted R-factor (wR) and goodness of fit (S) are based on F^2 , conventional R-factors (R) are based on F , with F set to zero for negative F^2 . The threshold expression of $F^2 > 2\sigma(F^2)$ is used only for calculating R-factors(gt), etc., and is not relevant to the choice of reflections for refinement. R-factors based on F^2 are statistically about twice as large as those based on F , and R-factors based on ALL data will be even larger.

All esds (except the esd in the dihedral angle between two l.s. planes) are estimated using the full covariance matrix. The cell esds are taken into account individually in the estimation of esds in distances, angles and torsion angles; correlations between esds in cell parameters are only used when they are defined by crystal symmetry. An approximate (isotropic) treatment of cell esds is used for estimating esds involving l.s. planes.





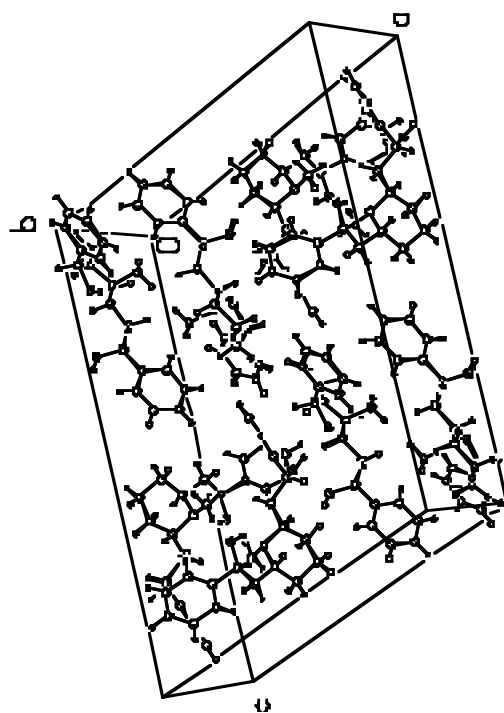
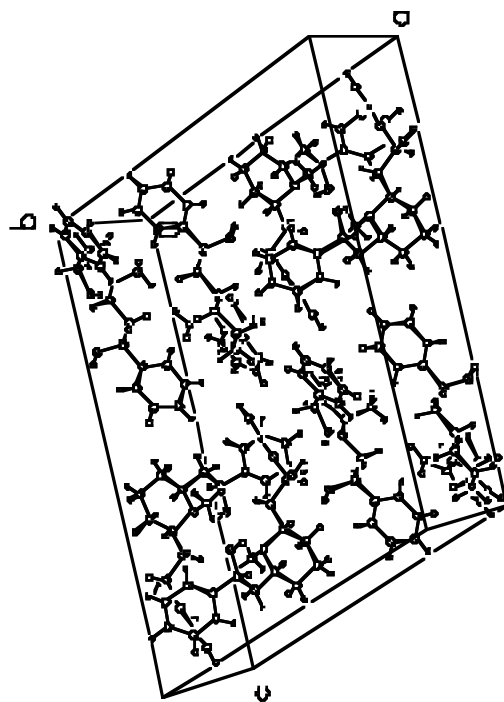


Table 2. Atomic coordinates ($\times 10^4$) and equivalent isotropic displacement parameters ($\text{\AA}^2 \times 10^3$) for JTB03 (CCDC 269741). U_{eq} is defined as the trace of the orthogonalized U^{ij} tensor.

	x	y	z	U_{eq}
O(1A)	5202(2)	8135(3)	2305(1)	22(1)
O(2A)	3653(2)	4333(3)	3134(1)	23(1)
N(1A)	3881(2)	7265(3)	3355(1)	17(1)
C(1A)	3788(2)	10989(4)	1490(2)	20(1)
C(2A)	3386(2)	11328(4)	928(2)	20(1)
C(3A)	3386(2)	10331(4)	493(2)	21(1)
C(4A)	3791(2)	8978(5)	628(2)	20(1)
C(5A)	4194(2)	8652(4)	1193(2)	18(1)
C(6A)	4208(2)	9646(4)	1629(2)	16(1)
C(7A)	4629(2)	9284(4)	2243(2)	16(1)
C(8A)	4056(2)	8722(4)	2541(2)	18(1)
C(9A)	4411(2)	8294(4)	3170(2)	15(1)
C(10A)	4659(2)	9651(4)	3571(2)	25(1)
C(11A)	5026(2)	9139(4)	4188(2)	25(1)
C(12A)	4521(2)	7973(4)	4376(2)	23(1)
C(13A)	4301(2)	6699(4)	3936(2)	20(1)
C(14A)	3843(2)	5399(4)	4088(2)	21(1)
C(15A)	3818(2)	3994(4)	3721(2)	18(1)
C(16A)	3242(2)	2838(4)	3806(2)	18(1)
C(17A)	3403(2)	2090(4)	4325(2)	21(1)
C(18A)	2867(2)	1088(4)	4429(2)	26(1)
C(19A)	2180(3)	826(4)	4009(2)	29(1)
C(20A)	2021(2)	1536(4)	3489(2)	27(1)
C(21A)	2556(2)	2551(4)	3388(2)	21(1)
C(22A)	3136(2)	7975(5)	3322(2)	25(1)
O(1B)	-236(2)	8086(3)	2650(1)	23(1)
O(2B)	1339(2)	11950(3)	1875(1)	24(1)
N(1B)	1148(2)	9012(4)	1656(1)	20(1)
C(1B)	1194(2)	5341(4)	3534(2)	19(1)
C(2B)	1570(2)	5082(4)	4104(2)	21(1)
C(3B)	1523(2)	6094(5)	4517(2)	27(1)
C(4B)	1089(2)	7408(4)	4352(2)	22(1)
C(5B)	727(2)	7684(4)	3783(2)	18(1)
C(6B)	756(2)	6679(4)	3361(2)	17(1)
C(7B)	361(2)	6970(4)	2741(2)	19(1)
C(8B)	947(2)	7579(4)	2464(2)	19(1)
C(9B)	616(2)	8002(4)	1839(2)	18(1)
C(10B)	379(2)	6655(4)	1436(2)	24(1)
C(11B)	44(2)	7143(5)	813(2)	25(1)
C(12B)	557(2)	8299(4)	641(2)	23(1)
C(13B)	760(2)	9576(4)	1072(2)	20(1)
C(14B)	1236(2)	10882(4)	932(2)	20(1)
C(15B)	1218(2)	12304(4)	1291(2)	21(1)
C(16B)	1817(2)	13457(4)	1240(2)	20(1)
C(17B)	2481(2)	13750(4)	1686(2)	20(1)
C(18B)	3029(2)	14769(4)	1616(2)	24(1)

C(19B)	2918(2)	15495(4)	1108(2)	25(1)
C(20B)	2256(2)	15235(4)	661(2)	26(1)
C(21B)	1708(2)	14226(4)	725(2)	24(1)
C(22B)	1902(2)	8306(5)	1717(2)	28(1)

Table 3. Bond lengths [Å] and angles [°] for JTB03 (CCDC 269741).

O(1A)-C(7A)	1.432(4)	C(18B)-C(19B)	1.367(5)
O(2A)-C(15A)	1.418(4)	C(19B)-C(20B)	1.379(5)
N(1A)-C(22A)	1.474(5)	C(20B)-C(21B)	1.384(6)
N(1A)-C(13A)	1.488(4)		
N(1A)-C(9A)	1.496(5)	C(22A)-N(1A)-C(13A)	113.0(3)
C(1A)-C(2A)	1.385(5)	C(22A)-N(1A)-C(9A)	113.0(3)
C(1A)-C(6A)	1.399(5)	C(13A)-N(1A)-C(9A)	108.0(3)
C(2A)-C(3A)	1.388(5)	C(2A)-C(1A)-C(6A)	120.8(4)
C(3A)-C(4A)	1.393(5)	C(1A)-C(2A)-C(3A)	120.6(4)
C(4A)-C(5A)	1.390(5)	C(2A)-C(3A)-C(4A)	119.2(4)
C(5A)-C(6A)	1.384(5)	C(5A)-C(4A)-C(3A)	119.7(4)
C(6A)-C(7A)	1.506(5)	C(6A)-C(5A)-C(4A)	121.6(4)
C(7A)-C(8A)	1.531(5)	C(5A)-C(6A)-C(1A)	118.1(4)
C(8A)-C(9A)	1.533(5)	C(5A)-C(6A)-C(7A)	121.9(3)
C(9A)-C(10A)	1.533(5)	C(1A)-C(6A)-C(7A)	120.0(4)
C(10A)-C(11A)	1.529(5)	O(1A)-C(7A)-C(6A)	112.8(3)
C(11A)-C(12A)	1.544(5)	O(1A)-C(7A)-C(8A)	107.4(3)
C(12A)-C(13A)	1.531(5)	C(6A)-C(7A)-C(8A)	109.9(3)
C(13A)-C(14A)	1.533(5)	C(9A)-C(8A)-C(7A)	115.3(3)
C(14A)-C(15A)	1.531(5)	N(1A)-C(9A)-C(10A)	111.7(3)
C(15A)-C(16A)	1.525(5)	N(1A)-C(9A)-C(8A)	110.3(3)
C(16A)-C(21A)	1.377(5)	C(10A)-C(9A)-C(8A)	114.0(3)
C(16A)-C(17A)	1.390(5)	C(11A)-C(10A)-C(9A)	111.2(3)
C(17A)-C(18A)	1.399(6)	C(10A)-C(11A)-C(12A)	112.2(3)
C(18A)-C(19A)	1.376(5)	C(13A)-C(12A)-C(11A)	109.3(3)
C(19A)-C(20A)	1.377(5)	N(1A)-C(13A)-C(14A)	109.3(3)
C(20A)-C(21A)	1.401(6)	N(1A)-C(13A)-C(12A)	112.3(3)
O(2B)-C(15B)	1.422(4)	C(14A)-C(13A)-C(12A)	115.1(3)
O(1B)-C(7B)	1.435(4)	C(13A)-C(14A)-C(15A)	112.7(3)
N(1B)-C(22B)	1.472(5)	O(2A)-C(15A)-C(16A)	110.0(3)
N(1B)-C(9B)	1.487(5)	O(2A)-C(15A)-C(14A)	112.9(3)
N(1B)-C(13B)	1.482(5)	C(16A)-C(15A)-C(14A)	111.3(3)
C(1B)-C(2B)	1.381(5)	C(21A)-C(16A)-C(17A)	119.2(4)
C(1B)-C(6B)	1.419(5)	C(21A)-C(16A)-C(15A)	121.7(3)
C(2B)-C(3B)	1.378(5)	C(17A)-C(16A)-C(15A)	119.1(4)
C(3B)-C(4B)	1.396(5)	C(18A)-C(17A)-C(16A)	120.6(4)
C(4B)-C(5B)	1.376(5)	C(19A)-C(18A)-C(17A)	119.5(4)
C(5B)-C(6B)	1.382(5)	C(20A)-C(19A)-C(18A)	120.4(4)
C(6B)-C(7B)	1.498(5)	C(19A)-C(20A)-C(21A)	119.9(4)
C(7B)-C(8B)	1.530(5)	C(16A)-C(21A)-C(20A)	120.3(4)
C(8B)-C(9B)	1.517(5)	C(22B)-N(1B)-C(9B)	112.7(3)
C(9B)-C(10B)	1.528(5)	C(22B)-N(1B)-C(13B)	113.2(3)
C(10B)-C(11B)	1.532(5)	C(9B)-N(1B)-C(13B)	109.6(3)
C(11B)-C(12B)	1.530(6)	C(2B)-C(1B)-C(6B)	120.2(4)
C(12B)-C(13B)	1.517(5)	C(1B)-C(2B)-C(3B)	121.3(4)
C(13B)-C(14B)	1.546(5)	C(2B)-C(3B)-C(4B)	119.0(4)
C(14B)-C(15B)	1.545(5)	C(5B)-C(4B)-C(3B)	119.8(4)
C(15B)-C(16B)	1.525(5)	C(4B)-C(5B)-C(6B)	122.4(4)
C(16B)-C(17B)	1.386(5)	C(5B)-C(6B)-C(1B)	117.3(4)
C(16B)-C(21B)	1.399(5)	C(5B)-C(6B)-C(7B)	122.7(3)
C(17B)-C(18B)	1.394(6)	C(1B)-C(6B)-C(7B)	120.0(3)

O(1B)-C(7B)-C(6B)	112.4(3)
O(1B)-C(7B)-C(8B)	106.6(3)
C(6B)-C(7B)-C(8B)	109.5(3)
C(9B)-C(8B)-C(7B)	115.1(3)
N(1B)-C(9B)-C(8B)	111.2(3)
N(1B)-C(9B)-C(10B)	110.7(3)
C(8B)-C(9B)-C(10B)	114.3(3)
C(9B)-C(10B)-C(11B)	112.2(3)
C(12B)-C(11B)-C(10B)	112.2(3)
C(13B)-C(12B)-C(11B)	110.1(3)
N(1B)-C(13B)-C(12B)	111.7(3)
N(1B)-C(13B)-C(14B)	109.7(3)
C(12B)-C(13B)-C(14B)	115.7(3)
C(15B)-C(14B)-C(13B)	111.7(3)
O(2B)-C(15B)-C(16B)	109.7(3)
O(2B)-C(15B)-C(14B)	112.1(3)
C(16B)-C(15B)-C(14B)	111.0(3)
C(17B)-C(16B)-C(21B)	118.3(4)
C(17B)-C(16B)-C(15B)	122.1(4)
C(21B)-C(16B)-C(15B)	119.6(4)
C(16B)-C(17B)-C(18B)	120.4(4)
C(19B)-C(18B)-C(17B)	120.4(4)
C(18B)-C(19B)-C(20B)	120.1(4)
C(19B)-C(20B)-C(21B)	120.0(4)
C(20B)-C(21B)-C(16B)	120.8(4)

Table 4. Anisotropic displacement parameters ($\text{\AA}^2 \times 10^4$) for JTB03 (CCDC 269741). The anisotropic displacement factor exponent takes the form: $-2\pi^2 [h^2 a^{*2} U^{11} + \dots + 2hka^*b^*U^{12}]$

	U^{11}	U^{22}	U^{33}	U^{23}	U^{13}	U^{12}
O(1A)	185(15)	181(15)	325(17)	69(14)	133(13)	52(13)
O(2A)	287(17)	146(16)	269(17)	-40(14)	96(14)	-99(13)
N(1A)	130(18)	173(19)	220(20)	13(16)	103(15)	17(15)
C(1A)	180(20)	150(20)	290(30)	0(20)	110(20)	-63(19)
C(2A)	170(20)	160(20)	290(30)	10(20)	100(20)	-22(18)
C(3A)	200(20)	210(20)	210(20)	70(20)	48(19)	-40(20)
C(4A)	140(20)	230(30)	280(30)	-30(20)	130(20)	-62(19)
C(5A)	160(20)	130(20)	310(30)	0(20)	130(20)	-41(18)
C(6A)	130(20)	120(20)	270(20)	10(20)	118(19)	-60(18)
C(7A)	140(20)	100(20)	270(20)	6(18)	114(19)	16(17)
C(8A)	120(20)	130(20)	320(20)	-59(19)	92(19)	-25(18)
C(9A)	130(20)	110(20)	210(20)	27(18)	48(18)	-10(17)
C(10A)	290(30)	210(20)	250(30)	-20(20)	100(20)	-30(20)
C(11A)	270(20)	190(20)	330(30)	-60(20)	130(20)	-60(20)
C(12A)	250(20)	190(20)	280(20)	10(20)	110(20)	30(20)
C(13A)	220(20)	170(20)	210(20)	10(20)	68(19)	-23(19)
C(14A)	240(20)	170(20)	230(20)	0(20)	60(20)	-6(19)
C(15A)	200(20)	170(20)	190(20)	-10(20)	79(19)	-62(19)
C(16A)	170(20)	90(20)	280(30)	0(20)	90(20)	45(18)
C(17A)	140(20)	210(20)	300(30)	-20(20)	90(19)	7(19)
C(18A)	260(30)	200(20)	340(30)	60(20)	120(20)	0(20)
C(19A)	350(30)	110(20)	430(30)	0(20)	160(20)	-90(20)
C(20A)	250(20)	200(20)	350(30)	-60(20)	80(20)	-70(20)
C(21A)	270(30)	130(20)	230(20)	-26(19)	90(20)	3(19)
C(22A)	130(20)	360(30)	300(30)	80(20)	97(19)	60(20)
O(1B)	206(16)	187(16)	354(17)	45(14)	162(14)	36(13)
O(2B)	325(17)	150(16)	322(18)	-31(14)	220(14)	-41(13)
N(1B)	169(19)	190(20)	210(20)	-9(17)	45(16)	-37(16)
C(1B)	200(20)	150(20)	250(30)	-20(20)	110(20)	8(19)
C(2B)	180(20)	160(20)	280(30)	20(20)	60(20)	32(18)
C(3B)	220(20)	310(30)	260(30)	50(20)	40(20)	-20(20)
C(4B)	270(20)	130(20)	270(30)	-37(19)	100(20)	-61(19)
C(5B)	210(20)	80(20)	250(30)	28(19)	70(20)	-9(18)
C(6B)	170(20)	110(20)	270(30)	-1(19)	111(19)	-25(18)
C(7B)	150(20)	120(20)	330(30)	20(20)	98(19)	34(18)
C(8B)	170(20)	150(20)	240(20)	-20(19)	58(19)	16(18)
C(9B)	140(20)	160(20)	250(20)	-47(19)	91(19)	-36(18)
C(10B)	280(20)	160(20)	270(30)	-50(20)	90(20)	30(20)
C(11B)	270(20)	200(20)	270(30)	-70(20)	60(20)	-40(20)
C(12B)	200(20)	230(30)	240(20)	-20(20)	50(20)	-3(19)
C(13B)	120(20)	190(20)	270(30)	-10(20)	49(19)	-33(19)
C(14B)	150(20)	210(20)	260(20)	10(20)	85(19)	-3(18)
C(15B)	210(20)	140(20)	280(30)	0(20)	100(20)	7(19)
C(16B)	210(20)	150(20)	250(30)	6(19)	120(20)	37(19)
C(17B)	260(20)	130(20)	200(20)	-14(19)	80(20)	4(19)
C(18B)	160(20)	240(30)	270(30)	-40(20)	10(20)	40(20)

C(19B)	250(20)	140(20)	400(30)	30(20)	160(20)	-25(19)
C(20B)	300(30)	180(20)	340(30)	80(20)	170(20)	110(20)
C(21B)	220(20)	230(30)	270(30)	-10(20)	70(20)	10(20)
C(22B)	200(20)	400(30)	250(20)	50(20)	70(20)	0(20)

Table 5. Hydrogen bonds for JTB03 (CCDC 269741) [\AA and $^\circ$].

D-H...A	d(D-H)	d(H...A)	d(D...A)	<(DHA)
O(1A)-H(1AA)...O(2A)#1	0.84	1.99	2.830(4)	176.3
O(2A)-H(2AA)...N(1A)	0.84	1.95	2.660(4)	141.5
O(1B)-H(1BA)...O(2B)#2	0.84	1.96	2.801(4)	176.5
O(2B)-H(2BA)...N(1B)	0.84	1.88	2.658(4)	154.4

Symmetry transformations used to generate equivalent atoms:

#1 $-x+1, y+1/2, -z+1/2$

#2 $-x, y-1/2, -z+1/2$

Notebook Cross-reference

Compound 33	JTB3-071
Compound 37	JTB2-289
Compound 57	JTB1-243
Compound 58	JTB3-053
Compound 59	JTB3-057
Compound 63	JTB2-227
Compound 64	JTB2-295
Compound 65	JTB3-049
Compound 72	JTB20-205
Compound 88	JTB21-111
Compound 96	JTB20-125
Compound 98	JTB20-129
Compound 99	JTB20-135
Compound 100	JTB20-147
Compound 101	JTB20-149
Compound 102	JTB20-159
Compound 103	JTB20-161
Compound 104	JTB21-115
Compound 105	JTB20-253
Compound 106	JTB20-257
Compound 107a	JTB20-179
Compound (-)-107	JTB20-199
Compound (-)-108	JTB20-201
Compound 109a	JTB20-177
Compound (-)-109	JTB20-197
Compound 110a	JTB21-119
Compound (-)-110	JTB21-119
Compound 111	JTB20-155
Compound 112	JTB20-169
Compound 113	JTB20-157
Compound 114	JTB20-173
Compound 145	JTB19-159
Compound 146	JTB21-045
Compound 159	JTB20-251
Compound 162	JTB20-119
Compound (-)-163	JTB20-065
Compound (+)-163	JTB20-065
Compound 177	JTB5-211
Compound 180	JTB9-275
Compound 182	JTB9-277
Compound 186	JTB17-185

Compound 187	JTB19-205
Compound 188	JTB19-239
Compound 190	JTB19-301
Compound 191	JTB19-295
Compound 193	JTB20-263
Compound 194	JTB20-265
Compound (-)-194	JTB20-265
Compound (\pm)-195	JTB19-269
Compound (-)-195	JTB20-065
Compound (\pm)-196	JTB20-269
Compound (\pm)-199	JTB19-271
Compound (-)-201	JTB21-107
Compound (\pm)-202	JTB19-287
Compound (\pm)-203	JTB19-289
Compound (\pm)-204	JTB19-291
Compound 205	JTB19-295
Compound 206	JTB20-121
Compound (-)-207	JTB19-301
Compound 208	JTB19-301
Compound (-)-209	JTB20-053
Compound 218	JTB20-031
Compound 219	JTB20-299
Compound (-)-225	JTB21-101

About the Author

Jeffrey Thomas Bagdanoff was born on September 3, 1976 in the Los Angeles area city of Bellflower, CA. At the age of 5, he was transplanted to northern California, where he experienced his childhood and adolescence in the city of Modesto, home to Gallo wineries, Gary Condit, Chandra Levey, and Lacy and Scott Peterson (to whom he bears no relation). Tragically uncoordinated in team sports, he established his physical development through running track and cross country, swimming, weightlifting, waterskiing, bicycling, martial arts, and mischief.

While Modesto provided a good environment for his early interests, he was drawn to UC Davis in 1994 to cultivate his interest in science generally and chemistry specifically. Along the way, he found himself in a number non-academic of occupations including home painter, small business owner, bus driver, forest fire-fighter, resident advisor and pizza chef. Ultimately, he found chemistry to be an exciting and noble pursuit when he began undergraduate research in the laboratory of Mark Kurth.

After obtaining his B.S. in chemistry from UC Davis in 1998, he moved to the San Francisco Bay area to work in the small molecule drug discovery department at Chiron Corp. in Emeryville, CA. It was there that his desire to pursue a career in pharmaceutical development was cemented. To further this goal, he pursued graduate studies at Caltech in 2000 and completed his Ph.D. studies in the laboratories of Brian Stoltz in the summer 2005. One week later, he married Claire V.A. Weatherhead, set off on an extended honeymoon cruise of the Bahamas, then moved to Princeton, New Jersey to continue his career in the pharmaceutical industry, and lived happily ever after.